Assessing uncertainty in co-heating tests:

Calibrating a whole building steady state heat loss measurement method

Samuel Francis Stamp

A dissertation submitted in fulfillment
of the requirements for the degree of
Doctor of Philosophy
of
University College London.

UCL Energy Institute
University College London

September 29, 2015

I, Samuel Francis Stamp, confirm that the work presented in this thesis is my own.
When information has been derived from other sources, I confirm that this has been indicated in the thesis.

Samuel Stamp

London, September 29, 2015

Abstract

Co-heating is a method of estimating the whole building heat loss coefficient (*HLC*) of a dwelling using constant internal temperatures and steady state analysis. Use of the co-heating method in the UK has provided significant evidence of a fabric performance gap and identified unexpected mechanisms for heat loss, such as the party wall bypass. However, to date there has been little assessment of the uncertainties associated with this method, leading to considerable debate and lack of understanding over its use.

This research draws on the use of both simulated co-heating tests and case study field tests to understand uncertainty within the co-heating method. A broad range of uncertainties are assessed under three themes: weather driven, experimental and statistical uncertainties. For each source of uncertainty identified, the nature, direction and scale is considered. Interactions to key building characteristics are then explored, including the thermal mass, fabric insulation and airtightness of a test dwelling. In addition, approaches to both identifying and limiting these errors are discussed.

In particular, the impact of the prevailing test weather conditions are shown to influence *HLC* estimates, particularly solar radiation. These include: the estimation of solar gains, the imperfect measurement of solar radiation, the influence of stored solar heating contributions and the influence of solar driven overheating restricting when reliable *HLC* estimates can be obtained. Furthermore, in non-airtight dwellings, the impact of wind is shown to increase variation in heat loss. Incomplete knowledge of secondary heat flows driven by the external environment lead to definitional uncertainty in *HLC* estimates and make comparisons to predicted or design *HLC*s more complex. Experimental uncertainties, from non-uniform internal temperatures, equipment measurement errors and uncoupled heat losses are also shown to potentially provide large systematic uncertainties if unchecked.

Having established the presence and nature of these uncertainties the application of the co-heating method is reviewed. This includes suitable environmental testing conditions, the required duration for testing and the ability to perform comparisons to design and determine retrofit improvements. As such issues are a function of the building being tested and its characteristics, a number of archetype dwellings are used to show how the requirements and the general suitability of co-heating varies between dwellings. However, within a suitable external environment and avoiding experimental uncertainties, accurate *HLC* can be obtained with just 72 hours of monitoring. In addition, an approach to providing appropriate uncertainty estimates to a given co-heating test is developed and the interpretation of the measured *HLC* is shown to be when compared to both design predictions and when examining retrofit improvements.

To summarise, theoretically, this research establishes the bounds of the co-heating method and demonstrates the effectiveness of co-heating tests in understanding building fabric heat loss. Methodologically, it establishes the role of simulation in the estimation of errors associated with measurement procedures and demonstrates the value of applying multi-method approaches to complex problems arising from the physical performance of buildings. Substantively, this research highlights the need for researchers working in the field to be mindful of the uncertainty in co-heating tests and understand limits of the measurement and its interpretation.

Acknowledgements

I would like to thank all those who helped and support me during the course of the PhD. Firstly, I owe gratitude to my supervisors Prof. Bob Lowe and Dr. Hector Altamirano-Medina, for their insightful guidance, encouragement, understanding and support throughout this research. I would also like to thank Dr. Ian Ridley, my supervisor for the first few months of this work and to Dr. Jez Wingfield for his support during and after his time at UCL. I would also like to thank my colleagues at the UCL Energy Institute, in particular Dave, Ed, Carrie, Faye and Sofie. My thanks also goes to the administrative staff in the UCL Energy Institute and LoLo CDT for their support, particularly Alison Parker, Mae Oroszlany and Rosanna Seels.

The research conducted as part of this thesis would not have been possible without support from a number of people and organisations including: the NHBC and participants of the NHBC co-heating field trial, David Butler and Andy Dengel at BRE, Justin Bere and Sarah Lewis of Bere Architects, Elizabeth Ness and Julia Plaskett of Crest Nicholson, Owen Daggett of Joseph Rowntree Housing Trust, Neil May and Chris Eaton of Natural Building Technologies, Dominic Miles-Shenton at Leeds Beckett University, John Palmer of AECOM, and Richard Jack at Loughborough University.

I would like to acknowledge the financial contribution of the UK Engineering and Physical Sciences Research Council in supporting the London-Loughborough Centre for Doctoral Research in Energy Demand that provided the necessary financial means for this PhD research (grant number EP/H009612/1).

Finally, I must thank my parents Sheila and Nick, brothers Oliver and Elliot, family, friends and most of all Stephanie for supporting me throughout the last 4 years.

Contents

List of Figures

List of Tables

Acronyms

DER = Dwelling Emission Rate

TER = Target Emission Rate

DFEE = Dwelling Fabric Energy Efficiency

TFEE = Target Fabric Energy Efficiency

SA = Simple average analysis method

SLR = Simple linear regression

MLR = Multiple linear regression

iMLR = Multiple linear regression including intercept

cSLR = Solar corrected simple linear regression

MLR$_{wind}$ = Multiple linear regression including wind speed

SOLR = Solar load ratio

SBLR = Solar load ratio including baseload

PSTAR = Primary and Secondary Terms Analysis and Renormalisation

STEM = Short Term Energy Monitoring

CWI = Cavity Wall Insulation

TMP = Thermal Mass Parameter

HLP = Heat Loss Parameter

TFA = Total Floor Area

LBU = Leeds Beckett University

NREL = National Renewable Energy Laboratory

SERI = Solar Energy Research Institute

GHA = Good Homes Alliance

BPE = Building Performance and Evaluation

EST = Energy Savings Trust

GHA = Good Homes Alliance

NHBC = National House Builders Council

TSB = Technology Strategy Board

BRE = Building Research Establishment

JRHT = Joseph Rowntree Housing Trust

SAP = Standard Assessment Procedure

RdSAP = Reduced Standard Assessment Procedure

Nomenclature - Common Terms

Symbol	Description	S.I. Units
HLC	The heat loss coefficient of a dwelling	(W/K)
HLC_{True}	The true heat loss coefficient of a dwelling	(W/K)
HLC_{meas}	The measured heat loss coefficient of a dwelling	(W/K)
HLC_{pred}	The predicted heat loss coefficient, based upon either design or as-built assumptions	(W/K)
HLC_{TOT}	The total heat loss coefficient of a dwelling	(W/K)
HLC_{inf}	Infiltration heat loss coefficient	(W/K)
HLC_{trans}	The transmission heat loss coefficient of a dwelling	(W/K)
HLC_{fabric}	The fabric heat loss coefficient of a dwelling, i.e. HLC_{TOT} - HLC_{inf}	(W/K)
HLC_{adj}	The heat loss coefficient between a dwelling and an adjoining space	(W/K)
HLC_{unc}	The heat loss coefficient between a dwelling and a unconditioned space	(W/K)
HLC_{unc}	The heat loss coefficient describing heat transfer to an connected, unheated space	(W/K)
HLC_{adj}	The heat loss coefficient describing heat transfer to an adjoining, heated space	(W/K)
T_i	Internal air temperature	(°C)
T_e	External air temperature	(°C)
T_{si}	Internal surface temperature	(°C)
T_{se}	External surface temperature	(°C)
T_{sky}	Effective sky temperature	(°C)
$T_{setpoint}$	Experimental setpoint temperature	(°C)
T_g	Ground temperature	(°C)
T_{adj}	Air temperature of adjoining heated space	(°C)
T_{unc}	Air temperature of connected unconditioned space	(°C)
ΔT	Is the temperature gradient between internal and external air temperatures	(K)
R	The solar aperture	(m^2)
R_{GHR}	The solar aperture based upon S_{GHR}	(m^2)
R_{GVS}	The solar aperture based upon S_{GVS}	(m^2)
R_{GVM}	The solar aperture based upon S_{GVM}	(m^2)
R_{ISO}	The solar aperture numerically calculated using ISO 13790:2008	(m^2)
R_{SAP}	The solar aperture numerically calculated using SAP	(m^2)
R_{PHPP}	The solar aperture numerically calculated using PHPP	(m^2)

Symbol	Description	S.I. Units
Q_{elec}	Electric heating load	(W)
$Q_{baseload}$	Non-thermostatically controlled electric heating load	(W)
Q_{trans}	Transmission losses	(W)
Q_{inf}	Infiltration losses	(W)
Q_g	Heat flow to the ground	(W)
Q_{adj}	Heat flow to adjoining spaces	(W)
Q_{unc}	Heat flow to unconditioned spaces	(W)
Q_{sol}	Solar heat gains	(W)
$Q_{sol,true}$	True solar heat gains through glazed elements	(W)
Q_{sky}	Het flow to the sky	(W)
S	Incident solar radiation	(W/m^2)
S_{GHR}	Global horizontal radiation	(W/m^2)
S_{GVP}	Global vertical radiation in the orientation of the principal facade	(W/m^2)
S_{GVS}	Global vertical south-facing radiation	(W/m^2)
S_{GVE}	Global vertical east-facing radiation	(W/m^2)
S_{GVW}	Global vertical west-facing radiation	(W/m^2)
S_{GVN}	Global vertical north-facing radiation	(W/m^2)
S_{GVM}	Global mean vertical radiation	(W/m^2)
S_{Diff}	Diffuse horizontal radiation	(W/m^2)
S_{Dir}	Direct normal radiation	(W/m^2)
U	Thermal transmittance / U-value	(W/m^{2}K)
R	Thermal resistivity / R-value	(m^{2}K/W)
h_r	Radiative heat transfer coefficient	(W/m^{2}K)
h_c	Convective heat transfer coefficient to the external environment	(W/m^{2}K)
α	Absorptance of the surface for solar radiation	(0-1)
R_{se}	External surface heat resistance	(m^{2}K/W).
U_w	Average wind speed	(m/s).
A	Area of surface	(m^2).

Chapter 1

Introduction

Chapter Overview

1.1 Context and relevance of research

This research aims to understand the uncertainty, accuracy and limitations of co-heating heat loss measurements. Through better understanding it is hoped this method can become a more valuable tool; improving our knowledge of actual building performance and how to consistently achieve truly low energy dwellings. Improved thermal performance of the building fabric may translate to improved thermal comfort and economics of the individual occupants, reduced energy demand, lower infrastructure costs and improved energy security at a regional and national level and reduced global pressures on fuels and resources.

A fuller discussion of the surrounding context and motivation for this study can be found at the beginning of the literature review (section 2.1).

1.2 Problem statement

Co-heating tests have been used to measure the total building heat loss coefficient, or *HLC*, since their inception and early development in the 1980s (Palmiter, 1979; Siviour, 1981). Recently, particularly in the UK, the adoption of co-heating tests has increased following their use in a number of successful research programmes that uncovered significantly higher measured heat losses than predicted and unveiled significant unpredicted heat loss pathways (Bell and Lowe, 1998; Lowe et al., 2007; Wingfield et al., 2011). As further dwellings have undergone testing this trend for measuring higher than predicted heat loss has persisted, enhancing the evidence of a fabric performance gap (Stafford et al., 2012; Johnston et al., 2013). Understanding and closing this gap is now thought crucial in meeting reduction targets not just in theory but in practice.

However, without a full understanding of the accuracy of co-heating heat loss measurements and estimates of their errors, it has been difficult to define the significance of such measured discrepancies between predicted and measured heat loss. It has therefore been difficult to persuade the industry to act. Whilst previous work revealing a fabric performance gap has increased the use and prominence of co-heating tests, it has also highlighted a lack of current understanding over the reliability of the method and the accuracy of its results. This is confounded by a lack of research into the method itself, an absence of any official standards, leading to inconsistent usage, and a lack of published material.

As such, a problem statement can be formulated as follows:

Although a number of co-heating tests have been performed and their results have provided significant evidence of a fabric performance gap, the method itself has not been rigorously evaluated to date. This leaves ambiguity over the accuracy and validity of results and uncertainty over how the method should be applied to help resolve the performance gap it has previously helped to identify.

1.3 Research questions

Following from the problem statement presented above, the research question defining the central core of this thesis can be written as:

How accurate and reproducible is the steady-state co-heating method at determining a dwelling's heat loss coefficient?

The terms accurate and reproducible need careful consideration. We can consider the term *accuracy* to describe the closeness of measurement to the unknown *true value*, a combination of the *trueness*, reflecting the degree of systematic errors, and the *precision*, reflecting the presence of random errors - see ISO 5725-1:1994 (JCGM, 2008a, ISO, 1994;). In any physical experiment, as the true value cannot be known, the error between the measured and true values remains equally unknowable. Instead, it is the *uncertainties* associated with the random and systematic effects that give rise to the error that can be evaluated. It is only in simulations carried out in this work that the true *HLC* can be known and the accuracy assessed more directly.

The term *reproducible* then refers to the the ability to replicate a measurement within a difference set of conditions. It therefore describes the sensitivity of the co-heating *HLC* measurement to the external environment, internal experimental conditions, construction of the test dwelling, experimental conditions and analysis techniques. These terms and further definitions for terms describing the uncertainty of measurements can be found in section 3.5.

To fully answer this research question a number of further issues must be addressed. The answer to this question will very much be a function of the building being tested and the conditions, both environmental and experimental, in which it is tested. This leaves a broad research landscape that requires narrowing. Firstly, the definition of a dwellings heat loss coefficient needs to be considered. Providing the first secondary research question:

- **A0)** How is the *HLC* defined, in terms of its *predicted*, *measured* and *true* value?

The remaining secondary research questions can be split into two branches, the first, investigated in chapters 5 - 8, is concerned with understanding the uncertainties in the co-heating method:

- **A1)** What is the impact of the non-steady state external environment upon the steady state *HLC* estimate? (Chapters 5 and 6)
- **A2)** How do the experimental conditions achieved in reality deviate from the theoretical heat balance model and what uncertainties are created as a result? (Chapter 7)
- **A3)** How do building characteristics of the test dwelling interact with parts A1 and A2 and dictate the accuracy and reliability of the *HLC* measurement? (Chapters 5 - 7)
- **A4)** How can sources of uncertainty be identified and subsequently addressed (Chapters 5 - 7)

The second branch, forming the basis of chapter 9, concerns the impact of these uncertainties on the application and use of the co-heating method (chapter 9):

- **B1)** Under what environmental conditions can co-heating tests be performed to reliably estimate a building *HLC*? (Section 9.1)
- **B2)** When tested under suitable environmental conditions, how long is required to accurately determine a building *HLC*? (Section 9.2)

- **B3)** Given the uncertainties that exist, what is the optimum co-heating method, both in terms of experimental protocol and analysis techniques, within the existing steady state approach? (Section 9.3)
- **B4)** How can appropriate uncertainty estimates be derived and stated? (Section 9.4)
- **B5)** How do the sources of uncertainties identified limit the use of co-heating in comparisons to design and to before and after retrofit cases? (Section 9.5)

1.4 Objectives

A number of objectives can be drawn from these secondary questions. The first branch of research questions (A1 - A4), focus on investigating the sources of uncertainties present in co-heating tests. Here the first step is to establish the range of environmental and experimental uncertainties that exists. Subsequently, for all sources identified, determine and demonstrate the following:

- The nature of the uncertainty (i.e. systematic or random).
- The scale and direction of error.
- The relationship with key building characteristics of the test dwelling and with other sources of uncertainty.
- The approach to identifying, minimising, correcting or accounting for each source of uncertainty.

For the second branch of secondary research questions (B1-5), focused on the application of the methods, the objectives of this work can be defined as follows:

- To define the likely testing season and duration with which reliable *HLC* estimates can be made for a representative range of test dwellings.
- To define the optimum analysis method (covering questions such as data aggregation period and regression type).
- To define requirements of the experimental protocol adopted.
- To demonstrate an appropriate method of uncertainty analysis based upon suitable literature.

1.5 Scope

The scope of this thesis is defined by a number of further considerations, defining the boundaries of this research:

- The co-heating test method considered principally within this thesis is that used most predominantly in the UK, based upon the early work of Siviour (1981) and Everett (1985) and later incorporated into the Leeds Metropolitan University Protocol (Wingfield, 2010a; Johnston et al., 2013). This consists of quasi-steady state conditions, i.e. constant internal temperatures, data aggregated across periods of at least 24 hours[1], and steady state analysis is conducted through linear regression. Dynamic methods using short periods of co-heating amongst other sequences are not the focus of this research, although parallels are drawn and relevant literature reviewed.

- This thesis is concerned with the measurement, through co-heating, of the total building heat loss or *HLC* as defined fully in section 3.1. Whilst other parameters and disaggregated heat flows are discussed throughout this work, it is the uncertainties surrounding the estimation of the whole building *HLC* that is chiefly of interest.

- The focus of this thesis is on UK housing and a UK climate. Most instances of co-heating tests, using the method as considered in this thesis, conducted to date have been performed in the UK, making these conditions the most relevant. Additionally, these are the conditions in which the author is both most likely to be able to conduct field tests and in which they have the most familiarity. Many of the issues identified will apply to a broader scope, albeit their relative significance may alter. An extreme period of weather in one country may represent typical conditions in another.

- As understanding *as-built* building heat loss is crucial to closing the fabric performance gap and therefore to reducing energy demand, this thesis addresses the use of co-heating as a tool for measuring 'real' dwellings *in the field*. This is as opposed to simply evaluating the use of co-heating in laboratory tests or in dedicated test dwellings. Field tests conducted as part of this research constitute such tests in dwellings constructed under normal conditions, reflecting the complexities this may bring.

[1] Typically meaning daily aggregation (e.g. 24 hours), although periods which are an integer multiple of 24 hours are also used on occasion (e.g. 48 hours, 72 hours, 1 week etc.)

- As most co-heating tests to date been performed on modern, low heat loss dwellings, this type of dwelling represents the main focus of this research. However, more traditional and higher heat loss dwellings are considered later in the thesis, particularly in reference to the application of co-heating tests to measuring retrofit improvements.

1.6 Thesis overview

Chapter 2 - Literature review

This chapter reviews the broad context and motivation behind this study (section 2.1) before covering the history and development of co-heating (2.2) and the details of the co-heating method as considered in this thesis (2.3). Further details of the co-heating method and its variations are then discussed (2.4), along with supporting measurements (2.5). To provide a more rounded perspective on co-heating and to draw useful parallels, both alternative methods for estimating heat loss (2.6) and dynamic *HLC* methods (2.7) are reviewed. To complete the literature review the subject of this thesis is addressed more directly through reviewing work on uncertainty in co-heating (2.8). The chapter itself is then concluded with major themes discussed (2.9).

Chapter 3 - Defining the *HLC*, *R*, *S* and uncertainty

To allow subsequent discussions and investigations the building heat loss coefficient, *HLC*, solar aperture, *R*, and the measured solar radiation, *S*, all need to be considered and properly defined. This chapter begins by defining the *HLC* (3.1) as set out in ISO 13789:2007 and further calculation methodologies (ISO, 1997). This is compared to the definition formed by the co-heating measurement and the definition of the true *HLC*, to which measured values can be assessed. This then includes a brief consideration of the measurement of temperature and how this relates to definitions of heat loss (3.2).

Subsequently, solar gains, and the second parameter estimated by co-heating tests, the solar aperture are defined (3.3) from the perspective of both their formal calculation and the statistical co-heating measurement. The measurement of solar radiation and its various components and forms are then reviewed (3.4), providing the foundations for their use in the rest of the thesis.

Chapter 4 - Research method

Chapter 4, defining the research method adopted for this study, begins by re-stating the research questions (4.1) defined earlier in this chapter. Following this, a number of potential research methods are considered, with their strengths and limitations laid out (4.2). This proceeds a discussion of the research method selected (4.3) and details of both the simulated co-heating tests (4.4) and field test cases studies (4.6) that make up the full research method. Specific elements of the research method may be included later with the relevant analysis. The chapter is again finished with a chapter conclusion (4.7).

Chapters 4, 5, 6 and 7 then explore sources of uncertainty. These are themed around solar sources of uncertainty, further weather driven sources of uncertainty, experimental sources of uncertainty and regression based uncertainties.

Chapters 5 - Solar driven sources of uncertainty

Chapter 5 examines the impact of solar radiation on a test dwelling and *HLC* estimates. This includes a consideration of solar radiation incident upon a test house under co-heating conditions (5.1) and the resulting uncertainties in determining solar gains through measuring solar radiation (5.2) and from determining the solar aperture of a dwelling (5.3). Further solar driven sources of uncertainty are considered in the form of stored solar heating contributions (5.4) and solar driven experimental overheating (5.5). The main conclusions drawn then close the chapter (5.6).

Chapters 6 - Further weather driven sources of uncertainty

Chapter 6 considers further weather driven sources of uncertainty, including those from wind and stack driven infiltration (6.1), dynamic external temperature (6.2) and from long-wave radiation exchange with the sky (6.3), again with the chapter then concluded (6.4).

Chapters 7 - Experimental sources of uncertainty

Chapter 7 concerns experimental sources of uncertainty. This begins with uncoupled heat loss pathways (7.1), such as ground losses and heat transfer to adjoining spaces (7.2). Subsequently, non-uniform (7.3) and non-constant internal temperatures are investigated, including heating to a quasi-steady state (7.4). Uncertainty associated with equipment measurement errors (7.5), moisture and latent loads (7.6) and operational uncertainties (7.7) conclude this chapter on experimental uncertainties, with the outcomes discussed in (7.8).

Chapters 8 - Regression based uncertainties

Chapter 8 considered a number of uncertainties within the regression process itself, including those from a forced intercept model (8.1), from attenuation bias associated with errors in the independent variable S and ΔT (8.2) and from collinearity between S and ΔT (8.3).

Chapter 9 - The application of co-heating

Chapter 9 uses the sources of uncertainty revealed in chapters 5 to 8 to readdress the application of the co-heating method. Importantly, this is considered across a wider range of buildings. This begins with a consideration of the required environmental conditions (9.1) and monitoring duration (9.2) for reliable *HLC* estimation. Subsequently, the optimum co-heating experimental protocol, analysis technique and reporting standard are reviewed (9.3). A method for calculating appropriate uncertainty estimates for co-heating tests is then developed (9.4) before the impact of uncertainties upon comparisons to design and pre and post retrofits (9.5) are considered. The chapter itself is then again concluded (9.6).

Chapter 10 - Conclusions This thesis is then concluded with a summary of the findings (10.1) and key conclusions (10.2). The limitations of the research are then discussed (10.3) along with recommendations for further research (10.4).

1.7 Outputs from this thesis

A number of peer reviewed conference papers have been written as part of this thesis, including:

- *Using simulated co-heating tests to understand weather driven sources of uncertainty within the co-heating test method* (ECEEE Summer Study Proceedings, Presqu'ile de Giens, Toulon/Hyres, France, June 3-8) Initial exploratory work into the impact of various weather variables upon co-heating tests through full building simulation (Stamp et al., 2013d).

- *An investigation into the role of thermal mass on the accuracy of co-heating tests through simulations and field test results* (IBPSA Building Simulation 2013, Chambery, France, August 25-28): An comparative examination of the accuracy of co-heating *HLC* measurements upon a dwelling of varying thermal mass (Stamp et al., 2013a).

- *Solar driven uncertainty in co-heating* (IEA Annex 58, 4th Meeting, April 8th - 10th, Holzenkirchen, Germany, 2013) Investigation of the solar driven uncertainness upon co-heating tests (Stamp et al., 2013b).

Additionally, results from this work have fed into the Zero Carbon Hub Performance Gap Project - Working Group 5b - Testing (see ZCH, 2013; ZCH, 2014a; ZCH, 2014b) and into the IEA Annex 58 - Subtask 1 - An overview of state-of-the art methods to analyse data of in-situ measurements for energy performance quantification.

Further papers are also planned from the work within this thesis.

Chapter 2

Literature review

Chapter Overview

Chapter 2, the literature review, is split up into eight parts, each listed below with a brief description for guidance:

- **2.1 Context & motivation:** In which the context behind this thesis is discussed, including: space heating demand, building regulations, fabric performance, the performance gap and verifying performance.
- **2.2 The history & development of co-heating:** Reviews the initial development of the co-heating method from its US and UK origins. Contemporary and future uses are then discussed.
- **2.3 The co-heating method:** The key components of the co-heating method are described in full detail, including both the experimental protocol and analysis techniques.
- **2.4 Discussion of the method:** The requirements for co-heating testing are reviewed from literature, including: the duration, testing season, aggregation length and intervals.
- **2.5 Additional co-heating test protocols:** Supporting tests typically used in tandem with co-heating tests are discussed, both in relation to the support they provide to *HLC* estimates and for broader context around the use of co-heating tests. This includes infiltration measurements, party wall heat transfer and a review of further supporting methods.
- **2.6 Alternative method of estimating heat loss:** In situ U-value measurements and infrared thermography are briefly discussed to provide comparisons and further context around co-heating.

- **2.7 Dynamic methods of estimating building *HLC*:** Dynamic experimental protocols and analysis techniques are discussed to provide a contrast to the steady state co-heating method. In particular this includes the PSTAR method.

- **2.8 Research into Uncertainty:** Narrowing the focus of the literature review onto the precise subject of this thesis, pieces of work investigating uncertainty either directly or indirectly are reviewed.

- **2.9 Conclusions from the literature review:** Key conclusions, gaps in the literature and emergent themes are considered at the end of the chapter.

2.1 Context & motivation

A residential building is intended to provide its occupants with shelter, security and thermal comfort. To limit both financial and environmental costs, thermal comfort should be achieved through minimised energy consumption.

Space heating in dwellings forms a significant part of total UK energy demand. Whilst the domestic sector accounts for 29% of the UK final energy demand (DECC, 2014), records from 1970 show around two-thirds of household energy use is associated with space heating, accounting for 62% of the domestic energy consumption, and 19% of the UK's total energy consumption in 2013 (DECC, 2013b, table 1.1.5). Reducing domestic energy use and space heating demand therefore forms a fundamental element in reaching emission reductions laid out in the 2008 climate change act, i.e. a 34% cut in 1990 greenhouse gas emissions by 2020 and at least an 80% cut by 2050 (DECC, 2013b).

Reducing space heating demand is not only imperative to reaching emission targets and ensuring energy security but also impacts individual households. In 2013, there were 2.35 million households in fuel poverty, 10.4% of total UK households (DECC, 2015). Adding significant weight to this statistic, previous studies have shown that between 1988 and 1997 an average of 37,000 annual excess winter deaths have been recorded in the UK (Healy, 2003). The benefits of healthy, comfortable and thermally efficient homes therefore extend from the health, comfort and economics of the individual, to national and global issues of energy demand, security of supply and CO_2 emission targets.

Space heating demand itself is dictated by three factors: the building fabric, the heating system and the behaviour of the dwelling's occupants, all within a set of climatic conditions. This thesis will be focusing on one of these components in isolation - the building fabric. The rest of section 2.1 will review how space-heating demand may be reduced through improvements in fabric efficiency, evidence of a fabric performance gap and finally the role of feedback and verifying performance.

2.1.1 Improved fabric efficiency: Regulation & calculation

To promote cost-effective measures for improved energy performance the Energy Performance of Buildings Directive (EPBD) was brought into force on the 4th January 2003 and recast in 2010, with the aim of moving towards new and retrofitted nearly-zero energy buildings by 2020, or 2018 in the case of Public buildings (BRE, 2006; EU, 2010). This has driven the national targets and calculation methodologies for member states, forming the overarching driver for improved fabric efficiency.

2.1.1.1 Scrapping of zero carbon homes by 2016

There have been significant recent policy changes altering the UK's path to meeting the European Directive. In a policy first announced in 2006, the UK had targeted all new homes to meet the Zero Carbon Standard by 2016. However, shortly following the election of a new conservative government, in July 2015 this was effectively scrapped in an effort to reduce 'net regulation' on house builders, with the government no longer intending to *"proceed with the zero carbon Allowable Solutions carbon offsetting scheme or the proposed 2016 increase in on-site energy efficiency standard, but will keep energy efficiency standards under review, recognising that existing measures to increase the energy efficiency of new buildings should be allowed time to become established"* (HM Treasury, 2015, p.46).

Whilst this announcement has caused uncertainty within the industry, it does not alter the fundamental context of the research conducted in this thesis. Rather, fabric performance remains a key factor in overall energy performance and without measurements of thermal performance control over the delivery of efficient buildings is weakened. In fact, with less ambitious targets there is perhaps more onus to ensure existing fabric heat loss standards are met. Further, if current regulations are failing to deliver homes that consistently meet the current standards, then robust evidence from measurements is needed to inform and amend regulations.

2.1.1.2 Heat loss calculations within regulation

The EPBD requires the implementation of a calculation methodology and setting minimum energy requirements, although the directive does not specify how these requirements should be set or how they should be arrived at. This is instead decided at a national level.

In the UK these energy requirements are established by the Building Regulations Approved Documents (DCLG, 2013), with a calculation methodology defined by the Standard Assessment Procedure, SAP (BRE, 2011; BRE, 2014), based upon the BRE domestic energy model, BREDEM (BRE, 2015). Presently, Building Regulations define a number of backstop U-values for individual elements, whilst the building as a whole is addressed through its annual CO_2 emissions per m^2 of floor area. Essentially, the emissions from a proposed dwelling, the dwelling emission rate (DER), are compared to a notional dwelling, of the same size, shape and orientation. The notional dwelling is based upon the requirements of the 2002 Building Regulations, giving a target emissions rate (TER) which the DER should not exceeded. Both the TER and DER must be set out and supplied to the Building Control Board prior to construction, and again in an updated as-built version within 5 days of completion, including any changes made to the specification.

An overall emissions approach is designed to leave plenty of flexibility for designers and developers. However, in 2013, target and dwelling fabric energy efficiency (TFEE & DFEE) ratings were introduced into Part L to sit alongside the DER and TER, operating in much the same way. This increased emphasis on energy efficient building fabric was then slightly downgraded following responses to this consultation, with a 15% shortfall allowed between the TFEE & DFEE to restore some design flexibility (BRE, 2014).

Thermal characteristics used as inputs into SAP heat loss calculations (e.g. U-values) are defined by further calculation methodologies (Anderson, 2006), based on European and International standards, e.g. ISO 6946:2007 (ISO, 2007). This is the first point at which physical measurements are required and form inputs into the chain of calculations used to determine a building's total heat loss. Thermal properties, such as the thermal conductivity of the constituent materials or sample elements, are measured in certified laboratories under prescribed methodologies, e.g. guarded hot box, ISO 8990:1996 (ISO, 1996). Whilst such measurements are well defined, the conditions in which they are performed are likely to differ from the deployment of such materials in both a full building system and in the full external environment.

In this framework, thermal performance is then only measured outside of the construction process, testing individual materials and components in laboratories under certain sets of conditions and only on selected samples. These measured thermal parameters are then adopted into simplified equations along with further assumptions to yield a whole building heat loss estimate. If unsuitable, these assumptions and simplified heat loss models may lead to discrepancies between the predicted or modelled heat loss and the as-built dwelling. In addition, thermal parameters measured in laboratories may no longer be fully applicable, with the materials now sitting within different constructions, sets of environmental conditions and in a state influenced by their handling in the construction process. Without measurements within the construction process and of full buildings, design calculations and assumptions are left unchecked and may fail in delivering targeted energy performance.

2.1.2 Actual performance and the performance gap

The regulation to drive improved fabric thermal performance discussed so far only enforce these targets, and the subsequent demand reduction is therefore only met on paper. However, for almost as long as energy use has been measured, evidence of significant variation from design predictions has been evident (see Socolow, 1978; Norford et al., 1994; Bordass et al., 2001). This variation can be driven by all three components that dictate space heating demand: occupier behaviour, heating system efficiencies and fabric performance. More alarmingly, in recent years evidence of a 'performance gap' has increased, with higher than predicted energy use potentially undermining the targets set through regulation. For example, assumptions over assumed occupant behaviour have been found to be limited or unrepresentative (DECC, 2013a; Huebner et al., 2015; Fabi et al., 2012) and field trials have found evidence of underperformance across a range of heating systems (Orr et al., 2009; EST, 2010; Trust, 2011). Disentangling the different contributions to the performance gap from occupant behaviour and system and fabric performance has proved a difficult task, particularly as a large number of interactions are present. Direct measurements may therefore be key to improved building performance.

Centrally to this thesis, evidence of a fabric performance gap has emerged through both indirect and more direct evidence. There is considerable evidence of fabric defects occurring from stages across construction (Calcutt, 2007; Josephson, 1999) and of non-compliance with part L (EEPH, 2006; Mawditt and Palmer, 2008). Further, the expected reductions from retrofit interventions have not yielded the improvements in airtightness predicted (Hong et al., 2006).

More directly, in situ U-value measurements of cavity walls have been reported as significantly higher than predicted (Siviour, 1994; Doran, 2001). Drivers for poor performance have been demonstrated in twin test houses and laboratory settings, relating complex heat loss processes to poor workmanship (Rayment, 1995; Hens et al., 2007). In fact links between workmanship and complex heat transfer processes across a wall, such as forced convection, have been in established in a laboratory setting and shown to reduce thermal performance almost four decades ago (Bankvall, 1977).

Such measurements have not exclusively revealed underperformance. In situ U-value measurements of traditional and solid brick walls (Rye, 2010; Baker, 2011; Birchall, 2011; Li, 2014), have shown significantly better thermal performance than predicted, findings that have significant policy and economic implications.

Significant evidence of a fabric performance gap has also come from measurements of whole building heat loss coefficients through the use of co-heating. Researchers at Leeds Beckett University[1] drove much of this work and with over 50 tests performed, hold the largest database of measured *HLC*s. Whilst such a sample is not representative, the consistency of higher measured values and the scale of this gap became a source of great concern (Johnston et al., 2012a). The figure below, taken from Stafford et al. (2012) shows 22 of 34 tested dwellings with measured values 20% higher than predicted and 14 of the 34 more than 60% higher. More recent analysis from this database has begun to examine the measured gap together with built form and construction types (Johnston et al., 2015).

It can be noted here that figure 2.1 does not include any error estimated for either measured of predicted *HLC*s, potentially undermining confidence in the evidence presented. Error estimates, typically based upon statistical standard errors, are given in a number of the individual LBU tests and other practitioners (see table 2.1), but generally this remains an inconsistent and poorly understood aspect of co-heating tests and is not included in the LBU protocol.

[1] Formerly Leeds Metropolitan University

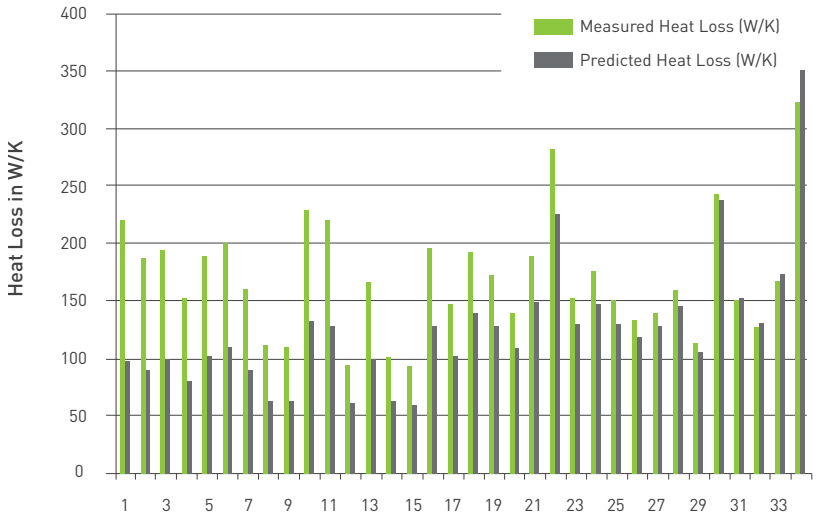

Figure 2.1: *Measured vs Predicted HLC values for 34 dwellings measured by LBU. Note this includes both new builds and existing dwellings. Taken from Stafford et al. (2012)*

2.1.3 Verifying performance & feedback

With growing evidence of a fabric performance gap there is a significant risk that regulatory work is undermined by actual performance. The impact of this risk is magnified by the long physical lifetimes of dwellings, slow replacement cycles and high costs of retrospective repairs or improvements, potentially leaving a legacy of poorly performing building fabrics for generations to come (Johnston et al., 2015).

A review into the performance gap was conducted by the Zero Carbon Hub, collating the views of experts from academia and industry, including insulation manufacturers and associations, house builders, architects, government and certification and testing organisations (ZCH, 2013; ZCH, 2014a; ZCH, 2014b). This report argued that, *"in order to close the Performance Gap it is critical that real performance can be assessed, measured, tested and demonstrated"* (ZCH, 2014a, p.43). This coincides with an ambition of ensuring designed performance is met in reality.

> *"From 2020, be able to demonstrate that at least 90% of all new homes meet or perform better than the designed energy / carbon performance" (ZCH, 2014a, p.3)*

This represents a significant challenge and requires an array of suitable methods for demonstrating performance. Even prior to this, a better understanding of how this ambition might be consistently met is required, meaning improved understanding of actual building heat loss and

the processes behind it. The same report notes *"existing diagnostic tests need to be more useful, useable and consistent, through standardising the application of tests and the interpretation of results*" (ZCH, 2014a, p.43), with a particular need for fabric and services tests at a systems level to be developed.

There is one area in which thermal performance is already tested as part of the building regulations. Air permeability can be measured through pressure or blower door tests and since 2006 (HM Government, 2006a; HM Government, 2006b), it has been required that an appropriate sample[2] of new builds are tested to ensure they meet a backstop compliance value, and the results are re-inputted into SAP to ensure the overall TER is met. This process is supported by defined standard protocols (ATTMA, 2010) and requirements for trained persons. Importantly, a required number of tests must be carried out early enough in the construction process to prevent repeated failures. When tests do fail, remedial work should be conducted until a passing test result is obtained.

However, there are fundamental differences between airtightness and whole house fabric heat loss tests; namely the timescales and complexity of measured parameters. As a result the use of co-heating tests have remained limited and within a research domain. Furthermore, the experimental protocol is not as well established or consistently adopted. However, to ensure that buildings are meeting performance targets overall, not just on airtightness alone, some type of whole building assessment may be required. To address this, it was suggested as part of the 2012 Building Regulation Consultation that in the future they:

> *"...might specify a level of sample testing (e.g. whole house fabric co-heating tests or equivalent carried out post completion but pre-occupation)" (DCLG, 2012, p.51)*

Such a statement has perhaps led to concern and debate over the suitability of the co-heating method. Assurances over the reliability and accuracy of the test method and an understanding of its limits are required, including the adoption of appropriate estimates of the error within *HLC* measurement. It is unlikely policy or developers themselves will act upon any evidence unless it is robust and can be stated with some estimate of the uncertainty in the measurement. Furthermore, it needs to be established how and when co-heating tests can best be used. It is these two themes that this thesis addresses, understanding the uncertainties in the co-heating method and determining how they can inform its application within the context defined here.

[2]Either on 3 units of each dwelling type or 50% of all instances of that dwelling type, whichever is less.

2.2 The history & development of the co-heating method

2.2.1 Early development 1979 - 1988

In the late 1970s, researchers in the US, described a method known as electric co-heating (Sonderegger and Modera, 1979; Sonderreger et al., 1980). Following studies that had demonstrated high diversity in the energy used by energy efficient buildings there was growing interest in being able to disaggregate the potential causes via in situ-measurements of both heating system efficiencies and building heat loss coefficients. A method was developed in which a test dwelling was heated via portable electric heaters to a constant internal temperature. Heaters were thermostatically controlled with electricity consumption monitored by kWh meters and external temperatures recorded to allow a building heat loss coefficient to be estimated across either a single or set of consecutive nights. Subsequently, the regular heating system was operated and the ensuing load reduction seen in the electric heaters was used to determine the net heat gain into the house, with the fuel provided to the heating system then used to determine the heating system efficiency. The term co-heating was adopted to describe this method and its adoption of this dual heating approach.

This basic method was extended to incorporate sections of not only constant internal temperatures, termed co-heating periods, but with thermal decays or cooldowns and free-floating periods, a combination developed by Duffy and Saunders (1987) amongst others. This test procedure was used to recalibrate a building model based on an audit description, in the PSTAR[3] method, section 2.7.3 (Subbarao, 1988a; Subbarao, 1988b; Subbarao, 1988c). These additional stages in the experimental protocol allowed estimates of further parameters, namely the effective solar gains and effective building thermal mass. Ultimately, this provided a re-calibrated building model used to improve predictions of long-term energy use.

Meanwhile, researchers in the UK were interested in the performance of passive solar houses and began to develop similar test methods with which to estimate the building heat loss coefficient and the solar aperture, R, of test dwellings. This work began with Siviour (1981) who developed a method that adopted an experimental protocol similar to Sonderegger and Modera (1979)., i.e. constant internal temperatures and electric heating, albeit over much longer time periods ($>$1 week) and using the full data set within the analysis, rather than simply night time data. A simplified energy balance was used (see equation 2.5, section 2.3.1), with both building parameters then determined via steady state regression analysis, using a form of energy balance

[3] Primary and Secondary Terms-Analysis and Renormalisation

previously suggested by Palmiter (1979).

Everett (1985), attempted to speed up and simplify Siviour's method to expand its application, with the goal of allowing 'architects to test their own designs'. However, Everett discovered a number of challenges within the test procedure, not only experimental but also theoretical and statistical in nature, concluding that further work was needed. Lowe and Gibbons (1988) then looked further into the duration required for testing through examining weather statistics, also at this point apparently applying the name co-heating into UK nomenclature to describe this longer form of the test.

As funding dropped off, interest in the development and validation of such procedures faded. In fact, following the Pennyland and Linford projects (Everett, 1985; Chapman et al., 1985), SERC[4] decided that there would be no further large scale and expensive field trials, instead focusing on dynamic thermal simulation (Bowman and Lomas, 1985; Bowman and Lomas, 1986). Thus the use of co-heating became more sporadic until activity resumed around the turn of the millennium, particularly in the UK. Before reviewing this more contemporary work, it is worth briefly defining co-heating as considered in this thesis and noting some broader uses of the term and method.

2.2.2 Defining co-heating & further afield examples

Typically, but not exclusively, the term co-heating is used to describe periods of constant internal temperatures, certainly the case within this thesis. The UK method used by Siviour, Everett and researchers at Leeds Beckett University (LBU) researchers then used a steady state energy balance and regression to determine the heat loss coefficient, typically over periods exceeding a week and using data aggregated to at least 24 hour integer periods. This method is described fully in section 2.3. In contrast, the PSTAR method, utilises short (overnight) co-heating periods along with further dynamic sequences and parameter identification techniques (see section 2.7).

It is the long-term co-heating method that is the subject of this thesis, although the use of shorter periods is considered to provide further insight and comparisons. This typically refers to the use of the PSTAR method, although variations on this method have been used. In addition, this work centres upon the testing of domestic dwellings, although these have not been tested exclusively.

[4]SERC - Science & Engineering Research Council, now the Engineering & Physical Science Research Council

For example, wider uses of the co-heating method have included the testing of schools; or rather single classrooms, using overnight periods (Zabot, 1987). In one example, Masy and Lebrun (2004) adopted a 5 day test sequence, with a night time set back, using network analysis to account for attic and grounds heat transfer pathways.

2.2.3 Contemporary use: 1998 - present

Interest in the UK was revised around the turn of the millennium through work from a team of researchers at Leeds Beckett University (LBU) with notable projects at the York Demonstration Project (Bell and Lowe, 1998), Stamford Brook (Lowe et al., 2007), Elm Tree Mews (Wingfield et al., 2011) and Temple Avenue (Miles-Shenton et al., 2010; Miles-Shenton et al., 2011). Researchers adopting the long-term co-heating tests developed by Siviour and Everett, produced significant pieces of work through over 50 tests (Johnston et al., 2013), amassing evidence of a fabric performance gap between designed and measured heat loss (Stafford et al., 2012) and identifying the party wall bypass (Lowe et al., 2007). In this context co-heating tests were typically performed alongside further fabric tests, construction observations, forensic investigations and further building performance evaluation (BPE) techniques.

Interest further peaked following these studies and a wider range of UK based university research teams adopted the method, particularly through the Good Homes Alliance BPE programme, 2009 - 11 (GHA, 2011b), in which LBU participated and provided advisory support, the AIMC4 Project (AIMC4 Partners, 2013) and the Technology Strategy Board BPE programme, 2010 - 2014 (TSB, 2015). This led to a series of guidelines being published by researchers at LBU, often referred to as the LBU protocol (Wingfield, 2010a; GHA, 2011a; Johnston et al., 2012b; Johnston et al., 2013). A number of commercial organisations also began to offer a co-heating testing service, including: BRE, BSRIA, Stroma, Gastec, NBT Consult (GHA, 2011b) as well as at least one house developer, Wilmott Dixon, testing their own dwellings.

2.2.4 Reported co-heating tests within the literature

Published literature on co-heating tests is scarce and of variable depth and quality. This is for a number of reasons. Firstly, tests have traditionally been performed in partnership with house builders, architects, etc. This means many of the details, or entire projects, are left unpublished under confidentiality agreements. Additionally, co-heating results will typically be published as part of broader BPE reports or papers, with only the inclusion of headline figures and an absence of technical details. When technical reports are available, without a standard reporting criteria or even methods, they can be uninformative, often missing information on key pieces of data. Without adequate details it becomes impossible to assess the reliability of a test and its result. Co-heating tests that are reported in available literature, along with any relevant details supplied, are shown in tables 2.1 - 2.5. What is clear is that drawing comparisons between tests, or performing any meta-analysis, is limited by the lack of consistent details, variations in method and the small sample size.

Notes on tables 2.1 to 2.5:

- Predicted *HLC*s are based upon either SAP calculations or Passivhaus Planning Package (PHPP) calculations, operating along similar lines. Occasionally, these values have been adjusted to incorporate measured in situ U-values, air infiltration or to account for construction defects.
- Error estimates are based upon either the standard error of regression (1) or on the standard deviation of daily estimated *HLC*s.
- For explanation of analysis methods, MLR, cSLR, Sviour, Simple Average see section 2.3.3.
- For definitions of types of measured solar radiation see section 3.4.
- Infiltration measurements are described in section 2.5.1.

Table 2.1: Review of published co-heating tests. Part 1 - summary of results.

Project	Building	Testing Organisation	Predicted W/K	Calculation Method	Coheating Test W/K	Error W/K	Variation from Predicted %
Sigma House		Oxford Brookes	98	SAP	144.0	-	47%
GHA Monitoring Programme 2009-2011	A	LMU, UCL, Oxford Brookes	129.9	SAP / Adapted SAP	149.5	-	15%
	B		118.4		132.9	-	12%
	C		111.8		110.2	-	-1%
	D (CASE-G)		37.8		48.9	9.9 [2]	29%
Stamford Brook	A	LMU	63.8	SAP	111.7	5.9 [1]	75%
	E		75.2	SAP	153.4	3.3 [1]	104%
Elm Tree Mews		LMU	127.5	Adjusted SAP	196.4	5.74 [1]	54%
Temple Avenue	A1 (CASE-E)	LMU	129.3	Adjusted SAP	149.5	-	16%
	A2 (CASE-F)		120.2		132.9	-	11%
	Retrofit - Phase1		341.43		312.2	-	-9%
	Retrofit - Phase2		238.67		241.8	-	1%
	Retrofit - Phase3		107.18		147.5	-	38%
Ebbw Vale	Lime House	WSA	37.2	PHPP	45.0	2 [1]	21%
	Larch House		57.6	PHPP	62.0	4 [1]	8%
LEVH		UCL	300	Adapted SAP	280.0	-	-7%
Rowner	Flat 8	BSRIA	37.9	SAP	122.0	-	222%
Passivhaus Tests	Racecourse Dwelling 1	LMU	43.4	-	46.7	-	8%
	Racecourse Dwelling 2		36.6	-	38.1	-	4%
	Ford Close	WARM	45.6	-	50.4	-	11%
York Energy Demonstration Project	Chapel Fields B - Before	LMU	266	-	218.0	3 [1]	-18%
	Chapel Fields B - After		149	-	133.0	1 [1]	-11%
	Bell Farm A - Before		300	-	229.0	4 [1]	-24%
	Bell Farm A - After		132	-	121.0	4 [1]	-8%
Heusden Zolder (Belgium)	Passivhaus	KU Leuven	0.179 W/m^{2}K	-	0.15 W/m^{2}K	0.0037 W/m^{2}K [1]	-16%
Natural House (CASE-D)		-	-	-	93.8	-	-
NHBC Field Trial	BRE Swedish Test House	A	68.4	SAP	64.4	-	-
		B			65.3	-	-
		C			70.0	2.6 [1]	-
		D			65.2 / 73.4	-	-
		E			61.2	9.1 [1]	-
		F			52 / 52 / 70 / 57	-	-
		G			78 / 77 /73.9	-	-
Thesis Case Studies	CASE-C	UCL - Stamp	78	SAP	134.8	13 [2]	73%
	CAM-PH2		66	PHPP	35.0	15 [1]	-47%
	CAM-PH		66	PHPP	56.0	5 [1]	-18%
	CASE-B		205	Adjusted SAP	231.0	6 [1]	13%
	NHBC		68.4	SAP	70.0	2.6 [1]	2%
	CASE-A1		112	Adjusted SAP	245.0	6 [1]	118%
	CASE-A2				144.0	3 [1]	29%

Table 2.2: Review of published co-heating tests. Part 2 - test durations and analysis used.

Project	Building	Duration	Warm Up	When	Analysis Method	Forced Intercept	Aggregation	Measured Solar
Sigma House		-	-	-	-	-	-	-
GHA Monitoring Programme 2009-2011	A	32	-	Jan-Feb	-	-	-	-
	B	32	-	Jan-Feb	-	-	-	-
	C	18	-	Mar-April	-	-	-	-
	D (CASE-G)	28	-	Mar-April	MLR - Party Wall Corrections	-	12-12am & 6-6am	-
Stamford Brook	A	11	-	February	MLR	y	-	Vertical South
	E	22						
Elm Tree Mews		11	-	Feb - Mar	MLR	y	-	Vertical South
Temple Avenue	A1 (CASE-E)	24	2	Jan - Feb	MLR	y		-
	A2 (CASE-F)	24	2	Jan - Feb	MLR	y		-
	Retrofit - Phase1	9	-	Oct-Nov	MLR + Wind & Party Wall Correction	y	-	-
	Retrofit - Phase2	6	-	December		y		-
	Retrofit - Phase3	8	-	March		y		-
Ebbw Vale	Lime House	18	-	Feb - Mar	Siviour + SA	NA	12pm - 12pm	-
	Larch House	15	-	Feb - Mar	Siviour + SA	NA	12pm - 12pm	-
LEVH		-	-	-	-	-	-	Inside Windows, Vertical
Rowner	Flat 8	7	-	April - May	MLR + Wind	y		Vertical
Passivhaus Tests	Racecourse Dwelling 1	33	-	-	-	y	-	-
	Racecourse Dwelling 2	-	-	-	-	-	-	-
	Ford Close	11		-	Siviour	NA	24 hour 6am-6am	-
York Energy Demonstration Project	Chapel Fields B - Before	20	-	Dec-Jan	MLR	n	-	-
	Chapel Fields B - After	6	-	March	MLR	n	-	-
	Bell Farm A - Before	20	-	Dec-Jan	MLR	n	-	-
	Bell Farm A - After	11	-	March	MLR	n	-	-
Heusden Zolder (Belgium)	Passivhaus	43	-	-	MLR + Wind	-	-	-
Natural House (CASE-D)		18	-	Feb-12	MLR + Wind	y	24 hour / Nightime	Horizontal
NHBC Field Trial	BRE Swedish Test House	-	-	December	MLR	y	24 hour	-
		10	-	January	MLR + Wind	y	24 hour	-
		13	2	February	MLR / Siviour	y	24 hour	Vertical South Facing
		15	-	Feb - Mar	Siviour (Vertical / Horizontal Solar)	NA	24 hour	Vertical S + Horizontal
		14	3	March	MLR + Wind	y	24 hour	Horizontal - Coverted to Vertical
		13	-	April	SLR / MLR / cSLR / Siviour	y	6pm - 6pm	Vertical - South & North
		13	2	April - May	MLR / Siviour / Nightime (10pm-4am)*	y	24 hour / Nightime	Horizontal
Thesis Case Studies	CASE-C	17	4	December	MLR	y	24 hour	Horizontal
	CAM-PH2	8	5	March	Numerical cSLR + Corrections	y	24 hour	Vertical South
	CAM-PH	6	1	December	MLR	y	24 hour	Vertical South
	CASE-B	15	5	March	MLR / Siviour	y	24 hour	Vertical South
	NHBC	13	2	February	MLR / Siviour	y	24 hour	Vertical South Facing
	CASE-A1	26	5	Jan - Feb	MLR / Siviour	y	24 hour	Vertical South Facing
	CASE-A2	15	2	March - April	MLR / Siviour	y	24 hour	Vertical South Facing

Table 2.3: Review of published co-heating tests. Part 3 - details of test dwellings.

Project	Building	Construction	Built Form	Glazing Ratio (Window/Total Floor Area)	Total Floor Area	Airtightness $m^3/h/m^2$	Floors
Sigma House		Closed Panel Timber Frames With Phase Change Material	Detatched	-	116	-	4
GHA Monitoring Programme 2009-2011	A	• Thin joint Masonry, Concrete Slab Floor	Detatched	-	152	-	2 1/2
	B	• SIP - External Brick Cladding	Detatched	-	155	-	2 1/2
	C	• Timber-Frame	Detatched	-	139	-	2
	D (CASE-G)	• Clay block in concrete frame	Corner Apartment	-	63	-	1
Stamford Brook	A	Masonry	Semi	-	73	3.3-4.2	-
	E	Masonry	End-of-terrace	-	106	5.3-5.9	-
Elm Tree Mews		Timber Frame Closed Panel	End-of-terrace	-	113	5.39 - 6.67	3
Temple Avenue	A1 (CASE-E)	• Masonry Thin Joint	Detached	19.5%	151	3.98 - 4.17	3
	A2 (CASE-F)	• SIP	Detached	17.8%	154	2.21 - 2.42	
	Retrofit - Phase1	• 1930s Brick Cavity, Double Glazing, Loft Insulation	Semi Detached	14.4%	112	20.7	2
	Retrofit - Phase2	• Blown Mineral Fibre, Increased Loft Insulation, Sealed Flooring, Draughtproofing				10.3	
	Retrofit - Phase3	• EWI, Floor Insulation, Triple Glazing				5.7	
Ebbw Vale	Lime House	Timber Frame	Detatched		2 bed		2
	Larch House	Timber Frame	Detatched		3 bed		2
LEVH		Solid Wall Victorian Retrofit - IWI,Floor Insulation Airtightness	Semi Detached	-	250	6.5	4
Rowner	Flat 8	Render - Hemelite Block - Full Fill - Thin Block	Corner Flat	-	2 Bed	5.77	1
Passivhaus Tests	Racecourse Dwelling 1	-	End of Terrace	-	-	-	-
	Racecourse Dwelling 2	-	Mid Terrace	-	-	-	-
	Ford Close	-	Terrace	-	-	-	-
York Energy Demonstration Project	Chapel Fields B - Before	• 1950s Cavity Crickwork, concrete floor, pitched roof	Semi	-	70	19.3	-
	Chapel Fields B - After	• Improved loft ins, CWI, double glazing, draughtproofing, sealed suspended floor		-		7.5	-
	Bell Farm A - Before	• 1930s Cavity Brickwork, pitched roof, part solid part suspended timber	Semi	-	75	16.9	-
	Bell Farm A - After	• Improved loft insulation, CWI, double galzing, draughtproofing		-		4.9	-
Heusden Zolder (Belgium)	Passivhaus	Passivhaus, Timber Frame - Brick Clad	Detached	5% South, 6% Nort	-	0.2	2
Natural House (CASE-D)		Lightweight, Aerated Timber Blocks	Semi	-	-	-	2
NHBC Field Trial	BRE Swedish Test House	Brick Clad Timber Frame	Detached	15.5%	84	2.2	2
Thesis Case Studies	CASE-C	Aircrete Thin Joint - Concrete Floor Slab	Detached	20.4%	132	-	4
	CAM-PH2	Timber Frame, Partially Excavated	Detached	35.3%	99	0.59	2
	CAM-PH						
	CASE-B	Thin Joint Masonary - Partial Fill Cavity - Brick	Detached	25.1%	192	2.93	3
	NHBC	Brick Clad Timber Frame	Detached	15.5%	84	2.2	2
	CASE-A1	Brick - Cavity - Block (Unisulated)	Semi	14.3%	103	8.4	3
	CASE-A2	Brick - Polybead - Block					

Table 2.4: Published co-heating tests. Part 4 - measurements & environmental conditions.

Project	Building	Measured Solar	Infiltration Measurement	Mean Ti °C	Mean Solar W/m²	Mean ΔT K	Mean Te °C
Sigma House		-	None	-	-	-	-
GHA Monitoring Programme 2009-2011	A	-	-	-	-	-	-
	B	-	-	-	-	-	-
	C	-	-	-	-	-	-
	D (CASE-G)	-	Tracer Gas Decay	25	-	-	-
Stamford Brook	A	Vertical South	Pressure Tests	-	-	-	-
	E						
Elm Tree Mews		Vertical South	Pressure Tests + Tracer Gas Decay	-	-	-	-
Temple Avenue	A1 (CASE-E)	-	Pressure Tests	25	43	21.5	-
	A2 (CASE-F)	-		25	43	21.8	-
	Retrofit - Phase1	-		24	-	-	10.8
	Retrofit - Phase2	-	Pressure Tests	23.1	-	-	3
	Retrofit - Phase3	-		25	-	-	7.9
Ebbw Vale	Lime House	-					
	Larch House	-					
LEVH		Inside Windows, Vertical	Pressure Test	21	-	-	-
Rowner	Flat 8	Vertical	Pressure Test + Tracer Gas Decay	-	168	10.2	-
Passivhaus Tests	Racecourse Dwelling 1	-	-	-	-	-	-
	Racecourse Dwelling 2	-	-	-	-	-	-
	Ford Close	-	-	-	-	-	-
York Energy Demonstration Project	Chapel Fields B - Before	-	Pressure Tests	-	-	-	-
	Chapel Fields B - After	-		-	-	-	-
	Bell Farm A - Before	-		-	-	-	-
	Bell Farm A - After	-		-	-	-	-
Heusden Zolder (Belgium)	Passivhaus	-	Pressure Test	22-24	-	-	-
Natural House (CASE-D)		Horizontal		25	62.3	18.7	-
NHBC Field Trial	BRE Swedish Test House	Horizontal	-	-	-	-	-
		-	-	-	44	26.12	-
		Vertical South Facing	Tracer Gas Decay	25			
		Vertical South + Horizontal	Tracer Gas Decay	-	-	-	-
		Horizontal - Coverted to Vertical	-	-	190	17.8	-
		Vertical - South & North	Pressure Test + Tracer Gas Decay	25	97	-	7.3
		Horizontal		26	-	-	-
Thesis Case Studies	CASE-C	Horizontal	None	24.5	14.5	20.6	3.7
	CAM-PH2	Vertical South	Tracer Gas Decay	27.0	84.4	14.2	12.8
	CAM-PH	Vertical South	None	24.5	4.6	16.9	7.6
	CASE-B	Vertical South	Tracer Gas Decay	24.0	90.3	16.0	8.0
	NHBC	Vertical South Facing	Tracer Gas Decay	25.3	82.0	20.3	5.0
	CASE-A1	Horizontal & Vertical South Facing	Pressure Test + Tracer Gas Decay	23.8	37.0	20.1	3.7
	CASE-A2	Vertical South Facing	Pressure Test + Tracer Gas Decay	24.0	37.0	21.2	2.8

Table 2.5: Review of published co-heating tests. Part 5 - notes and references.

Project	Building	Notes	Reference
Sigma House		Noted difficulty in keeping unoccupied and accounting for variation in solar	(Stevenson & Rijal, 2008)
GHA Monitoring Programme 2009-2011	A	-	(GHA, 2011)
	B	-	
	C	-	
	D (Case-G)	Partial Guarding - Not Above or Below	
Stamford Brook	A	-	(Lowe et al., 2007)
	E		
Elm Tree Mews		Could not control next door, Builders had to access so data had to be removed	(Wingfield et al., 2011)
Temple Avenue	A1 (CASE-E)	-	(Miles-Shenton et al., 2010)
	A2 (CASE-F)	-	
	Retrofit - Phase1	Adjacant property was at mean temperature of 21.4, 19.8, 20.4^{o}C respectively, giving a ΔT_{adj} of 2.6-4.8 ^{o}C	(Miles-Shenton et al., 2011)
	Retrofit - Phase2		
	Retrofit - Phase3		
Ebbw Vale	Lime House	Overheating due to solar gains, does not carry over more than a day, simple hourly average gave 60 ± 14 W/K	(Siddall et al., 2012)
	Larch House	Overheating due to solar gains, does not carry over more than a day, simple hourly average gave 41 ± 8 W/K	
LEVH		Occupied for security	(Makrodimitri, 2010)
Rowner	Flat 8	No note on T_{adj}	(TSB Report, Confidential)
Passivhaus Tests	Racecourse Dwelling 1	Refer to short term overheating, sky losses, wind variation	(Siddall et al., 2012)
	Racecourse Dwelling 2		
	Ford Close		
York Energy Demonstration Project	Chapel Fields B - Before	Mention Theft of equipment	(Bell & Lowe, 1998)
	Chapel Fields B - After		
	Bell Farm A - Before		
	Bell Farm A - After		
Heusden Zolder (Belgium)	Passivhaus	Disturbances due to essential work access, non-uniform Ti, required to adjust heating power, short term overheating	(De Meulenaer et al., 2005)
Natural House (CASE-D)			(Confidential Report)
NHBC Field Trial	BRE Swedish Test House	-	(NHBC, 2012), (Jack et al., 2015)
		High Range in ΔT and S	
		High Range in ΔT and S	
		-	
		Very Unstable internal temperatures, short term overheating everyday	
		Empirical Calculation of Solar Gains used measured Solar on all glazed orientations	
		Sensor Failures + Loss of Data	
Thesis Case Studies	CASE-C	-	-
	CAM-PH2	Long Term Overheating	
	CAM-PH	Overcast - No Overheating	
	CASE-B	High Moisture Content, Spatial Variation in T_i	
	NHBC	High Range in ΔT and S	
	CASE-A1	Similar Conditions to CQ2, Complex Party Wall Heat Transfer	
	CASE-A2	-	

2.2.5 Obstacles to the adoption of co-heating

Returning to the context discussed at the beginning of this chapter, there remains considerable debate over the future use of co-heating, particularly whether its role lies within a research or a compliance landscape. It is worth initially considering the obstacles to wider adoption that have been cited within relevant literature.

A number of obstacles have been cited as not only having an impact on the tests conducted to date, but also significantly limiting the wider adoption of co-heating tests. These are summarised below:

- **Unoccupied test dwellings:** The requirement that buildings are left unoccupied and inaccessible for the entire test period, limits opportunities to test occupied dwellings and disrupts the construction and sale of new builds (GHA, 2011b; De Meulenaer et al., 2005).

- **Duration of testing:** Tests typically take in the region of 1-3 weeks (Johnston et al., 2013), exacerbating the disruption caused and increasing the overall cost of the test.

- **Limited testing season:** The limited testing season, approximately October to March in the UK, places a strain upon the scheduling of tests and site progress. Additional pressure is exerted if a gap must be left between applying wet finishes, and testing with reasonable residual moisture (Johnston et al., 2013). In particular, developments finished in the summer and immediately occupied will likely be left untested (GHA, 2011b; ZCH, 2014b).

- **Cost:** Tests as part of the GHA BPE programme costs as much as £30-50,000 (GHA, 2011b), although this is dependent upon the depth and scale of investigation, the size of test dwellings, additional tests performed and required reports and further project commitments. Stand-alone tests cost in the region of £5,000 (GHA, 2011b).

- **Non-standard protocols:** Whilst a number of guidance documents have been published by LBU, a central official standard does not exist. This inevitably has led to variations in experimental protocol, equipment, analysis techniques and report content (Butler and Dengel, 2013; ZCH, 2014b). This can lead to both difficulties in comparisons but also misunderstanding and a lack of trust in the results.

- **Absence & lack of understanding of uncertainties:** The majority of the work conducted to date has focused on the use of co-heating tests in evaluating building heat loss, rather than directly investigating the method itself, see section 2.8. In many cases, reported *HLC*s are absent of any uncertainty estimate, whilst in others only rudimentary discussions may be included. Importantly, variations due to weather and across a variety of house types are not well understood (Butler and Dengel, 2013; ZCH, 2014b).

- **Risk & reliability:** Organising a co-heating test requires co-ordination from a number of partners and may incorporate a significant amount of effort and investment (GHA, 2011b). Tests themselves may then prove unreliable due to unsuitable weather, equipment malfunction or experimental difficulties. Particularly for new research teams and in new partnerships with house builders, these risks can dissuade both from pursuing co-heating tests.

In response to these difficulties in conducting tests the TSB BPE programme downgraded co-heating tests from a mandatory to an optional element (Birchall, 2011).

2.2.6 Future use

It has been suggested that a full blown research co-heating test, incorporating a variety of further research tools, should be differentiated from a simpler one-off or industry test, reducing the overall cost and potentially further demands (JRHT, 2011). The GHA Monitoring Programme argued that there would be benefit in exploring development of a simplified test which had the target to provide 80% of the accuracy/results with only 20% of the commitment and complexity in terms of time, resources and cost (GHA, 2011b, p.24).

Therefore there remains a potential role for co-heating tests, both in a research context and more controversially in some type of compliance role. Opposition to such usage is considerable, with the costs of remedying any misfiring dwellings likely to be sizeable and the potential for damaging the reputation of designers, developers and contractors. It is evident that clarity is needed on the accuracy and reliability of the test and its application in the spectrum of research, regulation and construction industry practice.

2.3 The co-heating method

The co-heating test considered in this thesis is based on the method developed by (Siviour, 1981) and (Everett, 1985) and later used by researchers at LBU and across the UK. This uses a constant internal temperature throughout the test period, and is therefore set in quasi-steady state conditions, 'quasi' being an implicit recognition of the presence of dynamic outdoor conditions. The method consists of long monitoring periods (typically 1-3 weeks) and uses aggregated data of at least 24 hour periods (or multiples thereof) as opposed to selected night time periods.

The principal result of such co-heating tests is the building heat loss coefficient, *HLC*, a parameter describing the heat loss across the entire building envelope, via all heat transfer mechanisms, in units of W/K. Secondary to this is the solar aperture of the test dwelling, *R*, a term used to define solar gains for given incident solar radiation. Both terms are in fact complex, and emergent properties of the interaction between building fabric and external environment. Therefore they need careful definition, in terms of both in their measured and theoretical values. This is more fully discussed in chapter 3.

2.3.1 Experimental protocol

With the aim of measuring the total heat loss across the full building envelope it should be clear that direct measurement is not possible without coating the entire building with heat flux sensors. Instead, heat loss must be inferred from an energy balance, essentially forming the assumption that *heat in* equals *heat out*.

A simple analogy can come in the form of a leaking swimming pool. Directly measuring the rate of water leakage through the base of the pool and into the ground below may prove impossible. However, by maintaining a constant water level and monitoring the amount of water required to achieve this, one could infer the rate of water leakage from the pool. A more direct building analogy can be made to pressure testing, operating on the principal of the conservation of mass rather than energy, where *air in = air out.*

In an occupied building, any energy balance must incorporate a wide range of interacting terms. The co-heating experimental protocol therefore consists of a number of techniques that aim to simplify the energy balance equation used to evaluate the building *HLC*, consisting of:

- **Constant internal temperatures:** to reduce the dynamic heat flows associated with the charging and discharging of the building's thermal mass. Often T_i is slightly elevated to enhance heat flows (typically $T_{setpoint}$= 25°C)
- **Long aggregation periods:** typically 24 hours, to further smooth dynamic heat flows and allow steady state analysis.
- **Uniform internal temperatures:** to allow treatment of a test dwelling as a single zone, facilitated by multiple heaters and mixing fans.
- **Unoccupied test dwellings:** to avoid behaviour driven heat flows (i.e. natural or mechanical ventilation) and metabolic gains.
- **Electric heating:** such that the heating efficiency = 1, avoiding unknown and variable efficiency factors.

When met, these conditions allow a simplified analysis in which to determine the *HLC* of a test dwelling (figure 2.2), with a simple steady state energy balance, equations 2.1 - 2.5.

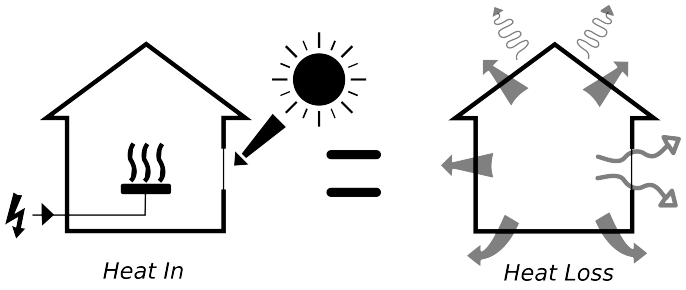

Figure 2.2: *Co-heating test principal in which the heat in, consisting of electrical heat and solar gains, is equated to the total building heat loss, from convection, conduction and radiation across the entire building envelope.*

$$Q_{elec} + Q_{sol} = Q_{loss} \tag{2.1}$$

$$Q_{elec} + R \cdot S = HLC \cdot (T_i - T_e) \tag{2.2}$$

$$Q_{elec} + R \cdot S = HLC \cdot \Delta T \tag{2.3}$$

Where,

Q_{elec} (W) is the electric heat input, from both thermostatically controlled heaters and non-thermostatically controlled equipment, $Q_{baseload}$, i.e. mixing fans and data loggers.

Q_{sol} (W) represents the solar heat gains, determined by the measured incident solar radiation, *S* (W/m^2) and the solar aperture, *R* (m^3/s), the latter being a secondary building parameter derived from co-heating.

Q_{loss} (W) is the net heat flow out of the building.

HLC (W/K) is the heat loss coefficient of the test dwelling, the primary parameter to be derived through co-heating tests.

T_i (°C) is the representative internal temperature, which will approximately represent the chosen internal thermostat setting, $T_{setpoint}$.

T_e (°C) is the measured external temperature.

ΔT (K) is the inside-outside air temperature gradient, defined as (T_i- T_e)

2.3.2 Equipment & sensors

To meet the requirements of the experimental protocol further equipment is required. Firstly, to provide a constant and uniform T_i, sets of heating and mixing equipment are required throughout a test dwelling. Typically a test dwelling will be divided into a number of zones, each with a heater, mixing fan and thermostatic controller in order to provide a constant and uniform internal temperature (see figures 2.3 and 2.4).

In addition to satisfy equation 2.5 for the *HLC* and *R*, data from four measurement channels are required:

1. **Internal Temperature, T_i:** measured at various locations inside the dwelling. Averaged to provide a representative value for the whole dwelling. In units of °C.

2. **External Temperature, T_e:** measured externally in a Stevenson screen. In units of °C.

3. **Electric Heat Input, Q_{elec}:** measured via kilowatt hour meters, in which all electronic equipment is plugged into, and/or at the main service meter. In units of W.

4. **Solar Radiation, *S*:** measured externally via a solar pyranometer, to allow the determination of solar gains into the energy balance, either numerically or statistically through incorporating S into regression analysis. In units of W/m^2, measured in a number of orientations, see chapter 3.

Figure 2.3: *Co-heating internal equipment: a mixing fan, electric heater, PID thermostatic controller with temperature sensor on tripod, all plugged into a kilowatt-hour meter.*

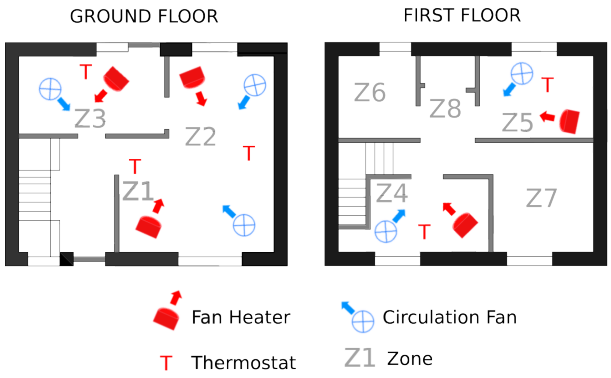

Figure 2.4: *Example of the layout of co-heating equipment.*

2.3.3 Principal analysis methods

Once a suitable analysis period has been determined co-heating data is predominantly analysed in four different ways. The type of analysis is primarily dependent upon the treatment of solar gains. In simple averaging (SA) or corrected simple linear regression (cSLR) the solar gains are typically calculated from numerically modelled solar gains (section 3.3.1). In either Siviour or multiple linear regression (MLR), solar gains are accounted for through the inclusion of S as an independent regression variable, allowing R to be determined as a separate regression coefficient. Figure 2.5 illustrates the three main methods of regression analysis.

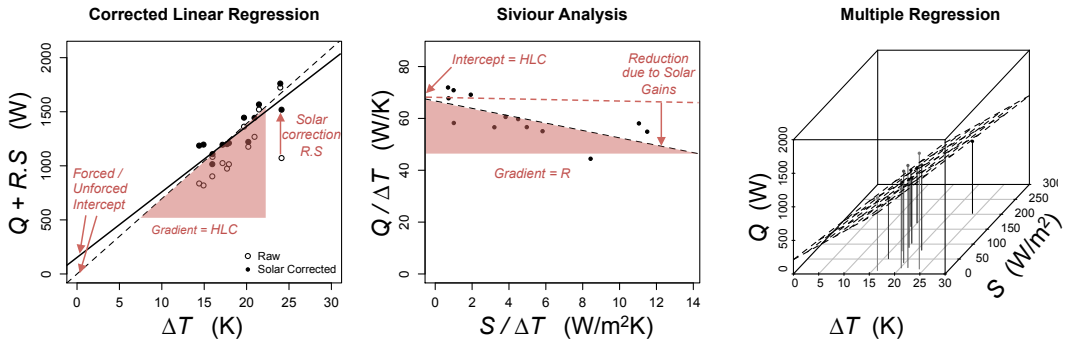

Figure 2.5: *Main Types of Co-heating Analysis. Left - Corrected simple linear regression (cSLR), Centre - Siviour Analysis. Right - Multiple linear regression (MLR).*

2.3.3.1 Simple Average (SA)

The simplest method is to obtain a simple average of the power input, Q_{elec}+ *R.S*, divided by the temperature difference across this period, equation 2.4. Guerra Santin et al. (2013) use hourly averages to determine the *HLC* via this method, although it is important that integer 24 hours are used to avoid bias from dynamic effects, as with in in-situ U-value measurements, see ISO 9896:2014 (ISO, 2014). Solar gains must be estimated numerically (3.3.1).

$$HLC = \frac{\sum_{0}^{j=t}(Q_j + R \cdot S_j)}{\sum_{0}^{j=t}(T_{i,j} - T_{e,j})} \tag{2.4}$$

Where: Q_j, S_j, $T_{i,j}$and $T_{e,j}$ are the electrical heating power, solar radiation, internal and external temperatures at time step *j*, where there are a total of *t* time steps and *t* consists of integer 24 hour periods.

2.3.3.2 Corrected Simple Linear Regression (SLR & cSLR)

More commonly, co-heating data is analysed through linear regression. The simple linear regression (SLR) model plots the heating power, Q (W) against ΔT (K), such that the gradient of the regression least squares fit represents the *HLC* (W/K). A corrected heating power must then be calculated by combining heat input from the electric heaters, Q_{elec}, and from solar gains, Q_{sol}= *R.S*, allowing regression of the corrected data (cSLR). Typically, these solar gain corrections will be made from exogenous numerical calculations (section 3.3.1). Often MLR plots incorporating solar corrections will be seen projected onto a 2D plot, although it is important not to confuse the two. It must be decided whether the regression model allows

a non-zero intercept or if the intercept is forced (section 2.3.4.1). Johnston et al. (2013) states that the cSLR approach, using numerical calculations of Q_{sol}, is useful when it is not possible to undertake effective MLR analysis.

$$Q_{elec} + R \cdot S = HLC \cdot \Delta T \tag{2.5}$$

$$Q_{elec} + R \cdot S = HLC \cdot \Delta T + c \tag{2.6}$$

Where c represents the intercept value in units of W.

2.3.3.3 Siviour or Biaxial Regression Analysis

A further form of regression analysis rearranges the energy balance in equation to allow a biaxial regression, commonly referred to as 'Siviour' analysis (Siviour, 1981; Palmiter, 1979). In this case the heat loss coefficient is depicted by the y-intercept and the solar aperture, R, is statistically derived from the regression, forming the slope of the line of best fit in this case (figure 2.5).

$$\frac{Q}{\Delta T} = -R \cdot \frac{S}{\Delta T} + HLC \tag{2.7}$$

2.3.3.4 Multiple Linear Regression (MLR)

Finally, and perhaps most commonly, multiple linear regression (MLR) can be carried out between the electric power Q_{elec} and two independent variables ΔT and S (Everett, 1985; Wingfield, 2010a). This extracts both the parameters, HLC and R through regression. Again, the regression model can incorporate either a forced or unforced intercept.

The Siviour and MLR approaches are considered to give similar results (Deconinck and Leunis, 2012; Bauwens et al., 2011). Baker (2015) states that MLR represents a better statistical representation as both ΔT and S are independent variables, although Siviour analysis perhaps offers clearer visualisation of the results. As each approach handles the errors within the regression variables differently, they are compared directly in section 9.3.2.1.

2.3.4 Variations & additional analysis methods

2.3.4.1 Forced vs un-forced regression models

There is some debate over the use of forced intercept models. Forced intercepts have predominantly been used (table 2.2) on the assumption that at ΔT = 0, the required heating power will also be zero, Q_{elec} = 0. Such an assumption is based on the fact that all heat losses are directly coupled to T_e. Therefore, there are a number of reasons why it is physically possible for a non-zero intercept to exist (Johnston et al., 2013; Bauwens and Roels, 2014). The suitability and uncertainty in each approach is considered in sections 8.1 and 9.3.2.

2.3.4.2 Subtracting heat losses

Everett (1985) experimented with subtracting combinations of secondary heat flows, including to the ground, Q_g (W), party wall, Q_{adj}, and infiltration losses, Q_{inf}, prior to regression, equation 2.8. This alters the definition of the *HLC* being measured (see section 3.1.3) and is not commonly adopted, although it represents an important concept.

$$\frac{(Q_{elec} - Q_g - Q_{inf} - Q_{adj})}{\Delta T} = -R \cdot \frac{S}{\Delta T} + HLC \tag{2.8}$$

Where,

Q_{inf} is the infiltration heat loss (W)

Q_g is the ground floor heat loss (W)

Q_{adj} is the heat flow to adjoining spaces/ dwellings (W)

2.3.4.3 Night time data

The NHBC[5] co-heating field trial report (Butler and Dengel, 2013) states that averages from 'quiet' periods of weather can be used to determine the *HLC*. This is particularly useful as night time periods incorporate no incident solar radiation. This then more closely follows the short term co-heating periods used in the PSTAR method, although without any corrections from dynamic and secondary heat flows. Whilst it is possible that such periods will elicit accurate estimates of the *HLC* it is also possible that they will be subjected to a number of the sources of uncertainty documented in this thesis. Analysis of such arbitrary selected periods is typically avoided, unless care is taken over the proceeding conditions, for example shielding solar gains (Zabot, et al., 1987), or filtering out biased data (Judkoff et al., 2000).

[5]National House Building Council

2.3.4.4 Additional independent regression variables

On occasion wind speed has been included as a third independent regression variable (see table 2.2). The latest LBU protocol (Johnston et al., 2013) refers to the option of including wind speed but states experience shows such a correction is problematic. Alternatively, high wind speeds can be filtered out of data sets or losses subtracted prior to regression (Judkoff et al., 2000; Butler and Dengel, 2013).

Other researchers (Deconinck and Leunis, 2012; Bauwens et al., 2012) have suggested the use of multiple solar regression variables, for example incorporating the solar radiation incident on all facades, e.g. N, S, E, W. Such an approach is explored, along with further considerations of solar radiation measurements, in section 5.4.8.

2.3.4.5 Lagged T_e and solar terms

Attempting to account for the dynamics that remain within a test dwelling Everett (1985) suggested the use of external response function to account for the lag in a building's response to dynamic T_e. This gave a T_e that incorporated parts of the T_e measured in previous aggregation periods, although this was more of a mathematical exercise than a full evaluation of such an approach.

More recently, Bauwens et al. (2012) and Deconinck and Leunis (2012) applied weighting factors to both the previous ΔT and solar input (see eq 2.9-2.13). Whilst this approach may have elicited more accurate results and shorter time periods in simulations, as Deconinck & Leunis point out, it is not so easy to determine the length of time lags in field tests of full size dwellings. Within a simple simulated test wall, Bauwens found considerable uncertainty in these additional lagged coefficients (α, β) for tests lasting less than 3 weeks (Bauwens et al., 2012).

$$Q = (\alpha_1 \Delta T_t + \alpha_2 \Delta T_{t-1}) + (\beta_1 S_t + \beta_2 S_{t-1}) \tag{2.9}$$

$$\alpha_1 + \alpha_2 = 1 \tag{2.10}$$

$$\beta_1 + \beta_2 = 1 \tag{2.11}$$

Where *t* represent the current time step (day) and (*t* - 1) represents the previous and α and β represent the coefficients for these lags.

2.4 Further discussion on the co-heating method

2.4.1 Required environmental conditions and monitoring durations

2.4.1.1 Suggested testing season

On the subject of a suitable testing season, the LBU protocol states the typical testing season is restricted from October/November to March/April (Wingfield, 2010a; Johnston et al., 2013). The most recent iteration gives some consideration to building type, particularly south facing, highly glazed and well insulated dwellings, e.g. Passivhaus, stating they may need to be tested during the lowest levels of insolation (Johnston et al., 2013).

2.4.1.2 Required mixes in weather and solar radiation

The testing period defined by LBU corresponds to the earlier work of Everett (1985) and Lowe & Gibbons (1988), who set criteria for suitable numbers of consecutive dull and sunny days (see section 9.1.5) to predict both when successful testing could be performed and how long was likely to be required. This work additionally stated that whilst mid-winter may be most fruitful for *HLC* estimates, September, February and March were likely to be the best periods in which to determine R due to the higher range in solar radiation. The parameter R may not be sufficiently determined in mid winter, owing to the lack of sunny days. This highlights the fact that regression analysis requires variation in external conditions (see also section 5.3.1). It is an interesting paradox that the steady state regression method does typically benefit from a some dynamic behaviour in external conditions.

2.4.1.3 Required ΔT

Often the value of ΔT across a test period is considered as an indication of when tests can be performed. The LBU protocol argues that the testing season is dictated by the requirement for a reasonable ΔT which should generally be 10K or more, such that most heat flow is from inside to outside (Johnston et al., 2012b; Wingfield, 2010a). Baker and Dijk (2008), referring to testing in outdoor test cells, considered ΔTs of at least 10K were required, with 20K preferable. Judkoff et al. (2000) filtered out tests with a ΔT lower than 20°F ($\sim$11°C) when testing office cells with the STEM method (see section 2.8.5).

2.4.1.4 Required monitoring duration

The LBU protocol states that between 1 - 4 weeks of monitoring, with a minimum of 1 week of data following the building reaching quasi-steady state, is typically required for a co-heating

test (Johnston et al., 2013). In the latest LBU protocol, Johnston et al., also remark how the actual duration required is dependent upon a range of factors: the thermal characteristics of a test dwelling, environmental conditions, warm up period, residual moisture in the building fabric and the actual objectives of the test. This corresponds to earlier work by both Everett (1985) and Lowe and Gibbons (1988) who looked at the expected duration from a statistical perspective, examining weather files for periods that met criteria over numbers and combinations of dull and sunny days. Periods of 1-3 weeks were thought to be sufficient in mid winter, whilst longer periods might be required in Spring / Autumn.

Table 2.1 shows durations ranging from as few as 6 days to as many as 41 days. These durations are likely to be largely influenced by the available time and depth of study - practically rather than theoretically driven.

2.4.2 Aggregating data

2.4.2.1 Aggregation length

The duration of testing will be linked to the aggregation length, i.e. the period of time averaged into a single regression data point. Siviour (1981) and Everett (1985) used 6 day or weekly aggregation lengths, similar to Palmiter (1979), who suggested 5 - 10 day aggregation lengths. For testing building components in outdoor test cells aggregating 10 days together into a single measurement point has been suggested for steady state analysis (Baker and Dijk, 2008). In most recent outdoor co-heating tests 24 hour periods have been used almost exclusively (table 2.1), allowing a larger number of data points but also increasing the risk of any dynamic heat flows across the aggregation interval. However, Everett (1985) reported that he found consistent *HLC* estimates between weekly, 2 day and daily aggregations. Confusing the issue, variations in *HLC* due to different aggregation lengths, or even the actual period used in analysis, are rarely reported.

2.4.2.2 Aggregation interval

Similarly, data can also be aggregated across different intervals of the same length, i.e. 24:00 - 24:00 or 06:00 - 06:00. As early as Everett (1985), it has been pointed out that dawn-dawn aggregation may be preferable, allowing more time for solar gains to remerge from the mass of a test dwelling within the same aggregation period. The current LBU protocol also indicates this may be preferable in some test dwellings. However, as Deconinck and Leunis (2012) point

out, and as can be seen in table 2.2, a number of aggregation intervals are still regularly used. With various aggregation intervals used in the NHBC Field Trial, Butler and Dengel (2013) conclude more research is needed to determine optimal start and end times.

2.5 Supplementary co-heating test protocols & measurements

2.5.1 Measuring and disaggregating infiltration losses

The vast majority of co-heating tests have incorporated some type of measurement of air infiltration (e.g. Siviour (1981), Subbarao (1988a), Wingfield (2010a), and Johnston et al. (2013)). This has the dual advantage of providing information on infiltration losses themselves, Q_{inf} and HLC_{inf}, and allowing disaggregation of transmission losses[6], HLC_{trans}, from the total measured building heat loss, HLC_{TOT}. Additionally, depending upon the timescale of the infiltration measurement, variation in the measured total *HLC* can be related to the variation in infiltration rate across the test period. A number of methods have been used with which to measure infiltration either outside or during the co-heating test. The main methods used to determine infiltration rate during co-heating tests are compared in table 2.6, with the first two approaches, pressure tests and tracer gas decays, the most commonly adopted (table 2.4).

Table 2.6: Methods of measuring air infiltration

Method	Timescale	Advantages	Disadvatages	Examples of Use in Co-heating	Standards/ Protocol
Pressurisation / Depressurisation Test	Spot Measurement	• Low Cost • Quick • Allows identification of leakage paths • Measure increase in air leakage over co-heating test (pre & post)	• Uncertainty in conversion to ACH under natural conditions, i.e. n/20 approximation • Does not indicate the effects of weather, sheltering or terrain (Younes et al., 2011) • No information on daily variation	• Current co-heating LBU protocol - (Johnston et al., 2013) • PSTAR (Subbarao, 1988a & 1988b)	• ATTMA TSL1 (2010) • BS EN 13829:2001 (BSI, 2001)
Tracer Gas Decay	~4-12 hours	• Utilises co-heating mixing strategy • Low / moderate cost • Allows multiple measurements across test period	• Measurements do not cover whole test period, i.e. must be extropolated to daily values • Difficulties in very airtight dwellings (Laussmann & Helm, 2011; Guerra-Santin et al., 2013)	• Current Co-heating LMU Protocol (Johnston, 2013) • PSTAR (Judkoff et al., 2000)	• BS EN ISO 12569:2012 (ISO, 2012) • Sherman, 2000 • Roulet & Foradini, 2002
Passive Tracer Gas	Test Duration i.e. 2 Weeks	• Allows continuous measurement across test	• Systematice error in representivness of sampling points (Styme et al., 1994) • Single measurement, low time resolution	• Siviour (1981) • Palmer et al. (2011)	• BS EN ISO 12569:2012 (ISO, 2012) • Styme et al (1994)
Constant Concentration	Hourly	• Low time resolution • Continuous measurement across test period	• Expensive • Requires sophisticated/ expensive equipment	• Everett (1985)	• BS EN ISO 12569:2012 (ISO, 2012)

[6] As discussed in section 3.1, this method of disaggregation rather separates the direct infiltration losses, HLC_{inf} from HLC_{fabric} a combination of all other losses, including transmission and radiation losses, rather than transmission losses alone.

It should be noted that the aim of this thesis is not to assess the uncertainties of these supplementary methods or with the estimation of HLC_{inf} and hence HLC_{trans}. Rather the focus is on the determination of the total building heat loss via all mechanisms, HLC_{TOT}. These methods should however be considered to better understand the context in which co-heating tests are used and when dealing with uncertainty associated with infiltration losses.

2.5.2 Party Wall Heat Transfer

Co-heating tests performed on semi-detached and terraced dwellings or apartments require researchers to consider how to address party wall/ floor heat transfer. Clearly this can add complications to both the experimental protocol and the energy balance and *HLC* analysis.

A number of researchers have suggested heating the neighbouring spaces to the same internal temperature as the test dwelling itself (Feuermann, 1989; Ridley et al., 2010a; Wingfield, 2010a). This approach of 'guarding' party wall heat transfer will attempt to minimise any heat flow across such elements, although this cannot be completely avoided, particularly as temperatures are unlikely to be precisely matched and heat flows will not be purely horizontal across the walls. Restricted access to occupied neighbouring spaces ultimately limits the experimental control and measurements that an be taken.

In addition to this approach of guarding, particularly in cases when the temperatures in neighbouring spaces cannot be fully controlled, it has been recommended that heat flux and temperature sensors should be positioned across any party walls (Everett, 1985; Johnston et al., 2013; Wingfield, 2010a). Corrections can potentially be made to account for the heat flow(s) across party elements, either from audit descriptions of the UA values and monitored temperatures, equation 2.12 (Feuermann, 1989), or from measured heat flux, equation 2.13 (Ridley et al., 2010a):

$$Q_{adj} = \sum_{j} U_j \cdot A_j (T_{i,j} - T_{adj,j}) \tag{2.12}$$

$$Q_{adj} = \sum_{j} q_j \cdot A_j \tag{2.13}$$

Where:

Q_{adj} (W) is the net heat flow across the total part wall/floor area, composed of *j* elements.

U_j (W/m^{2}K) and A_j (m^3/s) are the respective U-values and area of each party wall/floor element.

$T_{i,j}$ and $T_{adj,j}$ ($^\circ$C) are the representative internal temperatures on either side of the party element.

q_j (W/m^2) is the measured heat flux across the element. In cases of multiple measurements this is likely to take an averaged form.

Wingfield (2010a) and Johnston et al. (2012b) and Johnston et al. (2013) note problems may exist with the representativeness of any sensor positioning and the difficulties in accounting for thermal bridges and other thermal bypasses between dwellings. In addition Johnston et al. (2013) remarks on the potential for solar induced temperature differences and heat transfer between adjoining spaces. Therefore, these authors recommend such corrections be avoided and a strategy of minimising heat transfer pursued. Such difficulties testing apartment dwellings during their monitoring programmes, led the GHA to suggest a *"robust and simple test methodology for apartments therefore needs to be developed for more widespread application"* (GHA, 2011b, p.25).

To further understand inter-dwelling heat transfer, pressure equalisation tests can seek to establish if there is any inter-dwelling air leakage and estimate its likely impact. In addition, Feuermann (1989) suggests after maintaining equal temperatures across party walls, a constant temperature difference (i.e. 10K) can be induced across the party wall in order to then estimate the heat flow across such elements. Such an approach may well provide more reasonable estimates of party wall heat transfer, better capturing the full heat transfer across the element, whilst providing an opportunity for better qualitative understanding through thermal imaging. However, this will likely extend the overall duration of monitoring and any external systematic bias between the two distinct test periods may have to be considered.

The influence of party wall heat transfer is addressed in section 7.2, with a more general assessment of testing dwellings with high party wall areas considered in chapter 9, including the estimation of their additional uncertainty (section 9.4.7.2).

2.5.3 Co-heating in occupied dwellings

Whilst most current usage of the co-heating method involves unoccupied houses, as is the focus in this thesis, the initial development did incorporate occupied dwellings. Chapman et al. (1985), under the Pennyland project, monitored 80 houses with basic monitoring equipment. Using 6 day aggregations, the *HLC* estimates showed reasonable correlation to the results from unoccupied dwellings (Everett, 1985). Everett concluded that whilst this monitoring strategy could not produce hard estimates ($\pm 10\%$) of the heat losses of individual houses, or determine solar gains, it could distinguish houses to within three basic levels of insulation.

Masy (2005) using a shorter (5 day) method similar to the PSTAR approach, suggested tests could performed in either occupied or unoccupied dwellings. Here, a questionnaire was used to help estimate metabolic free gains, although the accuracy of such a reported approach is highly questionable. As Lowe and Gibbons (1988) remark the presence of occupants can mean variations in T_i and heat flows into and from the thermal mass can no longer be regarded as negligible. Further, ventilation rates can vary strongly with window opening and all internal heat gains need to be reliably estimated. Such behaviour will also provide uncoupled heat losses and gains, weakening the relationship between heat loss and ΔT and making statistical regression analysis very difficult (Lowe and Gibbons, 1988; Everett, 1985). Some current work is attempting to understand the sensitivities to these issues and occupant behaviour during *HLC* estimates (Jack, 2015a).

2.5.4 Supporting tools

Since the early development of the co-heating test methodology, it has frequently been deployed not as an isolated tool but as a central element of a wide range of investigative methods. Additional tools have been adopted in tandem to co-heating measurements to provide qualitative information, disaggregate heat flows and extended protocols have been adopted to elicit further information on the building. Often it is through these methods that real understanding of heat loss and the underlying processes can be gained. Successful and informative projects are likely to be those in which a variety of tools are at the hands of the researchers, with adaptable research programmes allowing for further testing.

This is reflected in the latest LBU co-heating protocol in which a number of additional tools are listed (Johnston et al., 2013). A full list of additional procedures used by LBU and other researchers include:

During Co-heating:

- Background infiltration measurement, i.e. tracer gas (e.g. Everett, 1985).
- Measurement of in situ U-values (e.g. Everett, 1985).
- Localised heating loads, when separately logged, have been compared to identify the respective heat loss of internal zones (Sonderegger and Modera, 1979), although internal mixing must be considered.
- Air flows, i.e. cavities, floor voids (e.g. Wingfield et al., 2007).
- Forensic temperature measurements i.e. cavity/party wall, (Johnston et al., 2013).
- Thermography surveys to qualitatively identify heat loss paths, i.e. defects, thermal bridges, air leakage (e.g. Siviour, 1981; Everett, 1985; Wingfield et al., 2007; Johnston et al., 2013).

Pre / Post Co-heating:

- Pressure tests (pre & post) to determine leakage area and any increase across co-heating period (e.g. Wingfield, 2010a).
- Use of thermography during pressure tests, providing useful qualitative information (Persily & Linteris, 1980)
- Identification of air leakage paths, i.e. smoke tests (e.g. Siviour, 1981; Everett, 1985; Johnston et al., 2013).

Additional Test Sequences:

- Cooldown tests to determine time constants and thermal capacitance (Subbarao, 1988a).
- Heating system efficiency (Francisco et al., 2006).
- Heating system distribution losses (Judkoff et al., 2000) - via strip heaters deployed alternatively at the point of heating within the ducts and directly in the conditioned space of the dwelling.
- Heat pump COP[7] (Judkoff et al., 2000)

[7] Coefficient of Performance

- Ventilation system air leakage (i.e tape them up and subtract the difference - repeat 4 times for accuracy (Judkoff et al., 2000)).

Wider Project Tools:

- Construction observations / 'buildability' assessments (Chapman et al., 1985; Everett et al., 1985; Johnston et al., 2013).
- Post-construction audits (Johnston et al., 2013).
- Non-destructive investigation, e.g. boroscope and partial deconstruction (Johnston et al., 2013).
- Air movement tests (Guerra Santin et al., 2013).
- Acoustic tests (Wingfield et al., 2007).
- Wider BPE tools and social studies.

Synergies exist when adopting further tools and techniques. For example, the elevated and stable temperatures used in co-heating provide good conditions in which to perform thermography surveys. The presence of an infrared camera then allows more informed positioning of heat flux sensors for in situ U-value measurements.

This thesis focuses on the use of co-heating to determine an estimate of the *HLC*, although it is important to understand this measurement, and co-heating testing, within the wider context in which they are usually deployed, a theme revisited in the conclusion chapter.

2.6 Alternative methods of estimating heat loss

In this section two alternative methods of examining building heat loss are briefly considered, namely in situ U-values and infrared thermography. Some parallels can be drawn between these and co-heating tests, whilst it is also important to understand the role of co-heating within the context of these alternatives.

2.6.1 In situ U-values

The measurement of in-situ U-values with the use of heat flux plates has been commonly applied to test cells as well as field measurements, with guidance given by ISO 9869:2014 as well as a number of practical field examples (Doran, 2001; Baker, 2008; Baker, 2011; Rye, 2010;

Birchall, 2011). A number of parallels can be drawn with co-heating. Using steady state analysis, similar monitoring durations are required (typically >7 days), with measurement durations requiring 24 hour integer periods, across similar periods of cold weather. An advantage is that measurements can be taken less intrusively and in occupied dwellings with varying heating patterns. To avoid the influence of solar radiation and wind, sensors are often placed on north facing, sheltered facades. Alternatively, a number of dynamic analysis protocols can be used (Jimenez and Madsen, 2008; Biddulph et al., 2014; Naveros et al., 2014, ISO 9869:2014), typically retrieving results within a shorter time frame and providing information on the capacitance of the measured section of wall as an additional extracted parameter.

Significantly, heat flux measurements only represent the heat flow through the section of wall covered by the sensor. This can mean a large number of sensors are required to reliably estimate heat flow across large elements, particularly when non-uniform constructions and indirect heat flows exist. This last point means that when heat flux is not normal to the surface of the wall the measurement becomes more difficult to interpret. In addition, measurements of thermal bypasses, 2D/3D heat loss, thermal bridges and windows are all difficult to perform.

2.6.2 Thermography

Infrared thermography allows visual checks on heat loss across the building fabric. The use of thermography is increasing as prices reduce and equipment becomes more user friendly. The method itself is governed by international standards (ISO 13187:1999).

Whilst thermography can be an excellent tool in visually identifying defects, the absence of evidence is not evidence of absence. This particularly applies as it is only the external surface that is visualised. This can hide thermal bypasses, particularly when ventilated air gaps exist, and the influence of sun, rain, long wave radiation losses and wind shear are all capable of masking underlying effects. This means that not only are skilled and experienced operatives required but also external conditions must be right, with ΔT >10K (Titman, 2001) and with an absence of stored effects. This means testing must be conducted late at night or early in mornings, again limiting available testing time slots and the testing season.

Potentially a bigger limitation is the qualitative nature of the information gathered. Whilst thermography can be an exceptional tool in qualitatively determining areas of heat loss, it cannot quantitatively estimate heat loss.

Clearly, each of these methods, and co-heating itself, have their own limitations. Some of these limitations are shared, meaning for example that testing is restricted to colder parts of the year. Others are mutually supportive, providing greater information on tested buildings. This is perhaps why they have worked so effectively when used together along with other methods, providing both overall and detailed heat loss measurements, as well as a visual understanding of the fabric performance.

2.7 Dynamic methods of estimating building *HLC*

Heat loss measurements are not performed solely through steady state analysis. Dynamic approaches exist, both in terms of experimental protocols and analysis techniques. Bauwens et al. (2012), when reviewing the co-heating method, concluded that to improve the accuracy it might be advisable to go towards an intrinsically dynamic model, where detailed characteristics of the building envelope components can be determined in a distinguishable way and shorter time intervals to allow for more descriptive data points. In general, dynamic methods offer a number of advantages, as described by Baker and Dijk (2008):

- Results can often be obtained in shorter monitoring durations.
- More information can be yielded about the building or measured element, e.g. effective thermal capacitance.
- More accurate results can be obtained.
- Thermal processes can be 'de-coupled', e.g.. to separate thermal transmission and the solar aperture.
- Allows the option of adding specific non-linearities, such as specific thermal resistance changing with temperature or wind velocities.
- Often variables such as radiation exchanges with sky, ground and other terrestrial features and external surface convection variations are ignored in steady state methods but can be included in dynamic analysis.

Work through projects such as PASLINK, have aimed at defining common equipment and agreed test procedures, calibration, data processing and analysis. Largely, this work has looked at measurements made in labs or test cells. This does not mean whole building heat loss

measurements have not been made. The PSTAR method dates back to the 1980s (Subbarao, 1988a), whilst a recent IEA Annex 58 programme, 'Reliable Building Energy Performance Characterisation Based on Full Scale Dynamic Measurements', 2011 - 2015, has worked at pushing dynamic methods to full scale building measurements.

2.7.1 Dynamic test sequences

A number of dynamic testing sequences have been developed, with vary degrees of complexity, ranging from simple cooldowns and free floating periods to PRBS[8] sequences. Reviewing dynamic sequences, Baker and Dijk (2008) concluded appropriate dynamic test sequences should:

- Contain low and high frequency variations, to allow the identification of both steady-state and dynamic properties, covering the range of time constants in components of the system, i.e. 20 min - 50 hours.
- De-couple temperature and solar radiation signals to allow the identification of both the solar (gA) and thermal transmittance (UA).
- Yield sufficient signal-to-noise ratios, in particular in low frequency behaviour, because of the priority given to the accuracy in the identification of the steady state properties.

2.7.2 Analysis of dynamic data

A number of analysis methods then exist with which to determine building parameters from such test sequences. A common approach is to use a grey-box model and system identification. Models are often constructed as lumped capacitance models, ranging from simple first order RC[9] models to multi-node models, incorporating large numbers of resistances and capacitances as well as introducing heat sources such as solar gains. Tools such as LORD and CTSM-r, have been developed to support such approaches (Juhl et al., 2013; DYNASTEE, 2015).

Baker and Dijk (2008) again provide a useful review of the requirements for appropriate models:

- Model accurately reproduces the steady state and dynamic thermal processes.
- Should allow for the separation of physical properties.

[8] Pseudo Random Binary Sequence

[9] An RC model is one in which thermal resistances can capacitances are made analogous to their electrical equivalents.

- Avoid 'over-parameterisation', i.e. some of the parameters cannot be identified because of strong correlation with other 'free' parameters in the model.
- Preferably allow for prior knowledge.
- Allow option of adding specific non-linearities, such as specific thermal resistance changing with temperature or wind velocities.
- Often variables such as radiation exchanges with sky, ground and other terrestrial features and external surface convection variations are ignored in steady state methods but can be included in dynamic analysis.
- Some parameters can be fixed to reduced the model complexity, 'freezing' their values, (i.e. not assigned to be optimised in fitting process), this is seen in the PSTAR secondary terms.

Whilst dynamic methods are not the subject of this thesis it is useful to consider one example, the PSTAR method, which shares the same origins as the steady state co-heating method. This offers a number of contrasting notes, in terms of the application, the theoretical heat balance equation, the experimental test sequence and the analysis techniques adopted.

2.7.3 The PSTAR method

It is helpful to briefly review the PSTAR method, as it can provide a useful contrast and extension to the co-heating method. The PSTAR method is designed to estimate the building *HLC*, effective solar gains and effective building mass. This starts with an energy balance based upon an audit description of the test dwelling, such that this represents a grey-box[10]

An example of this heat flow balance equation can be found in, 2.14 (Subbarao, 1988b), and works such that the terms sum to zero at each time step, *t*, i.e. $\sum Q_{TOT} = 0$.

$$Q_{elec}(t) + p_0[-HLC(T_i(t) - T_e(t)] + p_{in}Q^{in}_{storage}(t) + p_{bsm}[-HLC_{bsm}(T_i(t) - T_{bsm}(t))] + Q_{bsm,storage}(t) + p_{sol}Q_{sol}(t) + Q_{inf}(t) + p_{out}Q^{out}_{storage}(t) + p_{sky}Q_{sky}(t) = 0 \quad (2.14)$$

[10] A black back model is one that is purely data driven, with no physical model. A white box model is then purely theoretical and a grey-box model therefore combines a partial theoretical structure with data to complete the model

Here,

$Q^{in}_{storage}$ and $Q^{out}_{storage}$ represent stored heat flows coupled with the internal and external air temperatures (W).

HLC_{bsm}, T_{bsm}, $Q_{bsm,storage}$ represent the heat loss coefficient, temperature and storage term for an unheated basement space.

Q_{sky} is the heat flow associated with radiation losses to the sky (W).

p_0, p_{in}, p_{sol} etc. are renormalisation terms for the heat loss coefficient, internal mass and solar heat flow terms respectively, initially set to unity.

Terms in the heat flow balance equation are deemed either dominant/ primary heat flows (typically Q_{elec}, Q_{sol}, $Q^{in}_{storage}$) or minor / secondary terms (Q_{sky}, Q_{bsm}, $Q^{out}_{storage}$) with their renormalisation factor remaining at unity.

The STEM[11] test sequence then runs through a number of phases, each designed to elicit a different renormalization factor for the primary terms in equation 2.14. This includes:

- An initial warm up to the set point temperature.
- An overnight *co-heating* period, with the last few hours for analysis to elicit p_0, (i.e. enhance Q_{elec} and minimise Q_{sol} and $Q^{in}_{storage}$).
- *Night of cooldown/decay*, approximately 16 hours (to elicit p_{in}).
- *Free floating period* with solar input signal (to elicit p_{sol}).
- *Pressurisation Test / Tracer gas* or both to determine infiltration rate.
- Optional second night of *steady state* using heating system to define efficiency

An example of the internal temperature, as measured, predicted by the initial building audit description and by the renormalised building is taken from (Subbarao, 1988c) and shown in figure 2.6.

[11] STEM: Short-term Energy Monitoring

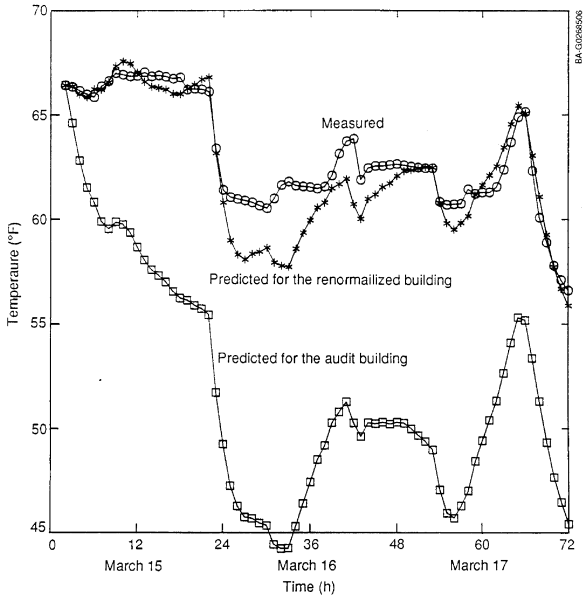

Figure 2.6: *Measured, audit and renormalised estimates for T_i in a PSTAR test, taken from Subbarao (1988c, p.25).*

The renormalisation parameters are estimated iteratively by least squares fitting. The *HLC* parameter p_0 is initially established from the end of the co-heating period, with p_{in} and p_{sol} then estimated, before the process starts again with p_0 estimated with the renormalised equation from the previous step until convergence is reached.

Drawing a comparison to co-heating a number of points can be considered:

- A significantly more complex energy balance in comparison to the co-heating balance equation, including the mass charging and discharging and a number of secondary terms: Q_{sky}, Q_{bsm}.
- A significantly shorter test period is required $\sim$ 72 hours, with an even shorter period of analysis actually used to determine the *HLC*.
- Further building parameters can be estimated, e.g. the effective thermal mass.
- An audit description of the building is required.

This thesis maintains a focus on the steady state co-heating heat loss measurement, rather than exploring alternative dynamic methods. Dynamic tests methods are however considered in reference to the uncertainties and limitations of steady state co-heating tests.

2.7.4 Dynamic vs steady state methods

As described earlier, there is a growing interest in developing full scale dynamic test procedures, particularly through the IEA Annex 58. Examples include the QUB (Quick U-value of Buildings) method (**Mangematin2012; Pandraud2013**), which uses heating and cooling curves over two nights of measurement, and the ISABELE method, which combines periods of heating, constant temperature and then free cooling with network analysis similar to ISO 13790:2013 (ISO, 2013; Bouchie and Boisson, 2014). With a number of potential benefits these methods may overtake the steady state co-heating method as a test for use in the field. However, there are a number of benefits to focusing on the steady state approach.

Firstly, this research will improve our understanding of the co-heating tests performed to date and therefore how to interpret the performance gap that has been measured. Secondly, there are numerous cross overs, between steady state and dynamic heat loss measurements including many of the sources of uncertainty identified and characterised later in this thesis. There are also complementary themes such as discrepancies between the definitions of design and measured *HLC*s. Ultimately, there are both strengths and weaknesses to a simpler experimental protocol and analysis methods within the context defined earlier in this chapter. It is therefore important to establish how and when co-heating tests can be used effectively and establish the limitations of the method. This can allow both the best use of this existing approach and inform areas for future development.

2.8 Research into uncertainty

Direct research into the co-heating methodology and the accuracy of *HLC* estimates has been relatively scarce since the early development work of Siviour (1981) and Everett (1985), which despite being three decades old still remains insightful and relevant. Contemporary research has been conducted since the start of this thesis, including, the NHBC Co-heating field trial (Butler and Dengel, 2013; Jack, 2015b) and by researchers at KU Leuven (Deconinck and Leunis, 2012; Bauwens et al., 2012; Bauwens and Roels, 2014). In addition, knowledge and experience have been gathered from tests performed as part of BPE projects, such as the GHA Programme (GHA, 2011b) and collated into iterations of the LBU protocol (GHA, 2011a; Wingfield, 2010a; Johnston et al., 2012b; Johnston et al., 2013).

Research into uncertainty can also be borrowed from dynamic methods that do not solely adopt a period of constant T_i and steady state analysis or which only use short term periods of overnight co-heating. This includes work reviewed by Andrews (1995) and periods of co-heating used in PSTAR validation work (Judkoff et al., 2000).

Research into the reliability and repeatability is summarised in the next section before an overview of the sources of uncertainty noted in literature is given, providing a basis for further investigation throughout this thesis.

2.8.1 Self-consistency at the Linford project - Everett 1985

Everett (1985), looking at 12 sets of test data, between March 1982 and May 1983, examined the self-consistency of the co-heating method at the Linford project (Everett et al., 1985). The results are shown in figure 2.7, with each data point consisting of approximately 2 weeks of data[12]. There are two points to note.

1. Firstly, there is a jump in estimated *HLC* ($\sim$ 20 W/K) coinciding with the floor being covered in insulation. In this example Everett is removing the estimated floor losses, equation 2.9, such that no change should be seen in the remaining *HLC* estimates despite the increased insulation. Everett puts this unexpected shift down to the treatment of floor losses, in particular the extrapolation of heat loss from two flux sensors across the entire floor. It is difficult to read too much into this without further details of the measurements, but if anything, it identifies the potential uncertainty in trying to disaggregate losses in analysis without precise measurements.

2. Secondly, there is a trend towards lower measured *HLC* moving towards spring, with estimates reducing from 155 to 125 W/K ($\sim 21\%$). Everett puts this down to 'unsuitable' weather. Similar behaviour is seen later in this thesis, but with the mechanisms driving underestimation explicitly identified (section 5.4).

Everett (1985) also included a statistical error estimate, using the standard error calculated from regression, to provide a reported value of 127 $\pm$ 5 W/K. Undefined estimations of uncertainty due to floor losses were then given as $\pm$ 10 W/K, with $\pm$ 8 W/K due to infiltration. Adding the error terms in quadrature to give a 'generous' estimate, Everett stated the overall result as 127 $\pm$ 20 W/K.

[12]The last data set incorporates 20 days

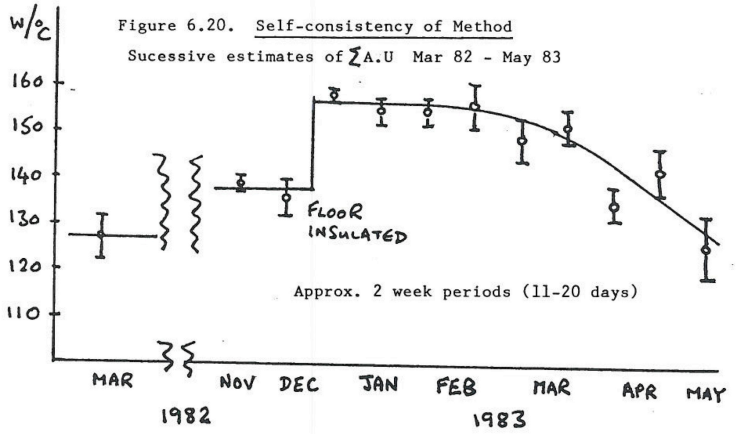

Figure 2.7: *Self-consistency of the co-heating method - from Everett (1985, figure 6.21)*

2.8.2 The NHBC co-heating field trial - 2013

Much like the objectives of this thesis, the NHBC field trial aimed to 'understand the accuracy of the co-heating test and its wider application' (Butler and Dengel, 2013). With twin test houses the project ran between December 2011 and May 2012, and offered scope to investigate the repeatability of the co-heating method and the sensitivity to different experimental and analytical approaches.

The project was structured such that 6 individual test organisations (of which UCL was one) were allotted two-week slots, whilst a control house was constantly kept in co-heating conditions by the BRE. The reported variation from the NHBC field trials was stated as between -17% to +11% of the SAP estimate, 68.4 W/K (Butler and Dengel, 2013) or within 15% of the mean (Jack, 2015b). The variation in results was principally put down to the analysis techniques used by the report's authors.

However, in the absence of 1) weather normalisation, 2) a consistent experimental protocol, 3) standardised analysis methods and 4) common equipment, it is not clear how the sensitivities of the *HLC* to each of the above can be clearly distinguished. Such considerations were not fully addressed when the project results were published (Butler and Dengel, 2013). In addition, results were compared to the SAP estimate of the *HLC* based on the assumption that the test dwellings were precisely constructed. Even where dwellings are very carefully constructed, there are dangers in this type of assumption, a fact that leads this thesis to utilise simulated co-heating tests, where accurate baselines or HLC_{True}, can be precisely known.

Data from this project is analysed later in this thesis, both the individual UCL test and the full dataset. The influence of inconsistent methods, analysis and varying weather conditions across this period upon results is made clear.

2.8.3 Research & development of co-heating at KU Leuven, Belgium

Research has been conducted by a number of researchers based at KU Leuven in Belgium. De Meulenaer et al. (2005) testing a passivhaus dwelling, noted difficulties in achieving constant and uniform internal temperatures, observing temperatures below the thermostatic set point, uneven temperatures distributions throughout the test dwelling and unstable temperatures resulting from midday peaks due to solar radiation. Deconinck and Leunis (2012) later removed such periods of overheating ($>$0.5 °C above set point) from their analysis.

Bauwens et al. (2012) and Deconinck and Leunis (2012) both looked at the reliability of co-heating tests and modified energy balances through examining simulated co-heating tests on a wall and small test box respectively. This included lagged ΔT and solar terms seen in equation 2.9.

Testing a full sized building in the same piece of work, Deconinck & Leunis, noted drastically different results between repeated tests, 200 - 268 W/K, which was largely put down to the use of unsuitable equipment in the first tests, with Bauwens and Roels (2014) also stating that tailored equipment is indispensable, although Deconinck & Leunis did not fully list both sets of equipment. It should also be noted that in this comparison the extent of variation in external conditions is not addressed and in addition, $T_{setpoint}$ was increased from 19-25 °C between the two tests.

Bauwens and Roels (2014) further re-examined the physics behind the simplified energy balance used in co-heating. An extended energy balance included a latent load term, Q_{latent}, to account for the hydroscopic loading and unloading of parts of a test dwelling. Additionally, solar radiation was considered over a number of orientations/projections, ΔT and S used lagged average values (see eq 2.9), an equivalent external temperature was used to account for external short and long wave radiation and the opaque and transparent components of transmission losses were separated out.

However, it is then remarked that when looking at daily data, due to the correlation between measured solar radiation across different orientations the respective projections of R cannot be determined separately, instead this second term is lumped into a single building solar aperture, at which point Bauwens (2014) states it has perhaps lost its physical relevance.

Furthermore, the opaque, transparent and ventilation heat loss terms cannot be separated in regression and are similarly lumped into a single building *HLC* parameter. At this point the extended balance equation has 'naturally evolved' back to the simplified balance. As Bauwens explains, linear regression only allows us to identify as many parameters as there are independent variables. Often, strong correlations are seen between the variables used in the extended balance equation, and thus cannot be used.

In conclusion, Bauwens (2014) states that more accurate predictions can be obtained by keeping the lagged average terms and that more reliable estimates may be made when c the intercept term is neglected from analysis. Finally, it is stated that a numerically calculated R should not be used as the assumptions used may not describe the complex phenomena lumped into this parameter.

2.8.4 Evidence from LBU Work

Researchers at LBU have not published any direct research into uncertainty in the co-heating method or its development. However, with significant practical experience, examples of uncertainty can be gathered from the review of test reports and the co-heating protocol.

In particular, the most recent LBU protocol (Johnston et al., 2013) lists a large number of uncertainties associated with co-heating tests. Systematic sources of uncertainty include the calibration of sensors, appropriate shielding of T_e sensors, the stability and spatial variation in T_i and the location of the pyranometer, including the presence of shading. Additionally, different weather conditions and unexpected thermal effects (e.g wind washing, thermal bypasses) are both cited as random sources of uncertainty.

Johnston et al. (2013) also include in these lists a number of uncertainties relating to the predicted *HLC* and thus present in any comparison to the measured value. Measurements and calculations of internal dimensions are cited as a systematic error, whilst construction defects, variability in construction tolerances and unexpected thermal effects can be considered as ran-

dom errors. Less directly, the LBU protocol discusses issues of moisture and drying out, stored solar contributions, thermal mass effects, varying external temperatures and the time taken for the test dwellings to become heat saturated.

Previous studies have shown the influence of wind speed on co-heating tests (Miles-Shenton et al., 2011) and numerically calculated the increase in stack losses with elevated internal temperatures (Lowe et al., 2007). Additionally, poor correlation has been identified in statistical solar aperture measurements, resulting in the need for a numerical approach. Finally, through examining results either side of interventions, particularly the presence of a cavity sock, $\sim$ 17 - 25 W/K differences were measured, and whilst there is no way to characterise the absolute accuracy of such differences, this does hint at the sensitivity of the *HLC* measurement.

Finally (Johnston et al., 2015), making references to the reproducibility of the test method, report that tests on the same dwelling four years apart yielded results of 132.9 W/K and 133.8 W/K. Repeated tests within the Salford Energy House environmental test chamber then were recorded as 224.4 W/K, 222.9 W/K and 222.2 W/K (Johnston et al., 2015).

2.8.5 Uncertainty in short term co-heating & the PSTAR method

In this section the relevant elements of literature using short term co-heating periods are considered. Andrews (1995) reviewed the various experimental methodologies used and the accuracy of short term co-heating tests to determine duct efficiencies as well as the building *HLC*. These methods are based upon the PSTAR method, i.e. night time co-heating data across typically 2 or 3 days, although the precise experimental and analysis methods varied.

Reviewing cases in which repeated *HLC* estimates were made, Andrews summarised the repeatability and random error through the standard deviation of *HLC* estimates, table 2.7. In uncorrected, raw data, the variation between estimates is quite high. Duffy and Puri (1985), reported that whilst *'coefficient values derived from only 24 hours of data were extremely erratic. Coefficient values estimated on the basis of 96 hours (4 days) of data were reasonably close to those based on data for the entire month'*. Subbarao et al., (1990), similarly stated *'repeated measurements have been known to show considerable variation from night to night'* due to *'storage effects due to variations in inside and outside temperatures, solar radiation, sky temperature depression, variable infiltration, and heat flow through the floor'* with a range in raw estimates of 121 - 207 W/K.

However, when these additional heat flows are corrected, limited or accounted for in the analysis, the majority of results demonstrate standard deviations in the region of 5%. For example, Subbarao et al. (1990) estimated raw results from 13 repeated tests as 146.9 $\pm$ 24.7 W/K. Accounting for infiltration and basement losses, this estimate was adjusted and the deviation reduced to 151.6 $\pm$ 7.8 W/K. Subsequently accounting for thermal storage coupled to outside (4.7 $\pm$ 2.3 W/K), inside temperatures (1.4 $\pm$ 5.3 W/K), solar gains (6.9 $\pm$ 3.1 W/K) and the sky temperature (-5.4 $\pm$ 3.5 W/K) gave a 'corrected' *HLC* of 159.3 $\pm$ 4.4 W/K. Andrews (1995) states that this effectively normalised the conditions under which tests were taken.

Table 2.7: Summary of short term co-heating test *HLC* estimates & their random error. Adapted from Andrews (1995) with additional cases. Note: Random error is defined as the standard deviation from the mean result.

	Random Error [1]	No. of Values	Range	Conditions	
Sonderegger 1979	9.0%	8	196 - 241 W/K	Tests on different heating systems (heating system, fireplace, cooling system, infiltration)	
	3.3%	4 pairs	-	Pairs from initial and end period of same night, for each test type	
Duffy 1989	3.3%	-	-	Engineering Judgement, ΔT = 16.7 °C (30F), further 10% at 5.5°C, 5% at 11°C, 2.5% at 22°C	
Jones 1984	1.3%	2	-	Two tests on same house, 20 days apart, at a mean ΔT = 22 °C	
Subbarao 1990	16.8%	13	121 - 206.7 W/K	Raw for repeated tests on same dwelling over 5 months	
	2.8%	13	-	Corrected - PSTAR Method	
Saunders 1984	4.0%	7	-	Raw	
	5.5%	7	-	Corrected for Infiltration	
Andrews et al., 1995b	3.9%	4	222 - 244 W/K	Mean ΔT = 17.8°C (32 F)	
	4.7%	2	175 - 193 W/K	Mean ΔT = 21.1 °C (38 F)	
Judkoff et al., 2000	5.3%	28	75 - 89 W/K	SIP Panel Office Cell	STEM: Three Day Test, 1am to dawn periods, filtered for high wind speed, low ΔT and max solar, sky radiation and mass heat flows
	4.7%	28	14%, mean 118 W/K	Timber Frame Office Cell	
Lloyd et al., 2007	18.9%	5	Mean = 438 W/K	Original	Retrofitted Dwelling in New Zealand, tested at various stages of retrofit. Brick clad timber frame with suspended timber floor.
	10.0%	7	Mean = 409 W/K	With Drapes/ Curtains	
	5.4%	4	Mean = 460 W/K	No Carpet	
	8.7%	10	Mean = 416 W/K	EPS Underfloor Insulation	
	4.2%	12	Mean = 401 W/K	Double Glazing	
	6.6%	5	Mean = 350 W/K	Wall Insulation	
	6.8%	3	Mean = 296 W/K	Drapes + Double Glazing	

Since Andrews review, Judkoff et al. (2000) has perhaps performed the most comprehensive validation of the PSTAR and STEM methods. Judkoff et al. (2000) tested SIP and timber frame cells both within a large environmental chamber, at close to true steady state conditions, and then within the outdoor environment.

For a month between March and May the test cells were constantly heated to the same internal set point, allowing some comparisons to the co-heating test method to be conducted. Night time data (1am to dawn) was used to analyse the cells *HLC*[13] across a three day period. Importantly, data was filtered for high wind speed, low ΔT and summed solar, sky and mass heat flows were less than a maximum value, with the results listed in table 2.7.

Judkoff et al. (2000) states this suggests that for a given test there is a 68% chance of being within $\pm$ 5% of the answer derived from multiple tests, as long as systematic errors can be ruled out. If multiple tests are conducted then there is a 95% chance of being within 2% of the mean. Whilst this shows there is promise in short term testing, the absence of systematic error is a crucial caveat and an element that must be investigated more thoroughly. Further, even the largest sample sizes seen in table 2.7 remain relatively small. There remains a lack in breadth of these studies. Questions would therefore remain over the impact of the proceeding environmental conditions, particularly in lower heat loss, thermally heavier and more complex structures than tested here.

2.8.5.1 Systematic error

Reviewing work into systematic error, Andrews cites Liu and Claridge (1995) who regarded systematic errors in overnight periods to occur from:

- Impact of solar radiation through windows.
- Impact of neglecting solar radiation through walls and roof.
- Impact of neglecting relatively higher daytime temperatures.

To reduce this first uncertainty, it was recommended to reduce solar gains introduced into the dwelling on the day before testing by covering the windows with reflective sheets. Solar radiation incident on opaque elements and changing external temperatures could not be reduced so easily. This could lead to bias or error in *HLC* / heating system efficiencies if, for example,

[13] US Literature often uses the BLC, Building Loss Coefficient, normally in unit of BTU/hr/F

a test was performed on a night following a warm sunny day, and the other test followed a dull cold day. The suggested approach to be adopted into the ASHRAE 152 Standard was to perform a 'flip-flop' test, or rather both a *HLC* and heating system test on the same night, with the order then reversed on the subsequent night. This would reduce any bias in the calculation of the heating system efficiency, but may not reduce the absolute error in *HLC* estimates.

Concluding his review, Andrews stated there are not enough test cases or houses to make a firm conclusion on the accuracy of the method, although the results showed promise. Clearly the presence of systematic errors needs to be addressed and a wider number of buildings, i.e. low energy, heavyweight, need to be explored to further validate such test methods.

2.8.5.2 Comparing PSTAR & co-heating

Palmer et al. (2011) performed a blind comparison of the PSTAR and co-heating method on a modern UK semi-detached dwelling. A 'consistent and systematic difference between the two sets of measurements' was found (Palmer et al., 2011, p.8). The co-heating tests estimated a *HLC* of 196.4 W/K (HLC_{inf} = 26.6 W/K) whilst the PSTAR method provided a much lower *HLC* of 125 W/K (HLC_{inf} = 17 W/K).

The two tests were performed over 12 months apart, with the initial co-heating tests performed on a newly finished, but uncarpeted and unpainted dwelling. Any changes to the building in this period, including the drying out of moisture, were cited as potential causes of such discrepancy. Consideration was also given to the nature of the two measurements and the difference between the 'heat soaked' co-heating dwelling and the much shorter time frame allowed in the PSTAR method to reach steady state. The elapsed time between the two tests mean that it is hard to assess the root causes of the difference between the two measurements. There are also details absent from the report, which make comparisons difficult, such as the environmental conditions during both tests and the treatment of the adjoining property and any associated heat transfer.

2.8.5.3 Comparing co-heating and LORD dynamic analysis

Baker and Morgan (2013) and Baker (2015) have used both steady state analysis and LORD (Gutschker, 2004) to measure the *HLC* of more traditional dwellings pre and post retrofit. More consistent estimates between the dynamic and steady state approaches are seen than in Palmer et al. (2011). The comparison of two symmetrical rooms with alternative retrofit strategies gave results of 62 and 98 W/K using co-heating analysis and 60 and 87 W/K using LORD. A similar

approach on a retrofit project gave pre and post results of 251 W/K and 143 W/K using LORD and 241 W/K and 126 W/K using co-heating analysis, where little difference was seen between Siviour and MLR results (Baker, 2015). A more significant difference was seen in the estimation of R, particularly post retrofit where the LORD value more than doubles the co-heating estimate. Baker (2015) states that both methods have their own 'benefits and problems', in particular noting the potential tendency for the steady state analysis to underestimate the *HLC* as a result of the external dynamics.

2.8.5.4 IEA Annex 58

Within the framework of IEA Annex 58, common exercises have focused on both a small test cell, which was transported and tested in different climates, and full scale test houses. Tests have been run using both constant internal temperatures and dynamic test sequences (e.g. ROLBS, Randomly ordered logarithmically distributed binary sequence). A variety of analysis technique have then been used, including autoregressive models (ARX and ARMAX), RC networks and state space models. Whilst the focus is on developing identification methods, rather than specifically on uncertainty, it is thought more work will be published as this annex draws to a close.

2.9 Conclusions from the literature review

It has been established that reducing space heating energy demand is crucial to achieving emission targets, ensuring energy security, delivering thermal comfort and alleviating fuel poverty. Reduction in space heating demand is central to this and is addressed through building regulations with specific requirements for the fabric performance. However, there is a large gap between the point at which thermal performance is measured and verified, typically at material or component level, and the point at which a building is completed. This gap is bridged by an array of simplified calculations and assumptions that perhaps inevitably result in a gap between measured and predicted performance. Recent measurements, including via co-heating, have revealed evidence of this fabric performance gap that represents a sizeable risk of undermining reduction strategies. Without any forms of measurement and feedback only limited control can be achieved, impairing the delivery of consistently thermally efficient dwellings to the housing stock.

Co-heating has been used as a measurement tool to determine total building heat losses through the estimation of a building *HLC*, particularly in the UK over the last decade. This has helped identify the fabric performance gap and the party wall bypass. There have been suggestions

that co-heating may therefore have a larger role, within compliance as well as research, with the Zero Carbon Hub stating that 90% of new homes should demonstrate actual performance meeting design by 2020. However, there are concerns, from industry in particular, over the accuracy and reliability of the co-heating method along with its suitability for wider adoption.

In order to determine what role the co-heating method has to play a number of gaps in our current knowledge need to be addressed. Firstly, the accuracy of the co-heating method has not been established. This will require determining the sources of uncertainty present in co-heating tests. Whilst many have been identified from previous work more research is required in order to identify their exact nature, scale, impact upon *HLC* estimates and relationship to building characteristics. In particular the presence and impact of systematic errors needs to be understood.

With a limited number of tests the accuracy and reliability of the co-heating method needs to be understood across a wider range of dwellings and built forms (GHA, 2011b; Andrews, 1995). Further, the impact of weather conditions need to be established (ZCH, 2014b). This can help establish what buildings can be tested and under what environmental conditions. Other limitations also require further research. Whilst the duration and environmental conditions required for testing are cited as major obstacles to the adoption of co-heating, no research has sought to establish the required monitoring duration or testing season beyond the examination of weather files (Lowe and Gibbons, 1988).

Finally, a consistent method is required. This includes optimum experimental protocols and forms of analysis, including data aggregation (Butler and Dengel, 2013). It needs to be established how uncertainties can be identified and addressed, including a method for suitable estimates of uncertainty - allowing co-heating results to be placed within the context of their uncertainties.

These issues form the basis of the research questions stated at the beginning of chapter 4. Prior to this, chapter 3 sets out a number of definitions describing heat loss, solar gains and uncertainty itself.

Chapter 3

Defining the Heat Loss Coefficient, the Solar Aperture, Measured Forms of Solar Radiation and Uncertainty

Chapter overview

This chapter reviews and defines a number of key terms and concepts, providing the foundations for work in this thesis. This includes key building parameters, namely the *HLC* and *R*, and the latter's relationship to the form of measured solar radiation. Subsequently, a number of terms used to describe uncertainty are considered. The chapter is therefore structured as follows:

- **3.1 The heat loss coefficient:** is defined and its underlying equations reviewed, including:
  - The formal definition of the predicted *HLC* as defined by ISO 13790:2008 (ISO, 2008). (Section 3.1.1)
  - A definition of the design or predicted *HLC* typically used in co-heating measurements, HLC_{pred}. (Section 3.1.2)
  - A definition of the *HLC* measured through co-heating tests, HLC_{meas}. (Section 3.1.3)
  - A definition of the true *HLC* of a test dwelling, HLC_{True}. (Section 3.1.4)
  - And a comparison of these three terms. (Section 3.1.5)
- **3.2 Definitions of both internal and external temperatures:** are considered in relation to the *HLC*.

- **3.3 The solar aperture *R*:** is defined through both its determination by numerical and statistical models:
  - Numerical calculations to determine solar gains using ISO 13790:2008, SAP 2012 and PHPP methods (ISO, 2008, BRE, 2014; Feist, 2007). (Section 3.3.1)
  - A definition of the statistically derived *R* as measured in co-heating tests. (Sections 3.3 and 3.4.4)
- **3.4 The components of solar radiation and its measured forms:** are reviewed and definitions of the statistically derived *R* are reconsidered.
- **3.5 Definitions of uncertainty:** are given along with a review of the science of measurement.

3.1 The heat loss coefficient, *HLC*

The heat loss coefficient or heat transfer coefficient is the principal parameter measured by co-heating tests. However, its definition, needs careful consideration. This can begin with the ISO description of the heat loss coefficient.

3.1.1 ISO model of the heat loss coefficient

The heat transfer coefficient or as it is referred to as in this thesis, the heat loss coefficient (*HLC*), is defined in both ISO 13789:2010 and ISO 13790:2008 as (ISO, 2008; ISO 2010):

> *"heat flow rate divided by temperature difference between two environments; specifically used for heat transfer coefficient by transmission or ventilation."* (ISO, 2008, p2)

As alluded to here, the *HLC* is typically decomposed into two principal components. The transmission heat transfer coefficient (HLC_{trans}), describes the heat flow rate due to thermal transmission through the building fabric, divided by the environmental temperatures[1] on either side of the construction. The ventilation heat transfer coefficient (HLC_{vent}), is the heat flow rate due to air entering a conditioned space, either through ventilation or infiltration, divided by the difference between internal air and supply air temperature. As ventilation systems are typically switched off and sealed during co-heating, the ventilation term consists of purely unintentional air leakage and can thus be represented by an infiltration heat loss coefficient (HLC_{inf}).

[1] See section 3.2 for definitions of these temperatures.

The sum of these two components is then occasionally referred to as the building or total heat transfer coefficient HLC_{TOT}, as in ISO 13790:2008 (ISO, 2008).

$$HLC_{TOT} = HLC_{trans} + HLC_{inf} \tag{3.1}$$

3.1.1.1 Transmission Heat Transfer Coefficient, HLC_{trans}

Considering the transmission heat flows through the building fabric, HLC_{trans}, can be broken down into four components:

$$HLC_{trans} = HLC_d + HLC_g + HLC_{unc} + HLC_{adj} \tag{3.2}$$

Here, HLC_d represents the most familiar direct heat transfer from the internal conditioned space across the fabric into the external environment through conduction. Further heat transfer coefficients then exist for heat flows through the ground (HLC_g), through unconditioned spaces (HLC_{unc}), and to heated spaces or conditioned adjoining buildings or spaces (HLC_{adj}).

These terms and their constituent parts are defined in more depth in appendix B.1 but at this point a number of concepts can be considered:

- The accuracy with which this model describes a real building depends upon:
  - The accuracy of the inputs, material properties, dimensions and environmental variables.
  - The extent to which the model captures the actual structural features of the heat transfer processes.
- Secondly, only the first of these four terms, HLC_d, is directly related to the external temperature, T_e, the variable used within co-heating analysis and in most definitions of the *HLC*. Heat transfer associated with the remaining three terms is dictated by their own respective temperatures: T_g, T_{unc} and T_{adj}.

3.1.1.2 Ventilation heat transfer coefficient, HLC_{vent}

The infiltration heat transfer coefficient can be calculated from:

$$HLC_{inf} = \rho_a c_p \, \dot{V} = \rho_a c_p \, nV \tag{3.3}$$

Where:

$\dot{V}$ is the airflow rate through the heated or cooled space, typically in m^3/h.

$\rho_a c_p$ is the heat capacity of air per unit volume, equal to one-third if $\dot{V}$ is in units of m^3/h, from the density, ρ_a, and heat capacity of air, c_p.

n is the air change rate, typically per hour (h^{-1}).

V is the volume of the space (m^3).

Both wind pressures and buoyancy or stack effects within the dwelling will then drive the infiltration rate of a test dwelling.

3.1.1.3 Wind and stack driven losses

Wind and stack driven infiltration losses can be modelled in a variety of ways, although in reality wind driven infiltration losses are one of the least understood and most difficult heat loss mechanisms to model (Deru and Burns, 2003). Here, the 'enhanced' model of Walker and Wilson (1997) is used, with stack and wind losses combined in quadrature (ASHRAE, 2013):

$$\dot{V} = \sqrt{\dot{V}_w^2 + \dot{V}_s^2} = \sqrt{(cC_w(sU_w)^{2n})^2 + (cC_s(\Delta T)^n)^2} \tag{3.4}$$

Here:

$\dot{V}$ is the airflow rate (m^3/s)

$\dot{V}_w$ is the wind airflow rate (m^3/s)

$\dot{V}_s$ is the stack airflow rate (m^3/s)

c is the flow coefficient ($m^3/(s/Pa^n)$)

C_w is the wind coefficient $(Pa.s^3/m^2)^n$

C_s is the stack coefficient $((Pa/K)^n)$

U_w is the average wind speed (m/s)

s is the shelter factor

n is a pressure exponent

Considering these equations in regards to co-heating tests, three conclusions may be quickly drawn:

- The stack airflow rate is a non-linear function of ΔT, meaning HLC_{inf} and therefore HLC_{TOT} are non-constant, increasing at higher ΔTs.
- Similarly, the relationship between wind-driven ventilation and wind speed is non-linear.
- The interactions between stack and wind driven infiltration, and therefore heat loss, are also non-linear, even in this simplified model, further increasing the non-constant nature of HLC_{TOT}.

3.1.2 The predicted heat loss coefficient, HLC_{pred}

These ISO calculations form the basis of the predicted heat loss coefficient, HLC_{pred}. The value of HLC_{pred} is in the majority of cases based upon ISO 13790:2008 (ISO, 2008) although various national models exist. In the UK, the ISO 13790:2008 compatible model is the Standard Assessment Procedure (SAP) and reduced SAP (RdSAP) (BRE, 2014). Most commonly, it is the SAP estimated HLC_{pred} or an adapted SAP estimate that is used as a comparison for the measured *HLC*, see table 2.1.

The inputs used for HLC_{pred} will then depend upon the objectives of the calculation and stage of construction. Calculations will be made at the design stage, for approval prior to construction, and will then subsequently be revised to represent any modifications made prior to completion. When calculated by the methods listed above the *HLC* can be based upon either design or as-built construction details. To avoid confusion between the two, this thesis will refer only to HLC_{pred}, assumed to be based upon the best details or information available. In simulated tests this will always represent an as-built calculation, with accurate information of the construction and thermal characteristics. Field tests are again based upon as-built details but the robustness of any inputs reduces the use of these values in any comparisons to measured values.

For example, research has shown that the inputs to SAP assessments are often missing, based on default values or do not match as-built details. A Zero Carbon Hub survey of SAP assessors identified that thermal bridging details, U-value calculations and window information was unavailable and missing in the majority of cases (ZCH, 2014b). The results of a SAP audit in the same project found U-values, linear thermal bridging and window g-values were wrong

in 100% of eight audited plots. These errors can be passed onto the comparisons between measured and calculated *HLC*s, such that SAP estimates are sometimes revised to incorporate as-built details and measured parameters, particularly air leakage, product substitutions and construction defects (Miles-Shenton et al., 2011).

The accuracy of HLC_{pred} is not the subject of this thesis, although it remains an important consideration throughout. One perspective of considering the required accuracy of whole building heat loss measurements is to consider the accuracy of predicted *HLC*s. There is little point in creating a test that is significantly more accurate than the baseline it is compared to.

In addition, these calculations of HLC_{pred} are often calculated under typical environmental conditions (e.g. wind speed, T_e). It is therefore important that inputs used in these calculations are adjusted to correspond to the conditions under testing or test results are normalised. If not, comparisons will be flawed.

3.1.3 The measured heat loss coefficient, HLC_{meas}

After defining the theoretical *HLC*, the *HLC* that is being measured by a co-heating test must also be considered and the two compared. Two heat loss models can be considered describing the measured heat loss coefficient, HLC_{meas}. In the no-intercept model ($Q + R \cdot S = HLC \cdot \Delta T$) all heat loss is dependent upon ΔT or rather T_e. In the intercept model ($Q + R \cdot S = HLC \cdot \Delta T + c$) heat loss not associated with T_e is lumped together into the intercept parameter, c (W).

Non-intercept regression models (MLR, SLR), assume all losses are direct to the external environment. However, as defined previously, there are a number of terms that, certainly over the course of a two-week test, are independent of ΔT. Such loss mechanisms can be considered 'uncoupled' from T_e and ΔT, but are nevertheless lumped together in the no-intercept model and assessed by the same internal-external ΔT.

$$HLC_{no-intercept} = \frac{(Q_{trans} + Q^*_{inf} + Q_g + Q_{adj} + Q_{unc})}{\Delta T} \tag{3.5}$$

Where Q_{trans} represents the heat flow (W) due to transmission losses across the building fabric, Q_g is the heat flow to the ground, Q_{adj} is the heat flow to adjoining heated spaces and Q_{unc} is the heat flow to connecting unheated or unconditioned spaces.

An intercept regression model (MLRi) may therefore provide a more elegant description of the numerous heat loss components, separating out the coupled and uncoupled heat flows within the gradient and intercept respectively:

$$HLC_{coupled} = gradient = \frac{(Q_{trans} + Q^*_{inf})}{\Delta T} \tag{3.6}$$

With the remaining uncoupled terms falling into the intercept, c:

$$c = (Q^*_{inf} + Q_g + Q_{adj} + Q_{unc}) \tag{3.7}$$

This defines losses in both a coupled *HLC* (W/K) and a net uncoupled heat flow (W). To combine the two and allow comparisons to a non-intercept model, the two regression coefficients must be added as below:

$$HLC_{intercept} = gradient + \frac{c}{\Delta T} = HLC_{coupled} + \frac{c}{\Delta T} \tag{3.8}$$

A comparison of the two models and the accuracy with which the values extracted from statistical analysis describe both the coupled and uncoupled losses is considered in section 8.1.

Note: The infiltration heat loss, Q_{inf} cannot be cleanly separated into coupled and uncoupled components in these definitions and hence is represented as Q^*_{inf} in the equations above 3.5 - 3.7. Equally, if infiltration measurements are made (see section 2.5.1), Q_{inf} can be estimated and subtracted from Q_{TOT}, potentially separating out HLC_{inf} from HLC_{TOT}. The assumption could be made that this then separates out HLC_{trans}, but it can be considered that the remaining heat loss incorporates radiative losses and thermal bypasses, rather than just straightforward transmission losses. The remaining heat loss component is therefore denoted HLC_{fabric} in this thesis. Equally, HLC_{inf} will not fully reflect the full range of heat losses induced by wind and stack effects, rather only the direct infiltration losses.

3.1.4 The true heat loss coefficient, HLC_{True}

"In fact, the true value of a measured quantity can almost never be known exactly and is, in fact, hard to define" (Taylor, 1997, p18)

When considering the *HLC* measured through co-heating, both elements in the above statement are particularly true. As the value of HLC_{True} can never be exactly known, and in the case of a field co-heating test there is potentially a large uncertainty over its value, assessing the error in a *HLC* measurement becomes challenging. This in part is justification for the use of simulated co-heating tests used in this thesis, as discussed in the methods chapter, section 4.4.

In simulated tests HLC_{True} can be known from simulation outputs (see section 4.3.3.1) and is defined as the sum of all heat flows through all elements of a test dwelling divided by ΔT. In field tests the theoretical, and unknown, HLC_{True} remains more conceptual, although can again be defined as the sum of the heat flows though the entire building envelope divided by ΔT. In both cases, HLC_{True} represents an average value across the test period.

The issue of definition is no less problematic. The value of HLC_{True} is not static, rather, as previously discussed, being a function not only of the internal and external environmental conditions but also the state of the testing dwelling itself and the form of the regression analysis (equations 3.5, 3.8 and 3.7). Care is therefore required when examining the reproducibility of tests, inter-test comparisons or comparisons to design. Again, this is discussed in more detail in section 9.5.

HLC_{True} can be considered generally as the value of a quantity that is believed to satisfy fully the definition of the measurand (JCGM, 2008a). In simulations, HLC_{True} is defined as the total heat flow out of the building, divided by ΔT. This can be precisely known from outputs of the simulation, as defined in section 4.3.3.1. In field tests this unknown value would again describe the total heat flow out of the building across the test period, divided by ΔT. Both HLC_{meas} and HLC_{pred} then fall unknown distances from this value.

3.1.5 Comparisons between HLC_{pred}, HLC_{meas} & HLC_{True}

Ultimately, in the majority of cases the measured value (HLC_{meas}) will be compared with a predicted or design value (HLC_{pred}), see figure 2.1). However, comparisons between HLC_{meas} and HLC_{pred} are not straightforward, even beyond the measurement errors that may exist within HLC_{meas}. Care must be taken to ensure that HLC_{pred} is representative of the actual as-built test dwelling, reflective of the environmental conditions under which it was tested and that assumptions used within the prediction calculation are reasonable. To allow appropriate comparisons the uncertainty in HLC_{pred} may also therefore need to be estimated. Comparing either of these two values with HLC_{True} is impossible, as not only is this parameter not known, but the variables that influence it are equally unknown.

Summarising issues related to HLC_{pred}:

- HLC_{pred} may not be reflective of actual build (ZCH, 2014b).
- HLC_{pred} may be calculated under different environmental conditions to HLC_{meas}.
- HLC_{pred} may not be capable of incorporating complex heat loss mechanisms, i.e. thermal bypasses, wind washing etc. (Johnston et al., 2013).
- HLC_{pred} can be improved through measured inputs (i.e. air change rate and in situ U-values) but their uncertainties and validity also need to be assessed.

These issues, along with further discussion on comparisons between HLC_{meas} and HLC_{pred}, and the role of feedback more generally can again be found in section 9.5.

3.2 Measuring & defining temperature

"The temperature of a fluid or object indexes its thermal energy, and in reference to its environment, is a measure of its ability to communicate this energy to other fluids or objects in the form of heat." (Thomas and Smoot, 2013, p.1)

In this section, the definition and measurement of internal and external temperatures are reviewed. This allows the definition of the *HLC* to be completed in the context of internal and external temperatures and provides further consideration of the measurement of these parameters and how they sit within the co-heating experimental method.

3.2.0.1 External temperature, T_e

The external temperature is defined as the dry-bulb temperature of the external air, measured within a *"thermometer screen fitted with louvers to allow a free flow of air"* (ISO 15927-1:2003, p.8; ISO, 2003). For transmission heat loss calculations the radiant temperature of the external environment is supposed to equal the external air temperature, with long-wave radiation to the sky handled separately. This definition leaves the exact height and positioning of an external sensor undefined. This may lead to issues relating to spatial variation in T_e, particularly in the presence of microclimates or in urban settings.

Thomas and Smoot (2013) states that the use of naturally ventilated enclosures can lead to uncertainties from inadequate airflows entering the enclosure and due to solar radiation penetrating the shield. The use of radiation shields with forced aspiration can avoid or significantly reduce these air temperature errors but come at an increased cost.

Sol-air temperature

An alternative concept is that of the Sol-Air Temperature. This is a hypothetical temperature that determines the rate of heat flow into an external surface by convection from the surrounding air, shortwave solar radiation and radiative exchange to the surrounding (other buildings, ground and sky) (ASHRAE, 2013, section 18.22).

$$T_{sol-air} = T_e + \frac{(\alpha \cdot S)}{h_e} - \frac{(\epsilon \Delta R)}{h_e} \tag{3.9}$$

Where h_e is the heat transfer coefficient for radiation and convection to the external environment (W/m^{2}K), α is the absorptance of the surface for solar radiation, *S* is the solar radiation incident upon the surface (W/m^2), ϵ is the hemispherical emittance of a surface and ΔR is the difference between long-wave radiation incident on surface from sky and surroundings and radiation emitted by blackbody at outdoor air temperature (W/m^2).

The use of $T_{sol-air}$, or a reference temperature in co-heating analysis was explored by Deconinck and Leunis (2012). Whilst there are potential benefits through incorporating shortwave and long wave radiation components, its calculation requires accurate knowledge of material absorptivity, heat transfer coefficients, the effective sky temperature (T_{sky}), surface temperatures (T_{se}) and incident solar radiation, all of which need to be measured or calculated over a range of building surface, making it fairly impractical in nature.

3.2.0.2 Internal temperature, T_i

As the objective of heating a space is to provide thermal comfort to its occupant, the heating load is calculated using the dwelling *HLC*, the external air temperature and an internal operative temperature, see equation 3.10 from ISO 13790:2008 (ISO, 2008). As the thermal sensation experienced by occupants is related to both the surrounding air temperature and that of the surrounding surfaces both are incorporated into the operative temperature, see equation 3.11 from ISO 7726:2001(ISO, 2001).

$$Q_{load} = HLC \cdot (T_o - T_e) \tag{3.10}$$

$$T_o = \frac{h_c \cdot T_i + \bar{h_r} \cdot \bar{T_r}}{h_c + h_r} \tag{3.11}$$

Or

$$T_o = a \cdot T_i + (1 - a)\bar{T_r} \tag{3.12}$$

Where

$$a = \frac{h_c}{(h_c + h_r) = \frac{1}{(1+\frac{h_r}{h_c})}} \tag{3.13}$$

Here, h_c and h_r are the internal convection and radiation coefficients, $\bar{h_r}$ is the mean radiant heat transfer coefficient and $\bar{T_r}$ is the mean radiant temperature.

At mean air velocities less than 0.2 m/s, a = 0.5, meaning T_o is an average of the mean radiant and air temperatures.

If it assumed that the internal air temperature is higher than the mean radiant temperature, then a *HLC* calculated using the internal air temperature would be marginally lower than one calculated using an operative temperature. Practically, the air temperature is a cheaper and more consistent variable to measure, both within a single test dwelling and across a range of tests. Temperature measurements are considered in section 9.3.1.

3.3 Solar gains, *R.S*, & the solar aperture, *R*

Solar gains form a fundamental part of the co-heating energy balance and the estimation of the solar aperture, *R*, through co-heating tests is often of interest, not only to determine solar gains and the building *HLC* but also as a unique parameter when evaluating passive solar buildings.

Both solar gains and the solar aperture can be determined through numerical calculations or derived statistically from regressing co-heating data. Traditionally, the solar aperture (*R*), within co-heating tests, is a building parameter that has been adopted to define this statistical relationship, with $Q_{sol} = R \cdot S$. However, once again the precise definition of this parameter is complex and must be considered in the context of the measured solar radiation during a co-heating test.

This section considers solar gains as they are calculated and defined numerically, before considering the definition of statistically calculated *R*s, which incorporates a review of incident solar radiation and its measurement.

3.3.1 Numerically calculating solar gains

Three methods of calculating solar gains can be considered, based on those used in co-heating tests to date. These include the methods detailed in ISO 13790:2008 (ISO, 2008), SAP and PHPP. The latter two methods are based upon the ISO method, albeit with simplifications and some additional terms as shown in equations 5.3 to 3.19.

3.3.1.1 Solar heat gains - ISO 13790 method

The solar heat gains to a building can be determined from ISO 13790:2008 (ISO, 2008):

$$Q_{sol,k} = F_{sh,ob,k} \cdot A_{sol,k} \cdot I_{sol,k} - F_{r,k} \cdot \phi_{r,k} \tag{3.14}$$

Here:

$Q_{sol,k}$ is the total heat gains through building element *k* (W).

$F_{sh,ob,k}$ is a shading reduction factor for external obstacles for the solar effective collecting area of surface *k* (0-1).

$A_{sol,k}$ is the effective collecting area of surface *k*, with a given orientation and tilt angle, in the considered zone or space (for glazed or opaque) (m^2).

$I_{sol,k}$ is the solar irradiance, the mean energy of the solar irradiation over the time step of the calculation, per square meter of collecting area of surface *k*, with a given orientation and tilt angle (W/m^2).

$F_{r,k}$ is a form factor between the building element and the sky.

$\phi_{r,k}$ is the extra heat flow due to thermal radiation to the sky from building element *k* (W).

Note: ISO 13790:2008 includes the thermal radiation to the sky from the building within solar heat gain calculations for convenience. This loss mechanism is further described in section B.3 of the appendix and the impact upon co-heating tests considered in section 6.3.

Through the term $A_{sol,k}$, gains through opaque and glazed elements can be considered separately. For glazed surface:

$$A_{sol} = F_{sh,gl} \cdot g_{gl}(1 - F_F)A_{w,p} \tag{3.15}$$

Here:

$F_{sh,gl}$ is a shading reduction factor for movable shading.

g_{gl} is the total solar energy transmittance of the transparent part of the element. Because the time averaged solar energy transmittance value, g_{gl}, is somewhat lower than g_n(the normal transmittance) a correction factor F_w is used, such that $g_{gl} = F_w \cdot g_n$

F_F is is a frame factor, the ratio of the projected frame area to the overall projected area of the glazed element.

$A_{w,p}$ is the overall projected area of the glazed element (m^2)

And for opaque element c:

$$A_{sol} = \alpha_{sol,c} \cdot R_{se} \cdot U_c \cdot A_c \tag{3.16}$$

Where:

$\alpha_{sol,c}$ is the dimensionless absorption coefficient for solar radiation of the opaque element.

R_{se} is the external surface heat resistance (m^2K/W).

U_c is the thermal transmittance of the opaque element (W/m^2K).

A_c is the projected area of the opaque part (m^2).

3.3.1.2 Solar heat gains - SAP 2012 method

SAP (BRE, 2011; BRE, 2014), the UK standard assessment procedure, bases its solar heat gain calculation on ISO 13790:2008 (ISO, 2008), albeit in a simplified form.

$$Q_{sol} = 0.9 \cdot A_w \cdot S \cdot g_{\perp} \cdot F_F \cdot Z \tag{3.17}$$

0.9 is a factor representing the ratio of typical average transmittance to that at normal incidence.

A_w is the area of an opening (m^2).

S is the solar flux on a surface (W/m^2).

$g_{\perp}$ the total solar energy transmittance factor for the glazing at normal incidence (0-1).

Z is the solar access factor (0-1).

To convert between solar radiation measured in the horizontal plane to that incident upon a vertical surface, either a horizontal-to-vertical (BRE, 2011) or horizontal-to-inclined-surface (BRE, 2014) conversion is used.

3.3.1.3 Solar heat gains - PHPP method

The Passivhaus House Planning Package (PHPP) calculates solar gains using the following equation (Feist, 2007):

$$Q_{sol} = A_w \cdot S \cdot g_{\perp} \cdot RF \tag{3.18}$$

This time, a reduction factor term, RF is included and incorporates shading (S_F), frame factors (F_F) and a 'dirt' factor (D_F) (Feist, 2007):

$$RF = S_F \cdot F_F \cdot D_F \tag{3.19}$$

The use and uncertainties of these three methods is discussed in section 5.3.3.

3.3.2 The statistically derived solar aperture, *R*

3.3.2.1 Definition

Statistically, the value of R is estimated from either MLR or a Siviour analysis of co-heating data. Through this regression, the term R is used to correlate reductions in Q_{elec} to the measured solar radiation S. The term R is well defined by Baker (Baker, 2015; Baker and Dijk, 2008) who refer to the solar aperture as the *'heat flow rate transmitted through the building envelope to the internal environment under steady state conditions, caused by solar radiation incident at the outside surface, divided by the intensity of incident solar radiation in the plane of the building ... It can be regarded as equivalent to a totally transparent area which lets in the same solar energy as the whole building'* (Baker, 2015, p.16).

The solar aperture therefore describes the gains for the building as a whole, including diffuse gains, direct gains through glazing of all orientations and those from solar radiation incident upon opaque elements. Typically calculated from daily aggregations, R will relate the total daily measured solar radiation to the heat gains on that day, accounting for the lag in absorbed and re-emitted gains - albeit only within that aggregation period.

To further understand the definition(s) of R, various forms of incident solar radiation and the associated types of measurement must be considered.

3.4 Solar radiation: definitions, calculations and measurement

3.4.1 Direct, diffuse and reflected radiation

Shortwave solar radiation incident upon a surface consists of three components: the *direct* or beam radiation coming in a direct line from the sun, *diffuse* radiation scattered within the atmosphere and radiation *reflected* by surrounding surfaces. The total or *global* irradiance (S_{Glb}) upon a surface is then equal to the sum of the direct (S_{Dir}), diffuse (S_{Diff}) and reflected components (S_{Ref}),with the irradiance generated by reception of solar radiation from the full hemisphere is given by ISO 15927-1:2003 (ISO, 2003):

$$S_{Glb} = S_{Dir} + S_{Diff} + S_{Ref} \tag{3.20}$$

The reflected component is often considered small relative to the other two unless the ground is highly reflective (i.e. snow). The proportion of diffuse radiation is dependent upon cloud cover and ranges from about 10-20% in clear skies to up to 100% for cloudy skies (NREL, 2015).

3.4.2 Measuring solar radiation

All of these components can be measured separately on-site. Global horizontal radiation (S_{GHR}) is in general the most commonly measured parameter and is obtained from a horizontally orientated pyranometer. Adding a shadow band onto a second horizontal pyranometer will block out direct beam radiation and will provide a measurement of diffuse horizontal radiation (S_{DHR}). Finally, a pyreheliometer with sun tracker can measure direct normal radiation (S_{DNR}), i.e. direct radiation received on a surface perpendicular to the sun's rays. This final quantity can also be arrived at through subtraction of diffuse from global, but whilst this is convenient, it is not necessarily accurate (Duffie and Beckman, 1991). The three components are related by considering the horizontal component of the direct normal radiation through the use of the zenith angle (θ_Z).

$$S_{GHR} = S_{DHR} + S_{DNR} \cdot cos(\theta_Z) \tag{3.21}$$

However, in most building applications we are interested in the incident solar radiation on glazed elements and therefore on vertically not horizontally orientated surfaces.

3.4.2.1 Direct incident radiation on a surface

Consider the incident direct solar radiation from the sun on a surface of given orientation and tilt angle, figure 3.1.

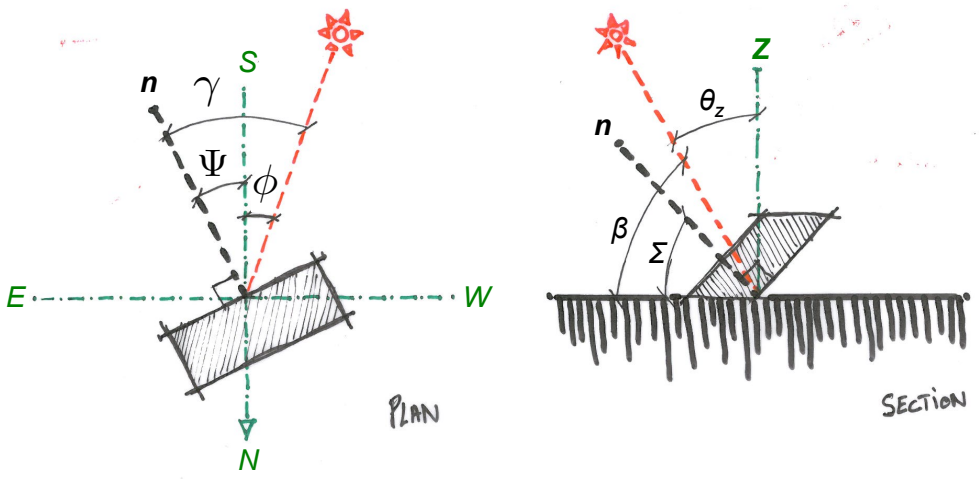

Figure 3.1: *Plan and section view of solar radiation incident on a tilted surface.*

To describe the position of the sun relative to the surface normal, and therefore the incidence angle, we must defined a number of additional angles.

- **Zenith Angle, θ_Z:** The Zenith angle is the angle between the sun's rays and the Zenith, **Z**, a point normal to the horizontal at the position of the observer.

- **Solar Altitude, β:** Is the angle in a vertical plane between the sun's rays and the projection of the sun's rays on a horizontal surface. Therefore:

$$\frac{\pi}{2} - \theta_Z = \beta \tag{3.22}$$

- **Solar Azimuth, ϕ:** The azimuth angle describes the suns position in the horizontal plane, (negative east of south and positive west of south).

- **Surface Azimuth, Ψ:** The angle between south and the horizontal projection of the normal surface, (east of south is negative and west of south positive).

- **Surface-Solar Azimuth Angle, γ:** It is then convenient to define an additional angle, γ, as the surface-solar azimuth angle, the angle between the horizontal projection of the solar rays and the horizontal projection of the surface normal.

$$\gamma = |\phi - \Psi| \tag{3.23}$$

- **Surface Tilt, Σ:** The angle of the surface from the horizontal, (i.e. horizontal = 0° and vertical = 90°).

Using these definitions the incident angle (θ), that between the sun's beam and normal of the surface, can be described by:

$$cos(\theta) = cos(\beta)cos(\gamma)sin(\Sigma) + sin(\beta)cos(\Sigma) \tag{3.24}$$

If the surface is vertical (i.e. Σ= 90 $^{\circ}$):

$$cos(\theta) = cos(\beta)cos(\gamma) \tag{3.25}$$

If the surface is horizontal (i.e. Σ= 0):

$$cos(\theta) = sin(\beta) = cos(\theta_Z) \tag{3.26}$$

3.4.2.2 Diffuse radiation on a surface

A number of simplified models exist to make it easier to predict the diffuse radiation on a vertical surface. A simple assumption is that the sky is a uniform radiator of diffuse radiation. Considering the sky as isotropic means that the vertical component of incident solar radiation upon a surface ($S_{Diff,sur}$) can be determined from a view factor (F_{view}) (Page, 1985). Therefore:

$$\frac{S_{Diff,sur}}{S_{DHR}} = F_{view} = \frac{(1 + cos(\Sigma))}{2} \tag{3.27}$$

Where, $S_{Diff,sur}$is the diffuse solar radiation incident upon a surface. Therefore, for a vertical surface (i.e. Σ= 90 $^{\circ}$) F_{view} = 0.5.

3.4.2.3 Reflected radiation on a surface

Similarly, the reflected radiation (S_{refsur}) can be determined by:

$$S_{refsur} = \rho_g \cdot S_{GHR} \cdot \frac{(1 + cos(\Sigma))}{2} \tag{3.28}$$

Where, ρ_g is the solar reflectance of the ground. This may be as low as 0.1 for bare soil, or 0.2 for browned grass, although fresh snow is considerably higher at 0.7 (Duffie and Beckman, 1991). The reflected component is generally ignored throughout this thesis, as it is not modelled in simulated tests, with ground reflectance set to zero (LBNL, 2014). The vertical component of reflected solar radiation is then incorporated into any vertically measured solar radiation in field tests.

3.4.2.4 Definitions of solar radiation incident on a surface

Considering the above, the following components of solar radiation on a test dwelling can be measured or calculated:

- The diffuse component, S_{Diff}.
- The direct component, S_{Dir}.

Both of which are included in the global solar radiation, measured as either:

- Global horizontal radiation, S_{GHR}.
- Global vertical radiation $S_{GV(N,S,E,W...)}$ for a given surface orientation:

$$S_{GV(N,S,E,W...)} = cos(\theta) \cdot S_{DNR} + F_{view} \cdot S_{DHR} \tag{3.29}$$

- We may choose to consider the mean vertical global radiation, S_{GVM}, considered over n^2 orientations, e.g.:

$$S_{GVM} = \frac{(S_{GVS} + S_{GVW} + S_{GVE} + S_{GVN})}{n} \tag{3.30}$$

- This mean value could then be weighted (S_{GVWM}) according to the proportion of total gains expected for each orientation, see section 5.2.5.2.

$$S_{GVWM} = \frac{(W_S \cdot S_{GVS} + W_W \cdot S_{GVW} + W_e \cdot S_{GVE} + W_N \cdot S_{GVN})}{n} \tag{3.31}$$

  Where weighting factors, $W_S + W_N + W_E + W_W = 1$. Each factor can be derived from numerically predicted gains, i.e. via ISO 13790:2008 (ISO, 2008).

Details and plots of the various forms of solar radiation can be seen in appendix A.1.0.1.

3.4.3 The measurement of *S* in co-heating tests

In general applications, global horizontal radiation (S_{GHR}) is the most commonly measured form of incident radiation. This is as it is often the cheapest, simplest and most widely recorded and therefore comparable form. However, when considering the thermal behaviour of buildings it is more common to consider the impact of direct and diffuse gains independently and to consider incident solar radiation on vertical surfaces or in the plane of glazed elements.

[2] n is likely to take a maximum value of four, although orientations may be offset from the four cardinal points to better reflect the orientation of a test dwelling and its glazing, e.g. NW, SE, NE, SW.

In the majority of cases to date a single pyranometer has been used in co-heating tests. This has either been horizontally orientated or orientated vertically, either south facing or on the plane *principal* glazed facade, S_{GVP} (i.e. facade with the highest expected gains due to orientation and glazed area, see figure 3.2). The two most commonly measured parameters are therefore:

- In the plane of the principal facade: S_{GVP}= S_{GVS} or S_{GVE} or S_{GVSW} ... etc.
- Global horizontal radiation: S_{GHR}.

Figure 3.2: *A vertically & horizontally orientated pyranometer*

Such measurements can be considered imperfect or incomplete, as not all orientations are considered and direct and diffuse components are not distinguished. Additionally, in most cases, the measured solar radiation will include an amount of shading from surrounding terrestrial objects. Without full weather station mounting equipment, the pyranometer will have to be placed within the height of the test dwelling. This means that the measured solar radiation will already incorporate some of the shading on the building, depending on its position (Stamp, 2011). This is potentially important when considering shading factors in numerical calculations of *R* and any bias in the positioning of the pyranometer.

3.4.4 The definition of *R* revisited

3.4.4.1 Definitions for statistically calculated *R*

The way in which *S* is measured and subsequently analysed will dictate the value and nature of the parameter *R*. If *S* was measured in the plane of all glazed and relevant opaque elements, then each associated *R* should remain constant across a year. However, as a single descriptive building parameter is sought, *R* will actually vary across the year and between days in which solar radiation is dominated by either the diffuse or direct component. The nature of this change will depend upon the orientation of the measurement of *S* and the respective orientations of glazed elements in relation to this measured surface.

Following the definitions of the measured solar radiation, we have now defined several associated versions of *R*:

- R_{GVP} Principal Facade, e.g. R_{GVS} or R_{GVE} or R_{GVSW} ... etc. Associated with S_{GVP}.
- R_{GHR} Global Horizontal Radiation, associated with S_{GHR}.
- R_{GVM} Mean Global Horizontal Radiation, associated with S_{GVM}.

3.4.5 Definitions for numerically calculated *R*

Ideally, when using numerical calculations, the incident solar radiation will be measured in the plane of every glazed facade or even opaque elements. A numerical value of *R* can be calculated for each orientation, taking components of equations 3.32 - 3.34, which would then allow a calculation of individual and total gains from the multiple measurements of *S*.

$$R_{ISO,k} = F_{sh,ob,k} \cdot A_{sol,k} \tag{3.32}$$

$$R_{SAP} = 0.9 \cdot A_w \cdot g_\perp \cdot F_F \cdot Z \tag{3.33}$$

$$R_{PHPP} = A_w \cdot g_\perp \cdot RF \tag{3.34}$$

With the total building solar aperture, R_{TOT}, equal to:

$$R_{TOT} = R_{north} + R_{south} + R_{east} + R_{west} + ... \tag{3.35}$$

When single solar measurements are taken, a single lumped value of *R*must be related to a single *S*, be it S_{GHR}, S_{GVP} or S_{GVM}. Therefore the relationship between the individual orientations and this single *S* must be defined and incorporated into the individual *R*through considering the ratio of solar radiation incident orientation to that of the considered facade - noting that this is

a dynamic ratio. For example, an orientation adjusted east facing glazed area dependent upon a measured S_{GVS}, represented by $R_{east}*$ would be defined as:

$$R_{east}* = R_{east} \cdot \frac{S_{GVE}}{S_{GVS}} \tag{3.36}$$

In either statistical or numerical cases, a number of values of *R* can be defined and measured or calculated. It is not their accuracy in relation to their 'true' value (which is in any case varying in time) but their ability to provide a solar correction to the *HLC* that is of importance.

3.4.6 The solar load ratio, SOLR

Finally, a useful metric can be introduced. Many solar driven sources of uncertainty scale with the size of solar gains in comparison to other heat flows. One way of predicting this is to examine the solar load ratio, a subset of the heat balance ratio as-defined in ISO 13790:2008 (ISO, 2008). The solar load ratio (SOLR), can be defined as the ratio of solar gains to the total building heating load (Q_{TOT}):

$$SOLR = \frac{Q_{sol}}{Q_{TOT}} \tag{3.37}$$

Most simply, in terms of a dwelling under co-heating this can be written as:

$$SOLR = \frac{R \cdot S}{\Delta T \cdot HLC} \tag{3.38}$$

Or incorporating the non-thermostatically controlled component of electricity use ($Q_{baseload}$) to define the ratio of solar gains to thermostatically controlled heating, a Solar and Base Load Ratio (SBLR) is defined below and can further help predicted solar driven experimental overheating, section 5.5:

$$SBLR = \frac{R \cdot S}{((\Delta T \cdot HLC) - Q_{baseload})} \tag{3.39}$$

In reality, when examining daily data points, the building's heat capacity and time constants may need to be accounted for. Additionally, as expressed elsewhere in the thesis, the *HLC* will not be a constant value rather varying with internal and external temperatures and with infiltration losses, such that the precise SOLR may be difficult to determine. It is particularly difficult to determine in field tests in which solar gains cannot be accurately estimated. However, without further complicating matters, this term remains a useful dimensionless ratio for examining the solar load and the impact of solar radiation across various environmental conditions and test dwellings.

3.4.7 The *HLC*, solar radiation and *R* - summary & conclusions

Summarising these considerations of *HLC* and *R*:

- The heat loss coefficient can be calculated numerically from ISO 13790:2008, SAP or PHPP. Co-heating measurements are most commonly being compared to SAP or an adjusted SAP *HLC*.
- This calculated value (HLC_{pred}), may not be reflective of the actual built dwelling and may contain errors within its inputs and will need to be reviewed, potentially incorporating error estimates.
- HLC_{pred} may not be calculated under the same environmental conditions as experienced by the tested building and incorporated into HLC_{meas}.
- HLC_{pred} will not be able to account for complex heat loss mechanisms, i.e. thermal bypasses. Robust measurements would help identify these.

In terms of solar radiation and the solar aperture *R*:

- Single measurements of solar radiation will imperfectly represent the solar radiation incident across the full building envelope and that entering the dwelling.
- The use of a single building parameter to determine solar gains is also an imperfect representation of the system.
- Solar Radiation can be measured in a number of forms:
  - In either a direct, diffuse or global form.
  - And across either horizontal or vertical orientation.
- Most commonly solar radiation is measured globally, either horizontally (S_{GHR}), or vertically in the plane of the principal facade (S_{GVP}), e.g. S_{GVS}, S_{GVE}, S_{GVSW} etc.
- The mean incident solar radiation can be calculated or measured via multiple pyrometers:

$$S_{GVM} = \frac{(S_{GVS} + S_{GVW} + S_{GVE} + S_{GVN})}{4} \tag{3.40}$$

- The mean value can be weighted by the predicted proportion of gains on each orientation (S_{GVWM}), equation 3.31.
- Statistically derived *R*s will be a function of the form of the measured *S* that they are based upon.

3.5 Defining uncertainty

To provide foundations for the discussion of uncertainty throughout this thesis, some background theory on metrology is reviewed alongside some formal definitions of terms relating to uncertainty and measurements. Much of this is drawn from the Guide to the Expression of Uncertainty in Measurement (GUM), a series of documents produced by the Joint Committee for Guides in Metrology (JCGM). These include JCGM (2008a) and JCGM (2009) and the guide to International vocabulary of metrology (VIM) (JCGM, 2008b). This work then forms the basis of further standards, including BSI PD 6461:2001 (BSI, 2001).

3.5.1 Metrology - the science of measurement

"The purpose of measurement is to provide information about a quantity of interest - a measurand." (JCGM, 2008b, p.17)

In the case of co-heating tests and this thesis, the quantity of interest and measurand is the *HLC*, a concept defined previously in section 3.1. Whilst an estimate of the *HLC* is sought, it stands that no measurement is exact, the outcome dependent upon the measuring system, the measurement procedure, operator skill, the environment, and other effects (JCGM, 2008a). Examples of these can be seen throughout this thesis, for example when considering the impact of the uncontrolled external environment upon *HLC* estimates (chapters 5 and 6), or through the experimental control over internal conditions (chapter 7).

3.5.2 Types of uncertainty

"Uncertainty: parameter, associated with the result of a measurement, that characterises the dispersion of the values that could reasonably be attributed to the measurand." (JCGM, 2008b, p. VIM 3.9)

Two types of measurement errors can be considered - *systematic* and *random*. A systematic error, or measurement bias, is associated with the fact that the value of the measured quantity is derived from indication values dispersed not about the true value but about some value offset from it. It is the difference between the offset value and the true quantity value that is referred to as the systematic error value.

A random error is associated with the fact that when a measurement is repeated it will generally provide a measured quantity value that is different, even when measured under the same conditions. Random error is then the result of a measurement minus the mean that would result

from an infinite number of measurements of the same measurand carried out under consistent conditions (JCGM, 2008b). As only a finite number of measurements can be made, it is only ever possible to determine an estimate of random error.

Definitional uncertainty is a component of measurement uncertainty resulting from the finite amount of detail in the definition of a measurand (JCGM, 2008b, p. VIM 2.27). For example, the incomplete knowledge of and inconsistencies between the definitions of the measured *HLC*, HLC_{meas}, the value of HLC_{True} and of design predictions, HLC_{pred}. Therefore, the finite amount of detail in the definition of a *HLC*, particularly without supplementary measurements of secondary heat flows, can lead to definitional uncertainties. Significantly, the definitional uncertainty is the 'practical minimum measurement uncertainty' achievable in any measurement (JCGM, 2008b, p. VIM 2.27).

Finally, the concepts of *repeatability* and *reproducability* are important when considering the application of co-heating tests. Under the GUM framework, a repeatable measurement is one that can replicate measurements using the same measurement procedure, operators, measuring system, operating conditions and the same location. With a test performed within the changing external environment, it is clear co-heating tests are never precisely repeated. Reproducibility however, describes the ability to replicate measurements even with these previous conditions changing. It is the reproducibility of co-heating tests that is therefore of interest.

3.5.3 Estimating uncertainty & error analysis

A basic premise of the GUM approach is that it is possible to characterise the quality of a measurement by accounting for both systematic and random errors on a comparable footing. A method for this is detailed in both JCGM (2008a) and BSI PD 6461:2001 (BSI, 2001), with this approach used later in this thesis (section 9.4).

3.5.4 Expressing uncertainty

A further basic premise of the GUM approach is that we cannot state how well the true value of a measurand is known, rather only how well it is believed to be known (JCGM, 2008a). This uncertainty reflects the incomplete knowledge of the measurand and the notion of 'belief' is an important one. The results of measurements need to be considered in terms of probabilities expressing degrees of belief.

Reflecting the belief in a measurement and its expression in probabilities, uncertainty is often expressed as a 'expanded uncertainty', an interval about the result of a measurement that may be expected to encompass a large fraction of the distribution of values that could reasonably be attributed to the measurand (e.g. 95% confidence intervals). The interval is also known as the coverage probability of confidence intervals, see BSI PD 6461:2001 (BSI, 2001).

3.5.5 Definitions of uncertainty terms

A number of terms that are used to describe uncertainty throughout this thesis are defined below, many of which are lifted from the 'International vocabulary of metrology' (VIM) (JCGM, 2008b):

- **Measured value / estimate of the measurand:** measured value of a quantity. (JCGM, 2008b, p. VIM 2.10)
- **True quantity value:** quantity value consistent with the definition of a quantity. (JCGM, 2008b, p. VIM 2.11)
- **Measurement error:** measured quantity value minus a reference quantity value (JCGM, 2008b, p. VIM 2.16).
- **Measurement uncertainty:** non-negative parameter characterising the dispersion of the quantity values being attributed to a measurand, based on the information used (JCGM, 2008b, p. VIM 2.26). Measurement uncertainty includes systematic effects as well as definitional uncertainty. When systematic effects are not corrected, their associated uncertainty can be incorporated. The measurement uncertainty can, for example, take the form of a standard deviation, or the standard measurement uncertainty and can include type A and type B uncertainty analysis, see section 9.4.3.
- **Random measurement error:** component of measurement error that in replicate measurements vary in an unpredictable manner, (JCGM, 2008b, p. VIM 2.19). Noting:
  - A reference quantity value for a random measurement error is the average that would ensue from an infinite number of replicate measurements of the same measurand.
  - Random measurement errors of a set of replicate measurements form a distribution that can be summarised by its expectation, which is generally assumed to be zero, and its variance.

  - Random measurement error equals measurement error minus systematic measurement error.

- **Systematic measurement error:** component of measurement error that in replicate measurements remains constant or varies in a predictable manner (JCGM, 2008b, p. VIM 2.17). Systematic errors can be known or unknown, often being hard to detect. A correction may be applied to compensate for a known systematic error, such as the heat flow across a party wall (section 9.4.7.2).

- **Measurement accuracy:** closeness of agreement between a measured quantity value and a true quantity value of a measurand (JCGM, 2008b, p. VIM 2.13).

- **Measurement bias:** bias estimate of a systematic measurement error.

- **Measurement precision:** closeness of agreement between indications or measured quantity values obtained by replicate measurements on the same or similar objects under specified conditions (JCGM, 2008b, p. VIM 2.15).

- **Definitional uncertainty:** component of measurement uncertainty resulting from the finite amount of detail in the definition of a measurand (JCGM, 2008b, p. VIM 2.27). As is seen, this is a particular issue within co-heating tests and the definition of HLC_{True}, which is influenced by unknown heat flows and environmental parameters. Significantly, the definitional uncertainty is the 'practical minimum measurement uncertainty' achievable in any measurement (JCGM, 2008b, p. VIM 2.27).

- **Standard uncertainty** measurement uncertainty expressed as a standard deviation.

- **Relative standard measurement uncertainty:** standard measurement uncertainty divided by the absolute value of the measured quantity value, typically expressed in percentages (JCGM, 2008b, p. VIM 2.32)

- **Combined standard uncertainty:** standard measurement uncertainty that is obtained using the individual standard measurement uncertainties associated with the input quantities in a measurement model (JCGM, 2008b, p. VIM 2.31)

- **Expanded uncertainty:** product of a combined standard measurement uncertainty and a *coverage factor* larger than the number one, (JCGM, 2008b, p. VIM 2.27), see equation 9.16.

- **Measurement repeatability:** measurement precision under a set of repeatability conditions of measurement
- **Measurement reproducibility:** measurement precision under reproducibility conditions of measurement (JCGM, 2008b, p. VIM 2.20).
- **Measurement model:** mathematical relation among all quantities known to be involved in a measurement.
- **Correction:** a compensation for an estimated systematic effect (JCGM, 2008b, p. VIM 2.53), e.g. see 9.4.7.2.
- **Repeatability condition of measurement:** condition of measurement, out of a set of conditions that includes the same measurement procedure, same operators, same measuring system, same operating conditions and same location, and replicate measurements on the same or similar objects over a short period of time. As the external environmental conditions cannot be precisely repeated, no co-heating measurement is perfectly repeatable.
- **Reproducibility condition of measurement:** condition of measurement, out of a set of conditions that includes different locations, operators, measuring systems, and replicate measurements on the same or similar objects (JCGM, 2008b, p. VIM 2.24). A co-heating test, and the *HLC* estimate, can therefore be considered to be reproducible, if a similar result can be obtained within differing environmental conditions.
- **Metrological comparability:** comparability of measurement results, for quantities of a given kind, that are metrologically traceable to the same reference (JCGM, 2008b, p. VIM 2.46). The comparability of sets of co-heating measurements, between dwellings or repeated measurements upon the same dwelling, is considered in section 9.5.2.
- **Steady-state operating condition:** operating condition of a measuring instrument or measuring system in which the relation established by calibration remains valid even for a measurand varying with time (JCGM, 2008b, p. VIM 4.8).

Chapter 4

Research Method

Chapter overview

This chapter describes the research method adopted for this thesis and consists of seven sections:

- **4.1 Research questions:** The chapter begins by stating the research questions that follow from the findings of the literature review and which were previously set out in the introduction chapter.
- **4.2 Potential research methods:** Following this, a number of potential research methods are considered. Their respective strengths and weaknesses in addressing the stated research questions are compared.
- **4.3 Research method:** An overview and discussion of the research methods used for this thesis are given.
- **4.4 Simulated co-heating tests - sources of uncertainty:** Details of the simulated co-heating tests used to investigate sources of uncertainty (chapters 5 - 8) are reviewed.
- **4.5 Simulated co-heating tests - the application of co-heating:** Details of the simulated co-heating tests used to investigate the application (chapter 9) of co-heating are reviewed.
- **4.6 Field tests:** Details of the field tests conducted as part of this thesis are stated.
- **4.7 Conclusions:** Brief conclusions concerning the research method are made.

4.1 Research questions

Following the review of the relevant literature and surrounding context, the main research question of this thesis can be stated as:

How accurate and reproducible is the steady-state co-heating method at determining a dwelling's heat loss coefficient?

To fully answer this single question a number of sub questions need to be answered, as previously stated at the beginning of this thesis. The first, A0, recurs throughout this thesis but has been initially addressed in chapter 3, providing definitions for the *HLC* and the basis for further analysis:

- **A0)** How is the *HLC* defined, in terms of its *predicted*, *measured* and *true* value?

The remaining questions can be split into two branches, the first, investigated in chapters 5, 6, 7 and 8, is concerned with understanding the uncertainties in the co-heating method:

- **A1)** What is the impact of the non-steady state external environment upon the steady state *HLC* estimate?
- **A2)** How do the experimental conditions achieved in reality deviate from the theoretical heat balance model and what uncertainties are created as a result?
- **A3)** How do building characteristics of the test dwelling interact with parts A1 and A2 to dictate the accuracy and reliability of the *HLC* measurement?
- **A4)** How can sources of uncertainty be identified and subsequently addressed?

The second branch, forming the basis of chapter 9, concerns the impact of these uncertainties on the application and use of the co-heating method:

- **B1)** Under what environmental conditions can co-heating tests be performed to reliably estimate a building *HLC*?
- **B2)** When tested under suitable environmental conditions, how long is required to accurately determine a building *HLC*?
- **B3)** Given the uncertainties that exist, what is the optimum co-heating method, both in terms of experimental protocol and analysis techniques, within the existing steady state approach?
- **B4)** How can appropriate uncertainty estimates be derived and stated?

- **B5)** How do the sources of uncertainties identified then limit the use of co-heating in comparisons to design and to before and after retrofit cases?

Answering these questions requires an appropriate research method, the focus of the rest of this chapter.

4.2 Consideration of potential research methods

In this section, potential research methods are reviewed, with consideration of their respective strengths, weaknesses and limitations. This includes a meta analysis of any available co-heating data (section 4.2.1), laboratory based testing (4.2.2) and outdoor tests (4.2.3). Outdoor tests can then be performed in either dedicated test houses or within 'typical' dwellings (4.2.4). Finally, the advantages and limitations of simulated co-heating tests are considered (4.2.5).

4.2.1 Meta analysis of co-heating tests

Only a limited number of co-heating tests have been performed to date, with a tentative estimate putting the figure somewhere upwards of 100. Unfortunately, only a fraction of these have been published in any detail (see tables 2.1 - 2.5). Further, a variety of experimental protocols and analysis methods have been adopted. Combined with the lack of reported details, this limits the usefulness of any comparisons drawn. This ultimately means that any meta-analysis of tests and their results is unlikely to yield any conclusive answers to the research questions proposed.

4.2.2 Laboratory co-heating tests

A number of researchers have examined both long and short term co-heating within a laboratory, typically across a single wall or within small test cells (Judkoff et al., 2000; Stamp, 2011; Deconinck and Leunis, 2012; Pandraud and Fitton, 2013). Such a method holds a number of advantages. A greater degree of control can be obtained over the variables present during testing, with close to steady state conditions replicated. Confounding variables (e.g. dynamic external temperatures) can then be varied systematically, on a one at a time basis, allowing a direct exploration of their effects. This can be compared to a baseline established by measuring the *HLC* in close to steady state conditions, allowing any deviations from this reference value and their scale to be determined.

However, a number of limitations with this approach can also be considered. Firstly, it is not possible to fully replicate the external environment within a laboratory. In particular, the impact of solar radiation and wind speed will be ignored or at least simplified, thus the research questions A1, A3, B1 and B2 cannot be answered, leaving the main research question only partially addressed. Further, the majority of laboratory facilities will only allow for component testing or scaled down test cells, simplifying losses and producing a relative shift in the scale of uncertainties. Uniquely, the Salford Energy House consists of a full sized dwelling, based on a traditional Victorian terrace, within an environmental chamber. Such a facility would provide a controlled laboratory setting at a full scale and utilising a dwelling built with some the complexities of real construction. The facility has therefore been used to test the dynamic QUB[1] heat loss method (Pandraud and Fitton, 2013). However, even within such a facility the ability to explore environmental uncertainties is limited and only a single test dwelling can be evaluated.

Finally, Judkoff et al. (2000), when assessing the PSTAR/STEM method, were able to test a number of office cells in both an environmental chamber at near ideal steady state conditions and outside in the full external environment. However, this does not allow simple comparisons between the two because, as Judkoff notes, the value of the HLC_{True} is not consistent in these two scenarios. Amongst other changes, the presence of wind driven pressure differences results in an increased infiltration rate and higher total losses. Even with the facilities and experimental design used here the value of HLC_{True} cannot be known within outdoor conditions. This leaves uncertainty, particularly systematic error, hard to characterise. To answer the specific research questions posed, some degree of testing must take place in the outdoor environment.

4.2.3 Outdoor testing

Tests can be performed within the outdoor environment, with a number of outdoor test facilities within research centres around the world (Janssens et al., 2011). These vary from experiments for single components and small test cells (Judkoff et al., 2000; Deconinck and Leunis, 2012) to full scale dedicated test dwellings (e.g. Butler and Dengel, 2013).

The advantage of outdoor testing is that co-heating tests can be evaluated in respect to full weather conditions, exposed to all the complexities that entails and reflective of the conditions of typical tests. However, again there are a number of limitations. As before, the majority of facilities focus on testing single components rather than full dwelling envelopes.

[1] QUB = Quick U-value of Buildings

As previously stated, a significant limitation with outdoor testing is that HLC_{True} cannot be known. It is particularly difficult to determine the impact of uncontrolled, interacting and correlated external variables. Very long monitoring durations and mixes in weather are likely to be required to allow any statistical analysis of such effects. The exploration of internal conditions or experimental protocol then requires separating or normalising the varying external environment - difficult without full knowledge of the impact of the external environments upon a test dwelling.

Similarly, the ability to alter building parameters is restricted and both cost and time constraints limit the number of test buildings that can be examined. Separating out the impact of dwelling characteristics and their relationship with weather variables is then an experimental challenge. This restricts the extent to which research question A3 can be addressed. Andrews (1995) reviewing the PSTAR method stated that the method needed to be assessed across a wider range of dwellings, a sentiment that can be extended to long term co-heating. In summary, the relationship between uncertainty and building characteristics can only partially be explored through field tests, whilst disentangling the impact of the external environment and identifying systematic errors remain equally challenging.

4.2.4 Test houses

Full-scale outdoor testing can be considered to take place in either dedicated, specifically built test houses or within 'typically' constructed dwellings. A number of dedicated outdoor full scale test houses exist within research institutions across the world. These can be highly instrumented and may have been previously characterised, allowing a better understanding of the dwelling and measurement of secondary heat flows. Twinned test houses (near identical dwellings), in particular offer a number of advantages. Internal conditions or dwelling characteristics can be varied and examined in comparison to a 'control' test house under the same environmental conditions (see Butler and Dengel, 2013). Unfortunately, the availability of such facilities is limited.

Rather than conducting tests within dedicated testing facilities, tests can be conducted in 'typical' dwellings, constructed for private use and therefore under processes reflective of the construction industry. This has the advantage of exposing the co-heating tests conducted as part of this research to more complex heat loss mechanisms, resulting from construction defects

and workmanship. These mechanisms will not only alter the dwelling *HLC* but may also add additional uncertainties to the co-heating method itself. A positive side effect of this approach is that the researcher gains more exposure to the context around the use of co-heating within the construction industry. However, the use of real world dwellings means that the construction and dwelling in general is less well known, making HLC_{True} even more of an unknown.

In either case, a number of factors can be considered which improve the benefit of conducting field tests. Firstly, long term data will allow a wider range of weather conditions to be considered. Secondly, consistent experimental protocol and analysis will allow more effective comparisons to be drawn. Finally, any additional tests or measurements that can be performed will improve the understanding of the dwelling and secondary heat flows - and hence their impact upon uncertainties. Referring to Everett: *'If you want to know one thing about a house, you have to know everything else'* (Everett, 1985, p.1).

Ultimately, the use of field tests is limited by a lack of breadth in terms of environmental conditions and dwelling characteristics. Without large ranges of data or knowledge of HLC_{True} it remains difficult to disentangle the drivers of uncertainty in *HLC* estimates or evaluate the accuracy of co-heating tests.

4.2.5 Simulated co-heating tests

Running simulated co-heating tests removes many of these practical constraints and allows a large range of weather conditions and building constructions to be evaluated - adding the breadth absent in other approaches. Simulated co-heating tests have been used since the start of this thesis, simulating co-heating tests across a single wall (Bauwens et al., 2012) and in a small test box (Deconinck and Leunis, 2012).

By adapting weather files the impact of a number of weather variables can be explored both in isolation and across a much wider range of conditions. Similarly, both single building parameters (e.g. glazed area, orientation, thermal mass) or experimental conditions can be systematically changed and the impact upon uncertainty assessed. This provides a systematic basis for investigating the impact of a wide range of variables upon a co-heating test dwelling and the accuracy of the estimated *HLC*.

This is particularly aided by the fact that in these simulated co-heating tests the input pa-

rameters are precisely known. This includes external weather conditions, internal temperatures and heating loads, but most importantly means an accurate value of HLC_{True} can be determined for each test dwelling (section 4.3.3.1). This allows effective assessments of the accuracy of co-heating *HLC* measurements and the identification of systematic errors and their scale.

As a large volume of data can be produced, data analysis tools can be used to write suitable algorithms to analyse data under a number of different methods. This can allow slight variations in data analysis techniques to be assessed over a large number of simulated tests with reasonable ease.

However, such an approach is not without limitations. In many cases simulated co-heating tests may demonstrate simplified physical mechanisms of heat loss compared to the reality of a field test. As previously discussed, a number of complex heat flows, such as bypasses within cavities or across party walls, may exist in real dwellings and may be difficult or impossible to model in simulated tests. In addition, without knowledge of the intricacies and practicalities of performing tests, the simulations may ignore experimental challenges met in physical tests. Therefore, performing simulated tests alone may not allow a full appreciation of the uncertainties and application of the co-heating method.

4.3 Selected research method

Following the review of potential methods along with their respective strengths and weaknesses, it was decided to use both simulated co-heating tests and a small number of field tests. Simulated co-heating tests provided the breadth in environmental conditions and dwellings that it is not possible to achieve in field tests. In addition, simulations have been used to examine the impact of sources of uncertainty in isolation or in reference to HLC_{True}, allowing systematic uncertainties to be identified. Field tests, largely performed in 'typical' dwellings, then provide supporting examples and introduce further complexities and experimental challenges that are not considered in the simulated tests.

Initially, simulated co-heating tests were conducted to understand the impact of environmental, experimental and building variables on the accuracy of the co-heating *HLC* estimates, addressing questions A1 to A4 in chapters 5 to 8. Systematically adjusting inputs to weather files and building characteristics within simulations allows the effects upon a dwelling under co-heating

conditions to be clearly demonstrated and the subsequent effect upon the *HLC* estimation made clear. Examples from field tests are then used throughout these chapters, particularly to demonstrate the more complex nature of wind driven heat loss, uncontrolled party wall heat transfer and non-uniform internal temperatures. Details of the simulations carried out in these chapters are described in section 4.4.

After understanding the nature of the uncertainties that may exist in co-heating tests, these simulations have been expanded across a wider range of weather conditions and building types. This particularly addresses research questions B1, B2 and B3 and is the subject of chapter 9. A range of weather conditions and a number of 'archetype' dwellings have been selected to represent the broad range in the UK housing stock. Again field test examples are used to further support this work. These simulations are discussed in more detail in section 4.5.

In total, five field tests have been conducted for this thesis with a further six secondary sources of data, from tests either performed previously by the author or by other research teams. The selection of tests was very much a result of the availability of test houses and resource constraints of this study, with many falling into wider BPE projects (section 4.6.3). All are therefore modern dwellings, with one test taking place in a twinned test house and the rest in typical dwellings. The advantage of field tests being performed under wider projects is that additional explanatory tests, such as in situ U-values, were also be performed. In addition, this increased the exposure of the author to other actors involved in conducting and learning from co-heating tests, allowing a better appreciation of the surrounding context. Field tests are discussed in more detail in section 4.6.

4.3.1 Experimental protocol & analysis methods

The method adopted throughout field and simulated co-heating tests follows the experimental protocol discussed in section 2.3. However, for clarity a number of default positions are stated below:

- An internal experimental setpoint of $T_{setpoint}$= 25 °C is adopted as a default.
- Solar radiation is measured vertically, on a south or near south orientation.
- Neighbouring properties have been heated to the same internal setpoint, limiting heat transfer.
- Throughout the simulated co-heating tests, unless specifically examining duration or aggregation lengths, 2 week test periods are used with 24 hour averages. Field tests ran for as long as possible, with the durations listed in table 2.2.
- The simple energy balance, $Q_{elec} + R \cdot S = \Delta T \cdot HLC$, is used.
- MLR analysis is conducted using Q_{elec}, ΔT and S. On occasion, Siviour analysis is used as it offers a useful visualisation of the test results. On other occasions, MLR is projected onto a 2D plot, with solar corrections applied.
- A forced intercept is adopted in all tests unless otherwise stated.
- A variety of supplementary tests (in situ U-values, tracer gas decays, thermography) have been used in field tests.

4.3.2 Simulation tools & simple building models

Full building simulations are carried out in EnergyPlus, a whole building dynamic thermal simulation programme, details of which can be found throughout appendix B. EnergyPlus has been part of a number of validation programmes, including Building Thermal Envelope and Fabric Load Tests from ANSI/ASHRAE Standard 140-2007 (ASHRAE, 2007), IEA BESTEST comparative tests (Henninger et al., 2004; Neymark and Judkoff, 2008; Neymark et al., 2009). Importantly, EnergyPlus allows full building simulations to take place under a wide range of weather files and with a range of materials and constructions. Furthermore, weather files can be easily adapted, data can be examined at various timesteps and outputs from the simulation allow heat flows to be disaggregated and for HLC_{True} to be determined. To build the test dwellings featured in simulations the Design Builder interface was used.

Some sections of analysis have adopted simple building models. These typically consist of a dwelling *HLC*, *R* and external variables from a weather file. Additional heat flows or error terms can then be applied to the models, e.g. wind driven infiltration. This can make isolating certain effects easier than in full building simulations, for example the relationship between the range in *S* and the accuracy of estimates of *R*. Figures and tables in this thesis are therefore labelled either *field test*, *modelled* or *simulated* depending on the approach used.

4.3.3 Determining HLC_{True} & solar gains in simulations

4.3.3.1 Determining HLC_{True}

EnergyPlus provides outputs for the net heat flow summed across each type of element in kWh, i.e. walls, ground, roof, windows. Similar outputs are available for infiltration and for solar gains through glazing. This means that net heat flow into/ out of the simulated test dwelling can be estimated at any given time.

Therefore, the net heat loss from the dwelling can be determined at each simulation time step and HLC_{True} determined by:

$$HLC_{fabric} = \frac{Q_{fabric}}{\Delta T} = \frac{Q_{walls} + Q_g + Q_{roof} + Q_{windows}}{\Delta T} \tag{4.1}$$

$$HLC_{True} = \frac{Q_{TOT}}{\Delta T} = \frac{Q_{walls} + Q_g + Q_{roof} + Q_{windows} + Q_{inf}}{\Delta T} \tag{4.2}$$

This form of HLC_{True} means that HLC_{True} is responding to external dynamics, such as the varying external temperature. Whilst this means the daily value of HLC_{True} is somewhat influenced by previous days, across the two week periods typically analysed these dynamics are averaged out.

4.3.3.2 Determining solar gains

The transmitted solar gains can therefore be determined directly from simulation outputs. Determining the opaque contributions to solar gains is more difficult as they cannot easily be separated from other heat flows (e.g. thermal radiation) Therefore, the estimated true gains ($Q_{sol,True}$) are defined as the solar heat gains received though glazed elements, with R_{True} calculated from:

$$R_{True} = \frac{Q_{sol,True}}{S} \tag{4.3}$$

4.4 Simulated tests - sources of uncertainty - chapters: 5 - 8

Chapters 5, 6, 7 and 8 examine the sources of uncertainty present within co-heating tests, both environmental and experimental in nature. To provide a level of consistency across these chapters a single core test dwelling is used in simulations (section 4.4.2) with individual parameters varied on a case-by-case basis. A similar approach is taken with the simulation weather file, where a primary weather file is used with a number of adaptions used in certain instances (section 4.4.1). This allows the sources of uncertainty identified to be explored in a similar context, with their sensitivities to single weather variables and individual building characteristics determined to provide insight towards a wider range of dwellings and conditions.

4.4.1 Weather files

4.4.1.1 Types of weather file

Various types of weather files exist, ranging from the short term (i.e. representative days) to long term (i.e. multiyear datasets). They can therefore be populated with directly monitored data or collated from a larger data bank (i.e. Design summer years, representative days, typical metrological years). The selection of the type of weather file therefore depends upon the purpose of the study.

A typical meteorological year (TMY) uses selected weather data for a specific location, generated from a larger data bank much longer than a year in duration. The selection is designed to represent the range of weather phenomena for the given location, while still giving annual averages that are consistent with the long-term averages. Typically these files are used in building simulation to assess predicted heating and cooling demand. For this thesis, TMY files are used in simulated co-heating tests to represent conditions likely to be experienced in field tests in the UK. These files will themselves contain weather conditions at the limits of suitable testing and beyond. This can be extended by using weather files from colder-duller and warmer-brighter locations.

4.4.1.2 UK climate zones

As laid out in the scope of this thesis, there is a focus on the UK climate. Predominantly using UK based weather files allows a better comparison with fieldwork, deals with conditions familiar to the researcher and covers the region in which most co-heating tests have been performed to date.

The UK Met Office divides the UK into 11 climate regions which form the basis of the 21 climate regions used in SAP (BRE, 2014) and the 18 in CIBSE Guide J (CIBSE, 2002). Here, the climate regions are designed to account for the different seasonal profiles in T_e, wind speed and solar radiation. As most buildings (64%) are in the southern parts of the UK (DCLG, 2014), an average weather file needs to be weighted to reflect this. Figure 4.1 compares the representative UK average used in SAP with the Finningley (FINN) TMY file available in EnergyPlus across monthly averages. Good correlation is seen between T_e, solar radiation and wind speed and this file is therefore used as the primary weather file throughout this thesis.

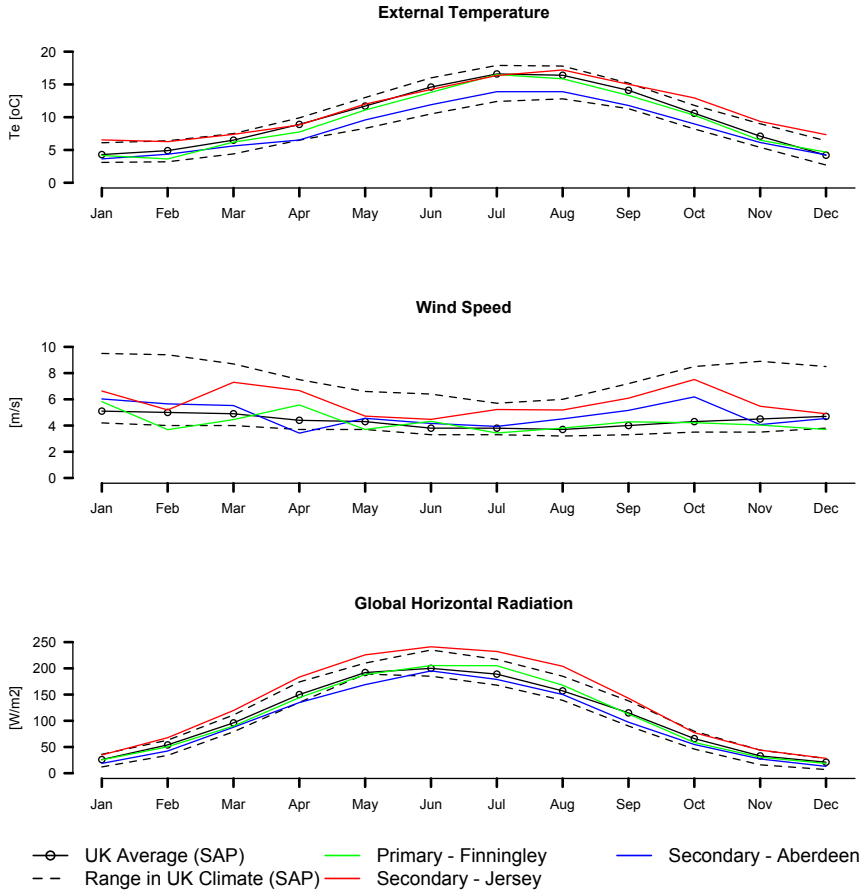

Figure 4.1: *Monthly T_e, S_{GHR} and wind speed used in SAP and in weather files used in this thesis.*

In addition, TMY weather files from Aberdeen (ABR) and Jersey (JER) are taken as colder and duller and warmer, sunnier examples respectively. These are used in chapter 9 when exploring suitable testing seasons. The thesis does not exhaustively explore ranges of weather conditions,

rather uses a small number of files as indicative examples of the uncertainties that exist.

Finally, simplified weather files have been created by adapting the Finningley file and setting variables to either zero or a constant value. Such an approach is used to examine the impact of dynamic external temperatures (Finn.T_e) and external sky temperatures (Finn.T_{sky}) in isolation from any other effects. These provide indicative examples before full simulations are carried out.

4.4.2 Simulated test dwelling - BRE test house

To investigate the nature of the sources of uncertainty identified in chapters 5 - 8 a single dwelling is simulated with the same basic form and overall *HLC* (*HLC*$_{pred}$ = 81 W/K) kept constant throughout. This is intended to provide a constant thread throughout these chapters.

This simulated dwelling, labelled BRE, follows the dimensions and form of the BRE[2] 'Swedish' test house used in the NHBC co-heating field trial (see Butler and Dengel, 2013). This dwelling, whilst fairly typical in scale, was selected here to provide better comparisons to the long term NHBC field data when possible and appropriate. The construction of the dwelling is however more conventional with respective elemental U-values obtained from the concurrent notional building regulation dwelling (DCLG, 2013), table 4.1, meaning this dwelling is likely to represent typical new builds.

The dwelling itself is shown in figure 4.2 along with a number permutations used to explore various sources of uncertainty. General building parameters are shown in tables 4.1 and 4.2 whilst details of the various weighted constructions used can be found later in table 4.3 along with calculated thermal mass parameters.

[2]BRE is the Building Research Establishment, based near Watford, UK

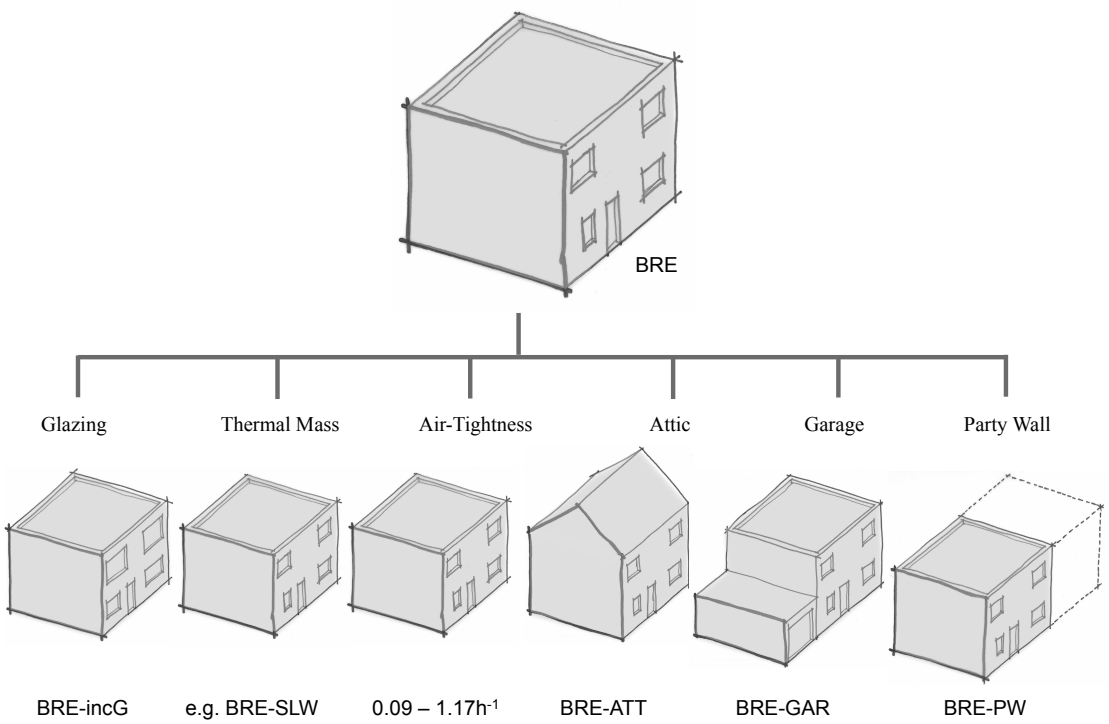

Figure 4.2: *BRE simulated dwelling and variations used.*

Table 4.1: Calculated *HLC* for primary simulated dwelling, BRE, based upon notional U-values, air permeability and thermal bridges. Notes: As EnergyPlus does not include linear thermal bridges within its calculations; the heat loss due to thermal bridges is incorporated into the external walls in actual simulations, but separated here for clarity. A value of y = 0.05 W/m^{2}K is used, as is practice for the notional dwelling if the actual dwelling uses a default of 0.15 W/m^{2}K (HM Government, 2006a). Only external door is included whereas the actual test dwelling has two.

Element or System	Values	Area, m^2	W/K
External Walls	0.18 (W/m^{2}K)	115.6	20.8
Party Walls	0 (W/m^{2}K)	0	0.0
Floor	0.13 (W/m^{2}K)	42.4	5.5
Roof	0.13 (W/m^{2}K)	42.4	5.5
Windows	1.4 (W/m^{2}K) *g value = 0.63*	13 -	18.2 -
Opaque Doors	1 (W/m^{2}K)	1.4	1.4
Air Permeability	5 (m^3/(hm^2))	-	17.9
Linear Thermal Transmittance	y = 0.05 (W/(m^{2}K))	-	11.6
		Total	**81 W/K**

Table 4.2: Basic building parameters for BRE simulated test dwelling.

Floor Area	42.4 m^2
Total Floor Area (TFA)	84.8 m^2
Volume	209.7 m^3
Envelope Area (exluding ground	171 m^2
Glazed Area	13 m^2
Glazed Fraction	15.40%
Glazing Distribution	57% - 43%
Heat Loss Parameter	0.96 W/Km^2

4.4.3 Variations to the BRE test house

As seen in figure 4.1, a number of variations are applied to the basic BRE test house used in simulations throughout chapter 5-8. These are detailed in sections 4.4.3.1 to 4.4.3.6.

4.4.3.1 Thermal mass of simulated test dwellings

The thermal mass parameter (*TMP*) is defined as the sum of the heat capacities (k (kJ/m K)), of elements in the buildings, multiplied by their respective areas (A), divided by the total floor area (*TFA*) of the dwelling.

$$TMP = \frac{\sum(k \cdot A)}{TFA} \tag{4.4}$$

SAP defines heavyweight, mediumweight and lightweight buildings as having TMPs of 450, 250 and 100 kJ/m^2K respectively. These approximately correspond to the values used for simulated test dwellings in this thesis, table 4.3, where additional super light and heavyweight constructions are also considered. These should allow typical buildings to be explored, with the addition of a further lightweight and heavyweight option for less conventional examples.

Table 4.3: Construction options leading to array of thermal mass parameters for the BRE simulated test dwelling.

Test Dwelling	Ground Floor	External Walls	Glazing	Roof	Internal Floors	Internal Partitions	TMP (kJ/m2K)
Super Lightweight (SLW)	Floating Floor	Timber Frame with Brick Outer Leaf - (single layer of plasterboard)	Simple U= 1.5 W/m2 g =0.63	Cold Deck Roof	Timber Flooring	Plasterboard & Timber Studs	**63**
Lightweight (LW)	Screed Floor	Timber Frame with Brick Outer Leaf - (two layers of plasterboard)	Simple U= 1.5 W/m2 g =0.63	Cold Deck Roof	Timber Flooring	Plasterboard & Timber Studs	**99**
Medium weight (MW)	Screed Floor	Full Fill Brick and Aircrete Block	Simple U= 1.5 W/m2 g =0.63	Cold Deck Roof	Timber Flooring	100mm Lightweight Block, Plastered both sides	**237**
Heavyweight (HW)	Concrete Slab	Full Fill Brick and Dense Aggregate Block	Simple U= 1.5 W/m2 g =0.63	Cold Deck Roof	Timber Flooring	100mm Lightweight Block, Plastered both sides	**470**
Super Heavyweight (SHW)	Concrete Slab	Full Fill Brick and Dense Aggregate Block	Simple U= 1.5 W/m2 g =0.63	Cold Deck Roof	Beam & Lightweight Block Floor	100mm Dense Block, Plastered both sides	**702**

4.4.3.2 Roof and attic space

While most UK houses have a pitched roof, with either a heated or unheated loft space, BRE incorporates a flat roof unless stated. This simplification removes any complexity from the attic space unless this is specifically being examined, as in section 7.1.

4.4.3.3 Airtightness

When examining varying infiltration rates, the airtightness of the dwelling is altered, shifting between values corresponding to airtight modern dwellings (mean ACH of 0.08 h^{-1}), through to to very poor airtightness associated with traditional dwellings (1.17 h^{-1}). The fabric itself is not altered, such that the value of HLC_{True} increases with infiltration losses. In simulations these can also be compared to a dwelling in which either no infiltration occurs, or in which the external wind speed is consistently set to zero.

4.4.3.4 Increased glazing

To examining the impact of a higher proportion of glazing, a increased glazing case (incG) is used to demonstrate the same dwelling with the south/east[3] facing glazing is increased (from 13.0 to 20.4 m^{2}and the glazing fraction 15% to 24%). The thermal performance of the walls is increased, such that the overall *HLC* remains constant for comparative purposes.

[3]The higher glazed facade always faces south in sourth-north (SN) facing dwellings and east in east-west (EW) orientation dwellings

4.4.3.5 Orientation

By default, the test dwelling is orientated on a south-north axis (SN). This influences both the amount and make up of solar gains received (i.e. direct/diffuse). To take account of this, an east-west (EW) orientated dwelling is also considered in chapter 5.

4.4.3.6 Adjoining spaces

For simplicity the test house is typically considered as detached, with no over shading from surrounding objects. In section 7.2, when the impact of adjoining spaces is considered, a second or third identical dwelling has been added to the east and west walls, creating a semi-detached or terraced test house.

4.4.4 BRE test dwelling - combinations & simulation codes

As seen, throughout chapters 5 - 8 a number of variations are applied to the basic BRE test house and a number of adapted weather files are used. In addition, the form of analysis used (regression type, test duration, aggregation, form of measured solar) may also be varied. To avoid confusion, each figure in chapters 5-8 will include a series of codes identifying the test dwelling, weather files and analysis. An overview is given in table 4.4.

Table 4.4: Options for simulations in chapters 5, 6, 7 and 8 along with identifying codes. Default options are marked with an *.

Method	Test Dwelling				Weather & Location		Analysis				
	Built Form	*Secondary Forms*	*Construction*	*Heat Capacity*	*Weather File*	*Orientation*	*Regression Method*	*Duration*	*Aggregation Interval*	*Aggregation Length*	*Solar Measurement*
Simple Model	Detached **(BRE)**	Attic **(ATT)**	Notional* **(NOT)**	Super Lightweight **(SLW)**	Finningley* **(FINN)**	South-North Axis **(SN)***	Multiple Linear Regression **(MLR)***	14 days* **(2w)**	24:00 - 24:00 **(24agg)**	24 hours* **(24h)**	Vertical South **(S_{GVS}*)**
Simulated		Garage **(GAR)**		Lightweight **(LW)**	All variable null or constant **(Ideal)**	East-West Axis **(EW)**	With Intercept **(MLRi)**		06:00 - 06:00* **(6agg)**	48 hours **(48h)**	Mean Vertical **(S_{GVM})**
Field Test		Increased Glazing **(IncG)**		Mediumweight **(MW)***	Ideal with only varying T_e **(FINN.T_e)**		Corrected Simple Linear Regession **(cSLR)**		12:00 - 12:00 **(12agg)**	72 hours **(72h)**	Horizontal **(S_{GHR})**
				Heavyweight **(HW)**	Ideal with only varying T_{sky} **(FINN.T_{sky})**		Siviour Analysis **(SIV)**		18:00 - 18:00 **(18agg)**	7 days **(1w)**	Mean Vertical East/ West **(S_{GVE} / S_{GVW})**
				Super Heavyweight **(SHW)**					Dawn - Dawn **(Dawn)**		Mean East & West **(S_{GVEW})**
											Vertical Weighted Mean **(S_{VWM})**

4.5 Simulated tests - application of co-heating - chapter 9

Chapter 9 focuses on the application of the co-heating method across a broader range of test dwellings and weather files. The simulated dwellings and weather files are described within this section.

4.5.1 Archetype dwellings

To consider the application of co-heating tests a wider range of dwellings are considered and used within simulations in chapter 9. These are selected to be somewhat representative of the UK housing stock, to reflect the type of dwellings commonly tested and to demonstrate variable behaviour under co-heating conditions. A number of 'archetype' dwellings are therefore used throughout chapter 9, described in the rest of this section.

4.5.1.1 The UK housing stock

In the UK approximately 65% of dwellings are constructed with masonry cavity walls, 27% are masonry solid walls and between 2 - 3% are timber frame (DCLG, 2014). Within these groupings the details of constructions vary, with materials, widths and depth of insulation varying according to the date and location of construction and any retrofit measures. With a large proportion of the UK housing stock dating back to pre 1919 (21%) (DCLG, 2014), dwellings made from traditional, solid walls, are an important component of the UK housing stock, particularly if regarding the use of co-heating to inform retrofit strategies. This equally applies to uninsulated cavity wall constructions, built later that century. Timber frame dwellings represent a smaller fraction of the total number of buildings but do offer variety in terms of the range in thermal mass.

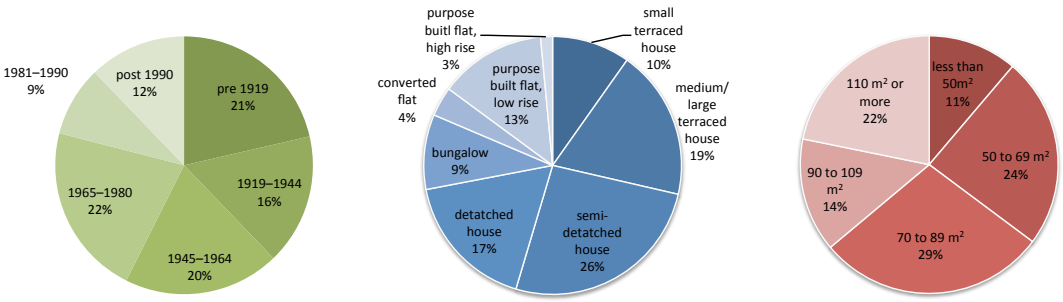

Figure 4.3: *Statistics of English housing stock (DCLG, 2014, Table11, p33)*

4.5.1.2 Archetype dwellings - built form

Four basic forms are used: a detached, semi, terraced and flat, with floor areas and layouts corresponding to the same example dwellings in the Zero Carbon Hub fabric energy efficiency guidance document (ZCH, 2012)[4]. This provide a range in sizes as well as increasing party wall areas. The four archetype dwelling built forms are shown in figure 4.4 with further details provided in table 4.5.

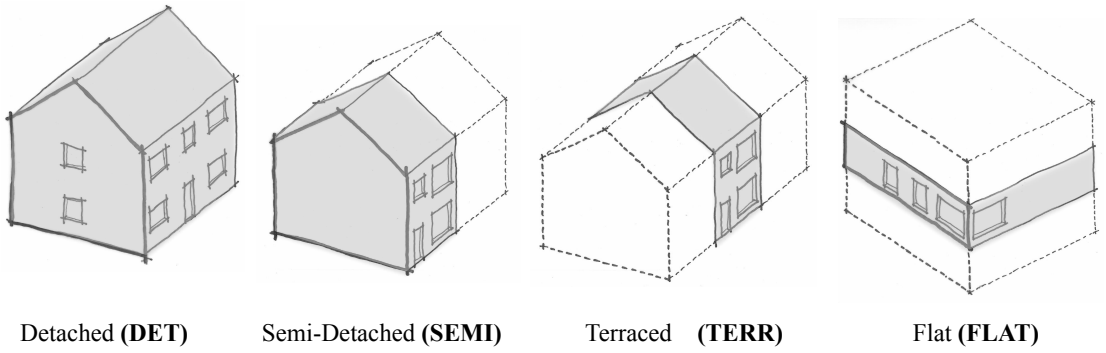

Figure 4.4: *Archetype dwellings used in simulations.*

Table 4.5: Summary of archetype dwellings used for simulations in chapter 9.

	Detached	Semi - Detached	Terrace	Apartment	
Floor Area	58.1	38.0	38.0	67.0	m^2
Total Floor Area (TFA)	116.3	76.0	76.0	67.0	m^2
Volume	348.9	190.1	190.1	167.5	m^3
Envelope Area (exc. ground floor)	242.0	127.3	92.3	55.0	m^2
Party Wall/Floor Area	-	35.0	70.0	190.3	m^2
Glazed Area	21.3	16.1	16.1	14.7	m^2
Glazing Fraction	18.3%	21.2%	21.2%	21.9%	%

4.5.1.3 Archetype dwellings - constructions

A number of different constructions can then be applied to each of these built forms. These feature a number of common constructions based on existing buildings, with fabric parameters based upon RdSAP and constructions from CIBSE Guide A (BRE, 2014; CIBSE, 2007). These consist of:

- *Victorian as-built* solid wall dwelling (VIC).
- *1960s as-built* brick cavity (SX).

[4]Floor plans for the archetype dwellings can be found in this reference.

- *Retrofitted 1960s* brick cavity (SXR).

A number of modern constructions, built to increasingly ambitious standards of fabric efficiency are then used:

- Built to *limiting* (L) 2010 UK building regulation fabric parameters (DCLG, 2013, p15, Table 2).
- Built to concurrent *notional* (NOT) fabric parameters (DCLG, 2013, p25, Table 4).
- Built to *Passivhaus* (PH) fabric standards (Feist, 2007).

These constructions have been chosen to both represent typical constructions in both existing and new build dwellings as well as providing a range in building characteristics to explore within simulations. Each of the modern dwellings can then be constructed from either lightweight or heavyweight materials. Details of the constructions of both existing and modern dwellings are then described in table 4.6.

Table 4.6: Constructions for archetype dwellings used for simulations in chapter 9.

Construction		Walls	Ground Floor	Glazing	Roof	Mean ACH	Partition Walls	Internal Floors
Victorian - As-built		*220mm Solid Brick - 13mm Plaster, (U = 2.1 W/m²K)*	*Uninsulated Suspended Timber Floor, (U = 0.82 W/m²K)*	*Single Glazing, (U = 4.8 W/m²K, g = 0.85)*	*Pitched Roof - Uninsulated, (U = 2.3 W/m²K)*	*~ 0.57 h⁻¹*	*110mm Solid Brick - 13mm Plaster each side*	*Timber*
1960s - Pre-Retrofit		*105mm brick - 50mm airspace - 105mm brick - 13mm plaster, (U = 1.6 W/m²K)*	*10mm Carpet - 50mm screed - 150mm cast concrete, (U = 1.2 W/m²K)*	*Double Glazing - Pre 2002, (U = 2.8 W/m²K, g = 0.76)*	*Pitched Roof - 12mm Insulation at ceiling level (U = 1.2 W/m²K)*	*~ 0.57 h⁻¹*	*13mm Plaster - Lightweight Block - 13mm Plaster*	*Timber*
1960s Retrofit		*105mm brick - 50mm polybead insulation - 105mm brick - 13mm plaster, (U = 0.5 W/m²K)*	*10mm Carpet - 50mm screed - 150mm cast concrete, (U = 0.3 W/m²K)*	*Double Glazing - Post 2002, (U = 2.0 W/m²K, g = 0.72)*	*Pitched Roof - Insulated at ceiling level (U = 0.13 W/m²K)*	*~ 0.2 h⁻¹*	*13mm Plaster - Lightweight Block - 13mm Plaster*	*Timber*
Modern (Limiting, Notional & Passhivhaus)	Heavywieght	*Full fill brick and aircrete block, (U = 0.3, 0.18, 0.15 W/m²K)*	*Concrete Floor - Insulated under screed (U = 0.25, 0.13, 0.15 W/m²K)*	*Double glazing, (U = 1.4 W/m²K, g = 0.63)*	*Pitched Roof - Insulated at ceiling level (U = 0.20, 0.13, 0.15 W/m²K)*	*~ 0.5, 0.2, 0.02 h⁻¹*	*13mm Plaster - Lightweight Block - 13mm Plaster*	*Timber*
	Lightweight	*Timber frame with brick outer leaf, (U = 0.3, 0.18, 0.15 W/m²K)*	*Floating Solid Floor - Insulated under flooring (U = 0.25, 0.13, 0.15 W/m²K)*				*Plasterboard on Studwork*	*Timber*

4.5.1.4 Archetype dwellings - heat loss & thermal mass parameters

The range in predicted heat loss coefficients for a combination of built forms and constructions used in chapter 9 are shown in figures 4.5 and 4.6. In addition, further building parameters, including glazing proportions and thermal mass parameters are included in tables 4.6, 4.7, 4.8 and 4.9.

4.5.1.5 Archetype dwellings - glazing

Details of the glazing and its distribution on each archetype dwelling is given in tables 4.8 and 4.9 respectively. The overall percentage of glazing alters slightly with age, according to RdSAP (BRE, 2014).

4.5.2 Weather Files

To briefly explore wider ranging weather conditions, two more extreme weather files are used in chapter 9. These are based on the TMY years for Aberdeen (ABR), representing colder external temperatures and lower solar isolation, and Jersey (JER) with a warmer and sunnier climate (EnergyPlus, 2015). The method adopted in this thesis could be extended over much wider range of conditions but this aspect is contained within the thesis.

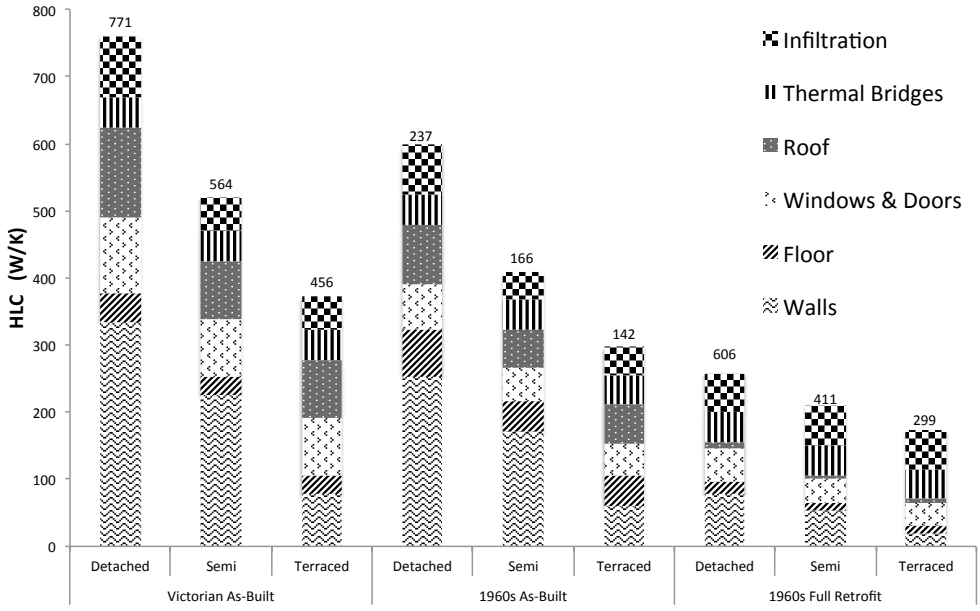

Figure 4.5: *Heat loss from archetype dwellings - traditional dwellings & retrofits. Based on ISO 13790:2008 calculations from simulation outputs.*

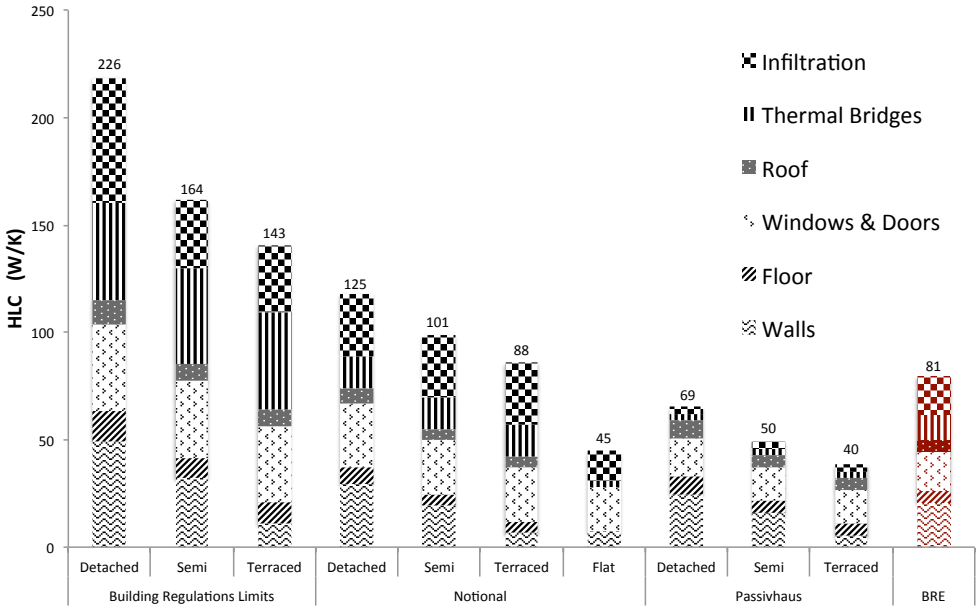

Figure 4.6: *Heat loss from archetype dwellings - modern dwellings. The BRE building used in chapters 5 to 8 is also shown in red. Note the flat is only considered as a notional construction.*

Table 4.7: Heat capacity and TMP for archetype dwellings used for simulations in chapter 9.

Construction	Form	Heat Capacity [kJ/K]	TFA [m^2]	TMP [kJ/m^2K]
Victorian	Detached	63732.1	116.3	548
	Semi	46512.7	76.0	612
	Mid Terrace	46512.7	76.0	612
1960s As-built & Retrofit	Detached	52138.4	116.3	448
	Semi	38140.3	76.0	502
	Mid Terrace	38130.0	76.0	502
Limiting, Notional & Passivhaus Heavyweight	Detached	37335.9	116.3	321
	Semi	29674.6	76.0	390
	Mid Terrace	32336.0	76.0	425
	Apartment	21291.1	67.0	318
Limiting, Notional & Passivhaus Lightweight	Detached	12971.8	116.3	112
	Semi	14279.9	76.0	188
	Mid Terrace	19123.5	76.0	252
	Apartment	10805.3	67.0	161

Table 4.8: Glazing parameters for archetype dwellings used for simulations in chapter 9. Existing dwelling values based upon BRE (Table S14 2014) for single glazed and double glazed pre & post 2002. Limiting and notional values from HM Government (2006b) and passivhaus values from Feist (2007).

Construction	Form	Glazed Area [m^2]	TFA [m^2]	Glazing Fraction [Glazing Area / TFA]	g value [0-1]	U-value [W/m^2K]
Victorian	Detached	21.0	116.3	18%	0.85	4.8
	Semi / Mid Terrace	16.1	76.0	21%		
1960s As-built & Retrofit	Detached	21.7	116.3	19%	0.76	2.8, 2.0
	Semi / Mid Terrace	16.2	76.0	21%		
Limiting, Notional & Passivahus	Detached	16.9	116.3	15%	0.76, 0.63, 0.5	2.0, 1.5, 0.85
	Semi / Mid Terrace	10.5	76.0	14%		
	Apartment	14.7	67.0	22%		

Table 4.9: Distribution of glazing for archetype dwellings used for simulations in chapter 9.

Form	Orientation of dwelling	Distribution of Glazing			
		North	South	East	West
Detached	*North - South*	45%	45%	5%	5%
	East - West	5%	5%	45%	45%
Semi / Mid Terrace	*North - South*	50%	50%	0%	0%
	East - West	0%	0%	50%	50%
Flat	*North - South*	66%	0%	0%	33%

4.5.3 Archetype dwellings - combinations & simulation codes

Throughout chapter 9 a number of different built forms, constructions, weather files and analysis methods have been adopted within a given simulation. These descriptive codes are given in each figure caption, with an overview provided in table 4.10.

Table 4.10: Options for simulations in chapter 9 along with identifying codes. Options marked with a * represent the default choice in simulations.

Method	**Test Dwelling**			**Weather & Location**		**Analysis**				
	Built Form	*Construction*	*Heat Capacity*	*Weather File*	*Orientation*	*Regression Method*	*Duration*	*Aggregation Interval*	*Aggregation Length*	*Solar Measurement*
Simple Model	Detached **(DET)**	Victorian Solid Wall **(VIC)**	Lightweight **(LW)**	Finningley* **(FINN)**	South-North Axis **(SN)***	Multiple Linear Regression **(MLR)***	14 days* **(2w)**	24:00 - 24:00 **(24agg)**	24 hours* **(24h)**	Vertical South **(S_{GVS}*)**
Simulated	Semi **(SEMI)**	1960s Cavity **(SX)**	Heavyweight **(HW)**	Aberdeen **(ABR)**	East-West Axis **(EW)**	With Intercept **(MLRi)**		06:00 - 06:00* **(6agg)**	48 hours **(48h)**	Mean Vertical **(S_{GVM})**
Field Test	Mid-Terrace **(TERR)**	1960s Cavity Full Retrofit **(SXR)**		Jersey **(JER)**		Siviour **(SIV)**		12:00 - 12:00 **(12agg)**	72 hours **(72h)**	Horizontal **(S_{GHR})**
	Flat **(FLAT)**	Building Regulations Limiting **(L)**						18:00 - 18:00 **(18agg)**	7 days **(1w)**	Mean Vertical East/ West **(S_{GVE} / S_{GVW})**
		Notional **(N)**						Dawn - Dawn **(Dawn)**		Mean East & West **(S_{GVEW})**
		Passivhaus **(PH)**								Horizontal **(S_{VWM})**

4.6 Field test case studies

4.6.1 Overview

The field tests conducted as part of this research were largely dictated by the availability of dwellings and limited by the time and resources required to conduct each test. As a result, five tests were conducted specifically as part of this research, with a number of secondary data sets used, either conducted previously by the author or by other organisations.

This small selection of field tests therefore relies on the range provided by simulated tests to fully answer the research questions of this thesis. However, within the 5 field tests conducted there is a wide range in measured *HLC*, varying from 56 to 231 W/K (HLP: 0.35 - 2.38 W/Km^2). In addition, there is a range in dwelling glazing fraction, ranging from 14% of the TFA (14.7 m^2) to 35% (38.8 m^2). Further details, including the built form, floor area and constructions of field test dewllings can be found in tables 2.1 to 2.5 alongside a review of other tests. Furthermore, a number of issues related to internal temperature distributions, wind driven cavity losses, party walls, moisture loads, unheated spaces and ground losses came to the fore as a result of the field tests.

Details of equipment used in field tests can be found in table 7.3 and in the two co-heating reports contained within appendix C and D. Each field test is documented in this section.

4.6.2 Field test method

Field tests conducted as part of this thesis follow the co-heating method set out by Johnston et al. (2013), following on from the work undertaken by Everett (1985) and Siviour (1981). This method is described in section 2.3. To maintain as much consistency as possible the same basic equipment was used in all tests, although some included additional measurement channels as their projects dictated and as further equipment became available. Details of the five field tests performed as part of this thesis can be found in tables 2.1 - 2.5. Unfortunately, due to confidentiality issues, most of the individual reports cannot be included, although two examples are contained within appendicies C and D.

Some details of the equipment used can be found elsewhere in this thesis, table 7.3, figures 2.3 and 2.4 as well as the reports in appendices C and D.

4.6.3 Field test research projects

The field tests conducted as part of this thesis came under three wider projects.

4.6.3.1 NHBC co-heating field trials

The NHBC Co-heating Field Trial was conducted as an investigation into the accuracy of the co-heating test and its application, see section 2.8.2 (Butler and Dengel, 2013). For the project, a set of twin test houses at BRE, Watford, were selected. These were built in 1995 based upon Swedish standards at the time. UCL was one of six participating organisations, each performing a single 2 week test under their own methodologies. An expanded data set gathered by the BRE, covering a longer but intermittent monitoring period for both test houses was provided to participants for further analysis. Both the individual UCL test and this expanded data set are used.

4.6.3.2 Joseph Rowntree Housing Trust - Derwenthorpe

A further case study formed part of a series of co-heating tests performed on phase 1 of the Derwenthorpe housing development in York. This followed on from earlier work incorporating co-heating tests by the Joseph Rowntree Housing Trust (JRHT) at Stamford Brook (Lowe et al., 2007) and Temple Avenue (Miles-Shenton et al., 2010; Miles-Shenton et al., 2011); the latter used to assess two prototype dwellings for the Derwenthorpe development.

The primary aim of the project was to *"inform the construction process and ensure that the building fabric of the units delivered will perform within a reasonable tolerance of the predictions in the compliance model"* (JRHT, 2011). However, based on their previous experiences JRHT held the opinion that *"a full research test is time consuming and restricted to the winter period. The industry needs a simple repeatable test that is less disruptive to the housebuilder"*. Therefore this project, hoped that *"by using several testing techniques at the same development some useful lessons can also be learned about the suitability of co-heating as a widespread compliance procedure"*.

It was this secondary aim of the project that was potentially more informative for this thesis. Plans initially aimed to have long (3 week) and detailed *research* tests as well as shorter ($\sim$1week) *industry* tests and even some *dynamic* tests using the PSTAR method. These were to be conducted across a large number of dwellings and by a number of organisations representing

both academia and industry. However, this was scaled back and in the end only a small number of co-heating tests were performed - 3 by two academic institutions. The UCL test conducted by the author is referred to in this thesis.

4.6.3.3 Technology Strategy Board Building Performance and Evaluation Programme

Three co-heating tests were performed under the Technology Strategy Board (TSB) Building Performance & Evaluation (BPE) programme (TSB, 2015). Co-heating tests formed a mandatory and subsequently optional element of these research programmes aimed at a number of high specification new dwellings. Performing field tests for this thesis within the framework of the TSB BPE programme provided available test dwellings, the support and involvement of architects and developers, as well as provided funding for the co-heating test, equipment and performing supplementary tests.

4.6.4 Test Dwellings

Details of all field tests conducted as part of this thesis can be found in ables 2.1 - 2.5, including total floor areas, built forms, glazing ratios, number of floors, air permeabilities, predicted *HLC*s, test lengths and environmental conditions during testing. More general descriptions can be found throughout the rest of this section.

4.6.4.1 The Camden Passivhaus (CAM-PH), 21st - 30th December 2012

Situated in London the Camden Passivhaus had initially been co-heating tested under the TSB BPE programme in April 2011, as part of a piece of Masters Research conducted by the author (Stamp, 2011). This test, performed at an unsuitable time of year, suffered from unstable internal temperatures. Therefore a follow up test was planned, conducted under more suitable environmental conditions. As the dwelling was occupied, this test had to be organised around the occupiers' holidays, resulting in a shorter test period (6 days).

As a Passivhaus, the dwelling has a large amount (32.3 m^2) of south-west facing glazing and a low designed *HLC* (HLC_{pred} = 66 W//K, HLC_{meas} 56 W/K). This combination of a high amount of glazing and very low heat loss represents perhaps the most challenging type of dwelling with which to conduct a co-heating test. The building is also partially excavated; meaning a large part of the fabric is connected to the ground (138 m^2, 36%), as opposed to ambient external air (see figure 9.17).

As part of the TSB BPE programme in situ U-values and CO_2 tracer gas decay measurements were also conducted by the author. Further pressure tests and thermography surveys were also carried out.

4.6.4.2 NHBC co-heating field trial (NHBC) - 10th - 24th February 2012

The test dwellings are detached and constructed from brick clad timber frames and. They are both approximately south facing with 13 m^2 of glazing split between the north and south facades. With a floor area of 42 m^2, and an airtight construction (2.2 m^3/h/m@50 Pa) the BRE dwelling has a relatively low heat loss (HLC_{pred} = 68.4 W/K, HLC_{meas} = 70 W/K).

The two week period allotted for the UCL test is perhaps most notable for the large range in ΔT experienced, a span of over 15K. The tests by the 6 participating organisations spanned between January and April 2012, with a control house operated by BRE running intermittently from December 2011 to September 2012. This gives a wide range of weather conditions. Participants were given access to this full dataset, although the test conditions were not kept consistent throughout this period, with internal temperatures increased and various shading devices trialled in the summer.

Additional tests again included in situ U-values (walls & ceiling), CO_2 tracer gas decays and a thermography survey.

4.6.4.3 CASE-A1 & CASE-A2- January & March 2013

Under another TSB BPE programme an end-of-terrace dwelling was tested in the south of England. Two tests CASE-A1 and CASE-A2 were performed in January and March 2013 upon the same dwelling, before and after a cavity insulation fill.

The dwelling is constructed with precast low density beam and block floors. The cavity walls contain 135mm Ecobead injected between an inner leaf of medium density blockwork and outer skin of brick, giving a calculated U-value of 0.22 W/m^2K. The roof structure consists of an unheated loft and pitched roof with 400mm of insulation at ceiling level.

In the first test, a vastly higher than predicted *HLC* was measured, 245 W/K (HLC_{pred} = 112 W/K). Further investigations revealed that the ecobead insulation had not actually been

injected into the cavities of the walls. This was subsequently rectified and a second test, CASE-A2 conducted under similar external conditions. This illustrates the effectiveness of co-heating tests at measuring fabric improvements, particularly with supporting in situ U-value measurements and pressure tests.

Additionally, as an end-of-terrace dwelling this is the only field test conducted for this thesis that involves any party wall elements and the guarding of a neighbouring property. Additionally, co-heating data from the neighbouring, guarded dwelling, can be analysed, with the limitation that the third dwelling in the row of terraces could not be accessed.

4.6.4.4 CASE-B - March 2012

Constructed from a thin joint masonry partial-fill cavity-brick wall system, the CASE-B test dwelling has a relatively high heat loss (Predicted 205 W/K, Measured 231 W/K), owing to its large size (TFA = 192 m^2).

The layout and form of the dwelling throw up a number of issues. Firstly, the dwelling is initially built to have an unheated attic space. However, the ability to convert the attic space into a heated, liveable space is built in. The result of this is that the building is insulated at roof and ceiling level. With just a small loft hatch connecting the attic to the rest of the dwelling, the attic space has a limited thermal connection to the rest of the dwelling.

Secondly, the dwelling is designed with a winter garden, a small, double height, and highly glazed, south facing space. Both these design features lead to lower control and a wider variation in internal temperatures. This makes this field test a useful example to illustrate the uncertainty in the representativeness of the chosen internal temperatures (see section 7.3).

Furthermore, the dwelling was recently constructed and had not been heated prior to testing, resulting in high amounts of residual moisture in the fabric and an increased initial heating period as the building slowly reached quasi-steady state. The result of this was both practical, with damage to internal fittings, and technical, with the addition of a latent load and increased thermal conductivity (see section 7.6).

On top of the co-heating test, in situ U-value measurements were made of the floor, external walls and roof along with daily CO_2 tracer gas decay measurements.

4.6.5 Secondary data

Some secondary analysis can be conducted on co-heating test data not conducted specifically as part of this thesis. This can be achieved when daily aggregated results are published, along with satisfactory supporting details, although such results need to be used with care. A limited number of secondary data, including some from the authors own tests, is listed below:

4.6.5.1 NHBC field trial - Dec 2011 to May 2012

Using the full data from this project, gathered by 6 other organisations between December 2011 and May 2012, further insights can be gained. This particularly comes from the long term monitoring of the control test house, collected by BRE, giving approximately 360 days of data split between the two test houses. In reality only part of this data can be used to perform useful comparisons but it does allow the best evaluation of the seasonable reliability and repeatability of co-heating tests from field measurements.

4.6.5.2 CAM-PH1- 20th March - 1st April 2011

An earlier test conducted in 2011 at the Camden Passivhaus can also be considered as an example of full overheating (section 5.5) and as a demonstration of the restricted testing season for low energy, highly glazed Passivhaus dwellings. This dwelling was tested previously by the author as part of a master thesis (Stamp, 2011).

4.6.5.3 CASE-C - 22nd December - 11th January 2011

Again tested previously by the author, CASE-C is a level 6 Code for Sustainable Homes dwelling built by a major developer. The structure is of aircrete masonry walls and a concrete slab floor, providing high thermal mass. The design heat loss is just 78 W/K, albeit the measured *HLC* was higher (130 W/K).

4.6.5.4 CASE-D

A semi-detached dwelling constructed from lightweight aerated clay blocks, with a measured heat loss of 94 W/K. Notable for the use of horizontally measured solar radiation. Further details can be seen in tables 2.1 - 2.5.

4.6.5.5 CASE-E

A detached dwelling constructed from a thin joint masonry-partial fill cavity-brick wall system, with a measured heat loss of 150 W/K. Further details can be found in tables 2.1 - 2.5 and (Miles-Shenton et al., 2010).

4.6.5.6 CASE-F

A detached dwelling constructed from structural insulated panels, with a measured heat loss of 133 W/K. Further details can be found in tables 2.1 - 2.5 and (Miles-Shenton et al., 2010).

4.6.5.7 CASE-G

A corner apartment (63 m^2) dwelling constructed from clay blocks and a concrete frame. With a small overall area and exposed fraction the heat loss is low (HLC_{pred} = 38 W/K, HLC_{meas} = 49 W/K). This example is most notable for some unguarded flows to surrounding apartments and the likely related non-convergence of results over time (section 9.2). Further details can be found in tables 2.1 - 2.5.

4.7 Chapter conclusions

The research conducted for this thesis uses both simulated co-heating tests and a number of case study field tests to investigate the uncertainty, accuracy and reliability of the co-heating method. Simulated tests offer the breadth in both external environmental conditions and in dwelling characteristics that it is not possible to achieve in field tests. Further, the ability to vary or isolate single parameters means simulated tests allow better insight into the impact of specific sources of uncertainty. Finally, as the value of HLC_{True} is a known simulation output, systematic errors and their scales can be observed directly.

Field tests are then used to provide supporting examples and to reveal complexities that occur in real tests but are ignored or simplified in the simulated tests. These include the impact of wind on cavity heat flows, party wall heat transfer, moisture, shading and internal temperature variations. Performing field tests has also exposed the author to the practicalities of performing co-heating tests and given insight into their use in the construction industry.

Chapter 5

Solar Driven Sources of Uncertainty

Chapter overview

Solar radiation incident on a test dwelling will provide solar gains to the dwelling and potentialy forms a major heat input into the co-heating energy balance. As solar gains cannot be directly measured they can result in a significant source of uncertainty. This uncertainty can take a number of forms, with solar radiation resulting in both measurement uncertainty and definitional uncertainty. Through increasing dynamic behaviour and interacting with the dwelling in non-linear ways, solar radiation can also lead to systematic bias in *HLC* estimates. These issues are explored in this chapter, under the following headings:

- **5.1 Solar radiation incident upon a dwelling:** to introduce solar sources of uncertainties, the response of a test dwelling to incident solar radiation is briefly considered.

- **5.2 Determination of solar gains - The measurement of *S*:** Uncertainty associated with the measurement of solar radiation incident upon a test dwelling and the resulting uncertainty in solar gains and *HLC* estimates.

- **5.3 Determination of solar gains - The estimation of *R*:** Uncertainty in solar gains due to uncertainty in the solar aperture *R*.

- **5.4 Stored solar heating contributions:** Heating contributions from solar radiation heating the building mass, stored and re-emitted in a subsequent day. These dynamics are not captured in the steady state energy balance.

- **5.5 Solar driven experimental overheating:** Instances in which solar radiation causes the internal temperature to rise above the experimental set point, causing the quasi steady state experimental conditions to be compromised and increase dynamic heat flows.

- **5.6 Chapter conclusions:** The chapter closes with a number of conclusions drawn from the proceeding sections.

5.1 Solar radiation incident upon a test dwelling

Upon reaching a dwelling, short-wave solar radiation will be incident upon either opaque or glazed building elements. Solar radiation incident upon a glazed element will be reflected, absorbed or directly transmitted into the internal space. The absorbed radiation will increase the temperature of the glazing and subsequently provide both convective and long wave radiant heat gains into the internal space. The transmitted solar radiation, excluding any that passes directly out of the space, is absorbed by internal surfaces or furnishings. This absorbed radiation then warms the internal surfaces and subsequently heats the internal air through convection and radiation. Through this cycle of absorption and re-emission of heat by the thermal mass of the test dwelling, there is a lag between the measured incident solar radiation incident upon the dwelling and the heat gains provided to the internal space.

The second component of the solar radiation, incident upon the opaque elements of the building, is either reflected or absorbed by the surface. These proportions depend upon the construction of the element and properties of its surface. For most opaque elements, the net solar heat gains are small and are in part compensated by long-wave losses to the sky (section 6.3). Absorbed radiation will increase external surface temperatures and thus reduce the heat flow through the opaque elements from the internal environment. In un-insulated, lightweight and thin elements (e.g. un-insulated roofs) the space may be heated more directly.

In both these processes it is clear that determining an exact heating contribution from solar gains is complex. Firstly, the solar gains admitted to a dwelling depends upon the distribution of incident solar radiation across the building fabric and the properties of the fabric itself. With multiple angles, local shading and variations in the fabric and glazing properties, this becomes complex, leading to uncertainty in *determining solar gains*. Accurately determining solar gains requires both an accurate and appropriate measurement of the incident solar radiation upon the dwelling, and a suitable conversion of this radiation into solar gains, via a solar aperture, R. This parameter can then be determined either statistically, or numerically modelled, with each approach containing its own uncertainties.

Secondly, as the heat input provided from a given period of solar radiation is lagged and released over an extended time period, the measured solar radiation and heating contribution do not fully coincide with one another. The nature of this lag is dependent upon the properties of materials contained within the building and the distribution of solar radiation across these surfaces. This leads to uncertainty from *stored solar heating contributions*.

A third source of solar driven uncertainty can also be considered. Applying steady state analysis to a co-heating test requires constant internal temperatures. As an uncontrolled heat input, solar radiation can force the internal temperature above the experimental set point, $T_{setpoint}$. When solar gains cause temperatures to rise above the experimental set point, i.e. $T_i > T_{setpoint}$, dynamic heat flows within the building are increased, causing major problems when attempting to resolve the energy balance. This can be defined as uncertainty due to *experimental overheating*. These issues are considered throughout the rest of this chapter.

5.2 Determining solar gains, R.S - The measurement of S

An accurate estimation of solar gains is dependent upon an accurate and appropriate measurement of the incident solar radiation, *S*, across a test period. The dependence of *HLC* estimates on the measurement of *S* will then scale with the SOLR[1] and should be considered in the context of the two forms of solar gain analysis - statistical and numerical.

When solar gains are accounted for by including *S* as an independent regression variable - a statistical approach (section 2.3.3) - definitional uncertainty arises in deciding which form of *S* to measure. For example, a single south facing vertical measurement, S_{GVS}, may provide a suitable explanatory variable for single aspect, south-facing dwellings. However, as will be shown, this statistical relationship becomes less clear in dwellings with windows on more than one orientation.

Alternatively, if a numerical calculation is used (based upon geometry and material properties, see 3.3.1), then the absolute value of *S* needs to be known accurately. Firstly, this increases the importance of suitable sensor accuracy and calibration. Secondly, suitable measurement and positioning of sensors remains crucial in order to accurately estimate gains across a range of glazing elements.

[1] See section 3.4.6 for the definition of the Solar Load Ratio.

5.2.1 Measuring Solar Radiation

Solar radiation can be measured on site in a number of different forms. Reviewing the discussion on forms of measured solar radiation in section 3.4, three forms of measured incident solar radiation can be considered:

- Global horizontal radiation, S_{GHR}
- Global vertical solar radiation, measured on a given vertical surface, typically that which is likely to experience the highest gains, termed the principal facade, S_{GVP}:

$$S_{GVP} = S_{GV(N,S,E,W,SW...)} = cos(\theta) \cdot S_{DNR} + F_{view} \cdot S_{DHR} \tag{5.1}$$

- Mean vertical global radiation, S_{GVM}, where:

$$S_{GVM} = \frac{(S_{GVS} + S_{GVW} + S_{GVE} + S_{GVN})}{n} \tag{5.2}$$

Where n is the number of orientations in which solar radiation was measured, here $n = 4$.

Any measurement is likely to only represent an estimation of the total solar radiation incident on a building, particularly when considering any practical and cost constraints placed on sensor deployment. Everett (1985) used a south facing vertical measurement, S_{GVS}, as a compromise between a meteorological and a building centred measurement. This approach is also adopted in the LBU protocol (Johnston et al., 2013) although as reported in Deconinck and Leunis (2012) and demonstrated earlier in this thesis (table 2.2) it is not consistently adopted.

Most commonly, in co-heating tests solar radiation in measured horizontally (S_{GHR}), or vertically in a single plane (S_{GVP}), typically south facing (see table 2.2). Both measurements can be considered imperfect in a number of ways. A measurement of S_{GHR} does not explicitly describe the direct solar radiation incident on vertical surfaces, the plane in which most gains are likely to enter a dwelling. However, measurements of vertical radiation on a single facade, S_{GVP}, may not represent the full incident solar radiation across the multiple orientations of a building. In addition, both measurements may be subjected to local shading effects and more importantly, neither fully considers the distribution of gains or glazing on each facade.

Measuring the mean solar radiation on all facades, S_{GVM}, will account for the solar radiation incident upon the full envelope. However, this measurement will not weight the total

measured solar radiation by the significance of each orientation, i.e. adjusting for facades with higher amounts of glazing, such that a single measurement may be preferable for dwellings with single dominant facades.

As in many cases within this thesis, this is an example of how the conceptual structure is being driven by the convenience of a measurement system and its analysis. In the rest of this section, the imperfect nature of these measurements are discussed and compared, with the impact upon *HLC* estimates shown.

5.2.1.1 Correlation between the measured *S* & the estimated true gains, $Q_{sol,True}$

In figures 5.1 and 5.2, the estimated true solar gains[2] are compared to three types of measured solar radiation (S_{GHR}, S_{GVP}, S_{GVM}), as well as the direct normal and diffuse horizontal solar components. This allows the correlation between each solar component and form of measured solar radiation to be compared with the estimated true solar gains. In addition, the correlation between the solar components and forms of measured solar radiation themselves can be observed. This is important when considering the use of multiple solar terms within regression analysis (section 5.2.5.1).

In figure 5.1 and 5.2, solar gains and associated scatterplots are considered for a simulated dwelling (BRE-NOT), orientated with the principal (7.4 m^2) and secondary (5.7 m^2) glazed facades facing either south-north or east-west respectively. Significant differences can be seen between the two orientations of the same dwelling.

A south-north orientated dwelling

Initially considering the south-north orientated dwelling (figure 5.1), it can be noted how the estimated true solar gains show a significantly higher correlation with direct gains than with diffuse. This can be understood from the building's characteristics, with most gains coming as direct gains through the vertical south facing glazing. The result of this is that S_{GVM}, and in particular S_{GVS}, provide a stronger correlation with the estimated true solar gains, both having a higher appreciation of direct gains. S_{GHR}, showing a stronger correlation with diffuse gains, has a weaker correlation with $Q_{sol,True}$, and importantly does not appear to demonstrate a straightforward linear relationship.

[2]The calculated solar gains are based on the solar gains (W) received through exterior windows, ignoring opaque gains, an output of the simulation tool, see section 4.3.3.2.

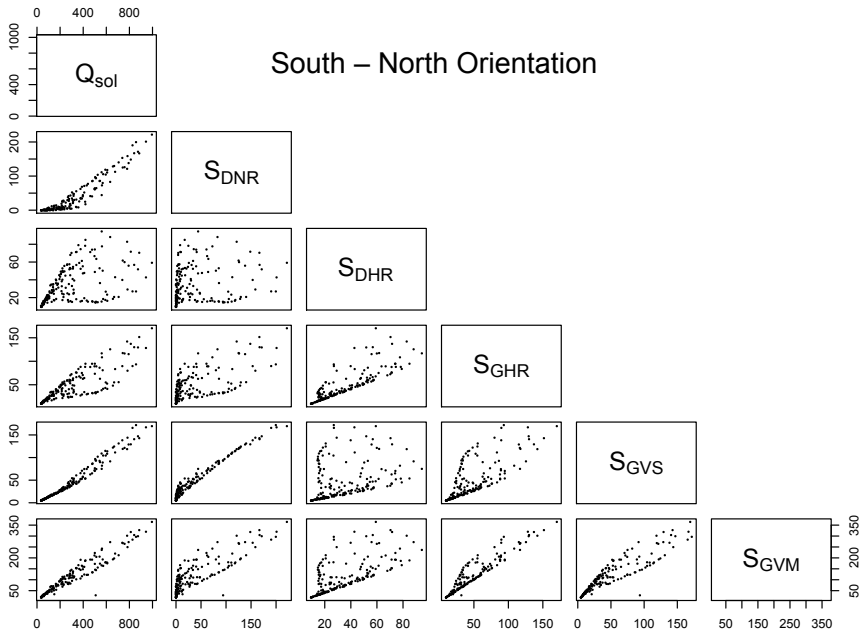

Figure 5.1: *Comparisons of estimated solar gains from various measurements of S across Oct-Mar.* (Simulation: BRE-NOT-SLW-FINN-SN-MLR-2w-24h-6agg)

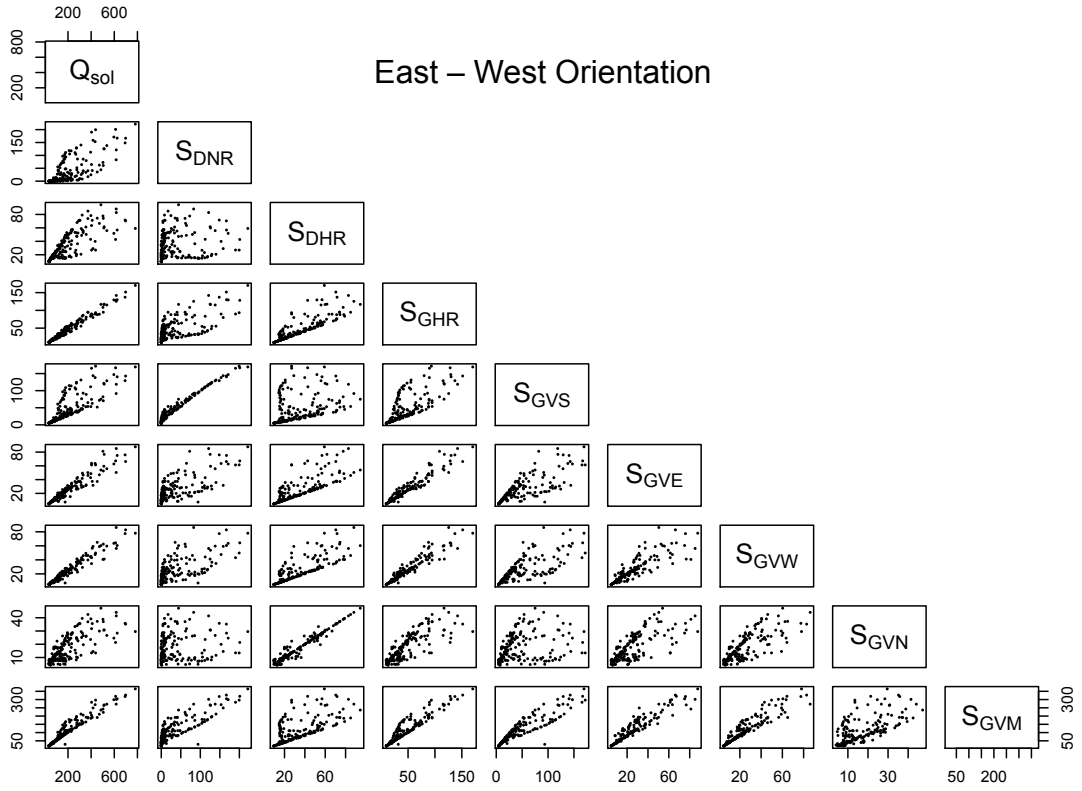

Figure 5.2: *Comparisons of estimated solar gains from various measurements of S for an east-west orientated dwelling.*(Simulation: BRE-NOT-SLW-FINN-EW-MLR-2w-24h-6agg)

An east-west orientated dwelling

Considering the east-west orientated test dwelling (figure 5.2), this behaviour changes somewhat. The correlation of solar gains with direct and diffuse radiation is split more evenly. Again, referring to the building characteristics, with the glazing and gains split over the east-west facades, diffuse gains are likely to have higher importance, whilst direct gains are reduced. The result is that this time S_{GVS} shows some non-linear behaviour, whilst S_{GHR} and any of S_{GVE}, S_{GVW} or S_{GVM} show improved correlation with the estimated true total gains.

These relationships, the interactions between these forms of measured solar radiation and the characteristics of the physical building are important to keep in mind as the resulting *HLC* estimates are reviewed (figures 5.3, 5.4, 5.5 and 5.6).

5.2.2 The impact upon *HLC* estimation

5.2.2.1 Fully simulated examples

Results from the same simulated co-heating tests are shown across the testing season in figures 5.3 - 5.6, with the orientation and the glazing fraction of the dwelling varied. Various forms of measured solar radiation can be compared in these plots and referred back to the plots in figures 5.1 and 5.2. What is perhaps most intriguing is that the most appropriate measurement of *S* depends very much on the specific test dwelling under consideration, its orientation and the distribution of glazing on each facade. When inappropriate measurements are made, the resulting bias in *HLC* estimates can be high.

HLC estimates using different forms of solar radiation are further compared for the four forms of this dwelling in table 5.1. Here, over the test period, the mean square errors (MSE) between HLC_{meas} and HLC_{True} have been compared, such that the most accurate form of solar radiation can be clearly identified. In addition to the previously discussed forms of solar radiation, a weighted mean, S_{GVWM} is considered, based upon the proportions of expected gains on each surface, as predicted by an ISO 13790 calculation (see table 5.1).

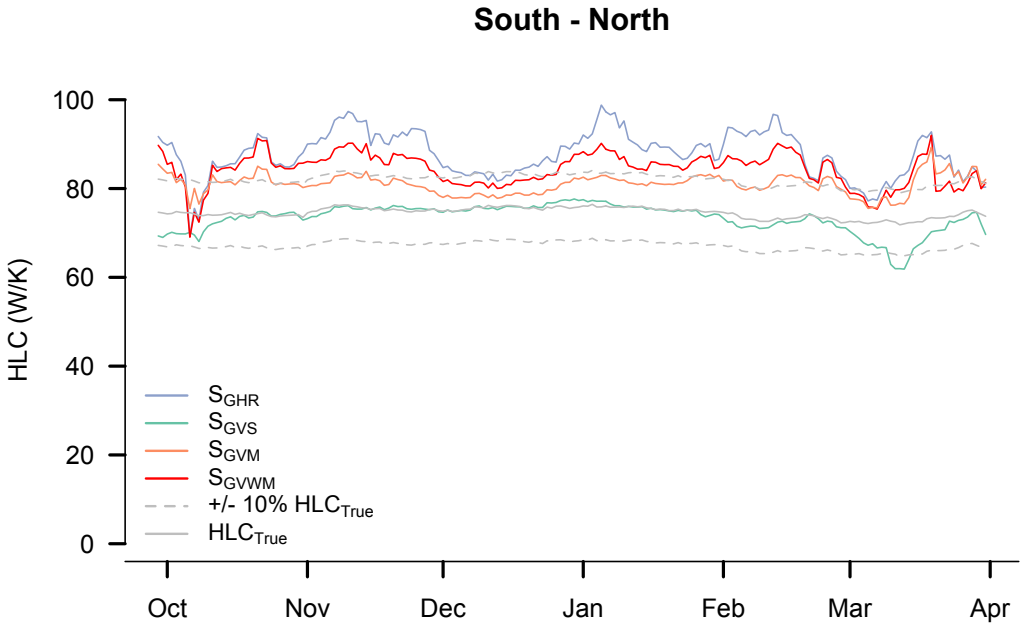

Figure 5.3: *Derived HLC using a variety of measured solar radiations, south-north orientated dwelling. Note data from simulations is analysed in 2 week segments running from day 1 to day 14, then day 2 to 15 and so on. This approach is repeated throughout this thesis.*(Simulation: BRE-NOT-SLW-FINN-NS-MLR-2W-24h-6agg)

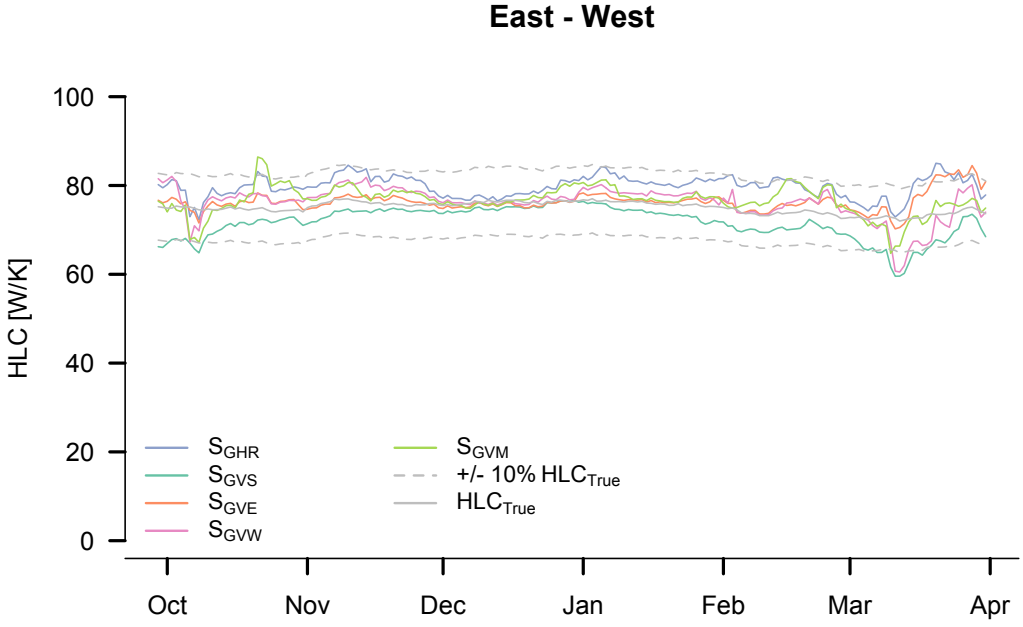

Figure 5.4: *Derived HLC using a variety of measured solar radiations, east-west orientated dwelling.* (Simulation: BRE-NOT-SLW-FINN-EW-MLR-2W-24h-6agg)

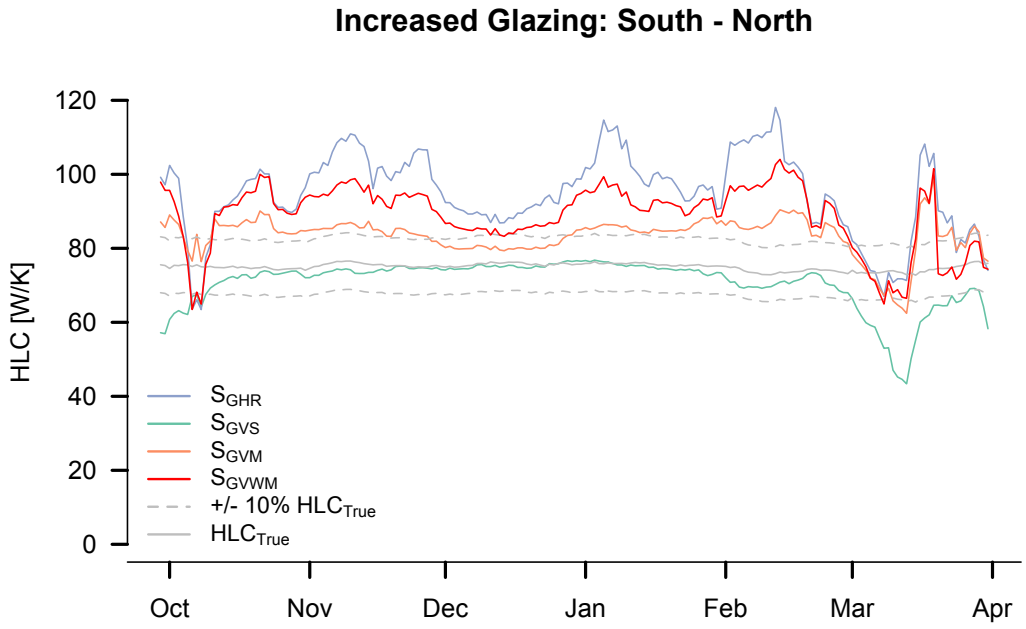

Figure 5.5: *Derived HLC using a variety of measured solar radiations, south-north orientated dwelling with increased glazing.* (Simulation: BRE-NOT-SLW-incG-FINN-NS-MLR-2W-24h-6agg)

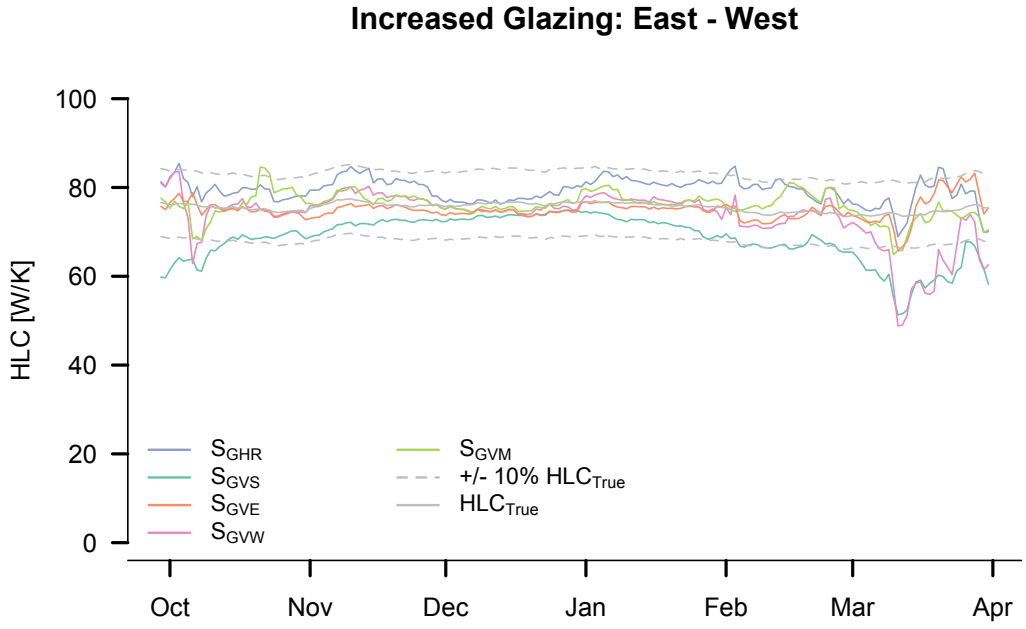

Figure 5.6: *Derived HLC using a variety of measured solar radiations, east-west orientated dwelling with increased glazing.* (Simulation: BRE-NOT-SLW-incG-FINN-EW-MLR-2W-24h-6agg)

Table 5.1: Corresponding mean square error for various forms of measured solar radiation. Note: Data is taken between 1st November and 28th February and a super lightweight dwelling (SLW) is used to minimise stored solar heat (see section 5.4) and examine the impact of the measured solar radiation more directly.

Dwelling	Orientation	Mean Deviation - $\lvert HLC_{True} - HLC_{meas} \rvert$						
		S_{GHR}	S_{GVS}	S_{GVE}	S_{GVW}	S_{GVM}	S_{GVEW}	S_{GVWM}
SLW	*North - South*	14.48	0.67	8.04	7.53	5.50	-	5.88
SLW Increased Glazing		23.95	1.57	12.37	11.18	9.17	-	16.92
SLW	*East - West*	4.71	2.17	2.23	1.92	0.97	3.12	2.84
SLW Increased Glazing		4.21	4.62	1.63	1.43	1.26	2.28	4.62

A south-north orientated dwelling

When a high proportion of total gains are associated with one facade, for example a highly glazed or near-south-facing facade, then a single vertical measurement, S_{GVP}, is the most reliable form (see figure 5.3 and table 5.1). This can be examined in the context of figure 5.1 where the strongest correlation was seen between S_{GVS} and the estimated true gains.

Measurements of S_{GVM} incorporate vertical solar radiation across the entire fabric, but as the majority of gains are through one facade, this correlates less well to the estimated true solar gains in figure 5.1 and the *HLC* estimate is marginally less accurate (see figure 5.3). Similarly, S_{GHR} shows even weaker correlation and less reliable *HLC* estimates.

Most significantly, in table 5.1, both S_{GVM} and S_{GHR} show a tendency to overestimate the *HLC* in the south-north facing test dwelling (by a mean of 6.5 and 13 W/K respectively across this test period), increasingly so in the increased glazing case ($\sim$ 9 and 21 W/K). This is further demonstrated in calculations of the solar aperture and solar gains, both of which are later seen to be overestimated by S_{GHR}, figures 5.12 and 5.13, section 5.3.2.

The mechanics behind this effect are perhaps clearest when the analysis of S_{GVS} and S_{GHR} are compared on the same plot. In the Siviour plot in figure 5.7, the same 2 week sample of data is plotted using both S_{GHR} and S_{GVS}. Two distinct groups of data can be perceived in each case, at both low and high S/ΔT, noting that it is only the measured form of the parameter S that is changing in these datasets. Approximately half the days, which appear to be dull, show similar distributions in both data sets. However, a second group, with their individual days labelled in the plot, show distinct differences between the two forms of measurement.

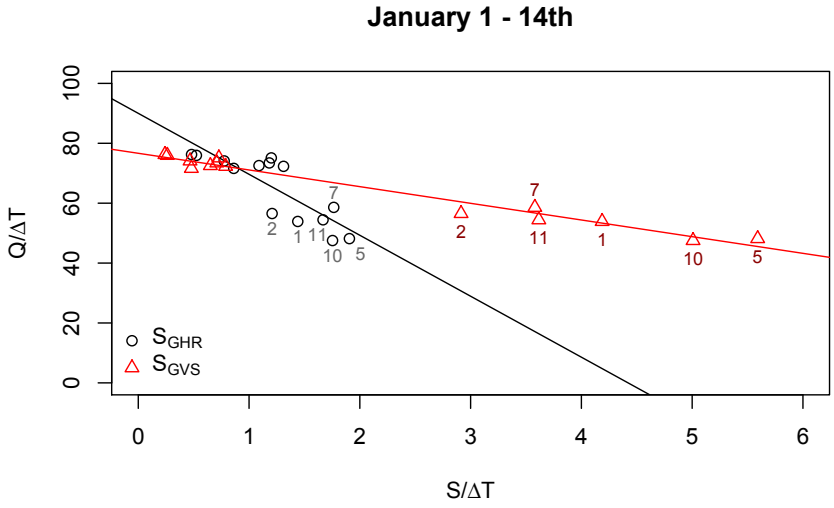

Figure 5.7: *Siviour plot comparing analysis using, S_{GHR} and S_{GVS}. Relevant days to figure 5.8 are labelled.* (Simulation: BRE-NOT-SLW-FINN-EW-MLR-2W-24h-6agg)

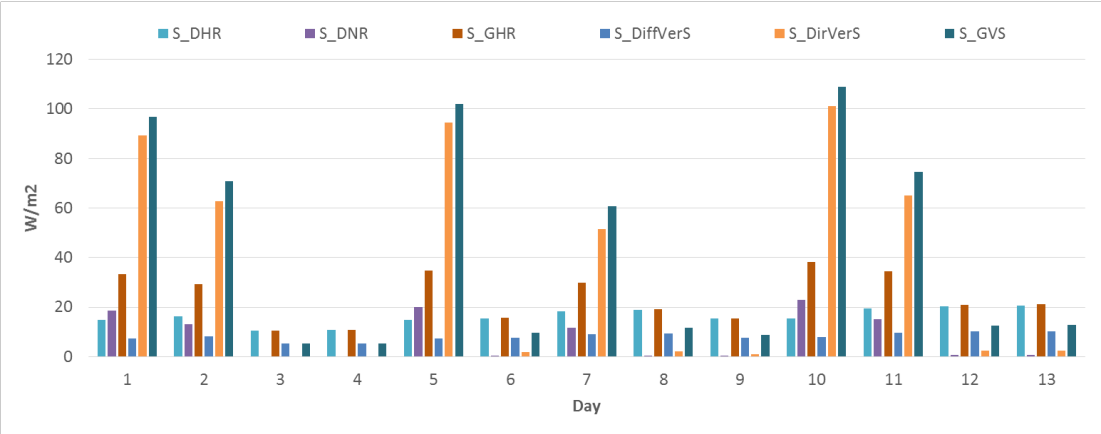

Figure 5.8: *Respective solar characteristics for days in figure 5.7.*

In figure 5.7, when the simulated co-heating test data is considered via a measurement of S_{GHR} the brighter days have only marginally higher measured solar radiation than the previous duller group, despite much higher reductions in Q_{elec}. When S_{GVS} is used this second group have considerably higher measured S, accounting for the higher reduction in Q_{elec}. The difference is most apparent when examining the different solar characteristics of these days, figure 5.8. Clearly, days 1, 2, 5, 7, 10 and 11 show significantly higher measured direct normal solar radiation, captured in measurements of S_{GVS} but not within S_{GHR}.

Measured horizontally, S_{GHR}, transforms direct gains into to a horizontal component. Particularly in the winter when the sun's position in the sky is low, S_{DirHor} is then similar in magnitude to the diffuse horizontal component, S_{DHR}. This means the measured value of S_{GHR} gives little weighting to the direct gains entering through the vertically aligned glazed elements. Conversely, S_{GVS}, gives far higher weighting to direct radiation incident in a vertical plane.

The result of this is that on overcast days, when large amounts of solar radiation is diffuse, both measurements give similar daily results (see 5.7) from similarly positioned data points. However, on sunny days, horizontal measurements are unable to fully appreciate the increase in direct gains. The result of this is the higher estimate of both *R* and the *HLC*, as seen in figures 5.3 and 5.4 and later in figures 5.12 and 5.13.

An east-west orientated dwelling

In east-west orientated test dwellings the majority of the total solar gains are split across two facades, neither of which is south facing. A number of observations can be made:

- As direct gains are reduced, S_{GHR}, shows improved correlation with the actual solar gains, now better representing the system and providing more accurate *HLC* estimates.
- In this case, S_{GVM} provides the most reliable *HLC* estimates (figures 5.4 and 5.6, table 5.1).
- East or west orientated solar measurements, S_{GVE} and S_{GVW}, provide improved *HLC* estimates in comparison to a south-facing measurement.
- In the example shown, east facing solar radiation measurements (with 7.4 m^2 of east facing glazing) provide marginally improved results to a west orientation with less glazing (5.7 m^2).
- Here, using a weighted mean, S_{GVWM}, or taking the mean of the east and west solar radiation, S_{GVEW}, does not provide any improvement upon the use of a single east facing measurement.

Clearly, without a dominant orientation in which gains are received, the choice of measured *S* is less obvious.

5.2.2.2 Evidence from field data

On a limited number of occasions field measurements have had access to both S_{GHR} and S_{GVP}. This was for repeated tests on CASE-A1, a northeast (9 m^2) - southwest (5.7 m^2) orientated dwelling and a number of periods in NHBC field trial, allowing the evaluation of the two test houses.

Table 5.2: Comparison of types measured solar radiation on field *HLC* and *R* estimates. Error estimates based upon 1 standard error. Both t-values and p-values are included as statistical tests of the inclusion of the respective solar radiation terms in regression[3]. (MLR-2w-24h-6agg)

Test Case				HLC	R	t value	P value (>|t|)	Mean S & s.d. (W/m^2)	Numerical R (m^2)
Case A1	*March*		S_{GHR}	143 ± 4 W/K	2.1 ± 1.4 m^2	-1.5	0.17	60 ± 26	3.0
			S_{GVSW}	143 ± 3 W/K	3.7 ± 1.5 m^2	-2.4	0.038*	37 ± 26	4.0
NHBC	*February*	*Test House*	S_{GHR}	73 ± 4 W/K	3.8 ± 1.4 m^2	-2.72	0.019*	62 ± 24	3.1
			S_{GVSSE}	69 ± 3 W/K	1.7 ± 0.6 m^2	-2.92	0.014*	82 ± 55	3.1
		Control	S_{GHR}	71 ± 5 W/K	4.6 ± 1.6 m^2	-2.9	0.013*	62 ± 24	3.0
			S_{GVSSE}	68 ± 2 W/K	2.7 ± 0.4 m^2	6.5	4.5e-5*	82 ± 55	3.1
	March	*Test House*	S_{GHR}	52 ± 8 W/K	1.1 ± 0.8 m^2	-1.4	0.203	166 ± 35	2.6
			S_{GVSSE}	44 ± 4 W/K	0.6 ± 0.8 m^2	-0.78	0.448	95 ± 50	3.4
			S_{GVNNW}	47 ± 6 W/K	2.6 ± 2.9 m^2	-0.927	0.372	34 ± 10	-
		Control	S_{GHR}	54 ± 6 W/K	2.2 ± 0.5 m^2	-4.1	0.002	166 ± 35	2.6
			S_{GVSSE}	31 ± 4 W/K	0.2 ± 0.8 m^2	0.2	0.845	95 ± 50	3.4
			S_{GVNNW}	34 ± 7 W/K	1.3 ± 3 m^2	-0.413	0.687	34 ± 10	-

In the case of the CASE-A1 test, there is no difference in the *HLC* estimates from the two measured solar approaches. This might be expected across a test period that was largely overcast, with solar gains estimated to be a very small percentage of Q_{elec} (SOLR= 0.04). However, even when a similar HLC_{meas} is obtained, the value of *R* varies through the use of either S_{GHR} (2.1 m^2) or S_{GVSW} (3.7 m^2). Here, it must be remembered that the definition, and therefore value, or *R* is dependent upon the measurement of *S* (see section 3.4.4). The difficulty in interpreting such parameters should be clear, particularly given their dynamic values.

In the February NHBC tests, S_{GHR} produces a marginally higher *HLC* ($\sim$ 3-4 W/K, SOLR = 0.14), an offset that increases ($\sim$ 20 - 23 W/K) in tests performed in a significantly sunnier March period (SOLR $\sim$ 0.30 - 0.42). Clearly, and as would be expected, the impact of the form measured solar radiation increases as the proportion of solar gains and the SOLR increases. The general trend towards lower *HLC* estimates in March is considered in chapter 5.4.

[3]The p-value for each independent regression term tests the null hypothesis that the coefficient is equal to zero, i.e. has no effect on the dependent variable. A low p-value (< 0.05) indicates you can reject this null hypothesis and the term is likely to be a meaningful addition to the regression model. Conversely, a high p-value suggests the predictor is not associated with changes in the response.

Interestingly, this overestimate using S_{GHR}, can mean that in periods when we expect an underestimate from other sources (i.e. section 5.4), an apparently more accurate *HLC* can be retrieved. The right answer from the wrong method so to speak.

5.2.3 Interactions with weather & building type

5.2.3.1 Interactions with test weather

As previously seen, and as with all solar driven sources of uncertainty, the scale of any errors associated with measured solar radiation is likely to be larger in sunnier periods and when solar gains represent a larger fraction of the total heat input or SOLR. Considering the sun's position, a horizontal solar measurement might be least appropriate in mid winter, although this may be mitigated by such periods having minimal solar radiation. An overestimate will only occur during sunny periods with significant proportions of direct solar radiation. Potentially the largest error exists in highly glazed south facing facades, in which S_{GHR} is measured.

Measuring S_{GVS} may create the largest uncertainty towards spring/autumn, as higher gains can be expected on east-west facades. Again, the distribution of glazing between these facades will dictate the uncertainty. In both cases, these solar generated errors will reduce relatively in test dwellings with lower glazed areas and higher overall *HLC*s.

5.2.3.2 Relationship to building type

The need to assess test dwellings on a case-by-case basis is perhaps not more evident than in this example of uncertainty. Identical buildings, under identical weather conditions, but with a different orientation would require different considerations when it comes to measuring *S*.

When the majority of solar gains are linked to one facade, then a single vertical measurement is likely to be most accurate. In cases in which there are multiple glazed facades, S_{GVM} or S_{GVP} maybe more suitable, although this results in a less clear definition of *R*.

5.2.4 Identifying the presence of uncertainty & estimating error

It is extremely difficult to assess uncertainty from the measurement of solar radiation without comparing multiple forms of measured solar radiation to gauge any uncertainty in a particular test dwelling and period of weather. Even then, it is impossible to fully establish the suitability of the measured form used. There are therefore significant risks that this form of uncertainty

goes unnoticed in otherwise well conducted tests, giving the impression of accurate results despite significant systematic bias. For example, in the NHBC field trial only a measurement of S_{GHR} is available across the full data set. This makes estimating the uncertainty across this period difficult as significant bias may occur undetected, as seen later in figure 9.5. Appropriate experimental set-up, analysis and documentation are therefore vital.

5.2.5 Addressing uncertainty from the measurement of *S*

To reduce this type of uncertainty appropriate solar radiation measurements should be taken, carefully considering the distribution of glazing and the orientation of the test dwelling. In most cases, additional solar measurements are likely to improve the reliability of results. Either vertical solar radiation measurements on each glazed facade or measurements of direct and diffuse solar radiation, S_{DHR} & S_{DNR}, allowing these components to be calculated, should be adopted if possible. This is likely to increase the cost and time taken to set up a co-heating test.

5.2.5.1 Multiple solar terms

Incorporating multiple solar terms intro regression analysis , e.g. S_{GVE}, S_{GVW} etc. has been investigated in the past (see (Deconinck and Leunis, 2012)). Results from such an approach can be seen the appendix A.2.1. Negligible improvement or even degradation of *HLC* estimates are seen. Often, these solar components are likely to be highly covariant on a daily basis, particularly under overcast skies. Deconinck and Leunis (2012) found that in some simulated cases multiple solar terms provided more accurate *HLC* estimates, despite low solar regression coefficient p-values. Within field tests, the returned regression coefficients from such an approach were then found to be nonsensical, suggesting additional solar terms were not suitable as explanatory variables.

5.2.5.2 Weighted facades

Everett (1985) suggested a method in which facades were weighted by their respective glazing proportions (equation 3.31). This approach has again been investigated, with a weighted mean, S_{GVWM}, used in table 5.1 and figures 5.3 and 5.5. This has not found to be more appropriate than other approaches and in addition, as these weightings are based on audit descriptions, there is a chance they may actually introduce further uncertainty.

5.3 Determining solar gains - The estimation of *R*

The determination of solar gains equally depends upon the calculation of the parameter *R*. As stated, this can be achieved either through statistical analysis, using either MLR or Siviour regression, or through numerical calculations.

Each approach has its own challenges. Statistical estimation requires a mix in solar radiation, including bright and dull days. Numerically modelled values of *R* sidestep these demands on the available weather but are susceptible to the equations adopted and their assumptions which describe complex geometry and varying material properties. Additionally, numerical estimates of solar gains require that accurate absolute value(s) of *S* are used rather than simply relying on the statistical correlation. The two approaches can therefore be considered separately.

5.3.1 Uncertainty using a statistically derived *R*

As noted, statistically estimating the solar aperture is dependent upon the range in solar radiation across a measurement period, the mix between sunny and dull days. Whilst strictly overcast, dull days tend to provide a strong basis for *HLC* estimates they do not necessarily allow for accurate estimates of *R*. When trying to establish the relationship between solar radiation and heating power through regression, a range of data points is required. This relationship is illustrated in the two Siviour plots in figure 5.9.

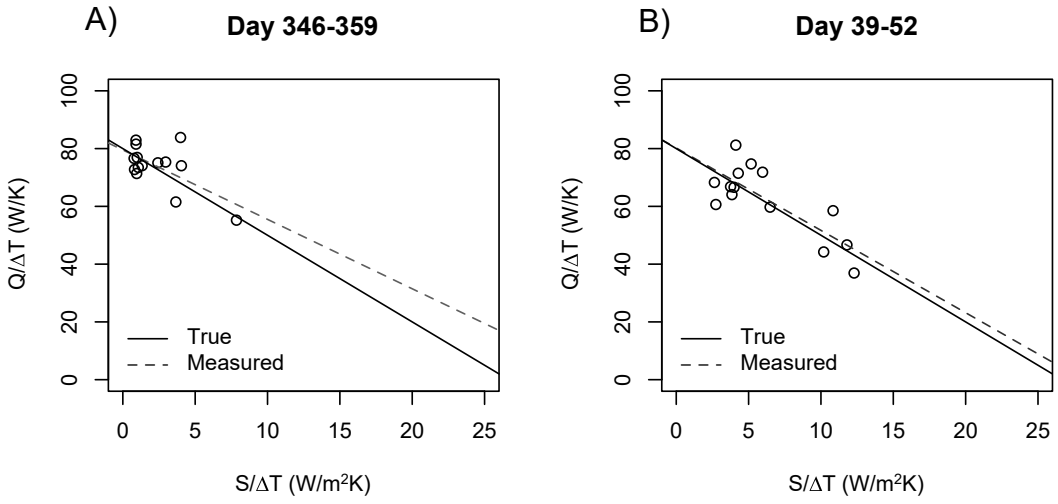

Figure 5.9: *Examples of Siviour regression and determination of the solar aperture. The figure on the left consists of only one non-dull day, a day that therefore has large influence over the estimation of R (see figure 9.11 and table 9.2). The right figure has more sunny days, reducing the propensity for error in the estimation of R.* (Modelled: Siviour-2w-24h-6agg-S_{GVS})

The range in solar radiation is then shown across the Finningley weather year, for both S_{GVS} and S_{GHR}, figure 5.10. There is a distinct difference as S_{GHR} increases into the summer months whilst S_{GVS}, relying on a mix between direct sunlight and overcast days, shows a higher range in early spring and autumn.

From a simple model (*HLC* = 80 W/K, R = 6 m^2), with an error term applied to Q_{elec} ($\pm$ 10% [4]) the estimated value of *R* for both MLR and Siviour analysis is shown across the heating season and across a full year in figure 5.10. The estimated value of *R* is compared to the range in *S* or (*S*/ ΔT) in each given test. It can be seen that the probability of estimating an accurate value of *R* increases as these ranges expand.

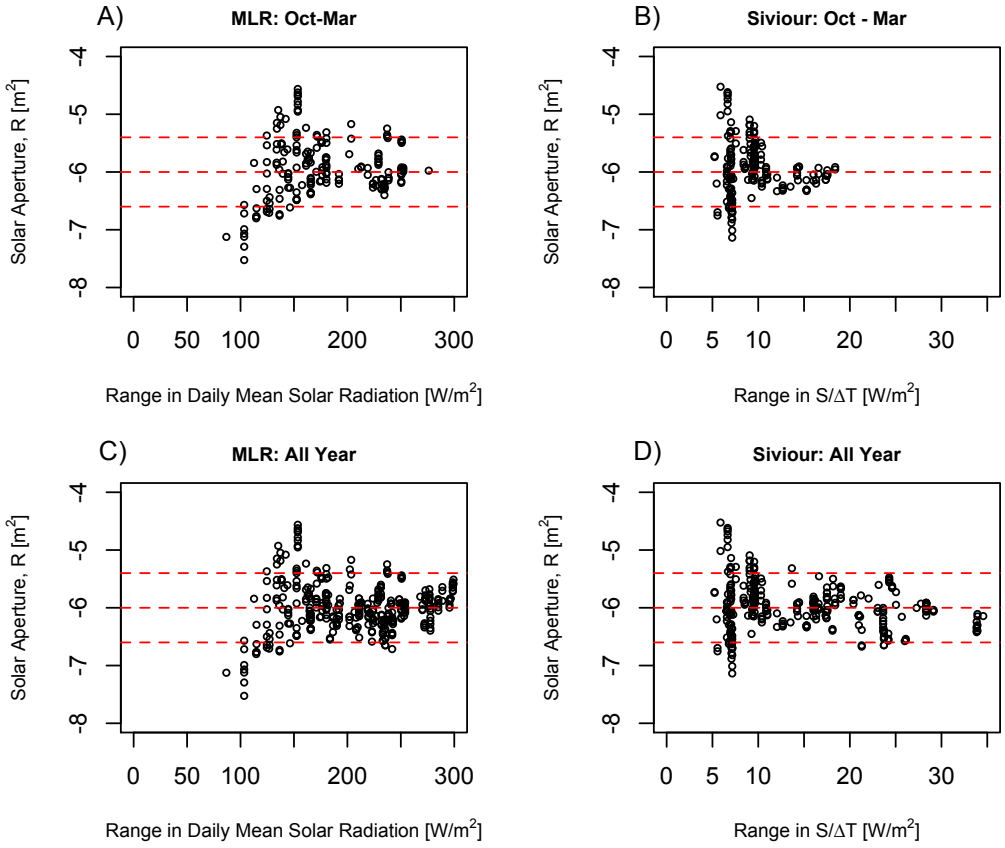

Figure 5.10: *Estimated value of R plotted against range in ΔT or (S/ΔT). Red lines indicate the value of R inputted into the model (6 m^2) and $\pm$ 10% bands about this.* *(Modelled: FINN-2w-24h-6agg-S_{GVS})*

[4] Standard deviation = 10% of Q_{elec}.

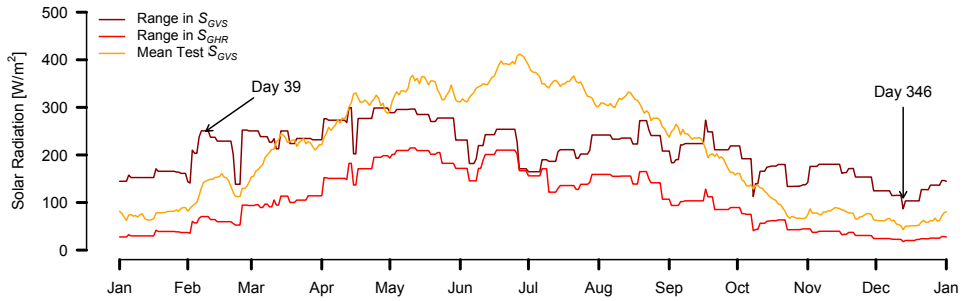

Figure 5.11: *Mean solar radiation and range in daily solar for 2 week tests. Finningley TMY weather file. Data sets from figure 5.9 are identified.*

In this exploratory example, more consistent estimates of R approximately correspond to ranges of $S >$150 W/m^2. The relationship between the range in solar radiation and estimates of R will depend upon the characteristics of the test dwelling and the scale of other uncertainties present. Everett (1985) and Lowe and Gibbons (1988) both set out criteria for a minimum range in daily solar radiation, i.e. that a number of dull (<42 W/m^2) and sunny (>125 W/m^2) days were needed to calculate the solar aperture (see section 9.1.5.1). The results of the analysis in figure 5.10 are broadly consistent with the criteria set out by both Everett (1985) and Lowe and Gibbons (1988).

With two-week test periods, such ranges can be achieved across large parts of the year, although this is very much a function of the test duration and the uncertainty in Q, ΔT and S. If an objective of test researchers is to determine an accurate estimate of R then long periods of data collection may be required. On a final note, if uncertainty in either S or ΔT are included in the previous model, then attenuation bias occurs, biasing the estimates of R. Attenuation bias is discussed in general terms in section 8.2, whilst examples corresponding to figure 5.10 can be seen in appendix (section A.2.2), along with similar examples exploring the required range in S using S_{GHR}.

5.3.2 Results for the statistical estimation of *R*

The estimated solar aperture and solar gains from full building simulations are shown in figures 5.12 and 5.13. Reasonable estimates can be achieved across large parts of this testing period, although underestimates are recorded when stored solar heating contributions and solar driven experimental overheating increase (e.g. early October and March).

Additional figures using S_{GVM} and S_{GHR} are shown in the appendix (A.2.3), further demonstrating the previous overestimated R and Q_{sol} from horizontally measured solar radiation.

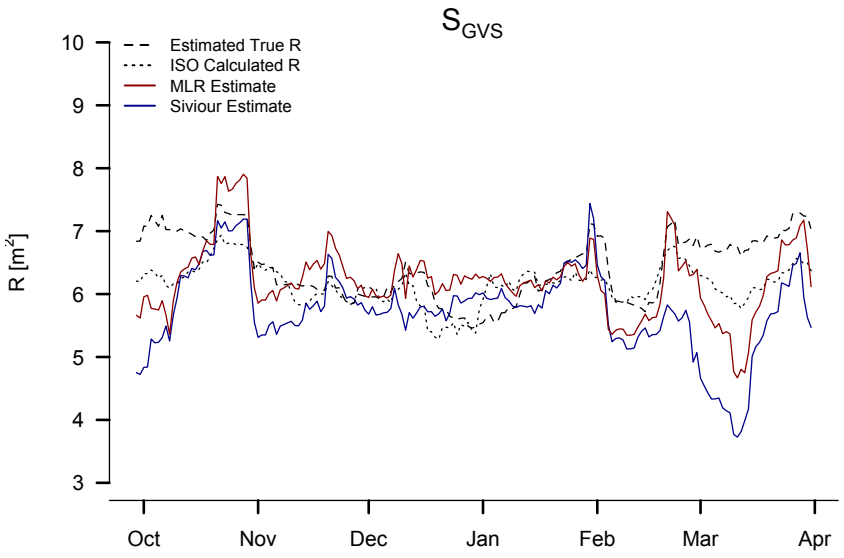

Figure 5.12: *Estimated solar aperture from MLR and Siviour analysis, using S_{GVS}.* (Simulation: BRE-NOT-SLW-FINN-SN-MLR-2w-24h-6agg-S_{GVS})

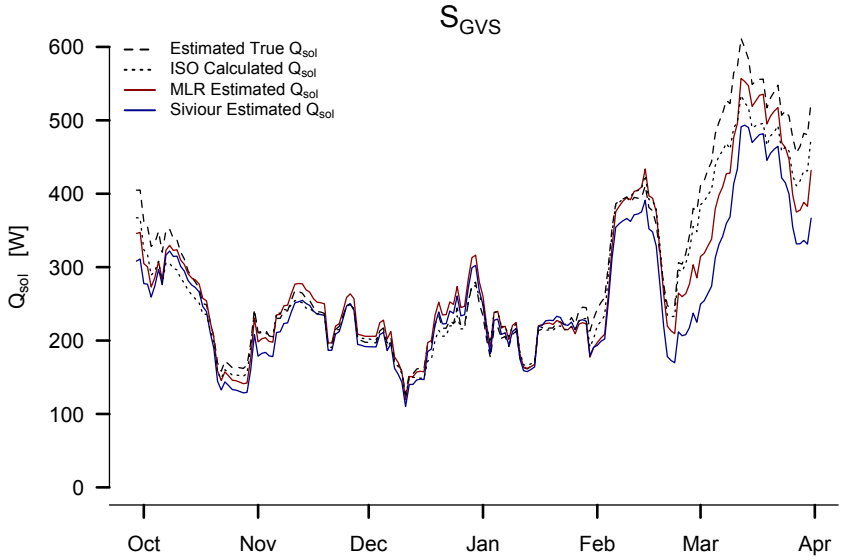

Figure 5.13: *Estimated solar gains from MLR and Siviour analysis, using S_{GVS}.* (Simulation: BRE-NOT-SLW-FINN-SN-MLR-2w-24h-6agg-S_{GVS})

5.3.3 Uncertainty using an numerically calculated *R*

Numerical solar apertures can be calculated according to ISO 13790:2008 (ISO, 2008), SAP (BRE, 2011; BRE, 2014) and PHPP (Feist, 2007) as discussed in full detail in section 3.3.1. The three methods give equations to calculate solar gains as follows:

ISO 13790:

$$Q_{sol,k} = F_{sh,ob,k} \cdot A_{sol,k} \cdot I_{sol,k} - F_{r,k} \cdot \phi_{r,k} \tag{5.3}$$

Where

$$A_{sol} = F_{sh,gl} \cdot g_{gl}(1 - F_F)A_{w,p} \tag{5.4}$$

and

$$A_{sol} = \alpha_{sol,c} \cdot R_{se} \cdot U_c \cdot A_c \tag{5.5}$$

SAP:

$$Q_{sol} = 0.9 \cdot A_w \cdot S \cdot g_{\perp} \cdot F_F \cdot Z \tag{5.6}$$

PHPP:

$$Q_{sol} = A_w \cdot S \cdot g_{\perp} \cdot RF \tag{5.7}$$

There are a number of uncertainties we can consider to be likely when adopting these equations. For example, SAP and PHPP equations ignore any opaque gains, albeit these are also in some part counteracted by the similarly ignored long wave radiation losses. The ISO calculation for an example test house (BRE-NOT-SLW-SN) would indicate $\sim$ 17% of the total solar contribution across the testing season comes through opaque gains (table 5.6). Ignoring these gain mechanisms is likely to lead to underestimated total solar contributions and therefore underestimating the total *HLC* by a similar amount as previously suggested by Liu and Claridge (1995) and Bauwens and Roels (2014). This contrasts to the previously considered statistical estimation of solar gains, in which any opaque contributions are incorporated through the regression of *S*.

Calculations of factors such as shading, solar access or dirt are bound to be complex leading to the adoption of arbitrary values with significant errors. Without complex solar simulations of shading devices and surrounding terrestrial objects, it is very difficult to accurately determine a shading or access factor. This is further complicated as any on-site measurement of solar radiation may incorporate a percentage of the total shading factor within the measured value(s)

of *S*. In an example from a field test conducted as part of this research, shading from scaffolding on a construction site was removed half way through the testing period. Such practical considerations cannot simply be dismissed when conducting fieldwork of this nature.

Even more simply, it is not uncommon to find that the windows that have been installed differ in size, location or product, from the specifications. This means that, in practice, window specifications, areas and frame fractions should be verified on site. EST (2008) recommend using a tool capable of measuring glazing and air gap thickness, such as a laser glass measurement gauge (e.g MerlinLazer, 2015). Such a device may be useful to reduce uncertainty in the properties of the installed glazed products, although not all glazing properties may be easily checked.

5.3.4 Impact upon a test dwelling

Tables 5.3, 5.4, 5.5 and 5.6 demonstrate calculations, including errors, for SAP and ISO calculated solar gains, Q_{sol}. Parameters are given approximated percentage errors, although there may be reasons why these can be significantly higher when taking into consideration the conversation above. The total error is then calculated via error propagation techniques (Taylor, 1997; JCGM, 2008a).

Table 5.3: SAP calculated solar aperture and gains. *Solar gains listed are the mean global vertical solar radiation incident on each orientation over the testing season.

SAP Calculation								
	0.9	**A_w (m^2)**	**S* (W/m^2)**	**g**	**FF**	**Z**	**R (m^2)**	**Q_{sol} (W)**
South	0.9	7.373	69.08	0.63	0.8	0.8	2.68	184.82
	1%	*5%*	*10%*	*5%*	*10%*	*20%*	*23%*	*26%*
North	0.9	5.67	35.96	0.63	0.8	0.8	2.06	73.99
	1%	*5%*	*20%*	*5%*	*10%*	*20%*	*23%*	*31%*
						Total	**4.73**	**258.81**
						+/-	1.11	79.81

Table 5.4: ISO calculated solar aperture and gains - glazed gains.

			$F_{sh,gl}$	**g_{gl}**	**1-FF**	**$A_{w,p}$ (m^2)**	**$A_{sol,k}$ (m^2)**
Glazed Elements	**S**	Estimated Value	1	0.567	0.8	7.37	3.34
		Uncertainty	*0%*	*5%*	*10%*	*5%*	*12%*
	N	Estimated Value	1	0.567	0.8	5.67	2.57
		Uncertainty	0%	5%	10%	5%	12%

Table 5.5: ISO calculated solar aperture and gains - opaque gains.

			α	R_{se} (m^2K/W)	U ($W/m^2/K$)	A_c (m^2)	$A_{sol,k}$ (m^2)
Opaque Elements	N	Estimated Value	0.9	0.04	0.18	31.312	0.20
		Uncertainty	10%	10%	20%	5%	25%
	S	Estimated Value	0.9	0.04	0.18	28.166	0.18
		Uncertainty	10%	10%	20%	5%	25%
	E	Estimated Value	0.9	0.04	0.18	28.072	0.18
		Uncertainty	10%	10%	20%	5%	25%
	W	Estimated Value	0.9	0.04	0.18	28.072	0.18
		Uncertainty	10%	10%	20%	5%	25%
	Roof	Estimated Value	0.9	0.04	0.18	42.37	0.27
		Uncertainty	10%	10%	20%	5%	25%

Table 5.6: ISO calculated solar aperture and gains - combined gains.

ISO Calculation													
		$F_{sh,ob,k}$		A_{sol} [m^2]		S* [W/m^2]		Q_{sol} [W]			R [m^2]		
		$F_{sh,ob,k}$	±	A_{sol}	±	S*	±	Q_{sol}	±	%	$F_{sh,ob,k}$ * A_{sol}	±	%
Glazed Elements	S	0.80	0.16	3.34	0.41	69.08	6.91	184.75	47.10	25.5%	2.67	0.58	21.5%
	N	0.80	0.16	2.57	0.31	35.96	7.19	73.99	22.80	30.8%	2.06	0.44	21.5%
Opaque Elements	S	0.80	0.16	0.18	0.05	69.08	6.91	10.09	3.60	35.7%	0.15	0.04	27.7%
	N	0.80	0.16	0.20	0.05	35.96	7.19	5.84	2.11	36.1%	0.16	0.04	25.1%
	E	0.80	0.16	0.18	0.05	52.64	10.53	7.66	2.89	37.7%	0.15	0.04	26.3%
	W	0.80	0.16	0.18	0.05	52.75	10.55	7.68	2.90	37.7%	0.15	0.04	26.3%
	Roof	0.80	0.16	0.27	0.07	107.57	21.51	23.63	8.92	37.7%	0.22	0.06	26.3%
						Quadratic Sum		**313.63**	**53.41**	**17.0%**	5.55	0.73	13.2%
						Arithmetic Sum		**313.63**	**90.32**	**28.8%**	5.55	1.23	22.2%

In both SAP and ISO calculations there is a large expected error in the estimated solar gains $\sim$13-22%, depending on whether the uncertainty is combined in quadrature or arithmetically[5]. Clearly, equivalent uncertainty will be incorporated into the *HLC* estimate, with the total uncertainty then a function of the ratio of the SOLR.

5.3.5 Impact upon *HLC* estimates

5.3.5.1 Fully Simulated Examples

The estimated *HLC*s from numerically calculated solar gains are shown across a full year in figure 5.14. This time data is shown across the full year as regression of $Q + R$. S vs ΔT works in instances of experimental overheating (Q_{elec}= 0 or $Q_{baseload}$), where MLR approaches are of little use. In the figure, the ISO *HLC* calculation is accompanied by maximum and minimum error bands, based on the percentage errors in tables 5.3, 5.4, 5.5 and 5.6.

[5]Here, the respective solar components from each orientation and glazed or opaque elements are combined additively. In cases of independent errors, a quadratic sum can be adopted (Taylor, 1997). However, if, for example, a single pyrometer was used and extrapolated to multiple orientations, or an inaccurate g-value used across all windows, then the errors are no longer independent and should be added arithmetically.

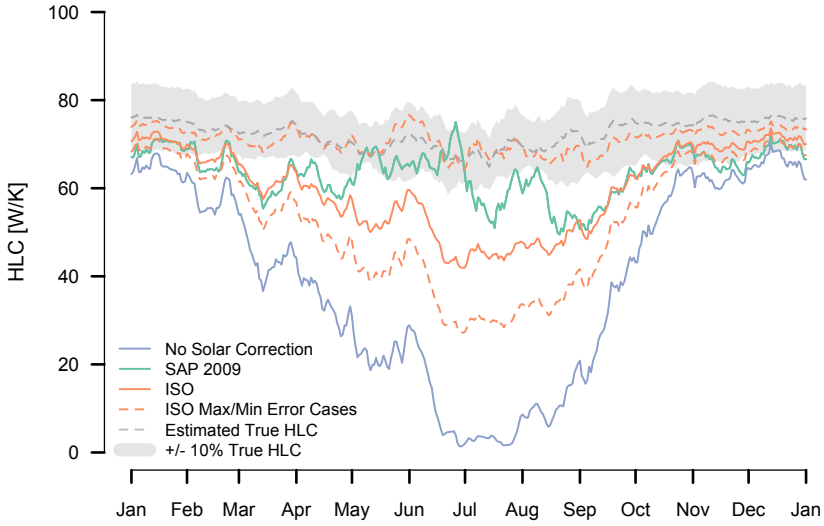

Figure 5.14: *Numerically modelled solar gains used to estimated HLC. Error applied to ISO calculation at 95% confidence intervals. A full year is plotted, demonstrating the effectiveness of numerically calculated solar gains outside of periods when a statistical approach is possible.* (BRE-NOT-SLW-FINN-SN-cSLR-2w-24h-6agg;S_{GVS})

As can be seen, the estimated range in *HLC* from the ISO calculation increases vastly as Q_{sol} becomes dominant. This means that outside of valid periods for MLR analysis, numerically calculated gains are unlikely to provide more accurate *HLC* estimates. During the period in which MLR can achieve satisfactory results, the numerical approach is unlikely to provide more accurate or robust results. Instead an offset error will likely exist dependent upon the assumptions made and how they differ from reality. It is therefore not thought that a numerical approach offers any advantages in the majority of cases, although comparisons between the numerical and statistically calculated *R* may be useful.

Additionally, the calculated Q_{sol} in the simulated test in figure 5.14 utilise solar radiation measured on all facades (i.e. north, south, east, west, horizontal). When considering the measurement of *S*, these may vary significantly from one another. In addition, local effects may mean the solar radiation received by two openings on the same orientation may receive differing incident radiation. Extrapolating from a single measurement to multiple orientations is likely to significantly increase the uncertainty in this approach. Therefore, multiple orientated solar radiation measurements are thought to be essential if numerical calculations are used. In addition, any calibration error associated with the pyranometer used will transfer an offset into the numerically calculated gains. Measuring devices therefore need to be suitably calibrated and uncertainty from calibration accounted for in *HLC* uncertainty statements (see section 9.4).

5.4 Stored solar heating contributions

In this section we can consider the uncertainty generated within *HLC* estimates from fractions of solar heat, absorbed on a given day but re-emitted by the building's thermal mass as useful gains on a subsequent day. These fractions can be referred to as *stored solar heating contributions* and can be shown to cause a systematic underestimation of the *HLC*.

Stored solar heating contributions carried forward to subsequent days will form an unregulated heat flow into the building under steady state analysis, which assumes daily aggregated data points to be independent of one another. This leads to an underestimation of the total heating power on the subsequent day and therefore of the *HLC*. The energy balance equation could potentially be restated as:

$$Q_i + R_1 S_i + R_2 S_{i-1} + R_3 S_{i-2} + ... + R_n S_{(i-(n-1))} = HLC \cdot \Delta T_i \tag{5.8}$$

Here, *i* denotes a given 24 hour aggregation period and R_1, R_2, and R_3 represent solar aperture values for the current, previous, and two day previous days, such that $R_2 S_{i-1}$ represents the stored solar heating contribution from the previous day/ aggregation period. This can be taken back *n* days, but as is shown in figure 5.16 and table 5.7; fractions stored beyond the third day are typically negligible but included here for completeness.

In addition, the time varying T_e will cause similar lags across hourly periods, potentially extending between days. This issue is explored separately in section 6.2.

The presence of stored solar contributions has been noted by Everett (1985) and Lowe and Gibbons (1988) and in the most recent LBU protocol (Johnston et al., 2013), which states that solar heating contributions re-emitted the next day need to be considered in analysis. However, it is not stated how these may impact a *HLC* estimate or how they can be considered within the analysis. This section aims to clearly demonstrate the nature of this uncertainty, its scale and interaction with both the prevailing weather conditions and characteristics of test dwellings.

5.4.1 The impact upon a test dwelling

The impact of solar radiation on a test dwelling and the lag between measured solar input and its full heating contribution is explored in this section. A *dull*, *medium* and *sunny* day of solar radiation are used as input for a simulated test dwelling in steady state conditions with T_e = 5 $^{\circ}$C. These solar inputs are taken from days with similar statistics to the respective lower (0.4

kWhm^{2}d^{-1}), median (2.4 kWhm^{2}d^{-1}) and upper quartiles (3.4 kWhm^{2}d^{-1}) of the Finningley weather file and correspond to definitions used throughout this thesis[6]. Alternatively, these can be viewed in terms of their daily calculated SOLR (section 3.4.6), corresponding to SOLR = 0.1, 0.46 and 0.71 respectively. The response in required electrical heating power Q_{elec} is seen in lightweight (LW), mediumweight (MW) and heavyweight (HW) constructions of the same form (BRE-NOT-SN).

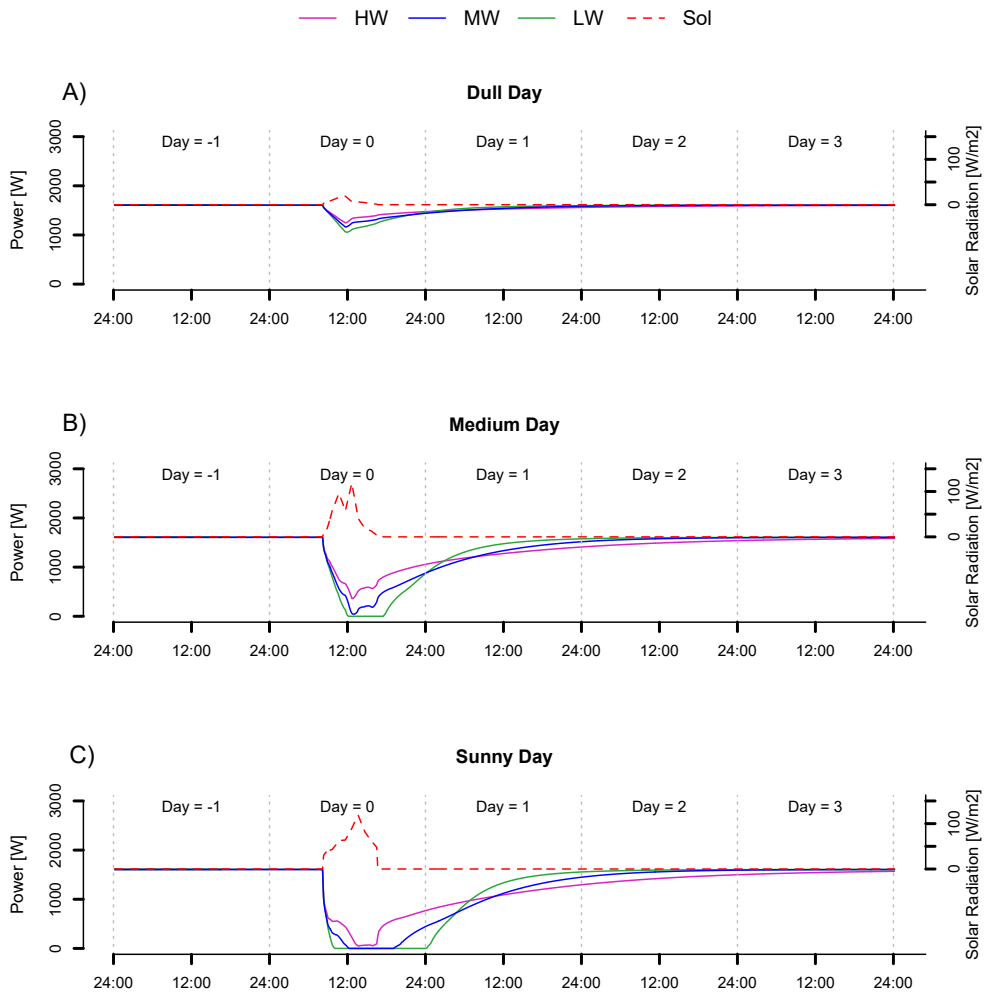

Figure 5.15: *Building response to a dull, medium and sunny solar input. Buildings are under steady state co-heating conditions with an internal temperature of 25 °C and a constant external temperature of 5 °C.* (Simulation: BRE-NOT-SN)

[6]These also correspond to the criteria of dull <1 kWhm^{-2}, medium >1 kWhm^{2}d^{-1} & <3 kWhm^{2}d^{-1} and sunny >3 kWhm^{2}d^{-1} set out by Everett and Lowe & Gibbons, discussed in section 9.1.5.1

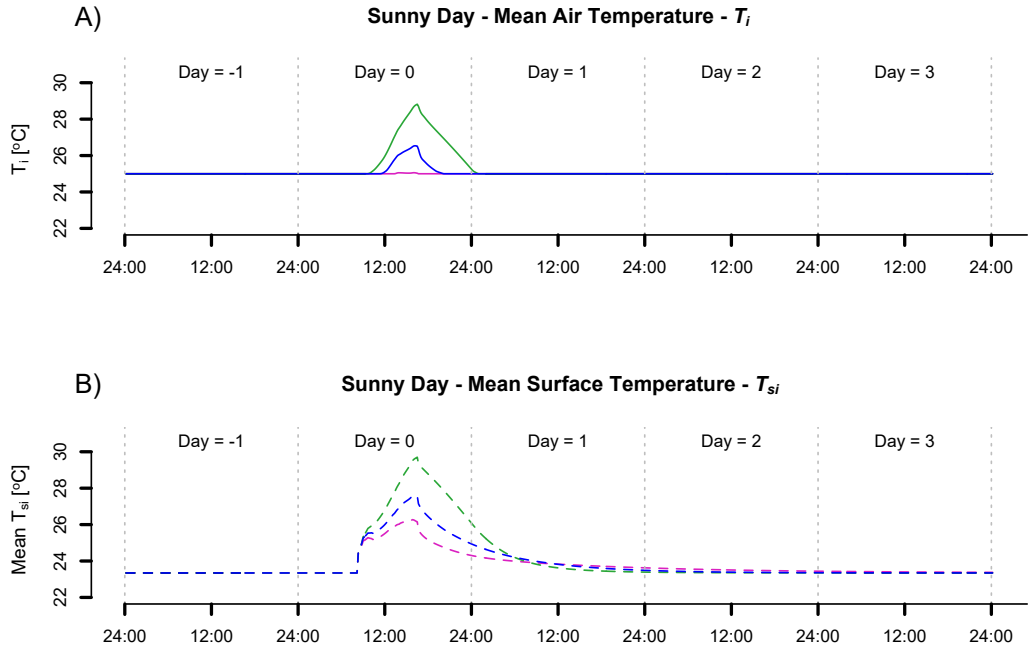

Figure 5.16: *Mean internal Air (T_i) and the average internal surface temperature of external walls (T_{si}) are shown for a simulated test dwelling on a sunny solar day.* (Simulation: BRE-NOT-SN)

Table 5.7: Heating power in simulated test dwelling resulting from various sized solar inputs. The solar input occurs on day 1, as seen in figure 5.15. Percentages indicate the heating power required relative to days in which no solar radiation is incident. (Simulation: BRE-NOT-SN)

		HEATING POWER [W]				
		Day -1	**Day 0**	**Day 1**	**Day 2**	**Day 3**
Dull	**HW**	1617 *(100%)*	1484 *(92%)*	1536 *(95%)*	1590 *(98%)*	1608 *(99%)*
	MW	1617 *(100%)*	1443 *(89%)*	1543 *(95%)*	1608 *(99%)*	1616 *(100%)*
	LW	1617 *(100%)*	1408 *(87%)*	1571 *(97%)*	1614 *(100%)*	1617 *(100%)*
Medium	**HW**	1617 *(100%)*	1089 *(67%)*	1274 *(79%)*	1496 *(92%)*	1575 *(97%)*
	MW	1617 *(100%)*	921 *(56%)*	1302 *(80%)*	1582 *(98%)*	1614 *(100%)*
	LW	1617 *(100%)*	788 *(49%)*	1413 *(87%)*	1606 *(99%)*	1616 *(100%)*
Sunny	**HW**	1617 *(100%)*	854 *(53%)*	1083 *(67%)*	1426 *(88%)*	1551 *(96%)*
	MW	1617 *(100%)*	653 *(40%)*	1068 *(66%)*	1558 *(96%)*	1612 *(100%)*
	LW	1617 *(100%)*	576 *(36%)*	1160 *(72%)*	1600 *(99%)*	1616 *(100%)*

Figure 5.15 shows how the electrical heating power, Q_{elec}, reduces as the incident solar radiation is received by the test dwellings. The reduction is large on the day of the solar input, although in theory this will be corrected using either numerical solar corrections or regression analysis methods. However, the impact of the solar radiation clearly lasts longer than this input signal, with a significant proportion of the subsequent day's heating power also reduced. This is dependent upon the thermal mass of the test dwelling and the size of the solar input, with the precise shape of the response function a result of the internal mass and its distribution within

the dwelling. Whilst there is little reduction from a dull day, for days following medium or sunny days there is a significant stored heating contribution, ranging from 13-21% following a medium day and 28-33% following a sunny day. This would result in a similar underestimate of required heating power and therefore heat loss on these days.

A second key concept here is that a fraction of a building's response to a solar input becomes disassociated from the measured solar input. Regression relates the measured solar radiation to the heating contribution supplied to the building only within the same aggregated period. The further these two become disassociated, the less accurately the derived solar aperture describes the system. The impact of the stored solar heating contribution and its disassociation with the measured *S* within the regression model will then also depend upon the solar radiation received in the subsequent day and the general distribution of daily data points and mix in weather. Both these issues allude to the benefits of performing dynamic methods of analysis.

5.4.1.1 Internal Air and Surface Temperatures

Figure 5.16 shows the internal temperatures during this period for a sunny day, further illustrating the problem. In the case of the sunny day, both the lightweight and mediumweight test dwellings experience periods of experimental overheating (i.e. $T_i > 25$ °C, see section 5.5)[7]. Whilst these internal air temperatures return to the experimental set point within the aggregation period (e.g. by 24:00) the average internal surface temperature does not.

In figure 5.16, the average internal surface temperature of external walls, T_{si}, initially sits at 23.3 °C, in equilibrium between T_i and T_e. When solar radiation is received by the building, T_{si} increases above this resting point and above the experimental set point. Note that this even occurs in the HW case, where T_i remains constant. The contribution to the subsequent day can then be understood from the tail into the subsequent 24 hour aggregation period, as the internal surfaces cool to the resting equilibrium temperature. It is important to note that this average T_{si} is a difficult parameter to measure in practice, as different surfaces within the building will warm and cool at different rates. However, measurements of T_{si}, where possible, throughout the dwelling may allow more subtle cases of stored solar contributions to be identified.

[7]Note here that this definition of overheating assumes that the electrical heating is controlled by a thermostat measuring the internal air temperature, rather than being influenced by any radiant surfaces

5.4.2 The impact upon *HLC* estimates

5.4.2.1 Stored Solar Contributions in a Simple Model

Initially, the effect on *HLC* estimates can be observed in a very simple model analysed through MLR and consisting of only a *HLC* (80 W/K) and a solar aperture R_1 (6 m^2). An extra solar term is then introduced, based on a secondary solar coefficient, R_2, related to the previous days solar radiation, S_{i-1}. The Finningley weather file is again used to provide inputs for ΔT and S. Figure 5.17 below shows the results with R_2 = 0 - 3 (m^2)[8].

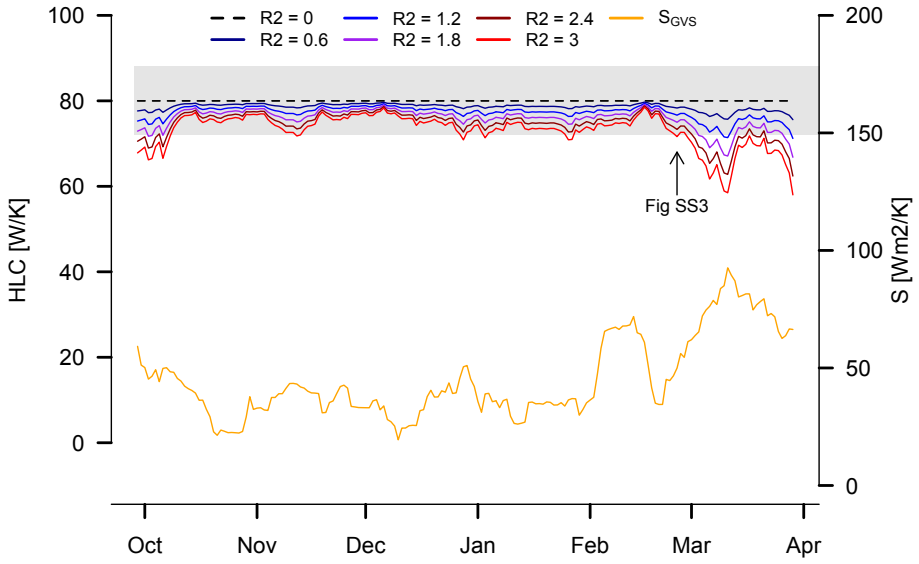

Figure 5.17: *Effect of stored solar contributions on HLC estimates.* (Modelled: FINN-MLR-2w-24h-6agg-S_{GVS})

It is clear that as soon as there is any fraction of stored solar energy, an underestimation of the *HLC* is seen, increasing with the stored fraction. Significant underestimation therefore occurs towards either end of the testing season (Oct & Mar).

[8]The values of R_2 used here are based on the reductions seen in day 1 in table 5.7.

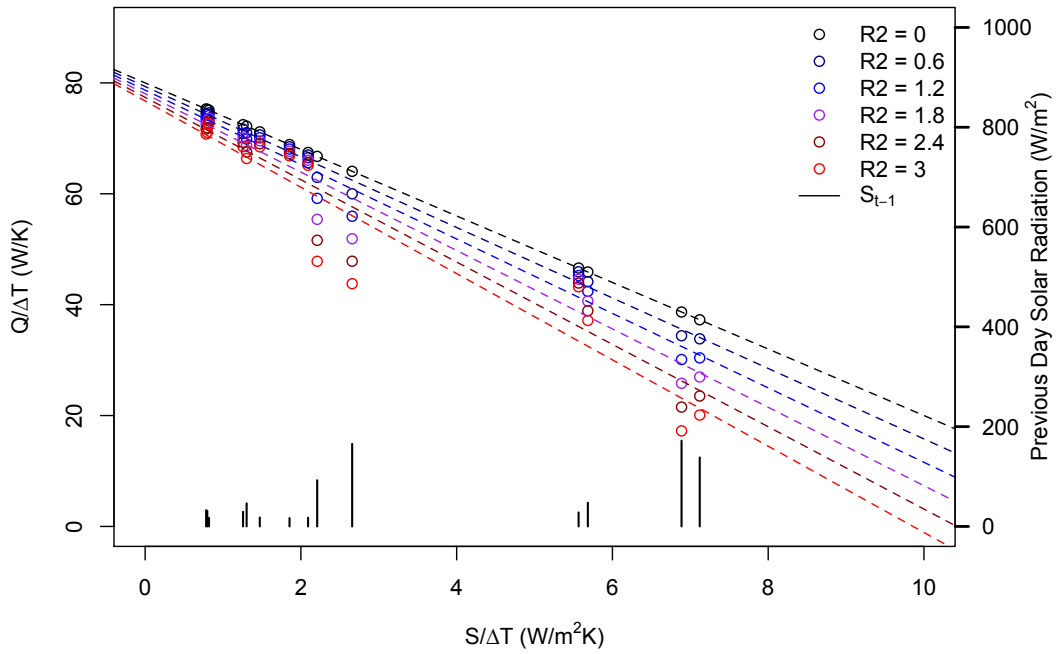

Figure 5.18: *Example of stored solar contributions reducing the subsequent day's power consumption and therefore HLC estimate.* (Modelled: FINN-MLR-2w-24h-6agg-S_{GVS})

A selected 2-week period is plotted in figure 5.18 and demonstrates how daily data points are affected by stored solar contributions. There is little impact on days preceded by dull days, but data points preceded by sunny days can be significantly affected. This figure also hints at the consideration that must be given to both the distribution of dull, medium and sunny days and their ordering. Days after sunny or even medium days can become unreliable, whereas days with preceding dull days do not significantly suffer from this type uncertainty. Noting the relationship between the distribution of data points and the estimation of parameters, we can consider two points:

- For an accurate *HLC* estimate, a significant proportion of dull days unaffected by stored solar contributions are required (i.e. with dull days preceding them).
- For accurate *R* estimations, a number of unaffected sunny days are required, again with dull days preceding them.

Similar criteria have been considered in the past in order to estimate when co-heating tests can be performed and how long they may require (Everett, 1985; Lowe and Gibbons, 1988). With more complete knowledge of the impact of stored solar heating contributions, and of other uncertainties, these issues are revisited in the context of the requirements and application of co-heating in sections 9.1 and 9.2.

5.4.3 Fully simulated examples of stored solar heating contributions

Now that the nature and direction of this uncertainty is understood it can be observed in full building simulations with full weather files. To explore the effect of thermal mass and glazing area a number of otherwise identical buildings are simulated across the same weather conditions (figure 5.19). The resulting mean *HLC*s from MLR are shown in table 5.8, along with the respective standard deviations. Across this entire October-March period, HLC_{True} is underestimated by between 3.4 - 14.6 W/K. However, if data in which short term overheating occurs (mean T_i >25.1 °C) is removed, this is reduced to just 1 - 10 W/K.

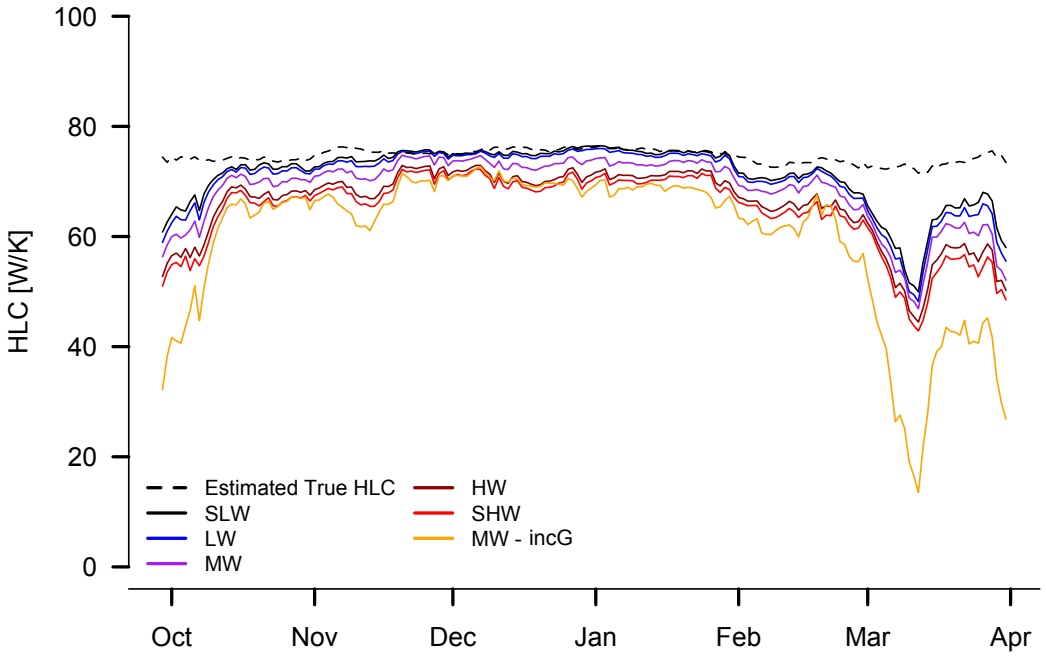

Figure 5.19: *Stored solar contributions in full building simulations. Six data sets are shown for an identical building (BRE-NOT), with varying thermal mass, e.g. super lightweight (SLW), lightweight (LW), medium weight (MW), heavyweight (HW), super heavyweight (SHW) and medium weight with increased glazing (MW - incG) - see section 4.4.3.1* Simulation: BRE-NOT-FINN-SN-MLR-2w-24h-GVS)

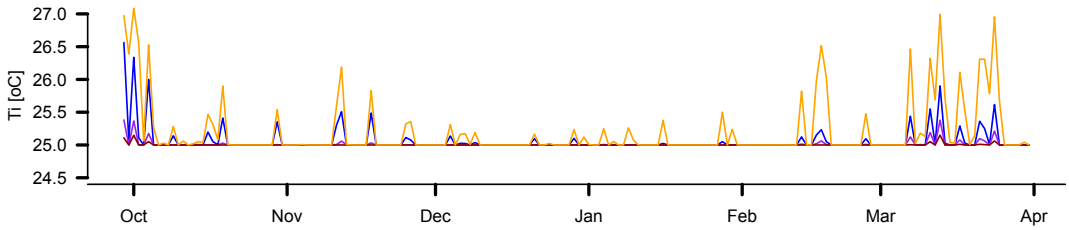

Figure 5.20: *Corresponding internal temperatures.*

Table 5.8: Corresponding mean *HLC* and standard deviation of results.

	October - March		**Excluding Mean Ti > 25.1**	
	HLC [W/K]	*s.d. [W/K]*	*HLC [W/K]*	*s.d. [W/K]*
HLC_{True}	74.6	1.2	74.6	1.2
SLW	71.2	5.5	73.7	2.4
LW	70.4	6.0	72.3	3.5
MW	68.6	6.3	68.6	6.3
HW	66.0	6.6	66.0	6.6
SHW	64.7	7.0	64.7	7.0
MW incG	60.0	13.2	67.7	2.0

A similar trend to the simple model can be observed and four conclusions derived:

- Test buildings with higher thermal mass consistently measure lower *HLC* despite the fact that HLC_{True} is identical for each.
- All buildings show higher probability of underestimating the *HLC* during sunnier, warmer periods.
- The test dwelling with a higher amount of glazing shows a higher consistent underestimate. It is also more sensitive to sunnier periods.
- Corresponding T_is in figure 5.20 show periods of greater underestimation, associated with rises in internal temperature, or periods of experimental overheating. Periods of stored solar contributions and of short term experimental overheating are strongly connected, as defined and discussed further in section 5.5.

5.4.4 Evidence in field data

The same trend can also be seen in field data, the most complete example of which is the NHBC field trial data. Figure 5.21 shows the familiar pattern of underestimated *HLC*s with increasing solar radiation; despite an unfortunate gap in data collected under the constraints of this project. Data shows the results from two twin test houses, with individual tests also shown (Butler and Dengel, 2013). Troughs in *HLC* estimates are often seen to correspond to peaks in mean solar radiation during each test.

Examining this effect in single test data sets is more challenging. Plotting previous days' solar radiation vs. daily *HLC* is one potential way of identifying this source of uncertainty (Stamp et al., 2013a). This is perhaps made clearer by assessing the variation in estimated *HLC* by shifting the aggregation interval. This method is discussed in more detail in figure 5.24. In table 5.9, section 5.4.7.1, four different aggregation intervals are assessed for the 9 case study dwellings. Minor shifts in estimated *HLC* are seen when shifting from 24:00-24:00 hour intervals to 06:00-06:00. This would indicate in 7 of the dwellings there are potentially stored solar effects.

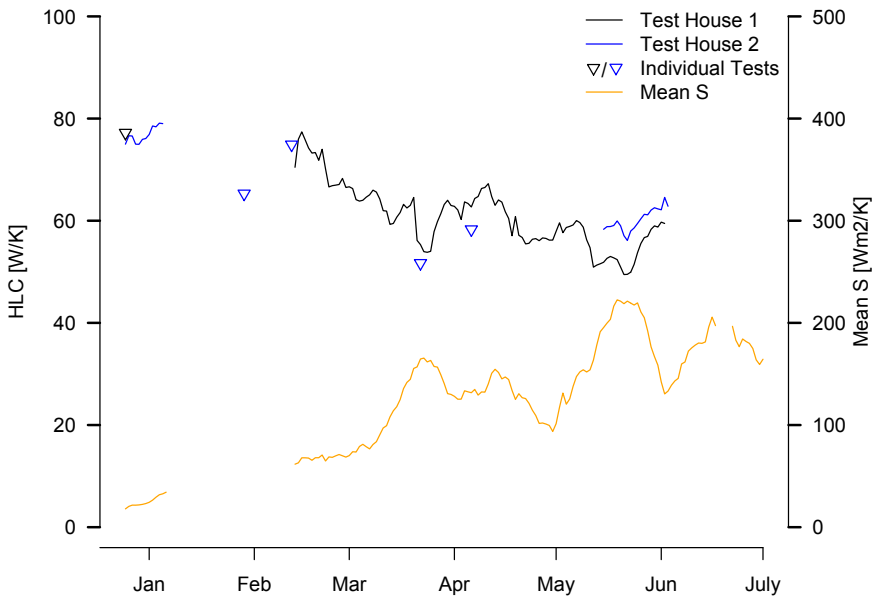

Figure 5.21: *Seasonal variation in NHBC field data HLC estimates.* *(MLR-2w-24agg-S_{GHR})*

5.4.5 Interactions with weather

The limit of when stored solar heat begins to significantly underestimate the *HLC* depends very much on the nature of the building but this is also likely to coincide with short-term periods of overheating. As an approximate estimate, the MLR estimated *HLC* is compared to the mean test solar radiation (S_{GVS}), figure 5.22. To a first approximation the majority of results fall within 10% of the true value for all dwellings shown until mean solar radiations of 44 W/m^2. Beyond this point, the extent of the underestimate depends upon the thermal mass and glazing characteristics of the test dwelling - as seen in figure 5.22. This mean test solar radiation of 44 W/m^2 corresponds to the level earlier defined as a dull day, (<42 W/m^2, <1 kWhm^{-2}), although this point undoubtedly will shift as the building characteristics change and in particular short term overheating takes place.

Alternatively, figure 5.23 shows the discrepancy between HLC_{meas} and HLC_{True} for these dwellings, plotted against the mean SOLR across the test period. Again the underestimate appears to be a function of the SOLR, with increasing systematic error as the SOLR increases.

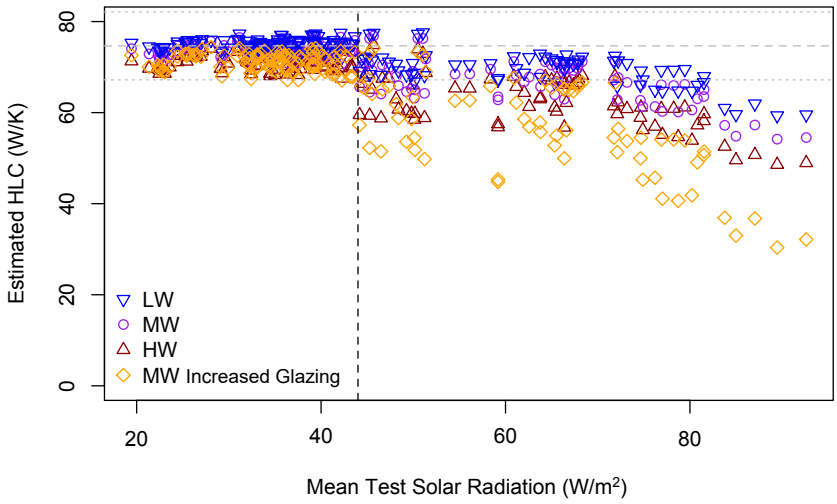

Figure 5.22: *MLR derived HLC and mean test solar radiation.* (Simulation: BRE-NOT-FINN-SN-MLR-2w-24h-24agg-S_{GVS})

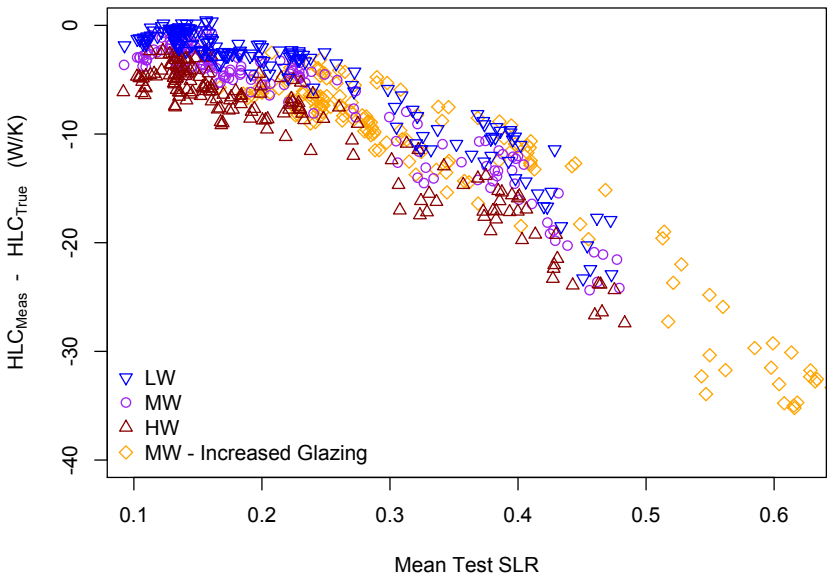

Figure 5.23: *Deviation between HLC_{meas} and HLC_{True} vs. mean test SOLR.* (Simulation: BRE-NOT-FINN-SN-MLR-2w-24h-24agg-S_{GVS})

5.4.6 Identifying the presence of uncertainty

A number of methods could be adopted to potentially show the presence of stored solar heating contributions and assess the likelihood of an underestimated *HLC*. Many of which are demonstrated in figures used in this discussion:

- Observe T_i to identify periods of short-term overheating (figures 5.16 and 5.20).
- Observe T_{si} (figure 5.16).
- Observe any heat flux sensor readings.
- Adjust aggregation interval (figure 5.24) and check for systematic changes in *HLC*.
- Increase aggregation length (figure 5.25) and check for systematic changes in *HLC*.

5.4.7 Addressing stored solar heating contributions

Beyond experimentally avoiding or limiting solar gains, there are a couple of subtle ways in which data can be analysed to reduce any stored solar contributions. By either shifting or extending the aggregation interval, the stored solar contributions can be better captured, and any trend towards underestimating the *HLC* reduced. An example is also included in which the previous day's solar is included as a regression variable, although little improvement is seen.

5.4.7.1 Adjusted aggregation interval

Referring back to the solar inputs in figure 5.15, one can imagine how if the aggregation interval was adjusted forward from 24:00 to 24:00 (e.g. to 06:00 to 06:00) the correlation between the lagged heating contribution and solar input signal would rise. This approach was noted as early as Everett (1985) but is not consistently adopted in tests (Deconinck and Leunis, 2012) with a variety of intervals used, including 12:00 - 12:00 and 18:00-18:00 (Butler and Dengel, 2013; Jack, 2015b), see also table 2.2.

Figure 5.24 demonstrates the MLR estimated *HLC* from four aggregation intervals across the day, and one set to match dawn to dawn for each test period. From figure 5.16, and reconsidering the solar inputs in figure 5.15, it can be understood that an aggregation interval that begins at the start of the solar input will incorporate the largest portion of the full resulting solar heat input. Whilst a dawn-dawn approach shows the best results here, improvements can be gained if the interval begins one or two hours after dawn (see section 9.3.2.4). Often the first few hours solar input is small and less important than capturing additional hours of lagged heat input. However, this might vary depending upon glazing orientation and cloud cover, such that a dawn-dawn aggregation may be the most robust approach.

Table 5.9 compares aggregation intervals for 9 field tests. In some cases, there is negligible difference between the four aggregation intervals analysed (e.g. CASE-C). However, in others the highest *HLC*s are typically obtained with 06:00-06:00 or 12:00-12:00 intervals, with the lowest estimates obtained using 18:00-18:00 (e.g. CAM-PH, CASE-A1, CASE-A2, NHBC, CASE-D). The fraction of stored solar heat, and therefore the size of any underestimate bias, changes across these different aggregation periods. Optimum aggregation intervals are discussed later in this thesis (section 9.3.2.4) but here it is important to recognise this means the method does not remain robust or reproducible across these variations in analysis. Consistency and clear report are crucial to avoiding any artificial bias from the analysis.

5.4.7.2 Increased aggregation period

An alternative approach would be to increase the length of the aggregation period, although this would need to be by 24 hour integer periods. There is however a direct trade-off between the length of aggregation period and either the number of available data points or the total length of the measurement regime.

In figure 5.25, the same simulated test data as figure 5.24 is analysed this time with different aggregation lengths (with the same total days of data). Moving towards longer aggregation lengths, the underestimate in *HLC* associated with stored solar contributions again decreases, particularly in the 3 day aggregation. It is important to note here that the start-end interval in figure 5.25 is 24:00-24:00. When a dawn-to-dawn or similar interval is used the improvement seen in longer aggregation lengths is reduced and vice versa. These issues are discussed further in section 9.3.2. Similar results with shifted aggregation intervals can be seen field data from the NHBC field trial in figure 5.26.

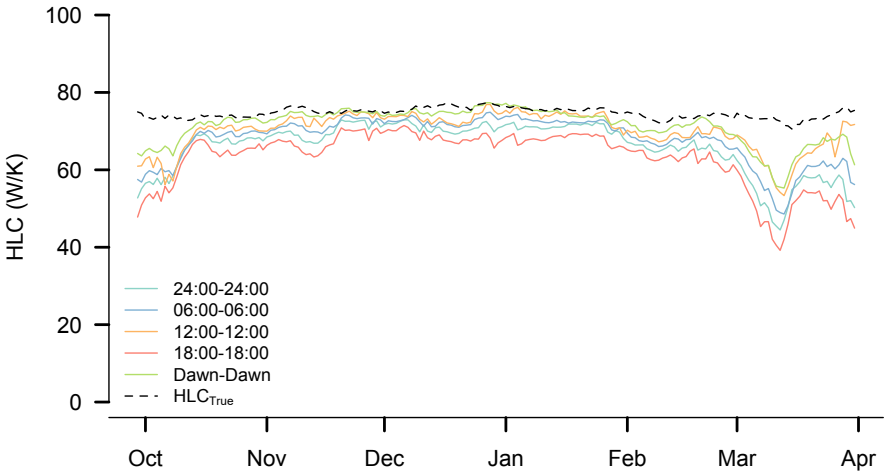

Figure 5.24: *Reducing underestimate from stored solar contributions due to various aggregation intervals.* (Simulation: BRE-NOT-HW-FINN-SN-MLR-2w-24h–S_{GVS})

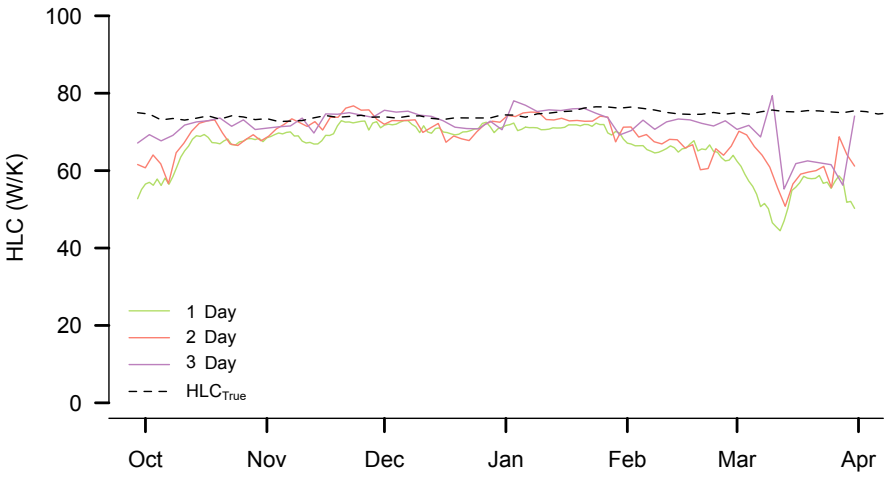

Figure 5.25: *Reducing underestimate from stored solar contributions using increased aggregation length.* (Simulation: BRE-NOT-FINN-SN-MLR-2w-24agg-S_{GVS})

Table 5.9: Field test estimated *HLC* s with various aggregation intervals. (Field Test: MLR-2w-24agg)

Case Study	Aggregation Interval	HLC Estimate (W/K)	Standard Error (W/K)	95% c.i. (W/K)	Glazed Area (m^2)	Mean Solar Radiation (W/m^2)
CAM-PH	24:00 - 24:00	55.9	1.9	3.8	38.8	5.4
	06:00 - 06:00	59.0	2.7	5.2		
	12:00 - 12:00	60.4	4.0	7.9		S_{GVS}
	18:00 - 18:00	52.7	11.4	22.3		
NHBC	24:00 - 24:00	67.4	2.9	5.7	13.2	82.0
	06:00 - 06:00	71.1	2.3	4.5		
	12:00 - 12:00	74.8	3.9	7.7		S_{GVS}
	18:00 - 18:00	64.3	4.9	9.6		
Case-A1	24:00 - 24:00	245.0	6.3	12.3	14.7	37.3
	06:00 - 06:00	247.2	7.0	13.6		
	12:00 - 12:00	241.7	6.9	13.6		S_{GVS}
	18:00 - 18:00	240.5	6.4	12.5		
Case-A2	24:00 - 24:00	143.3	3.0	5.9	14.7	37.1
	06:00 - 06:00	144.7	2.8	5.4		
	12:00 - 12:00	144.1	3.9	7.7		S_{GVS}
	18:00 - 18:00	142.7	4.0	7.7		
Case-B	24:00 - 24:00	243.0	7.0	13.6	48.2	92.6
	06:00 - 06:00	244.1	6.8	13.4		
	12:00 - 12:00	243.7	8.9	17.5		S_{GVS}
	18:00 - 18:00	241.0	7.7	15.0		
Case-C	24:00 - 24:00	125.4	2.6	5.1	26.9	12.8
	06:00 - 06:00	124.2	2.6	5.1		
	12:00 - 12:00	124.1	6.6	12.9		S_{GHR}
	18:00 - 18:00	127.4	6.2	12.1		
Case-D	24:00 - 24:00	108.1	10.1	10.7	-	67.9
	06:00 - 06:00	108.4	11.1	9.8		
	12:00 - 12:00	113.7	18.2	6.2		S_{GHR}
	18:00 - 18:00	100.5	11.5	8.8		
Case-E	24:00 - 24:00	149.0	1.9	3.7	-	42.2
	06:00 - 06:00	149.1	2.1	4.1		
	12:00 - 12:00	148.5	2.4	4.7		S_{GVS}
	18:00 - 18:00	148.1	2.3	4.6		
Case-F	24:00 - 24:00	127.0	2.4	4.6	-	42.2
	06:00 - 06:00	126.8	2.2	4.4		
	12:00 - 12:00	125.9	2.5	4.9		S_{GVS}
	18:00 - 18:00	125.9	2.3	4.5		

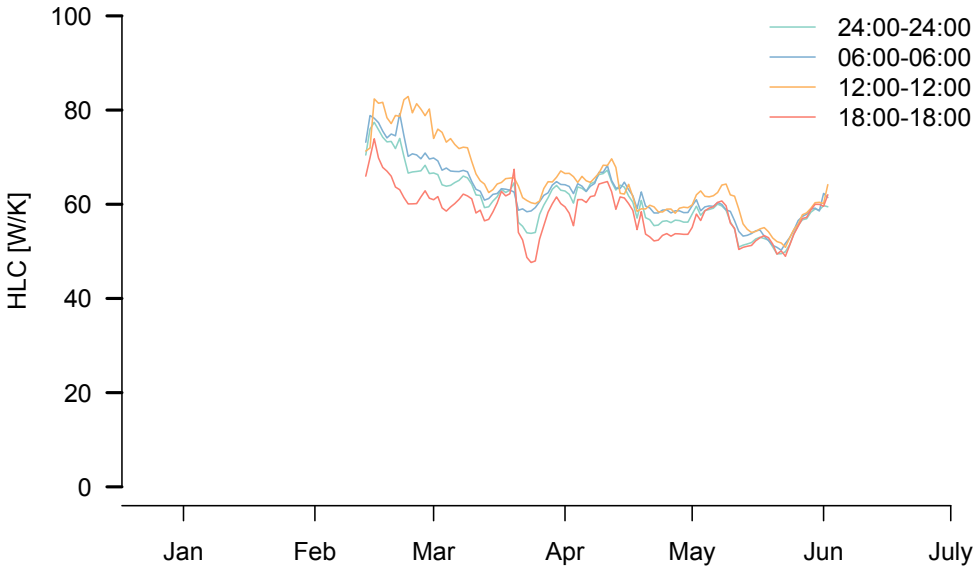

Figure 5.26: *Estimated HLC from NHBC field trial with varying aggregation intervals.* (Field Test: MLR-2w-24h-S_{GHR})

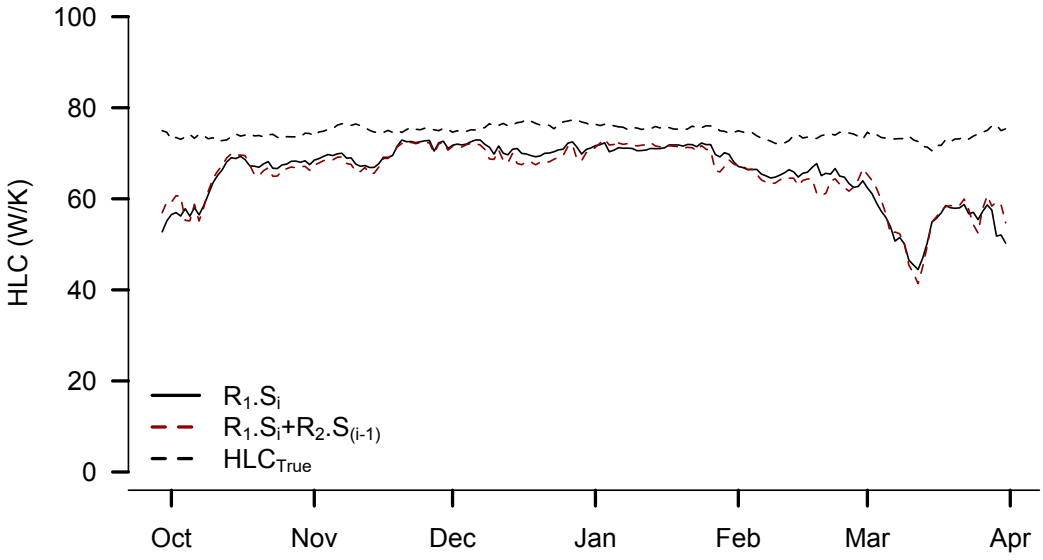

Figure 5.27: *Addressing stored solar contributions with a previous day's solar regression term.* (Simulation: BRE-NOT-FINN-SN-MLR-2w-24h-24agg-S_{GVS})

5.4.8 Additional regression variable

Finally, a further approach might be to include an additional regression variable for the previous day's solar radiation, adding the term $R_2 S_{i-1}$ to the traditional energy balance. A similar approach is suggested by Bauwens et al. (2011).

Figure 5.27 shows the traditionally MLR estimated *HLC* compared to MLR with a second solar term. Little difference is seen between the two, with the second solar regression variable not identified as significant. For example, MLR of a 2 week period gives R_2 a p-value of 0.66, whilst for R_1 the p-value = 0.000973, and R_2 has significant standard error in its estimation (R_2 = 0.3 $\pm$ 0.7 m^2). Furthermore, the relationship between Q_{elec} and the lagged solar term, $R_2 S_{i-1}$, would appear more strongly non-linear than Q_{elec} and $R_1 S_i$. This would suggest that estimates of R_2 and any corrections provided will be unreliable.

5.5 Solar driven experimental overheating

The third and final solar driven source of uncertainty concerns experimental overheating. The co-heating method assumes that a constant internal temperature is maintained in order to limit dynamic behaviour and allow the use of a steady state analysis. Although achieving this assumption is dependent on experimental technique and heating strategy, uncontrolled heat input from solar radiation is commonly the main driver of significant periods of non-constant internal temperature. High solar gains, particularly coupled with warm external temperatures, can cause the internal temperature to rise above the experimental set point. In such instances of *experimental overheating* the dynamic heat flows within the building are increased. Significantly these heat flows are not captured in the steady state energy balance or analysis, potentially resulting in large errors. Ultimately, this is a major limiting factor on when co-heating tests can be performed, particularly in low heat loss, highly glazed buildings.

5.5.1 The impact upon a test dwelling

Under quasi steady state conditions the internal air temperature is approximately constant and in approximate equilibrium with the internal mass it is in contact with. The thermal mass within the external envelope then sits at a lower temperature, reflecting its properties and the state of the internal and external environments. If too much heat input is supplied into the building, internal temperatures will rise. If this heat source is solar in nature then initially the temperature of some internal surfaces will increase; subsequently heating the internal air such that it rises above the experimental set point, switching off thermostatically controlled electric heaters.

During the warming phase, there are additional heat flows into the thermal mass of a test dwelling. Internal temperatures will continue to rise until the heat input is no longer sufficient

to increase or maintain internal temperatures. At this point, the building will begin to cool until internal air temperatures return to the experimental set point, $T_{setpoint}$.

As the building cools, the internal air, with a lower heat capacity, will cool quicker than the surrounding mass. Importantly, this means that whilst internal air temperatures may appear to have returned to the experimental set point temperature, the building's mass may still be warmer and still provide a heating contribution to the internal space. Here, the experimental overheating is associated with stored solar heating contributions and shows the same tendency to underestimate the *HLC* (section 5.4).

5.5.2 Types of experimental overheating

Periods in which the internal air temperature is above the experimental set point can thus be defined as instances of experimental overheating. The scale of any related uncertainty will depend on the extent of the overheating. It is quite common for brief overheating to occur around midday, following the peak in solar gains. This may occur just within single zones or throughout the entire dwelling (fig 5.30).

When experimental overheating does occur, the building may cool back down to the experimental set point after just a brief period, i.e. within the 24 hour aggregation period. The duration of overheating will then influence the depth and penetration of heat into the thermal mass of the dwelling, and hence the duration of the solar driven event. In more severe cases, experimental overheating will be such that internal temperatures do not cool to the experimental set point until a subsequent aggregation interval, severely effecting *HLC* estimates.

It is therefore useful to classify occurrences of experimental overheating, as the scale of the uncertainty generated varies with the extent of experimental overheating.

- In *short term* experimental overheating T_i may rise temporarily around midday before reducing back down to the experimental set point within the same 24 hour aggregation period, figure 5.28. This is often associated with stored solar heat (section 5.4).
- With high enough solar radiation there will be *long term* experimental overheating, in which the building does not cool back down to $T_{setpoint}$ by the end of the aggregation period. This will typically then last for successive days (see figure 5.29).

Figures 5.28 and 5.29 show examples of short term and long term overheating in 2 week simulated co-heating tests. In the short-term case, midday peaks in T_i can be associated with brief periods in which Q_{elec} = 0 or Q_{elec} = $Q_{baseload}$[9]. Essentially, periods of short term overheating will be associated with significant cases of stored solar contributions, operating and affecting *HLC* estimates in the same way.

In the long term overheating case, temperatures stay above 25 °C for extended periods of time, with entire days of data with Q_{elec} = $Q_{baseload}$. In such cases, when Q_{elec} is either zero or constant, no longer varying with ΔT and therefore regressing Q_{elec} vs. ΔT will not produce reliable *HLC* estimates - a co-heating test, along the lines set out in the experimental objectives, effectively no longer taking place.

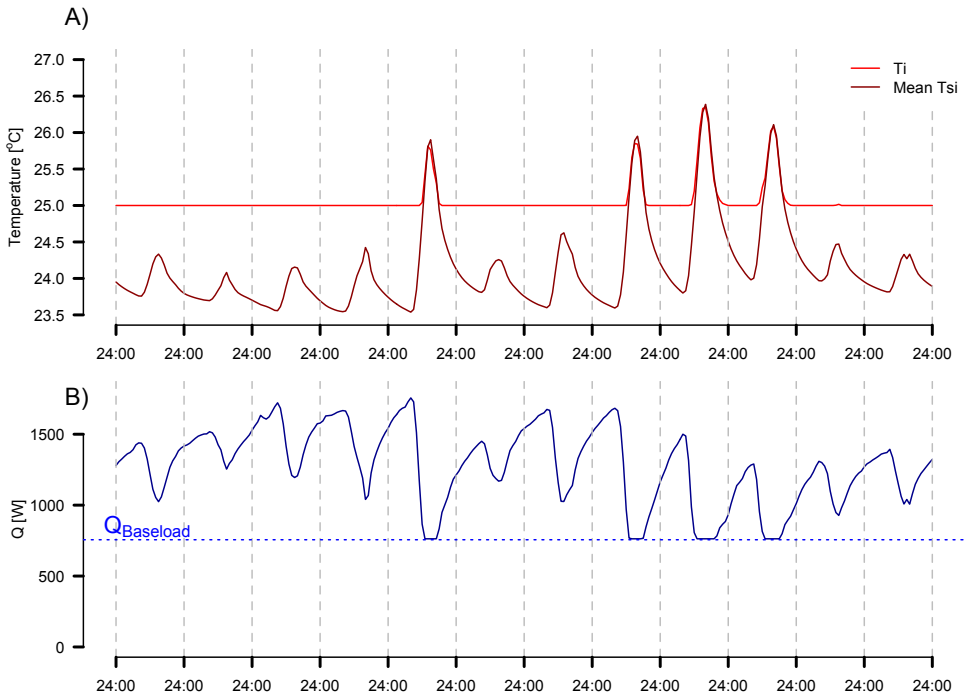

Figure 5.28: *Simulated co-heating data with evidence of short-term overheating. A base load of 750W or 9 W/m^{2}of floor area is applied based on the load during a field test of the same property.* (Simulation: BRE-NOT-MW-FINN-SN)

[9]i.e. non-thermostatically controlled equipment: loggers, mixing fans etc.

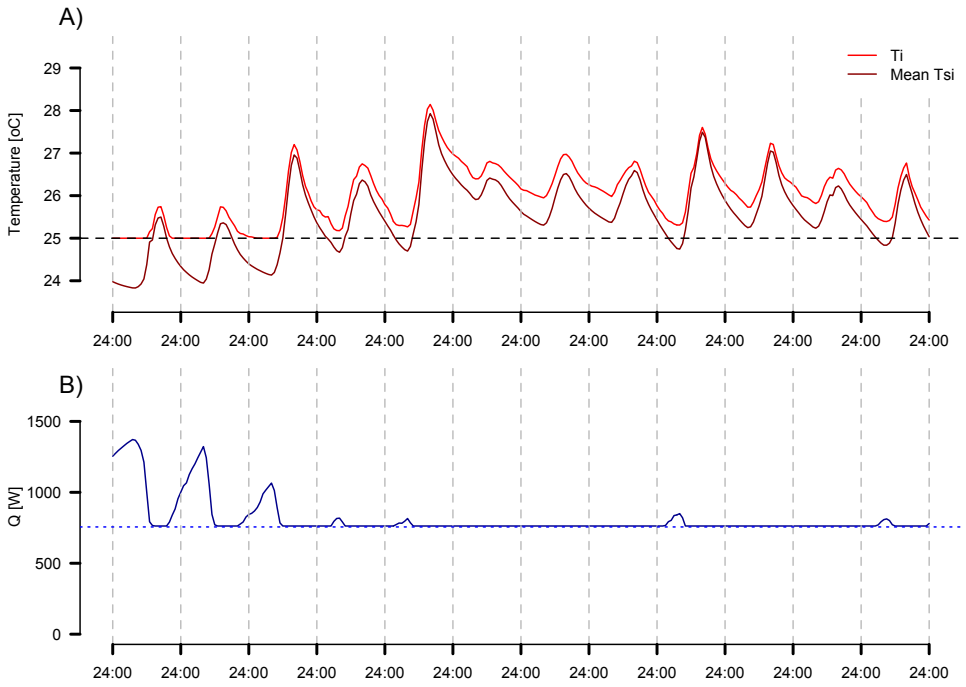

Figure 5.29: *Simulated co-heating data with example of long term overheating.* (Simulation: BRE-NOT-MW-FINN-SN)

However, the presence of multiple zones makes experimental overheating a less clear phenomenon in field data. Figures 5.30 show the same phenomenon but within the context of temperature sensors located throughout a dwelling. It should be clear that:

- The achieved $T_{setpoint}$ is harder to define and may from vary zone to zone due to equipment layout and calibration.
- Overheating may only occur in a fraction of zones.
- Zones will cool at different rates and across different timeframes.

To observe and identify occurrences of experimental overheating it is clear that the time resolution of such plots needs to be short, $\sim$1 hour or less, and that time series temperature measurements should not be spatially averaged. This is considered later in a section on reporting co-heating tests, section 9.3.3.

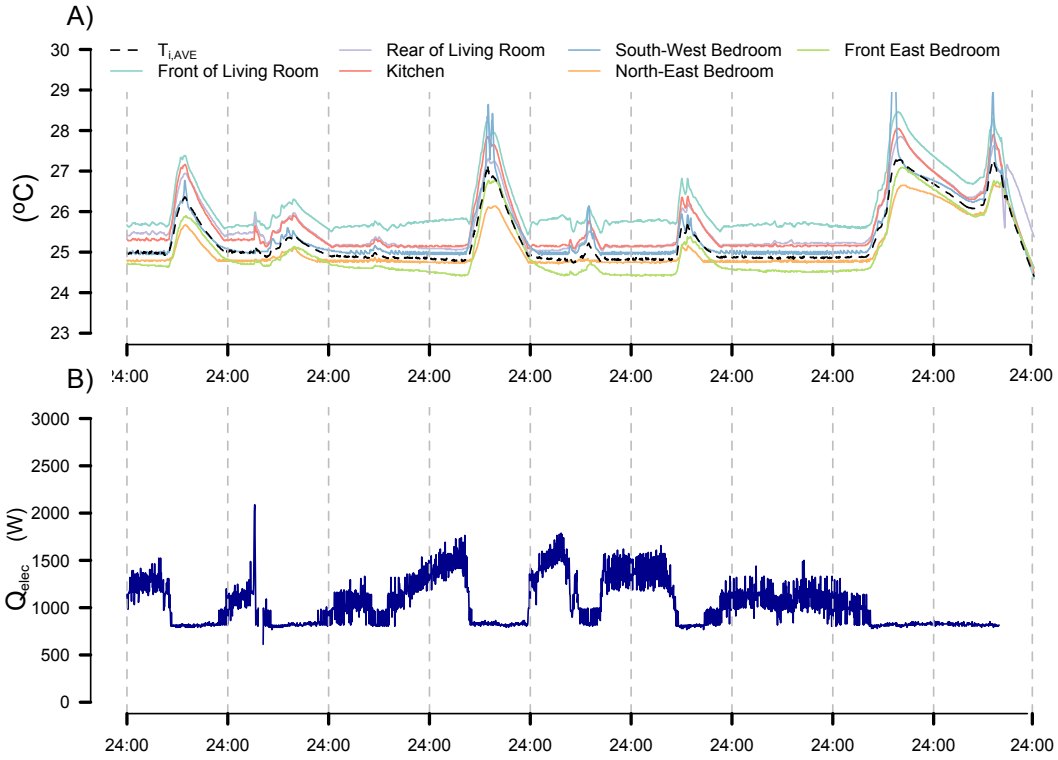

Figure 5.30: *Field test showing short and long term overheating. Short term overheating is seen throughout the test period, with an incidence of long term overheating occurring at the end. Floor plans and equipment positioning can be seen in appendix D.* (Field Test: NHBC)

5.5.3 The impact upon *HLC* estimates

5.5.3.1 Fully simulated examples

Figure 5.31 shows the estimated *HLC* from simulated co-heating tests, this time across a full year. The percentage of total hours and days, in which experimental overheating occurred, within each two-week test period are plotted in figures 5.31b and 5.31c respectively. Three periods can be identified:

- **No experimental overheating:** In which HLC_{meas} is relatively consistent and accurate (Mean HLC = 69 +/- 3 W/K standard deviation). The mean solar load ratio across this period gives SOLR = 0.16.

- **Short term overheating:** In which HLC_{meas} significantly underestimates HLC_{True} (Mean *HLC* = 43 +/- 12 W/K standard deviation). Mean SOLR = 0.54.

- **Long term overheating:** In which valid *HLC*s cannot be obtained. Mean SOLR = 0.95.

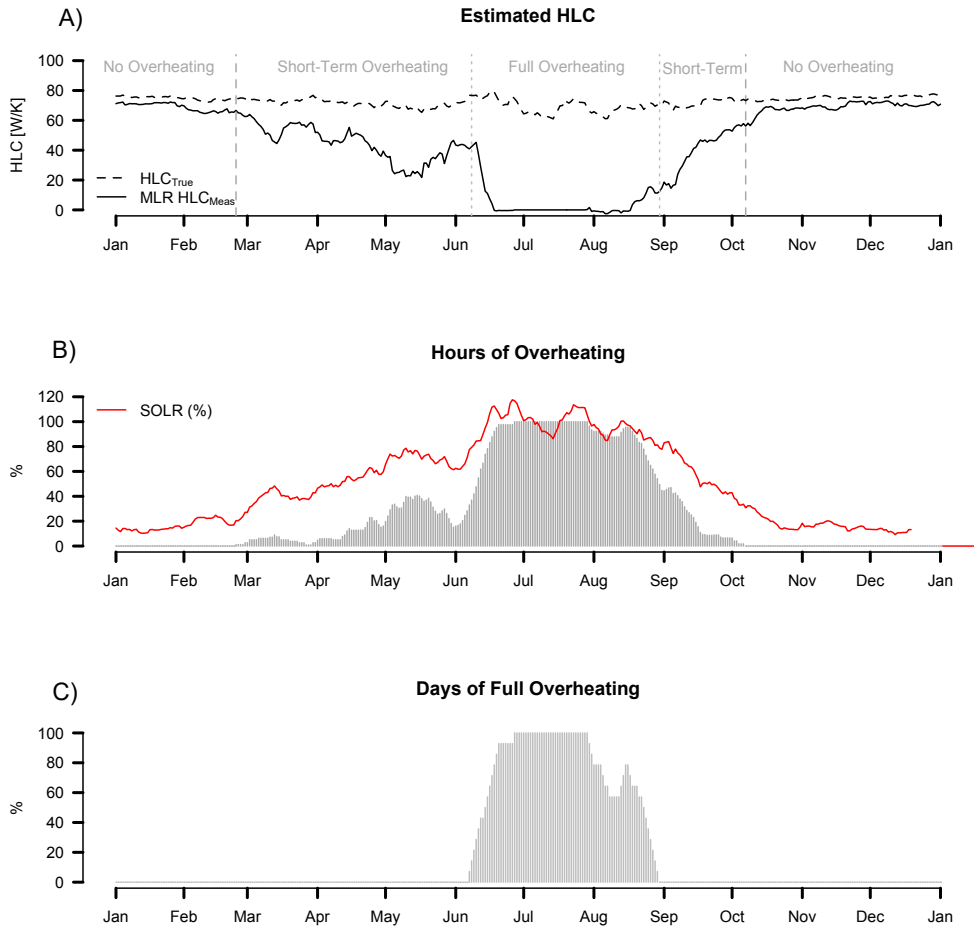

Figure 5.31: *Estimated HLC across a full year with hours of overheating and days of full overheating. The mean test SOLR is also included as a percentage.* (Simulation: BRE-NOT-HW-FINN-SN-MLR-2w-24h-24agg-S_{GVS})

5.5.4 Occurrences of experimental overheating

Experimental overheating will occur when solar gains provided to the building exceed the total heating requirement, most simply on an instantaneous basis when the SOLR or SBLR is greater than 1 (although this ultimately depends upon the thermal mass heat flows and the SOLR across longer periods of time):

$$SBLR = \frac{R \cdot S}{((\Delta T \cdot HLC) - Q_{baseload})} > 1 \tag{5.9}$$

This means a test dwelling is more likely to experimentally overheat, and will do so more severely when:

- *HLC* is low.
- *R* is high.

- $Q_{baseload}$ is high.
- S is high.
- ΔT is low i.e. T_e is high and/or T_i is low.

More completely, the thermal mass of a dwelling will influence the propensity for it to overheat and the duration of overheating. Table 5.10 shows the occurrences of both short and long term experimental overheating from simulated co-heating tests of a number of test dwellings. As can be seen, lightweight dwellings with little mass are more susceptible to short term overheating. Heavyweight buildings are, however, more likely to experience long term overheating.

Additionally, despite showing less evidence of short-term overheating, heavyweight buildings are more likely to suffer from underestimated *HLC* due to stored solar heating contributions (figure 5.19). This means that whilst periods of short term overheating may be associated with stored solar contributions, the mass of a test dwelling needs to be taken into consideration. Dwellings of various forms and constructions are assessed in section 9.1, where the limits upon suitable testing conditions enforced by experimental overheating can be seen.

Table 5.10: Instances of overheating for simulated BRE test house of various thermal mass and glazing fractions. (Simulated: BRE-NOT-FINN-MLR-2w-24h-6agg-S_{GVS})

		Jan	Feb	Mar	Apr	May	Jun	Jul	Aug	Sep	Oct	Nov	Dec
Lightweight (LW)	*Days of Full Overheating*	0	0	10	20	31	30	31	31	30	15	0	0
	Hours Of Overheating	108	152	481	652	744	720	744	744	720	509	175	131
Mediumweight (MW)	*Days of Full Overheating*	0	0	12	21	31	30	31	31	30	17	0	0
	Hours Of Overheating	76	117	478	666	744	720	744	744	720	514	145	101
Heavyweight (HW)	*Days of Full Overheating*	0	0	16	25	31	30	31	31	30	20	0	0
	Hours Of Overheating	42	70	487	696	744	720	744	744	720	554	95	50
Mediumweight + Increased Glazing (MW-incG)	*Days of Full Overheating*	1	5	22	30	31	30	31	31	30	23	7	2
	Hours Of Overheating	215	308	617	720	744	720	744	744	720	613	329	229

Importantly the propensity of a test dwelling to overheat is influenced by the amount of non-thermostatically controlled equipment or the baseload, $Q_{baseload}$. This is particularly evident in low heat loss dwellings, where a high proportion of the total load may be met by the power of mixing fans alone. This makes successfully establishing a uniform temperature and avoiding experimental overheating a fine balance. The value of $Q_{baseload}$ even with conservative numbers of mixing fans can equal approximately equal 9 W/m^2[10]. Such loads may need to be

[10]Estimate based on average base load per m^2 in field tests conducted as part of this thesis.

considered when evaluating the likelihood of experimental overheating, section 9.1.3.4.

5.5.5 Identifying the presence of uncertainty

Identifying long term overheating should be straightforward. Care has to be taken that once long term overheating has occurred, sufficient time is given to allow the building to fully cool before valid data can be analysed.

Short term experimental overheating is harder to identify. If peaks in T_i, either in the building average or within zones are present, then there is potential that the *HLC* has been underestimated. Data should be analysed sub hourly and across all temperatures sensors to properly observe this. If peaks are seen, then checks for stored solar contributions should be performed (section 5.4.6).

5.5.6 Addressing uncertainty from solar driven experimental overheating

Essentially avoiding experimental overheating is largely dependent upon reducing the total solar gains into a test dwelling. As such, methods considered here may help to reduce all sources of solar driven uncertainty.

Approaches to handling experimental overheating generally fall into two categories. The first, *avoidance* includes the scheduling of tests, increasing internal temperatures and deploying shading devices. The alternative would be to perform some *correction*, accounting for the dynamic heat flows, a much more complex task involving knowledge of the thermal mass and its associated heat flows. Sticking within a steady-state perspective, it is the strategy of avoidance that is discussed here.

5.5.6.1 Scheduling tests

The simplest solution to avoid cases of overheating is through more carefully defined suitable testing seasons. This relies on correctly scheduling a test to limit likely solar gains and to maximise heating demand. Any such scheduling is obviously susceptible to the risk of uncharacteristic weather, but utilising simulations similar to those shown in figure 5.31 can help identify the conditions likely to be required for testing and have been used before (Stamp et al., 2013c), see the co-heating report in appendix C.

5.5.6.2 Increasing $T_{setpoint}$

Attempts at avoiding experimental overheating can be aided through adapting the experimental test protocol. For example, raising the internal experimental set point will increase ΔT and therefore reduce the likelihood for overheating. This approach has occasionally been adopted to aid tests performed in warmer weather (Butler and Dengel, 2013). In principal this can increase the periods in which co-heating can successfully be conducted.

However, in practice there are reasons to limit the internal set point. Some of these are practical, i.e. increasing shrinkage and cracking during testing, whilst others are concerned with the concept of HLC_{True}, as a higher internal temperature will increase the value of HLC_{True} through both increased stack infiltration losses and increased thermal conductivity of materials (see section 7.7.1).

5.5.6.3 Blocking solar radiation

An alternative method to reduce the likelihood of overheating is to reduce solar gains through blocking or reflecting solar radiation. Previous thermal characterisation studies, including some co-heating tests, have attempted to block out solar gains. This can be through the use of whole building shading, e.g. scaffold and opaque sheets (Santamouris, 2005) or through shading around windows (Butler and Dengel, 2013). The BRE, as part of the NHBC field trail, examined methods of shielding a test dwelling from solar radiation. This data was made available to the participants of this project and is re-analysed in the appendix, section A.2.4. Shading devices deployed in this work appear to assist in reducing experimental overheating, but it is not clear from the experimental design how much of this results from the devices themselves and how much from raised internal set point temperatures, both occurring at the same time. When using side-by-side test dwellings to examine changes to co-heating methods, care needs to be taken to ensure other sources of variation or uncertainty, of the type discussed throughout this thesis, are minimised such that reasonable comparisons of methods can be made.

When providing additional shading to the test dwelling it is important to consider how the introduction of shading may alter the heat loss system. The addition of shading may alter the external surface resistances, ventilation rates and the external air temperature surrounding the house. Adequate ventilation may be required to ensure the heat loss through shaded elements is not significantly altered. Furthermore, if shading is only provided to glazed openings, rather then the full building, then consideration of the solar heating contribution to the opaque ele-

ments of a test dwelling may still be required. It is key here to consider the context of the heat loss measurement, the required accuracy, any comparisons to be drawn and the feedback, both quantitative and qualitative, that can be achieved.

5.6 Chapter conclusions

Several key conclusions can be made from this chapter on solar sources of uncertainty. In terms of the measurement of solar radiation these include:

- Any measurement of solar radiation will only be an imperfect representation of the complex distribution of *S* and solar gains across the building fabric. This results in definitional uncertainty in the variable *S* and the model in which it is used.

- If a dwelling has all or the majority of its glazing, and therefore predicted solar gains, on the south facade, then a single solar measurement of S_{GVS} is likely to give the most accurate *HLC* estimates.

- When the glazing and gains are split around a dwelling, e.g. east and west glazed facades, the choice of measured solar radiation is more complex. A mean vertical measurement (S_{GVM}) is likely to give the most accurate result. If only a single measurement is possible then vertical measurement of the principal gains facade is likely to produce the most accurate results.

- The use of multiple orientations as independent regression terms is unlikely to achieve improved results, as multiple solar terms are expected to show collinearity.

- Significantly, if a horizontal measurement of *S* is used for a building receiving predominantly direct gains, then a significant overestimate of the *HLC* may be estimated, even in otherwise ideal conditions.

Considering the derivation of the solar aperture, *R*:

- Statistical estimation of *R* will improve with higher ranges of *S* within a test period. Ranges $>$150 W/m^2 are likely to yield more accurate estimates of *R*.

- If only a small number of bright days are present, the influence of extreme data points can be evaluated and bright days checked for any bias, particularly from stored solar radiation. Checks are particularly required when extreme or influential data points are proceeded by another sunny day.

- If R is calculated from numerical models, the assumed parameters need to be checked on site and should be used with appropriate error estimates.

- The use of a numerically calculated R is unlikely to improve results when compared to an appropriate measurement of solar radiation used within MLR or Siviour analysis. Instead a systematic offset is likely, as a result of the inputs used to calculate R and any offset in the measurement of S.

Stored solar heating contributions were identified with the following implications:

- Fractions of solar gains received on one day can be re-emitted on subsequent days. As this heat flow is not captured in steady state analysis, an underestimate of the *HLC* can occur.

- This underestimate is more likely and more significant in heavyweight dwellings and those that admit more solar radiation into the internal space.

- Aggregating data from dawn-dawn will help reduce any underestimate. Additionally, comparing various aggregation periods may help identify the presence of stored solar heat.

- Increasing the aggregation period to 2 or 3 days may again reduce the underestimate caused by stored solar heat.

Finally, solar radiation can cause a rise in internal temperatures above the experimental set point:

- When internal temperatures rise above the experimental set point, dynamic heat flows are increased as the building both warms up and subsequently cools.

- Short term periods of solar overheating last less than a day and are associated with stored solar heating contributions.

- Longer term overheating result in Q_{elec} = 0 or a constant, meaning MLR can no longer be used. It could be stated that a co-heating tests is effectively no longer being carried out.

- Overheating therefore plays a strong role in determining when co-heating tests can be successfully performed, particularly for low heat loss and highly glazed dwellings.

- The best strategy may be to avoid overheating through more careful scheduling of tests. Providing shading may be beneficial and extend testing seasons, but any changes to the dwellings heat loss need to be considered.

Chapter 6

Further Weather Driven Sources of Uncertainty

Chapter overview

Chapter 6, the second chapter examining sources of uncertainty within the co-heating method, explores and evaluates the uncertainty generated by three additional weather variables. These include uncertainty from:

- **6.1:** Wind & stack driven heat loss.
- **6.2:** Dynamic external temperatures.
- **6.3:** Sky temperature & radiative heat loss.

The chapter is then concluded in section 6.4.

6.1 Uncertainty from wind and stack driven heat loss

Wind and stack driven infiltration losses for a test dwelling are not fully described by the co-heating energy balance. As a result, both effects increase the variation in daily data points and act to increase the overall heat losses, or HLC_{True}. As such, two branches of uncertainty can be considered:

1. Daily variation and random uncertainty.
2. Both increasing the value of and variation in HLC_{True}, therefore introducing definitional uncertainty affecting comparisons to design or between tests/dwellings .

The ability of wind to influence heat losses is well known. Everett (1985) considered varying infiltration losses as a major source of uncertainty in co-heating tests and evidence from a number of field tests have shown correlation between both daily estimated *HLC* and ACH with the

measured wind speed (e.g. Miles-Shenton et al., 2011; Palmer et al., 2011; Siddal et al., 2011; Butler and Dengel, 2013). However, accounting or correcting for such losses is not trivial, and may introduce additional uncertainties (Stamp et al., 2013d; Butler and Dengel, 2013) and therefore should be avoided (Johnston et al., 2013).

Stack losses have been considered less commonly, with Lowe et al. (2007) using calculations based on a semi-analytical model of air flow to suggest that the slightly elevated internal temperature (25 °C) used in co-heating tests is likely to increase heat loss by the order of 3 W/K for a two-storey house and 15 W/K for a three-storey house.

This section aims to clarify the impact of wind losses upon a test dwelling and upon *HLC* estimates. This begins with a simple and hypothetical consideration of the impact of modelled wind losses upon infiltration (section 6.1). Stack losses are then given a similar hypothetical treatment (6.1.2) before both forms of infiltration are combined in full building simulations (6.1.3.1). Subsequently, more complex interactions with heat loss are considered through an example from a field test (6.1.4.1). Finally, a number of approaches to addressing wind losses in co-heating tests are considered (6.1.6).

6.1.1 The impact upon a test dwelling

As defined in sections 3.1.1.2 and 3.1.1.3 the infiltration heat loss coefficient can be written as:

$$HLC_{inf} = \rho_a c_a \dot{V} \tag{6.1}$$

Where the wind and stack components of infiltration airflows can be described by (Walker and Wilson, 1997):

$$\dot{V} = \sqrt{\dot{V}_w^2 + \dot{V}_s^2} = \sqrt{(cC_w(sU_w)^{2n})^2 + (cC_s(\Delta T)^n)^2} \tag{6.2}$$

From equation 6.2 it can be seen how at low wind speeds or still conditions (i.e. $\frac{dt}{U^2} \rightarrow \infty$) that stack losses will dominate. Equally, as $\frac{dt}{U^2} \rightarrow 0$ the wind losses dominate. Additionally, if $\dot{V}$ is in units of m^3/h, $\rho_a c_a$= 0.33 Wh/$(m^3 K)$, such that the resultant heat flow, Q_{inf}:

$$Q_{inf} = \frac{1}{3}\dot{V}\Delta T \tag{6.3}$$

Figure 6.1 calculates the wind driven losses using equations 6.2 and 6.3 with stack losses omitted from equation 6.2, demonstrating the impact of wind driven losses in isolation across the testing season. As stack driven infiltration is ignored here, figure 6.1 represents a purely hypothetical case, but is illustrative of the impact of wind losses upon a test dwelling. A house with

a mean AHC of 0.27 h^{-1} is shown in this case and there are three points to note, relating back to the three previous forms of uncertainty:

1. Wind driven losses are associated with increased random error and scatter in daily data points.

2. There is an overall increase in heat loss due to the presence of the additional wind driven losses, Q_{wind}. Higher wind speeds = higher HLC_{True}.

3. As wind losses are non-linear with ΔT, they increase the value of the intercept (see section 8.1).

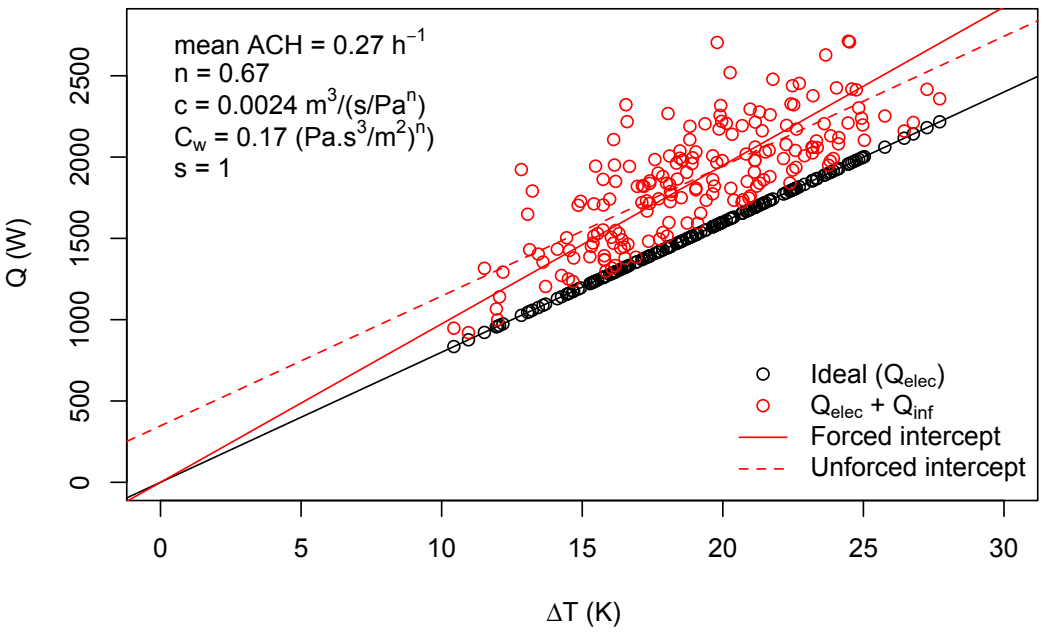

Figure 6.1: *Effect of wind losses on co-heating analysis. Q_{elec} represents the heating load due to the ideal conditions, with Q_{inf} resulting entirely from wind driven infiltration as defined in equations 6.2 and 6.3.* (Modelled: FINN-24h-6agg)

Of course, this example is only representative of simple wind losses, ignoring the interactions with stack driven infiltration and more complex interactions with the building fabric. The former is discussed in the next section, whilst a field study example of more complex wind losses is discussed in section 6.1.4.

6.1.2 Stack driven losses

Stack losses, are dependent upon ΔT but, as internal temperature is assumed constant during co-heating tests (although deviations from this assumption may occur 5.5), this means a higher heat loss would be expected with a lower T_e and vice versa. This is demonstrated in figure 6.2, in which the non-linear behaviour and increasing stack losses can be seen, based on the equation dictating stack losses (equation 6.2), this time with windspeed, U_w, set to zero.

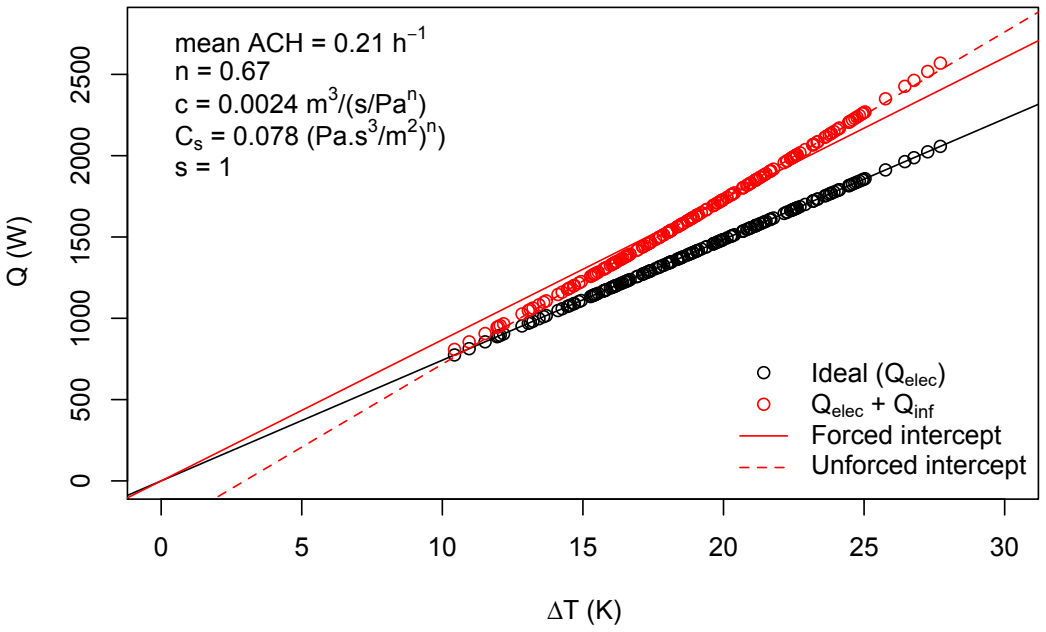

Figure 6.2: *Q vs ΔT - plot for ideal case and with stack losses included.* (Modelled: FINN-24h-6agg)

Again, figure 6.2 is purely demonstrative, representing simplified stack losses in isolation. However, the impact of stack losses can be noted as:

1. A systematic increase in HLC_{True} at higher ΔT.
2. Non-linear relationship of Q and ΔT.

Analysing this data across a full testing season (Oct-Mar) shows a difference of 6.4 W/K (8%) between the highest and lowest HLC_{True} across two week test intervals. This range will then increase as the proportion of stack losses to total losses increases.

To further explore the impact of stack and wind driven infiltration upon *HLC* estimates, both effects are combined within a full building simulation[1].

[1] Details of the simulation treatment of stack and infiltration losses can be found in appendix B.2.1.2.

6.1.3 The impact upon *HLC* estimates

6.1.3.1 Simulated results

The estimated *HLC*s for four simulated test dwellings are considered in figure 6.3. The buildings are again identical apart from their airtightness characteristics, and therefore total heat loss. The four dwellings have various flow coefficients and flow exponents used in EnergyPlus simulations. For comparison, the mean ACH for each across the period shown is included in the figure. This includes a test dwelling with ACH = 0.22 h^{-1}, approximately corresponding to a dwelling with notional airtightness standards of 5 $m^3/(hm^2)$ and a dwelling of ACH = 0.54 h^{-1}, roughly corresponding to the building regulation limit of 10 $m^3/(hm^2)$. Two additional cases then provide further variation, with an air change rate of just 0.08 h^{-1} in the most airtight example and 1.17 h^{-1} in a dwelling with similar leakage to a traditional build[2].

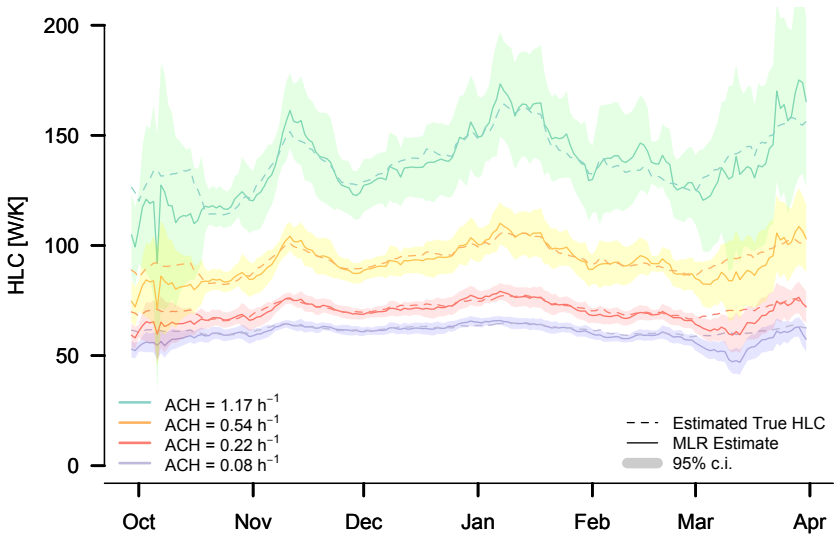

Figure 6.3: *Estimated HLC due to wind uncertainties for various test dwelling leakiness.* (Simulated: BRE-NOT-SLW-FINN-SN-MLR-2w-24h-6agg-S_{GVS})

[2]These air change rates do not necessarily correspond precisely to the equivalent $m^3/(hm^2)$ @50 Pa above. It should be noted these are mean values across the period plotted in figure 6.3 and additionally that this factor of 20 can vary significantly in reality. Further, the most leaky case may represent an unlikely dwelling, given its low conductive heat loss, but is included as an illustrative example of the uncertainty infiltration losses create.

In general the airtightness of most dwellings will approximately correlate to its level of insulation, although the ratio of Q_{inf} to Q_{TOT} may vary with construction types and fabric efficiency targets (e.g. Passivhaus dwellings, with high airtightness targets, are likely to have a low Q_{inf}:Q_{TOT}). Therefore the impact of wind and stack losses is likely to be highest in highly insulated dwellings in which airtightness targets are missed, leaving high ratios of Q_{inf}:Q_{TOT}.

Table 6.1: Estimated *HLC* for various airtightness test dwellings. Mean and standard deviations calculated from 2 week tests across Oct-Mar. (Simulated: BRE-NOT-SLW-FINN-SN-MLR-2w-24h-6agg-S_{GVS})

Airtightness	ACH (h^{-1})	MLR Estimate			Estimated HLC¢ith$		
		Mean HLC (W/K)	s.d. (W/K)	s.d/ Mean HLC (%)	Mean HLC (W/K)	s.d. (W/K)	s.d/ Mean HLC (%)
Very Poor	1.17	137.2	16.0	11.7%	138.2	11.7	8.5%
Poor	0.54	92.4	7.8	8.4%	93.9	5.9	6.3%
Medium	0.22	69.7	4.7	6.7%	71.4	2.9	4.0%
Good	0.08	60.1	3.9	6.5%	61.7	1.7	2.8%

As can be seen in figure 6.3 and the corresponding table (6.1), HLC_{meas} shows good agreement with HLC_{True} across 2 week test periods, with no significant bias, albeit the remnants of stored solar contributions can be seen in figure 6.3. The distinction that must be made is that these results show a reliable measure of their HLC_{True}, but this can cause difficulties in comparisons to HLC_{pred} or between tests. For a dwelling such as the very poor airtightness example above, the variation in HLC_{True} across this period is over 50 W/K. If infiltration losses are not separated from total losses, then repeated tests could show significant disparity from their respective environmental conditions and varying infiltration rates, despite the building actually itself remaining constant. This could lead to a lack of reproducibility and therefore biased estimates of retrofit improvement or a bias between two dwellings tested under different conditions (see section 9.5.2). Further, as discussed in section 9.5.1.1, relating this measurement to the HLC_{pred} is equally complex and prone to comparison errors.

Strategies to resolve these comparison errors may include attempting to remove wind losses or adjusting design values to match the test weather. However, further difficulty exists in the later approach. To readjust the HLC_{pred} would require knowledge of the pressure coefficients that determine wind driven ventilation losses. Again we can see that to fully understand a *HLC* measurement, more information on the test dwelling is needed. This is another example of a definitional uncertainty from incomplete knowledge of the HLC_{True}.

In buildings meeting notional airtightness standards, the variation in HLC_{True} may be small (s.d. 4%) and measured values accurate. This presents less of a problem in interpreting test results. However, wind effects should be considered in all test dwellings, as the airtightness certificate may hold incorrect or out-dated information and complex effects can occur (see section 6.1.4). Indeed, the simulated wind driven losses here are likely to represent a simplest case scenario. Further studies may be required to understand wind driven heat loss in dwellings.

6.1.3.2 Evidence in field data

The correlation between the daily, solar corrected, *HLC* from field tests can be plotted against daily wind speeds to assess the potential scale of wind driven losses. All the field tests in which wind speed was locally measured are included in figure 6.4 below. Whilst in some cases there appears to be no correlation, in others there appears to be a relationship between the daily *HLC* and daily mean wind speed. Whilst figure 6.4 can be a useful qualitative assessment of the relationship between the building heat loss and wind speed, caution is needed in making any further assumptions over the nature of this relationship.

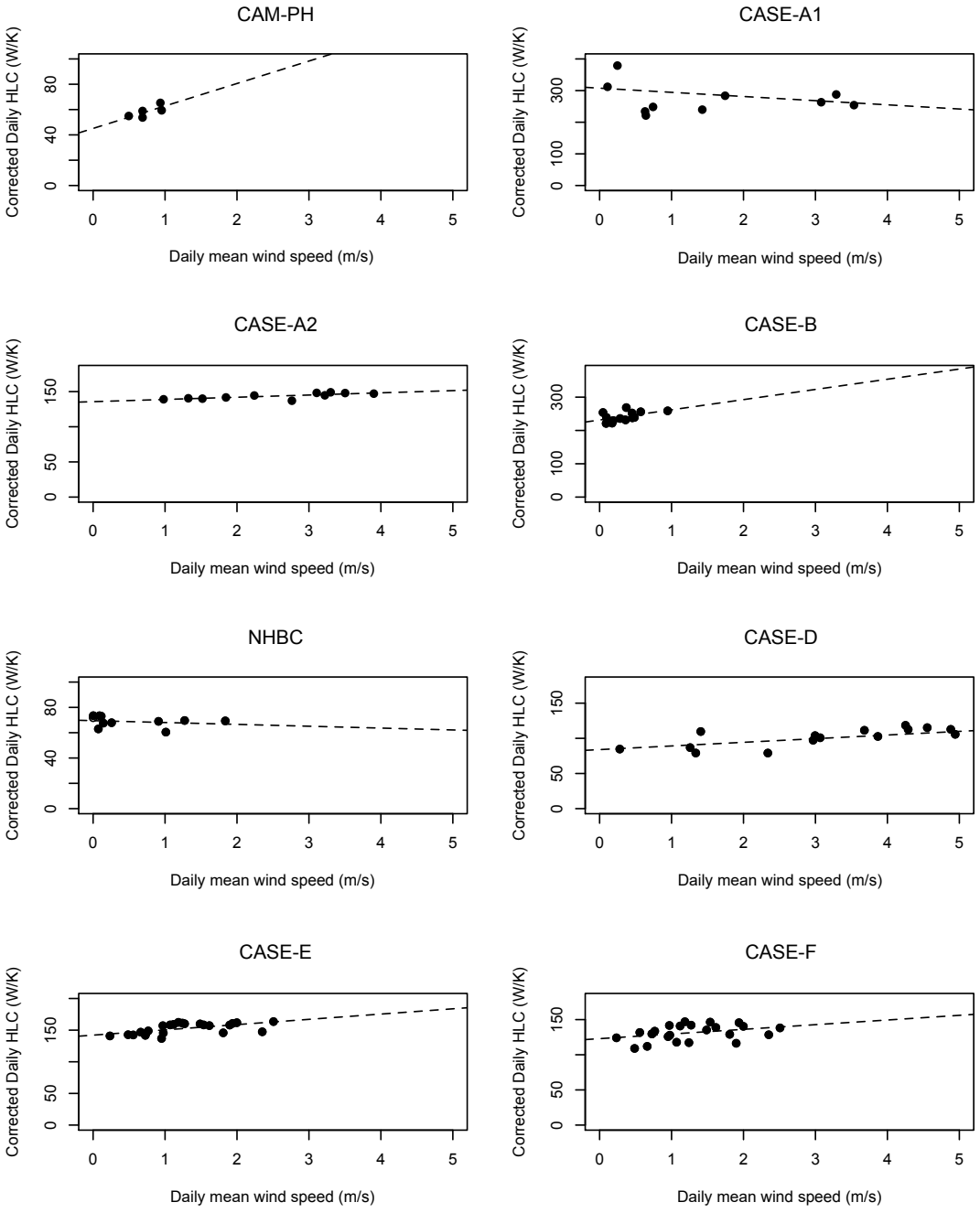

Figure 6.4: *Correlation between solar corrected daily HLC and mean daily wind speed in eight field tests.* (Field Tests: MLR-24h-6agg)

6.1.4 Complex wind driven heat loss mechanisms and further uncertainty

So far, the impact of wind and stack effects has been treated in a simple manner, assessing their impact on air infiltration. In reality, both processes and their interactions with the building fabric are more complex and harder to model. Complex heat loss mechanisms may exist, particularly in voids such as wall cavities. These may include wind washing, air looping and convective bypasses. Such processes are harder to identify in the field or to model in simulations and whilst they may be absent from well-designed and built dwellings, building science does not only concern itself with such dwellings.

As an example, air can loop around the cavity insulation, a process often linked to bad workmanship when an air layer is left between the fill and inside leaf. This can have devastating effects on the actual U-value of a partially filled wall (Bankvall, 1977). Experimental work in a lab showed that this can increase the measured U-value of a partial fill cavity wall by 250%, compared to the intended value (Lecompte, 1989; Hens et al., 2007).

Within field data collected for this thesis similar effects can be seen. In CASE-A, the measured in situ U-values in an empty cavity can be compared to those in a fully filled (Eco-bead) cavity. Figure 6.5 shows the correlation between the hourly measured in situ U-value and measured wind speed for both cases during two successive co-heating tests of the same dwelling. Between the two tests, the house remained almost identical apart from the cavity insulation fill, with pressurisation results of 8.1 and 8.4 $m^3/(hm^2)$ @50 Pa and tracer gas decay air change rates of 0.62 h^{-1} and 0.60 h^{-1}respectively. Despite no significant change in airtightness, we can see in figures 6.5a and 6.5b the empty cavities show a more pronounced correlation with wind speed than in the filled insulated cases, 6.5c and 6.5d. The corresponding co-heating test data is shown later in this thesis, section 9.5.2.3, figure 9.25.

Such wind driven loss mechanisms are hard to predict or model in simulated co-heating tests. Information from field tests is then needed to begin to understand how such process may introduce uncertainty into co-heating *HLC* measurements beyond the examples in figures 6.1 and 6.3. For example, in this case, even perfectly accurate infiltration measurements would not remove all the wind driven variation and uncertainty from *HLC* estimates.

This also demonstrates how additional measurements, in this case local wind speed, can help us understand more about the heat loss processes within the as-built building, providing better

feedback and identifying areas for further forensic testing. It may be noted how the co-heating *HLC* result in this case may be higher than predicted, but this in itself tells us little of why this may be. More detailed measurements, such as these on the cavity wall and of the environment (i.e. wind speed), may help unlock the processes behind this number.

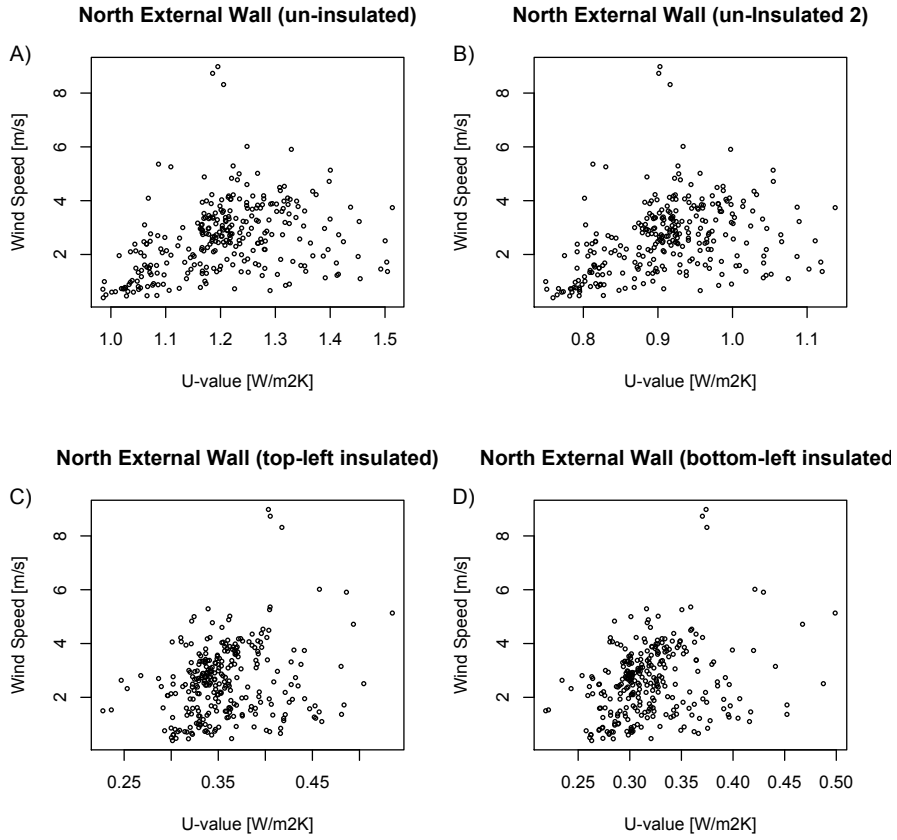

Figure 6.5: *In situ U-value measurements as part of a co-heating test. Showing correlation of hourly calculated U-values to wind speed for a cavity when un-insulated and then insulated.* (Field Test: CASE-A1 and CASE-A2)

6.1.4.1 Complex stack effects

It is also worth mentioning that the stack losses considered previously only represent those associated directly with infiltration. However, ΔT may affect convective bypassing. Again, from most empirical datasets it may not be possible statistically to disentangle the two effects and therefore further measurements and modelling may be required, such as those performed in work identifying the cavity wall bypass (Wingfield et al., 2007; Lowe et al., 2007; Winfield et al., 2009).

6.1.5 Identifying the presence of uncertainty

Plotting results as in figure 6.5 or as in figure 6.6 below should allow any correlation with wind speed to be identified. Plots such as figure 6.6 can potentially be used to identify and then remove extreme data points (Judkoff et al., 2000; Butler and Dengel, 2013). These points are not necessarily erroneous, as they will describe heat loss under the conditions in which it was measured. They maybe removed to allow better comparisons to HLC_{pred} or HLC_{fabric} in a given limit of low wind speeds.

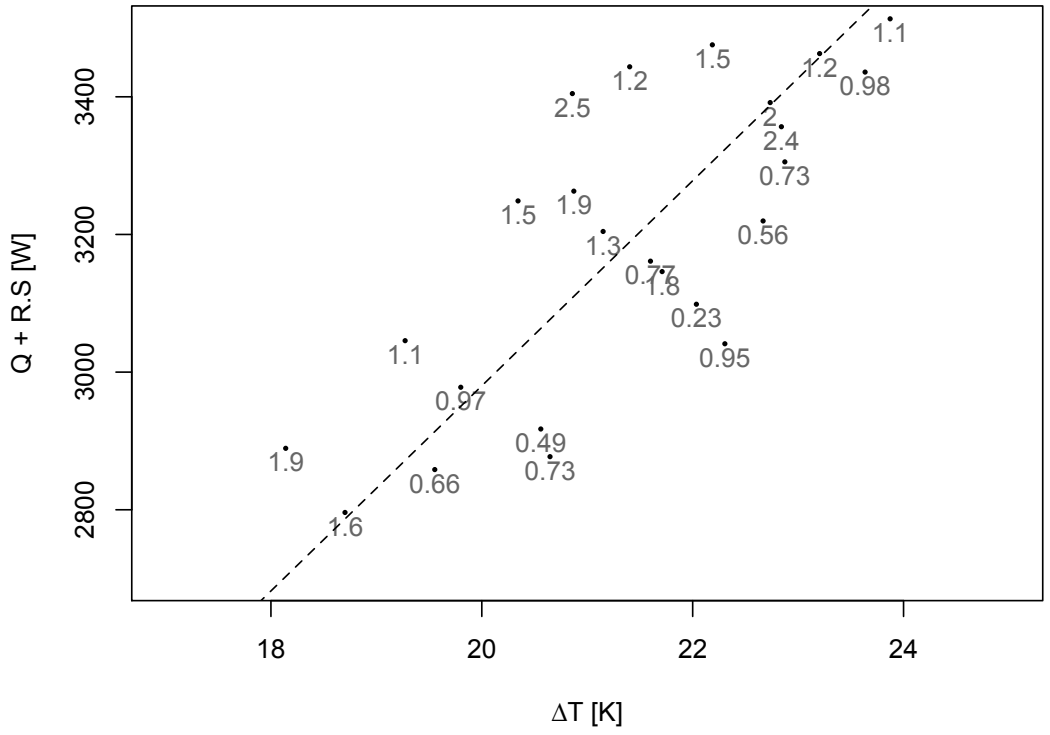

Figure 6.6: *Solar Corrected Regression with daily mean wind speed included on plot. Data from LBU, (Miles-Shenton et al., 2010)* (Field Test: MLR-2w-24h-S_{GVS})

6.1.6 Addressing uncertainty from wind driven losses

6.1.6.1 Measuring wind speed

Different approaches can be used to examine the presence of wind driven uncertainty and indeed to understand the interaction between wind conditions and heat loss from a test building. In all cases, it is essential that on site, local wind conditions be measured, as stated in the LBU protocol (Wingfield, 2010a; Johnston et al., 2013). This allows an understanding of when wind conditions may be behind variable heat loss, creating uncertainty in the co-heating *HLC* measurement.

The location of an anemometer is often imperfect due to practical constraints. Mounting above the roofline of a test dwelling may not be feasible for short term tests. Equipment may also have to be in a location where it does not attract attention or can be stolen. Similarly to solar radiation measurements, the measurement of wind speed is likely to incorporate some of the local sheltering effects at the precise position of the sensor. If local conditions are likely to vary across different locations around a building, then if possible more than one monitoring station should be used, e.g. in front of each elevation.

6.1.6.2 Removal of data points

A simple and commonly used approach to data points with high wind driven losses is to simply remove affected daily data points from the analysis. Such analysis has been performed when using short, night time periods of co-heating in the STEM method, at various wind speed thresholds (Judkoff et al., 2000) and also within full co-heating data sets (Butler and Dengel, 2013). It is important to note that the level of any wind speed threshold is dependent upon the height and location of the sensor and the building and the sensitivity of the test dwelling to wind pressures. In such cases, aggregated daily data points in which the wind speed is thought to be over a threshold level and therefore unduly high due to additional wind speed losses can be removed after being identified in regression plots, as demonstrated in figure 6.6. However, considerable care has to be taken that the cause of higher than expected losses is indeed through high wind speed and not through any other sources of uncertainty identified throughout this thesis.

This approach also means that the full heat loss across the test period is no longer measured, rather a *HLC* representing the filtered data or the new mean wind speed. This is perhaps only useful for comparison purposes where a set wind speed is desired, although as discussed, care is needed comparing design wind inputs and those measured on site. This means that the filtering of data may only be useful for inter-test comparisons. In general, this approach reduces the number of data points and does not necessarily clarify comparisons to design. Further, data revealing a dwelling's sensitivity to wind speed may prove more valuable as feedback than a simple *HLC* estimation at low wind speeds, even if the form of the relationship or quantitative assessments are not clear. Often the most important information in sets of measurements is contained in the outliers.

6.1.6.3 Measurement of infiltration rates

If infiltration measurements are made throughout the co-heating test (see section 2.5.1 for example techniques) then the daily infiltration losses comprising of both stack and wind driven components can be disaggregated. In theory these losses could be subtracted from the total heating power, leaving a regression free of the variation caused by infiltration losses, i.e. Q_{elec} - Q_{inf}, measuring HLC_{fabric}, as defined in section 3.1.3. An example of daily tracer gas decay measurements from a field test are shown in figure 6.7. Figure 6.8 shows a simulated test in which accurately derived infiltration losses have been subtracted out prior to regression.

The difficulty with this approach is that other than with sophisticated and expensive methods the infiltration measurements are not made on the same time scale as the co-heating test. For example, the most commonly used tracer gas tests only measure the infiltration rate over a period of a few hours, rather than the daily aggregated 24 hour periods used in co-heating. Such measurements are also subject to their own uncertainties, particularly achieving satisfactory mixing in the dwelling, sensor location bias and the measurement and calculation of a tracer gas concentration representative of the dwelling as a whole. It is more likely that measured high daily infiltration measurements will correlate with periods of high wind speed and therefore re-enforce the decision to remove data points rather than correct data.

A further weakness with this approach is that the measured air change rate may not fully correspond to the actual heat loss out of the dwelling. Infiltration heat recovery, the recovery of heat as warm air passes out through cracks in the cooler building fabric, can mean that approximately 20%, or even higher fractions, of the heat lost through infiltration is recovered (Claridge and Liu, 1995; Judkoff et al., 2000).

The results from daily tracer gas decays in a field test (CASE-A1) are shown in figure 6.7. The decay curves show some variation between daily measurements in the left figure, which shows some correlation to the measured daily wind speed in the right figure. This variation will also incorporate some experimental error associated with the tracer gas decay technique.

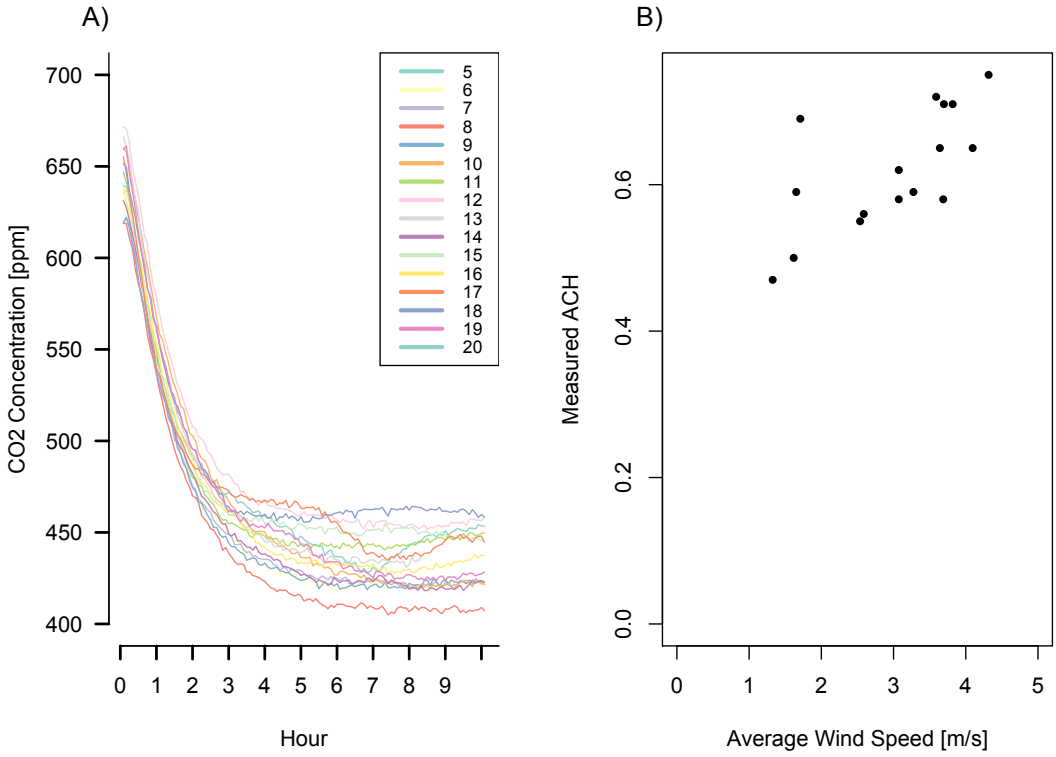

Figure 6.7: *Daily CO_2 decays and the measured air change rates correlation with wind speed. Each daily measurement of the test sequence is identified in the legend, with measurements starting on day 5 and running till day 20.* (Field Test: CASE-A2-MLR-2w-24h-6agg-S_{GVS})

6.1.6.4 Wind speed as a regression variable

In many reported co-heating tests the measured wind speed has been used as an additional independent regression variable when using MLR, denoted MLR$_{wind}$ (see table 2.2). This attempts to correlate the deviation in measured heat loss with measured wind speed. However, as previously seen there is no reason to suspect that the relationship between wind driven heat loss and wind speed is linear - selecting the wrong functional form is in itself an error that is likely to bias parameter estimates.

Under conditions of constant stack losses, infiltration losses could appear approximately linear with wind speed. Estimated *HLC*s from figure 6.3 are reassessed with the inclusion of wind speed as an independent regression variable and compared to the original estimate. The results are presented in figures 6.8 and 6.9. Of course, here HLC_{True} also changes. In traditional

MLR, the *HLC* incorporates all wind and infiltration losses (Q_{inf}). If wind speed is included as an additional independent regression variable then the associated *HLC* does not incorporate wind losses, albeit with other infiltration losses remaining. So whilst a number of these cases show that wind speed is a potentially suitable explanatory variable, such an approach will not separate the effects of the wind on infiltration losses or the wind's impact on U-values or in other heat loss processes, e.g. external surface resistances and wind washing. How these regression coefficients can then be interpreted into any physical meaning and useful feedback is then unclear.

Figures 6.8 and 6.9 show the calculated *HLC* from traditional MLR, MLR$_{wind}$ and from MLR in which all infiltration losses are subtracted before regression (i.e. if a perfect tracer gas measurement was made). These are all compared to their respective true heat loss coefficients, *HLC*$_{TOT}$, *HLC*$_{excWind}$[3] and *HLC*$_{fabric}$.

Including wind speed as a regression variable does allow an estimate of the *HLC* without wind speed, and therefore of the wind driven losses. However, regression estimated wind coefficients will typically have large errors and low significance (see Table 6.2). Furthermore, the remaining estimated *HLC* still incorporates stack infiltration losses and the calculated losses associated with wind are partly related to infiltration and partly related to the influence of wind on the building fabric, e.g. wind washing or thermal bypasses.

[3]This is calculated by setting the wind factor to 0 in the simulation.

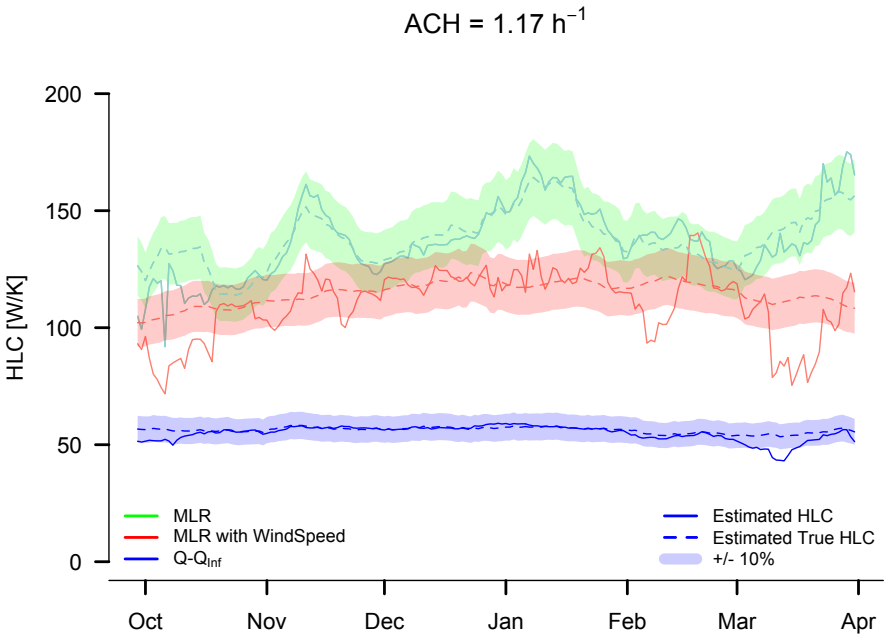

Figure 6.8: *Leaky test dwelling - Mean ACH 1.17 h^{-1} - Approaches to addressing wind driven uncertainty - regressing against wind speed and removing infiltration.* (Simulation: BRE-NOT-SLW-FINN-SN-2w-24h-S_{GVS})

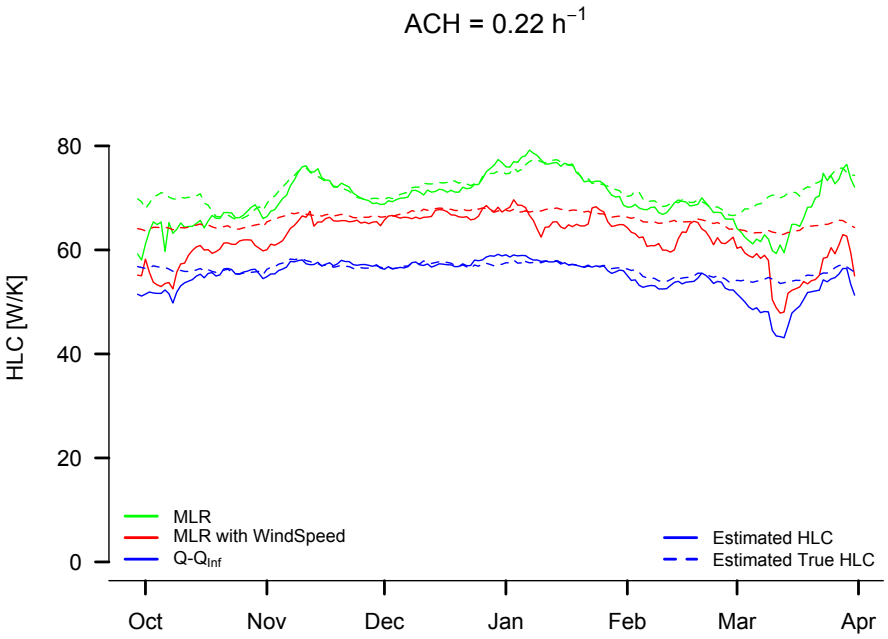

Figure 6.9: *Airtight test dwelling- Mean ACH 0.22 h^{-1} - Approaches to addressing wind driven uncertainty - regressing against wind speed and removing infiltration.* (Simulation: BRE-NOT-SLW-FINN-SN-2w-24h-S_{GVS})

Table 6.2: Impact of MLR with wind speed as a independent regression variable upon field tests. Note: The infiltration *HLC* calculated from measured air changes per hour, derived from the tracer gas decay measurements. The estimated wind *HLC* is based on the difference between MLR and MLR with wind speed.

Case Study	Analysis Type	HLC Estimate (W/K)	Standard Error (W/K)	95% c.i. (W/K)	Wind Coefficient	Standard Error	t	P-value	Tracer gas measured ACH (h^{-1})	Air Permeability @50 $m^3/(h.m^2)$	Infiltration HLC - (1/3)nV (W/K)	Estimted Wind Loss Coefficient (W/K)	% Infiltration Losses	Mean Wind Speed (m/s)
CAM-PH	*MLR*	55.9	6.8	13.3	-	-	-	-	-	0.53	-	14.5	26%	0.8
	MLR with Wind Speed	41.4	5.8	11.4	227.0	89.0	3.1	0.085	-					
NHBC	*MLR*	71.1	2.9	5.7	-	-	-	-	0.07 +/- 0.02	2.14	4.9	-	-	0.6
	MLR with Wind Speed	72.9	2.5	4.9	43.8	41.0	-6.2	0.326						
Case-A1	*MLR*	248.0	11.3	22.1	-	-	-	-	0.62 +/- 0.08	8.10	53.9	20.0	8%	3.0
	MLR with Wind Speed	228.0	15.6	30.6	192.0	107.0	1.8	0.088						
Case-A2	*MLR*	144.6	2.8	5.5	-	-	-	-	0.60 +/- 0.04	8.40	52.2	11.6	8%	2.5
	MLR with Wind Speed	133.0	4.5	8.8	74.7	25.6	2.9	0.0196*						
Case-B	*MLR*	243.0	7.0	13.6	-	-	-	-	0.39 +/- 0.09	2.93	66.9	6.0	2%	0.4
	MLR with Wind Speed	237.0	6.6	12.9	698.0	284.0	-3.0	0.0339*						
Case-D	*MLR*	108.1	10.1	10.7	-	-	-	-	-	-	-	14.8	14%	3.4
	MLR with Wind Speed	93.3	7.6	9.8	83.7	24.0	3.5	0.0037**						
Case-E	*MLR*	149.0	1.9	3.7	-	-	-	-	-	-	-	9.2	6%	1.3
	MLR with Wind Speed	139.8	2.8	5.5	136.7	42.0	-5.0	0.0008***						
Case-F	*MLR*	127.0	2.4	4.6	-	-	-	-	-	-	-	6.0	5%	1.3
	MLR with Wind Speed	121.0	4.0	7.8	102.0	62.0	1.6	0.1161						

6.2 Uncertainty from dynamic external temperatures

In true steady state conditions, the external temperature remains constant, whilst in any outdoor field test it is inevitably dynamic, varying on a diurnal and seasonal basis. As observed with stored solar contributions, applying a steady state analysis to dynamic data can introduce error and bias into *HLC* estimates. The following source of uncertainty can therefore be considered:

- Uncertainty from dynamic external temperatures - the lagged response of a test dwelling and its heating demand to changing T_e.

Additionally, the external temperature, through defining ΔT and the scale of overall heat loss, will have an impact on the scale of almost all other sources of uncertainty. Here however, it is only the impact of the dynamic T_e in producing a lagged response from the test dwelling that is assessed.

6.2.1 Dynamic external temperatures

Dependent upon the characteristics of a test dwelling, there will be a lag between the measured ΔT and the required heating power (Q_{elec}). Therefore, instantaneously the measured heat loss shows a poor match with steady state energy predictions (see section 6.2.2, figure 6.10). Daily aggregations should allow better predictions. However, as in the case of stored solar contributions, fractions of heat may be stored between successive days, say from a day with a warm mean T_e to a subsequently cold day and vice versa.

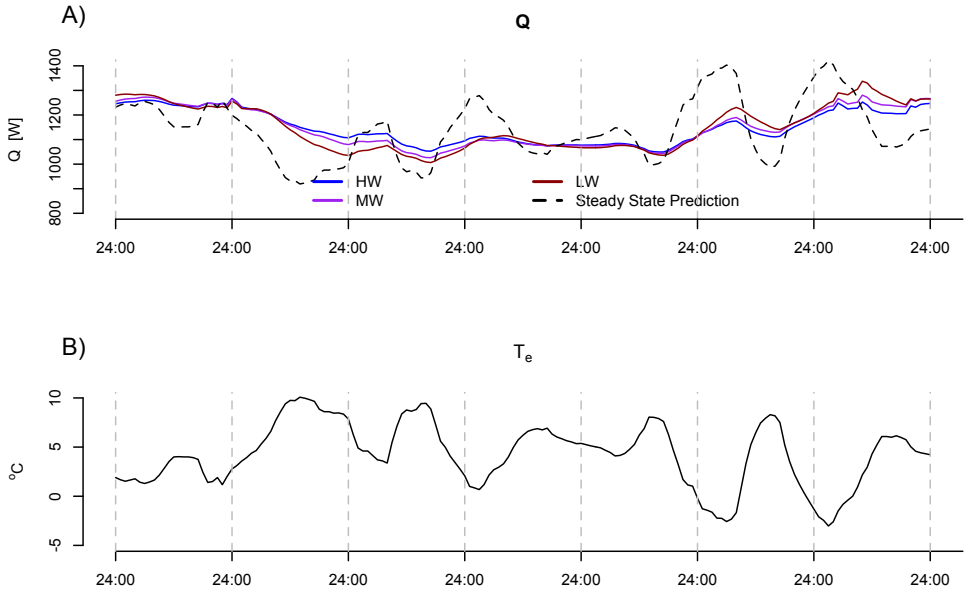

Figure 6.10: *Simulated heating power, Q_{elec}, due to dynamic T_e. Data is generated through an adapted weather files with a varying T_e other variables null or constant (FINN.Te). Light, medium and heavyweight buildings are shown for a selected seven day period.* *(Simulated: BRE-NOT-FINN.Te)*

The presence of uncertainty in steady state heat loss estimates due to such dynamics are well known, meaning even longer periods (i.e. 10 days) are often used for accurate heat loss measurements in controlled test cell measurements (Baker and Dijk, 2008). Other researchers (Everett, 1985; Deconinck and Leunis, 2012; Bauwens and Roels, 2014) have suggested incorporating the ΔT from previous time steps into heat balance equations.

A major confounding factor to understanding the impact of a dynamic T_e on *HLC* estimates is that T_e is often correlated with incident solar radiation, which has been shown to be a major source of uncertainty. The simulation approach in this thesis allows a hypothetical weather file

in which only dynamic external temperatures are present. Whilst this is hypothetical, it does allow the impact of dynamic T_e to be explored in isolation from S and stored solar heating contributions.

6.2.2 The impact upon a test dwelling

Figure 6.10 below shows the heating power required for a building simulated in conjunction with a weather file in which T_e is the only variable present or non-constant (FINN.T_e). The lag between peaks in the predicted instantaneous and actual heating demand for LW, MW and HW buildings can be seen ($\sim$ 2 hours). As expected, lower amplitude profiles occur with higher mass dwellings, with a steady state prediction differing significantly from the simulated dwellings across hourly and daily periods.

As seen in figure 6.10, there is a discrepancy between the steady state predicted heat loss and that experienced with a building with thermal mass. This is shown in the familiar regression plot for a medium weight (MW) dwelling (see figure 6.11).

Figure 6.11 suggests there is not any systematic bias in *HLC* estimates due to dynamic external temperatures, rather random error in the form of daily variations is seen. This random error marginally reduces using dawn-to-dawn aggregation periods, as the diurnal profile of T_e is better matched within the aggregation periods. Further, if the aggregation period is increased the variation further reduces, as can be seen in figure 6.12, in which 3 day and 7 day aggregations are shown for the same dataset as in figure 6.11.

Table 6.3 shows the *HLC* estimates for 1, 2, 3 and 7 day aggregation periods, along with a number of regression statistics. Whilst there is no discernible bias in the four approaches, the dispersion of data points is seen to reduce at higher aggregations, with the mean sum of squared errors decreasing and the aggregation length increases.

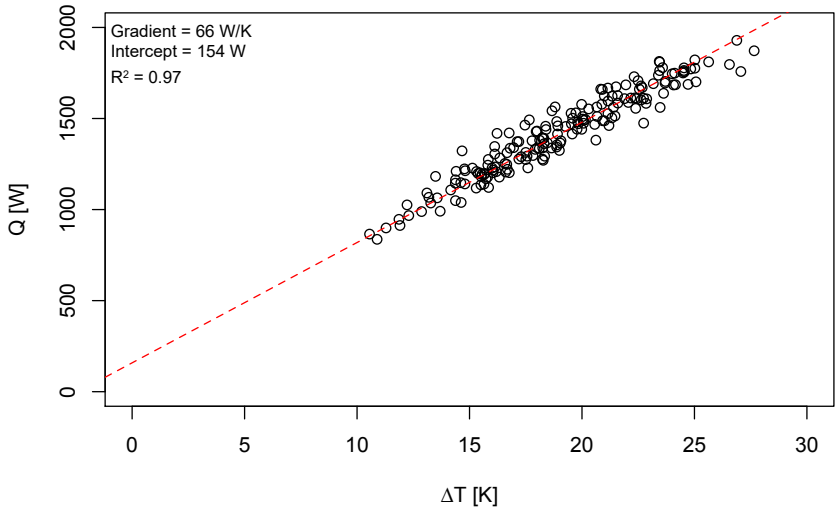

Figure 6.11: *Regression plot showing random error in regression due to dynamic T_e.* *(Simulation: BRE-NOT-MW-FINN.T_e-SN-MLR-2w-24h-6agg)*

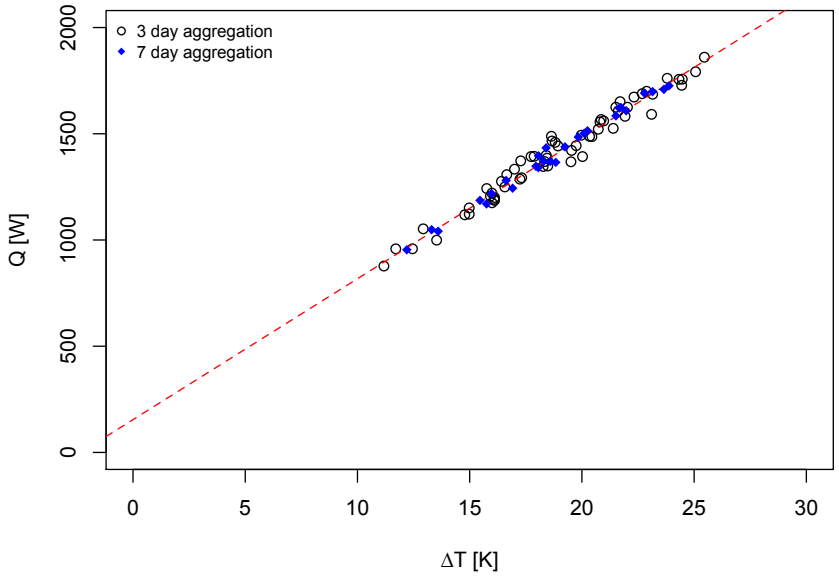

Figure 6.12: *Random error in regression due to dynamic T_e is reduced using 3 and 7 day aggregation periods.* (Simulation: BRE-NOT-MW-FINN.T_e-SN-MLR-2w-24h-6agg-S_{GVS})

Finally, the residual plots in figure 6.13 (based on figure 6.11) show that the uncertainty is related to the difference between the mean daily T_e on successive days, rather than the amplitude of the variation of T_e on a single day. Days that are colder than the previous require less heating power than predicted in the steady state energy balance and vice versa for warmer days. It can be imagined how this might further compound the error from stored solar contributions with the correlation between warm and sunny days and cold, dull days.

Table 6.3: Regression statistics comparing 1 day, 2 day, 3 day and 7 day aggregation periods. Includes sum of squared errors (SSE) and the mean SSE for each aggregation length. (Simulation: BRE-NOT-MW-FINN.T_e-SN-MLR-2w-6agg-S_{GVS})

	Aggregation	Hours	HLC (W/K)	Standard Error (W/K)	Residual Standard Error	Degrees of Freedom	SSE	Mean SSE
Non-intercept (MLR)	*1 Day*	24	74.2	0.3	77	183	1089578	5954
	2 Days	48	74.4	0.3	61	91	341711	3755
	3 Days	72	74.4	0.3	50	60	149195	2487
	1 Week	168	74.6	0.3	32	26	25986	999

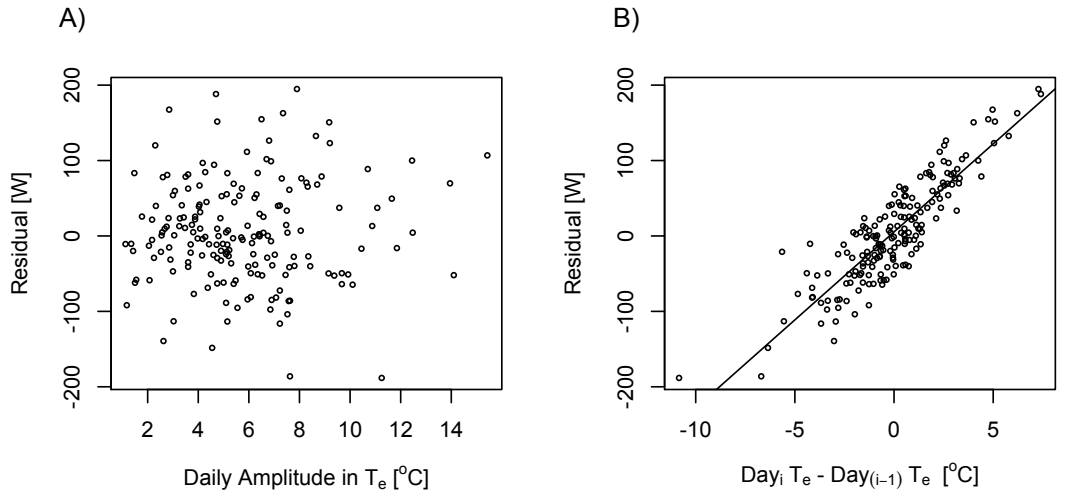

Figure 6.13: *Residual plots showing impact of daily amplitude in T_e to difference between mean T_e across two days.* (Simulation: BRE-NOT-MW-FINN.T_e-SN-MLR-2w-24h-6agg-S_{GVS})

6.2.3 The impact upon *HLC* estimates

Alone, the dynamic T_e causes only negligible error in *HLC* estimates (appendix A.3.1). Two week monitoring periods of 24-hour aggregations are sufficient to give accurate *HLC* estimates despite any random variation. If shorter monitoring durations were used, or even filtered data (i.e. night time), then the uncertainty could be considerably higher, with a bias depending upon the direction of changing T_e, in most cases an underestimate in the *HLC* for night time data as T_e is expected to be moving from warm to cold.

An important note is that the correlation between T_e and S makes analysis of the impact of a dynamic T_e upon *HLC* estimates difficult to quantify, particularly in field data. Creating a proxy variable for the changing external temperature between two successive days, ΔT_{i-1}, and plotting it against residuals from a co-heating test regression, can give the impression that the impact of the dynamic external temperature is large (Stamp et al., 2013a). Although these can be separated in simulations, in reality these effects will combine with each other in ways that

are difficult or impossible to disentangle in the field, meaning their respective contributions cannot be determined.

6.3 Radiative losses & apparent sky temperature

Long-wave radiative heat transfer will exist between the external surfaces of a building and the external environment including surrounding building surfaces, the ground and, in particular, the sky. Discussed in further detail in appendix B.3, long-wave sky losses are a function of the 'apparent sky temperature', which varies both hourly and seasonally with changes in humidity and cloud cover (Sicart et al., 2010). Losses are also driven by the temperature difference between external surface temperatures and the apparent sky temperatures (ΔT_{sky}) rather than directly by ΔT. Again, this represents a loss mechanism not described in the co-heating energy balance equation and uncoupled from ΔT, causing minor random uncertainty and increased heat loss.

Long wave radiation exchange with the sky therefore causes uncertainty in the form of:

1. Daily variation and random uncertainty.
2. Increasing and varying HLC_{True}, introducing definitional uncertainty concerning reproducibility and comparability to design estimates or HLC_{pred}.

Modelling sky losses is problematic (Adelard, 2010) and complex as the external surface temperature (T_{se}) is dependent upon incident solar radiation, external air temperatures and the heat flow through the element itself. This makes the impact of sky radiation hard to detect and considering the heat flow in isolation from these other variables incomplete. However, the impact of the long-wave radiative heat flow to the sky (Q_{sky}) can be briefly considered, using equations 6.4 and 6.5:

$$Q_{elec} + R \cdot S = HLC \cdot \Delta T + Q_{sky} \tag{6.4}$$

Where ISO 13790:2008 (ISO, 2008) defines Q_{sky} as:

$$Q_{sky} = F_{sky} \cdot R_{se} \cdot U_c \cdot A_c \cdot h_{r,sky} \cdot (T_{sky} - T_{se}) \tag{6.5}$$

Here, F_{sky} is a view factor between a surface and the sky (1 for an unshaded roof, 0.5 for an unshaded vertical wall), R_{se} is the external surface resistance of a surface, U_c is the U-value of the surface, A_c is the surface area, $h_{r,sky}$ is the external radiation heat transfer coefficient, T_{sky} is the apparent sky temperature and T_{se} is the temperature of the surface.

6.3.1 The impact upon a test dwelling

Using equation 6.5 and weather data from the Finningley weather file, Q_{sky} can be plotted as in figure 6.14. Between two week test periods, Q_{sky} remains approximately constant across the year, albeit with significant day-to-day variation. Within the testing season (October - March), the mean heat flow is calculated to be 80 W, approximately 6% of the total building losses, but ranging from 48 to 121W between individual days. The variability is reduced when considering the mean flow from two week monitoring periods, Q_{sky}, 64 - 87W, preserving the repeatability of the test across this period and only introducing a small comparison error.

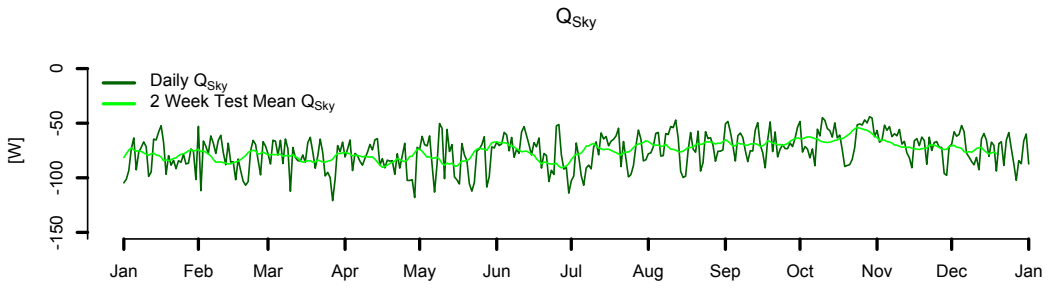

Figure 6.14: *Q_{sky} across a year in an ideal weather file with only varying T_{sky}.* (Simulation: BRE-NOT-SLW-FINN.T_{sky}-SN-MLR-2w-24h-6agg)

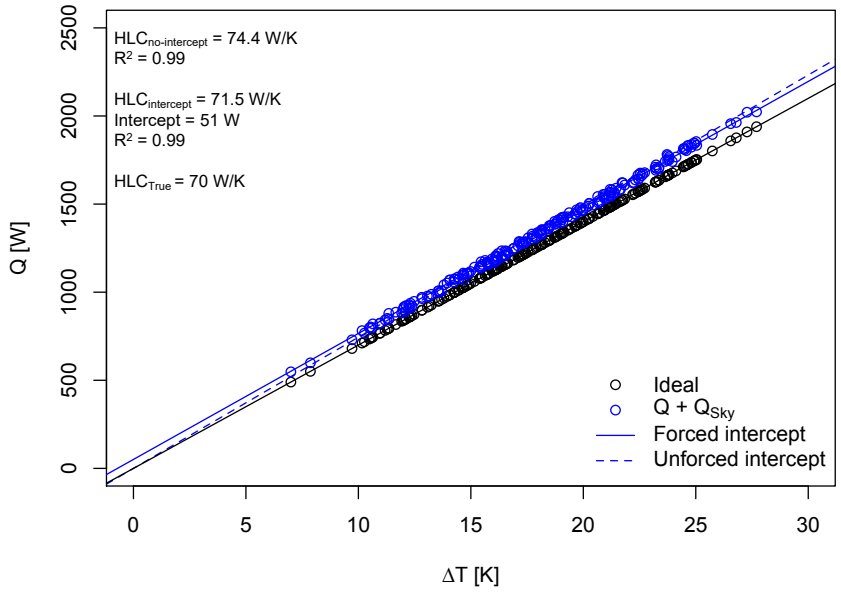

Figure 6.15: *Effect of long wave thermal sky radiation losses on co-heating test, in an ideal weather file with only varying T_{sky}* (Simulation: BRE-NOT-SLW-FINN.T_{sky}-SN-MLR-2w-24h-6agg)

Figure 6.15 expands on this in the familiar form of a corrected linear regression plot, with comparisons of this added Q_{sky} heat flow to an ideal case. The daily variation seen is small compared to the effects from other weather driven sources of uncertainty (e.g. figure 6.1) - perhaps to be expected given the relatively small associated heat flow. There is again an increase at the expected intercept associated with the increase in uncoupled losses but again, this is likely to be a smaller effect than seen in other heat loss mechanisms.

6.3.2 The impact upon *HLC* estimates

In figure 6.16 the estimated *HLC* using MLR for the same test dwelling (BRE-NOT-SLW) are compared for full building simulations in which sky losses are either present or absent (i.e. external surface emissivity = 0). The HLC_{meas}, estimated from MLR across the simulation data, shows a similarly accurate description of HLC_{True} in each case, indicating the random effect over two week periods is negligible. The most significant point to note is that, in the case considered here, there is a 4.5 W/K (6%) mean difference between the HLC_{True} of each case across the testing season [4]. This has again thrown up considerations of the definition of HLC_{pred}, HLC_{True} and HLC_{meas} and how the term Q_{sky} is incorporated into each. A difficult to measure and model heat flow, sky radiative losses lead to incomplete knowledge of the definitions of HLC_{meas} and HLC_{True} for the test dwelling and the conditions in which it was measured. For example, we could not distinguish between the build quality of two test dwellings by a heat flow smaller than the variation in Q_{sky}. Without consideration of sky losses, there is an inherent difference between the definitions of HLC_{pred} and HLC_{meas} and therefore definitional uncertainty and potential bias in their comparisons.

6.3.3 Addressing uncertainty from long-wave sky radiation losses

Losses due to Q_{sky} are challenging to measure. Estimating the effective sky temperature involves measurements of long wave radiation (via pyrgeometer or radiometer) or establishing the level of cloud cover to use with models of sky emissivity (see section B.35). Even then, the response of various building surfaces to this effective sky temperature has to be established. Incorporating T_{sky} as an independent regression variable is unlikely to be fruitful, given its the relatively small size of the associated heat flow (Q_{sky}) and correlation with T_e and S.

[4] Subbarao (1988a) assigned an audit term of similar magnitude to account for long wave sky radiation losses

The PSTAR method adopts an audit term to describe Q_{sky}, an approach that may help reconcile HLC_{meas} with HLC_{pred}, particularly if sky losses are ignored within the design calculations (e.g. BRE, 2014). However, this relies on assumptions over the building fabric and external environment and therefore may not actually provide any improvement in this reconciliation. Without significant investigations, perhaps the most appropriate approach would be to acknowledge the presence and uncertainty of Q_{sky} through the inclusion of error terms to either measured or predicted *HLC*s (see section 9.4).

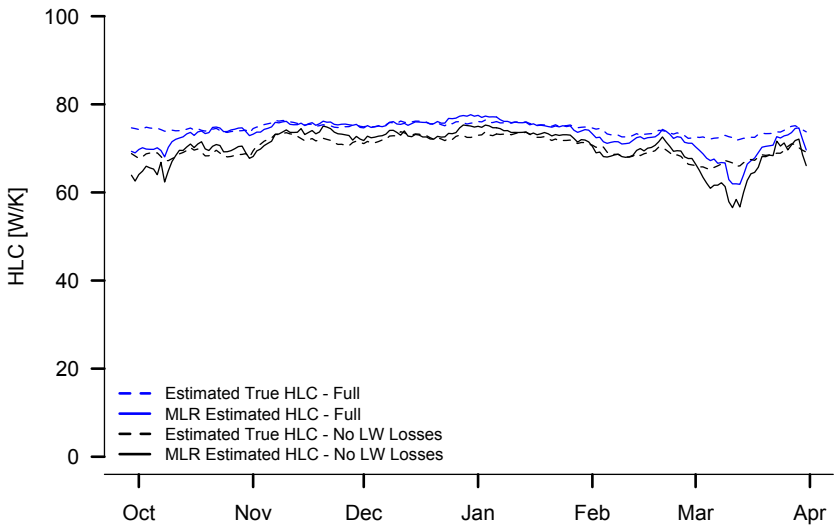

Figure 6.16: *HLC_{meas} in full weather file and with radiative losses removed.* (BRE-NOT-SLW-FINN.T_{sky}-SN-MLR-2w-24h-6agg)

6.4 Chapter conclusions

Several conclusions can be drawn from each of the three sections of this chapter, before a brief, more general discussion is given.

Conclusions drawn from the section on uncertainty due to stack and wind driven infiltration can be stated as:

- Stack and particularly wind losses increase the variation in daily data points, increasing the random error.
- The nature of the random error means HLC_{meas} shows an accurate measure of HLC_{True} as infiltration losses vary, without systematic bias, although the dispersion of data points increases.

- However, stack and wind losses increase and vary HLC_{True}, leading to definitional uncertainty and comparison errors between tests and to HLC_{pred}.

- More complex heat loss processes, driven by wind pressures and stack effects, can exist within the building fabric. These may include: wind washing, air looping or convective bypassing, and are unlikely to be modelled in simulations. These can further increase HLC_{True} and daily variation. In depth monitoring in the field may be required to identify and understand such effects.

- Infiltration measurements may help to disaggregate losses, reduce comparison errors and improve overall understanding of the test dwelling. However, the uncertainties and timescales of these measurements need to be considered and incorporated into uncertainty analysis.

- Regression using wind speed needs to be done with the possibility of a non-linear underlying relationship between wind speed and heat loss in mind. Filtering data may help with comparisons but is compromised by inconsistent wind measurements and unclear revised *HLC* definitions.

Further, uncertainty from dynamic external temperatures leads to the following conclusions:

- Dynamic external temperatures increase daily variation and random errors, with cold days following a warmer day underestimating steady state heating demand and vice versa.

- In short testing periods (e.g. single nights), bias may occur, depending on the direction of changing temperatures.

- Random error is reduced at longer aggregation intervals or across longer monitored durations, meaning *HLC* estimates are likely to remain accurate.

- The impact of dynamic T_e is likely to compound the underestimate from solar stored heat.

Finally, uncertainty from long-wave radiative sky losses can be considered as:

- Long wave sky radiation losses will increase the daily variation in heat loss and also influence HLC_{True}.

- Variation in Q_{sky} is likely to be small across two week monitoring periods.

- When monitoring for shorter periods, including just overnight, the variation in Q_{sky} is likely to be larger, increasing bias and comparison errors.

- Q_{sky} is hard to measure in field tests, although T_{sky}, cloud cover, long wave radiation and T_{se} can all be measured to begin to understand this heat flow.

- Including an audit estimate of Q_{sky} in HLC_{pred} calculations may provide a fairer comparison with HLC_{meas}.

6.4.1 Discussion of Uncertainty from Weather

The uncertainties considered in this chapter are typically random in nature, formed from heat flows outside those predicted in the simplified energy balance, rather than providing any systematic bias in *HLC* estimates (i.e. HLC_{meas} is an unbiased reflection of HLC_{True}). Rather, the most significant uncertainties take the form of *definitional* and *comparison* errors. As shown in this chapter, HLC_{True} is a function of the external environment during testing, including ΔT and therefore T_e, wind speed U_w and T_{sky}. This means that HLC_{meas} may vary between two identically performed tests, on an identical dwelling, performed under varying external conditions. The challenge this presents is in interpreting the test results. Without knowledge of these secondary heat flows within the dwelling comparisons between HLC_{meas} and HLC_{pred}, or even between sets of dwellings for which a HLC_{meas} has been obtained, may be biased themselves.

Solutions to this problem include incorporating additional terms into the heat balance equation and regression analysis - problematic when terms may be expected to be non-linear, vary on short timescales, correlate with other explanatory variables or a single weather variable drives heat loss in a number of ways. Alternatively, supplementary measurements of these heat flows may be performed, e.g. infiltration measurements. Here, the timescales or measurements need to correspond to the co-heating aggregated data points and any measurement uncertainty will need to be assessed, e.g. constant concentration tracer gas techniques. Such supplementary measurements may be crucial to precisely understand HLC_{meas}. Potentially, the feedback gained from such supplementary measurements may even outweigh the value of the HLC_{meas} determined. However, these supplementary measurements cannot be performed without additional time and resources and the overall purpose of the test must be considered.

The assumption that this error can be considered as random fails when long aggregations and monitoring periods are not adopted. Over short time frames, e.g. single days or night time periods, bias may occur due to the dynamic T_e proceeding the test and analysis period. Additionally, Q_{sky} is also likely to be largest during the night, leading to further definitional

and comparison errors. In fact, these errors are likely to be larger in shorter monitoring durations, where the test result may be susceptible to higher variations in the external environment.

Finally, there are a number of weather conditions that have not been considered in this chapter. Periods of high rainfall will increase the moisture content within the fabric of a test dwelling. The increased moisture content in the building fabric is likely to reduce thermal performance and there may be some additional latent heating loads associated with driving out the moisture from the fabric. The extent and duration of this increased heat loss will depend upon the precise construction of a test dwelling and the hygrothermal properties of its external elements. Whilst rain is not directly considered in this thesis, the issue of moisture more generally is addressed in section 7.6.

Chapter 7

Experimental Sources of Uncertainty

Chapter overview

In addition to uncertainty generated by weather and external boundary conditions there remain a number of sources of experimental uncertainty. These are presented and discussed within this chapter and include:

Uncertainties related to indirect or uncoupled heat loss to the external environment:

- **7.1 Uncoupled heat loss:** Losses to the ground & unconditioned spaces.
- **7.2 Party wall heat transfer:** Uncertainty due to heat losses and gains across party elements.

Deviations from the experimental assumptions:

- **7.3 Non-uniform internal temperatures:** Spatial variation in internal temperatures throughout a test dwelling.
- **7.1 Achieving quasi-steady state:** Uncertainty in heating a test dwelling to quasi steady state.

Further experimental uncertainties, including:

- **7.5 Equipment measurement errors:** From measureing Q_{elec}, S, T_i and T_e.
- **7.6 Moisture:** Uncertainty from latent loads and reduced thermal conductivity.
- **7.7 Operational uncertainties:** Uncertainties from the experimental set-up: elevated T_i and the presence of mixing fans.

7.1 Uncoupled heat loss

As identified when examining the heat loss from a dwelling, a number of heat loss pathways exist that, rather than being directly to the external environment and coupled to T_e, take indirect routes through elements such as the ground, unheated or unconditioned spaces (attics, garages, voids) or through adjoining heated spaces (neighbouring properties). Both Q_g and Q_{unc} can be considered losses uncoupled from T_e, at least across two week test periods and are therefore represented in the regression intercept, rather than the gradient (for further details see section 8.1). In the case of heat flow to adjoining neighbouring spaces (Q_{adj}), the temperature of an adjoining space (T_{adj}) can be higher than T_i, such that heat transfer may exist in either direction across the party wall. Party wall heat transfer is therefore treated separately in section 7.2.

These uncoupled losses can be considered as additional heat flow terms in the energy balance equation and may be better written as:

$$Q_{elec} + R \cdot S = HLC \cdot \Delta T + Q_g + Q_{unc} + Q_{adj} \tag{7.1}$$

A number of uncertainties can therefore be associated with these uncoupled losses:

- Variations in HLC_{True} creating comparison errors between tests and to HLC_{pred}.
- Uncertainty in HLC_{pred} due to treatment of uncoupled heat flows and expected thermal resistance.
- Uncertainty from dynamic uncoupled heat flows.
- Bias if T_g and T_{unc} have not yet been heated to a constant temperature (see section 7.4).

7.1.1 Ground losses

Everett (1985) was particularly concerned over the impact of ground losses on *HLC* estimates, especially the impact of their dynamics. Everett took the approach of subtracting out ground floor losses prior to regression (see equation 2.8) and estimated the uncertainty related to Q_g as 10 W/K for a 127 W/K dwelling. Such an approach is no longer normally adopted, although in other dynamic *HLC* estimation methods, an audit term is often used to describe floor losses (Subbarao, 1988a; Masy and Lebrun, 2004).

Much of Everett's uncertainty seemed to result from the 'complex' dynamics of the floor heat loss. However, Everett was initially testing an un-insulated floor and he himself questioned the accuracy and positioning of a small number of heat flux sensors on the floor. As seen

throughout this thesis, inaccurate measurements of secondary heat flows used to correct *HLC* estimates are only likely to introduce further uncertainty. Although ground temperatures and floor losses may change seasonally, in both the simulated and field test cases considered here, approximately constant losses across a test period are seen.

7.1.1.1 Measured ground floor losses

Ground temperatures vary with the annual mean temperatures, approximating the mean annual external air temperature and following a lagged response to seasonal changes in T_e. The seasonal change in T_g is likely to influence the value of HLC_{True} across a year or testing season. A dwelling tested in March is likely to experience lower ground losses than a dwelling tested in February, when T_g is lower. The scale of this effect will depend upon the area and U-value of the floor and its scale in respect to the total building heat loss.

Across a single test, the heat flow across a floor element is thought to be relatively constant after the initial heating period. Data from this initial heating period must be removed from analysis to avoid bias (see section 7.4). The measured heat flux from two field tests is shown in figure 7.1, each including two measurements on the ground floor, with one also incorporating measurements taken on a retaining wall. These measurements are shown to be constant throughout the test analysis period, with deviations due to short term solar overheating in CASE-B. Further, ground temperatures recorded during CASE-B and CASE-A2 tests can be seen in, figure 7.2 and 7.3.

In the case of suspended floors, particularly suspended timber floors, losses are more closely associated with T_e but are mediated by a more complex heat loss system (CIBSE, 2007; Pelsmaker, 2015a). Suspended timber floors could therefore be treated as unconditioned spaces, but as little is understood about their characteristics, they are considered beyond the scope of this research. In fact, ground losses in general are complex, hard to define and challenging to measure. Rather than any specific interest in determining ground losses, this thesis is concerned with the impact of ground losses on overall *HLC* estimates.

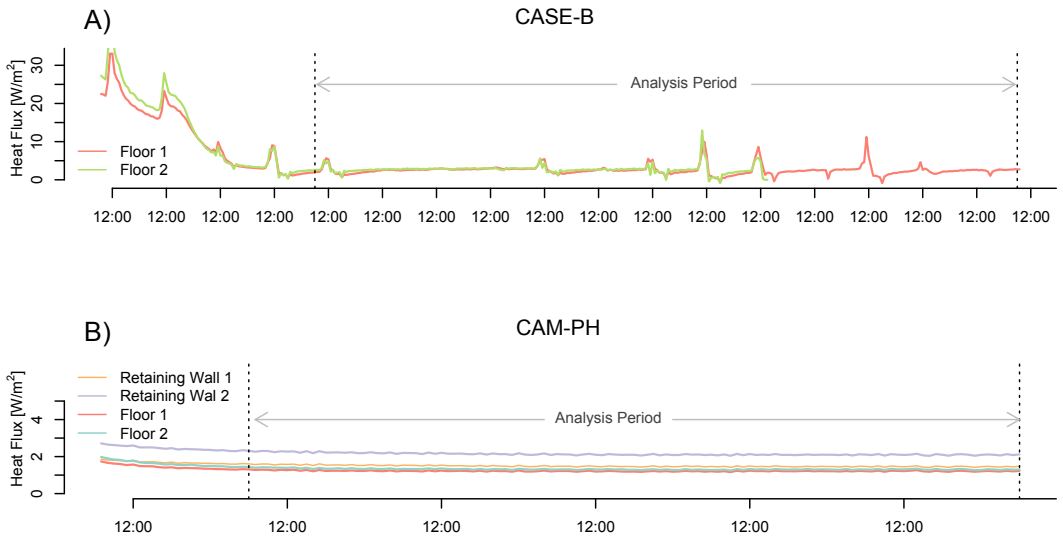

Figure 7.1: *Measured heat flux through ground elements from two field tests.* (Field Tests: CASE-B & CAM-PH)

7.1.2 Unconditioned spaces

Many dwellings will have unheated or unconditioned adjoining spaces, be they attics, garages or conservatories. In the UK, 93% of dwellings have a pitched roof often creating unheated attics and additional void spaces within the roof structure (DCLG, 2014). Further, 18% have conservatories and 40% have access to a garage[1] (DCLG, 2014). Typically these will fall outside the insulated envelope and therefore will also be unheated during a co-heating test. Therefore, such unconditioned spaces form indirect heat loss pathways to the external environment.

The temperature profile within each of these unheated spaces will depend upon the rate of heat transfer from within the heated dwelling into the space, the heat transfer (both conductive and infiltration) with the external environment and the influence of solar radiation, acting to heat the space.

Examples of such temperatures during co-heating field tests are shown for an unheated attic space (CASE-A2) and for an adjoining garage (CASE-B) in figures 7.2 and 7.3. Ground temperatures, T_g and adjoining heated spaces, T_{adj} are also included.

[1] This number includes non-adjoining garages.

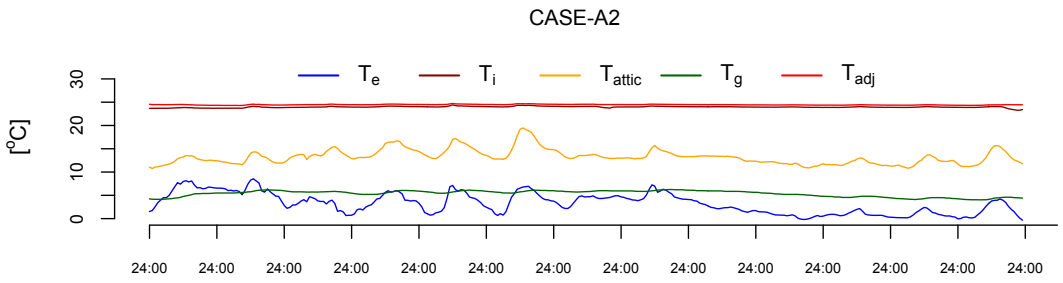

Figure 7.2: *Examples of uncoupled temperatures from field test. T_g is measured at an approximate 5cm depth and 3m from the perimeter of the test dwelling.* (Field Test CASE-A2))

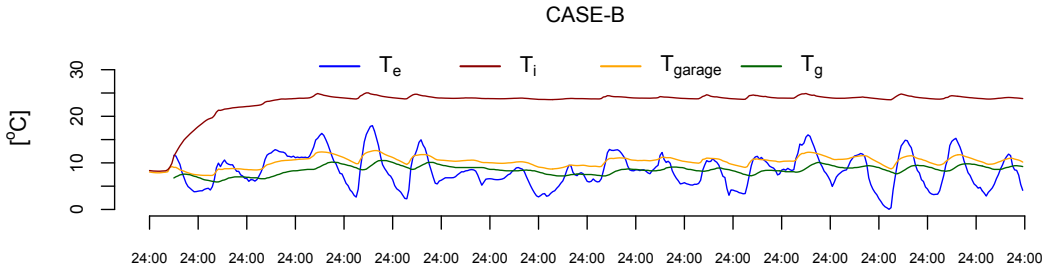

Figure 7.3: *Examples of uncoupled temperatures from field test. T_g is measured at an approximate 5cm depth and 3m from the perimeter of the test dwelling.* (Field Test CASE-B)

The garage temperature in 7.3, unglazed and with no insulation, stays at a relatively constant temperature, often below T_e. The attic, as illustrated in 7.2, shows a profile more similar in shape to T_e, at a higher average temperature. In this case, the attic shows a mean temperature (13.3 °C) approximately 10 °C warmer than the external air (mean = 3.3 °C) whilst in the CASE-B test the garage (mean = 10.3 °C) has a smaller discrepancy with the external air (mean = 8.3 °C). In either case, across 24 hour aggregation periods, these temperatures remain approximately constant. This is consistent with results seen during other co-heating tests (Miles-Shenton et al., 2010).

7.1.3 Impact upon a test dwelling & *HLC* estimates

Generally, if losses are constant across the aggregation periods and the ratio of uncoupled to coupled losses is small, the uncertainty from uncoupled losses is restricted. However, there are a couple of issues to consider.

The first point to note is that whilst the test dwelling itself may have reached quasi steady state, the surrounding unconditioned spaces may still be warming up, see figures 7.10 and 7.11. This is considered further in section 7.4.

Secondly, HLC_{True} will vary with both T_g and T_{unc}. For example, testing a building in early October, the ISO 13770:2007 (ISO, 2007) calculated Q_g is approximately 20W less than for the same dwelling in February. This is small for the BRE dwelling considered in this chapter, with a well-insulated floor. However, this can increase if the relative proportion of the floor area is increased or if it is uninsulated, with a difference of 173W observed in an uninsulated floor (1.2 W/m^{2}K).

Similarly, T_{unc} may vary seasonally with T_e, but also with the internal T_i and with the solar radiation received by the space. Temperature traces can be useful in determining any differences between tests or to the predicted performance of such spaces.

Design calculations will normally have accounted for the improvement in thermal performance of unconditioned spaces outside the insulation zone. In the simulated examples in figure 7.4, the addition of a garage space reduces the mean HLC_{True} from 74.5 W/K to 72.7 W/K (2%) and an attic space reduces the mean HLC_{True} to 70.1 W/K (6%). The SAP calculation methodology does not account for additional thermal resistance for non-integrated garages (BRE, 2014). To reconcile and understand any gap between HLC_{meas} and HLC_{pred}, the predicted thermal resistance of such zones could be reassessed from temperature traces or heat flux measurements.

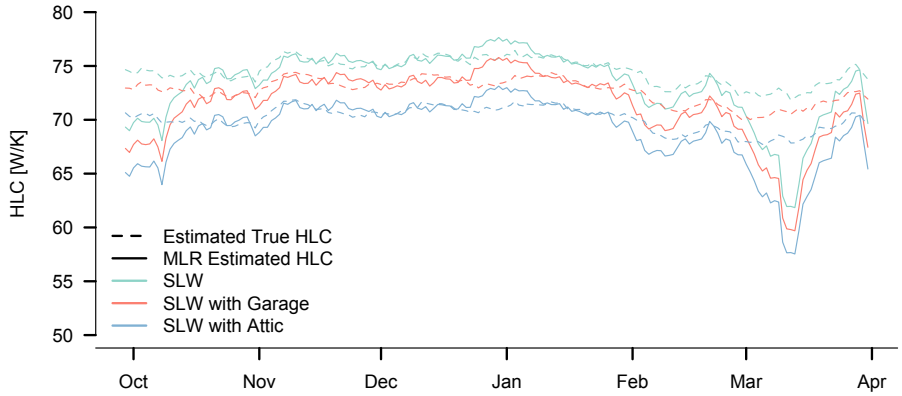

Figure 7.4: *HLC estimates with unconditioned spaces.* (Simulation: BRE-NOT-MW-ATT/GAR-FINN-SN-MLR-2w-24h-6agg-S_{GVS})

In reality, as shown in figure 7.4, many of these considerations are likely to be small unless large proportions of a building's heat flow are to uncoupled spaces. Such examples may exist however, including excavated dwellings, flats connected to corridors or bungalows with attics. Full consideration of how these 'buffer' spaces change the overall *HLC* may be required to accurately estimate and compare *HLC*s for such building types.

Further, in some cases the heat flows to the ground or unconditioned spaces may demonstrate more dynamic behaviour. For example, many existing dwellings have conservatories and some modern dwellings are constructed with design features such as sunspaces or winter gardens. These spaces may have highly variable temperatures, due to both high heat losses and high solar gains. These are likely to introduce more dynamic heat flows than the examples above, making monitoring temperatures and heat fluxes more important. Such dynamic uncoupled losses are largely ignored here, as careful and tailored monitoring and simulation may be required to evaluate their impact. However, it can be said that when such features exist, dense measurements of both temperatures and heat fluxes is likely to be beneficial, if only from a qualitative perspective.

7.2 Party wall heat transfer & unregulated gains

Considering adjoining heated spaces, in the current UK housing stock, detached dwellings only account for 17% of total dwellings, with a large proportion having some type of adjoining neighbouring dwelling: 26% semi, 29% terraced and 20% flats[2] (DCLG, 2014). Therefore, to evaluate the full range of the UK building stock and to assess construction details associated with party walls, tests methodologies must allow the testing of non-detached dwellings.

Performing co-heating tests on test dwellings with adjoining heated spaces creates a number of problems. Firstly, the overall envelope area connected to the external environment is reduced, decreasing the fraction of the envelope associated with ΔT. This can increase the scale of a number of other sources of uncertainty, including uncoupled heat transfer. Depending upon the temperatures of the test dwelling and adjoining spaces there maybe uncoupled heat gains or losses into the test dwelling. When testing a multifamily dwelling, Feuermann (1989) reported a vaguely estimated 21% error in the estimated *HLC* due to party wall heat transfer.

[2]The remaining 8% are classed as bungalows.

The experimental protocol adopted by Feuermann and the LBU protocol (Wingfield, 2010a; Johnston et al., 2013) attempts to 'guard' heat transfer across party walls and floors by heating any adjoining spaces or properties to the same experimental set point temperature. This then creates the assumption that these guarded party walls and floors are zero heat transfer elements. In practice, with variations in internal temperatures, solar gains and complex heat flow paths it is unlikely that heat transfer is completely avoided or that the direction of net heat flow is knowable by inspection or even clear through measurements. Nevertheless, Q_{adj} should be reduced, focusing the co-heating measurement on the external fabric.

Co-heating strategies for adjoining spaces then often extend to monitoring heat transfer, through surface temperature and heat flux measurements. On occasion these have been used to correct for heat transfer by extrapolating heat flux measurements across party walls (Ridley et al., 2010a), although correcting for any heat transfer detected may only lead to further uncertainty (Johnston et al., 2013).

Party wall heat transfer can be complex, showing behaviour beyond that of simple conductive heat transfer. Air movement and convective bypassing within the party walls, the presence of thermal bridges and 3-dimensional heat transfer can make guarding, understanding and measuring these heat flows more challenging. Party wall heat flows can be categorised as either co-planar or perpendicular. Whilst co-planar flux ends up next door, perpendicular flux can be further divided into i) predominantly vertical flow due to convective bypassing and ii) horizontal flow driven by windward-to-leeward pressure differences. To begin with, this section will examine co-planar party wall heat transfer from a simple, conductive perspective, before contemplating these further, more complex issues, although a full analysis is avoided.

7.2.1 Practicalities of guarding

To successfully guard adjoining spaces, access is required to one (or potentially more) dwellings. This may not always be possible, particularly when neighbouring dwellings are already occupied.

There are also cases in which there has been no access to neighbouring adjoining spaces, meaning that temperatures cannot be controlled or in some cases even temperature sensors cannot be deployed (e.g. Palmer et al., 2011). In these cases, there is high potential for uncertainty in *HLC* estimates and dynamic heat flows.

Considering uncertainties due to adjoining heated spaces, three cases can be considered:

1. *Ideal guarding:* no heat transfer across the party walls/ ceiling.

2. *Offset guarding:* adjoining spaces are at temperatures just above or below the test dwelling experimental set point.

3. *Zero guarding:* adjoining spaces cannot be accessed and are heated by the occupant.

4. *Variable guarding:* taking account of the variation e.g. of party wall temperature across the surface of the party wall.

7.2.2 Impact upon a test dwelling & *HLC* estimate

If we consider equation 7.2, using a non-intercept regression model[3], in its simplest form the nature of the uncertainty from party wall heat transfer is straightforward. If there is a net heat flow into the test dwelling, the *HLC* will be underestimated. Equally, if the net heat flow is out of the dwelling then the *HLC* will be overestimated.

$$Q_{elec} + R \cdot S = HLC \cdot \Delta T + Q_{adj} \tag{7.2}$$

Furthermore, the scale of this under /overestimation will approximately scale with the percentage Q_{adj} makes up of the total heat input, $Q_{elec} + R \cdot S$. Uncertainty due to party wall heat transfer therefore increases with:

- Uninsulated party walls / higher party wall U-value.
- Higher party wall area.
- Higher ΔT_{adj}.
- Lower ΔT.
- Lower coupled heat loss.
- The presence of a cavity or cavities within the party wall.

[3] As discussed later (see section8.1), if an intercept model is used, Q_{adj} will likely end up in the intercept as the dwelling-dwelling heat transfer is unlikely to be proportional to ΔT. However, if convective bypassing occurred, then this may be expected to show some correlation with ΔT. This is one reason to examine both models (see fig 9.17)

7.2.3 Simple models of the uncertainty from party wall heat transfer

To initially explore the impact of party wall heat transfer, the same simple building model (80 W/K, 6 m^2) across the Finningley Weather file is explored with various party wall heat flows. Figure 7.5 shows the estimated *HLC* with an un-insulated party wall (U-value = 2.33 W/m^2K) (CIBSE, 2007) across a number of temperature differences and with increasing party wall area (representing a semi to a terrace dwelling). An example with a lower party wall U-value (0.30 W/m^2K), from a wool sound insulation system (Knauf, 2015) is then shown with a high ΔT_{adj}. Note the *HLC* of 80 W/K, which relates to the area of the dwelling exposed to the external environment is not altered, with party wall heat flows acting as additional heat flows.

Considering the well insulated party wall, even with large temperature differences (ΔT = 5 K) Q_{adj} is small (39 W) relative to the mean total heat input (1238 W) and therefore the impact on HLC estimates is small ($\sim$ 3%). When the party wall has a high U-value, with a small temperature difference (ΔT_{adj} = 1) a similar scale of systematic error is seen ($\sim$ 4%).

If ΔT_{adj} increases then the size of the heat flow increases with the systematic error in *HLC* scaling approximately with $(\frac{Q_{adj}}{Q_{elec}+R \cdot S})$. For a terraced dwelling, with uninsulated party walls and with ΔT_{adj}= 2 °C, this gives a mean shift of 19% in *HLC*, certainly not insignificant. Clearly, the size of Q_{adj} needs to be assessed as a significant shift in *HLC* can occur. This means that accurately testing buildings with either large party wall areas, and/or uninsulated party walls, is more challenging and requires higher experimental control.

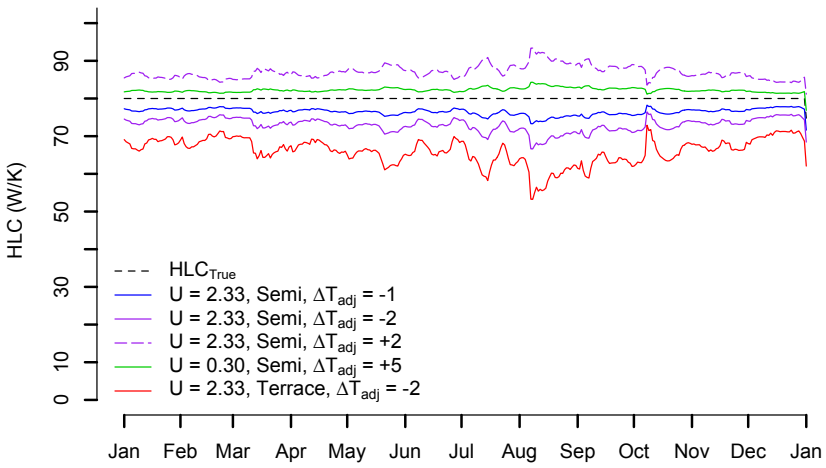

Figure 7.5: *Estimated HLC due to varying ΔT_{adj} and party wall UA from calculations.* (Modelled: FINN-MLR-2w-24h-6agg)

7.2.4 Example of party wall heat transfer from field data

Two field tests conducted as part of this thesis were on a semi-detached dwelling, as such having one party wall (CASE-A1& CASE-A2). Temperatures were guarded, and the party wall heat flux was also measured at four points. For CASE-A2, an estimated Q_{adj} was calculated from the mean of these sensors and extrapolated across the area of the party wall (figure 7.6).

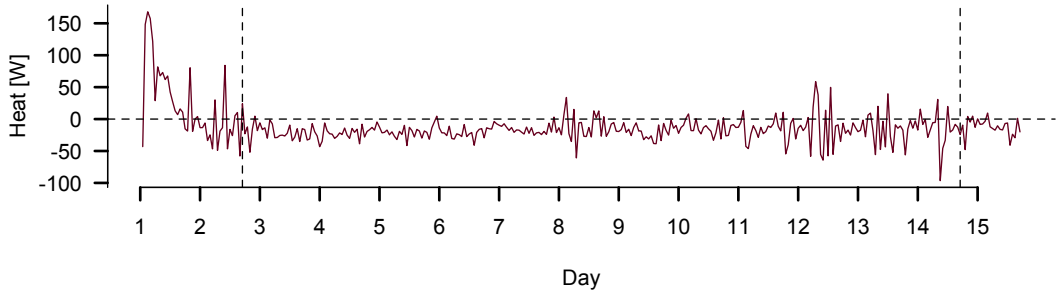

Figure 7.6: *Heat flow across party wall. Vertical dotted lines indicate period used in analysis.* (Field Test: CASE-A2)

The mean estimated party wall heat transfer, calculated from equation 7.4 for the four heat flux sensors, was -22 W, less than 1% of the average total heat input into the house. This would indicate any uncertainty from the party wall is negligible. Similarly, whilst there are small hourly variations, across daily aggregations the heat loss is approximately constant. However, as seen in figure 7.7 these sensors may not fully explain the heat transfer across the party wall.

In an earlier test of the same dwelling (CASE-A1), before the external walls were insulated, the estimated Q_{adj} was 214 W, attributed to a higher ΔT_{adj}. This still represents a small but perhaps not insignificant proportion of the total heat input (4%). These results illustrate how party wall heat flows may need to be estimated and their uncertainty considered within *HLC* statements, particularly in retrofit cases (see section 9.4.7.2).

7.2.5 Non-constant & non-homogenous party wall heat transfer

So far, Q_{adj} has been considered constant and simple, relating to the U.A value of the party wall and the temperature difference, ΔT_{adj}. In reality, we can expect party wall heat transfer to be far more complicated, featuring multidirectional heat flows and air movement within and across the party wall. Additionally, even when guarded, solar heat may introduce unstable temperatures and dynamic heat flows. To begin to explore such issues, an example from field data is considered.

Figure 7.7, shows heat transferred across the top of the party wall of the test dwelling, into the neighbouring dwelling. The second thermogram, taken whilst the test house was under pressurisation, shows warm air leaking into the first floor void of the neighbouring dwellings, likely to be the result of floor beams penetrating the party wall. Such complex heat flows may make it impossible to accurately calculate party wall heat transfer. However, the measurement process often qualitatively identifies a problem that can subsequently be fixed, if not in the dwelling under test, then in all future dwellings of a similar construction, through changes in regulation and construction practice. Through attempting to account for such heat transfer, the processes within the party wall may be better understood, even if just qualitatively, potentially providing useful and effective feedback.

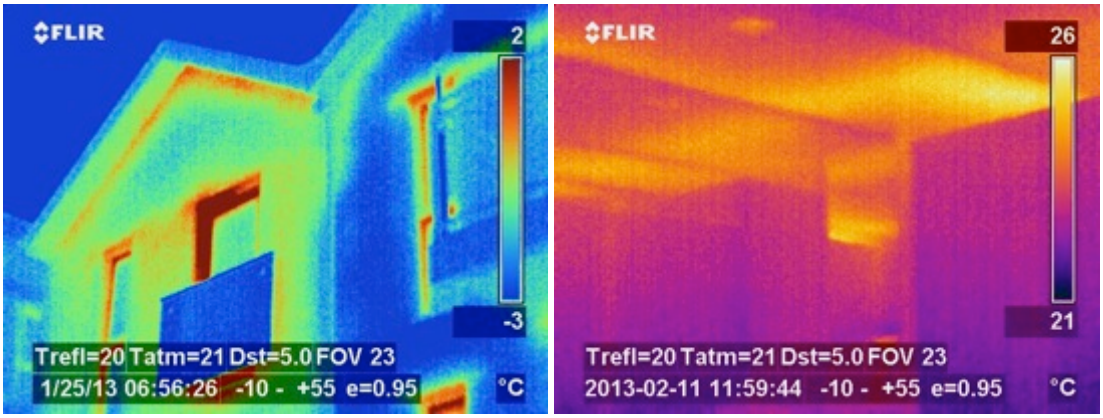

Figure 7.7: *Heat transfer across top of party wall and within an internal floor space. The image on the right shows the test dwelling (left) with heat being lost across the top of the party wall into the attic of the adjoining, guarded dwelling. The image on the right has been taken inside the adjoining property, whilst the test dwelling is being pressurised. Warm areas appear within the floor space of the adjoining property, whilst this the test dwelling is pressurised.* (Field Test: CASE-A)

7.2.6 Identifying and accounting for party wall heat transfer

If the adjoining space can be guarded with carefully matched internal temperatures, then the uncertainty generated will be significantly reduced. To adequately monitor this, T_i needs to be monitored on both sides of the party wall, ideally with the deployment of both surface temperature and heat flux sensors. In such cases, the representativeness of the sensors' locations must be considered. Ideally, to fully assess the heat transfer, the party wall should be saturated with sensors. Even then, there may be complex heat exchanges that cannot be measured. When effects such as convective bypassing are present, they may induce a more complex and variable

temperature field across the surface of the party wall, making adequate sensor placement and supporting thermographic investigations even more important.

Parallel pressure tests may also allow the estimation of air leakage between two dwellings, as well as the identification of air leakage paths. Finally, thermal imaging, preferably both with and without a temperature difference between the dwellings, could help reveal any thermal bridges and bypasses. Such methods may also help to qualitatively distinguish between heat flows across party walls to the external environment and those direct to the neighbouring dwelling.

For these more complex heat transfer pathways it may not be possible to calculate their scale, only on the likely direction of impact on *HLC* estimates. For more straightforward conduction across the party wall, Q_{adj} can be estimated (see equations 7.3 and 7.4).

Alternatively, Feuermann (1989), suggested initially testing a dwelling with guarded temperatures, $T_i = T_{adj}$, but then increasing T_i (or decreasing T_{adj}) by 10 °C to then estimate the party wall heat transfer. In the absence of a convective bypass, this method may allow estimation of the heat loss coefficient (HLC_{adj}), incorporating perpendicular heat flux through the party wall. When heat flow is not completely co-planar across the party wall elements, and some convective bypassing exists, the quantitative measurement of Q_{adj} achieved through this method may be prone to bias or not represent the actual heat flows present. Additionally, this measurement may not represent the heat flows across the same period and will further prolong the overall testing duration. However, it may be a useful technique to shift focus and attention to the issue of party walls, allowing both quantitative and better qualitative (i.e. thermal imaging, air leakage paths) understanding of party wall constructions and thermal performance.

7.2.6.1 Audit terms for uncoupled heat transfer

Most simply, the expected ground, unconditioned or net party wall heat transfer can be calculated from a U.A value and ΔT_{unc}. This can be used to estimate Q_{unc}, the percentage of $Q + R \cdot S$ this represents and then the likely reduction/ increase in *HLC*. For each element *k*:

$$Q_{k,g/unc/adj} = \sum_{0}^{k} (U.A(T_{i,k} - T_{k,g/unc/adj})) \tag{7.3}$$

Alternatively, Q_{adj}, can be determined from measured heat fluxes (q_k), extrapolated across the party wall area.

$$Q_{k,g,unc,adj} = \sum_{0}^{k}(q_k A_k) \tag{7.4}$$

All these methods will be subject to their own uncertainties, due to error in the measured/ assumed values and the representativeness of sensors locations (Johnston et al., 2013). Therefore, any corrections made may actually increase the overall bias in *HLC* estimates, particularly where incorrect functional forms have been adopted. The recommendation therefore would be to state both uncorrected values, and estimates of Q_{unc} and the corrected *HLC*, along with appropriate uncertainty estimates for both (see section 9.4.7.2 for an example). By at least reporting either of these two estimates, it is possible to understand the potential direction and scale of any bias. This is likely to be significant if the party wall has a high U-value, or party wall areas constitute a large percentage of the total envelope of a test dwelling. The application of co-heating to flats, one extreme example of this, is discussed in further detail in section 9.1.3.2.

7.3 Non-uniform internal temperatures

The co-heating experimental protocol incorporates a number of heaters, thermostats and mixing fans to create as uniform an internal temperature as possible. This allows the building to be considered as a single zone in the energy balance equation.

However, in practice internal temperatures are likely to vary, depending upon the location of the heating and mixing equipment and due to the layout and characteristics of the rooms within a test dwelling. A spread of internal temperatures can therefore exist within a zone/ room or between zones. When the variation in T_i is significant, this can present problems in determining a representative T_i for analysis and bias *HLC* estimates. This can be particularly problematic in cases in which the heat loss is unevenly distributed across the building fabric (Mangematin et al., 2012), instances in which several constructions are used, differing floor and roof thermal performance, concentrations of lower performing glazing elements, or potentially where the structure is more complex and leads to higher number thermal bridges, faults and air leakage paths. Such instances place a higher significance on the derivation of a representative internal temperature, while making it more difficult to achieve this in practice.

7.3.1 Impact upon a test house

The internal temperatures from two field test dwellings (NHBC & CASE-B) are shown in figures 7.8 and 7.9 respectively. Figure 7.8 is a useful example, as the first four days show particularly poor mixing, which improves after fan and heater locations are adjusted. This reinforces the extent to which both researcher experience and a watchful, rather than fit and forget, approach is preferable, a recommendation of the LBU protocol (Wingfield, 2010a; Johnston et al., 2013).

In particular, lower temperatures are associated with zones or rooms in which heaters were not directly deployed. The relatively tight floor plan[4] makes mixing between rooms tricky and therefore lower and less controlled temperatures are seen in these rooms (Z3, Z4 and Z7).

The second figure, 7.9, shows similar mixing profiles across a larger dwelling. In particular, the winter garden is a small but relatively high heat loss zone. This zone is small but highly glazed and was not sufficiently heated by the heating strategy adopted, resulting in lower temperatures. This is likely due to a combination of its high heat loss, lack of connection to the rest of the dwelling and a lack of equipment used in the test. The handling of this zone in the representative T_i then becomes significant.

When internal temperatures show a wider variation, calculating a representative internal temperature for use in analysis becomes more important. Three approaches can be taken (Palmer et al., 2011). A simple arithmetic mean, a volume weighted or a heat loss weighted T_i can be determined, all of which are shown on both figures, calculated from the equations below. The resulting *HLC* estimates from each approach are then shown in table 7.1. This also includes a partial arithmetic mean case, in which a mean is taken from temperature sensors deployed only in directly heated zones. The potential flaws in such an approach are clear. However, it is included for consideration here, as this approach has been noted in some test reports (see Jack, 2015b).

$$T_i^{SA} = \frac{\sum_j^n T_{i,j}}{n} \tag{7.5}$$

$$T_i^{vol} = \frac{\sum_j^n (T_{i,j} \cdot w_{vol,j})}{n} \tag{7.6}$$

$$T_i^{HLC} = \frac{\sum_j^n (T_{i,j} \cdot w_{HLC,j})}{n} \tag{7.7}$$

[4]Floor plans can be seen in the appendix, A.4.1

Where:

$$\sum_{j}^{n}(w_{vol,j}) = 1 \tag{7.8}$$

And:

$$\sum_{j}^{n}(w_{HLC,j}) = 1 \tag{7.9}$$

Where there are *n* sensors, with weighting factors based on either the volume, w_{vol} or heat loss, w_{HLC}, of the respective zones, *j*.

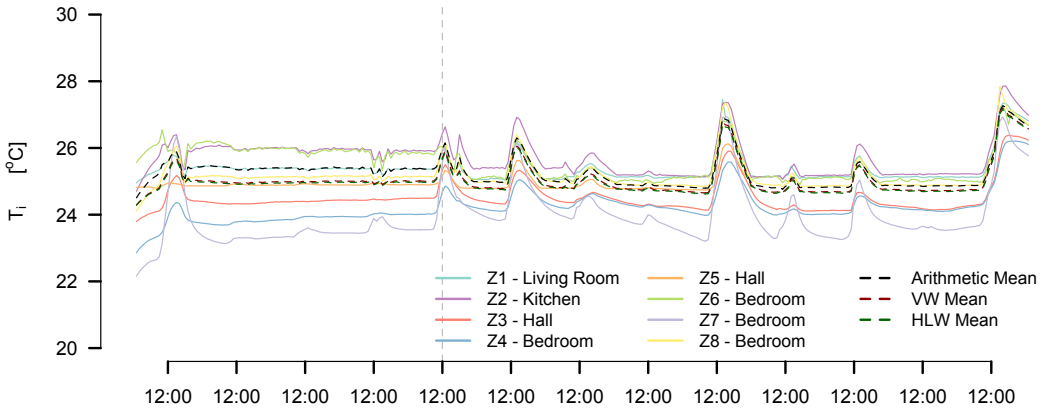

Figure 7.8: *Temperatures throughout a test dwelling. The eight zonal temperatures are shown (Z1-Z8) along with various calculated internal temperatures (arithmetic mean, volume weighted and heat loss weighted). The vertical dotted line indicates when the researcher adjusted the position of heating and mixing equipment.* (Field Test: NHBC)

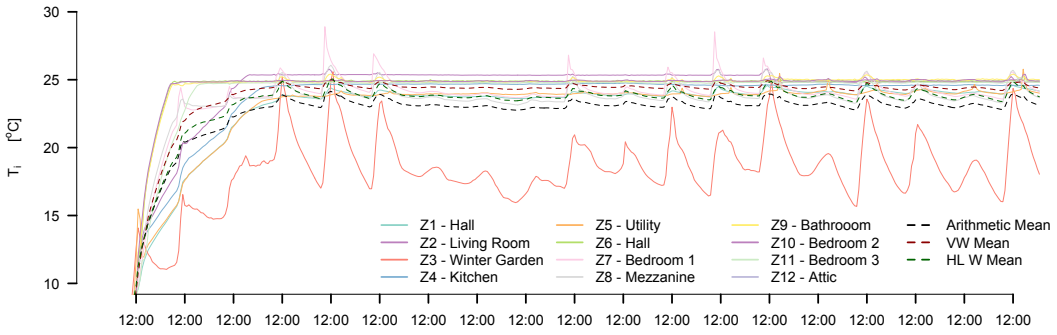

Figure 7.9: *Temperature distribution throughout second test dwelling.* (Field Test: CASE-B)

Table 7.1: *HLC* estimates from different T_i calculation methods

	Calculation Method	Mean T_i (°C)	HLC (W/K)
NHBC	*Arithmetic*	25.3	69.4
	Volume Weighted	25.0	70.4
	Heat Loss Weighted	25.0	70.4
	Partial Arithmetic	25.5	68.7
CASE-B	*Arithmetic*	23.2	255.8
	Volume Weighted	24.5	236.1
	Heat Loss Weighted	23.9	245.8
	Partial Arithmetic	24.8	231.0

In the BRE test dwelling the various approaches make minor differences to the estimated *HLC*, a range of 1.1 W/K between the three full approaches. In the CASE-B test dwelling more significant variations are seen, with a range of 19.7 W/K (8%), or 24 W/K if only a partial arithmetic mean T_i is taken. This is principally as a result of the winter garden, and the attic, a single zone that accounts for a quarter of the total heat loss and has poor thermal exchange with the rest of the dwelling[5].

Such variations are not insignificant, enforcing the need to consider the approach adopted to calculate T_i and for successful mixing strategies. These are compared and discussed in the light of simulations in the following section. Furthermore, if temperatures are not recorded throughout the test dwelling, then increased errors may occur and more damagingly may not be observed.

7.3.2 Impact upon *HLC* measurement

Comparisons of T_i calculation methods are easier in simulated test dwellings where HLC_{True} can be determined. Initially, this can be considered in the simplest case in which the temperature difference exists between two zones, specifically, the ground and first floor zones of a simulated test dwelling (BRE-NOT-MW). Two constructions are considered. In the first, the test dwelling is as used elsewhere in this thesis is used, in which the respective heat loss is split at 46% and 54% for the ground and first floors respectively - resulting in a 'minor bias'. In the second 'bias' case, these percentages are further spread to 40% and 60%, still ensuring the overall *HLC* remains the same. Finally, a 'high bias' case increases these percentages further, such that 25% of heat is lost from the ground floor and 75% from the first floor.

[5]This particular test dwelling had a large attic, insulated at both the pitched roof and ceiling level, as the attic was not sold as a living space, but the option to convert was built-in. The only direct connection was therefore through a small loft hatch

Table 7.2: Estimated *HLC* from two zone model. (Modelled: BRE-NOT)

Construction	HLC1 (W/K)	HLC2 (W/K)	T1 (°C)	T2 (°C)	Te (°C)	Q1 (W)	Q2 (W)	Q_{Tot} (W)	Arithmetic Mean Estimated HLC (W/K)	HLW Estimated HLC (W/K)
Minor Bias	32.4 (40%)	48.6 (60%)	25	25	8	551	826	1377	81.0	81
			24	26	8	518	875	1393	82.0	
			23	27	8	486	923	1409	82.9	
Bias	27.0 (33%)	54.0 (66%)	25	25	8	459	918	1377	81.0	
			24	26	8	432	972	1404	82.6	
			23	27	8	405	1026	1431	84.2	
High Bias	20.3 (25%)	60.7 (75%)	25	25	8	344	1033	1377	81.0	
			24	26	8	324	1094	1418	83.4	
			23	27	8	304	1154	1458	85.8	

In table 7.2 three distributions of internal temperatures on the ground (T1) and first floor (T2) are considered. These are calculated using a constant T_e, representative of the mean T_e across Oct-Mar of the Finningley weatherfile. Equation 7.10 is then used to determine the heating loads for each of the three cases.

$$Q_{elec} + R \cdot S = HLC_1 \cdot \Delta T_1 + HLC_2 \cdot \Delta T_2 \tag{7.10}$$

This basic example further demonstrates the issue. The higher the variation in internal temperatures, and the higher the heat loss bias of zones, the further the arithmetic mean is from the input *HLC*. Correctly weighting temperatures by heat loss consistently provides this input *HLC*. In many cases, with small variations in T_i, and similar constructions throughout the test dwelling, such errors will be small. However, if the mixing strategy is less successful and the building contains complex structures, the error can be significant.

7.3.3 Approaches to non-uniform T_i

Three approaches to reducing errors from non-uniform T_i can be considered: (1) measuring T_i, (2) mixing strategies and the (3) calculation of T_i.

In terms of temperature measurements, it is important reliable measurements are made in all rooms. If possible, several measurements can be made in large rooms, depending on practical, time and cost constraints. Measurements within rooms should also provide information on the uncertainty of temperature distributions within zones and the suitability of sensor locations.

Regarding mixing strategies, sufficient and suitably placed heaters, thermostats and mixing fans are required, although the impact these have on internal surface resistances may need to be considered (section 7.7.2). The analysis in 7.2 would suggest that if possible temperatures should be within a spread of at least 2 °C throughout a test dwelling. This is achievable but requires a suitable number of well placed heaters and fans. Both examples in figures 7.8 and 7.9 utilised too few heaters and fans[6]. The size of the domestic ring main can also be an obstacle in deploying sufficient equipment (Johnston et al., 2013). Traditionally, fan heaters have been used, but more success maybe gained using heaters with variable output (Johnston et al., 2013) or through using low temperature radiant mats (Pandraud and Fitton, 2013), although the impact of higher radiant fractions need to be considered as heat will be delivered more directly to the internal surfaces of external walls. Figure 7.8 also suggests the importance of monitoring the initial internal temperature profiles and making adjustments if required.

Finally, it is useful to consider the calculation of T_i. In general, an arithmetic mean may not suitably weight the size of the zones and their respective heat loss. Volume weighting may provide too high weightings for zones, which actually have little heat loss, i.e. bathrooms and cupboards with little or no envelope area. Weighting by heat loss is likely to provide the best estimate of the building *HLC*. However, it is worth remembering that it is impossible to precisely heat loss weight zones, as their actual heat loss is not known and is rather the subject of the test. In such cases, an exposed envelope area weighting systems can be used.

7.4 Achieving quasi steady state

The co-heating method also assumes that internal temperatures are approximately constant with time across the monitoring period. In reality, there are likely to be deviations from this, as seen earlier in instances of solar driven overheating (section 5.5). Examining the results of field tests conducted as part of this research, it is this solar driven overheating and the initial test period, as the building heats up to quasi steady state, that are the major instances of non-constant temperatures. Experimental control may also drive non-constant temperatures, although this is likely to be a result of inadequate equipment and heating strategy. This may particularly apply to tests which use the existing domestic heating system and therefore lack temperature control. In most cases however, this is though to be a minor effect and it is the initial warm up period and any uncertainty it introduces that is examined in this section.

[6] Sets of thermostatic controllers, heaters and fans cost in the region of £400

7.4.1 Heating to quasi-steady state

In the majority of cases, test dwellings will need to be heated to reach the experimental set point. This will mean heating their internal mass to $T_{setpoint}$ and the thermal mass within the envelope to a temperature in an approximated equilibrium with the internal and external temperatures. This can take anywhere from a day (Andrews, 1995) to a week (GHA, 2011b), depending on the original temperature of the building, the heating capacity installed and the mass of the dwelling. Johnston et al. (2013) also points out that this will be dictated by the residual moisture within the building fabric, although this issue is considered separately in this thesis (section 7.6). Importantly, this warm up period can set a limit upon the total time to conduct a test (section 9.2), although this may be reduced by pre-heating the dwelling.

During the heating phase, additional heating power is required, associated with heating the thermal mass of the dwelling. This period of data will then have to be removed from analysis and is often identified through observing internal air temperatures or electric heating loads. However, internal air temperatures can appear to have reached equilibrium whilst some of the heaviest building elements are still being heated. This means data points, biased by the additional heat flows into the thermal mass, remaining within *HLC* analysis.

7.4.2 Impact upon *HLC* estimates

Daily data points in which the thermal mass of a test dwelling is still being heated will require higher heat input (Q_{elec}) than predicted in the co-heating energy balance. If these data points are included in non-intercept MLR, then they will influence a higher *HLC* estimate.

7.4.2.1 Evidence in field data

Figure 7.10 shows the daily MLR results from a field co-heating test, including the initial warm up days that are excluded from analysis. Figure 7.11 then shows the corresponding internal air temperature, Q_{elec} and readings from heat flux sensors located in the test dwelling. It is clear that day 1 should be removed from the data set from either the T_i or Q_{elec} plots. However, these both appear flat for day 2, the removal of which can more easily be justified from the heat flux plot, figure 7.11c. Further examples from heat flux measurements can be seen in the discussion on ground losses, figure 7.1.

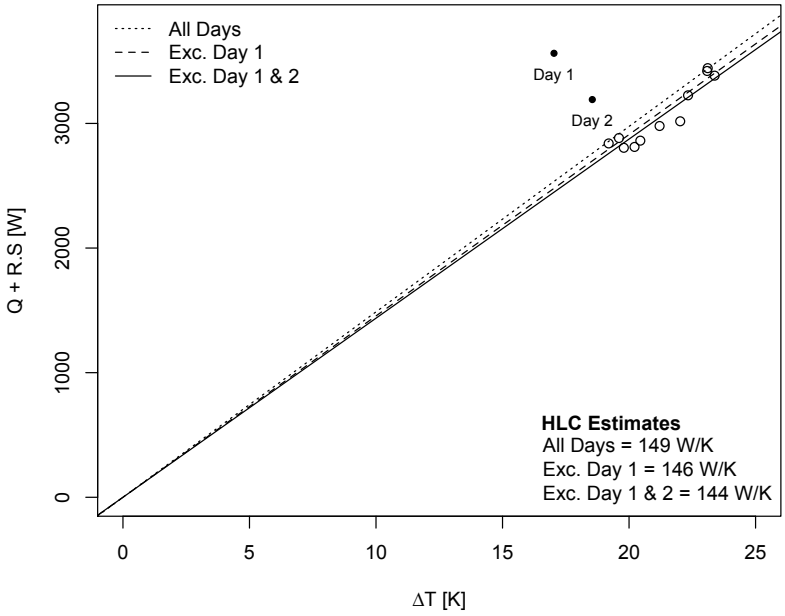

Figure 7.10: *Field test with initial heating phase included. MLR analysis with solar corrections has been applied to all data points.* (Field Test: CASE-A2-MLR-11d-24h-6agg-S_{GVS})

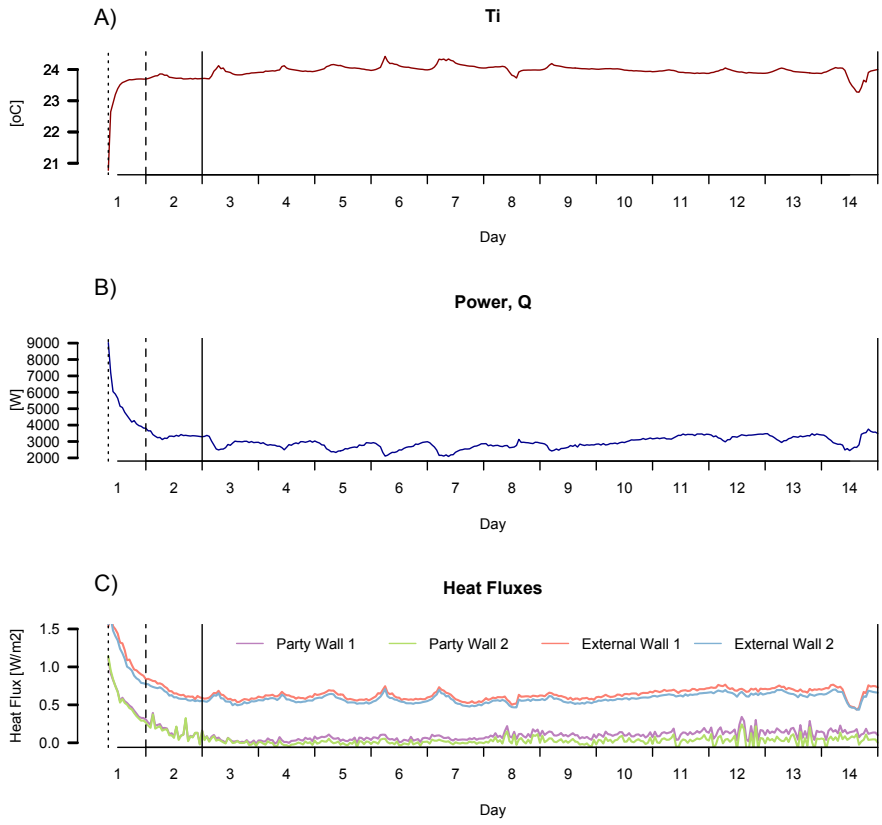

Figure 7.11: *Corresponding T_i and heat flux measurements.*

7.4.3 Identifying, estimating & reducing error

The approach to equilibrium and quasi-steady state will be asymptotic. Judgement is therefore required to define when suitable conditions have been reached. The shape of the approximately exponential heating curve will depend upon the ratio of mass to excess heating capacity. This may therefore vary considerably throughout a dwelling, as the constructions and distribution of heating equipment varies. Whilst some rooms have reached quasi steady state, others may still be warming up. Whilst heavyweight dwellings and rooms may require the longest warm up, it is potentially lightweight constructions with heavyweight elements (i.e. timber frame with concrete floor) where the bias from heat flows into thermal mass are most likely missed.

Surface temperature or heat flux measurements can help identify when some elements are still being heated (see figure 7.10). This re-enforces the benefit of deploying a higher number of heat flux sensors across the building farbic. Additionally, the influence of the initial data point(s) on the *HLC* estimate should be checked. This error is likely to be small, and only effect a single day of data. In such cases, these data points need to be removed from analysis.

7.5 Equipment measurement errors

Estimating the *HLC* depends upon the measurement of four key variables: Q_{elec}, the electric power input (units of W or Wh), ΔT consisting of T_i and T_e (°C) and the solar radiation (W/m^2). Each measured variable will be associated with a degree of sensor measurement uncertainty, the scale of which depends upon the sensors used and the monitoring strategy adopted. The sensitivity of the *HLC* estimation to uncertainties in each of these variables is explored in this section. Whilst a wide variety of different sensing equipment is used by various research teams, for guidance, table 7.3 sets out the listed accuracies of sensors used by the author in field co-heating tests conducted as part of this thesis.

Table 7.3: Example of instrument sensor accuracies.

Measurement Variable	Sensor Model	Stated Accuracy
Ti	*Eltek GC10*	± 0.10°C
	Onset Hobo U12-012	± 0.35 °C
Te	*Eltek OD43-J*	± 0.20 °C
	Davis Vantage Vue	± 0.50°C
ΔT	Combined Accuracy	± 0.22 - 0.40 °C
S [W/m^2]	*Kipp & Zonen CMP3 Pyranometer*	3-6%
Q [W]	*Elster AC100*	1-2.5%

7.5.1 Systematic measurement uncertainties

Any random sensor errors are likely to be averaged out due to the large number of readings taken and aggregated into a single daily measurement. However, a number of systematic errors may occur, effecting all measurements. These include:

External temperature, T_e

- *Calibration offset:* Particularly important if only one sensor deployed.
- *The influence of solar radiation:* Most commonly, external sensors are shielded in Stevenson screens but not ventilated. Solar radiation may still have an impact on such devices. (Everett, 1985) suggested the use of aspirated external temperature sensors. Similarly, placing sensors too close to the external building fabric can falsify readings.

Internal temperature, T_i

- *Calibration offset:* Reduced by using multiple sensors.
- *The influence of solar radiation:* Typically sensors are placed in positions out of the way of direct solar radiation. Palmiter (1979) referenced lab work showing that without any shielding, even small sensors placed out of direct sunlight displayed a 3 $^{\circ}$F (1.7 $^{\circ}$C) higher temperature than doubly shielded sensors.
- *Sensor location & heaters:* If sensors were placed in front of heaters, then a systematic bias would occur. More generally, the location of sensors throughout the test dwelling may exhibit a systematic bias, if for example T_i was measured at a set height and strong stratification occurred.
- *Radiant fractions:* Some large air temperature sensors may in fact measure a proportion of the radiant heat. Typically, if surrounded by cold walls, this would lead to a negative bias.

Heating power, Q_{elec}

- *Calibration offset:* Again, potentially high if a single meter is used for whole electrical load.
- *Logger bias:* Pulse outputs may have to be individually calibrated within logging programmes, leading to additional calibration offsets.

- *Unregulated gains:* Gains not plugged into kWh meters, including missed internal equipment, lights, battery operated equipment.
- *Surplus loads:* Loads outside the thermal envelope, particularly susceptible if using main electric meter, e.g. external security light, garage or attic equipment/ lights.

Solar radiation, *S*

- *Calibration offset:* Zero offsets can occur due to thermal radiation and the temperature of the device.
- *Directional error:* Error in measuring solar radiation received from wide angles (Zonen, 2013).
- *Location bias & Shading:* A reduced measurement due to local shading, not reflective of the building as a whole.

The sensitivity of *HLC* to these systematic uncertainties is modelled over the same weather file (Finningley), with the same building parameters as in previous simple building models (*HLC* = 80 W/K, $R = 6$ m^2). Typical uncertainties are used with both absolute and percentage systematic sensor errors explored. The results are shown in table 7.5.

Table 7.4: Estimated *HLC* due to systematic sensor measurement uncertainties. (Modelled: FINN-MLR-2w-24h-6agg-S_{GVS})

	Systematic Error	Mean HLC Estimate [W/K]			Mean R Estimate [m2]		
		Full Year	*Oct-Mar*	*Apr-Sep*	*Full Year*	*Oct-Mar*	*Apr-Sep*
Q	± 50 W	± 3.0	± 2.7	± 3.4	± 0.08	± 0.04	± 0.20
	± 100 W	± 6.1	± 5.4	± 6.8	± 0.16	± 0.06	± 0.40
	± 2.5%	± 2.0	± 2.0	± 2.0	± 0.16	± 0.16	± 0.16
	± 5%	± 4.0	± 4.0	± 4.0	± 0.30	± 0.30	± 0.30
ΔT	+ 0.5 oC	- 2.4	- 2.1	- 2.7	+ 0.06	- 0.02	+ 0.16
	- 0.5 oC	+ 2.5	+ 2.2	+ 2.8	- 0.08	+ 0.02	- 0.16
	+ 1.0 oC	- 4.6	- 4.1	- 5.2	+ 0.10	- 0.06	+ 0.28
	- 1.0 oC	+ 5.2	+ 4.5	+ 5.8	- 0.16	+ 0.04	- 0.16
	+ 1.5 oC	- 6.7	- 6.0	- 7.5	+ 0.16	- 0.08	+ 0.40
	- 1.5 oC	+ 8.0	+ 7.0	+ 9.0	- 0.24	+ 0.06	- 0.56
	+ 2.0 oC	- 8.8	- 7.8	- 9.8	+ 0.20	- 0.10	+ 0.52
	- 2.0 oC	+ 10.9	+ 9.5	+ 12.3	- 0.36	+ 0.08	- 0.80
S	+ 20 W/m2	+ 3.5	+3.2	+ 3.9	- 0.12	+ 0.00	- 0.24
	- 20 W/m2	- 3.8	- 3.2	- 4.4	+ 0.08	- 0.08	+ 0.22
	+ 40 W/m2	+ 6.7	+6.2	+ 7.2	- 0.28	- 0.06	- 0.50
	- 40 W/m2	- 7.8	- 6.3	- 9.3	+ 0.12	- 0.20	+ 0.44
	± 3%	0	0	0	± 0.18	± 0.18	± 0.18
	± 6%	0	0	0	± 0.38	± 0.38	± 0.38

In terms of the measured electric load, any unregulated devices could provide 50 or 100 W offsets and produce 3-7% systematic errors in the *HLC*, although these will obviously have a lower impact in higher heat loss dwellings. Percentage errors in measured Q_{elec}, such as calibration offsets, will equally impact higher heat loss dwellings, offsetting the result approximately by the scale of their own uncertainties. Some of these calibration errors will be reduced by the use of multiple kWh meters.

Internal and external temperature measurements, making up ΔT, show a higher influence over *HLC* estimates. A 1.0 °C shift in ΔT leads to a 4.6 - 5.2 W/K (6 - 7%) under or overestimate in *HLC*. If the calibration uncertainties in table 7.3 are considered, it can be imagined how significant measurement errors could occur within the estimated ΔT, particularly as a single sensor often measures T_e.

The measurement of *S* makes an interesting case. If the uncertainty in the measurement of *S* is fractional, i.e. 3% across all measurements, the estimated value of the *HLC* does not change, with the offset accounted for in the change in estimated *R*. Conversely, an absolute offset will alter the *HLC* estimate, but have less of an impact on *R* (see appendix A.4.2 for an example plot).

Recent work by Jack (2015a) has performed some sensitivity analysis on the NHBC field trial data, a building with similar properties to that modelled here ($\sim$ 67 W/K). Jack notes that shifting ΔT by 1 °C would shift *HLC* estimates by between 1.8 - 4 W/K (4-8%) depending on the analysis adopted. Similarly, service meters with a 5% error give between a 2 and 3 W/K (3 - 6%) shift in *HLC*.

7.6 Moisture & latent loads

The effect of moisture within the building fabric and inside the test dwelling upon thermal performance is complex, but two sources of uncertainty can be considered:

1. A latent load associated with the energy required to evaporate moisture within the building fabric.

2. Reduction in conductivity of materials due to increased levels of moisture.

Both the presence of a latent load (Bauwens and Roels, 2014) and increased thermal conductivity (Johnston et al., 2013; Wingfield, 2010a; Deconinck and Leunis, 2012) have been considered in the context of co-heating or alternative whole building heat loss assessments. The LBU protocol has recommended monitoring RH (Wingfield, 2010a) but recognises the uncertainty in trying to account for what is a complex process (Johnston et al., 2013). Issues with moisture are given additional significance as many newly built dwellings, the type most commonly being tested at present, will have increased moisture content resulting from their construction and are still 'drying out'.

Both these sources of uncertainty are addressed briefly here. A full understanding of the effects of drying out will require more dedicated and high quality monitored research projects. It is thought that major uncertainty can be sidestepped by improved scheduling and test preparation, particularly in trying to ensure the building is sufficiently dried out prior to testing. This is essential as much for the practical costs as the theoretical uncertainty (see figure 7.15).

7.6.1 Uncertainty from a latent load

Wet finishes (plaster, mortar, concrete, etc.) will initially contain high moisture contents. During a co-heating test, the evaporation of moisture from such surfaces will add an additional load to the energy balance, Q_{latent}. As the latent evaporation of moisture is not accounted for in the co-heating energy balance equation, it can potentially lead to higher *HLC* estimates. A latent load could therefore be described by:

$$Q_{elec} + R \cdot S = HLC \cdot \Delta T + Q_{latent} \tag{7.11}$$

Where:

$$Q_{latent} = mL_{water} \tag{7.12}$$

Where, m is the mass of the water present (kg) and L_{water} is the specific latent heat of water (kJ/kgm).

To consider the impact of a latent load on *HLC* estimates, we can refer to literature and consider examples from field tests conducted as part of this research.

7.6.2 Evidence of latent loads

Researchers at BBRI (Belgian Building Research Institute), in the framework of the PLEIADE project reported the drying power in an unoccupied dwelling, for a construction less than a year old. Across a 30 day, dynamic monitoring period, the estimated latent load corresponded to 9% (700MJ) of the total heating load (BBRI, 1997; Santamouris, 2005). Using parameter identification techniques, this fraction was determined in respect to transmission (71%, 5,700MJ) and ventilation (20%, 1,600MJ) losses. Further, Deconinck and Leunis (2012), conducting co-heating tests in a small test box, remarked that the estimated *HLC* of their test box was higher during a particularly wet month, although the difference is not stated and no further analysis was offered.

7.6.2.1 Field tests

Evidence of high moisture content is clear in the CASE-B field co-heating test but without high quality and high-resolution measurements it is difficult to determine the latent load. The difficulty with calculating the size of any latent load is the limited number of locations, depths and number of materials in which moisture can be monitored without significant investment and intrusive sensor placement. Rather than providing an accurate correction, calculations are perhaps more useful for defining sensitivities and likely directions of error.

The measured internal RH for CASE-B, including a number of internal zones and additional environmental variables, can be seen in figure 7.14. Such measurements allow an elementary assessment of the moisture content of the test dwellings. Here, CASE-B can be seen to have significantly higher levels of internal RH than two other case studies, CASE-A1 and NHBC (figures 7.12 and 7.13). Further cases can be found in the appendix (section A.4.3).

In CASE-B, the mean internal RH is approximately 80% at the beginning of testing, reducing slowly to around 70% after 22 days. The measured RH, particularly looking at individual sensors, also shows some diurnal variation, correlating with high solar radiation and brief periods of midday overheating.

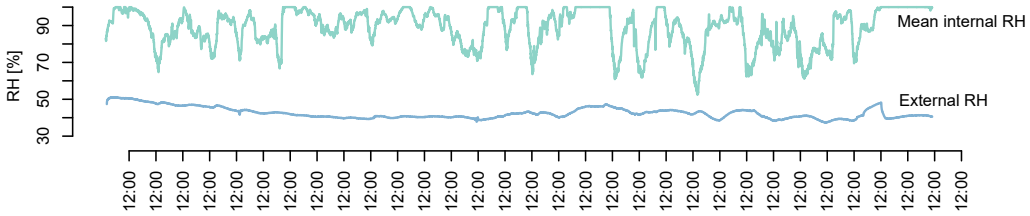

Figure 7.12: *Mean internal and external RH for CASE-A1 field test dwellings.* (Field Test)

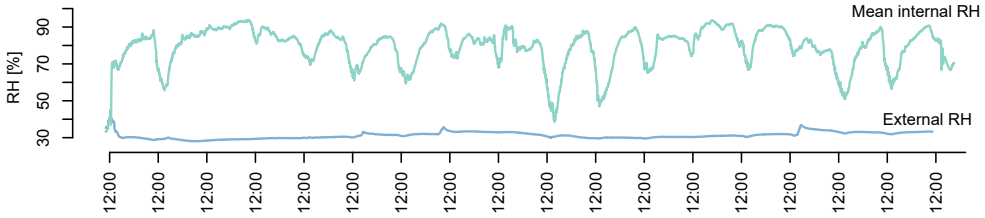

Figure 7.13: *Mean internal and external RH for NHBC field test dwellings.* (Field Test)

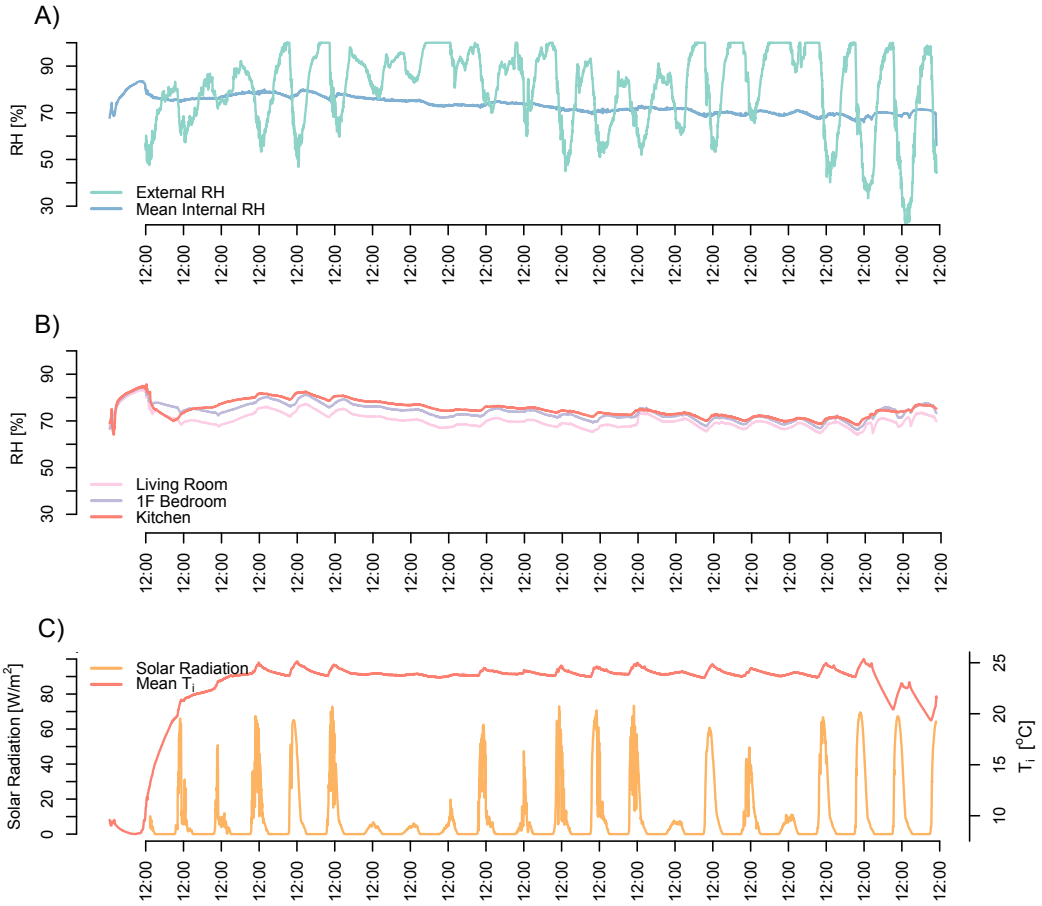

Figure 7.14: RH and associated measurements in CASE-B test dwelling. (Field Test)

7.6.2.2 A practical note

During co-heating tests, if a large amount of moisture remains in the fabric, this can lead to high internal humidity and when mixed with high internal temperatures and little ventilation, mould can form inside the dwelling - see figure 7.15. This poses serious practical and ethical problems regarding the application of co-heating tests and in particular when they should be scheduled to take place in the lifetime of the dwelling. Extra work and expense through moisture damage is problematic for developers, whilst the presence of mould should be avoided for the health of the occupants.

Figure 7.15: Mould forming due to high internal temperatures and RH during co-heating test.

7.6.3 Moisture and reduced thermal performance

The thermal conductivity of most materials diminishes with increasing moisture levels, with some materials more sensitive than others. A newly built dwelling with higher than normal moisture content would therefore be expected to have a higher heat loss than an otherwise identical building 5 years further down the line. In addition, wet/rainy periods, either during or proceeding co-heating tests are likely to further increase the moisture content of external materials.

Rhee-Duverne and Baker (2013) investigating the thermal properties of three types of traditional bricks, measured the conductivity after both oven drying and complete saturation. The resulting thermal conductivities ranged from 0.55 - 1.56 W/mK, corresponding to wall U-values of $\sim$ 1.2 - 2.5 W/m^{2}K. This would provide a huge increase in heat loss due to the change in thermal conductivity. For example, the detached Victorian test house considered in chapter 9, based on the above solid wall U-values would have a range in *HLC* of 703 - 936 W/K

from these extremes. In such cases, HLC_{meas} should reflect the true state of the building and therefore HLC_{True}. However, the definitional uncertainty in both parameters is significant and makes performing any comparisons extremely difficult. For example, consider two similar test dwellings, reported to have HLC_{meas} = 700 W/K and 900 W/K respectively, with HLC_{pred} = 800 W/K for both. The proportion of the discrepancies between these figures could result from the thermal performance of the fabric of each dwelling, or from the respective moisture content within the fabric. Without further measurements and analysis this remains unknown, captured within the definitional uncertainty of each parameter.

In such cases, the moisture content of a building cannot be ignored and will need to be measured or monitored over the test period. Rainfall measurements both during and proceeding the test may also prove useful. The difficulty, as stated above, is that recording moisture content measurements representative of the full building fabric is challenging and requires intensive measurements. Without the ability to weigh materials in the lab, it is likely any estimates of the moisture content during testing will be highly uncertain. More work may be required to adequately investigate the state of the building during the co-heating measurement.

7.6.4 Addressing latent loads

Given the complex nature of latent loads, the sophisticated monitoring equipment and the practical risks, the most appropriate strategy appears to be to avoid the presence of significant latent loads and monitoring a dwelling to determine the likelihood of moisture related bias.

7.6.4.1 Avoiding high moisture content

Heating a test dwelling, with adequate ventilation and ideally with the deployment of dehumidifiers, prior to conducting a co-heating test, will act to dry out the building prior to testing. This can be done with the building's own heating system, enabling access to the dwelling to be maintained. This also means that the test dwelling can be pre-heated to a higher resting temperature before testing, reducing the amount of test data that needs to be removed as the building warms to a quasi steady state.

Figure 7.14) shows a case (CASE-B) in which this approach was not adopted. In a further case (CASE-A1, figure 7.13), the test dwelling was similarly newly finished and in fact had had significant water leakage into the internal fabric during construction. To avoid any practical

issues, the building was pre-heated and dehumidified for a period of 2 weeks prior to testing. Previous reports (GHA, 2011b) have suggested a period of three-months between a building being made weather tight and performing co-heating tests in order to let the building dry out. This is dependent upon the construction and the internal conditions in the dwelling during this period, so this may need to be accelerated via heating, etc. The period of time required to dry out a building depends upon its construction and environmental and internal conditions. Generally, this it is though to take in the region of 9 months to a year (NHBC, 2015), but more work is needed to understand drying rates and their impact upon heat loss. If dwellings are to be tested post-completion and prior to occupation, some degree of uncertainty due to the unknown moisture content of the building is almost inevitable.

7.6.4.2 Monitoring internal conditions - standardised excess vapour pressure

Rather than monitor internal relative humidity, an alternative method is to calculate the vapour pressure excess (*VPX*) or a standardised vapour pressure excess (*SVPX*). The internal and external saturated water pressure (*SVP*) can be calculated from equation 7.14 (ISO 13788:2012; ISO, 2012) and subsequently the internal and external vapour pressures (*VP*) determined along with *VPX*(see equation 7.15). This allows the moisture content of the internal environment to be defined with respect to the external conditions during testing. Such a method has been suggested to evaluate the likelihood of mould in UK dwellings (Altamirano-Medina et al., 2008).

$$SVP = 610.5 \cdot \exp \frac{17.269 \cdot T}{237.3 + T} \tag{7.13}$$

$$VP = \frac{RH}{100} svp \tag{7.14}$$

$$VPX = svp_{int} - svp_{ext} \tag{7.15}$$

The vapour pressure excess can then be standardised to specific external conditions (e.g. 5 $^{\circ}$C and 80% RH) and the dwellings classified through a number of approaches (BSI 5250:2011; BSI, 2011 Janssens and Hens, 2007; Ridley et al., 2010b). BSI 5250:2011 proposes five humidity classes of increasingly humid internal conditions (BSI, 2011). Janssens and Hens (2007) then suggest four indoor climate classes (ICC) and Ridley et al. (2010b) three, with spaces with VPX ¿ 500 being classed as 'undefined' under the latter system. These classifications allow a test dwelling to be assessed for high moisture content and therefore potential bias in the *HLC* estimate to be categorised, if not fully estimated or corrected. Six field tests conducted as part of this thesis are analysed and classified in tables 7.5. As expected from the RH measurements, CASE-B is classed within the highest humidity classification under each system. Within

ICC4 surface condensation and mould formation can be expected, with the BSI class 5 corresponding to laundries, swimming pools or breweries. The remaining dwellings fall into BSI class 2/3 (ventilated offices/ low occupancy dwellings). We therefore might consider these test dwellings to be operating within conditions approximating with normal operation and humidity.

Table 7.5: VPX and SVPX for Field Tests.

Field Test	Mean RH	Mean External RH	Mean SVP_{INT}	Mean SVP_{EXT}	Mean VPX	Mean SVPX	Classification		
	%	%	(Pa)	(Pa)		(Pa)	ICC	BS5250	Ridley
CAM-PH	49	96	1489	1019	471	662	ICC3	Class 3	Undefined
Case-A1	43	89	1218	719	499	468	ICC3	Class 3	Wet
Case-A2	42	78	1178	595	583	536	ICC3	Class 3	Undefined
NHBC	32	79	965	735	253	251	ICC2	Class 2	Average
Case-C	41	83	1255	671	584	533	ICC3	Class 3	Undefined
Case-B	73	81	2055	877	1232	1247	ICC4	Class 5	Undefined

Concluding this section, despite the challenges in taking representative moisture content measurements of materials, any that can be taken, even manually measured pre and post testing, are likely to increase understanding, if not fully resolve the issue of moisture. As much measurement as possible is likely to assist in sensitive constructions and the change in thermal performance of buildings overtime, from newly finished constructions to aged dwellings remains an interesting research question.

7.7 Operational uncertainties

The co-heating experimental protocol is designed to simplify heat flows in a test dwelling but by doing so it also creates its own set of uncertainties - so called operational errors. These include:

1. The presence of mixing fans decreasing internal surface resistances.

2. The influence of an elevated T_i on the thermal performance of materials and elements within the test dwelling.

7.7.1 Increased internal temperatures

7.7.1.1 Increased thermal conductivity

To achieve a reasonable ΔT, but to limit cracking and shrinkage of the internal fittings and finishes, an internal temperature of 25 °C is typically used as the experimental set point, although experimental set points of 30 °C or higher have been used (Butler and Dengel, 2013). As a

materials thermal conductivity is a function of its temperature, the elevated internal temperature will increase the temperature of materials within the building fabric, altering the materials resistivity[7]. The effect of temperature can be described by a temperature conversion factor, F_T and conversion coefficient, f_t (ISO 10456:2007; ISO, 2007).

$$\lambda_2 = \lambda_1 F_T \tag{7.16}$$

$$F_T = e^{f_t(T_2 - T_1)} \tag{7.17}$$

Where λ is the thermal conductivity of a material (W/mK) and (T_2 -T_1) is the respective temperatures of the material.

A post-construction guidance document by the EST (2008) notes that despite any perceived benefits, internal temperatures during co-heating tests should not be elevated well above normal levels, as the thermal performance of many insulations deteriorates with increasing temperatures. It notes that the lambda value of one 'popular foam insulation board' increases by approximately 6% for every 10 °C in mean working temperature. Similar sensitivities are reported in general, with a 5% change in conductivity with a 10 °C change in temperature in many materials (CIBSE, 2007), although this is much lower in concrete and other inorganic materials.

The EST report does not consider the fact that the external temperature will also drive the temperature of an insulation layer. In the following example, a brick-insulation-brick wall is considered (U = 0.30 W/m^{2}K). Temperature across each material interface are then calculated using equation 7.18 (Hagentoft, 2001):

$$T = \frac{R_- \cdot T_i + R_+ \cdot T_e}{R_- + R_+} \tag{7.18}$$

Where R_- is the sum of the thermal resistances of each layer from outside to the point of consideration and R_+ is an equivalent metric, working from the inside layer.

This allows the mean temperature of the insulation, T_{ins}, to be calculated based upon a mean of the two relevant interfaces. T_{ins} is plotted alongside T_e across the Finningley year, for various T_is (see figure 7.16). As can be seen in figure 7.16, the temperature of the insulation in this simple model will have higher variability from the changing T_e across even just the heating season, than from changing $T_{setpoint}$ from 20 to 35 °C.

[7] Although the raised temperatures may reduce the moisture content of the material and therefore act to increase resistivity.

This is further summarised in table 7.6. The influence of T_i on the mean U-value of the wall (mineral wool λ_1 = 0.04 W/mK, f_t = 0.0056, $\sim$ 5% change in conductivity with a 10 °C change in temperature) is seen to be minor, with a difference of $\pm$ 3% between 20 - 35 °C. A similar spread is seen due to the seasonal range in T_e. However, the significance seen here is likely to reduce when considering the building *HLC*, with elements such as windows accounting for large percentages of total losses and not showing the same susceptibility to temperature. In addition, the mean U-value at 25 °C is just 2% higher than at the calculated design conductivity (10 °C, ISO 12667:2001 (ISO, 2001)).

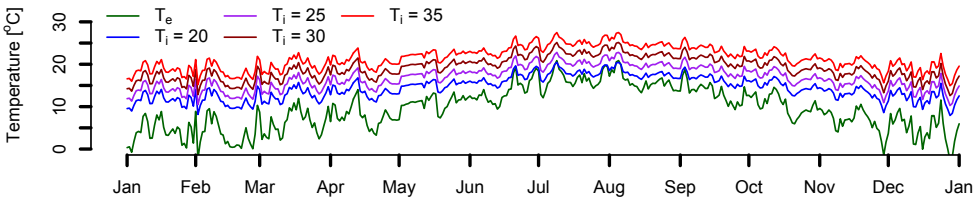

Figure 7.16: *Temperatures of insulation at various internal set points.* *(Modelled: FINN)*

Table 7.6: Summary statistics for insulation temperature for two week periods across Oct-Mar.

Ti [°C]	Max [°C]	Mean [°C]	Min [°C]	Range [°C]	Mean U-Value [W/m²K]
20	15.8	12.6	10.2	5.6	0.336
25	18.1	14.9	12.5	5.6	0.339
30	20.5	17.3	14.9	5.6	0.343
35	22.8	19.6	17.2	5.6	0.347

7.7.1.2 Stack losses

The experimental set point temperature will also influence the average ΔT across a test period and therefore the expected stack losses. If the building considered in figure 6.2 is again used as a reference (mean ACH = 0.21 h^{-1}), the mean heating season stack *HLC* changes from 14.4 W/K at 25 °C to 11.4 W/K at 20 °C and 17.2 W/K at 30 °CȦgain, such changes are likely to be smaller than the seasonal variation in stack losses at the same internal temperature, 10-19 W/K.

For the majority of modern houses ($<$ 5 $m^3/(hm^2)$) the difference between stack losses incurred at 25 °C will show only a small deviation from set points at 20 or 30 °C, $\sim \pm$ 20% change in stack HLC or $\pm$ 3% of total. The variation in HLC_{True} across the testing season is

likely to have a marginally higher influence, $\sim \pm 5\%$ change in total *HLC*. If a test dwelling is very leaky, i.e. a Victorian dwelling, and susceptible to high stack losses, i.e. chimneys, 4 storeys, etc., then the overall heat loss is likely to be significantly higher too. It is difficult to calculate stack coefficients in practice and hence estimate the subsequent stack losses. As with such buildings in windy conditions, co-heating tests performed in such dwellings may therefore require better measurements of infiltration rates and losses, particularly if effective comparisons to design or between tests are to be conducted. Nevertheless, details of ΔT throughout the test period can be reported, infiltration measurements made, and simple estimates of stack losses can be made as seen in Lowe et al. (2007).

7.7.2 Mixing fans disrupting the boundary layer

In the case of mixing fans, whilst their primary objective is to provide uniform temperatures, a potential side effect is the disruption of the boundary layer where the internal air and internal surface of walls meet.

The percentage of the total thermal resistance of a building element that the internal surface accounts for depends upon the element's composition. At the building regulation backstop (0.3 W/m^{2}K), the default internal surface resistance (0.13 m^{2}K/W) this accounts for 4% of the total thermal resistance. For an un-insulated solid wall (U-value = 2.09 W/m^{2}K) the R_{si} accounts for approximately 27% of the total thermal resistance.

The value of the internal surface resistance R_{si} can be calculated from the internal radiative (h_r) and convective (h_c) heat transfer coefficients, see equation 7.19 (CIBSE, 2007; CIBSE, 2007).

$$R_{si} = \frac{1}{h_c + \frac{6}{5} \cdot \epsilon \cdot h_r} \tag{7.19}$$

Where ϵ is the emissivity of the surface and:

$$h_r = 4\sigma T_{si}^3 \tag{7.20}$$

Where σ is the Boltzmann constant and T_{si} is the internal surface temperate. Equally, if the mean air velocity, v < 5 m/s, then:

$$h_c = 4 + 4v \tag{7.21}$$

It can therefore be seen how the convective component will change with air velocity. To assess typical airflow next to the surface, induced by mixing fans the air velocity was measured 2cm from the surface of a wall in a laboratory setting. A mixing fan, the same as used in co-heating field tests, was positioned 1.5m away from the wall, and pointed at a 45° angle to the wall surface. In reality, the majority of external wall areas are not likely to experience such air velocities. In this case, the mean parallel air velocity across this period was 0.22 m/s. When the fan was moved to just 0.75m, and pointed directly at the measured surface, a situation unlikely to occur in real tests, the mean air velocity increased to 1.65 m/s. This higher value is taken as an extreme airflow to evaluate the reduction in thermal resistance.

If these air velocities are used in equations 7.19 to 7.21, R_{si}, the U-value, and the associated heat loss can all be re-evaluated. The effect on a building meeting the current building regulation backstop of 0.30 W/m^{2}K is negligible. The reduction in thermal resistance in the uninsulated cavity ranges from 5 - 11%, whilst in a solid wall this is between 9 - 17%.

Table 7.7: Changes in thermal transmittance with airflow across surface.

Construction	Default U-value	Rsi Contribution	Typical Airflow (Cs = 0.22 m/s)	Extreme Airflow (Cs = 1.79 m/s)	Rsi = 0
	W/m2K	%	W/m2K	W/m2K	W/m2K
Solid Wall	2.09	27%	2.31 (+10%)	2.6 (+24%)	2.87 (+37%)
Unisulated Cavity	1.44	18%	1.54 (+7%)	1.66 (+15%)	1.77 (+23%)
Building Regulation Backstop	0.3	4%	0.303 (+1%)	0.308 (+3%)	0.311 (+4%)

In reality, only small proportions of the external envelope are likely to be directly influenced by the mixing fans. In general, to facilitate the mixing strategy, most mixing fans will be positioned near external walls, pointing inwards. Thus this increased thermal transmittance is likely to be of a much smaller scale than seen here and unlikely to be significant across the whole fabric.

Two recommendations can be offered, applying to poorly insulated buildings, with U-values at least > 0.3 W/m^{2}K.

- Mixing fans should not be pointed directly at external elements.
- Air velocity can be measured during set up, through a hand held hot-wire anemometer, to ensure low air velocities at internal surfaces.

7.8 Chapter conclusions

From the range of experimental uncertainties covered in this chapter, a number of conclusions can be drawn. Firstly, considering uncoupled heat losses:

- Heat loss to unconditioned spaces and the ground may not be coupled to T_e across a test period.
- If heat loss to unconditioned spaces is dynamic, such heat flows may introduce significant uncertainty into *HLC* estimates - therefore they may need to be monitored (e.g. temperature or heat flux).
- Uncoupled heat losses can cause definitional uncertainty and bias comparisons. Assumptions in HLC_{pred} may need also to be checked.

And heat transfer across party walls/ floors:

- Systematic bias can occur in either direction as a result of net party wall heat transfer. This is particularly important in flats and terrace dwellings, where temperature gradients exist and when party elements are uninsulated.
- Any heat transfer should be monitored and investigated qualitatively (thermography, air leakage paths).
- Estimated heat flows, Q_{adj}, can be incorporated into *HLC* estimates and/or introduced as additional uncertainty (section 9.4.7.2).
- This source of uncertainty can be particularly hard to account for if heat flows are not acting directly across the party wall, but instead involve perpendicular heat flows within the cavity.

In terms of the experimental assumptions during co-heating, temperatures are likely to deviate somewhat from their assumed uniformity:

- Non-uniform internal temperatures can bias *HLC*, particularly if variations in T_i are high and in dwellings with inhomogeneous heat loss.
- Suitable mixing strategies should be implemented to reduce any variation along sufficient with sensor coverage.
- Heat loss weighted internal temperatures should be derived to reduce bias.

And achieving a quasi-steady state for analysis also needs consideration:

- Heating to quasi steady state can take a number of days and data points will be biased during this period.
- Internal temperatures and heating power should be observed to identify when a suitable level of quasi steady state has been reached.
- Heavyweight elements may need to be monitored through heat flux sensors to determine when unbiased data collection can begin.

Experimentally, the uncertainty of sensors deployed to measure S, T_i, T_e and Q_{elec} need to be considered:

- Sensors used to measure key variables for co-heating analysis can cause systematic bias due to calibration offsets, bias within the sensor characteristics or due to location bias.
- The measurement of T_e is particularly prone to error as only a single measurement is often taken.
- Uncertainties from sensors should be incorporated into any uncertainty analysis (section 9.4).

Excess moisture within the building fabric is one of the most difficult uncertainties to account for and has the potential for highly biased measurements:

- Latent loads will increase the heating requirement during co-heating and therefore overestimate the *HLC*.
- Similarly, high moisture content within the building fabric will increase thermal conductivity and overall heat loss.
- Determining the moisture content of various materials within the fabric of a building and estimating the impact on heat loss is complex.
- High moisture content can also cause mould and damage internal fittings.
- Attempting to dry out a dwelling prior to testing is therefore preferable, although this makes scheduling tests more prohibitive.
- Monitoring RH or calculating the vapour pressure excess can help identify tests in which there may be increased uncertainty due to excess moisture.

Finally, the conditions imposed by co-heating will potentially provide operational uncertainties:

- Elevated internal temperatures will increase both the thermal conductivity of some materials and stack infiltration.
- This causes definitional uncertainty, although this is likely to be of a smaller scale than the result of natural variations in external temperature. Reporting internal and external conditions is important to allow interpretation of *HLC* measurements.

7.8.1 Discussion of experimental sources of uncertainty

Many of the uncertainties discussed in this chapter again represent definitional uncertainties in the HLC_{True}. The HLC_{True} can be influenced by the state of the test dwelling (moisture content, temperature of materials, internal temperature) and by the form of the dwelling and its losses (unconditioned spaces, ground losses). With incomplete knowledge of these influencing factors, the definitional uncertainty can be considered high. Supplementary measurements may again help improve our understanding of the *HLC* but require more time and resources.

Systematic uncertainties due to party wall heat transfer must be addressed and tests involving party elements will therefore require more extensive monitoring, experimental control and careful analysis. Testing flats or dwellings without access to neighbouring properties will be inherently more prone to error such that the use of co-heating may exclude such dwellings.

Chapter 8

Regression Based Sources of Uncertainty

Chapter overview

In this chapter, which concludes the series of chapters on sources of uncertainty, a number of uncertainties formed or consolidated within the regression analysis process are discussed. These include:

1. **Uncertainty from a forced intercept:** emanating from uncoupled losses and gains.
2. **Attenuation bias:** trend to underestimate the *HLC* due to error in the independent variables.
3. **Collinearity:** uncertainty due to the correlation between the independent regression variables T_e and S.

8.1 Uncertainty from a forced intercept

In the previous three chapters a number of uncoupled losses, in which the losses are not directly dependent upon T_e, have been described. In addition, there may be unregulated gains into the dwelling. Both uncoupled losses and unregulated gains are not represented by the gradient of a SLR or MLR regression but rather by the intercept (see figure 8.1). The non-zero intercept will become positive or negative depending on the net uncoupled gains/ losses. Uncoupled losses include:

- Ground losses
- Radiative sky losses
- Wind driven losses
- Losses to unconditioned / adjoining spaces

And un-regulated gains:

- Un-metered equipment
- Un-corrected solar gains
- Gains from heated adjoining properties

In addition, the intercept can be influenced by offsets in sensors and by biased data points, say from the building still warming to quasi steady state or cooling from a previous day. This will influence the intercept depending upon whether they under or overestimate the predicted heat loss and at whether the data points sit at high or low ΔT.

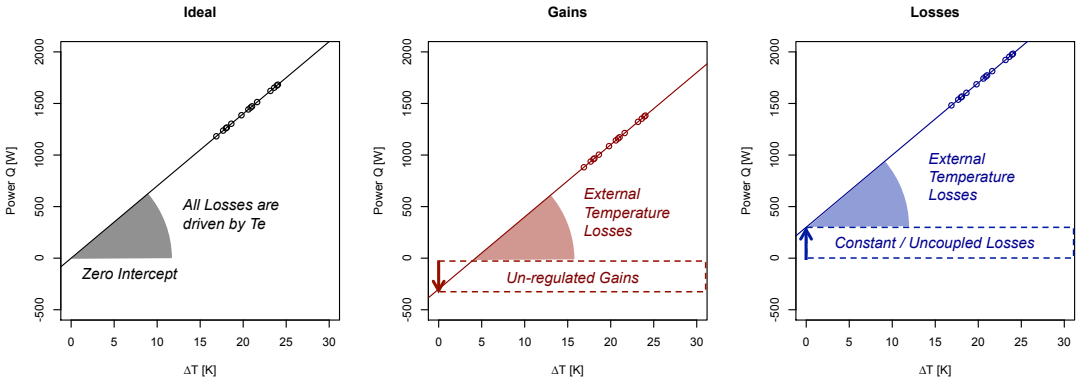

Figure 8.1: *Demonstration of un-coupled losses and unregulated gains impact on the intercept.*

Statistics literature will often warn against using no-intercept models, particularly if there are few data points near the origin and without physical reasoning to do so (Draper and Smith, 1998). Both clauses apply in co-heating tests.

Forced intercepts have predominantly been used (table 2.2) in co-heating tests on the assumption that at $\Delta T = 0$, the required heating power will also be zero, $Q_{elec} = 0$. Such an assumption is based on the fact that all heat losses are directly coupled to T_e and all gains are accounted for. However, as noted throughout this chapter, there exist a number of reasons why it is physically possible that a non-zero intercept exists (Bauwens and Roels, 2014; Johnston et al., 2013).

8.1.1 Impact upon *HLC* estimates

Definitions of the heat loss from a dwelling resulting from non-intercept (MLR) and intercept (iMLR) models have been stated previously (see equations 3.5 - 3.7, section 3.1.3). In an ideal case, an intercept model would allow the net unregulated gains or uncoupled losses to be disaggregated from coupled ΔT driven losses, providing more information on the test dwelling.

The two approaches are comparable if the intercept losses are combined with the gradient in an iMLR approach (i.e. $(\frac{Q_{elec}+R\cdot S}{\Delta T})$ + $(\frac{c}{\Delta T})$).If an iMLR approach is taken, and uncoupled losses are not considered, i.e. the *HLC* is estimated from the gradient of the slope alone without the addition of $(\frac{c}{\Delta T})$, then HLC_{True} will be:

- Underestimated if there are net uncoupled losses.
- Overestimated if there are net uncoupled gains.

Figures 8.2 and 8.3 demonstrate the estimated *HLC* from both methods across the Finningley year. Here, a modelled dwelling (*HLC* = 80 W/K) is driven by changes in ΔT and combined with the uncoupled losses from modelled wind losses (equation 6.2, section 6.1.1). As can be seen, even in this simple scenario, the iMLR approach shows poor estimation of both the coupled and uncoupled heat losses. Despite the clumsy definitions using either MLR or an adjusted intercept MLR i.e. $(\frac{Q}{\Delta T} + \frac{c}{\Delta T})$ give accurate estimates of the HLC_{True} defined by lumping losses together.

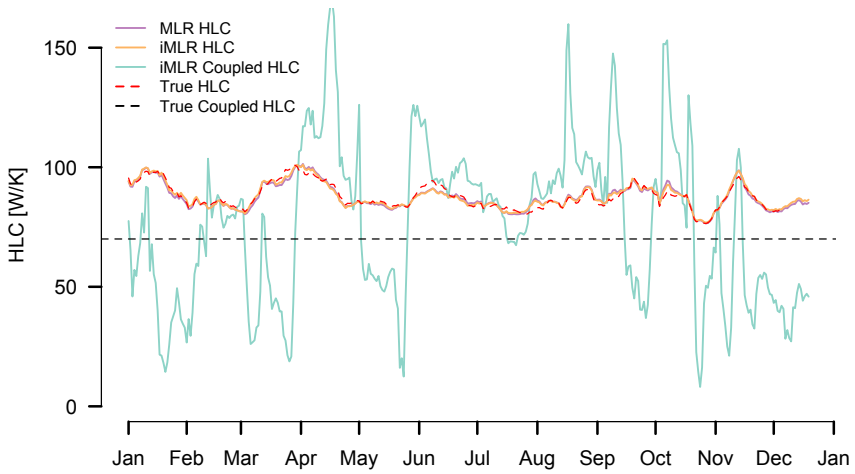

Figure 8.2: *Estimated HLC by MLR and iMLR, examining co-heating data set with uncoupled wind losses.* (Modelled: FINN-MLR-2w-24h-6agg)

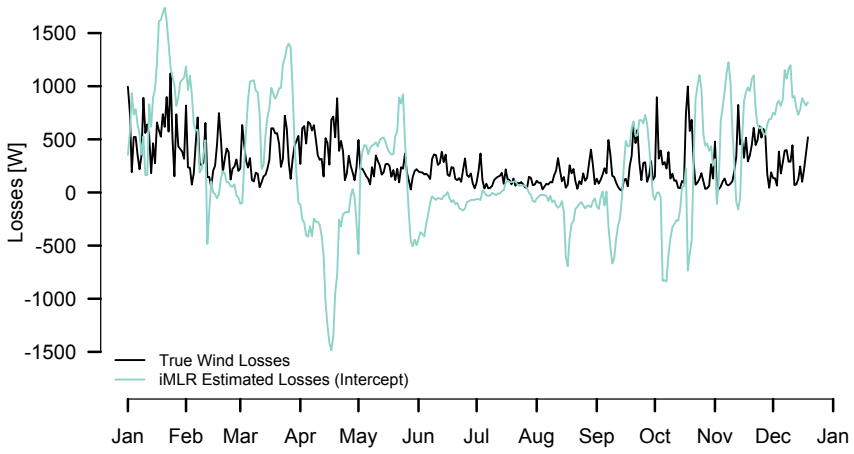

Figure 8.3: *Estimated uncoupled wind losses from iMLR.* (Modelled: FINN-MLR-2w-24h-6agg)

It can therefore be concluded that little error occurs in the choice of the model as long as an intercept MLR *HLC* incorporates uncoupled losses and that the HLC_{True} is carefully and clearly defined. Furthermore, the use of intercept MLR to disaggregate uncoupled and coupled losses is not likely to yield any benefit, unless all uncoupled losses are all constant across the test period and there is little measurement uncertainty - conditions unlikely to be met in outdoor testing. A further example in a full building simulation can be found in section 9.3.2.1.

Finally, applying Siviour analysis will effectively combine the coupled and uncoupled losses together. In reality, the difference between no intercept MLR and Siviour derived *HLC*s are very small (section 9.3.2.1).

8.2 Attenuation bias: Error in S and ΔT

An assumption of linear regression is that measurement error exists only in the dependent variable, Q_{elec}. However, with measurement errors and the uncertainties discussed in this chapter, it is clear that a degree of error also exists in the independent variables: ΔT, S or $(\frac{S}{\Delta T})$.

Linear regression is not symmetric, such that the line of best fit for predicting y from x is not the same as the line of best fit for predicting x from y. Error present in the independent variables causes regression attenuation or regression dilution, a biasing of the regression slope towards zero and therefore an underestimation of the coefficients true value, i.e. underestimation of the *HLC* and *R*. Such an effect is noted by Everett (1985) and more recently by Bauwens and Roels (2014), although the likely scale is not investigated in either case.

Here, the effect of error in the independent variables S, $\Delta T$and $(\frac{S}{\Delta T})$ is explored through generating modelled co-heating data on the previously studied building characteristics and weather data (HLC = 80 W/K, R = 6 m^2). The error in each variable is incrementally increased, with 1000 randomly generated data sets (gathered from the Finningley weather file) assessed at each error band. The mean estimated HLC is then shown in tables 8.1 - 8.4, along with the percentage of regressions performed that underestimate the value of HLC_{True}.

Table 8.1: Summary of mean estimated HLC and R due error in S. Mean taken from 1000 simulations performed at each level of error, with random days taken from FINN weatherfile (Oct-Mar) for each simulation. (Modelled: FINN-2w-24h-6agg-S_{GVS})

Error in S	Siviour		MLR		Siviour	MLR
	Mean HLC Estimate	*% Under True HLC*	*Mean HLC Estimate*	*% Under True HLC*	*Mean R Estimate*	*Mean R Estimate*
0%	80.0	-	80.0	-	-6.00	-6.00
5%	79.4	62%	79.5	62%	-5.95	-5.76
10%	78.1	69%	78.3	70%	-5.85	-6.09
15%	76.0	77%	76.2	81%	-5.67	-5.54
20%	72.7	83%	73.4	87%	-5.42	-5.45
25%	68.5	90%	69.8	93%	-5.05	-5.34
30%	64.5	94%	66.6	96%	-4.75	-4.81

Table 8.2: Summary of mean estimated HLC and R due to error in ΔT. (Modelled: FINN-2w-24h-6agg-S_{GVS})

Error in ΔT	Siviour		MLR		Siviour	MLR
	Mean HLC Estimate	*% Over True HLC*	*Mean HLC Estimate*	*% Under True HLC*	*Mean R Estimate*	*Mean R Estimate*
0%	80.0	-	80.0	-	-6.00	-6.00
5%	79.8	59%	79.5	55%	-5.96	-6.01
10%	79.0	69%	77.6	60%	-5.84	-6.07
15%	77.4	77%	75.0	66%	-5.62	-5.78
20%	75.1	83%	71.2	71%	-5.33	-4.54
25%	70.2	91%	66.4	80%	-4.76	-3.98
30%	65.4	94%	61.7	82%	-4.21	-4.48

Table 8.3: Summary of mean estimated HLC and R due error in Q. (Modelled: FINN-2w-24h-6agg-S_{GVS})

Error in Q	Siviour		MLR		Siviour	MLR
	Mean HLC Estimate	*% Under True HLC*	*Mean HLC Estimate*	*% Under True HLC*	*Mean R Estimate*	*Mean R Estimate*
0%	80.0	-	80.0	-	-6.00	-6.00
5%	79.9	51%	79.9	50%	-6.00	-5.57
10%	79.8	52%	79.7	51%	-5.97	-6.31
15%	79.6	52%	79.7	50%	-5.97	-6.93
20%	80.0	50%	79.9	50%	-6.00	-6.79
25%	80.3	50%	79.9	51%	-6.03	-2.89
30%	79.5	51%	79.6	49%	-5.94	-3.61

Table 8.4: Summary of mean estimated *HLC* and *R* due error in *S* and ΔT. (Modelled: FINN-2w-24h-6agg-S_{GVS})

Error in S	Error in ΔT	Siviour		MLR		Siviour	MLR
		Mean HLC Estimate	*% Under True HLC*	*Mean HLC Estimate*	*% Under True HLC*	*Mean R Estimate*	*Mean R Estimate*
0%	0%	80.0	-	80.0	-	-6.00	-6.00
5%	5%	79.4	58%	79.0	63%	-5.93	-5.76
10%	10%	77.0	70%	75.7	79%	-5.69	-6.04
15%	15%	73.3	78%	71.0	87%	-5.28	-5.06
20%	20%	68.2	84%	65.0	93%	-4.80	-4.04
25%	25%	62.7	89%	59.3	97%	-4.14	-3.51
30%	30%	57.2	93%	53.8	98%	-3.60	-3.75

In general, any underestimation caused by attenuation bias will be small (e.g. $<3\%$) if the errors in these parameters are less than 10%. What is interesting is that the increase in underestimation from attenuation bias is non-linear, increasing at a faster rate as the uncertainty in each parameter increases at regular intervals. The average underestimate in the *HLC* and *R* is only likely to be greater than 10% if there is a 20% error in both measured values. At such measurement sensitivities it is likely the *HLC* estimate will be inaccurate regardless. However, the trend to underestimate both parameters is still an important consideration and reinforces the need to reduce the uncertainties in the measurement of each parameter.

8.3 Collinearity in *S* and ΔT

In regression analysis, multicollinearity exists when two or more predictor variables in a MLR model are highly correlated. In such cases the estimated parameters may change erratically in responses to small changes in the model or data.

Both Everett (1985, p.6.5) and Johnston et al. (2013) point out that whilst ranges in both ΔT and *S* are required, covariance between the two can lead to regression errors. It is therefore also important that the same relationship between the two is not displayed across a given data set, i.e. sunny days are not all also warm. Everett also points out that:

- If *S* shows positive covariance with ΔT, both *HLC* and *R* are underestimated.
- If *S* shows negative covariance with ΔT, the *HLC* is underestimated and *R* is overestimated.

The correlation between, S and ΔT is shown in figure 8.4 for various aggregation intervals and times across the year. It can be seen that whilst there is reasonable negative correlation between S and ΔT on a monthly and even weekly aggregation, across daily data points little covariance is seen.

This can be further assessed within the statistics of MLR regression analysis across the year. In figure 8.5 the estimated R^2 between S and ΔT is shown, along with the Variance Inflation Factor (VIF), a statistic that quantifies the severity of multicollinearity (Draper and Smith, 1998). In almost all cases, and all cases that will be valid for co-heating analysis, the calculated VIF is less than a conservative 2.5 limit. This would further indicate that effects of multicollinearity are not generally an issue in co-heating tests, although such a statistical test can easily be performed on a given data set as a check.

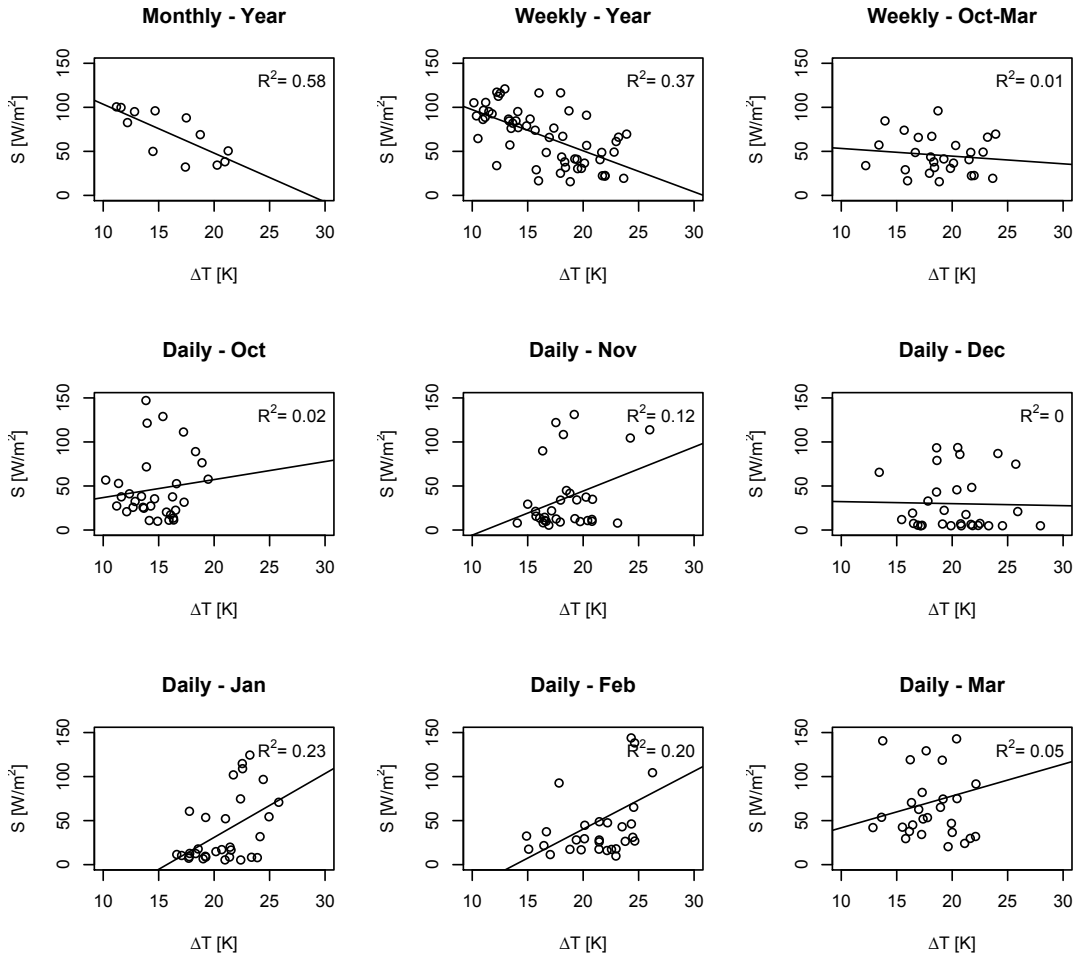

Figure 8.4: *Covariance between S and ΔT.*

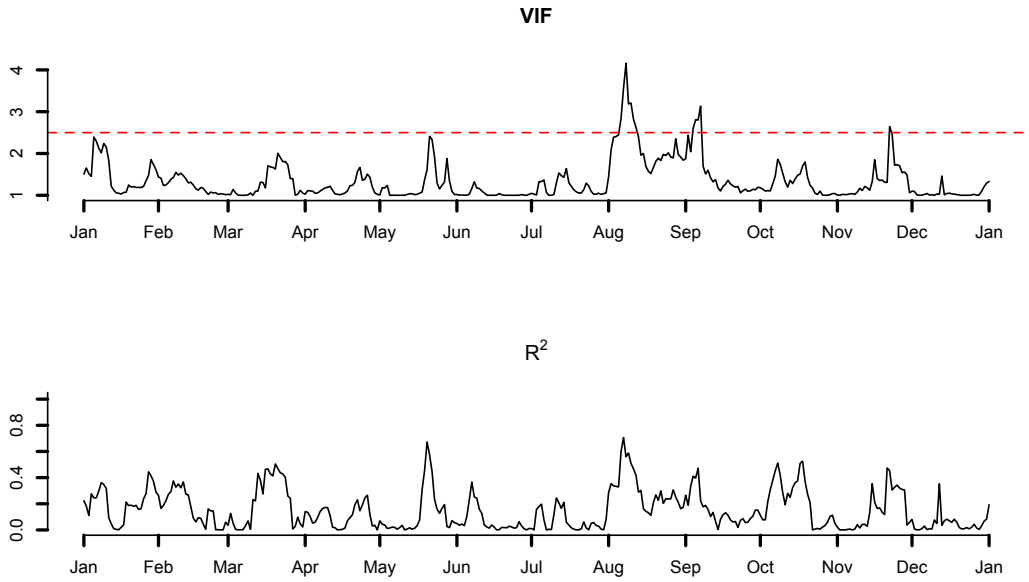

Figure 8.5: *Statistics to demonstrate the presence of multicollinearity between S and ΔT for the Variance Inflation Factor (VIF) and R^2 respectively.*

8.4 Chapter conclusions

Concluding this chapter, and the series of chapters of this thesis investigating sources of uncertainty within the co-heating method, the impact of forced intercept models, attenuation bias and covariance can be considered.

By adopting a forced intercept the regression model is assuming all losses are dependent upon ΔT, a fact demonstrated not to be true throughout chapters 5 - 7. However, whilst the forced intercept model is perhaps inelegant, an intercept model is likely to provide poor estimates of both the coupled and uncoupled losses (figures 8.2 and 8.3). This means that the non-intercept model provides a more consistent estimate of the dwellings heat loss, although care is then needed in the interpretation of this lumped result. It stands that a complete and precise knowledge of the heat loss of a dwelling can only be achieved with supplementary measurements of secondary heat flows.

An assumption of linear regression is that measurement error exists only in the dependent variable, Q. However, in co-heating test a degree of error in the independent regression variables (S, ΔT, $\frac{S}{\Delta T}$) is unavoidable. Uncertainty in such parameters has been explored throughout this thesis and includes sensor measurement errors (section 7.5), stored solar heating contribu-

tions (section 5.4), variations in T_e (section 6.2) and the measurement of S (section 5.2).

The presence of errors in the independent regression variables can lead to attenuation bias within the regression engine. This will lead to underestimates of both the extracted regression parameters, *HLC* and *R*. However, as long as both the error in S and ΔT are less than 10% any bias is likely to be small (see tables 8.1, 8.2, 8.3 and 8.4). Such an effect is likely to increase at low ΔT, further limiting the use of co-heating to sufficient temperature gradients. The introduction of further systematic error through attenuation bias reinforces the need to reduce other forms of uncertainty with accurate sensors, appropriately measured solar radiation and adequate aggregation.

Multicollinearity, or covariance between independent regression variables, can similarly cause bias in the regression estimators. Bright, sunny days (high S) may be expected to correlate with warmer days (higher T_e, lower ΔT). However, whilst the variables S and ΔT may show significant covariance in weekly or monthly data, this is not apparent in daily data points. Nevertheless, the correlation between S and ΔT can be checked for any given data set by plotting the two variables and examining both the R^2 and the variance inflation factor regression statistic. This may be particularly important for extensions of the co-heating method or similar regression based energy balance models using longer monitoring periods with higher aggregation.

Chapter 9

The Application of Co-heating Tests

Chapter overview

Chapters 5 - 8 have previously established the sources of uncertainties that may exist within a co-heating test, demonstrating when they are likely to occur, the direction of error and approximating their scale. With this knowledge we can further look into the practical application of co-heating tests and consider how the method can most suitably be adopted.

The application of the co-heating test is considered along a number of themes in this chapter, set out as follows:

- **9.1 Required external environmental conditions:** Here the environmental conditions required to successfully estimate the *HLC* are reviewed and explored over a range of test dwellings, corresponding to research question B1.
- **9.2 Required duration for accurate *HLC* estimation:** Given the previous discussion concerning suitable external conditions, how long is required to determine the *HLC* accurately? Cited as a major limitation in the application of co-heating test, this little explored requirement is shown to be significantly shorter than previously suggested. This addresses research question B2.
- **9.3 Recommendations for experimental protocol and analysis:** Given the earlier discussions in this chapter, and the review of uncertainties in chapters 5 - 8, what recommendations can be made to optimise the steady state co-heating method? This also includes a framework for reporting tests and addresses research question B3.
- **9.4 Estimating uncertainty:** Addressing research question B4, this section reviews relevant literature then develops and demonstrates how the uncertainty in co-heating tests can be appropriately calculated and stated.

- **9.5 Comparisons to design & measuring retrofit interventions:** This section initially explores the comparison of HLC_{meas} with HLC_{pred}. Subsequently, the use of co-heating to measure retrofit improvements is demonstrated, answering the final research question, B5.

This chapter ends with a short summary in section 9.6, preceding the final concluding chapter of this thesis.

9.1 Required external environmental conditions

We can begin by re-stating the research question defined in chapter 3:

B1) Under what environmental conditions can co-heating tests be performed to reliably estimate a building HLC?

A number of weather driven uncertainties have already been explored in chapters 5 and 6 of this thesis. Here, this evidence is used to explore the range of suitable testing conditions across a broad range of test archetype dwellings (see section 4.5). Firstly, the environmental limits to testing and the relevant uncertainties can be reviewed. This section is therefore an examination of the reproducibility (see section 3.5.5) of the co-heating method, or its ability to achieve accurate results in a range of environmental conditions and a range of test dwellings.

9.1.1 Environmental limits to testing

Reviewing the work laid out in chapters 5 - 8, a number of sources of uncertainty have been determined that can lead to unreliable or inaccurate *HLC* estimates. In general, dull and cold periods are required to achieve reliable *HLC* measurements, with systematic underestimates or unreasonable results increasingly likely in warmer, sunnier periods. However, the limits of suitable testing conditions are a function of the construction and form of the test dwelling, as well as further environmental and experimental conditions.

In this section, the focus is upon the environmental conditions and weather driven uncertainties, such that the estimated testing periods are theoretically based, i.e. without experimental uncertainties incorporated into the simulations. It should be kept in mind that experimental uncertainties may elicit inaccurate *HLC* estimates, even within ideal external environmental conditions.

9.1.1.1 Experimental overheating

As seen in section 5.5, experimental overheating will have significant impacts upon *HLC* estimates with unreliable results obtained when internal temperatures are consistently unstable. This is largely driven by periods of high solar radiation and low ΔT, particularly restricting the available testing periods for low heat loss, highly glazed dwellings. In many cases, the need to avoid experimental overheating will stipulate the strongest restriction upon when co-heating tests can be performed.

9.1.1.2 Stored solar heating contributions

More subtly, cases of short term overheating and stored solar heating contributions can cause systematic underestimates and unreliable *HLC* estimates during sunny periods - particularly in heavyweight dwellings where there is likely to be more stored heat flows and peaks in internal air temperature may not be so obvious. Identifying this effect is more complex but it can be reduced by taking appropriate aggregation periods (see section 5.4).

9.1.1.3 Mixes in weather - ΔT and S

A suitable mix in both ΔT and S may be required to accurately retrieve regression coefficients. This is particularly important when solar gains make up a significant part of the total heat input. Generally, this is more important if estimations of R are required, or if there is an absence of dull days, leading to a higher probability of uncertainty in *HLC* estimates. A method of determining suitable testing periods using criteria for weather mixes, set out by Everett (1985) and Lowe and Gibbons (1988), is reviewed later in section 9.1.5.

9.1.2 Suitable testing conditions in the literature

Cited as a major obstacle in increased adoption of co-heating tests, a limited testing 'season' restricts opportunities for testing, increases scheduling pressures and increases the risk of test failures. However, a robust and broad analysis of what may represent suitable conditions has not been fully performed to date.

Everett (1985) and later Lowe and Gibbons (1988) deduced a thermal calibration season in the UK that was largely dictated by the requirement for dull days, running through September - March[1]. Exploring weather mixes across a number of weather files and locations, criteria for

[1] All periods are stated inclusively.

dull days were used to identify the likely testing seasons and therefore durations required for *HLC* estimates (see section 9.1.5). Including an additional criteria for sunny days allowed the optimum testing periods and durations required to estimate *R* to be equally assessed. Typically, September, February and March are cited as preferred periods in which to determine *R*, with mid-winter often proving an unfruitful period due to a lack of sunny days, despite the benefits associated with estimating the *HLC*.

The LBU protocol adopts a similar testing season, stating that the typical testing season is restricted from October/November to March/April (Wingfield, 2010a). The most recent iteration of the LBU protocol further considers building type, noting in particular that south facing, highly glazed and well insulated dwellings, e.g. Passivhaus, may need to be tested during the lowest levels of insolation (Johnston et al., 2013). In reality, as seen in table 2.2, it is suspected that when tests are conducted is largely dependent upon practical constraints - the completion of test dwellings, availability of test teams and equipment, occupation and funding deadlines, rather than any theoretical basis.

Often the value of ΔT across a test period is considered as an indication of when tests can be performed. The LBU Protocol argues the testing season is dictated by the requirement for a reasonable ΔT, which should generally be 10K or more, such that most heat flow is from inside to outside (Johnston et al., 2012b; Wingfield, 2010a). Baker and Dijk (2008), when referring to testing in outdoor test cells, considerer ΔTs of at least 10K are required, with 20K preferable. In similar test cell work, Judkoff et al. (2000) recommends ΔTs of 30 °F (16.6 °C), filtering out data with a ΔT lower than 20 °F ($\sim$ 11 °C).

Whilst these examples from the literature provide useful guidance, they are largely based upon experience and suitable testing conditions have not been explored fully, leaving the industry uncertain over the scale of this methodological limitation. The methods adopted in this thesis provide the opportunity to review suitable testing conditions across a wider range of building types and constructions, as well as weather conditions. Importantly, this can be assessed within simulated co-heating tests, allowing the respective testing seasons to be defined across a number of weather files and dwelling types. Significantly, these assessments can be made in respect to a known HLC_{True}. This should provide insight to allow test practitioners and developers to better plan and schedule tests as well as informing policy strategies regarding the use of co-heating tests.

Finally, it must be remembered that within any given test, highly unseasonal weather may be experienced. Equally, the actual thermal performance of the dwelling may vastly differ from predictions, altering what may have been regarded as suitable conditions prior to testing. This places the onus back on understanding the impact of all types of weather upon a variety of test dwellings, detecting and defining uncertainty and defining valid tests - issues discussed throughout this thesis.

9.1.3 Evidence of when a test can be conducted - simulated examples

In this section, a wide range of dwelling constructions and forms are simulated across a full year with the results shown in figures 9.1-9.4. These dwellings are based on the forms and constructions set out in section 4.4. In each case, HLC_{True} is identified along with a $\pm$ 10% band. The point at which the estimated HLC_{meas} first strays beyond this $\pm$ 10% band for two consecutive days is then marked with a vertical line - visually identifying the approximated testing season.

9.1.3.1 Construction type

As seen in figure 9.1, there is a vast difference between the suitable testing conditions for different constructions. For example, a semi-detached as-built Victorian dwelling may accurately measure the *HLC* ($<\pm$ 10%) for up to 62% of the year, whilst for a heavyweight Passivhaus construction of the same built form this may only be for 19%. Findings such as those from the solid wall field trial (Birchall, 2011) and from in situ measurements of further traditional constructions (Baker, 2011; Rye, 2010), have shown there is certainly a need to better understand the level of, and variation in, performance of existing dwellings. There is potentially a large window of opportunity to examine such dwellings through co-heating, although there is often a significant range in the value of HLC_{True}, a complication discussed in section 9.5.

Conversely, some very low heat loss dwellings, particularly those with substantial glazed areas and heavyweight constructions, are unlikely to be tested without significant risk of failure. Careful planning is likely to be required in such cases.

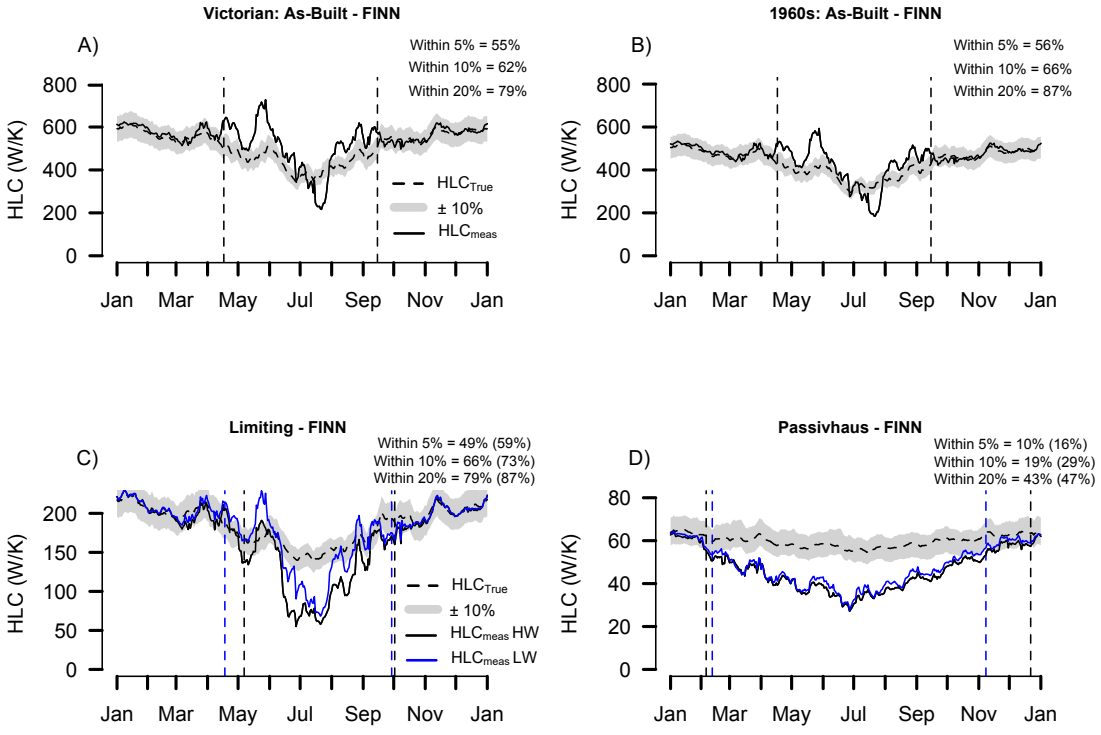

Figure 9.1: *Extent of suitable testing conditions for four different constructions with the same form, using the same weather file (Finningley) and analysis. Dashed lines indicate when results first consecutively fall outside ± 10% of HLC_{True}, for both light and heavyweight constructions where appropriate. This is a somewhat arbitrary boundary but kept consistent throughout to allow comparisons with other figures. The heat loss parameters HLP (W/Km^2) are as follows: VIC = 6.4, SX = 4.9, L = 1.8, PH = 0.6. In cases when both lightweight and heavyweight results are shown, the percentages of the lightweight dat ais given in brackets.* (Simulations: FINN-SN-MLR-2w-24h-6agg-S_{GVS})

9.1.3.2 Built form

Figure 9.2 displays the same construction type across a number of built forms: large detached, semi, terraced and corner 2 bed flat. As can be seen, as the exposed envelope area is reduced, thus reducing the *HLC*, the range in suitable conditions also reduces accordingly. In this case, whilst a heavyweight detached dwelling can be tested (to $<\pm$ 10%) for approximately 38% of the selected year, this decreases to 36% ($<\pm$ 10% HLC_{True}) in a semi of the same construction, 14% in a mid-terrace and just 3% in an apartment. The range of suitable conditions drops significantly in the latter two cases.

Further compounding these difficulties, these simulations are assuming zero heat transfer associated with party walls. In realistic conditions, the experimental uncertainties in these cases have the potential to be far higher, see section 7.2.

Clearly testing apartments and terraced dwellings is likely to be more restrictive, higher risk and more equipment intensive than detached or semi-detached dwellings. It is important to be aware of this and take appropriate steps, both in the timing of tests and supplementary measurements. Testing single flats, such as the example in figure 9.2c, simply may not be possible to any significant accuracy. In some cases, testing dwellings with limited fractions of their envelope exposed to the external environment, co-heating may simply not represent an appropriate tool.

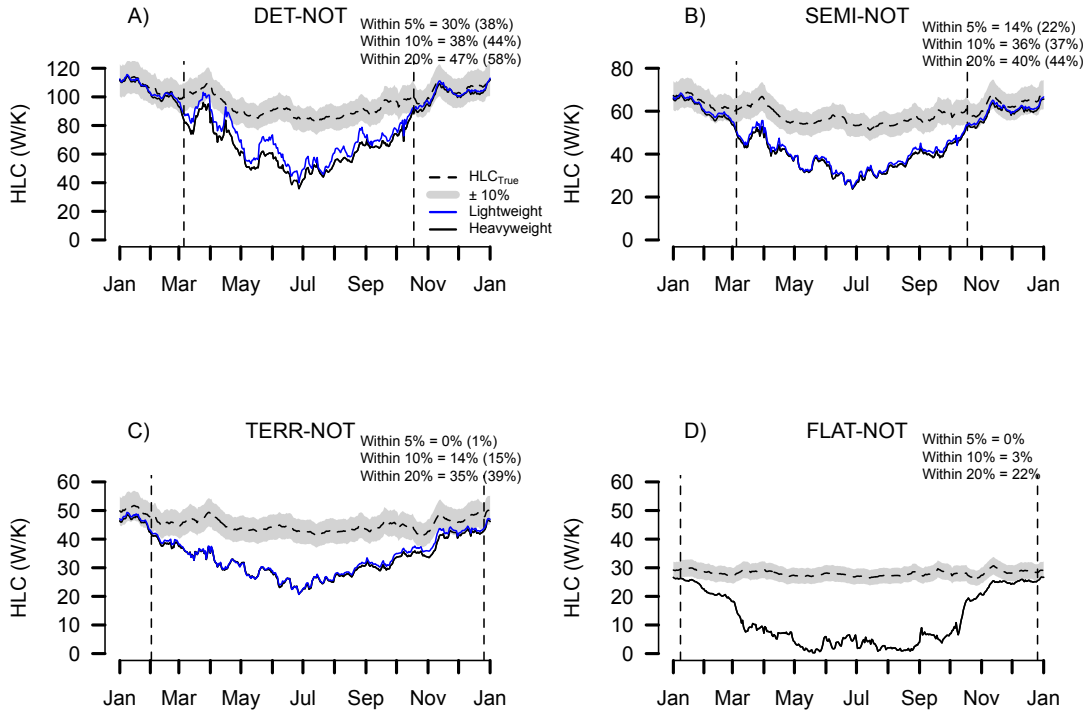

Figure 9.2: *Extent of suitable testing conditions for four dwelling forms of the same construction (Notional) using the same weather file (Finningley) and analysis.* Ratio of party elements to exposed envelope: DET = 0, SEMI = 0.37, TERR = 1.02, FLAT = 3.46. (Simulations: NOT-FINN-SN-MLR-2w-24h-6agg-S_{GVS})

9.1.3.3 Across wider ranges of weather

In figure 9.3, the same dwelling (SEMI-NOT-HW), is tested across 3 weather files. This includes a typical year in Aberdeen (ABR) and Jersey (JER), at opposing ends of the UK. The warmer and sunnier climate of Jersey has a a higher propensity for underestimation, as would be expected given the solar driven uncertainty discussed throughout this thesis.

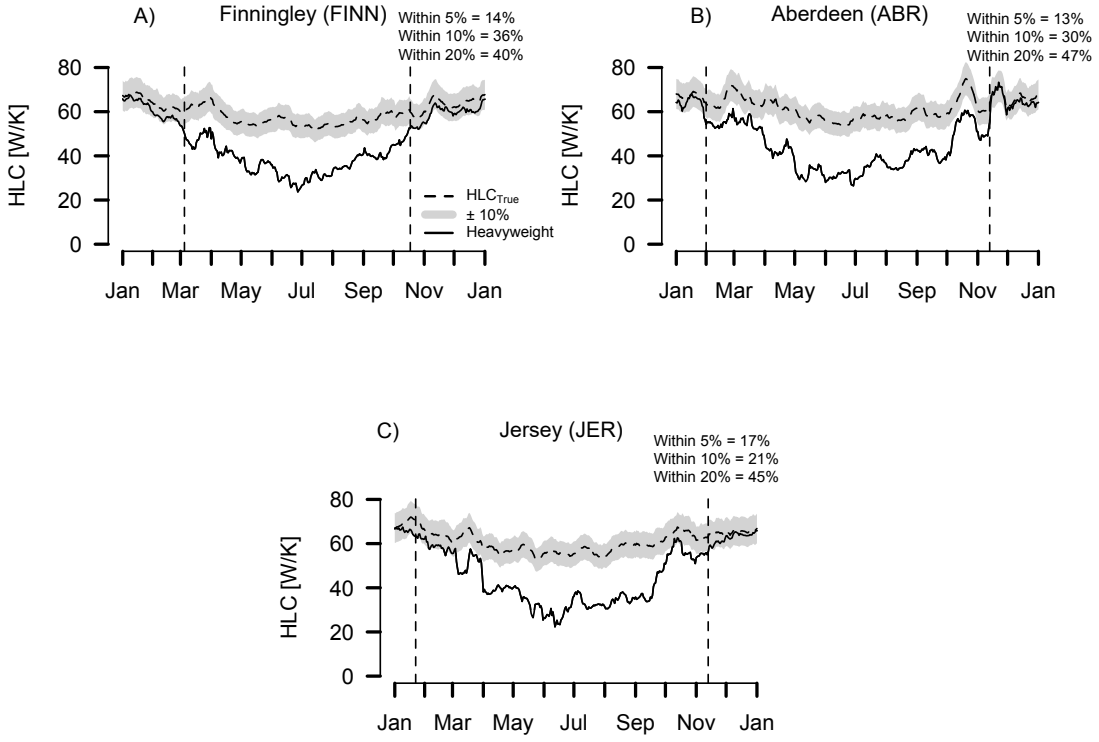

Figure 9.3: *Extent of suitable testing conditions for the same construction (Notional), heavyweight (HW) and built form (semi) using three different TMY weather files (Finningley, Aberdeen and Jersey).* (Simulations: SEMI-NOT-SN-MLR-2w-24h-6agg-S_{GVS})

9.1.3.4 Experimental influences: $Q_{baseload}$, $T_{setpoint}$ & shading

Several experimental choices will also influence the range of environmental conditions suitable for testing (see figure 9.4). Firstly, a fraction of the total electrical heat input, Q_{elec}, coming from mixing fans and loggers, will not be thermostatically controlled. The size of this baseload ($Q_{baseload}$) will influence the point at which a building will begin to experimentally overheat. In high heat loss dwellings, this is likely to be unimportant, but in small, low heat loss dwellings some consideration should be given to the size of $Q_{baseload}$ and the expected total heating load. Whilst allowing all equipment (including mixing fans) to be thermostatically controlled may avoid overheating, it will potentially result in higher variations in internal temperatures throughout a dwelling (section 7.3).

Secondly, the choice of $T_{setpoint}$ will again influence the point at which a dwelling begins to experimentally overheat (see figure 9.4). Higher internal temperatures will extend the range of suitable conditions but this process requires thought. On a practical level, increased temperatures may further increase the drying and cracking of the building's fabric and fixtures. On

a theoretical note, elevated temperatures will increase heat loss through enhanced stack flows (see sections 6.1 and 7.7.1.2) and reduced thermal resistance with warmer materials (see section 7.7.1.1). Corrections for these operational errors may need to be made into the calculation of HLC_{pred}, along with measurements of the infiltration rate during testing.

Finally, external shading can be provided, reducing gains and extending the range of suitable conditions. Previous examples have shaded an entire dwelling (BBRI, 1997) or simply the glazed elements (Butler and Dengel, 2013). Again, consideration of the impact upon the predicted *HLC* under these conditions is required. However, this may represent a necessity in highly glazed dwellings when there is little option over when they can be tested.

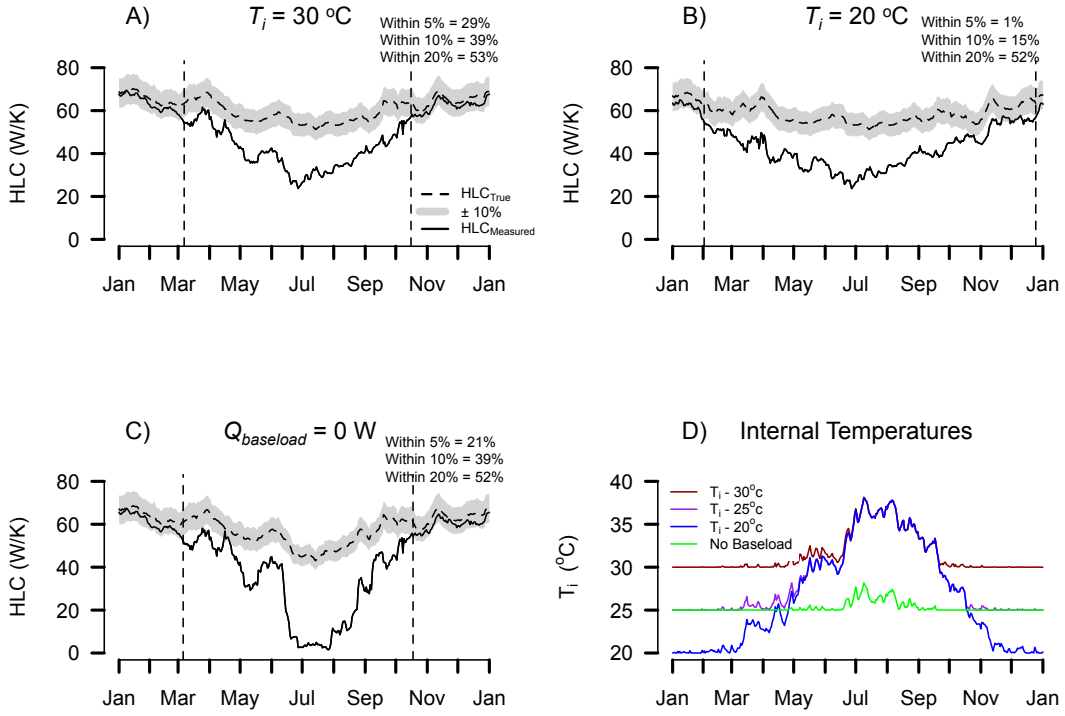

Figure 9.4: *Extent of suitable testing conditions for a test dwelling of the same construction (Notional) and form (detached) using the same weather file (Finningley) and analysis. The experimental conditions are changed through the internal setpoint ($T_{setpoint}$= 20, 25 & 30 °C) and baseload ($Q_{baseload}$= 9 or 0 W/m^2 in the no baseload case).* (Simulations: DET-NOT-SN-MLR-2w-24h-6agg-S_{GVS})

9.1.4 Evidence of when tests can be conducted - field tests

The long-term co-heating data collected as part of the NHBC co-heating field trial was also examined to further explore the range of acceptable environmental conditions. The full results of this project (including analysis periods of less than 2 weeks) are shown in figure 9.5, along with a simulated comparison of the test dwelling[2].

The internal temperatures of both field test dwellings were increased in the summer months from 25 °C to 30 °C and 32 °C respectively. Along with a number of trialled shading systems (Butler and Dengel, 2013), this potentially allowed more reliable testing to be performed over the summer months. Shading was only performed in BRE Test House 2; although temperatures were increased in both test houses, making it difficult to precisely determine which experimental change provided what benefit. It is also worth noting that HLC_{True} is likely to also have increased during this period.

A BRE dwelling has been simulated in the same weather conditions and with the same construction details as the field trial test houses. Whilst not fully calibrated simulations of the field test dwellings, or including the periods of increased internal temperatures and shading, the simulated dwelling offers a useful comparison. Here, suitable conditions occur for approximately 30% of the year in which HLC_{meas} is within 10% of HLC_{True} (see figure 9.5). Significantly, this period does not cover all the measurements taken by individual organisations as part of the NHBC project.

One of the most critical issues in 9.5 is that even in potentially suitable conditions, a significant overestimate ($\sim$ 9 W/K, $\sim$ 14%) is seen when taking the horizontally measured solar radiation (S_{GHR}). This was the only form of measured solar radiation taken across the entire period monitored for this field trial. As a result HLC_{meas} is likely to be a significant overestimate of the HLC_{True}, as demonstrated in the simulated case using S_{GVS} and S_{GHR} (section 5.2).

[2]See appendix A.5.1 for details of this simulation

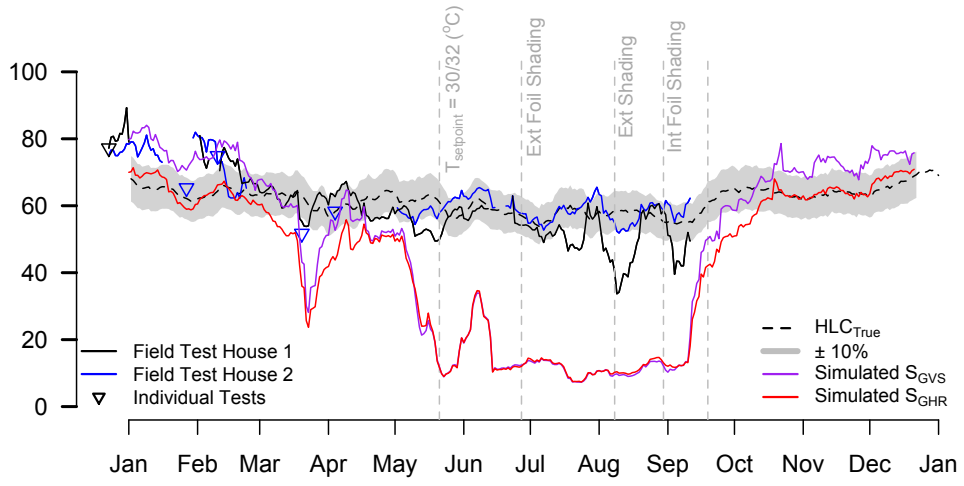

Figure 9.5: *NHBC field trial test houses estimated HLCs across part of a year. A simulated dwelling based upon the test houses is also considered for comparison, using both $S_{GHR}$and S_{GVS}. See Appendix A.5.1 for details of the weather files.* (Field test & Simulation: (BRE-MLR-2w-24h-6agg)

9.1.5 Criteria for suitable testing conditions

9.1.5.1 Required mixes in weather: Everett, Lowe & Gibbons

As previously discussed, both Everett (1985) and later Lowe and Gibbons (1988) set out criteria defining the weather mixes required to estimate both the *HLC* and *R*. These are worth considering briefly as guides for when tests can be performed. The criteria set out are as follows:

Everett, to establish when the *HLC* could be determined, set out two conditions (E1a & E1b):

- **E1a:** Monitor until three very dull days have occurred (i.e. S <0.5 kWhm^{2}d^{-1}or 21 W/m^2).
- **E1b:** None of these days should be proceeded by a sunny day (S >3 kWhm^{2}d^{-1} or 126 W/m^2).

To subsequently determine *R* required two further criteria (E2a & E2b):

- **E2a:** Two moderately dull days (<1 kWhm^{2}d^{-1} or 42 W/m^2), again not proceeded by a sunny one.
- **E2b:** Two sunny days (S >3 kWhm^{2}d^{-1} or 126 W/m^2).

Lowe and Gibbons (1988) adopted a further, more stringent test (LG1 & LG2):

- **LG1:** Pair of consecutive dull days (S <1 kWhm^{2}d^{-1}) and
- **LG2:** Two sunny days (S >3 kWhm^{2}d^{-1} or 126 W/m^2)

In both cases, the criteria attempt to allow for the provision of dull days in which to accurately determine the *HLC*. These days are to be preceded by a further dull day in order to avoid any bias from stored solar heat, reducing the underestimate bias demonstrated in chapter 5.4. The second set of criteria attempts to allow enough sunny days, and therefore a wide enough range in S in order to estimate R. The required range in S with which to determine R to within 20%, was shown to be approximately 150 W/m^2 in chapter 5.2, roughly agreeing with these criteria. However, whilst in both sets the dull days are protected from bias by proceeding dull days, the sunny days are not. In a set of consecutive sunny days, the second of which biased by the stored heat of the first, could give an overestimate of R, with potentially high influence over both regression parameters.

In general, whilst these criteria show agreement with the suitable conditions for relatively high heat loss dwellings >200 W/K, without any adjustment they perhaps unsurprisingly do not appear suitable for very low energy dwellings, as illustrated in figure 9.6. Additionally, with 2 weeks of data the periods deemed suitable for determining R are short, lying between dull and overly sunny periods in which overheating occurs.

9.1.5.2 Overheating criteria

A better indication of suitable testing conditions is achieved through examining the internal conditions of a given test house. As indicated throughout this section, the point at which a dwelling begins to experimentally overheat largely dictates the range of suitable environmental conditions. In figure 9.7, data filtered for experimental overheating is identified.

Periods excluding any full overheating (24 hours of $T_i > T_{setpoint}$) are identified alongside periods consisting of even fewer hours of experimental overheating (<12 hours of $T_i > T_{setpoint}$). Both a heavyweight and a lightweight dwelling are considered.

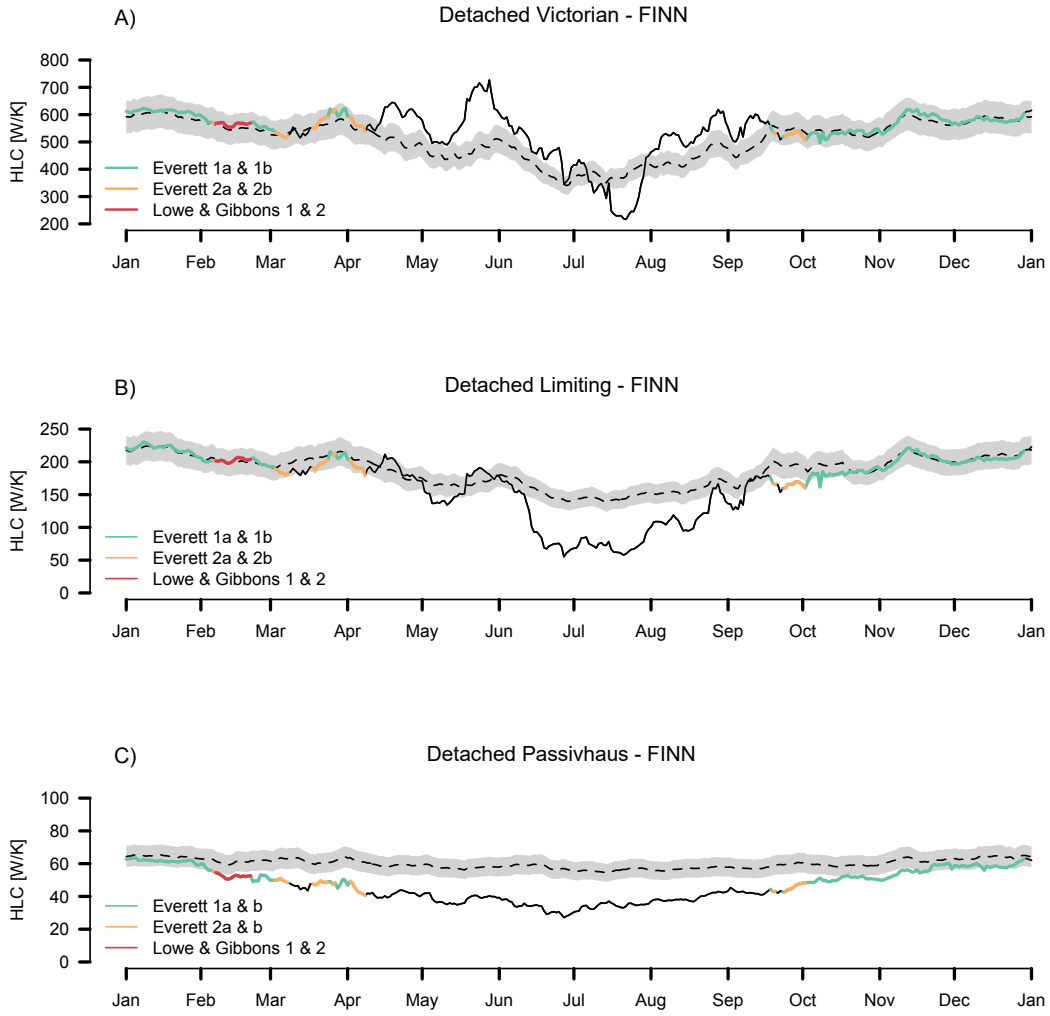

Figure 9.6: *Criteria for required mixes in weather (dull and sunny days) suggested by Everett (1985) and Lowe and Gibbons (1988)). Dashed line again represents* HLC_{True} *with* $\pm$ *10% bounds indicated.* (Simulation: DET-FINN-SN-MLR-2w-24h-6agg-S_{GVS})

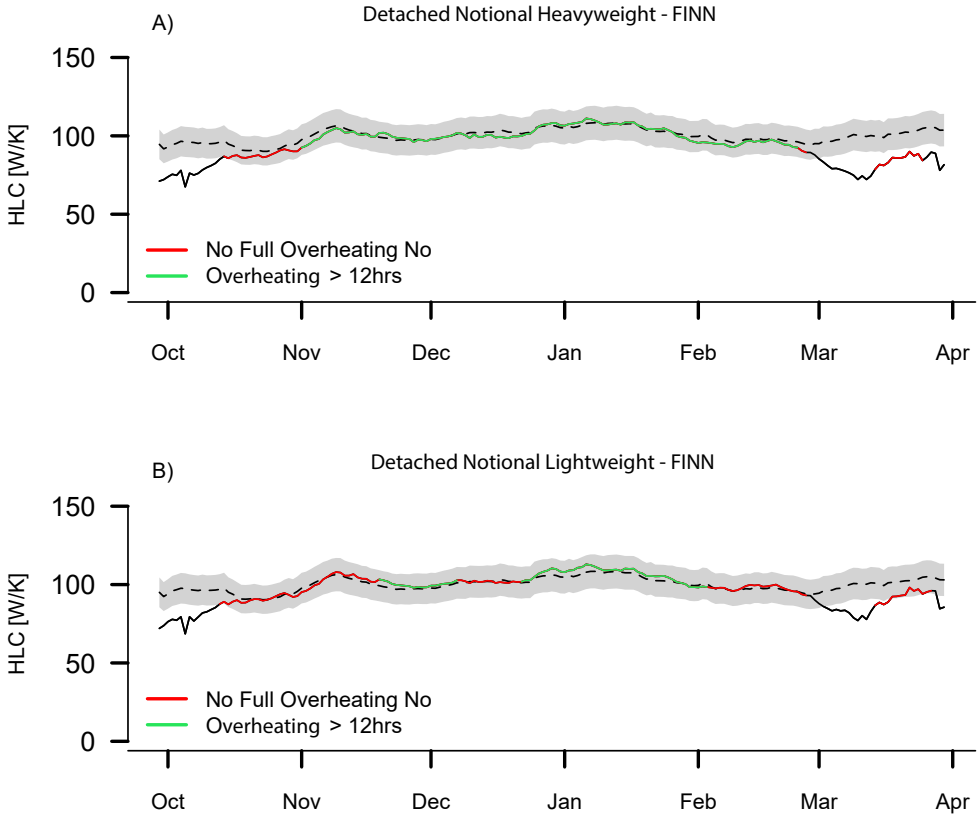

Figure 9.7: *Criteria for experimental overheating to determine valid testing periods. Dashed line again represents* HLC_{True} *with* $\pm$ *10% bounds indicated.* (Simulation: DET-NOT-HW-FINN-SN-MLR-2w-24h-6agg-S_{GVS})

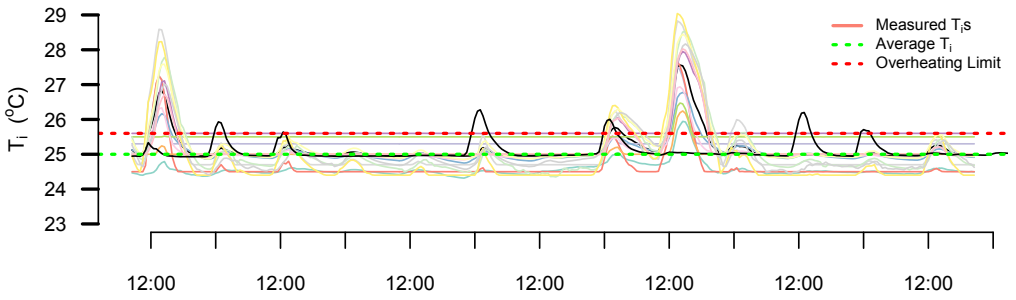

Figure 9.8: *The internal temperatures for each zone of the simulated dwelling in figure 9.7. Variations caused by zones being non-directly heated or through variations in thermostat settings/ calibration. A representative sample for 6 days taken from figure 9.7. Solid coloured lines represent various zones throughout the simulated dwelling.* (Simulation: DET-BR-HW-FINN-SN)

Outside periods of full overheating there are generally accurate results (within $\pm$ 10% of HLC_{True}) for both cases. When there are less than 12 hours of overheating within a given day, then even more accurate results are achieved. However, this is dependent upon the selection of $T_{setpoint}$. The simulations in figures 9.7a and 9.7b were performed with varying internal set points and with only some zones heated directly. This gives a distribution of temperatures equivalent to those likely to be experienced in a field test (the simulated temperatures are shown in figure 9.8).

For the cases seen in figure 9.7, to establish when overheating occurs, $T_{setpoint}$ has been set as the highest base temperature seen in any zone (25.6 $^{\circ}$C). In the simulated case shown this proves the most effective definition of experimental overheating, rather than in respect to the average T_i. However, if thermostatic controllers and zonal temperatures drift over the test period, such a decision is even more complex.

It is also worth noting that in periods with $T_i > T_{setpoint}$ when full overheating does not occur, a systematic underestimate associated with stored heating contributions can still occur. This is reduced with appropriate aggregation intervals but may still be significant, as in the case seen in the heavyweight dwelling (figure 9.7). Here there is a period in March in which HLC_{meas} underestimates HLC_{True} by more than 10% despite no full overheating occurring.

9.1.5.3 Investigating underestimate bias through various aggregations

The limitation with the overheating criteria is that there will be instances, particularly in heavyweight dwellings, in which the air temperature may not appear to overheat but a significant underestimate from stored solar heat may occur. Generally, in cases where systematic errors such as this are thought to exist they can be examined by slightly altering the data set in a way that theoretically should not demonstrate systematic differences. Such an approach has already been discussed, in which co-heating test data can be analysed through various aggregation intervals or through increased aggregation length.

Theoretically, if any dynamics were small then there should be no difference between 18:00 - 18:00 aggregation and 06:00 - 06:00 aggregation or equally between 1 day and 2 day aggregations. If stored contributions are high, then the difference between these two methods may be expected to be large.

9.1.6 Conclusions on suitable environmental conditions

It can be seen throughout this section that the range of suitable testing conditions varies significantly based on the built form, construction type and typical weather conditions expected for a test dwelling. Whilst this leaves a reasonably long testing season for high heat loss, large dwellings (approximately $>$50% of a year), this is reduced to short suitable testing periods with significant risks of failure when testing very low energy dwellings ($\sim$ 20%), or apartments ($\sim$ 3%). As a result, it is unlikely such dwellings can be tested at any significant scale.

Test dwellings with high exposed envelope areas, low thermal mass and small glazed areas will typically represent dwellings in which more accurate results can be achieved more often. In addition, adjusting experimental conditions in dwellings prone to experimental overheating (such as reducing the electric baseload, $Q_{baseload}$, or increasing $T_{setpoint}$) can extend the range of suitable conditions. In the case of the latter option, an adjustment for increased heat loss from increased stack effects and adjusted thermal conductivities may need to be calculated.

Finally, whilst noting that the number of dull days may prove useful, monitoring internal temperatures for periods of experimental overheating is likely to be the most effective method of determining if suitable environmental conditions existed, and whether a *HLC* is likely to be reliable. This is best judged by taking the temperature of the warmest zone and counting the umber of hours above this temperature the mean T_i achieves across each day. If this is 24 hours, then the day should be removed from analysis, along with any subsequent days that are also affected.

9.2 The required duration for accurate *HLC* estimates

Having established the range of suitable environmental conditions and how a limited testing season may restrict the application of co-heating, this section addresses another major limitation, that of the required testing duration and thus the research question:

B2) When tested under suitable environmental conditions, how long is required to accurately determine a building HLC?

9.2.1 Literature on the required test duration

Cited as a major limitation for the wider adoption of co-heating, tests are typically performed with between 1 - 4 weeks of monitoring, with a minimum of 1 week of data following the building reaching quasi-steady state said to be required (Siviour, 1981; Johnston et al., 2013). Johnston et al. (2013) further remark that the duration required is dependent upon a range of factors: the thermal characteristics of a test dwelling, environmental conditions, warm up period, residual moisture in the building fabric and the actual objectives of the test. Table 2.2 of the literature review shows that published tests ranged significantly in durations, taking between 6 and 32 days. In the majority of cases, it is suspected that the duration of monitoring is actually dictated by practical constraints and the availability of the test dwellings, rather than considerations of the building and incumbent weather.

Again, the guidance above is largely based upon experience or through the evaluation of weather mixes rather than the evaluation of actual test data. As a result, the relationship between the duration of testing and the accuracy of the *HLC* estimate from the results have hitherto not been fully and formally addressed in the literature, perhaps strangely so as it is considered such a constraint upon the method. The required duration is addressed directly in this section, with field test data reviewed and a number of simulated test dwellings examined.

9.2.2 The required duration amongst field tests

The relationship between the duration of testing and the derived *HLC* can be determined here using the field tests conducted as part of this thesis and a number of secondary data sets in which daily Q, S and ΔT were documented. Figures 9.9 and 9.10 show the estimated *HLC* as a function of the duration of testing for 12 field tests. The results are then summarised in table 9.1.

In this case, error bars corresponding to the standard error of each measurement are also included (at 63% confidence intervals). Prior to a full discussion on estimated uncertainty in section 9.4, it can be noted that the error bars do not significantly reduce with increasing duration and secondly, that in many occasions they are smaller than the subsequent variation in the result.

The following discussion on the required duration cannot be conducted without a consideration of the experimental uncertainties present. Therefore, criteria from the ISO 9869:2014 (ISO, 2014) on in situ U-values are briefly discussed below and used in figure 9.9. These

allow checks for convergence and non-constant conditions or longitudinal changes across the monitored period, assisting in the discussion of these results.

9.2.2.1 ISO 9869 in situ U-value criteria

Drawing parallels with the steady state in situ U-value measurement protocol,ISO 9869:2014 (ISO, 2014) defines three criteria with which to assess whether a valid in situ U-value or R-value measurement has been achieved. These include:

a) The test duration exceeds 72 hours.

b) The R-value obtained at the end does not deviate by more than $\pm$ 5% from the value obtained 24 hours before.

c) The R-value obtained by analysing data from the first time period during two-thirds of measurement does not deviate by more than $\pm$ 5% from the values obtained from the data of the last two-thirds.

Here, criteria b) essentially checks that the calculated U-value has settled whilst criteria c) attempts to establish whether the long-term conditions during monitoring have significantly changed. Both criteria can be borrowed to establish whether the co-heating test has suitably converged and conditions within a test period appear consistent. Both checks are therefore considered in this section.

9.2.2.2 Field test durations

Figures 9.9 and 9.10 show the results of 12 field tests, representing either tests conducted as part of this thesis or from secondary data. For comparative purposes and to investigate experimental errors, this includes the adjoining test dwelling for the tests CASE-A1 and CASE-A2, which is a mid terrace with one guarded and one unguarded and uncorrected party wall.

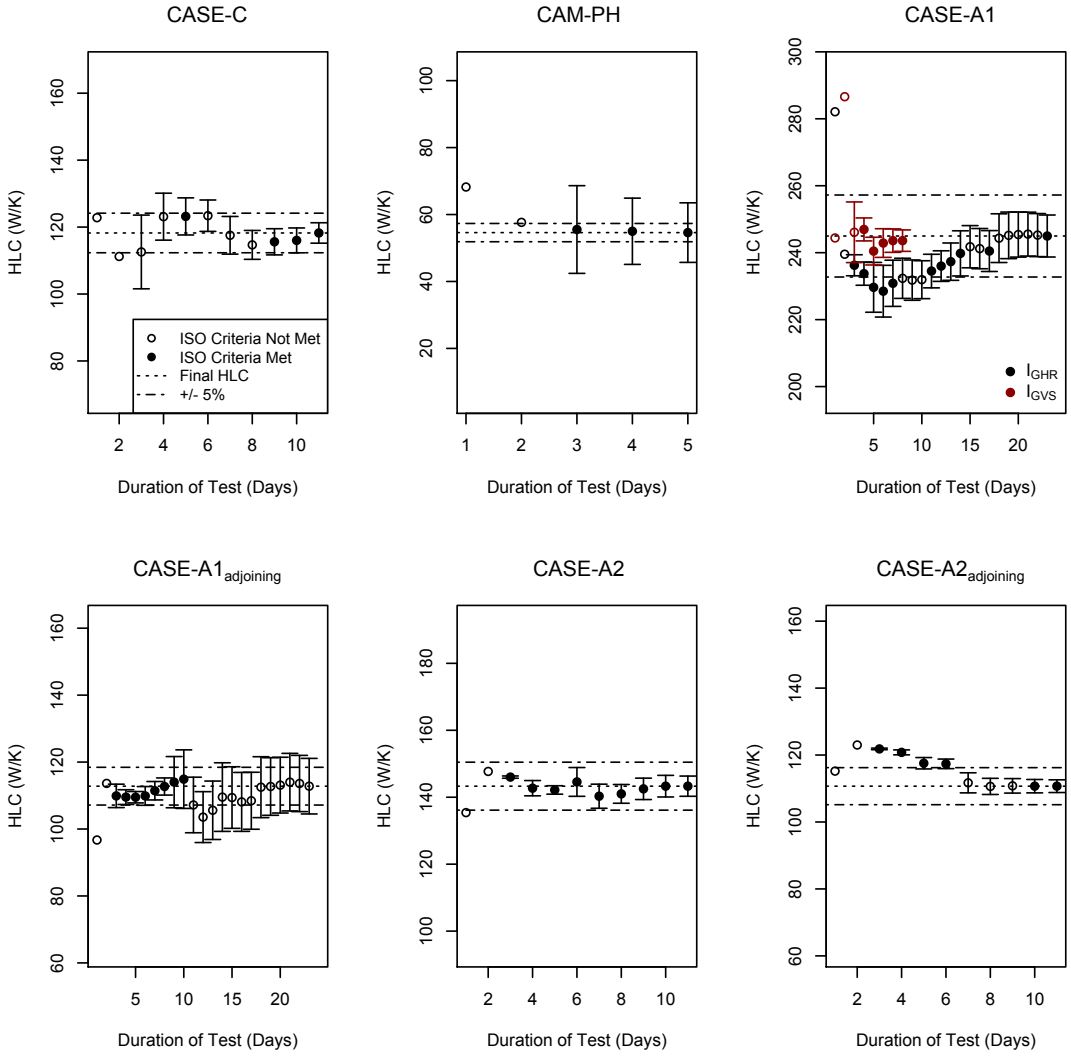

Figure 9.9: *Required duration for field tests. The estimated HLC after each day is shown, along with error bars corresponding to a single standard deviation. Additionally, ISO 9869:2014 (ISO, 2014) criteria for convergence and longitudinal drift (section 9.2.2.1) are shown.* (Field Tests: MLR-24h-6agg)

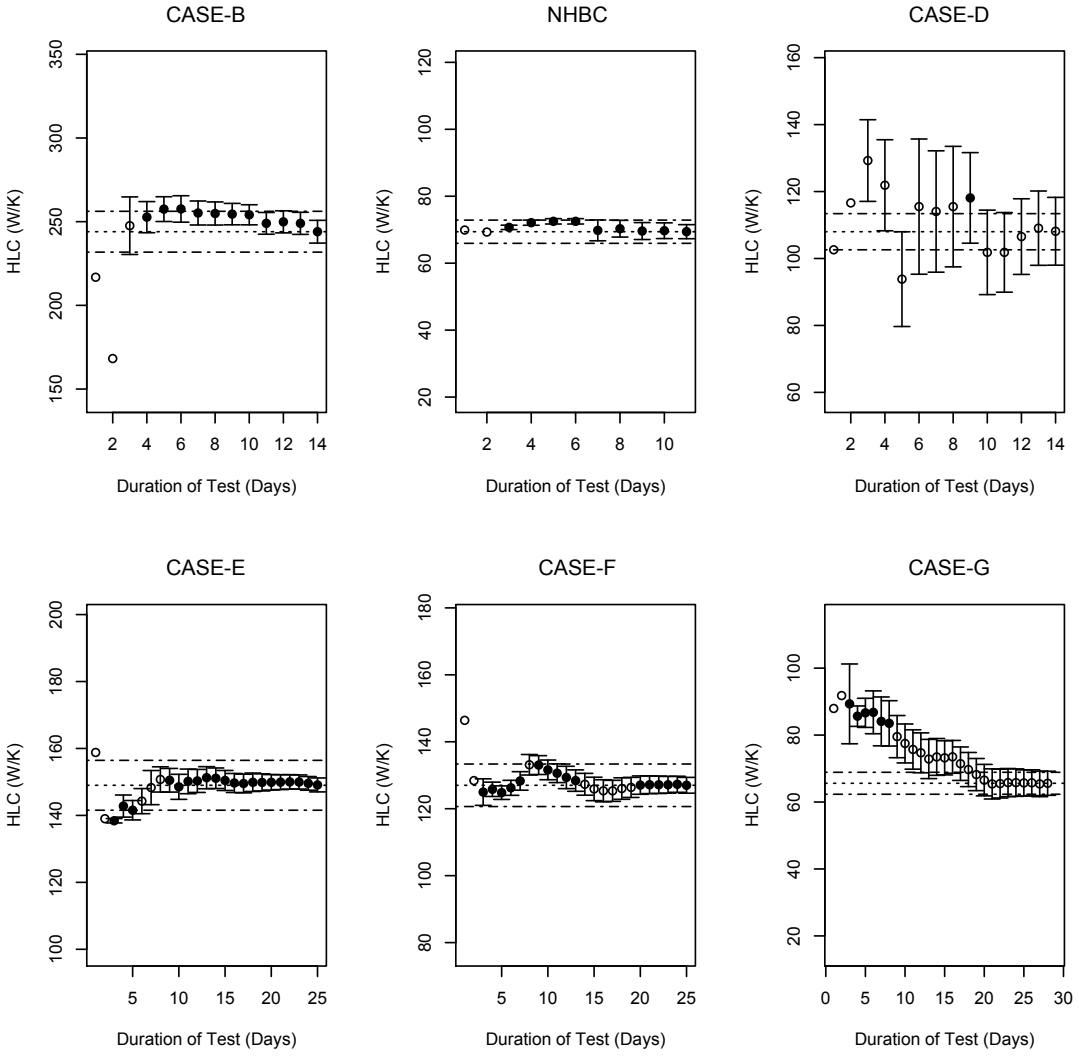

Figure 9.10: *Required duration for field tests. The estimated HLC after each day is shown, along with error bars corresponding to a single standard deviation. Additionally, ISO 9869:2014 (ISO, 2014) criteria for convergence and longitudinal drift (section 9.2.2.1) are shown.* (Field Tests: MLR-24h-6agg)

Table 9.1: Required duration for field tests. *For instances in which the criteria are initially met, but the result subsequently drifts and the criteria no longer met, all instances are recorded, with the day at which the results finally settles within the relevant criteria marked with a *.

Test Case	Days < 20%	Days < 10%	Days < 5%	Days to ISO	Monitoring Duration	Warm Up Period
CASE-C	1	1	1, 3*	5, 9*	13	5
CAM-PH	2	2	3	3	5	1
CASE-A1 - S_{GHR}	1	2	2, 11*	8	24	5
CASE-A1 - S_{GVS}	1	3	3	4	8	5
CASE-$A1_{adj}$	1	2	2, 14*	3	24	5
CASE-A2	1	1	2	3	11	2
CASE-$A2_{adj}$	1	3	1, 6*	3	11	2
CASE-B	1, 3*	3	3	3	14	4
NHBC	1	1	1	3	11	1
CASE-D	1	5	12	9	14	-
CASE-E	1	1	4	3, 9*	25	-
CASE-F	1	2	2	3, 9, 19*	25	-
CASE-G	10	17	19	3	29	-

Several conclusions can be made. Firstly, in the majority of cases, results within 20% of the final result can be obtained within a 72 hour or even a single 24 hour period. Accuracy to within 10% of the final result can be achieved within similar periods, with 10 of 12 cases requiring 72 hours or under. For higher degrees of convergence (within 5%) longer periods may be required - this being achieved within a week in 8 of the 12 cases. The important caveat here is that data prior to reaching approximate steady state, the warm up period, is removed from analysis, such that any associated errors (section 7.4) are absent and the total duration required is not fully reflected.

9.2.2.3 Non-convergence and experimental uncertainties

In fact, of the cases that do not quickly converge upon a result and fail to meet to ISO 9869 criteria, a number of experimental faults can be attributed. The examples $CASE - A1_{Adj}$, $CASE - A2_{Adj}$ (a mid-terrace house with one guarded and one unguarded party wall) and in particular CASE-G (a corner apartment with unguarded flats above and below) shows longitudinal variations, likely associated with non-constant heat transfer to these unguarded spaces. In the case of CASE-G, this means a result cannot be converged upon even after 29 days of monitoring.

In the example of CASE-D, high variability and a jump of -17 W/K and then +15 W/K in the estimated *HLC* is seen after days 5 and 6 respectively (see figure 9.11a). A similar shift (-18 W/K) is then seen following day 9 (see figure 9.11b). Each instance corresponds with significant jumps in the estimation of *R* (-3.8, +4.9 and -5.4 m^2 respectively), and therefore a large readjustment of the solar gains across the entire period and hence *HLC* estimate. The change in estimated *HLC* and *R* before and after these points are demonstrated in figures 9.11 below, where relevant daily data points are identified.

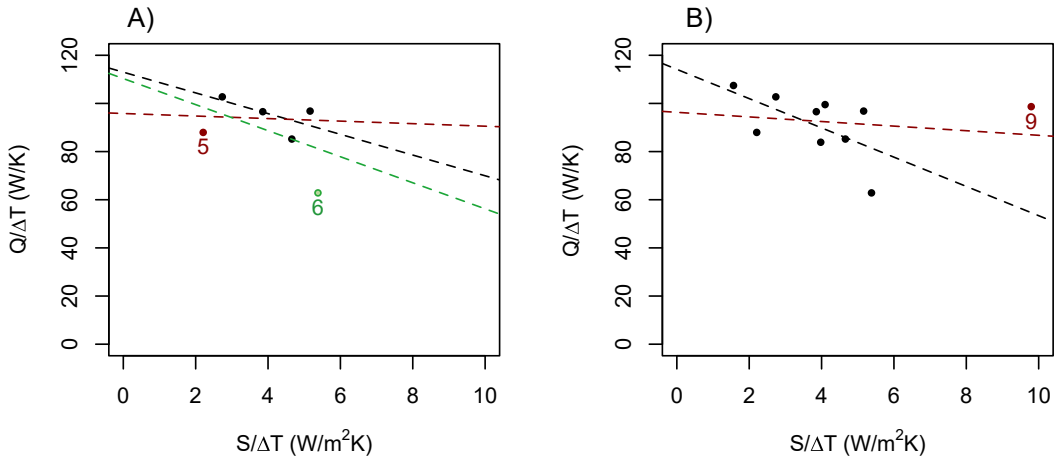

Figure 9.11: *Field test data from CASE-D, in which outlier data points have a high influence over R and hence the HLC. Red and green lines indicate the regression lines before/after the red and green data points,* (Field Test: SIV-24h-6agg-S_{GHR})

Table 9.2: The calculated influence for each daily data point in the CASE-D data set.

Day	Influence	
	HLC	R
	(W/K)	*(m^2)*
1	2.41	-0.35
2	0.99	-0.10
3	-0.14	0.00
4	0.38	0.11
5	-1.94	0.30
6	-0.36	-0.29
7	-0.68	0.06
8	1.28	-0.10
9	4.27	-0.70
10	-16.99	4.51
11	-0.07	0.00
12	2.17	-0.83
13	2.38	-0.86
14	-0.54	0.08
Full Result	**101.0**	**-2.99**

Similar effects can be seen within the result for CASE-A1, where using horizontally measured radiation again demonstrates difficulties in describing solar gains across a number of largely dull days, with the regression estimate of *R* evolving from +15 to -1.3 m^3/s across the period shown in figure 9.9. When S_{GVS} is used, albeit across a shorter monitoring duration[3], a similar overall *HLC* can be retrieved under a significantly shorter time frame.

Plotting results, as in figures 9.9, 9.10 or 9.11, can prove useful in determining whether conditions have changed throughout the monitoring period, either through varying weather conditions (i.e. windy periods), shifting experimental conditions (i.e. temperatures of adjoining spaces) or the estimation of solar gains through the solar aperture. Furthermore, table 9.2 shows the influence of each data point, a measure of the change in the estimated regression parameters due to the presence or absence of the respective day. This proves useful in determining which days are critical to the result, providing grounds for further investigation.

9.2.2.4 Conclusions from field test re-analysis

The evidence from this re-analysis of field data would therefore suggest that short periods of monitoring of just 72 hours can elicit *HLC* estimates similar to those achieved after much longer monitoring periods. Cases in which this is not true often demonstrate high experimental uncertainties. The ISO criteria appear to be useful in identifying convergence, non-constant experimental conditions and unsuitable estimations of solar gains.

Of course, analysis of field data is limited, as there is no certainty that the value converged upon is a good representation of HLC_{True} across this period. To further assess the duration required for accurate *HLC* estimation, the next section examines simulated co-heating tests.

9.2.3 The required test duration in simulated test cases

In the following set of figures, 9.12 - 9.15, the monitoring duration required to achieve an estimated *HLC* within $\pm$ 10% of HLC_{True} is plotted across a Finningley weather year for three archetype test dwellings. In the vast majority of cases, when reliable measurements can actually be made, these can be done to within an accuracy of $\pm$ 10% of HLC_{True} within a week or typically within 72 hours. Long durations (>1week) are not required unless the external conditions are unsuitable.

[3]Resulting from sensor failure

Of course, these simulations assume ideal measured quantities and zero experimental errors as externalities. Accurate *HLC* estimates, in short time periods or otherwise, can only be achieved if systematic offsets that may exist due to a number of experimental uncertainties can be avoided.

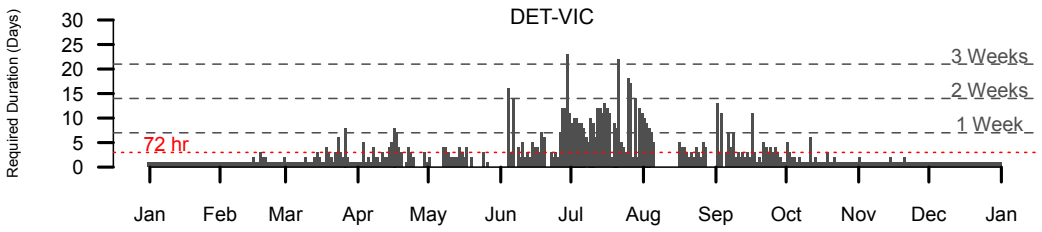

Figure 9.12: *Required duration across Finningley year for an as-built Victorian detached test dwelling. Duration required to achieve ± 10% of* HLC_{True}. (Simulation: DET-VIC-AB-FINN-SN-MLR-2w-24h-6agg-S_{GVS})

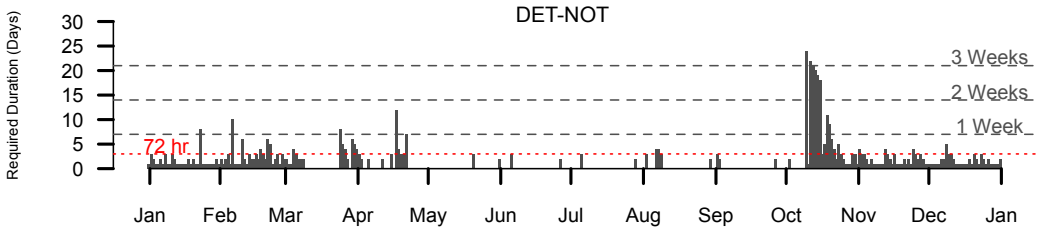

Figure 9.13: *Required duration across Finningley year for a heavyweight notional detached test dwelling. Duration required to achieve ± 10% of* HLC_{True}. Note: results are not normally possible in the summer months, but maybe achieved over short, dull, cold periods. Longer periods are more susceptible to bias from warm, sunny weather. (Simulation: DET-NOT-HW-FINN-SN-MLR-2w-24h-6agg-S_{GVS})

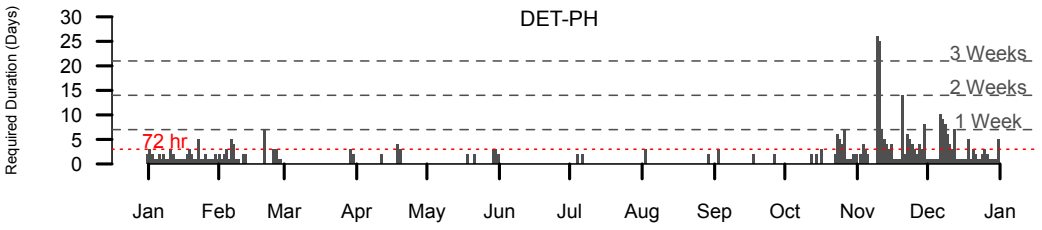

Figure 9.14: *Required duration across Finningley year for a heavyweight Passivhaus detached test dwelling. Duration required to achieve ± 10% of* HLC_{True}. (Simulation: DET-PH-HW-FINN-SN-MLR-2w-24h-6agg-S_{GVS})

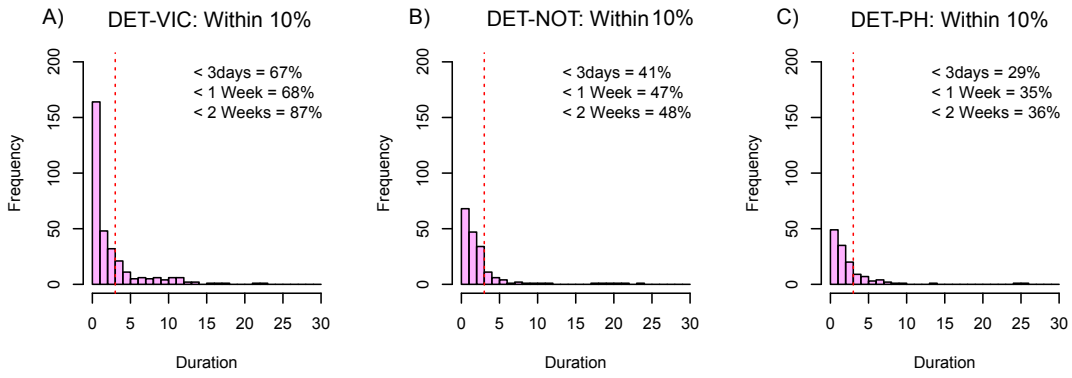

Figure 9.15: *Corresponding histograms for each case in figures 9.12, 9.13 and 9.14.*

9.2.4 The total time required for testing

Unfortunately, the monitoring duration required for analysis only tells half the story. The total length required to test a dwelling will also depend upon the time taken to install and dismantle monitoring equipment and to heat the house to a stable, quasi steady state. To fully appreciate not only the theoretical but the practical drivers for test duration, these must also be considered.

Estimates for researchers setting up and dismantling equipment typically range between 1/2 and 1 full day (Masy and Lebrun, 2004). In the experience of the author, 1/2 a day is normally sufficient for a single researcher to install basic co-heating equipment, exclusive of travel time. If additional data channels or tests (e.g. pressure test, in situ U-values, tracer gas decays) are to be carried out, then typically two researchers are required for a full day at either end of the test period.

To warm up a house sufficiently to a quasi steady state can take as little as 1 day (Andrews, 1995) but can take significantly longer (e.g. 1 week (GHA, 2011b)), depending upon the initial T_i, *HLC*, thermal mass, T_e and installed heating power. For tests conducted as part of this thesis, the range is between 1-5 days (table 9.2). This warm up period is generally reduced if the dwelling has been pre-heated by the existing heating system prior to testing and if researchers can access the dwelling after 24 hours to make any necessary adjustments to the test heating system. The pre-heating phase may have to be significantly longer if moisture must be driven out, although this can be achieved with the existing heating system and with the provision for access maintained. However, it is these practicalities that define an absolute limit on the required test time.

9.2.5 Conclusions on the required testing duration

The results of both the field tests and the simulated results would seem to suggest that in many cases co-heating tests can be performed in shorter time periods than previously suggested, particularly if the required accuracy is set at $\pm$ 20%. In many cases, accurate results to within $\pm$ 10% of a longer dataset can be achieved with 72 hours of measurement.

There are instances in which this is not the case. In particular, this includes tests in which conditions are not constant throughout monitoring, such as variable party wall heat transfer and non-constant internal conditions. Additionally, in cases in which solar gains are providing significant heat input into a test dwelling, but solar gains and *R* are poorly defined, there may be significant jumps in *HLC* estimation throughout the monitoring period. Data sets may therefore need to be examined for outliers with large influence over *R* and therefore the *HLC*.

Such durations are on a par with those of the short term co-heating tests, where night time monitoring periods and dynamic test sequences and analysis techniques are deployed, although there remain other advantages and disadvantages between the two approaches. The real limit then becomes the total time for testing, setting up equipment and achieving steady state conditions and avoiding bias in the result from any warm up period (section 7.4).

Taking this finding back to the context in which co-heating tests are applied, one could imagine the ideal length of testing would be just 48 hours. This would allow testing to be conducted across a single weekend, during which most construction sites are shut down, causing minimal disruption to construction works. If a house could be pre-heated whilst works access was maintained, potentially with the existing heating system, then testing across a weekend may be feasible. The addition of one or two additional weekdays, if required, would then not seem overly disruptive and could result in a reasonably accurate *HLC* assuming the experimental and environmental conditions were suitable.

9.3 Recommendations for experimental protocol and analysis

This chapter reviews and adds depth to the approaches, both experimental and within analysis, which can be made to limit the impact of the sources of uncertainty described in chapters 5 - 8. Thus addressing the question:

B3) Given the uncertainties that exist, what is the optimum co-heating method, both in terms of experimental protocol and analysis techniques, within the existing steady state approach?

This begins with a consideration of alterations or additions to the experimental protocol and measurements (section 9.3.1) before an investigation of the optimal analysis methods (9.3.2). Finally, section 9.3.3 describes a suggested reporting criteria. Without clear guidance, crucial details of tests can be ignored and it becomes extremely difficult to review either the success or uncertainty in a given test.

9.3.1 Experimental protocol

In addition to the LBU protocol, and in reference to the uncertainties documented in this thesis, the following experimental issues should be considered.

9.3.1.1 Measurement of solar radiation

The measurement of solar radiation is one of the most important components for a researcher to get right. As seen elsewhere in this thesis (section 5.2), significant errors can result if solar radiation is measured inappropriately, particularly if a horizontal measurement is applied to a test in which large proportions of solar gains are received directly and vertically.

If a single solar radiation measurement is made, this should occur in the plane of the expected dominant gains. This is likely to be vertical and lie either on the south, east or west facades.

If possible,multiple solar radiation measurements may be made, particularly if the glazing and shading of a building are complex. If, for example, the shading on the east and west facades was significantly different, then both orientations could be measured; although they would have to be combined into a single variable for analysis, as they are likely to be highly correlated and unsuitable as separate MLR variables. If full direct normal and diffuse horizontal radiation can be made, then any desired component can be constructed.

In many cases, it may be difficult to avoid shading completely. Furthermore, some shading may only be temporary, particularly when testing on operational construction sites. Mounting a pyranometer above the roofline will help reduce the impact of shading but may not always be possible from a practical perspective.

9.3.1.2 Measurement of T_e

As the measured parameter is used directly in the analysis and estimation of a building *HLC*, any systematic error or calibration offset is directly transferred into this result.

External temperature sensors should be suitably shielded and ideally, aspirated (Everett, 1985). In addition, an external temperature sensor should ideally be placed away from the building fabric so as not to be affected by any boundary heat flows or radiation from the external building fabric.

It is also important that any external temperature sensors deployed are well calibrated and able to measure T_e to a good accuracy ($<$0.5 °C). Commonly, a single sensor may be used but it would be prudent to use at least two external sensors to reduce any calibration error, location bias and risk of failure. In any case, the error associated with calibration and spatial variation should be incorporated into the uncertainty evaluation of the *HLC* parameter.

9.3.1.3 Measurement of T_i

To ensure a representative internal temperature is used in analysis, T_i should be monitored throughout the dwelling, with a minimum of one sensor per room. Ideally, to avoid any location bias from stratification, sensors should be deployed at various heights or temperature stratification checked manually.

In general, temperature sensors should be positioned out of direct sunlight, away from any heating elements or radiant sources of heat. Palmiter (1979) notes that even in positions out of direct solar radiation, unshielded internal temperatures may measure artificially high air temperatures (when tested sensors recorded temperatures 3.4 °C higher when in direct sunlight and 1.7 °C higher when shaded, compared to a double-shielded sensor).

9.3.1.4 Calculation of a representative T_i

In cases where internal temperatures show a spread in values, the calculation of T_i gains increasing significance. A simple average may lead to bias, as may a volume or floor area weighted average in a building with inhomogeneous heat loss. A heat loss weighted average T_i(see equation 9.10), is likely to yield the best results, even if it is itself based on predicted, rather than measured heat loss characteristics.

9.3.1.5 Heating & mixing strategy

Insufficient heating and mixing equipment is likely to lead to higher variation in internal temperatures, increasing the uncertainty in the measurement and calculation of T_i. In particular dwellings with tight floor plans and thermally disconnected spaces may experience high temperature variations. In many cases, the heating and mixing equipment may need to be adjusted after a short period of heating ($\sim$ 24 hours) to improve the mixing strategy. Ideally, internal temperatures should not vary by more than 2 $^{\circ}$C throughout a test dwelling.

In uninsulated dwellings, to avoid the effect of mixing fans on the internal surface resistance, mixing fans should be aimed inwards, away from external walls. Air velocity at internal surfaces can be measured if necessary. Unfortunately, there is no perfect solution to this problem, only a range of compromises.

Further, if radiant heaters are used then the internal surface temperatures may be higher than when convective heaters are deployed. This could result in higher heat flows through the external walls, even at the same internal air temperature, biasing *HLC* estimates. Radiant and surface temperatures may need to be monitored to evaluate any differences in the two heating strategies.

9.3.1.6 Experimental setpoint temperature $T_{setpoint}$

Low experimental set points ($T_{setpoint}$) will reduce ΔT and therefore reduce the availability of a dwelling for testing, increasing the risk of failure and increasing the scale of many uncertainties. However, if $T_{setpoint}$ is above typical occupied temperatures for extended periods, then increased shrinkage and cracking can occur within the dwelling. In addition, $HLC_{True}$is likely to increase with higher stack effects and increased thermal conductivity of materials at higher temperatures. In such cases, adjustments may need to be made to HLC_{pred} or the infiltration measurements that are taken.

9.3.1.7 Achieving quasi-steady state

Periods in which the mass of a dwelling is still warming up will bias any *HLC* estimate if included in the analysis (section 7.4). Internal air temperatures can be used to identify when an adequate quasi steady state is reached, although for heavyweight elements it may be useful to use either monitored heat flux or surface temperatures.

9.3.1.8 Moisture

High moisture content within the building fabric will add an additional latent load, which will lead to an overestimate of the *HLC*. Further, higher moisture contents within the building fabric will reducing the thermal resistance of many building materials, further increasing this overestimate. Under warm, poorly ventilated co-heating conditions, damage may occur to internal fittings (see section 7.6, figure 7.15).

With difficulties in estimating these effects, the most suitable approach is therefore to try and remove as much residual moisture from the building fabric as possible prior to testing. This will always be challenging when wanting to test new builds, with a limited window of time available for testing post-completion but pre-occupation. Pre-heating the test dwelling, under suitably ventilated conditions and using dehumidifiers may help to reduce residual moisture.

Additionally, internal relative humidity should be monitored and reported. The internal and external vapour pressures can then be evaluated and the vapour pressure excess determined. Converted to a standardised value, this can help determine whether the internal environment of a test dwelling has a high moisture content with respect to the external environment. If possible moisture content measurements can be made manually or at logged intervals of representative points of the fabric.

9.3.1.9 Pre-heating & drying out

Heating a test dwelling to a quasi steady state can take a significant amount of time (as long as 5 days), in fact potentially longer than is required to attain an accurate *HLC* estimate (see table 9.1). It therefore makes sense to heat a test dwelling to a temperature at least close to $T_{setpoint}$ prior to testing. This can be carried out with the existing heating system and with access maintained, reducing disruption and overall cost. Temperatures may still take some time to stabilise, but in general, the overall time required to conduct a co-heating test can be

significantly reduced, whilst this may help remove excess moisture.

9.3.1.10 Measuring Q_{elec}

Measurement of the electrical heat input Q_{elec} is relatively straightforward but holds the potential for mistakes to be made. Suitable accuracy (better than $\pm$ 3%) and appropriate resolution (in Wh) pulse kWh meters should be used. In addition, care needs to be taken that logging devices for pulse inputs are set up correctly. Reconciliation of individual kWh meters with the main meter can be performed, although the possible presence of metered loads outside the thermal envelope should be checked.

9.3.1.11 Baseloads

Part of the internal electrical equipment, all of which provides internal heat gains to the test dwelling, will not commonly be thermostatically controlled. This may include mixing fans, loggers and sensors. This provides a constant baseload that will affect the point at which experimental overheating will occur. In very low heat loss dwellings, researchers may have to limit the amount of equipment to sensible levels to limit the probability of experimental overheating.

9.3.1.12 Party walls

In most cases, uncertainty from perpendicular (i.e. house-to-house) party wall heat transfer can be reduced by guarding any adjoining spaces and enhancing the scale of the heat flow to the external environment. To validate the success of this approach, air temperatures should be recorded on either side of the party element. Additionally, surface temperatures and heat flux sensors deployed on party wall elements can prove helpful.

Unfortunately, heat flows across any party elements may not be uniform or be represented by simple one directional conductive processes. The heat flow through a party wall may better be understood though thermal imaging, particularly if a temperature difference is imposed or during pressure testing of one property. The potential for coplanar heat transfer can be assessed from a knowledge of the likely party wall construction, supplemented if necessary by visual inspection using a borescope.

If party wall heat transfer is of particular interest, then a second period of co-heating can be conducted, this time with any surrounding spaces at a lower temperature than the test dwelling. In simple cases, this approach, suggested by Feuermann (1989) may further indicate the scale of the full heat transfer across these elements. However, any variation between internal and external conditions during the periods needs to be assessed and non-direct heat flows will undermine this measurement.

9.3.1.13 Unconditioned spaces

In many cases, heat transfer may not exist directly to the external environment but via an unheated space such as an attic, roof void, garage or conservatory. In such cases, the first step is to establish whether the temperatures of such spaces, and therefore heat transfer, is approximately constant across the test period or if it is strongly coupled to T_e. It might be useful to check the the predicted heat loss through such elements (see appendix equation B.10) and the temperature difference ratio, as used in Lowe et al. (2007) and defined in Harrje et al. (1979):

$$\frac{T_{unc} - T_e}{T_i - T_e} \tag{9.1}$$

If dynamics exist then significant uncertainty may be introduced into the *HLC* estimate. This may be the case for spaces receiving high amounts of solar gains, such as conservatories of sunspaces. In such cases the heat flows to and from the spaces may be calculated from the properties of the connecting envelope or through measured heat fluxes, in similar approaches to party wall heat transfer.

Even when temperatures in these unconditioned spaces remain relatively constant across a test period (see figures 7.2 and 7.3), this may not correspond to the assumed thermal resistance of such a space in heat loss calculations. The value of HLC_{pred} may therefore need to be adjusted.

9.3.1.14 Infiltration measurements

Infiltration measurements allow infiltration losses to be disaggregated from the total heat loss measured through the co-heating tests. If there is likely to be high variability in daily measurements due to varying infiltration rates, then daily estimations may provide an explanation of the variation, although the estimated *HLC* should still accurately reflect the losses throughout this period. Finally, with accurate infiltration heat loss measurements, HLC_{pred} and HLC_{meas} may also be better reconciled.

A number of measurements can be undertaken. Pressure tests may indicate the likely scale of infiltration losses but converting this measurement into an infiltration rate under natural conditions is problematic and likely to lead to significant uncertainty. Additionally, this does not allow any explanation of daily variation. Nevertheless, performing pressure tests allows the visual identification of leakage paths, an effective form of feedback in general.

Daily tracer gas decays can provide an infiltration measurement under natural conditions and allow a partial expression of daily variation. This latter fact is limited by the duration of the decay and indeed of the period analysed. If infiltration losses were thought to be particularly important or of interest, then a more sophisticated method of infiltration measurement could be used, i.e. constant concentration.

9.3.1.15 Ground heat losses

Again, it should be established whether ground floor losses (Q_g), are approximately constant or dynamic across the test period. Further, measurements of Q_g will reduce any comparison errors to both design and repeated tests. Any quantitative treatment of floor losses may require high density monitoring of both heat flux and temperatures (Pelsmaker, 2015b).

9.3.1.16 Measuring wind speed

Wind speed measurements can be used to explain variation in daily aggregated heat loss and also provide further evidence of the processes of heat loss present in a test dwelling, including air flows in cavities (see section 6.1.4.1). Again, measured wind speed can reduce comparison errors, acting as a check on the conditions throughout testing.

9.3.1.17 Data collection

Data should be collected at sub hourly intervals (a time step of at most 10min), to avoid large sampling errors and to allow smooth time series plots of temperatures and heat flux. Further, if data can be accessed remotely, it will reduce the number of site visits required and allow preliminary data analysis during data collection, allowing adjustments and additional measurements to be taken. This can turn a simple result into a far more productive investigation.

9.3.1.18 Repeated tests

If tests are going to be repeated upon the same dwelling, either as validation of an original test, measuring longitudinal degradation or retrofit measures, then conditions need to be kept as consistent as possible. Internally, the same average internal temperature should be pursued. It may make sense to deploy heaters and mixing fans in the same locations, such that any bias in internal temperature variations from the building layout will be consistent. External conditions cannot be controlled, but similar conditions should be targeted as far as possible and well documented with any discrepancies made clear.

9.3.2 Analysis techniques

9.3.2.1 Form of regression analysis

As seen in the literature review table 2.1, a number of different regression analysis techniques may be used. Most commonly, this consists of either MLR or Siviour analysis, unless solar gains are calculated analytically.

These two methods can be compared across a wide range of data using simulated co-heating tests, thus facilitating comparisons to the true heat loss. An example is shown in figure 9.16, in which it can be seen that there is generally very little difference between either MLR or Siviour analysis. This result is supported by recent findings of other researchers, noting the similarities between the two methods (Bauwens et al., 2011; Deconinck and Leunis, 2012; Baker, 2015).

In figure 9.16 MLR is also performed with the inclusion of an intercept. As previously discussed (see section 8.1), the slope determined from this is a poor match with HLC_{True}, largely due to the discrepancy in their definitions. When the intercept losses are combined with the slope (slope + Intercept/ΔT) then a more accurate estimate of HLC_{True} is achieved, albeit less accurate and more volatile than a non-intercept model.

Whilst this means that in general analysis of co-heating data should take the form of either MLR or Siviour analysis, there is perhaps some benefit in including an intercept model. Figure 9.17 below shows two field tests, one of which (CAM-PH) has 35% of its external envelope and approximately 30% of losses in contact with the ground rather than the ambient air. The other, NHBC, has 29% of the envelope but just 5% of the total losses represented by the uncoupled heat flow to the ground. This difference is demonstrated by the difference between the forced and unforced intercepts in figure 9.17.

The inclusion of an unforced intercept model may therefore be useful for assessing the appropriateness of the co-heating test and *HLC* definition for a given test house. However, as seen earlier (see section 8.1), the estimated intercept remains a poor indication of either the coupled or uncoupled losses. Here the intercept of CAM-PH is 780 $\pm$ 157 W, vastly higher than the 211 W predicted from heat flux measurements.

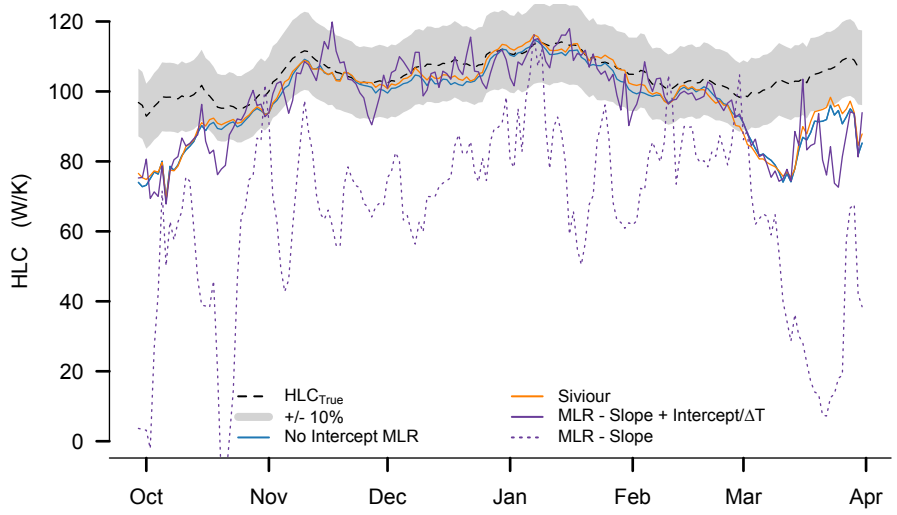

Figure 9.16: *Comparison of MLR, Siviour and MLRi.* (Simulated: DET-NOT-HW-FINN-SN-2w-24h-6agg-S_{GVS})

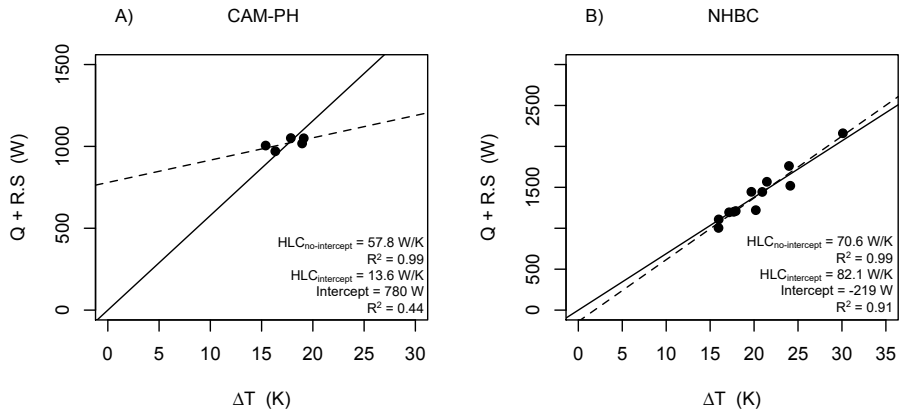

Figure 9.17: *Forced (solid) and unforced (dashed) regressions for two field tests with differing proportions of uncoupled heat losses.*

9.3.2.2 Subtracting out losses prior to regression

On occasion, for example Everett with floor losses (Everett, 1985), components of the total heat loss have been subtracted prior to regression analysis (see sections 2.3.4.2). If such an approach is taken then a number of issues need to be considered. Firstly, the measured quantities that are subtracted, whether floor losses or infiltration heat loss, must be measured robustly. A limited number of heat flux sensors deployed on a large and varied floor element are unlikely to aid any *HLC* estimations, instead increasing the uncertainty in the measurement. Similarly, infiltration measurements representing short periods of a daily data point may not represent the full losses in that period.

This leads to the second point, that appropriate error estimates must be included in any such adjustment and subsequently incorporated into the uncertainty in the *HLC*. If the uncertainty in estimated heat flow can be determined, then this can be converted into the uncertainty in the *HLC* estimation through a process equivalent to that seen in section 9.4.

Finally, as always, care needs to be taken to ensure any comparisons between HLC_{meas} and HLC_{pred} remain equivalent.

9.3.2.3 Aggregation interval

As previously identified, the selection of aggregation interval can help reduce the uncertainty from dynamic effects, e.g. stored solar heating contributions and dynamic T_e (see sections 5.4, 6.2). This analysis can be extended here by evaluating the optimum aggregation interval within simulated tests. Surprisingly, sunrise to sunrise aggregations do not necessarily yield the best results as the initial hours of low sunlight are outweighed by the additional hours of stored solar heat being re-emitted to the internal space. This is demonstrated in figure 9.3.2.4 and table 9.3 for a detached, notional, heavyweight dwelling in which a 12:00 - 12:00 aggregation interval is shown to be optimal, or 4 hours after sunrise in an evolving interval. However, the optimal delay in starting an aggregation interval reduces in dwellings or periods in which less solar heat is stored and it is stored for shorter periods (e.g. lightweight, less glazing, east-west orientated). Therefore, unless there is specific reasons to suspect high amounts of stored solar heat, a sunrise to sunrise aggregation would allow a consistent and perhaps purer approach. Pragmatism is again required.

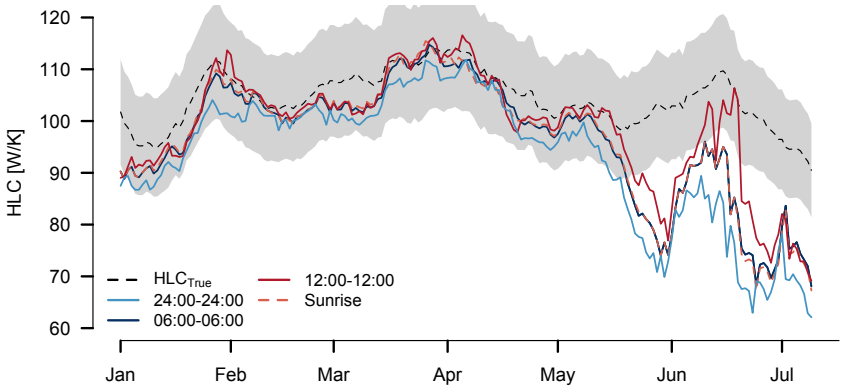

Figure 9.18: *Optimum aggregation intervals in a simulated co-heating test.* (Simulated: DET-NOT-HW-FINN-SN-MLR-2w-24h-S_{GVS})

Table 9.3: Optimum aggregation intervals in a simulated co-heating test. (Simulated: DET-NOT-HW-FINN-SN-MLR-2w-24h-S_{GVS})

Aggregation Interval	*24:00-24:00*	*01:00 - 01:00*	*02:00 - 02:00*	*03:00 - 03:00*	*04:00 - 04:00*	*05:00 - 05:00*	*06:00 - 06:00*	*07:00 - 07:00*	*08:00 - 08:00*
Mean Square Error - MSE	11.3	11.3	10.6	10.1	9.5	9.0	8.5	8.1	7.6

Aggregation Interval	*09:00 - 09:00*	*10:00 - 10:00*	*11:00 - 11:00*	*12:00 -12:00*	*13:00 - 13:00*	*14:00 - 14:00*	*15:00 - 15:00*	*16:00 - 16:00*	*18:00-18:00*
Mean Square Error - MSE	7.2	6.9	6.4	5.9	6.1	8.4	12.0	14.5	15.0

Aggregation Interval	*Sunrise*	*Sunrise +1h*	*Sunrise +2h*	*Sunrise +3h*	*Sunrise +4h*	*Sunrise +5h*	*Sunrise +6h*
Mean Square Error - MSE	7.9	7.6	7.2	6.7	6.7	7.3	9.0

9.3.2.4 Aggregation length

Similarly, the optimum aggregation length can be assessed using 1 day, 2 day and 3 day aggregations. Again, rather than this being clear, the optimum method depends upon the dwelling. In a well insulated dwelling, where stored dynamics are likely to be relatively larger heat flows, a 2 day aggregation provides more accurate results. However, in a higher heat loss dwelling, with relatively smaller storage heat flows and higher variability due to varying infiltration, the higher number of data points provides a more accurate result. It is therefore thought that unless stored dynamics are thought to be significant, 24 hour aggregations are used. In any case, comparisons of aggregation lengths and intervals should help identify these systematic errors.

Table 9.4: Optimum aggregation lengths in a simulated co-heating test. (Simulated: DET-NOT-HW-FINN-SN-MLR-2w-6aggS_{GVS})

	DET-NOT-HW			**DET-VIC**		
Aggregation Interval	*1 Day*	*2 Day*	*3 Day*	*1 Day*	*2 Day*	*3 Day*
Mean Square Error - MSE	8.0	6.2	8.3	18.4	26.4	33.6

9.3.2.5 Night time data

As expected from the discussion on stored solar dynamics and dynamic T_e, any analysis of night time data on its own is likely to underestimate HLC_{True}, (see figure9.19). This means utilising segmented night time periods should be avoided. Testing over such short periods is likely to increase any definitional uncertainty from unknown heat flows (e.g. sky radiation) as the results are more susceptible to extremes, as seen by the variation in the two day averaged night time *HLC* estimates in figure 9.19. If a night time strategy is adopted for any such method, it would be recommended that dull days, with little variation in T_e are used, and shading deployed during the day to further reduce any stored solar effects (see Zabot, 1987).

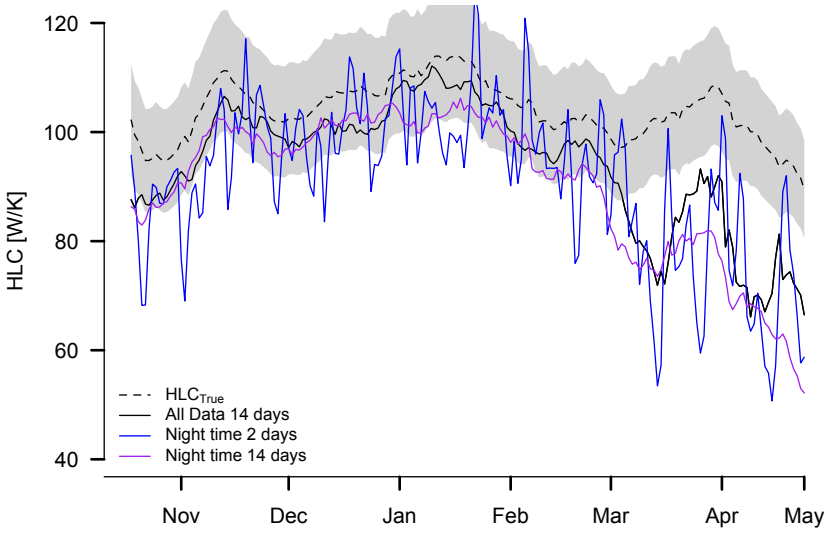

Figure 9.19: *Analysis of night time data, using the 4 hours proceeding dawn. 2 night and 14 night averages shown. These are compared to a MLR using 14days, 06:00 - 06:00 aggregation.* (Simulated: DET-NOT-HW-FINN-SN-SLR)

9.3.3 Reporting

Suitable reporting of co-heating tests is essential to reviewing their validity and gaining an improved understanding of the method itself. Currently, the depth and level of reporting is variable and often leaves results difficult to interpret. To address this, a set of reporting criteria are set out in table 9.6 below, drawing on conclusions throughout this thesis and ISO 9869:2014 (ISO, 2014) reporting criteria. These cover details on the test dwelling, the project aims, the experimental protocol, conditions during testing, analysis method, results (including uncertainty estimates) and comparisons to design and other tests.

Table 9.5: Reporting Criteria for Co-heating Tests, part 1.

Reporting Checklist
a) Data on the test dwelling
• Location of building & Orientation
• Purpose of test (i.e. suspected bad workmanship, building system, retrofit measures,ageing of the materials, etc.)
• Design HLC - including calculation method, input assumptions and appropriate error bars
• Further Whole Building Parameters: Floor Area, Volume, Envelope Area, Glazed Area, TMP, Volume, Air Leakage, party wall area.
• Size and Locaion of glazed elements and (R)
• Probable structure of elements: walls, floor, roof, party walls, glazing, internal partitions
• Predicted relative size of heat flows coupled to ΔT and to other temperatures (Tg etc.)
b) Description of the Experimental Set-up
• Name of the measuring institution
• Type and characteristics (make, serial number, calibration factors, history) of the temperature sensors, electricity meters, heaters, fans etc.
• Details of precise variables measured:
- Orientation and type of measured solar radiation (i.e. South/North, Vertical/Horizontal, Global/Diffuse/Direct)
- Type of temperature measured (air, radiant, surface etc.)
• Locations of internal sensors, heaters and mixing fans (diagram & photographs)
• Locations of external sensors (diagram & photographs)
• Interval between records and number of measurements averaged or sampled in each record
c) Conditions during testing
• Date and time of the beginning and end of measurement (entire period)
• Identification of period of data to be used within analysis
• Timeseries graphs of the recorded data (at no more than hourly intervals) - showing also the data discarded before and after analysis period, including:
- Internal Temperatures in all zones
- RH / VPX
- Electrical Heating Power
- Any relevant heat flux measurements
- Temperatures from adjoining heated or unconditioned spaces (i.e. attics, conservatories, garages, voids)
• And Environmental Variables including:
- External Temperature
- Solar Radiation
- Wind Speed & Direction
Additionally, useful measurements may be taken of:
- Surface Temperatures
- Ground Temperature
- Effective Sky Temperature
d) Description of the method of analysis
• Calculation method for the average internal temperature (i.e. heat loss / volume weighted)
• Assumed heat balance equation
• Calculation method (i.e. MLR, Siviour, Simple Average)
• Forced or unforced intercept
• Aggregation interval used (i.e. 06:00 - 06:00)
• Aggregation length used (i.e.24hours, 48hours etc)
• Description of any filtering of the data
• Details of any corrections made (i.e. party wall heat flows, ground losses, infiltration)
• Details of Error Analysis Calculations

Table 9.6: Reporting Criteria for Co-heating Tests, part 2.

Reporting Checklist
e) Results
• Plot of results (Siviour or 2D MLR) showing aggregated data points including omitted data and appropriate error bars
• Estimated HLC
• Estimated R
• Intercept (if appropriate)
• Regression Statistics
- Standard errors for regession variables
- t-value & p-value
- Influence of data points
• Appropriate Error Estimation and error statement at appropriate coverage (i.e. 95% confidence intervals)
• Discussion of undefined uncertainties that require type B uncertainty analysis (e.g. moisture)
• Details of any alternative results (i.e. alternative aggregation periods, periods of analysis or the use of an intercept)
• Aggregated Data Used in Calculations (Daily or otherwise) for:
- Ti
- Te
- Solar Radiation
- Electric Power
- Wind Speed
- Calculated ACH
- Estimated party wall heat flows (if appropriate)
f) Comparisons to design
• Details of calculation proceedure used for $HLC_{predicted}$ (i.e. ISO , SAP, PHPP)
• Details of any verification of on site details
• Estimated corrections due to elevated internal temperatures: increased stack effect & adjusted thermal resistances
• Adjustments for het transfer through unconditioned spaces
• Estimated Infiltration losses under the conditions of testing
• Predicted HLC, with appropriate error bands
• Discrepancy between $HLC_{measured}$ and $HLC_{predicted}$
• Discussion of the significance of this discrepancy and potential causes
g) Comparisons between tests (if appropriate)
• Comparison of conditions during testing:
- Internal (Temperature, RH, moisture, T_{adj}, T_{unc})
- External (T_e, Solar Radiation, T_g, RH)
• Details of any deviations in method
• Changes to dwelling between tests (changes to fabric, glazing, thermal mass etc.)
• Full results, including error analysis
h) Details of any supplementary tests
Description of supplementary tests (i.e. in situ u-values, pressure tests, tracer gas decays)
- Methods & Appropriate Standards Adopted
- Results from tests
- Comparisons to co-heating results (i.e. adjusted $HLC_{predicted}$ based upon measured u-values)

9.4 Estimating uncertainty

9.4.1 The importance of uncertainty statements

It is worth beginning this section on estimating uncertainty by formally defining measurement uncertainty:

"uncertainty (of measurement): a parameter, associated with the result of a measurement, that characterizes the dispersion of the values that could reasonably be attributed to the measurand"

(JCGM, 2008a, p.36)

Reasonable estimates of the uncertainty attributed to any measured parameter are crucial to understanding the trust held in the estimated result, the confidence within which a value can be stated and presenting the measured value in the context within which it was measured. An understatement of uncertainties might allow too much trust to be placed in the values reported, with potentially embarrassing or disruptive consequences. Similarly, an overstatement of uncertainties can have undesirable repercussions. In the context of co-heating *HLC* measurements, this can mean understating the likely performance gap and leaving the impression of an unreliable measurement and method.

9.4.2 Uncertainty estimates in co-heating

Generally, uncertainty estimates accompanying co-heating *HLC* and *R* estimates are either based upon statistical errors, the standard error or standard deviation, or are absent completely (see table 2.1). The prevalence of the latter has likely compounded the lack of trust in co-heating results, their accuracy and any estimations of the size of the performance gap. When statistical estimations of uncertainty are used, although they can be insightful, they do not incorporate or give any weight to the experimental sources of uncertainty that might be present in a result, e.g. sensor calibration and data acquisition system uncertainties. A more encompassing and consistent method of estimating uncertainty is required.

In general, uncertainty estimates are not applied consistently within thermal performance measurements, particularly amongst in situ field measurements and those using steady state calculations. There is certainly a preference within the wider building industry to state building and material properties as single values - neglecting the almost inevitable variations present and without stating any measurement uncertainties with which these values are determined. In the absence of an existing robust, formal framework for estimating uncertainty in co-heating *HLC* estimates, a number of examples from the broader literature are considered.

The first, reviews the generalised approach to measurement uncertainty contained within the de facto standard on the GUM[4] standards (JCGM, 2008a) which also provides the basis of the BSI PD 6461-4:2004 General Metrology - Part 4: Practical guide to measurement uncertainty (BSI, 2004). In particular this provides a framework for evaluating uncertainty both statistically (Type A uncertainty evaluation) and through past experience and knowledge (Type B), allowing a wider range of uncertainty sources to be incorporated into uncertainty estimates.

Following this, four cases from within the field of thermal performance testing are discussed. Firstly, uncertainty estimates within laboratory hot box and heat flow meter measurements are reviewed, providing a number of parallels to co-heating. Secondly, the assessment of in situ U-value measurements, as described in ISO 9869:2014 (ISO, 2014) are discussed before an alternative approach to in situ U-value error analysis is considered (Baker, 2011). Subsequently, the approach to uncertainty analysis proposed for system identification techniques within the PASLINK[5] network is also considered (Baker and Dijk, 2008; Baker, 1993).

9.4.3 The BSI and GUM approach to uncertainty analysis

Under the GUM and BSI framework, type A evaluation of uncertainty is based upon a statistical analysis of a series of readings, i.e. the standard deviation or standard error, and is therefore the type used most commonly to date when estimating the uncertainty in co-heating *HLC* measurements.

Whilst type A covers the random variations in the measurand it cannot readily be applied to the analysis of such parameters as the calibration of an instrument and further systematic errors and offsets. Such sources can be evaluated on the basis of the information available, which may come from calibration certificates, manufacturers specifications or professional judgement (BSI PD 6461-4:2004; BSI, 2004). These non-statistical sources of information lead to type B uncertainty evaluation, a concept absent from co-heating *HLC* estimates to date.

An important difference between type A and B uncertainty evaluation exists. Type A defines an interval, based upon a defined level of confidence, within which the true value of a measurand is expected to lie. In type B evaluation, the expert has to specify not only the interval

[4]GUM: the Guide to the expression of uncertainty in measurement

[5]PASLINK evloved from the PASSYS Project (Passive Solar Components and Systems Testing) which began in 1985.

but also the level of confidence that the value of the measurand will lie within, and whether it is likely to lie within one region or another. This requires the specification of an appropriate probability distribution, i.e. normal, rectangular, etc. Results then need to be reduced to the standard uncertainty so there is a common basis for combination.

A six step generalised framework is presented by the BSI documents and is used here to analyse the uncertainty within a number of co-heating tests after four examples of uncertainty analysis in thermal performance measurements are considered (see sections 9.4.7 & 9.4.7.2).

9.4.4 Methods of estimating uncertainty

9.4.4.1 Uncertainty Analysis in Hot Box, Hot Plates and Heat Flow Meters

The standard BS EN 1946:2000 (BSI, 2000) parts 1 to 4 document uncertainty evaluation in heat flow meters, hot plates and hot box measurements. With a number of fundamental similarities to the equipment and methods used in co-heating, these documents provide insight into how various sources of uncertainty can be estimated and combined.

Taking the guarded hot box as an example (BS EN 1946-4:2000), whilst the heat flow rate through the metered specimen area is of primary interest, a number of secondary heat flows may exist. These include: the heat flow at the edges of the specimen, due to insufficient guarding; lateral heat flow, across the specimen between the guarded and metered areas; and heat flow through the metering box walls.

The respective heat flows are calculated and determined as a percentage of the principal heat flow; that which flows through the metered area of the specimen. Each flow rate can be calculated from either 1) the thermal resistance, area and temperature difference across the element, 2) through measured heat flux or 3) determined experimentally. The latter method involves altering the temperature difference between the metered area and the surrounding guarded area to determine the size of the heat flow (as suggested by Feuermann (1989) when co-heating apartments). Secondary heat flows are summed to give the uncertainty in the heat flow through the specimen. Maximum limits can be defined for each flow, as a percentage of the primary heat flow to give acceptable limits on the size of these uncertainties. They are then combined into the uncertainty within the primary heat flow and the uncertainty of the estimated thermal characteristics.

Parallels between these secondary heat flows can be drawn to secondary indirect heat flows and their associated uncertainty in co-heating *HLC* measurements, particularly relating to party wall heat transfer. In terms of temperature measurement a degree of spatial variation is recognised within BS EN 1946-4:2000 (BSI, 2000), both in surface and more significantly in air temperatures, drawing another parallel to an uncertainty in co-heating tests. In such cases, the uncertainty is defined as the range in measured temperature, assumed to be constant and uniform, divided by 4, that is half the width of the range about the average[6]. Subsequently, this spatial temperature uncertainty is combined arithmetically with calibration and data acquisition errors to give the total uncertainty in the measured temperature.

Further errors, due to geometry (e.g. specimen thickness, metering area), power input, specimen inhomogeneity, drifts and fluctuations from steady state and moisture effects are also listed, with typical percentage values given for each, based upon previous studies or experience. Total uncertainty is calculated both as an *arithmetic* total and with the errors added in *quadrature*[7], the latter giving a smaller estimate defined by BS EN 1946-4:2000 as the 'maximum probable error' (BSI, 2000, B.9).

In conclusion, the framework for uncertainty analysis in laboratory tests, identifies the sources of uncertainty potentially present in a test and attributes a given uncertainty to each. These are based upon the measured or predicted size of the heat flows, from information such as calibration uncertainties or from professional judgement, following the form of type B uncertainty analysis. A number of parallels can be drawn to co-heating uncertainty estimation, with both variations in temperatures measurement and uncertainty from secondary heat flows.

9.4.4.2 Uncertainty analysis for in situ U-value measurements - ISO 9869-1:2014

To estimate the uncertainty in measured in situ U-values, ISO 9869-1:2014 (ISO, 2014) defines a list of sources of uncertainty, with estimated uncertainties, including:

- The calibration of heat flux meter and temperature sensors: Stated as a $\sim 5\%$ error for both heat flux and temperature sensors if the sensors are well calibrated.

- Accuracy of the data logging system: In which no estimated uncertainty is given.

[6]This width is not entirely clear, as it does not correspond to any of the GUM distributions.

[7]Random and independent errors can be added in quadrature, else, an arithmetic sum should be used (JCGM, 2008a; Taylor, 1997).

- Random variations due to changes in thermal contact of sensor and surface: Considered a $\sim 5\%$ error if carefully installed. This error is reduced if multiple measurements are conducted.

- Operational Uncertainty from heat flux meters: Gives a stated residual uncertainty of $\sim$ 2-3%.

- Errors from variation in temperatures and heat flows over time: These are said to be less than 10% if criteria 1, 2 and 3 are met (see section 9.2.2.1) or a dynamic method is adopted.

- Temperature variation within the space and differences between air and radiant temperatures $\sim 5\%$.

This uncertainty is then said to lie between the quadrature and arithmetic sums of the error, giving an overall error prediction of 14 - 28%, i.e.:

$$\sqrt{5^2 + 5^2 + 3^2 + 10^2 + 5^2} = 14\% \tag{9.2}$$

$$\sqrt{5 + 5 + 3 + 10 + 5} = 28\% \tag{9.3}$$

The uncertainty analysis here takes the form of Type B GUM analysis, with uncertainties derived from the professional experience of the authors (JCGM, 2008a). These estimates of uncertainties are often supplemented with somewhat arbitrary caveats, i.e. 'if carefully installed'. One would suspect that the uncertainty from poor thermal contact could be significantly higher if this definition of 'carefully' is not met. This runs the risk of providing unsuitable error estimates, particularly with inexperienced practitioners. Clearly, applying such a standard assessment across a range of tests, without any data input or supplementary measurements, is unlikely to fit all. However, no further indication is given over how these individual error components are estimated or indeed how they can be tailored for a given test.

Finally, and more generally, the ISO 9869 guidance provides a list of reasons that may further increase the probability of a larger uncertainty within U-value estimates beyond the bounds of the above assessment. These are often similar to the uncertainties within co-heating discussed in chapter 4, and include:

- If the temperatures (particularly T_i) show large fluctuations (before or during the test) compared to the temperature difference between both sides of the element.

- If the element is heavy and the duration of the test is too short - potentially controlled through the three ISO tests (section 9.2.2.1).
- If the element is submitted to solar radiation or other strong thermal influences.
- If no estimate is made of the operational error.
- The accuracy of the measurement of the U-value depends on the definition of the environment temperatures adopted for the U-value and their measurement.

In conclusion, ISO 9869:2014 (ISO, 2014) provides guidance for both reducing uncertainty and estimating the uncertainty from a number of key sources. This allows an estimate of the overall uncertainty based upon a quadratic or arithmetic sums - if errors are thought to correlate. However, this judgement of uncertainty is solely based upon professional judgement and does not provide any framework for feeding any of the measured data into uncertainty estimates and hence tailoring an error estimate.

9.4.4.3 Uncertainty Analysis for In situ U-value Measurements - Baker (2011)

Baker (2011) does incorporate the measured data into U-value uncertainty estimates. Here, U-values are calculated across long periods ($\sim$ 10 days) and estimated using an averaging method after ISO 9869:2014 (ISO, 2014). As the calculated averaged U-value contains all the information available, the uncertainty cannot easily be evaluated from the standard deviation.

Instead, Baker creates *N* periods from moving averages (days 1-7, 2-8 etc.). Such weekly periods are thought to be long enough to establish a steady state result, allowing a statistical comparison of a number of measurements to be performed. Whilst this approach allows a statistical assessment from a relatively short period of monitoring, it is unclear whether the use of overlapping periods can be considered valid, as the series of measurements may no longer be both random and independent.

To incorporate sensor and logger errors, type B uncertainty analysis, Baker adds the two components in quadrature:

$$\sqrt{E_{sensor}^2 + E_{logger}^2} \tag{9.4}$$

The data is analysed normally to give a basecase result, $U_{basecase}$. Further analysis is then conducted to produce an error case for each variable (i.e. T_i + $u(T_i)$). The overall error in the

U-value measurement is then defined by the root mean square of the deviations of each error case from the base case, combined with the standard deviation. For example:

$$\delta U = \sqrt{(U_{basecase} - U_{errQ})^2 + (U_{basecase} - U_{errTi})^2 + (U_{basecase} - U_{errTe})^2 + (s.d.)^2} \tag{9.5}$$

9.4.4.4 Uncertainty estimates in parameter identification and the PASLINK network

In a similar approach, Baker and Dijk (2008) provide a form of error analysis to be applied across the PASLINK network. This potentially deals with more complex models and larger numbers of parameters than the previously discussed examples. A step-by-step procedure, similar to Baker's U-value uncertainty evaluation, is set out as follows (Baker and Dijk, 2008):

- Step 1: For each signal used in the data analysis, its error is estimated as a single value, i.e. a combination of the following added in quadrature (See equation 9.4):
  - Sensor Error - U_{sensor}
  - Data acquisition measurement error - U_{logger}
- Step 2: The chosen identification technique is applied to obtain a set of base case results, *Y*, (e.g. U-value) using measured signals.
- Step 3: For each measured signal, *x*, in turn a maximum and minimum error case is calculated:
  1. Add error to each value of the signal - (x + *u(x)*)
  2. Re-run identification program to obtain new values - $Y(x + u(x))$
  3. Subtract error to each value of signal - (x − *u(x)*)
  4. Re-run identification program to obtain new values - $Y(x - u(x))$
- Step 4: to generate the error on each parameter, a matrix of results in an error propagation table is created which also includes the confidence interval from the identification. The following are calculated for each error input:
  - The deviation between the base case and the error case.
  - The effect of the (*x* + *u(x)*) and (*x* - *u(x)*) errors (combined by taking an average of the two deviations).
  - The quadratic sum of the deviations, to give the final error on each parameter.

The steps adopted here show a general agreement with those laid out in the generalised BSI and GUM guidance documents (see 9.4.3), with the identification of the model, the estimation of errors within each parameter and then the impact upon the final parameter identified from maximum and minimum error cases. In particular, this would allow the regression process to be examined through running error cases for each variable (Q, T_i, T_e, S). This also incorporates the statistical confidence intervals, as well as the experimental sensor errors, thus combining both type A and Type B error evaluation.

9.4.5 Estimating uncertainty in co-heating tests based upon the GUM and PASLINK methods

The GUM (JCGM, 2008a) and BSI (BSI, 2004) procedure consists of 6 steps:

1. Definition of the relationship between all the input measurements and the measurand, in our case the *HLC*:

$$HLC = \frac{Q_{elec} + R \cdot S}{\Delta T} \tag{9.6}$$

Where:

$$\Delta T = T_i - T_e \tag{9.7}$$

And depending on the calculation and weighting method for the representative internal temperature:

$$T_i^{SA} = \frac{\sum_j^n T_{i,j}}{n} \tag{9.8}$$

$$T_i^{vol} = \frac{\sum_j^n (T_{i,j} \cdot w_{vol,j})}{n} \tag{9.9}$$

$$T_i^{HLC} = \frac{\sum_j^n (T_{i,j} \cdot w_{HLC,j})}{n} \tag{9.10}$$

And

$$Q_{elec} = \sum_j^n Q_j \tag{9.11}$$

Where n represents the total number of sensors (j) used for each measurement variable.

2. For each quantity, compile a list of all the factors that contribute to uncertainty in that input, see tables 9.7 - 9.11, column *Input Quantity / Parameter of Uncertainty*.

3. For each of the input uncertainty sources, estimate the magnitude of the uncertainty. This can either be as a as a *standard uncertainty*, $u(x_j)$, or at a higher confidence interval as an *expanded uncertainty* (see 3.5.5 or equation 9.16). Both can then be stated in *absolute* $U(x_j)$ or *relative* terms $U^*(x_j)$. The form taken is likely to depend upon the source upon which it is drawn, i.e. calibration certificate, standard uncertainty of multiple measurements (see section 9.4.6). Ultimately, to be combined, all uncertainties must be converted to standard uncertainties in either an absolute or relative form.

4. From the relationship defined in step a), estimate the effect that each quantity has on the measurement result, the *HLC* or *R* (see table 9.12, column *'Sensitivity coefficients'*). The sensitivity coefficients ($c^*(x_j)$) are based upon maximum and minimum error cases, as seen in the PASLINK procedure, defining the sensitivity of the estimated *HLC* to errors in each parameter, (see table 9.13):

$$c(x) = \frac{Y(x\ + u(x)) - Y(x\ - u(x))}{2u(x)} \tag{9.12}$$

   The *contribution to uncertainty* can then be calculated from the sensitivity coefficient and the standard uncertainty, $c^*(x_j) \cdot u(x_j)$.

5. Combine the uncertainties in all the input quantities to obtain the uncertainty in the output quantity. If all sources of uncertainty are uncorrelated and random this can be achieved through the quadratic sum:

$$u(Y) = \sqrt{\sum_{j=1}^{N} u_j(Y^2)} = \sqrt{\sum_{j=1}^{N} (c_j u(x_j))^2)} \tag{9.13}$$

   If contributions to uncertainty are correlated, then a quadratic sum cannot be used. Instead, the correlated contributions must be combined arithmetically, before then being combined with other non-correlated sources in the standard quadratic sum:

$$c_j u(x_j) = c_1 u(x_1) + c_2 u(x_2) + ... \tag{9.14}$$

$$u(Y) = \sqrt{\sum_{j=1}^{N} (c_j u(x_j))} \tag{9.15}$$

6. Finally, the results should be expressed as an *expanded uncertainty* across an increased interval, about the measurement result within which it is anticipated, with a stated level of confidence that the measurand will lie within. The expanded uncertainty, and the stated confidence intervals are therefore dictated by the value of the divisor or coverage factor *k*.

$$U(Y) = k \cdot u(Y) \tag{9.16}$$

This final point requires consideration of the application and reporting of a result. For a standard uncertainty in a Gaussian distribution the true value only has a 68% probability of lying within the stated uncertainty interval. This is a level of risk that is unacceptable in almost all measurement situations (BSI, 2004). Therefore, the coverage is increased by a factor of *k*, based upon the degrees of freedom and the level of confidence required. Typically a value of *k* between 2 and 3 is adopted (BSI, 2004).

For the application of co-heating, the adoption of 95% confidence intervals appear more appropriate, and are adopted in the examples in section 9.4.7. It is however vitally important that any stated uncertainty includes the confidence levels in which it is estimated. For example:

the final HLC is measured to be 100 W/K with an expanded uncertainty at the 95% confidence interval of 10 W/K (10%).

9.4.6 Contributions to uncertainty for each variable

9.4.6.1 Sensor Calibration Uncertainty - T_i, T_e, Q_{elec} and S

From Baker (1993), the instrumentation or calibration uncertainty assigned to a measurement parameter where an average measurement (e.g. test room air temperature) is taken with *n* sensors, the calibration error for the average measurement may be taken as the standard deviation of the mean:

$$u(x)_{calibration} = \frac{Error_{calibration}}{\sqrt{n}} \tag{9.17}$$

Here, $Error_{calibration}$ can be taken as the uncertainty listed on the calibration certificate. What can be clearly seen here is that the more sensors deployed for a given measurement parameter, the lower the uncertainty due to any systematic calibration offsets. This means that the higher numbers of T_i sensors used, the lower the uncertainty. It also means that as fewer external temperatures are normally deployed, their uncertainty is likely to have a higher contribution to ΔT and the overall *HLC* estimate (see table 9.12).

It should be noted that when a calibration uncertainty is provided it should be provided at a quoted, confidence interval or coverage factor based upon a normal distribution. The standard uncertainty may then need to be reverse engineered from the listed expanded uncertainty from BSI PD 6461:2004 using the following formula (BSI, 2004):

$$u(x_j) = \frac{U(x_j)}{k} \tag{9.18}$$

Finally, the uncertainty is often quoted in percentage terms across a range (i.e. 0 - 40 °C). A 1% uncertainty is then the absolute uncertainty at this upper limit (i.e. 1% × 40 = 0.4 °C) across the entire range. Care is therefore often required when interpreting the stated uncertainty.

9.4.6.2 Spatial variation - T_i and T_e

As discussed in section 7.3, internal temperatures are unlikely to be consistent throughout a test dwelling. Effectively, the internal temperature, which has an unknown true mean and variance, will be sampled across a number of points, dependent upon the number and location of temperature sensors.

The measured locations may cause a distortion from the mean. A measure of this would be the standard deviation (*s(x)*), of the temperatures recorded by the sensors. Forming an analogy with measuring the diameter across a long rod at various locations, the uncertainty can be calculated from the standard deviation of the mean, $s(\overline{x})$ (BSI, 2004):

$$u(x)_{spatial} = s(\overline{x}) = \frac{s(x))}{\sqrt{n}} \tag{9.19}$$

Where the standard deviation of a series of *n* measurements, *s(x)*, is given by:

$$s(x) = \sqrt{\frac{\sum_{i=1}^{n}(x_i - \overline{x})^2}{n-1}} \tag{9.20}$$

Clearly, the more measurements taken or the more sensors deployed the more likely the measured mean will represent the true mean. The obvious problem is that just as one end of the pipe may have a significantly larger diameter, creating the risk of systematic bias from measurement locations, temperatures may vary with stratification or between rooms. It is therefore important that sensors are deployed evenly across the test dwelling and at a variety of heights.

There is however a significant departure from the analogy with a pipe's diameter. A consistent measuring device is not used across each measurement location; rather a number of different temperature sensors are deployed. The standard deviation in these measurements is

therefore a result of both the spatial variation and the calibration uncertainties. The uncertainty calculated in equation 9.19 is therefore not purely the spatial error but a combination of the two. However, as they are combined in quadrature, accounting for both the calibration and spatial uncertainties separately allows each to dominate when appropriate and consistently encourages higher deployment of sensors, lower calibration uncertainties and more uniform temperatures.

9.4.6.3 Sensor resolution - T_i, T_e, Q_{elec} and S

A combination of the sensor and logging device or data acquisition system will result in a value stored at a given resolution. The uncertainty associated with the resolution of a measurement follows a rectangular distribution, i.e. an equal probability of the true value being between measurement intervals. In temperature sensors, this will typically not be any greater than 0.005 °C, generally resulting in small contributions to the overall uncertainty. It does however remain important to maintain suitable sensor resolution, particularly when measuring Q_{elec} through pulse counts, where lower resolution meters are perhaps less commonly available and logged intervals on a kW scale could lead to more significant uncertainty. According to BSI PD 6461:2004 the resolution uncertainty is therefore defined by a rectangular distribution (BSI, 2004):

$$u(x)_{resolution} = \frac{a}{\sqrt{3}} \tag{9.21}$$

Where *a* is the semi-width of the rectangular distribution, e.g. 0.005 °C from the example above.

9.4.6.4 Sampling uncertainty - T_i, T_e and S

If a variable is measured at *n* points across an aggregated period, the measured value may deviate from the mean across this period, resulting in a degree of random uncertainty. If the measured parameter is approximately constant over the period then the sampling uncertainty may be defined as (BSI PD 6461:2004; BSI, 2004 Baker, 1993):

$$u(x)_{sampling} = s(\overline{x}) = \frac{s(x)}{\sqrt{n}} \tag{9.22}$$

Such an approach can be used for the approximately constant T_i but not for the varying external temperatures and solar radiation. For variables which follow real time series, the error can be estimated by assuming that, over a sufficient number of measurement intervals centred about each measurement point, the appropriate time series trend can be represented by a suitable

polynomial (Baker, 1993). The deviation, ρ, at each measurement point is then taken as the difference between the measured value and the trend value. An estimate of uncertainty in a variable described by a polynomial function is then given by:

$$u(x)_{sample} = \sqrt{\frac{\pi\rho}{2\sqrt{(n-1)}}} \tag{9.23}$$

In any case, as at least 24 hour integers will be used within co-heating analysis, and measurements are typically taken at sub hourly intervals, typically 5 or 10 min, the value of *n* is large ($\sim$ 144 - 288). In fact most data acquisition systems will log a 5-minute average based upon 10 or so samples across that interval meaning *n* is even larger in reality. The result, as seen in tables 9.7 - 9.8, is that the sampling error is small, particularly as uncertainties are combined via the quadratic sum, in which the largest sources dominate.

9.4.7 Estimating uncertainty in co-heating tests - field test examples

9.4.7.1 Estimating uncertainty in NHBC field tests

In this section an example field test (NHBC) is used to demonstrate the previously discussed method of estimating uncertainty. Steps 1 - 6 of the BSI procedure are followed within tables 9.7 - 9.13. Initially, uncertainties are identified and calculated from the data or through stated values from calibration certificates and input as either expanded or standard uncertainties and as relative or absolute quantities.

Once all components of each uncertainty have been converted into standard uncertainties, these can be combined into the total uncertainty in each parameter (Q, ΔT, S) by adding in quadrature or arithmetically as appropriate. Combining the uncertainties further will give the uncertainty in the parameters $R \cdot S$, ($\frac{S}{\Delta T}$) and ($\frac{Q}{\Delta T}$). If the uncertainty is calculated on a daily basis, then tailored error bars can be applied to the regression plots from Siviour and MLR analysis (see figures 9.20 and 9.21).

In figures 9.20 and 9.21, the uncertainty associated with solar radiation and the solar aperture results in daily data points from sunnier days having larger accompanying error bars. Similarly, days in which the internal temperature was more varied (see figure 7.8) incorporate higher error bars in the dimension of ΔT.

Following the equations in section 9.4.6, a total error quantity (*u(x)*) can be calculated for each variable (see table 9.7). Subsequently a maximum and minimum error case can be determined for each parameter (*x* +*u(x)*) (e.g. T_i + *u*(T_i) and T_i - *u*(T_i)).

The impact upon the *HLC* or *R* estimate for each error case can be calculated by running the regression analysis for each error case individually, e.g. *HLC*(T_i + *u*(T_i), T_e, Q_{elec}, *S*). A sensitivity coefficient, c, can then be determined for each variable via equation 9.12, with the results shown in table 9.12.

Writing out the sensitivity coefficients and subsequent contribution to uncertainty for each variable in this way means the contributions towards the total uncertainty in the *HLC* can be ranked. This can provide useful feedback on the relationship between the distribution of data points, a function of the incumbent weather, and the total uncertainties in each measured parameter. In the NHBC field test, the external temperature is shown to provide the highest contribution towards the overall uncertainty. This could be reduced in future tests if a higher number of sensors are deployed or the calibration uncertainty improved.

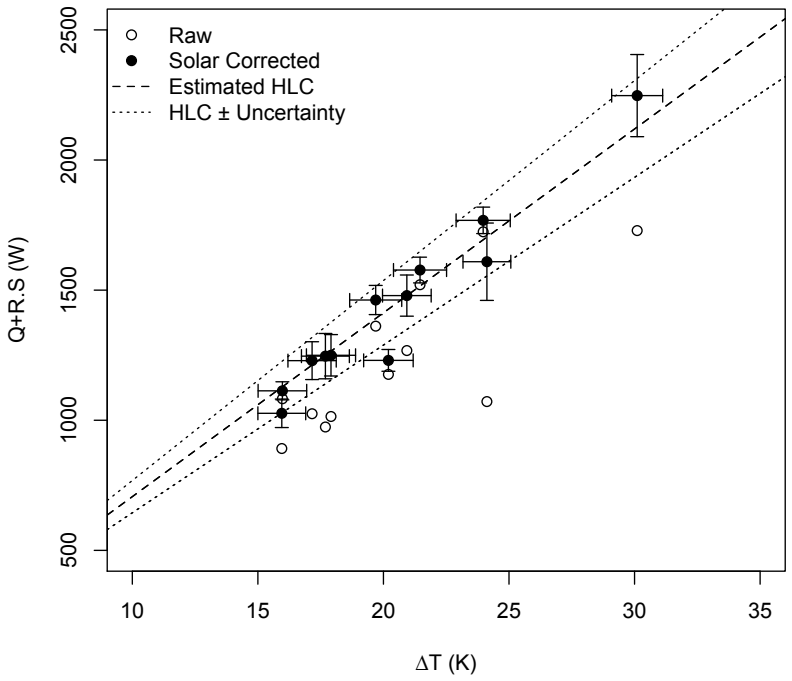

Figure 9.20: *Results from NHBC field test incorporating daily error bars and total HLC uncertainty estimates. No intercept MLR shown in a 2 dimensional form with solar corrections.* (Field Test: SIV-12d-24h-6agg-S_{GVS})

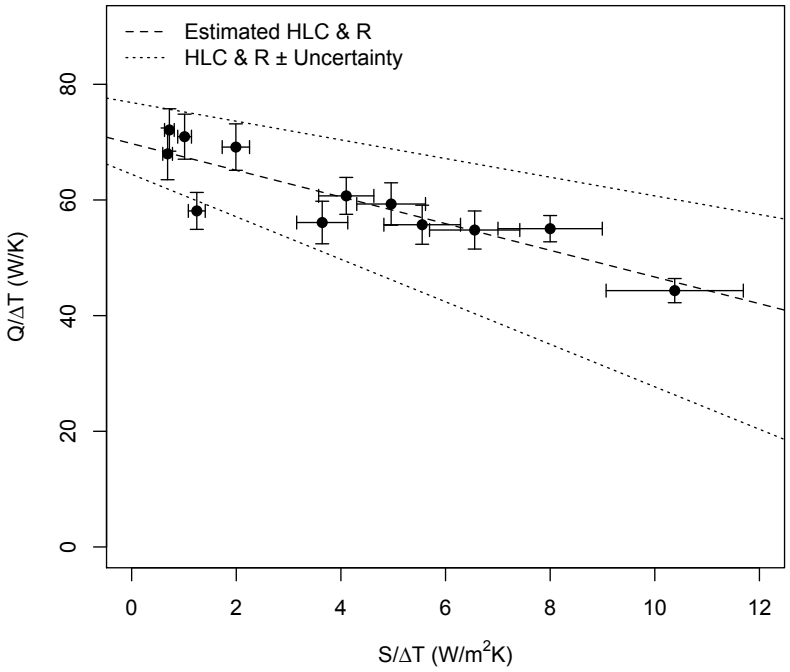

Figure 9.21: *Results from NHBC field test incorporating daily error bars and total HLC uncertainty estimates. Siviour plot.* (Field Test: MLR-12d-24h-6agg-S_{GVS})

The contributions to uncertainty are combined in quadrature, and then the total uncertainty, at 95% confidence intervals (k = 2) is calculated in table 9.12, giving results calculated via the GUM method (JCGM, 2008a) of:

$$70.6 \pm 4.2 \text{ (6\%) W/K}$$

And for R [8]:

$$\text{-}2.6 \pm 0.4 \text{ (15\%) m}^3\text{/s}$$

In such a case, the uncertainty associated with R is small, despite the statistical uncertainty calculated from the regression being much higher. If, as suggested by Baker (2011) the standard error (2.3 W/K & 0.49 m^2) is added in quadrature (equation 9.5), a GUM+ approach, then the results at a 95% confidence intervals increase to:

$$70.6 \pm 6.2 \text{ (9\%) W/K}$$

And for R:

$$\text{-}2.6 \pm 1.0 \text{ (37\%) m}^3\text{/s}$$

[8] Supporting tables calculating the uncertainty in R can be found in appendix A.5.2

This gives results effectively the same as by using equation 9.5 (Baker, 2011). This GUM+ approach gives a more reasonable estimate of the uncertainty in R above and is seen to be more suitable in simulated tests (see section 9.4.8).

Interestingly, looking at the sensitivity coefficients, the offset errors in S have no impact upon the estimated HLC, due to their use in regression. Other forms of error, such as directional bias, may have a slight impact, but are not considered here.

Table 9.7: Table combining the errors in T_i. NHBC Field Test

Input Quantity / Parameter of Uncertainty	Nominal Value	Expanded Uncertainty or limit relative	Expanded Uncertainty or limit absolute	Probability Distribution	Divisor	Standard Uncertainty	Sensitivity Coefficient	Contribution to Uncertainty	Correlated group contribution	Contribution Squared	Rank
	x_j	U*(x_j)	U(x_j)		k	u(x_j)	c(x_j)	u(x_j).c(x_j)	u(x_1).c(x_1)+u(x2).c(x2)...	$(u(x_j).c(xj))^2$	
T_i Spatial	25.20	-	-	Normal	2	0.160	1	0.1598	-	0.0255	*1*
T_i Calibration	25.32	-	-	Normal	2	0.080	1	0.0800	-	0.0064	*2*
T_i Sampling	25.20	-	-	Normal	2	0.012	1	0.0123	-	0.0002	*3*
T_i Resolution	25.20	-	-	Rectangular	1.732	0.000	1	0.0002	-	0.0000	*4*
		U*(y_j)	U(y_j)			u(y)				$\sum(u(x_j).c(xj))^2$	
T_i	**25.20**	**1.4%**	**0.358**	**Normal**	**2**	**0.179**				**0.0321**	

Table 9.8: Table combining the errors in T_e. NHBC Field Test

Input Quantity / Parameter of Uncertainty	Nominal Value	Expanded Uncertainty or limit relative	Expanded Uncertainty or limit absolute	Probability Distribution	Divisor	Standard Uncertainty	Sensitivity Coefficient	Contribution to Uncertainty	Correlated group contribution	Contribution Squared	Rank
	x_j	U*(x_j)	U(x_j)		k	u(x_j)	c(x_j)	u(x_j).c(x_j)	u(x_1).c(x_1)+u(x2).c(x2)...	$(u(x_j).c(xj))^2$	
T_e Spatial	4.77	-	-	**Normal**	2	0.163	1	0.1626	-	0.0264	2
T_e Calibration	4.77	-	-	Normal	2	0.424	1	0.4243	-	0.1800	*1*
T_e Sampling	4.77	-	-	Normal	2	0.058	1	0.0577	-	0.0033	*3*
T_e Resolution	4.77	-	-	Rectangular	1.732	0.000	1	0.0002	-	0.0000	*4*
		U*(y_j)	U(y_j)			u(y)				$\sum(u(x_j).c(xj))^2$	
Te	**4.77**	**19.2%**	**0.916**	**Normal**	**2**	**0.458**				**0.2098**	

Table 9.9: Table combining the errors in ΔT. NHBC Field Test

Input Quantity / Parameter of Uncertainty	Nominal Value	Expanded Uncertainty or limit relative	Expanded Uncertainty or limit absolute	Probability Distribution	Divisor	Standard Uncertainty	Sensitivity Coefficient	Contribution to Uncertainty	Correlated group contribution	Contribution Squared	Rank
	x_j	U*(x_j)	U(x_j)		k	u(x_j)	c(x_j)	u(x_j).c(x_j)	u(x_1).c(x_1)+u(x2).c(x2)...	$(u(x_j).c(xj))^2$	
Ti	25.20	1.4%	0.358	Normal	2	0.179	1	0.179	-	0.032	*2*
Te	4.77	19.2%	0.916	Normal	2	0.458	1	0.458	-	0.210	*1*
		U*(y_j)	U(y_j)			u(y)				$\sum(u(x_j).c(xj))^2$	
DT	**20.43**	**4.8%**	**0.984**		**2**	**0.492**				**0.242**	

Table 9.10: Table combining the errors in Q_{elec}. NHBC Field Test

Input Quantity / Parameter of Uncertainty	Nominal Value	Expanded Uncertainty or limit relative	Expanded Uncertainty or limit absolute	Probability Distribution	Divisor	Standard Uncertainty	Sensitivity Coefficient	Contribution to Uncertainty	Correlated group contribution	Contribution Squared	Rank
	x_j	U*(x_j)	U(x_j)		k	u(x_j)	c(x_j)	u(x_j).c(x_j)	u(x_1).c(x_1)+u(x2).c(x2)...	$(u(x_j).c(xj))^2$	
Q_Calibration	1236.56	-	-	Normal	2	43.28	1	19.36	-	374.62	*1*
Q_Resolution	1236.56	-	-	Rectangular	1.732	6.93	1	6.93	-	48.00	*2*
		U*(y_j)	U(y_j)			u(y)				$\sum(u(x_j).c(xj))^2$	
Q	**1236.56**	**3.3%**	**41.12**	**Normal**	**2**	**20.56**				**422.62**	

Table 9.11: Table combining the errors in *S*. NHBC Field Test

Input Quantity / Parameter of Uncertainty	Nominal Value	Expanded Uncertainty or limit relative	Expanded Uncertainty or limit absolute	Probability Distribution	Divisor	Standard Uncertainty	Sensitivity Coefficient	Contribution to Uncertainty	Correlated group contribution	Contribution Squared	Rank
	x_j	U*(x_j)	U(x_j)		k	u(x_j)	c(x_j)	u(x_j).c(x_j)	u(x_1).c(x_1)+u(x2).c(x2)...	$(u(x_j).c(xj))^2$	
S_Calibration	75.62	6.00%	4.54	Normal	1	4.54	1	4.54	-	20.59	*1*
S_Resolution	75.62	-	-	Rectangular	1	0.00	1	0.00	-	0.0000082944	*2*
		U*(y_j)	U(y_j)			u(y)				$\sum(u(x_j).c(xj))^2$	
S	**75.62**	**12.0%**	**9.07**	**Normal**	**2**	**4.54**				**20.59**	

Table 9.12: Combined Uncertainty in NHBC Field Test *HLC* Estimates. Sensitivity coefficients calculated in table 9.13

Input Quantity / Parameter of Uncertainty	Nominal Value	Expanded Relative Uncertainty	Expanded Absolute Uncertainty	Probability Distribution	Divisor	Standard Uncertainty	Sensitivity Coefficient	Contribution to Uncertainty	Correlated group contribution	Contribution Squared	Rank
	x_j	U*(x_j)	U(x_j)		k	u(x_j)	c(x_j)	u(x_j).c(x_j)	u(x_1).c(x_1)+u(x2).c(x2)...	$(u(x_j).c(xj))^2$	
T_i	25.32	1.4%	0.36	Normal	2	0.18	-4.03	-0.73	-	0.53	*3*
T_e	4.77	19.2%	0.92	Normal	2	0.46	3.808	1.75	-	3.06	*1*
Q	1236.56	2.5%	30.91	Normal	2	15.46	0.056112	0.87	-	0.75	*2*
S	75.62	6.0%	4.54	Normal	2	2.27	0	0.00	-	0.00	4
		U*(y_j)	U(y_j)			u(y)				$\sum(u(x_j).c(xj))^2$	
HLC	**70.69**	**5.9%**	**4.17**		**2**	**2.08**				**4.34**	

Table 9.13: NHBC *HLC* Sensitivity Coefficients

Input Quantity	Nominal Value	Expanded Uncertainty or limit relative	Expanded Uncertainty or limit absolute	x+Δx	x-Δx	Ynominal	Y +: (x + Δx)	Y -: (x - Δx)	c	c*
	xj		*Δx*			*HLC*			*(y1+-y1-)/2Δx1*	*c1x1/ynorm*
Ti	25.20	1.4%	0.18	25.38	25.02	70.64	69.92	71.38	-4.0343	-5.71%
Te	4.77	19.2%	0.46	5.23	4.31	70.64	72.43	68.93	3.8092	5.39%
Q	1236.56	2.5%	15.46	1252.02	1221.10	70.64	71.51	69.77	0.0564	0.08%
S	75.62	6.0%	2.27	77.89	73.35	70.64	70.64	70.64	0.0000	0.00%

9.4.7.2 Uncertainty in CASE-A1 field test - party walls

As a second example, the CASE-A1 field test can be considered. This is a more complex case, as horizontal solar radiation is used and additionally, the test dwelling features a guarded party wall. For the horizontally measured solar radiation, a higher statistical and therefore total uncertainty in *R* is seen (see table 9.14).

The party wall heat transfer (Q_{adj}) can be estimated from the temperature difference and expected thermal resistance of the party wall area, or, as in this case, from combining measured heat flux across the wall (see equation 7.4).

To incorporate any party wall heat transfer into either or both the *HLC* and uncertainty estimates three approaches have been compared. Firstly, *no adjustment* for party wall heat transfer is made (see table 9.14). Secondly, whilst no adjustment is made to the analysis or *HLC* estimate, the party wall heat transfer (Q_{adj}) and its own uncertainty are combined into an *expanded uncertainty* estimate for *Q*. This provides a greater uncertainty estimate without adjusting the estimated *HLC*. Potentially, an asymmetric uncertainty estimate could be provided, dependent upon the direction of the net heat flow. However, in many cases the direction of heat flow may not be entirely clear or consistent. Furthermore, stating uncertainty in such an asymmetric manner may not be easily interpreted.

Finally, a *correction for party wall* heat transfer can be subtracted prior to regression and uncertainty for the correction incorporated as a separate variable. The results for each approach are detailed in table 9.14, whilst full calculations can be seen in the appendix A.5.3.

Table 9.14: Estimated uncertainty for CASE-A1 field test, with three approaches for party wall heat transfer adopted. Uncertainty is stated at 95% (k = 2) confidence intervals.

Method	HLC	Expanded Uncertainty	R	Expanded Uncertainty
No Adjustment	247	± 19 (8%)	3.2	± 8 (244%)
Expanded Error	247	± 23 (9%)	3.2	± 9 (195%)
Corrected for Party Wall Heat Flow	242	± 19 (8%)	5.6	± 7 (133%)

In this case the party wall heat transfer is estimated to be only a small fraction of the total heat input ($\sim$ 4%). Therefore the correction and increased uncertainty are relatively small. However, ignoring such an uncertainty completely is likely to provide greater trust in a result

than should be attributed. This is particularly important if tests are performed in dwellings with high proportions of party walls or when there is poor guarding between properties. It is recommended therefore that either an expanded error or corrected party wall heat flow approach be adopted.

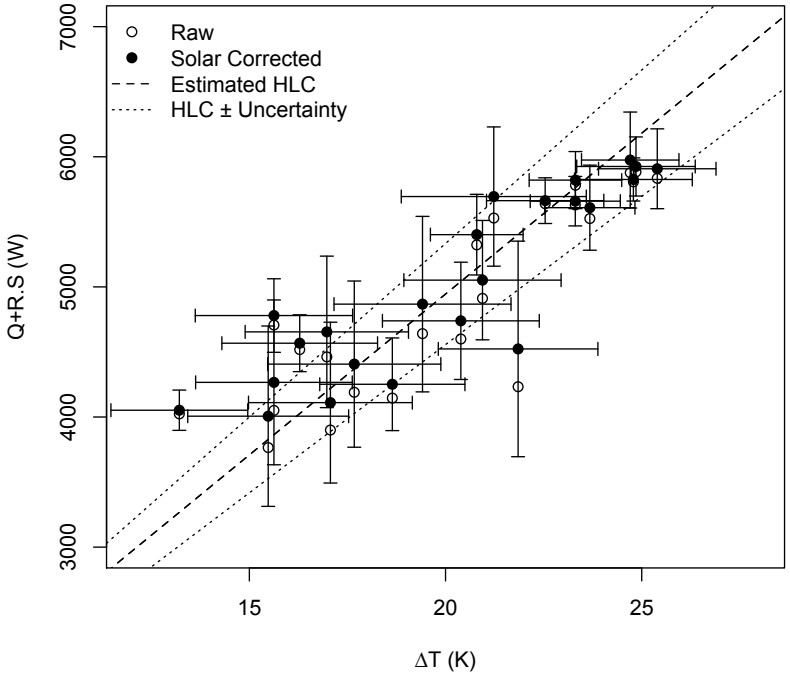

Figure 9.22: *CASE-A1 with party wall corrections and error bars for daily data points stated at 95% confidence intervals.*

9.4.8 Uncertainty analysis in simulated co-heating tests

To further test the appropriateness of this approach to error analysis, a number of simulated co-heating tests can be assessed. Here, simulated tests with precisely measured variables (Q_{elec}, ΔT, T_i and T_e) can be compared to those with randomly assigned measurement systematic offsets based upon the uncertainties defined in tables 9.7 - 9.11.

Two examples are shown in figures 9.22 and 9.23, with error bars based upon a quadratic combination of the GUM (JCGM, 2008a) calculated uncertainty and the standard error from regression at 95% confidence intervals. Further, results from over 1500 simulated tests are shown within table 9.15, demonstrating the suitability of each uncertainty estimate within valid periods (i.e. no full overheating). Here, errors in each variable have been applied according to the distributions in tables 9.7 - 9.11. The proportion of occasions within these periods in

which HLC_{True} falls within the estimated *HLC* and error bands is identified. Whilst the GUM or standard error bands contain slightly less than the 95% expected, the quadratic sum of the GUM uncertainty and standard error achieve slightly above this in a lightweight dwelling but marginally below in a heavyweight dwelling. This is likely a result of the systematic underestimate seen in heavyweight buildings due to stored solar heat. Whilst in general this GUM+ approach seems to be appropriate, accounting for further exogenous sources of uncertainty such as this are considered next.

Table 9.15: *Proportion of HLC_{True} within HLC estimated error bands - 95% confidence intervals (k=2).* (Simulation: DET-NOT-HW/LW-FINN-SN-MLR-2w-24h-6agg-S_{GVS})

Test Dwelling	Results within error estimate			
	GUM	Standard Error (95% c.i.)	GUM+	Baker
DET-NOT-LW	91.3%	95.2%	98.6%	98.6%
DET-NOT-HW	85.8%	86.8%	92.0%	92.0%

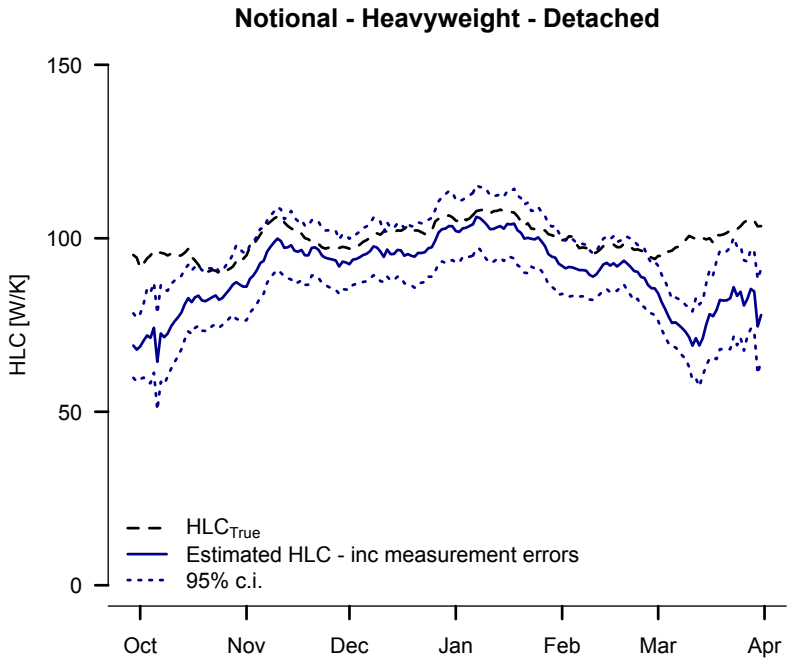

Figure 9.23: *Example of GUM+ uncertainty analysis for simulated dwelling, with experimental measurement errors. Heavyweight Notional Dwelling.* (Simulation: DET-NOT-HW-FINN-SN-MLR-2w-24h-6agg-S_{GVS})

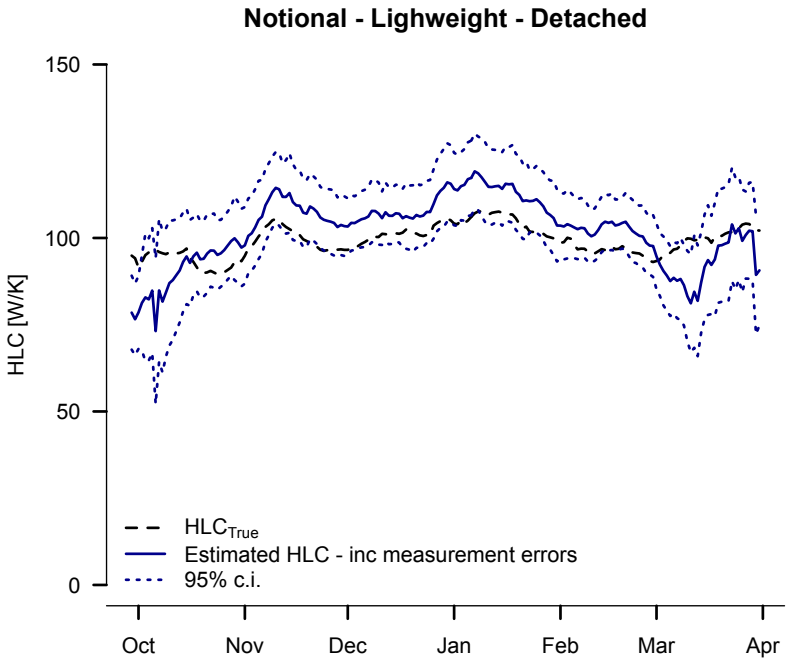

Figure 9.24: *Example of GUM+ uncertainty analysis for simulated dwelling, with experimental measurement errors. Lightweight Notional Dwelling.* (Simulation: DET-NOT-LW-FINN-SN-MLR-2w-24h-6agg-S_{GVS})

9.4.9 Additional Uncertainty Parameters

If type B uncertainty analysis was to be taken further, a number of other sources of uncertainty defined in chapters 5 - 8 could be incorporated, solely based upon judgements collated previously in this thesis. For example:

- Uncertainty due to stored solar fraction $\sim 5\%$
- Uncertainty due to high moisture content (latent load and increased thermal conductivity) $\sim 10\%$

These could be added to the standard GUM+ approach in quadrature following the form below:

$$\delta U = \sqrt{(GUM)^2 + (std.err)^2 + (5\%_{storedsolar})^2 + (10\%_{moisture})^2} \tag{9.24}$$

9.4.10 Discussion - estimating uncertainty

Combining the statistical uncertainty from regression into the GUM approach requires some thought. The statistical error is based upon the dispersion of points about the estimated *HLC*. This dispersion can be the result of uncertainties already accounted for in the GUM estimate,

e.g. calibration uncertainties, spatial variation. However, it may also be a result of sources of uncertainty identified within this thesis but not accounted for in the GUM analysis. These may include variable wind and stack losses, stored effects form S and T_e, variable radiative sky losses etc. Without further analysis, it is not possible to know if the dispersion is a result of uncertainties already accounted for, and therefore double counted, or these additional uncertainties. The pragmatic approach would therefore be to add both the GUM and statistical uncertainties together quadratically, assuming there is some overlap between the two but ensuring both elements are incorporated. This GUM+ approach then follows that of Baker and Dijk (2008) and the PASLINK network and seems the most appropriate approach.

9.5 Comparisons to design & measuring retrofit interventions

It is not just errors within the co-heating measurement that can misinform researchers. A number of comparison errors exist, relating to the weather driven and experimental sources of uncertainty in chapters 5 to 8, as well as the uncertainty in the calculation of HLC_{pred}. In terms of comparisons to design, these comparison errors can lead to an overestimate or underestimate of the discrepancy between HLC_{meas} and HLC_{pred}. When repeating tests on the same dwelling, or in particular measuring retrofit improvements, the net benefit can again be artificially over-or understated.

With knowledge of the sources of systematic bias in *HLC* estimates established in the previous chapters, the comparative errors in comparisons to design and for retrofit cases can be considered. Systematic bias leading to comparison errors seen in chapters 5 to 8 include:

- Variations in HLC_{True} due to:
  - Wind driven infiltration (section 6.1).
  - Stack driven infiltration (6.1).
  - Variable ground temperatures (7.1).
  - Variable cloud cover and effective sky temperature (6.3).
  - The temperature of unconditioned spaces and the associated heat transfer (7.2).
  - The moisture content of the dwelling fabric (7.6).
  - The internal temperature, which drives stack losses and influences the thermal conductivity of materials (7.7).

- Systematic measurement uncertainties, associated with:
  - Underestimate from stored solar contributions (5.4).
  - Internal spatial temperature distribution (7.3).
  - Orientation and measurement of *S* (5.2).
  - Measurement of T_i and T_e (7.5).
- Or variations due to the analysis method used and their respective handling of uncertainties, including:
  - Analysis type (MLR, Siviour) (9.3.2.1).
  - Aggregation intervals/ lengths (9.3.2.3, 9.3.2.4).
  - Calculation of T_i(7.3).

The following section discusses the uncertainties in comparisons between HLC_{pred} and HLC_{meas}, before the effectiveness of co-heating at measuring retrofit improvements is assessed.

9.5.1 Comparisons to design: HLC_{meas} vs HLC_{pred}

In the majority of cases, the measured and predicted *HLC*s will be compared, establishing whether the tested dwelling is thought to meet this prediction, and therefore is thought to be 'well built', or whether there is a single or combination of 'defects' that cause higher than predicted heat loss. In cases in which there is a big disparity, this can be cited as evidence of a performance gap, but care has to be taken to establish that this gap is related to the actual performance of the dwelling rather than any comparison errors.

As seen in figure 9.1, the variation in HLC_{True} is likely to be higher in higher heat loss and more traditional dwellings, where Q_{inf}, Q_{sky} and Q_g are likely to be higher. In many cases, the co-heating measurement will reflect these conditions, meaning HLC_{True} and HLC_{meas} show reasonable agreement under valid environmental and experimental conditions.

However, the inputs and assumptions used in HLC_{pred} may not reflect the conditions at the time of the measurement. For example, a given test may give a higher than expected *HLC* measurement due to high wind speeds and associated high infiltration losses. The value of HLC_{pred} may be based upon some default infiltration rate, wind speed or modelled response to wind pressures. Without knowledge of the infiltration losses themselves, or the ability to adjust

the HLC_{pred} calculation accurately, it is impossible to establish if a single *HLC* measurement is higher than design as result of defects in the fabric or just a reflection of the environmental conditions during testing.

Even with an accurate and reliable co-heating measurement, this can potentially lead researchers to either assume a poorly performing dwelling is satisfactory, or alternatively artificially give the impression a satisfactory performing dwelling is performing worse than design. To avoid such misinformation, the comparisons have to be made upon equal ground and clearly documented.

Ultimately, this is almost impossible to perform. For example, to revise a HLC_{pred} calculation to reflect the high wind speeds experienced during testing would require both accurate and complete measurements of local wind speeds and knowledge of the building's actual response to the complex array of wind pressures. The best we are likely to be able to do is apply simplified models with assumed parameters. These will almost inevitably require knowledge of more complex and harder to measure building parameters than the *HLC* we are trying to measure, or alternatively, the use of defaults with large uncertainties.

The alternative is to further inform the basis for HLC_{pred} with additional measurements. Continuing with the same example, infiltration losses can be disaggregated from total losses by either pressure test air leakage measurements or through tracer gas decay measured air change rate. Pressure test results undoubtedly hold significant uncertainty when converted into losses under natural conditions using the '$n_{50}/20$' rule of thumb and will only poorly reflect the actual conditions of measurement (Kronvall, 1978; Persily and Linteris, 1983). Models such as Walker and Wilson (1997) can calculate infiltration losses across the test period in response to measured wind speeds and temperature gradients. However, this requires knowledge of further unknown building parameters and careful positioning of anemometers. Tracer gas decay measurements will still contain their own measurement uncertainties and unless a constant concentration method is used, will have a potentially significant sampling error associated with the short periods used in analysis compared to the full test period.

9.5.1.1 Uncertainty in HLC_{pred}

Without attaching too much focus to the calculation of HLC_{pred} the uncertainty in this value can be briefly addressed.

Firstly, the assumptions and inputs into HLC_{pred} must reflect the as built dwelling, not the designed. Significant changes and material substitutions may have occurred during construction and need to be represented in any comparison. Further, recent research has shown much information is missing or incorrect in SAP information sheets (ZCH, 2014a) particularly U-values and thermal bridging details. Further, many parameters may just take on default values. In such cases, the uncertainty attached to the use of default values needs to be incorporated into any uncertainty estimates for HLC_{pred}.

Just as estimated uncertainties should be stated alongside HLC_{meas}, the uncertainties in the predicted side of this comparison should also be clearly stated, including details of the calculation method and with assumed inputs included and verified as far as possible on site. Further, measured components (i.e. in situ U-value, infiltration, temperatures, wind speed etc.) can be used to further adjust the as-built prediction; helping to further associate the areas of potential underperformance. This leaves a process as follows:

Design - As-built - Adjusted - Measured

This process involves verification of design details into the as-built calculation, updating any relevant values with measurements (i.e. infiltration, in situ U-values) and then an estimate of the uncertainty in this parameter from either the measurement uncertainty or from the calculated value, i.e. table 9.16.

In the appendix (section A.5.4), tables 9.16 to A.29 follow the GUM procedure to calculate the uncertainty in HLC_{pred}, based upon a SAP calculation (BRE, 2014). This begins with the example of the thermal resistances of materials in a wall, evolving to the wall U-value and the sum of all elements HLC_{trans}. The calculated thermal bridge losses and HLC_{inf}, calculated from a pressure test and $n_{50}/20$ assumption, are then combined with their respective uncertainties to give HLC_{pred} = 128 $\pm$ 26 W/K (20%), at 95% confidence intervals (see table A.27).

This uncertainty is largely related to the uncertainty in infiltration losses and thermal bridges. The former, allows for a $\pm$ 10 deviation to the $n_{50}/20$ rule (Sherman, 1987; Everett, 1985), whilst the later assumes large uncertainty around a default value. Whilst such calculations mainly serve to be demonstrative of a method of estimating the uncertainty in HLC_{pred}, they also show that in many cases, even simple calculations of HLC_{pred} have as high or higher uncertainty than the co-heating measurement. Combined with the variation in HLC_{True} seen in simulations, it can be argued that there is little point in targeting a *HLC* measurement to within less than 10%, as both HLC_{True} and HLC_{pred} are likely to contain higher variations and uncertainty. This unknown variation is carried forward into any comparisons, no matter the accuracy of the measurement.

Table 9.16: Example of the stages of HLC_{pred} calculation.

Component	Design	As-Built	Measured	With Uncertainty
i.e. external wall	0.18 W/m^{2}K	0.20 W/m^{2}K	0.35 W/m^{2}K	± 0.05 W/m^{2}K
...	...	...	...	...

9.5.2 Measuring retrofit improvements

Just as with comparisons to HLC_{pred}, a number of comparison errors may exist when comparing two tests performed at different times on the same, or retrofitted, dwelling. With knowledge of the sources of systematic bias in *HLC* estimates established in the previous chapters, the comparative errors in retrofit cases, as listed at the start of section 9.5, can be considered.

When pairs of co-heating tests are used to measure the impact of retrofit interventions, such issues need to be taken into account. It is important that we be sure the improvement seen is a result of the physical measures, rather than an artefact of any uncertainty bias within the test method. Without careful consideration there is a danger that rather than further empirical measurements informing retrofit strategies, they are instead providing misinformation.

9.5.2.1 The need to measure the performance of existing dwellings

Predictions based on currents trends estimate between 65 and 75% of the total UK building stock in 2050 will have been built prior to the turn of the millennium (Lowe et al., 2007). The UK has a large and inefficient historical housing stock, with approximately 5.7 million solid

walled dwellings accounting for 25% of the current total housing stock (DCLG, 2014). Clearly significant reductions across the built environment cannot simply focus on regulating new build but must address this significant retrofit challenge.

Retrofit programmes targeting demand reduction in the existing stock have discovered actual reductions often fall short of predicted targets, with areas of missing cavity and loft insulation and the gains from one intervention negated by another, i.e. airtightness improvements offset by new heating system installation (Hong et al., 2006). Further, recent solid wall insulation schemes have struggled with the aesthetic and economic complexities of increased wall thickness (Stevens and Bradford, 2013) as well as incomplete coverage and thermal bridges due to poor detailing, execution and a lack of technical solutions (Hopper et al., 2012). Of equal importance is the lack of empirical measurements of the existing stock, as demonstrated by the solid wall field trial (Birchall, 2011). Uncertainty within default assumptions of existing dwellings can misinform economic calculations and policy strategies for retrofit schemes. The need for empirical data to inform and evaluate retrofit strategies is clear (Lowe et al., 2007; Hong et al., 2006), as is the need for understanding the impact of retrofit measures on the building fabric as a whole system, rather than discrete components.

9.5.2.2 Co-heating measuring retrofit improvements: Examples from literature

Co-heating has largely been used as a tool for assessing new builds, although cases examining before and after *HLC*s for retrofit measures have been conducted (see table 2.1). However, with the focus of the measurement across the full building fabric, there are advantages in using co-heating tests to assess the full benefit delivered from retrofit interventions.

In work by LBU in the York Energy Demonstration Project (Bell and Lowe, 1998), a 1930s and 1950s dwelling were measured as-built and following subsequent retrofit improvements[9], showing reductions of 300 to 132 W/K and 266 to 149 W/K respectively. The Temple Avenue Project (Miles-Shenton et al., 2011) incorporated 2 steps of retrofit upon a 1930s brick cavity dwelling. Again, these targeted significant reductions, reducing from an initially measured 341 W/K, to 239 W/K (CWI, increased loft insulation, draught proofing) and finally to 107 W/K (external wall insulation (EWI), floor insulation and triple glazing). In perhaps the most sensitive measurement to date, the measured *HLC* reduced by as little as 10 W/K (139 - 129 W/K) after filling the party wall cavity with mineral wool insulation (Wingfield, 2010a).

[9]Including: increased loft insulation, cavity wall insulation, double glazing and draught proofing

9.5.2.3 Field test retrofit case study - CASE-A1 & CASE-A2

One field test conducted as part of this thesis features both pre and post co-heating tests around a single retrofit measure. CASE-A is a modern low energy new build with cavity-block walls with a 135mm cavity. The initial co-heating test discovered the polybead insulation had not been installed into the dwelling's cavity. This was then remedied and a follow-up co-heating test conducted a couple of months later, providing the opportunity to measure a single retrofit improvement.

The results of the co-heating test are shown in figure 9.25. The first test measured a *HLC* of 247 $\pm$ 23 W/K for the un-insulated dwelling, whilst after insulation was installed this was reduced to 144 $\pm$ 15 W/K, a difference of approximately 103 W/K. It is important to assess both the internal and external conditions in which the tests were conducted, particularly as one was performed in January and the other in March, a potentially less reliable month. External conditions during both tests were similar: mean ΔT = 23.6 & 21.4 K, mean solar radiation = 22 & 39 W/m^2, mean wind speed = 2.4 & 2.5 m/s respectively. Further, internal temperatures in both the test dwelling and neighbouring dwelling were consistently measured and calculated.

One such difference did occur within the estimated party wall heat transfer, from the test dwelling to either the adjoining dwelling or the cavity itself. In the first test Q_{adj}, is estimated to be 209 $\pm$ 104 [10] W, reducing to 5 $\pm$ 1.4 W in the second test respectively. This is likely due to better guarding of temperatures but even in the first case this represents a small fraction of the total heat input ($\sim$ 4%). If this party wall heat transfer is corrected, then the first test gives a result of 242 $\pm$ 19 W/K whilst the second remains as 144 $\pm$ 15 W/K.

[10] Uncertainties calculated according to the GUM+ method stated in section 9.4.7.2

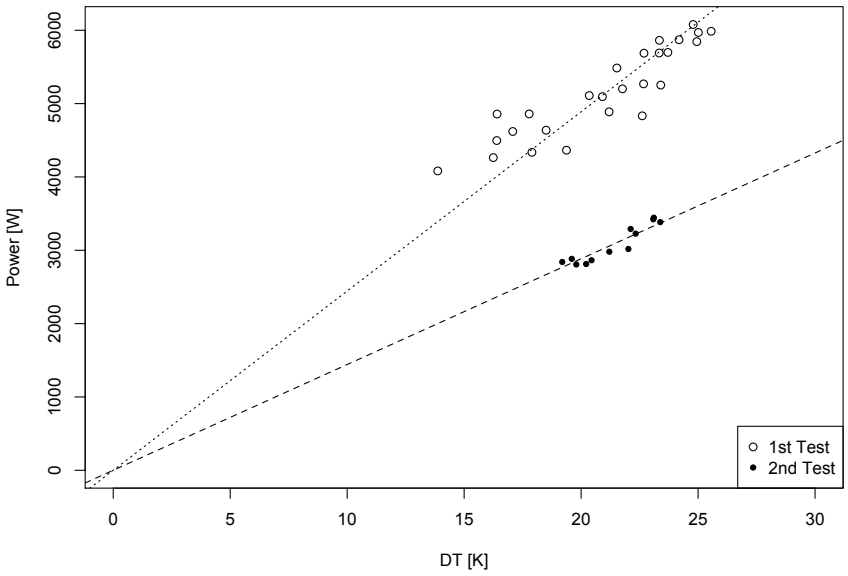

Figure 9.25: *Side-by-side co-heating results for the two tests, pre and post cavity wall insulation. Solar corrections applied.* (Field Test: CASE-A1 and CASE-A2MLR-24h-6agg S_{GHR} and S_{GVS} respectively.

Supplementary tests

The relative airtightness was measured by a series of pressure tests, which suggested the presence of cavity insulation had a negligible effect on the air leakage to the test dwelling, with average measurements of 8.1 $m^3/(hm^2)$ @50Pa pre and 8.4 $m^3/(hm^2)$ @50Pa post intervention. During the actual co-heating tests the mean air change rates, from tracer gas decays were measured as 0.62 $\pm$ 0.08 $h^{-1}$and 0.60 $\pm$ 0.04 $h^{-1}$for the first and second test respectively. This would suggest the HLC_{inf} is constant across the two co-heating measurements and the measured improvement is a result of changes to the fabric losses, rather than any disparity in infiltration due to weather or otherwise.

The co-heating result is then supported by a series of in-situ U-value measurements of the external walls. The mean U-value measured on insulated walls was 0.34 $\pm$ 0.1 [11] W/m^2K and 1.4 $\pm$ 0.3 W/m^2K across the un-insulated walls. This difference, extrapolated across the total wall envelope area would approximate to a 98 W/K difference.

[11] Uncertainties based upon measurement errors and standard deviation of multiple measurements of the same element.

Discussion of result

The co-heating result, and the measure of the absolute improvement from the insulation, would appear robust. However, a distinct difference can still be observed. Notably, in figure 9.25, the un-insulated dwelling shows significantly more variation in the daily averaged data points. There are two possible explanations. Firstly, in the first test there appears to be some wind driven influence upon the wall heat loss when the cavities are empty (figure 6.5). Alternatively, the first test here uses horizontally measured solar radiation. Whilst the overall result does not differ from a smaller data set using a vertical measurement, it is likely to increase the variation in data points.

If there were further discrepancies in experimental protocol or analysis technique then this difference between the two tests could be artificially increased or decreased. If, for example, the aggregation intervals used between the two tests were not consistent, this can give a difference as high as 105 W/K or as low as 95.8 W/K. This is not insignificant and the effect could be higher in other cases, supporting the need for consistent analysis and suitable reporting of the process used.

In this case, the two co-heating tests demonstrate a robust measurement of the benefit of the cavity wall insulation. However, this is dependent upon the control of the experimental method and analysis technique. The comparison is further supported by air leakage and infiltration measurements as well as complementary in situ U-value measurements. Finally, the suitability of the comparison depends upon the similarity of the test weather conditions, something altogether less controllable but nevertheless important to consider and to report accurately and discuss qualitatively in the absence of any quantitative estimates.

CASE-A1 & CASE-A2 and co-heating as a quality control tool

Taking a slight aside, the example of CASE-A provides a useful basis with which to discuss the application of co-heating for quality control. In this instance, the co-heating test *initially identified* higher than predicted heat loss for the building as a whole. In situ U-value measurements *narrowed down* the potential causes of this, *determining* the external walls were a likely and significant contributor. Thermograms provided further *qualitative evidence* for this conclusion, but the actual *cause*, the absence of cavity insulation, could only confirmed by an endoscope inspection.

Reaching this point does not require an accurate *HLC* estimate or full co-heating test. It was identified within a couple days of monitoring that heat loss was significantly higher than predicted, and a thermography survey, aided by co-heating conditions, quickly shifted interest to the external walls, with confirmation waiting till the end of the test and upon agreement for the more invasive testing.

Equally however, with knowledge of the method of construction process, i.e. insulation should be injected via the outside brick wall in a given drill pattern, the likely absence of insulation could simply have been observed visually though checking for the presence of repaired drill holes, a 5 minute process requiring no equipment or considerable expertise. Co-heating as an end-of-line test is clearly overkill in the case considered here and alternative quality assurance procedures could be applied to eliminate the repeating of such a mistake after its initial identification.

Whilst co-heating and supporting tools have helped to identify many of the causes of a fabric performance gap, for a number of the underlying processes, far simpler and more appropriate quality assurance systems need to be put in place to ensure that good thermal performance is achieved on a consistent basis.

9.5.2.4 Simulated measurements of retrofit improvements

To further examine the ability of co-heating measurements to determine retrofit improvements, a 1960s cavity wall dwelling is considered. This dwelling, detailed in table 9.17, is subjected to simulated co-heating tests as an as-built dwelling, with either some draught proofing or cavity wall insulation, and as a full retrofit, including: floor insulation, loft insulation, double glazed windows, draughtproofing and cavity wall insulation.

The simulated results, ignoring any experimental errors, are shown in figure 9.26. The reductions in *HLC* (draughtproofing = -22 W/K, CWI = -70 W/K, full retrofit = -147 W/K) are consistent across the period shown, in which there is no experimental overheating. This indicates that if a retrofit measure could be tested under the same experimental and environmental conditions, then an accurate estimate of the reduction in *HLC* from the improvement could be gauged. However, it is impossible to test a dwelling under either identical experimental or environmental conditions. Accurately gauging the *HLC* reduction then becomes more challenging.

Figure 9.27 shows the distribution in both HLC_{True} and HLC_{meas} for the same dwelling across the same testing period. In all cases, a range in HLC_{True} can be noted, particularly for initial high heat loss dwellings. There is then a wider distribution in the measured values, with a trend to underestimate seen, primarily associated with stored solar contributions. If the smallest improvement is considered, that of draught proofing ($\sim$ 22 W/K), it is clear that even an accurate measure of the HLC_{True} value might overestimate or underestimate the reduction in losses, even to the point of suggesting losses have increased. Clearly, whilst there is an opportunity to measure improvements at such a small scale, accurately estimating the magnitude of an improvement is subject to risk. Efforts will be needed to compare any disparities in the conditions of measurement.

Whilst larger reductions are likely to be identified clearly, again estimating their precise magnitude requires consideration of the testing conditions. The tendency for the measurement to underestimate the HLC_{True} is more likely to occur in lower heat loss dwellings. There is therefore a particular danger of testing the as-built dwelling in mid-winter and the retrofitted dwelling upon the completion of works in early spring. This may provide the environmental conditions for an underestimated *HLC* in the latter test and therefore an overestimate of the reduction in heat loss. However, if similar environmental conditions can be achieved, there is no reason the improvement cannot be accurately estimated. The previously discussed field test would represent such a case, additionally demonstrating the benefit of supplementary tests and measurements to support the co-heating result.

Table 9.17: Construction details for 1960s retrofit.

Construction	Walls	Ground Floor	Glazing	Roof	Mean ACH	Partition Walls	Internal Floors
1960s - Pre-Retrofit	*105mm brick - 50mm airspace - 105mm brick - 13mm plaster, (U = 1.6 W/m^{2}K)*	*10mm Carpet - 50mm screed - 150mm cast concrete, (U = 1.2 W/m^{2}K)*	*Double Glazing - Pre 2002, (U = 2.8 W/m^{2}K, g = 0.76)*	*Pitched Roof - 12mm Insulation at ceiling level (U = 1.2 W/m^{2}K)*	*0.5 h^{-1}*	*13mm Plaster - Lightweight Block - 13mm Plaster*	*Timber*
1960s - Draughtproofing	*As - above*	*As - above*	*As - above*	*As - above*	*0.2 h^{-1}*	*As - above*	*As - above*
1960s - Cavity Wall Insulation (CWI)	*105mm brick - 50mm polybead insulation - 105mm brick - 13mm plaster, (U = 0.5 W/m^{2}K)*	*As - above*	*As - above*	*As - above*	*0.5 h^{-1}*	*As - above*	*As - above*
1960s Full Retrofit	*105mm brick - 50mm polybead insulation - 105mm brick - 13mm plaster, (U = 0.5 W/m^{2}K)*	*10mm Carpet - 50mm screed - 150mm cast concrete, (U = 0.3 W/m^{2}K)*	*Double Glazing - Post 2002, (U = 2.0 W/m^{2}K, g = 0.72)*	*Pitched Roof - Insulated at ceiling level (U = 0.13 W/m^{2}K)*	*0.2 h^{-1}*	*13mm Plaster - Lightweight Block - 13mm Plaster*	*Timber*

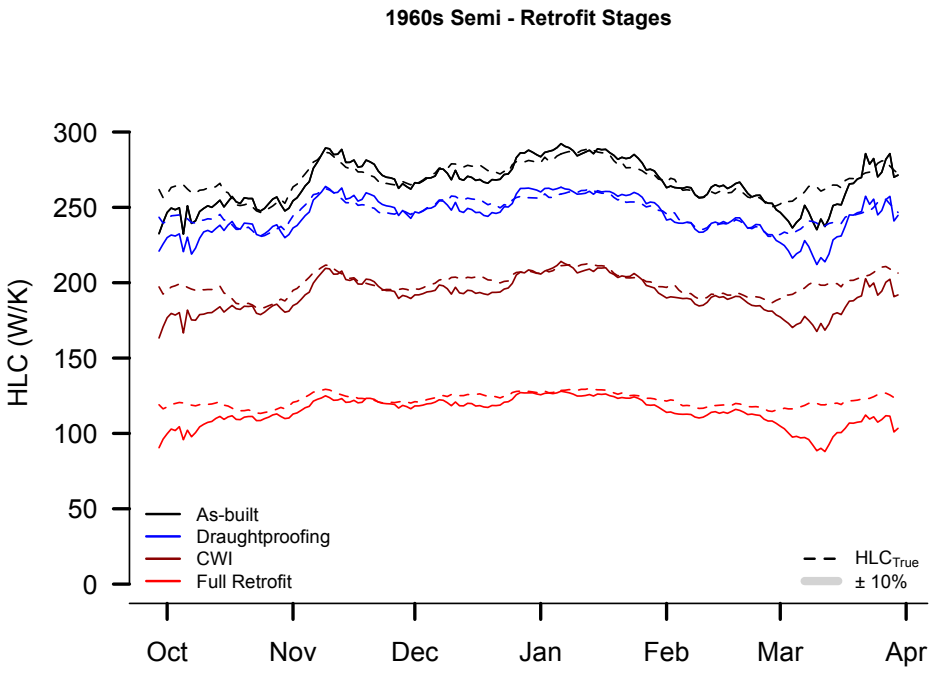

Figure 9.26: *Simulated retrofit improvements to a 1960s cavity wall semi detached test dwelling.* (Simulation: SEMI-SX-FINN-SN-MLR-2w-24h-6agg-S_{GVS})

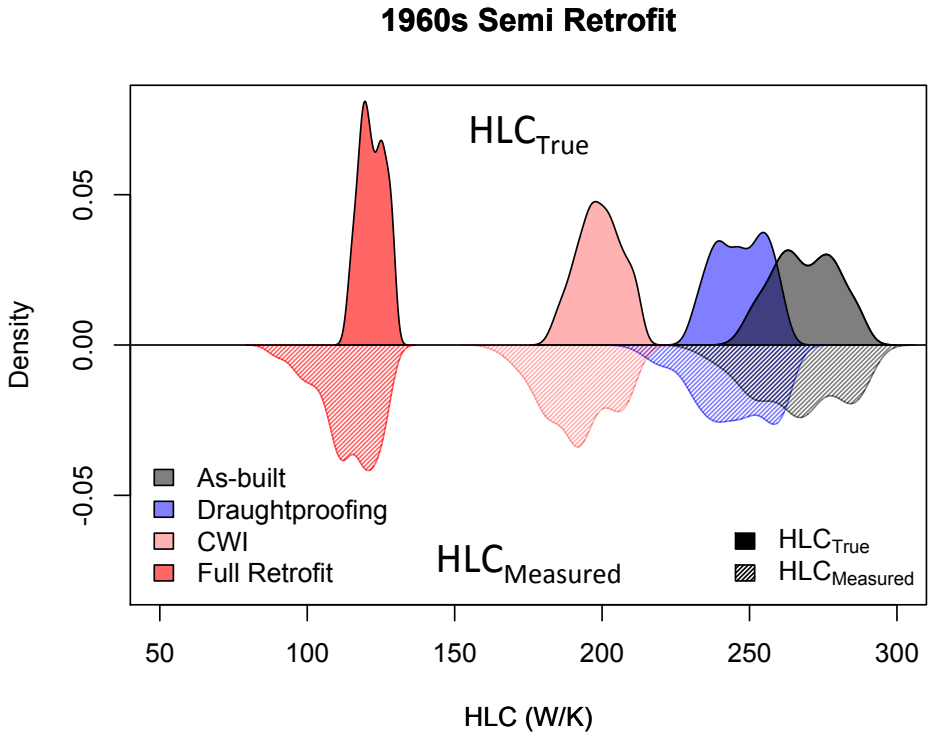

Figure 9.27: *Distribution of HLC_{True} and HLC_{meas} across the valid resting season shown in figure 9.26.* (Simulation: SEMI-SX-FINN-SN-MLR-2w-24h-6agg-S_{GVS})

Experimental bias

Figures 9.26 and 9.27 have only considered the measurement of retrofit improvements from a theoretical perspective, driven by environmental changes without any experimental measurement uncertainties. In particular, we could consider the bias in the two measurements from an external temperature offset. If the T_e sensor used in both the before and after tests is not the same, or the offset drifts, then further artificial bias into the improved *HLC* may occur. Adequate calibration and the use of multiple sensors is as important as ever.

Further experimental biases may exist, including further sensor offsets, the use of different solar radiation measurements, a difference in moisture content, or a difference in party wall heat transfer. It is therefore critical that these uncertainties are handled properly with appropriate uncertainty estimates.

9.6 Conclusions on the application of co-heating

This chapter has examined a number of issues related to the application of co-heating tests, based on the review of uncertainties in chapters 5 - 8.

Suitable environmental conditions

Suitable environmental conditions are driven very much by the propensity of a test dwelling to experimentally overheat. This means that highly glazed dwellings, with low heat loss, can only be tested in dull and cold conditions.

In the examples shown, a detached dwelling, either constructed as a Victorian solid wall, a 1960s uninsulated cavity wall or even to building regulation limiting values could be tested to within 10% of HLC_{True} for around two thirds of a typical year. This drops to just 38% of the year in a dwelling built to current national standards (see figure 9.2) and 20% of the year if the dwelling was constructed to Passivhaus standards (figure 9.1). Whilst there is a reasonable opportunity to test large amounts of the existing stock, testing modern dwellings is far more restrictive.

This theme continues as the external envelope area decreases, to smaller dwellings and importantly terraced dwellings and flats. For a flat with only a small exposed envelope, this can drop to as little as 3% of the year. It is unlikely, when considering experimental errors

associated with party wall heat transfer, that single flats can be successfully tested at scale and without risk of failure.

Experimental changes can be made to extend the range of testing conditions, either increasing $T_{setpoint}$ or providing shading. However, in both cases the impact on HLC_{True} needs to be considered.

Finally, observing whether a test is likely to have provided a reliable result in consideration of the environmental conditions requires investigation of the test data. Instances of full overheating are unlikely to yield sensible results and can be fairly easily identified. Determining periods of short term overheating is complex in test dwellings with a spread in T_i. Instances of overheating are then most clearly defined as occurrences of the mean T_i above the highest $T_{setpoint}$ seen in any zones. Even without significant periods of experimental overheating, the HLC_{True} can be underestimated by stored solar contributions. Here, it is important to use a dawn-dawn aggregation, and check the consistency of results across various aggregations.

Required duration of testing

It is shown that in both field tests and simulated tests that accurate *HLC* estimates can be achieved in 72 hours or under. This is significantly shorter than has previously been assumed or used (Everett, 1985; Lowe and Gibbons, 1988; Johnston et al., 2013) and table 2.2.

Most observed field tests achieved results within 10% of their final result within 72 hours or less. The exceptions to this, and those results that did not meet the ISO 9869:2014 criteria (ISO, 2014) adapted for co-heating, all showed experimental errors, either associated with inappropriate solar radiation measurements (S_{GHR}) or with party wall heat transfer. Plotting results as a function of duration, performing these ISO 9869:2014 checks and observing the influence of daily data points, all act as useful checks for experimental errors.

In reality, the duration required for testing also includes setting up the test and heating to steady state. To reduce the later, and help dry out the building, it is recommended that the dwelling is heated with its existing heating system prior to testing.

Recommendations for the co-heating method

A number of further recommendations to the co-heating method can be made, based on the sources of uncertainty chapters and the work in this chapter. These include recommendations to the experimental protocol: measurements of S, T_e and T_i, as well as monitoring party walls, infiltration rates, adjoining spaces and ground heat flows. Recommendations relating to the analysis procedure include: dawn-dawn aggregation intervals, 24 hour aggregation intervals, the use of forced intercepts. Importantly, this also includes a framework for reporting tests. This should allow a given test to be properly peer-reviewed and assessed, as well as allowing fairer comparisons between tests.

Uncertainty analysis

A method of assessing the uncertainty in a co-heating test is given, based upon the universal GUM and BSI standards (BSI, 2004 JCGM, 2008a), as well as work by Baker on in situ U-values and the PASSLINK network (Baker and Dijk, 2008). This allows type B uncertainties, such as calibration errors and party wall heat flows, to be combined with the standard error from regression. Two examples from field tests are shown and the method appears to be valid across simulated tests incorporating experimental errors.

Comparisons to design and pre/post retrofit

The variation in HLC_{True}, particularly in high heat loss dwellings, provides comparison errors in respect to design (HLC_{pred}), repeated tests and measures of retrofit improvements. Further, comparisons to HLC_{pred} are compromised by the difficulties in reconciling the prediction with the environmental conditions experienced during testing, particularly with measuring conditions and applying them to the building without knowledge of these minor heat flows and building parameters. Measuring minor heat flows (Q_{inf}, Q_g etc.) may assist such comparisons. Finally, comparisons to design should detail the calculations and assumptions forming HLC_{pred}, ideally incorporating error estimates as detailed in this chapter.

In terms of measuring retrofit improvements, again these minor heat flows and changes in HLC_{True} can misinform measurements. Ideally, similar internal and external conditions should be sought. Small retrofit improvements (i.e. draughtpoofing or loft insulation) may be difficult to pick up, but larger improvements (CWI) should be evident as long as conditions are similar. Supplementary tests and measurement are likely to assist in such comparisons.

Chapter 10

Conclusions

10.1 Summary of findings

10.1.1 Context of research (Chapter 2)

The benefits of energy efficient building fabrics are clear. However, as recent measurements have revealed, achieving high thermal performance and achieving it consistently is a complex and demanding challenge. Through measuring the total building heat loss across the entire building fabric, co-heating has been used to measure actual performance and, when combined with further investigations, revealing some of the mechanisms currently undermining performance and contributing towards a fabric performance gap.

Initially developed by researchers in both the US and UK in the early 1980s, the co-heating method uses unoccupied houses and constant internal temperatures to reduce and simplify heat flows within a test dwelling. The use of electric heaters and mixing fans provide accurately monitored heat inputs and uniform internal temperatures. Short term periods of co-heating (e.g. overnight) have been combined with further dynamic test sequences and analysis. However, the method considered throughout this thesis is the one that is predominantly used within the UK, consisting of constant internal temperatures, data aggregated into at least integer 24 hour periods, and steady state analysis conducted through linear regression.

The co-heating method has gained increased prominence over the last decade through its use by Leeds Beckett University and use within GHA and TSB building performance programmes. Whilst the results have amassed evidence of widely underperforming building fabrics and significantly helped identify the party wall bypass, the method is regarded to have a number of significant limitations preventing wider adoption. These include: long monitoring durations, a limited testing season, questionable reliability, high financial costs, an absence of any official

standard or consistently adopted methodology and notably, a lack of understanding over the accuracy and reliability of the measurement itself. To address these issues the following research question was proposed:

How accurate and reliable is the steady-state co-heating method at determining a dwelling's heat loss coefficient?

10.1.2 Research method (Chapter 3)

To address this question simulated co-heating tests have been conducted. This approach offers two significant advantages. Firstly, the combination of a known HLC_{True} and the ability to systematically vary individual parameters allows systematic errors to be identified and understood. Secondly, simulated co-heating tests can be performed across a wider range of environmental conditions and dwellings, providing breadth to this research and understanding how co-heating can be applied across a diverse housing stock.

To further support and inform simulated co-heating tests a number of field tests have also been performed. These have provided supporting evidence and unveiled complex effects not captured through simulated tests. In addition, conducting these field tests has provided further depth and discussion around the context in which co-heating tests are typically used.

10.1.3 Sources of uncertainty (Chapters 5, 6, 7 & 8)

The results of this thesis can be split into two parts. The first part reviews and investigates the sources of uncertainty that may exist within a co-heating test and *HLC* estimate, chapters 5 - 8. The second part examines the application of the co-heating method, chapter 9.

The review in chapter 4 and 5 reveals an extensive number of uncertainties that may or may not significantly impact given *HLC* estimates; these sources of uncertainties are summarised below.

10.1.3.1 Solar driven uncertainty (Chapter 5)

Accounting for the solar gains received by a test dwelling raises a number of significant issues. Inappropriate measurement of solar radiation, particularly using horizontal measurements for a building experiencing high direct gains will cause an overestimate of HLC_{True} even in otherwise ideal conditions. Determining gains from numerical calculations based upon building geometry and glazing properties is likely to bias the *HLC* with a number of arbitrary assumptions and higher demands for accurate measurements of incident solar radiation.

Some incident solar radiation will be absorbed and released during a subsequent aggregation period. Whilst in dull periods and lightweight dwellings this fraction is likely to be small, in sunnier periods and in heavyweight and highly glazed dwellings this can cause a significant underestimate. This will often be associated with short term periods of experimental overheating ($T_i > T_{setpoint}$). Longer periods of experimental overheating will provide seriously underestimated *HLC* and will restrict when tests can be reliably performed.

10.1.3.2 Further weather driven sources of uncertainty (Chapter 6)

Further environmental sources of uncertainty exist. Wind and stack infiltration will increase the variation in daily data points. Periods of higher infiltration will have an increased HLC_{True}. However, without explicit knowledge of this increase, definitional uncertainty increases and comparisons between tests or to HLC_{pred} can be biased. Similar but smaller effects are seen through long wave radiative losses to the sky. Finally, the dynamic external temperatures during co-heating will lead to bias in cold days following warmer ones and vice versa. This increases the random error in daily data points but is unlikely to produce significant bias across two week test periods. This may however act to compound bias from stored solar heat and bias short term heat loss measurements.

10.1.3.3 Experimental sources of uncertainty (Chapter 7)

Many heat flows do not occur directly to the external environment but rather to the ground or other unconditioned or heated spaces. Uncoupled losses, i.e. those not directly to the external environment and therefore correlated to T_e, would appear in the intercept if such a regression model was used. Ground losses and losses to unconditioned spaces can cause further comparison errors. Party wall heat transfer can cause further bias dependent upon the net direction of heat flow. This is particularly strong if there are large party wall areas, uninsulated constructions or high temperature differences through poor guarding or practical constraints. Perfect guarding of heat transfer across party walls is unlikely to be achieved in reality, particularly as complex heat transfer can occur within the party wall itself. Estimates should therefore be made for party wall heat transfer, incorporating this uncertainty into *HLC* estimates. Again, testing of terrace dwellings and flats is restricted by these uncertainties.

Furthermore, the simplifications used in co-heating analysis for a uniform and constant internal temperature will not be perfectly met in reality. Uniform temperatures are hard to achieve in dwellings with tight floor plans, thermally separated internal zones or either high heat loss or highly glazed zones. When internal temperatures vary, it is important to weight multiple measurements, preferably via the heat loss of the respective zones. This is particularly important in inhomogeneous constructions. Additionally, data from the period in which a test dwelling is warming up to a quasi-steady state needs to be removed from analysis to avoid bias. This can be assisted by heat flux measurements located on heavyweight elements.

The presence of higher than normal moisture content within the building fabric will add a latent load and increase the thermal conductivity of materials. Conducting suitable measurements of the moisture content of a dwelling is experimentally challenging, meaning any corrections are likely to have significant uncertainty. The most appropriate approach is to try and remove as much moisture as possible prior to testing and make rudimentary measurements of moisture content, RH and internal and external vapour pressures.

Sensor measurement errors also need to be considered with suitably calibrated sensors used in adequate numbers to monitor Q, ΔT and S. This is particularly true of T_e in which a single sensor is often deployed. Doubly shielding internal air temperatures may be required.

10.1.3.4 Regression based sources of uncertainty (Chapter 8)

The presence of errors in independent regression variables (S, ΔT, S / ΔT) can lead to attenuation bias within the regression engine and underestimates of both regression variables, *HLC* and *R*. However, as long as both the error in S and ΔT are less than 10% any bias is likely to be small.

Multicollinearity or covariance between independent regression variables can similarly cause bias in the regression estimators. The variables S and ΔT may have significant covariance in weekly or monthly data. This is not likely to be significant when looking at daily data, although this can be checked by the variance inflation factor regression statistic. However, this phenomenon does prevent the use of multiple solar terms within the regression model.

The sources of uncertainty identified and discussed throughout this thesis are summarised in tables 10.1 - 10.5.

Table 10.1: Table summarising solar driven sources of uncertainty.

SOLAR DRIVEN UNCERTAINTY											
Source of Uncertainty	**Sub category**	**Section**	**Description**	**Adjusted Energy Balance**	**Impact Upon Test Dwelling**	**Impact on HLC Estimates**	**Scale of Error (BRE - Finningley)**	**Influencing Building Characteristics**	**Influencing Weather**	**Identification**	**Addressing Uncertainty**
Determination of Solar Gains - R	*Statistical Calculation of R*	**5.3**	Uncertianty when calculating R and Q_{sol} statistically (i.e. Siviour or MLR)	-	Solar Gains are not accuraely determined	• Systematic error, variable direction, influenced by measured solar and attentuation bias	-	-	• Required range in S ~ 150 W/m^2 • Low ΔT • High S	• Regression outputs (Standard Error + p-value of R)	• Longer test periods • Targeted test periods to achieve mix in S • Alternative experimental protocol to determine R • Minimise S (testing season, blocking)
	Numerical Calculation of R		Uncertianty form empirical calcualtion of R and Q_{sol} (cSLR)	-	Solar Gains are not accuraely determined	• Systematic uncertainty, direction dependent upon assumptions used to determine R	~ 13% of Q_{sol}	• Hard to characterise gains, i.e: Complex Shading Devices, dirty windows. • Variation of as-built glazing from design	• High S • Low ΔT	• Include Error estimates for empirical R, and measured S	• Measure S on multiple orientations • Check Installled Glazing • Include Opaque Gains (ISO 13790) • Include Error Estimates in R • Minimise S (testing season, blocking)
Measurement of S		**5.2**	Imperfect nature and correlation between measured S and actual solar gains	-	Solar Gains are not accuraely determined	• The use of S_{GHR} overestimates HLC if direct gains are high • Inappropriate vertical measurements, S_{GVP}, can under/overstaimate HLC	As high as 13 - 21 W/K	• Highest in dwellings with high direct gains (i.e. large amounts of south facing glazing) with S_{GHR} • Can be significant in multiple glazed facades with a single vertical measurement, S_{GVP}	• Periods of mixed overcast & sunny days • High S • Low ΔT	Requires mulitple solar measurements	• Adopt appropriate solar measurement: S_{GVP} for high direct gains, S_{GVM} for mulipleglazed orientations • Measure multiple forms of solar (i.e. Direct & Diffuse) • Minimise S (testing season, blocking)
Solar Driven Experimental Overheating	*Short-Term*	**5.5**	Ti > $T_{setpoint}$ for less than 24 hours, Typically around midday	-	Lower Q/ heat loss on days preceeded by sunny days & short term overheating	Systematic underestimate of HLC	~ -27 W/K	• High thermal mass • Low HLC • High solar gains (glazing, south south facing)	• Consecutive days of high S • High S • Low ΔT	• Plot time series of all T_i and eyeball • Count number of hours, T_i > Tsetpoint	• Avoid high base loads • Minimise S (testing season, blocking) • Increase T_i • Reduce $Q_{baseload}$
	Long-Term		Ti > $T_{setpoint}$ for longer than 24 hours	-	Steady state conditions compromised	• Regression of Q becomes nonsensical, HLC severely underestimated • Empirical Calculations subjected to high error	Invalid Results				
Stored Solar Heating Contributions		**5.4**	Fraction of solar hear input carried forward to subsequent aggregation period	$Q_i = R_1.S_i + R_2.S_{i-1} + R_3.S_{i-2} + \Delta T.HLC$	Lower Q_{elec} on days preceeded by sunny days	Systematic underestimate of HLC	Consistent underestimate ~ 3 - 14 W/K (SLW - SHW)	• High thermal mass • High glazing fraction	• Successive sunny days • Lack of consectutive dull days • Mean test solar radiation > 45 W/m^2	• Check different aggregating intervals/ lengths • Plot (S-1) vs HLC • Check for short term overheating • Observe T_{si} and heat flux measurements	• Increased aggregation length • Optimise aggregation interval (i.e. Dawn-Dawn)

Table 10.2: Table summarising weather driven sources of uncertainty.

WEATHER DRIVEN UNCERTAINTY											
Source of Uncertainty	**Sub category**	**Section**	**Description**	**Adjusted Energy Balance**	**Impact Upon Test Dwelling**	**Impact on HLC Estimates**	**Scale of Error (BRE - Finningley)**	**Influencing Building Characteristics**	**Influencing Weather**	**Identification**	**Addressing Uncertainty**
Wind & Stack Driven Losses	*Stack Losses*	**6.1**	Increased stack driven heat loss at higher ΔT	$Q_{Stack} = (1/3).c.Cs.\Delta T^{n}.V$	• Higher infiltration losses, higher HLC_{True} • Daily variation in heat loss	• Change in HLC_{True} (Definitional uncertainty, comparibility, repeatibility) • Higher random error	Range across Oct-Mar in HLC_{True} ~ 6 W/K (8%)	Low airtightness/ high stack losses: e.g. chimneys, multistorey	• High change in mean ΔT between tests	-	• Recalculate HLC_{Pred} based on audit description of stack infiltration • Measure air infiltration during test
	Wind Losses		Increased and variable heat loss due to wind pressures	$Q_{w} = (1/3).c.Cw.(s.U)^{2n}.V$			s.d. 4-16 W/K (6.5-11.7%) (ACH 0.08 to 1.17)	• High ACH • Wind sensitive constructions (e.g. cavities & wind washing) • Exposed sites	• Variable wind speed • Periods of high wind speed	• Plot windspeed vs daily HLC • Plot infiltration vs daily windspeed	• Measure local windspeeds • Correction complex & needs consideration: • Infiltration measurments (potential to remove prior to regression) • Filter our periods of high windspeed • Wind Speed as regression variable
Dynamic External Temperature		**6.2**	• Variation in heat loss moving from warm to cold days, and vice versa • Lag between Q and ΔT	-	Increased random error in daily data points	Minor impact on its own, across 2 week tests, but likely to have cumulative impact with other uncertainties or impact shorter tests	Small over 2 week tests, increases standard error	High thermal mass	• Large change in T_e between successive days	Cannot easily plot residuals vs. $(\Delta T_i - \Delta T_{i-1})$	• Increased aggregation length • Minor improvement through optimise aggregation interval (i.e. Dawn-Dawn)
Radiative Sky Losses		**6.3**	• Increased heat loss due to radiative sky losses • Daily variations	$Q = Q_{Sky} + \Delta T.HLC$ $Q_{sky} = h_{r,sky}.A_s.(T_{sky}-T_{se})$	Overall increase/ variation in heat loss	• Increase in HLC_{True} compared to HLC_{Pred} • Definitional uncertainty, comparibilty & repeatibility	Mean 4.5 W/K (6%) increase in HLC_{True} due to sky losses	• High sky losses (i.e. relatively large roof area, uninsulated roof)	• Low Tsky & Low Cloud Cover	• Create audit term	• Measurement of T_{sky} to understand losses • Add losses to HLC_{Pred}

Table 10.3: Table summarising experimental sources of uncertainty - part 1.

EXPERIMENTAL SOURCES OF UNCERTAINTY											
Source of Uncertainty	**Sub category**	**Section**	**Description**	**Adjusted Energy Balance**	**Impact Upon Test Dwelling**	**Impact on HLC Estimates**	**Scale of Error (BRE - Finningley)**	**Influencing Building Characteristics**	**Influencing Weather**	**Identification**	**Addressing Uncertainty**
Uncoupled Heat Transfer	*Ground Losses*	**7.1**	Uncoupled losses related to T_g rather than T_e	$Q = Q_g + \Delta T.HLC$	• Change in Q_g • Potential for dynamics (uninsulated, suspended timber floors)	• *Variable HLC_{True} with T_g (Comparibilty & Repeatability)* • *Underestiamate warm up period included*	-	• Uninsulated floors / retaining walls • Large floor area • Q_F/Q_{Tot} large	• Variable T_g	Estimate audit term: • $Q_g = q_g.\Delta T$ • $Q_g = A_g.U_g.\Delta T$	• Measure T_g and heat flux across floor to establish any dynamics • Measure high density q_G • Consider changes in HLC_{Pred}
	Unconditioned Spaces		Uncoupled losses to unconditioned/ unheated spaces (i.e. attic, garage etc.)	$Q = Q_{unc} + \Delta T.HLC$	• Change in Q_{unc} • Potential for dynamics	• *Variable HLC_{True} with T_{unc} (Comparibilty & Repeatability)* • *Underestiamate from warm up period if unconditioned space has not reached quasi steady state*	Change in HLC_{True}: • ~ 2 W/K (2%) Garage • ~ 4.5 W/K (6%) Attic	• Scales with unconditioned/external envelope area, i.e.: large ground areas, excavated sites, large sloping roofs etc.	• Large difference between T_e and T_{unc}, likely at very cold T_e	Estimate audit term: • $Q_{unc} = q_{unc}.\Delta T$ • $Q_{unc} = A_{unc}.U_{unc}.\Delta T$	• Measure T_{unc} and heat flux across elements to establish any dynamics • Measure high density q_{unc} • Consider changes in HLC_{Pred}
	Adjoining (Heated) Spaces	**7.2**	Heat transfer to and from adjoining, heated spaces	$Q = Q_{adj} + \Delta T.HLC$	• Change in Q_{adj} (net losses or unregulated gains) • Potential for dynamics (i.e. solar heating of adjoining space, occupied adjoining spaces)	• *HLC can be over/underestimated depending upon direction of net heat transfer*	• Small if insulated: ~2.3 W/K (3%) • Large if uninsulated and poor guarding: ~15 W/K (19%)	• Uninsulated party walls • Complex party wall heat transfer • Dynamic heat transfer • Large party wall/floor area: semis, terrace, flats	• Low ΔT, increasing scale of Q_{adj}	Estimate audit term: • $Q_{adj} = q_{adj}.\Delta T$ • $Q_{adj} = A_{adj}.U_{adj}.\Delta T$	• Guard Q_{adj} by heating to same internal temperature, $T_{adj} = T_{setpoint}$ • Estimate party wall heat transfer & associated error
Non - Uniform Internal Temperatures	*Temperatures throughout a test dwelling*	**7.3**	Use of a single zone model to describe a spread of internal temperatures and their respective heat loss	$Q = \Delta T_1.HLC_1 + \Delta T_2.HLC_] + \Delta T_n.HLC_n \ldots$	• Variable T_i will result in variable heat loss in zones of different T_i • Spread in T_i must be converted into representative T_i	• *HLC can be over/underestimated depending upon the locations of higher/lower temperatures*	• Small if no bias in construction or low temperature spread ~ 1.9 W/K (2%) • High if large bias in heat loss locations and Ti ~ 4.8 W/K (6%) • Max in field ~ 20 W/K (8%)	• Non-homogeneous building construction, i.e. highly glazed zones, high air leakage zones. • Low thermal connectivity between zones (i.e. tight floor planes, small access openings)	-	• High resolution temperature measurement • Compare weighted temperatures	• Ensure sufficient mixing, target temperature spread of at least < 2°C • Check & adjust equipment as necessary • Ensure Ti recorded in each room, more if rooms are large • Volume or Heat Loss weight Ti
Non-Constant Ti	*Reaching Quasi Steady State*	**7.4**	Bias in the period in which the test dwelling is being heated to a quasi steady state	-	Additional heat flows into the dwellings mass	*HLC will be overestimated during these periods*	-	• Heavyweight constructions • Lighweight constructions, with single heavyweight element may be more difficult to observe error	• Low T_e at preceding test	• Examine T_i & heat flux into heavyweight elements (i.e. Floor slab)	• Remove data • Assisted by examining T_i & observing heat flux into heavyweight elements (i.e. Floor slab)

Table 10.4: Table summarising experimental sources of uncertainty - part 2.

EXPERIMENTAL SOURCES OF UNCERTAINTY											
Source of Uncertainty	**Sub category**	**Section**	**Description**	**Adjusted Energy Balance**	**Impact Upon Test Dwelling**	**Impact on HLC Estimates**	**Scale of Error (BRE - Finningley)**	**Influencing Building Characteristics**	**Influencing Weather**	**Identification**	**Addressing Uncertainty**
Equipment Measurement Errors	*Systematic Sensor Errors*	**7.5**	Uncertainty due to systematic erros in sensors (measureing Q, Ti, Te and S)	-	Bias measured values	*Over/underestimate based on direction of systematic sensor bias*	• 1°C in ΔT ~ 5 W/K (6%) • 2.5% in Q ~ 2 W/K (2%) • ±20 W/m2 ~ 3 W/K (4%)	-	-	-	• Calibrate Instruments • Measure via multiple sensors (including T_e) • Log at short intervals • Record T_i with doubly shielded sensors • Record T_e with ventilated & sheilded cover • Report sensor accuracies
Moisture	*Latent Loads*	**7.6**	A latent load associated with the energy required to evaporate moisture within the building fabric.	$Q = Q_{latent} + \Delta T.HLC$	Increased and unregulated increased heating load	*HLC_{True} is higher due to latent load*	~ 2-9% seen in literature and field tests	• New builds, wet finishes	Rain/ driving rain	• Measure RH and calculate vapour pressure excess	• Monitor RH • Measure moisture content of materials when possible • Estimate range in HLC_{Pred} • Dry out building prior to testing, (heat with adequate ventilation/ dehumidifcation)
	Increased Conductivity		Reduction in conductivity of materials due to increased levels of moisture in the fabric	-	Increased heat losses	*HLC_{True} increases, creating difficulties in design comparisons & definitional uncertainty*	¨• Solid Wall U-value 1.2 - 2.5 W/m2K (Baker, 2013) completely dry to saturated	• New builds, wet finishes • Solid / traditional brick walls		above	
Operational Errors	*Increased Internal Temperatures*	**7.7**	• Change in thermal conductivity of materials due to increased T_i • Increased stack losses due to increased T_i	-	• Higher HLC_{True}	Definitional uncertainty and comparison errors	• Conductivity < 3% between 20-35°C • Stack, ~ 6.2 W/K (8%) between 20-30°C) (ACH ~ 0.21)	• Temperature sensitive materials	• Varying Te will also change material conductivity and stack losses.	-	• Reflect variation in material performance in HLC_{Pred} • Test at realistic temperatures
	Influence of fans on boundary layer		Increase internal surface convection coefficient	-	• Higher HLC_{True}	Definitional uncertainty and comparison errors	• Low	• Uninsulated walls	-	-	• Avoid disrupting boundary layer (point fans inwards) • Measure internal surface air velocity (spot check)

Table 10.5: Table summarising regression based sources of uncertainty.

Regression Based Uncertainties											
Source of Uncertainty	**Sub category**	**Section**	**Description**	**Adjusted Energy Balance**	**Impact Upon Test Dwelling**	**Impact on HLC Estimates**	**Scale of Error (BRE - Finningley)**	**Influencing Building Characteristics**	**Influencing Weather**	**Identification**	**Addressing Uncertainty**
Regression Based Uncertainties	*Forced Intercept*	**8.1**	Error in using a forced intercept model	-	-	Coupled and uncoupled losses must be lumped into single HLC	-	• Large proportion of uncoupled losses	-	• Plot and compare MLR, iMLR and Siviour analysis	• Incoporate intercept losses (+ c/ΔT) • Use MLR • Use Siviour analysis
	Attenuation Bias	**8.2**	Uncertainty due to error in independent variables: S, ΔT and S/ΔT	-	-	• Underestimate HLC • Underestimate R	• < 3% if the errors in S and ΔT are less than 10%.	-	Sunny with significant uncertainty in Q_{sol}	-	• Ensure sensors are accurate & avoid other uncertainties
	Collinearity	**8.3**	Uncertainty due to covariance between S and ΔT	-	-	Over/underestimate HLC is covariance is positive/negative	Negligible	-	Warm & sunny/ cold and dull	• Check variance inflation factor (VIF) in regression package	• Avoid long (weekly or monthly) aggregations

10.1.4 The application of co-heating (Chapter 9)

This chapter reviews the advantages and limitations of the current application methods, and forms the second part of the thesis' results.

10.1.4.1 Suitable environmental conditions (Section 9.1)

What constitutes suitable environmental conditions for reliable *HLC* estimation depends upon the dwelling itself (i.e. *HLC*, thermal mass, glazing and orientation) and the experimental set up (i.e. $T_{setpoint}$, $Q_{baseload}$, shading). Whilst traditional constructions and even dwellings built to current building regulation limits can be tested for around 60% of the year, high performance dwellings, such as Passivhaus, and dwellings with high party wall areas, such as terraces and flats, can only be reliably tested in very small windows across a year. It is unlikely that these dwellings can be tested without a significant risk of failure or without adapting the experimental method.

10.1.4.2 Required monitoring durations (Section 9.2)

Assuming the building has adequately reached quasi-steady state, the duration of both field and simulated tests accurate results (to within $\pm$ 10%) can be achieved within just 72 hours. In cases when this is not achieved experimental errors are often found to interfere with the *HLC* estimate, namely, inappropriately orientated solar radiation measurements and party wall heat transfer. This result potentially means co-heating tests can be performed within much shorter time frames, particularly if the dwelling can be pre-heated, reducing the warm up time and data that must be removed from analysis.

10.1.4.3 Estimating uncertainty (Section 9.4)

A method of estimating the uncertainty in co-heating *HLC* estimates has been demonstrated and examined for both field and simulated tests. This is based upon the universal GUM standard (JCGM, 2008a) and error analysis within the field of thermal performance measurement, including in situ U-values and the PASSYLINK network (ISO, 2014; Baker and Dijk, 2008; Baker, 2011). A method is developed and demonstrated combing statistical error estimates and those from sensor measurement errors, temperature variations and party wall heat transfer. Uncertainty estimates can be further expanded through type B uncertainty analysis, incorporating set error estimates for more complicated and immeasurable effects, such as stored solar heating contributions and moisture, based upon expert judgement.

10.1.4.4 Comparisons to design & measuring retrofit interventions (Section 9.5)

Whilst the direct measurement errors in a *HLC* estimate i.e. the deviation of HLC_{meas} from HLC_{True}, are assessed throughout this thesis, the definitional uncertainty and comparison errors between repeated measurements or to design, HLC_{pred}, are also considered. Comparisons to HLC_{pred} are challenging as both environmental (i.e. windspeed, ΔT, T_{sky}, T_g) and experimental (i.e. $T_{setpoint}$, moisture content) conditions vary, altering HLC_{True}. Reconciling the conditions between two tests or from a single measurement to the conditions used as inputs in HLC_{pred} is almost impossible without further measurements and intimate knowledge of more subtle heat flows. A degree of uncertainty in these comparisons is therefore almost inevitable. Firstly, this reinforces the benefits in further complementary measurements and tests during periods of co-heating, estimating secondary heat flows and importantly the uncertainty in these estimates. Secondly, such definitional uncertainties set a 'practical minimum measurement uncertainty' achievable in any measurement (JCGM, 2008b, p. VIM 2.27). This therefore helps define the limit in accuracy *HLC* measurements should aspire to. There is little point in devising a test method that can measure a parameter to within 5% when the parameter itself varies by more than 20% in an unknown manner.

Definitional uncertainty can be further considered when specifically measuring pre and post retrofit interventions. Recent field measurements have caused us to reassess the long held assumptions of traditional constructions, whilst retrofit schemes have often been found to deliver lower levels of improvement than predicted. It has been shown that the reduction in heat loss can be artificially increased or decreased by variable external conditions and inconsistent analysis. Again, supporting measurements can reinforce the co-heating measurements and assist in understanding any comparison bias.

10.1.4.5 Recommendations for experimental protocol and analysis (9.3)

Finally, recommendations are made to both the experimental protocol and analysis techniques. In general, higher density of measurements will assist in understanding the uncertainties in the *HLC* estimate and comparison errors. This may include wind speed, infiltration rate, Q_g/T_g, Q_{unc}/ T_{unc} and moisture content. However, the deployment of sensors will depend upon financial constraints and the requirement for a refined *HLC* estimate and forensic investigation, or a simple quick check on the *HLC*.

In terms of analysis, it is recommended that dawn-dawn aggregation intervals are used to minimise stored solar effects, although aggregations lagged after sunrise may elicit better results in heavyweight dwellings. Aggregating 24 hour periods will usually suffice, although different aggregation intervals and lengths should be reported to display evidence of any systematic bias. In addition, calculating the statistical influence of each data point can determine whether a single outlier significantly effects the result.

From a theoretical point of view, the co-heating energy balance equation is overly simple, ignoring secondary heat flows and assuming a straightforward relationship. However, extending this equation through additional regression terms is often prohibited by multicollinearity (additional solar terms), weak signals (Q_{sky}) and non-linear relationships (Q_{wind}). Both Siviour and MLR regression produce similar results and whilst a forced intercept gives an inelegant description of HLC_{True}, it provides more consistent results as MLR with an intercept term will likely give poor estimates of both coupled and uncoupled losses.

Equally, subtracting out uncoupled terms prior to regression may provide information on disaggregated losses but the approach is prone to uncertainties not just in the co-heating measurement but also in the measurement of the secondary heat flows. Tracer gas decay infiltration measurements may contain significant measurement errors and represent different timescales to the daily aggregated co-heating measurements. Heat flux measurements may be biased by their location and may not capture bypasses within elements. In all cases, appropriate uncertainty analysis for each term and their combination is required. Consideration of the heat flows within a test dwelling and their relative scale from an initial audit description may be a useful starting set and help define which secondary heat flows are likely to be significant.

The current lack of understanding over the accuracy and reliability of co-heating tests has been increased by inconsistent reporting. As a result guidance for full reporting requirements is also given.

10.2 Key conclusions

The key conclusions from this research are stated as:

- Three types of uncertainties within co-heating tests can be defined. Many environmental or experimental sources of uncertainty impart **systematic measurement errors**, impairing the accuracy of HLC_{meas} in describing HLC_{True}. Others, e.g. wind losses, may cause **random error and variations in daily data points**, variation outside the co-heating energy balance but still allowing HLC_{meas} to accurately describe HLC_{True}, albeit at lower precision. This variation in HLC_{True}, leads to **definitional uncertianty** and comparison errors between successive measurements of the same dwelling (including retrofits), between different dwellings and to HLC_{pred}.

- Variations in HLC_{True} are driven by secondary heat flows typically ignored in co-heating analysis, including: wind and stack driven infiltration, ground losses, long-wave radiative sky losses, flows to adjoining heated and unconditioned spaces and the moisture content of the building fabric.

- *'If you want to know one thing about a house, you have to know everything else'* (p.1 Everett, 1985). Everett's statement remains as true as ever. Fully understanding a *HLC* measurement requires knowledge of several further heat flows. For this reason, high accuracy measurements and their interpretation require numerous supporting measurements and tests to reduce definitional uncertainties and to account for systematic uncertainties.

- Whilst the co-heating energy balance is overly simple, leading to a number of systematic measurement and comparison errors, adding further complexity within the steady state regression framework is unlikely to provide any benefits without additional costs. Additional regression terms are often restricted by multicorrelation, non-linear relationships and weak signal strengths. Disaggregating terms requires intensive additional monitoring regimes and test procedures.

- Definitional uncertainty can lead to the conclusion that there is little point in devising a test method that can measure a parameter to within 5% when the parameter itself varies by more than 20% in an unknown manner. Tests can either be conducted as quick, cheap and coarse measurements or alternatively require intensive monitoring of various heat flows in the dwelling. A balance must be sought between the investment into the measurement and the benefit of the output.

- Co-heating measurements can over or underestimate the HLC_{True} through a number of mechanisms, ranging from environmental (stored solar heating contributions, estimation of solar gains, dynamic T_e) to experimental uncertainties (measurement of solar radiation, party wall heat transfer, achieving quasi steady state, non-uniform T_i, sensor measurement errors) and even regression effects (attenuation bias, multicollinearity).

- Many of these effects can be reduced via suitable experimental protocol or optimum analysis techniques, meaning accurate *HLC* can be achieved for a wide range of dwellings across a range of conditions.

- Suitable testing conditions are largely dictated by the propensity of a test dwelling to overheat, meaning highly glazed and low heat loss dwellings carry higher restrictions and risks of failure. This particularly applies to Passivhaus dwellings, modern terraces and flats.

- In suitable conditions, co-heating tests can retrieve accurate results within shorter timeframes than previously suggested. Typically, results will converge to give a measured *HLC* within $\pm$ 10% of longer term monitoring within 72 hours. *HLC* estimates can be checked for convergence and variations over the test period, as in ISO 9869:2014 (ISO, 2014). Further evaluation of experimental overheating or aggregation intervals can identify the likelihood of any systematic bias due to stored solar heat. Remote monitoring and analysis during testing will be crucial to ensure valid results are achieved over these shorter timeframes and avoid tests ending before valid results are achieved.

- Full understanding of co-heating tests requires both appropriate error analysis and full reporting. Guidelines for both have been provided.

10.3 Limitations of the research

Simulated co-heating tests cannot fully replicate the complexities of real world testing. In particular, the analysis contained within this thesis does not fully explore the impact of high moisture content within the building fabric. Further work, both theoretical and with field measurements, is required to better understand and address the impact of moisture on a dwelling's heat loss, particularly for new builds. Additionally, the impact of wind pressures on a test dwelling is restricted to the modelling of infiltration, rather than interactions with the fabric such as wind washing. Field work has shown that these types of complex wind interactions

will increase the uncertainty in co-heating measurements, although they are omitted from simulations in this work. Furthermore, party wall heat transfer is largely considered as a simple dwelling-to-dwelling conductive heat transfer ignoring convective bypassing and further complications, with field work again identifying the more complex reality. Simulated tests therefore represent a somewhat idealised version of co-heating tests.

Only a small number of field tests (five) were conducted directly for the purpose of this research. In particular, no field data was taken from any traditional dwellings limiting the scope of investigation for such dwellings. Simulations have shown higher rates of infiltration and variability in HLC_{True} in more traditional dwellings. There may be uncertainties related to specific constructions, traditional and new, that have not been identified. For example, treatment of suspended timber floors or dwellings with strong stack effects in buildings with chimneys. The influence of a conservatory or sunspace is likely to be complex and may again require further simulations and field work.

There are a number of limitations with the use of the secondary data. Typically, only single internal temperatures were available and most data was only available at daily aggregations. In many primary and secondary cases, further measurements could have assisted this study, including multiple solar radiation measurements, increased use of heat flux sensors, measurement of fabric moisture content, higher resolution measurements of both T_e and T_i and improved infiltration measurements.

The scope of this research remained with UK dwellings and UK weather conditions. A wider variety of weather files could be used in simulated tests, with the three main files used allowing indicative examples rather than a large scale evaluation of the relationship between test conditions and the accuracy of *HLC* estimates. Further work would be needed to understand how the uncertainties identified and the application of co-heating changes in different climates and constructions.

10.4 Recommendations for further research

Following the outcomes of this research, several branches of future work can be considered, including:

- **Shorter, simpler co-heating tests:** There is potential for shorter monitoring periods ($\sim$ 72hours) if experimental challenges are met and suitable environmental conditions used. A larger number of dwellings could be tested relatively rapidly across a single site. Practical time and cost constraints then become more significant. One way to assist in both regards is to using the existing heating system. This will require factoring efficiencies but may be suitable for less accurate *HLC* measurements.

- **Testing en masse:** This idea can be extended to incorporate a wider range of dwellings. For example, over a weekend or slightly extended period, all or a large sample of dwellings on a site could undergo simultaneous co-heating testing potentially with existing heat systems. Outlier dwellings, with consideration to house types, could be subjected to further testing and inspection. This maybe aided by using a reference dwelling(s), that has already undergone more intensive testing. This might prove particularly effective at eliminating the worst performing homes and establish the variability of the *HLC* in supposedly identical dwellings.

- **Measurements of traditional dwellings and retrofit interventions:** Given the errors in assumptions over the performance of traditional buildings, variations in heat loss across the fabric, and challenges in delivering retrofit improvements, it is surprising more co-heating tests have not been conducted upon traditional dwellings or their retrofitted states. Co-heating tests, along with supporting measurements, could be used in a number of typical traditional constructions to improve our understanding of their expected heat loss and its variability. Further, these would provide a platform for further investigating the processes of heat loss forensically.

- **Measurements of dwellings under conditions of occupation:** The *HLC* currently measured represents a dwelling under unrealistic conditions. Co-heating tests could be performed in increasingly realistic conditions (e.g. typical temperature distributions, window openings etc), bridging the gap between a predicted *HLC* and the *HLC* under occupation.

- **Shading:** Testing highly glazed, low heat loss dwellings are likely to be restricted and carry significant risk. Methods of reducing solar gains through shading may provide a solution but need robust evaluation.

- **Infiltration measurements:** Definitional uncertainty is increased by variable infiltration rates, making it hard to compare to HLC_{pred} or between tests. At present, there is a lack of affordable and simple air infiltration methods that allow measurements across the same timescale as co-heating tests. This could assist in the interpretation of co-heating tests and provide further feedback.

- **Testing party wall and inter-dwelling heat transfer:** Party walls have already been shown to behave in a significantly different manner than expected, leading to higher than expected heat loss (see Lowe et al., 2007). Using a method suggested by Feuermann (1989), party wall and inter dwelling heat transfer could be assessed further by testing a dwelling through two periods of co-heating; the first fully guarded, the second with a temperature difference maintained between the test and surrounding dwellings.

- **Dynamic heat loss measurements:** There are certainly several benefits in utilising both dynamic experimental protocol and analysis techniques. These include shorter time-frames, more accurate results and the estimation of further building parameters. This is already an area of on-going research (IEA Annex 58). Options range from simple protocol, for example, a cooldown test is a simple addition to the end of the co-heating test, to more complex regimes. It is thought many of the findings of this thesis, whilst examining a steady state method, also apply to dynamic methods. This includes many of the sources of uncertainty but also issues relating to the definition of measured values and comparison errors. Similar reviews of the sources of uncertainty may need to be conducted for dynamic methods and simulations may again prove useful in identifying systematic errors.

- **Assessment of the use of performance measurements and estimated parameters:** There is a danger of focusing too much on the accuracy and number of parameters we can measure, rather than what constitutes effective feedback for the construction industry. For example, a co-heating *HLC* may have little value on its own. It is unlikely to be a consistent predictor of heat loss under occupation, as ventilation and window opening behaviour is excluded, internal temperature profiles may not be uniform and dynamics are not described. The main use of the *HLC* determined in co-heating tests is through comparisons to design predictions. However, as stated unavoidable comparison errors exist.

The question then is how can a single parameter describing many different heat flows and constructions provide effective feedback when used alone or with further tools? These issues also apply to dynamic test methods. Further research needs to determine how measured parameters can be used to better inform policy, manufacturers, designers, developers and contractors. Such a review would require a full multidisciplinary approach.

- **Development of fit for purpose quality control and in-line testing:** Over the last decade or so, a variety of contributors to the performance gap have been identified and reviewed. Whilst such investigations remain important and informative, there is a sufficient evidence base to begin to address these issues through improved quality control procedures and in-line testing. Many heat loss issues become invisible at certain stages of construction. The cost of rectifying defects also increases considerably as construction progresses. There is a need for research to identify and develop fit for purpose tools, testing and validating the product at crucial moments.

- **Whole building vs. component in situ measurements:** Further work could be performed to compare and contrast the whole building heat loss measurement with a *HLC* constructed from in situ U-value measurements, thermal bridging estimates and blower door tests. Would one approach be more suitable in certain dwelling types? How can comparisons of the two further identify areas of heat loss and issues that need addressing?

- **Consideration of extracted building parameters and their value:** With consideration of the *HLC*, its definition and the accuracy of the measurement, the usefulness of the metric itself can also be considered. Firstly, is a mean building U-value more useful for comparisons (see Johnston et al., 2015; Sutton et al., 2012)? Secondly, given the problems with the coupled and uncoupled components of heat loss, can this be expressed in alternative ways? More broadly, how useful is this number in terms of feedback, and how does the accuracy of the measurement correspond to the usefulness of its value?

To summarise, theoretically, this research establishes the bounds of the co-heating method and demonstrates the effectiveness of co-heating tests in understanding building fabric heat loss. Methodologically, it establishes the role of simulation in the estimation of errors associated with measurement procedures and demonstrates the value of applying multi-method approaches to complex problems arising from the physical performance of buildings. Substantively, this research highlights the need for researchers working in the field to be mindful of the uncertainty in co-heating tests and understand the limits of the measurement and its interpretation.

Bibliography

.

Adelard, L. et al. (2010). “Sky temperature modelisation and applications in building simulation”. In: *Renewable Energy* 15, pp. 418–430.

Altamirano-Medina, H. et al. (2008). “Mould Growth and Vapour Pressure Excess; A case Study of UK Apartments with Indoor mould Problems”. In: *11th International Conference on Indoor Air Quality and Climate, Denmark*.

Anderson, B. (2006). *Conventions for U-value calculations*. Tech. rep. Garston, Watford: Building Research Establishment Scotland.

Andrews, J.W. (1995). *Electric coheating as a means to test duct efficiency: a review and analysis of the literature*. Tech. rep. Upton, Long Island, New York, US: Brookhaven National Laboratories.

ASHRAE (2007). *ANSI/ASHRAE 140-2007 Standard Method of Test for the Evaluation of Building Energy Analysis Computer Programs*. Tech. rep. ASHRAE.

ASHRAE (2013). *2013 ASHRAE Handbook - Fundamentals*. Tech. rep. ASHRAE - American Society of Heating, Refrigerating and Air-Conditioning Engineers.

ATTMA (2010). *Technical Standard L1. Measuring Air Permeability of Building Envelopes (Dwellings) - October 2010 Issue*. Tech. rep. London, UK: Air Tightness Testing & Measurement Association.

Baker, P. (2008). *Technical Paper 2 - In situ U-value measurements in traditional buildings - preliminary results*. Tech. rep. Glasgow, UK: Historic Scotland, Technical Conservation Group & Glasgow Caledonian University.

Baker, P. (2011). *Historic Scotland Technical Paper 10 - U-values and traditional buildings*. Tech. rep. Historic Scotland & Glasgow Caledonian University.

Baker, P. (2015). *A retrofit of a victorian terrace house in New Bolsover: A whole house thermal performance assessment*. Tech. rep. Historic England & Glasgow Caledonian University.

Baker, P. and C. Morgan (2013). *FS42 - Co-heating test for Alternative Refurbishment Strategy on Hard to treat House on Uist*. Tech. rep. Historic Scotland & Glasgow Caledonian University.

Baker, P.H. (1993). "Error analysis of thermal performance characteristics determined from PASSYS test cell data - the effect of measurement errors". In: *Workshop on application of system identification in energy savings in buildings*.

Baker, P.H. and H.A.L. van Dijk (2008). "PASLINK and dynamic outdoor testing of building components". In: *Building and Environment* 43, pp. 143–151.

Bankvall, C. (1977). "Forced Convection. Practical Thermal Conductivity in an Insulated Structure Under the Influence from Workmanship and Wind". In: *ASTM symposium on Advances in Heat Transmission Measurement on Thermal Insulation Material Systems*.

Bauwens, G. and S. Roels (2014). "Co-heating test: A state-of-the-art". In: *Energy & Buildings* 82, pp. 163–172.

Bauwens, G., P. Standaert, S. Roels, and F. Delcuve (2011). "Reliability of Co-heating Measurements". In: *IEA Annex 58: Reliable Building Energy Performance Characterisation Based on Full Scale Dynamic Measurements, 2nd Meeting, April 2nd - 5th, Bilbao, Spain, 2012*.

Bauwens, G., P. Standaert, S. Roels, and F. Delcuve (2012). "Reliability of co-heating measurements". In: *First Building Simulation and Optimization Conference*. Loughborough, UK 10-11 September, 2012, pp. 348–355.

BBRI (1997). *Study and monitoring of the PLEIADE dwelling - Final report 1994-1996*. Tech. rep. Brussels, Belgium: Belgian Building Research Institute.

Bell, M. and R.J. Lowe (1998). *The York Energy Demonstration Project, Final Report*. Tech. rep. Leeds, UK: Leeds Metropolitan University.

Biddulph, P. et al. (2014). "Inferring the thermal resistance and effective thermal mass of a wall using frequent temperature and heat flux measurements". In: *Energy and Buildings* 78, pp. 10–16.

Birchall, S. (2011). "Co-heating Tests - what and how?" In: *52nd Annual General Meeting (AGM) for BSRIA, The Building Services Research and Information Association*. London,13th October 2011.

Bordass, B., A. Leaman, and P. Ruyssevelt (2001). "Assessing building performance in use 5: conclusions and implications". In: *Building Research & Information* 29(2), pp. 144–157.

Bouchie, R. and P. Boisson (2014). “In-situ measurements of the thermal performance of a non-occupied mock up - ISABELE method”. In: *IEA Annex 58*. 6th expert meeting, Gent, Belgium, April 14th.

Bowman, N. and K Lomas (1985). “Empirical Validation of Dynamic Thermal Computer Models in Buildings”. In: *Building Services, Engineering, Research and Technology* 6(4).

Bowman, N. and K. Lomas (1986). “Does Dynamic Simulation Work?” In: *Building Services* 8(3).

BRE (2006). *Energy Performance of Buildings Directive*. Tech. rep. Garston, Watford: Building Research Establishment.

BRE (2011). *SAP 2009 - The Government’s Standard Assessment Procedure for Energy Rating of Dwellings - 2009 Edition*. Tech. rep. Garston, Watford: Building Research Establishment.

BRE (2014). *SAP 2012 - The Government’s Standard Assessment Procedure for Energy Rating of Dwellings - 2012 Edition*. Tech. rep. Garston, Watford: Building Research Establishment.

BRE (2015). *BREDEM 2012 - A technical description of the BRE Domestic Energy Model*. Tech. rep. Garston, Watford: Building Research Establishment.

British Standards Institute (1998). *BS ISO 5725-5:1998 Accuracy (trueness and precision) of measurement methods and results - Part 5: Alternative methods for the determination of the precision of a standard measurement method*. Tech. rep. London, UK: BSI.

British Standards Institute (2000). *BS EN 1946-4:2000 - Thermal performance of building products and components - Specific criteria for the assessment of laboratories measuring heat transfer properties - Part 4: Measurements by hot box methods*. Tech. rep. London, UK: BSI.

British Standards Institute (2001a). *BS EN 13829:2001 - Thermal performance of buildings - Determination of air permeability of buildings - Fan pressurization method*. Tech. rep. London, UK: BSI.

British Standards Institute (2001b). *PD 6461-4:2004 General metrology. Practical guide to measurement uncertainty*. Tech. rep. London, UK: BSI.

British Standards Institute (2007). *BS EN 15242:2007 - Ventilation for buildings - Calculation methods for the determination of air flow rates in buildings including infiltration*. Tech. rep. London, UK: BSI.

British Standards Institute (2011). *Code of practice for control of condensation in buildings*. Tech. rep. London, UK: BSI.

Butler, D. and A. Dengel (2013). *Review of co-heating test methodologies*. Tech. rep. London, UK: NHBC Foundation.

Calcutt (2007). *The Calcutt Review of housebuilding delivery*. Tech. rep. London, UK: Department for Communities and Local Government.

Chapman, J., R. Lowe, and R. Everett (1985). *The Pennyland Project*. Tech. rep. Milton Keynes, UK: Energy Research Group, Open University.

CIBSE. Tech. rep. London, UK: The Chartered Institution of Building Services Engineers.

CIBSE (2002). *CIBSE Guide J: Weather, Solar & Illuminance Data*. Tech. rep. London, UK: The Chartered Institution of Building Services Engineers.

CIBSE (2007). *CIBSE Guide A: Environmental Design*. Tech. rep. London, UK: The Chartered Institution of Building Services Engineers.

Claridge, D.E. and M. Liu (1995). *The Measured Energy Impact of Infiltration in an Outdoor Test Cell*. Tech. rep. Energy Systems Laboratory, Texas A&M University.

D., Laussmann and D. Helm (2011). "Air change measurements using tracer gases: Methods and Results. Significance of air change for indoor air quality, Chemistry, Emission Control, Radiative Pollution and Indoor Air Quality". In: Intechopen. Chap. 14.

Davies, M.G. (1993). "Heat loss from a solid floor: A new formula". In: *Building Services Engineering Research and Technology* 14(2), pp. 71–75.

DCLG (2012). *2012 consultation on changes to the Building Regulations in England - Section 2 PartL - Conservation of fuel and power*. Tech. rep. London, UK: HM Government, Department of Communities and Local Government.

DCLG (2013). *The Building Regulations 2010 - Conservation of Fuel and Power - Approved Document L1A - Conservation of fuel and power in new dwellings - 2013 edition*. Tech. rep. Department of Communities and Local Government.

DCLG (2014). *English Housing Conditioning Survey - Headline Report 2012-2013*. Tech. rep. London, UK: HM Government, Department of Communities and Local Government.

De Meulenaer, V., J. Van der Veken, G. Verbeeck, and H. Hens (2005). "Comparison of measurements and simulations of a "Passivhaus"". In: *Ninth International IBPSA Conference, Montral, Canada, August 15-18, 2005*, pp. 769–776.

DECC (2013a). *The Future of Heating: Meeting the challenge*. Tech. rep. Department of Energy and Climate Change.

DECC (2013b). *United Kingdom housing energy fact file 2013*. Tech. rep. Department of Energy and Climate Change.

DECC (2014). *Digest of United Kingdom energy statistics 2014, Energy consumption by final user - energy supplied basis, 1970 to 2012 (DUKES 1.1.5)*. Tech. rep. Department of Energy and Climate Change.

DECC (2015). *Annual Report on Fuel Poverty Statistics 2015*. Tech. rep. Department of Energy and Climate Change.

Deconinck, A.H. and K. Leunis (2012). "Co-heating: a critical evaluation of data analysis methods." Masters Thesis. Katholieke Universiteit Leuven.

Deru, M. and P. Burns (2003). *Infiltration and Natural Ventilation Model for Whole-Building Energy Simulation of Residential Buildings*. Tech. rep. Golden, Colorado, US: NREL - National Renewable Energy Laboratory.

Doran, S. (2001). *DETR Framework Project Report: Field investigations of the thermal performance of construction elements as built*. Tech. rep. Glasgow, UK: Building Research Establishment.

Draper, N.R. and H. Smith (1998). *Applied Regression Analysis - Third Edition*. Wiley.

Duffie, J.A. and W.A. Beckman (1991). *Solar Engineering of Thermal Processes*. John Wiley & Sons.

Duffy, J.J. (1989). "Uncertainty in Passive Solar Systems Analysis". In: *Fourteenth National Passive Solar Conference Proceedings*. Denver, US.

Duffy, J.J. and H. Puri (1985). "Extrapolation of Short-Term Measurements to Long-Term Thermal Performance of Passive Buildings". In: *Solar 85, Tenth National Passive Solar Conference Proceedings, American Solar Energy Society*. Raleigh, NC, US, pp. 1371–1380.

Duffy, J.J. and D. Saunders (1987). *Low Cost Methods for Evaluation of Space Conditioning Efficiency of Existing Homes, Final Report to National Association of Home Builders (NAHB)*. Tech. rep. 400 Prince George Center Blvd., Upper Marlboro, MD 20772: NAHB Research Foundation, Inc.

DYNASTEE (2015). *DYNASTEE Software Tools*. http://dynastee.info/ (Access date: 2015-05-12).

EEPH (2006). *Compliance with Part L1 of the 2002 Building Regulations (An investigation into the reasons for poor compliance)*. Tech. rep. Oxford, UK: The Energy Efficiency Partnership for Homes.

EnergyPlus (2015). *EnergyPlus Weather Files*. URL: https://energyplus.net/weather (visited on 08/21/2015).

EST (2005). *Post-construction testing - a professional?s guide to testing housing for energy efficiency*. Tech. rep. Energy Saving Trust.

EST (2008). *Monitoring energy and carbon performance in new homes*. Tech. rep. Energy Saving Trust.

EST (2010). *Getting Warmer: a field trial of heat pumps*. Tech. rep. London, UK: The Energy Saving Trust.

EU (2010). *DIRECTIVE 2010/31/EU OF THE EUROPEAN PARLIAMENT AND OF THE COUNCIL of 19 May 2010 on the energy performance of buildings (recast)*. Tech. rep. Official Journal of the European Union.

Everett, R. (1985). *Rapid Thermal Calibration of Houses*. Tech. rep. Science and Engineering Research Council.

Everett, R., A. Horton, and J. Doggart (1985). *Linford Low Energy Houses*. Tech. rep. Milton Keynes, UK: Energy Research Group, Open University.

Fabi, V., R.V. Andersen, S. Corgnati, and B.W. Olesen (2012). "Occupants' window opening behaviour: A literature review of factors influencing occupant behaviour and models". In: *Building and Environment* 58, pp. 188–198.

Feist, W. (2007). *Passive House Planning Package 2007*. Tech. rep. Darmstadt, Germany: Passivhaus Institut.

Feuermann, D. (1989). "Measurement of envelope thermal transmittances in multifamily buildings". In: *Energy and Buildings* 13(2), pp. 139–148.

Francisco, P.W., J. Siegel, L. Palmiter, and B. Davis (2006). "Measuring residential duct efficiency with the short-term coheat test methodology". In: *Energy and Buildings* 38(9), pp. 1076–1083.

GHA (2011a). *Detailed Description of Coheating Test Procedure - indicative example*. Tech. rep. Good Homes Alliance & Leeds Metropolitan University.

GHA (2011b). *GHA Monitoring Programme 2009-11: Technical Report, Results from Phase 1: Post-construction testing of a sample of highly sustainable new homes*. Tech. rep. Good Homes Alliance.

Guerra Santin, O., C. Tweed, H. Jenkins, and S. Jiang (2013). "Monitoring the performance of low energy dwellings: Two UK case studies." In: *Energy and Buildings* 64, pp. 32–40.

Gutschker, O. (2004). *LORD - Modelling and identification software for thermal systems, User Manual*. Tech. rep. Brandenburg Technical University of Cottbus, Germany.

Hagentoft, C.E. (2001). *Introduction to building physics*. Studentlitteratur AB.

Harrje, D.T., S. Gauam, and J.E. Beyea (1979). "Locating and eliminating obscure but major energy losses in residential housing". In: *ASHRAE Transactions* 85(2), pp. 521–534.

Healy, J. D. (2003). “Excess winter mortality in Europe: a cross country analysis identifying key risk factors”. In: *Journal Epidemiology Community Health* 57, pp. 784–789.

Henninger, D., M.J. Witte, and D.B. Crawley (2004). “Analytical and comparative testing of EnergyPlus using IEA HVAC BESTEST E100-E200 test suite”. In: *Energy and Buildings* 36, pp. 855–863.

Hens, H. et al. (2007). “Brick Cavity Walls: A Performance Analysis Based on Measurements and Simulations”. In: *Journal of Building Physics* 31,2, pp. 96–124.

HM Government (2006a). *Building Regulations 2006: Approved Document L1A: Conservation of fuel and power in new dwellings*. Tech. rep. London, UK: HM Government, Office of the Deputy Prime Minister.

HM Government (2006b). *Building Regulations 2010: Approved Document L1A: Conservation of fuel and power in new dwellings*. Tech. rep. London, UK: HM Government.

HM Treasury (2015). *Fixing the Foundations: Creating a more prosperous nation*. Tech. rep. London, UK: HM Treasury, Presented to Parliament by the Chancellor of the Exchequer by Command of Her Majesty.

Hong, S.H., I. Ridley, and T. Oreszczyn (2006). “Measurement of envelope thermal transmittances in multifamily buildings”. In: *Energy and Buildings* 38(10), pp. 1171–1181.

Hopper, J. et al. (2012). “Assessing the execution of retrofitted external wall insulation for pre-1919 dwellings in Swansea (UK)”. In: *Paper presented and published in the conference proceedings for the Retrofit for the Future Conference*.

Huebner, G.M. et al. (2015). “The shape of warmth: temperature profiles in living rooms”. In: *Building Research & Information* 43,2, pp. 185–196.

International Organization for Standardization (ISO) (1994). *BS EN ISO 5725-1:1994 Accuracy (trueness and precision) of measurement methods and results - Part 1: General principles and definitions*. Tech. rep. Geneva, Switzerland: ISO.

International Organization for Standardization (ISO) (1996). *BS EN ISO 8990:1996 Thermal insulation - Determination of steady-state thermal transmission properties - Calibrated and guarded hot box*. Tech. rep. Geneva, Switzerland: ISO.

International Organization for Standardization (ISO) (1999). *BS EN ISO 13187:1999 Thermal performance of buildings Qualitative detection of thermal irregularities in building envelopes - Infrared method*. Tech. rep. Geneva, Switzerland: ISO.

International Organization for Standardization (ISO) (2001a). *BS EN ISO 12667:2001 Thermal Performance of Building Materials and Products. Determination of Thermal Resistance*

by means of Guarded Hot Plate and Heat Flow Meter Methods. Products of High and Medium Thermal Resistance. Tech. rep. Geneva, Switzerland: ISO.

International Organization for Standardization (ISO) (2001b). *BS EN ISO 7726:2001 Ergonomics of the thermal environment Instruments for measuring physical quantities*. Tech. rep. Geneva, Switzerland: ISO.

International Organization for Standardization (ISO) (2003). *BS EN ISO 15927-1:2003 Hygrothermal performance of buildings Calculation and presentation of climatic data Part 1: Monthly means of single meteorological elements*. Tech. rep. Geneva, Switzerland: ISO.

International Organization for Standardization (ISO) (2007a). *BS EN ISO 10456:2007 Building materials and products - Hygrothermal properties - Tabulated design values and procedures for determining declared and design thermal values*. Tech. rep. Geneva, Switzerland: ISO.

International Organization for Standardization (ISO) (2007b). *BS EN ISO 13789:2007 Thermal performance of buildings - Transmission and ventilation heat transfer coefficients - Calculation method*. Tech. rep. Geneva, Switzerland: ISO.

International Organization for Standardization (ISO) (2007c). *BS EN ISO 6946:2007 Building components and building elements - Thermal resistance and thermal transmittance - Calculation method*. Tech. rep. Geneva, Switzerland: ISO.

International Organization for Standardization (ISO) (2008). *BS EN ISO 13790:2008 Energy performance of buildings - Calculation of energy use for space heating and cooling*. Tech. rep. Geneva, Switzerland: ISO.

International Organization for Standardization (ISO) (2012). *BS EN ISO 13788:2012 Hygrothermal performance of building components and building elements - Internal surface temperature to avoid critical surface humidity and interstitial condensation - Calculation methods*. Tech. rep. Geneva, Switzerland: ISO.

International Organization for Standardization (ISO) (2014). *BS EN ISO 9869:2014 Thermal insulation: Building elements: In-situ measurement of thermal resistance and thermal transmittance*. Tech. rep. Geneva, Switzerland: ISO.

Jack, R. (2015a). "Building Diagnostics: Practical Measurement of the Thermal Fabric Performance of Houses". PhD thesis. Loughborough University.

Jack, R. (2015b). "The Co-heating Test for In-situ Measurements of Domestic Building Thermal Performance: A Comparative Evaluation".

Janssens, A. and H. Hens (2007). "Development of indoor climate classes to assess humidity in dwellings". In: *AIVC 24th Conference & BETEC conference*, pp. 41–46.

Janssens, A., S. Roels, and ed. Vandaele L (2011). *Full scale test facilities for evaluation of energy and hygrothermal performances*. University Press, Zelzate, Belgium.

JCGM (2008a). *Evaluation of measurement data - Guide to the expression of uncertainty in measurement*. Tech. rep. Joint Committee for Guides in Metrology (JCGM/WG1).

JCGM (2008b). *International vocabulary of metrology - Basic and general concepts and associated terms (VIM)*. Tech. rep. Joint Committee for Guides in Metrology (JCGM/WG1).

JCGM (2009). *Evaluation of measurement data - An introduction to the "Guide to the expression of uncertainty in measurement" and related documents*. Tech. rep. Joint Committee for Guides in Metrology (JCGM/WG1).

Jimenez, M.J. and H. Madsen (2008). "Models for describing the thermal characteristics of building components". In: *Building and Environment* 43, pp. 152–162.

Johnston, D., J. Wingfield, and D. Miles-Shenton (2012a). "Measuring the fabric performance of UK dwellings". In: *Egbu, C. (Ed) Procs 26th Annual ARCOM Conference, 6-8 September 2010, Association of Researchers in Construction Management*. Leeds, UK, pp. 1371–1380.

Johnston, D., D. Miles-Shenton, D. Farmer, and J. Wingfield (2012b). "Whole House Heat Loss Test Method (Coheating)". In: *IEA Annex 58: Reliable Building Energy Performance Characterisation Based on Full Scale Dynamic Measurements, 2nd Meeting, April 2nd - 5th, Bilbao, Spain, 2012*.

Johnston, D., D. Miles-Shenton, D. Farmer, and J. Wingfield (2013). *Whole House Heat Loss Test Method (Coheating)*. Tech. rep. Leeds, UK: Leeds Metropolitan University.

Johnston, D., D. Miles-Shenton, and D. Farmer (2015). "Quantifying the domestic building fabric 'performance gap'". In: *Building Services Engineering Research and Technology* 36(5), pp. 614–622.

Josephson P.E & Hammarlund, Y. (1999). "The causes and costs of defects in construction - A study of seven building projects". In: *Automation in Construction* 8, pp. 681–687.

JRHT (2011). *Tender Document for Dewenthorpe*. Tech. rep. York, UK: Joseph Rowntree Housing Trust.

Judkoff, R. et al. (2000). *Side-by-Side Thermal Tests of Modular Offices: A Validation Study of the STEM Method*. Tech. rep. Golden, Colorado, US: National Renewable Energy Laboratory.

Juhl, R., P. Bacher, and H. Madsen (2013). *ctsmr package - Continuous Time Stochastic Modelling in R*. Tech. rep. Copenhagen, UK: Department of Applied Mathematics and Computer Science, Technical University of Denmark.

Knauf (2015). *Party Wall Insulation Systems*. URL: http://www.knaufinsulation.co.uk/media/786492/3_4_2-separating-walls.pdf (visited on 08/21/2015).

Kronvall, J. (1978). "Testing of houses for air leakage using a pressure method". In: *ASHRAE Transactions* 84, pp. 72–79.

LBNL (2014). *EnergyPlus Engineering Reference - The Reference to EnergyPlus Calculations*. Tech. rep. University of Illinois Urbana-Champaign, Lawrence Berkeley National Laboratory.

Lecompte, J. (1989). "Influence of Natural Convection in an Insulated Cavity on the Thermal Performance of a Wall". In: *American Society Testing of Materials* STP 1030, pp. 397–420.

Li, F.G.N et al. (2014). "Solid-wall U-values: heat flux measurements compared with standard assumptions". In: *Building Research & Information* 43,2, pp. 238–252.

Liu, M. and D. E. Claridge (1995). *Improving Building Energy Performance Through Continuous Commissioning*. Tech. rep. Texas, US: Energy Systems Laboratory, Texas A & M.

Lloyd, B., T. Bishop, and M. Callau (2007). *Retrofit alternatives for State Houses in Cold Regions of New Zealand REPORT No 2*. Tech. rep. Dunedin, New Zealand: Energy Management Group, Physics Department, University of Otago.

Lowe, R. and C. Gibbons (1988). "Passive Solar Houses: Availability of weather suitable for calibration in the UK". In: *Building Services Engineering Research and Technology* 9,3, pp. 127–132.

Lowe, R.J. (2000). "Ventilation strategy, energy use and CO2 emissions in dwellings - a theoretical approach". In: *CIBSE A: Building Services Engineering Research and Technology*.

Lowe, R.J., J. Wingfiled, M. Bell, and J.M. Bell (2007). "Evidence for heat losses via party wall cavities in masonry construction". In: *Building Services Engineering Research and Technology* 28,2, pp. 161–181.

Makroddimitri, M. and I. Ridley (2010). "Energy efficient refurbishment of existing housing stock - the Victorian housing stock in the UK". In: *Consilience: The Journal of Sustainable Development* 4(1), pp. 33–59.

Mangematin, E., G. Pandraud, and D. Roux (2012). "Quick measurements of energy efficiency of buildings". In: *Comptes Rendus Physique* 13, pp. 383–390.

Masy, G. and J. Lebrun (2004). "Passive Solar Houses: Availability of weather suitable for calibration in the UK". In: *Proceedings of the Fourth International Conference for Enhanced Building Operations, Paris, France, October 18th - 19th, 2004*.

Masy, G. et al. (2005). “Residential Building Thermal Performances”. In: *IEA Annex 40, Final Subtask B2, Development of Functional Performance Testing procedures*, pp. 1–9.

Mawditt, I. and J. Palmer (2008). *EEPH/CLG Building Regulations Approved Document Part L1A Compliance Project - Pilot Study Report*. Tech. rep. Oxford, UK: The Energy Efficiency Partnership for Homes.

MerlinLazer (2015). *Merlin Lazer Glass Measurement Gauge*. URL: http://www.merlinlazer.com/Glass-Measurement-Gauge (visited on 08/21/2015).

Miles-Shenton, D., J. Wingfield, R. Sutton, and M. Bell (2010). *Project Title: Temple Avenue Project, Part 1: Temple Avenue field trial - Evaluation of design & construction process and measurement of fabric performance of new build dwellings*. Tech. rep. Leeds, UK: Leeds Metropolitan University.

Miles-Shenton, D., J. Wingfield, R. Sutton, and M. Bell (2011). *Project Title: Temple Avenue Project, Part 1: Temple Avenue field trial - Evaluation of design & construction process and measurement of fabric performance of new build dwellings Part 2: Energy efficient renovation of an existing dwelling: Evaluation of design & construction and measurement of fabric performance*. Tech. rep. Leeds, UK: Leeds Metropolitan University.

Naveros, I. et al. (2014). “Setting up and validating a complex model for a simple homogeneous wall”. In: *Energy and Buildings* 70, pp. 303 –317.

Neymark, J. and R. Judkoff (2008). *International Energy Agency Building Energy Simulation TEST and Diagnostic Method (IEA BESTEST) Multi-Zone Non-Airflow In-Depth Diagnostic Cases: MZ320 ? MZ360, NREL/TP-550-43827*. Tech. rep. National Renewable Energy Labatory, Golden, Colorado, US.

Neymark, J. et al. (2009). “IEA BESTEST In-Depth Diagnostic Cases for Ground Coupled Heat Transfer Related to Slab-on-Grade Construction”. In: *Building Simulation 2009 Conference Glasgow, Scotland, 27-30 July 2009*.

NHBC (2015). *Guide to your new home - A practical guide to looking after your new home*. Tech. rep. Milton Keynes, UK: National House Building Council.

Norford, L.K., R.H. Socolow, E.S. Hsieh, and G.V. Spadaro (1994). “Two-to-one discrepancy between measured and predicted performance of a ’low-energy’ office building: insights from reconciliation based on the DOE-2 model”. In: *Energy and Buildings* 21, pp. 121–131.

NREL (2015). *Shining On - Chapter 4 - What parts of solar radiation are measured*. URL: http://rredc.nrel.gov/solar/pubs/shining/chap4.html#fig3 (visited on 08/21/2015).

Orr, G., T. Lelyveld, and S. Burton (2009). *Final Report: In-situ monitoring of efficiencies of condensing boilers and use of secondary heating*. Tech. rep. GASTEC.

Page, J.K. (1985). *Statistics of Horizontal and Inclined Surface Irradiation in the UK with Consideration of Associated Temperatures, Long Wave Radiation and Wind Speed ETSU-51120*. Tech. rep. Abingdon, UK: Energy Technology Support Group.

Palmer, J., G. Pane, M. Bell, and J. Wingfield (2011). *Comparing primary and secondary terms analysis and re-normalisation (PStar) test and co-heating test results*. Tech. rep. London, UK: Department for Communities and Local Government, AECOM, Leeds Metropolitan University.

Palmiter, L.S. et al. (1979). *Low Cost Performance Evaluation of Passive Solar Buildings*. Tech. rep. Golden, Colorado, US: Solar Energy Research Institute.

Pandraud, G. and R. Fitton (2013). "QUB: Validation of a Rapid Energy Diagnostic Method for Buildings". In: *IEA Annex 58: Reliable Building Energy Performance Characterisation Based on Full Scale Dynamic Measurements, 4th Meeting, April 8th - 10th, Holzenkirchen, Germany, 2013*.

Partners, AIMC4 et al. (2013). *Lessons from AIMC4 for cost-effective, fabric-first, low-energy housing - Part1: Introduction to AIMC4*. Tech. rep. Garston, Watford, UK: AIMC4.

Pelsmaker, S. (2015a). "Pre-1919 suspended timber ground floors in the UK: measuring the in-situ thermal performance and heat-loss reduction potential of interventions (Confidential)". PhD thesis. University College London.

Pelsmaker, S. et al. (2015b). "Heat-loss from suspended timber ground floors: in-situ measurement, variability and uncertainty - Forthcoming".

Persily, A. and G. Linteris (1983). "A comparison of measured and predicted infiltration rates". In: *ASHRAE Transactions* 89, pp. 183–200.

Rayment, R. (1995). "The Use of Matched Houses to Investigate Energy Savings". In: *In Proc. CIBSE National Conference*. Vol. 1. Eastbourne, UK, pp. 52–63.

Rhee-Duverne, S. and P. Baker (2013). *Research into the thermal performance of traditional brick walls*. Tech. rep. Historic England & Glasgow Caledonian University.

Ridley, I., M. Davies, S.H. Hong, and T. Oreszczyn (2007). "Vapour pressure excess in living rooms and bedrooms of English dwellings: Analysis of the Warm Front Dataset". In: *Annex 41 Moist-Eng*. Florianapolis, Brazil.

Ridley, I., R. Lowe, and Z. Ye (2010a). *GHA Monitoring Programme - Post-construction testing - One Brighton (Confidential)*. Tech. rep. London, UK: UCL.

Ridley, I., R. Lowe, and Z. Ye (2010b). *GHA Monitoring Programme - Post-construction testing - One Brighton (Confidential)*. Tech. rep. London, U: UCL.

Rye, C. (2010). *The SPAB Research Report 1. U-value Report*. Tech. rep. Glasgow, UK: SPAB - Society for the Protection of Ancient Buildings.

Santamouris, M. (2005). *Energy Performance of Residential Buildings: A Practical Guide for Energy Rating and Efficiency*. Earthscan.

Sherman, M.H. (1987). "Estimation of Infiltration from Leakage and Climate Indicators". In: *Energy and Buildings* 10, pp. 81–86.

Sherman, M.H., P.E. Grimsrud, P.E. Condon, and B.V. Smith (1980). "Air infiltration measurement techniques". In: *Proceedings of the 1st IEA Conference of the Air Infiltration Centre, London. Report LBL-10705. Lawrence Berkeley National Laboratory, Berkeley, CA*.

Sicart, J. E., R. Hock, P. Ribstein, and J.P. Chazarin (2010). "Sky long-wave radiation on tropical Andean glaciers: Parameterization and sensitivity to atmospheric variables". In: *Journal of Glaciology* 56(199), pp. 854–860.

Siddal, M., J. Trinick, and D. Johnston. In:

Siviour, J.B. (1981). "Experimental Thermal Calibration of Houses". In: *Conference on Comparative Experimentation of Low Energy Houses*.

Siviour, J.B. (1994). "Experimental U-values of Some House Walls". In: *Building Services Engineering Research and Technology* 15,1.

Socolow, R.H. (1978). *Saving Energy in the Home, Princeton's Experiments at Twin Rivers*. Ballinger Publishing Company.

Sonderegger, R.C. and M. Modera (1979). "Electric Co-heating: A Method for Evaluating Seasonal Heating Efficiencies and Heat Loss Rates in Dwellings". In: *Second CIB Symposium on Energy Conservation in the Built Environment, Copenhagen, Denmark, May 28th - June 1st, 1979*.

Sonderreger, R.C., P. Condon, and M. Modera (1980). "In-Situ Measurement of Residential Energy Performance Using Electric Coheating". In: *American Society of Heating, Refrigerating and Air Conditioning Engineers Transactions* 86, p. 394.

Stafford, S., M. Bell, and C. Gorse (2012). *Building Confidence - A Working Paper*. Tech. rep. Leeds, UK: Leeds Metropolitan University.

Stamp, S. (2011). "The Error and Uncertainty in Coheating Tests". Masters Thesis. University College London.

Stamp, S., R. Lowe, and H. Altamirano-Medina (2012). "Derwenthorpe Co-heating Test - A report to the Joseph Rowntree Housing Trust. UCL Energy Institute - Confidential".

Stamp, S., R. Lowe, and H. Altamirano-Medina (2013a). "An investigation into the role of thermal mass on the accuracy of co-heating tests through simulations & field results". In: *Building Simulation and Optimization 2013*. Chambery, France, August 25-28.

Stamp, S., R. Lowe, and H. Altamirano-Medina (2013b). "Solar Driven Uncertainty in Co-heating". In: *IEA Annex 58: Reliable Building Energy Performance Characterisation Based on Full Scale Dynamic Measurements*. 4th Meeting, April 8th - 10th, Holzenkirchen, Germany, 2013.

Stamp, S., R. Lowe, and H. Altamirano-Medina (2013c). "TSB BPE Project - Camden Passivhaus - A report to the Technology Strategy Board as part of the Technology Strategy Board's Building Performance Evaluation Programme. UCL Energy Institute (Confidential)".

Stamp, S., R. Lowe, and H. Altamirano-Medina (2013d). "Using simulated co-heating tests to understand weather driven sources of uncertainty within the co-heating test method". In: *ECEEE Summer Study Proceedings*. Presqu'ile de Giens, Toulon/Hyres, France, June 3-8, pp. 2049–2055.

Stevens, G. and J. Bradford (2013). "Do U-value insulation? England's field trial of solid wall insulation". In: *ECEEE Summer Study Proceedings*. Presqu'ile de Giens, Toulon/Hyres, France, June 3-8, pp. 2049–2055.

Stevenson, F. and H. Rijal (2008). "Paper No 595: The Sigma Home: towards an authentic evaluation of a prototype building". In: *PLEA 2008 ? 25th Conference on Passive and Low Energy Architecture, 22nd to 24th October 2008*. Dublin, Rep. of Ireland.

Stymne, Y., C.A. Boman, and Kronvall J. (1994). "Measuring Ventilation Rates in the Swedish Housing Stock". In: *Building and Environment* 29(3), pp. 373–379.

Subbarao, K. (1988a). *PSTAR -Primary and Secondary Terms Analysis and Renormalization: A Unified Approach to Building Energy Simulations and Short - Term Monitoring*. Tech. rep. Golden, Colorado, US: Solar Energy Research Institute.

Subbarao, K. (1988b). *PSTAR -Primary and Secondary Terms Analysis and Renormalization: A Unified Approach to Building Energy Simulations and Short - Term Monitoring - A Summary*. Tech. rep. Golden, Colorado, US: Solar Energy Research Institute.

Subbarao, K., J.D. Balcomb, and J. Burch (1990). "Short-term energy monitoring summary of results from four houses". In: *ASHRAE transactions, 96(1)*, pp. 1459–1477.

Subbarao, K. et al (1988c). *Short-Term Energy Monitoring (STEM): Application of the PSTAR Method to a Residence in Fredericksburg, Virginia*. Tech. rep. Golden, Colorado, US: Solar Energy Research Institute.

Sutton, R., A. Stafford, and C. Gorse (2012). "The Coheating Test: The value of a number". In: *IEA Annex 58: Reliable Building Energy Performance Characterisation Based on Full Scale Dynamic Measurements, 2nd Meeting, April 2nd - 5th, Bilbao, Spain, 2012*.

Taylor, J.R. (1997). *An Introduction to Error Analysis - The Study of Uncertainties in Physical Measurements*. University Science Books.

Thomas, C.K. and A.R. Smoot (2013). "An Effective, Economic, Aspirated Radiation Shield for Air Temperature Observations and Its Spatial Gradients". In: *Journal of Atmospheric and Oceanic Technology* 30, pp. 526–537.

Titman, J. D. (2001). "Applications of thermography in non-destructive testing of structures". In: *NDT & E International* 34(2), pp. 149–154.

Trust, Carbon (2011). *Micro-CHP Accelerator*. Tech. rep. Carbon Trust.

TSB (2015). *TSB BPE Projects*. URL: https : / / connect . innovateuk . org / web / building - performance-evaluation (visited on 08/21/2015).

Walker, I.S. and D.J. Wilson (1997). "Field validation of algebraic equations for stack and wind driven air infiltration calculations". In: *International Journal of HVAC&R Research (now HVAC&R Research)* 4(2), pp. 119–140.

Winfield, J., D. Miles-Shenton, and M. Bell (2009). *Evaluation of the Party Wall Thermal Bypass in Masonry Dwellings*. Tech. rep. Leeds, UK: Leeds Metropolitan University.

Wingfield, J. (2010a). *In-situ Measurement of Whole House Heat Loss using Electric Coheating*. Tech. rep. Leeds, UK: Leeds Metropolitan University.

Wingfield, J. (2010b). "In situ Measurement of Whole House Heat Loss using Electric Coheating". In: *Dynastee Meeting*. Brussels,12th October 2010.

Wingfield, J. (2011). "Fabric Testing: Whole House Heat Loss". In: *GHA Closing the performance gap - Low Carbon 4 Real*. UCL, London, 14th April 2011.

Wingfield, J. et al. (2007). *Evaluating the Impact of an Enhanced Energy Performance Standard on Load-bearing Masonry Domestic Construction, Report Number 8 - Final Report,Lessons from Stamford Brook Understanding the Gap between Designed and Real Performance*. Tech. rep. Leeds, UK: Department for Communities and Local Government, AECOM, Leeds Metropolitan University.

Wingfield, J., M. Bell, D. Miles-Shenton, and J. Seavers (2011). *Elm Tree Mews Field Trial - Evaluation and Monitoring of Dwellings Performance Final Technical Report*. Tech. rep. Leeds, UK: Leeds Metropolitan University.

Younes, C., C.A. Shdid, and G. Bitsuamlak (2011). "Air Infiltration through building envelopes: A review". In: *Journal of Building Physics* 35(3), pp. 267–302.

Zabot, S. (1987). “A low-cost methodology for thermal performance monitoring of public schools in the Lombardy Region”. In: *Energy and Buildings* 10(1), pp. 59–157.

ZCH (2012). *Fabric Energy Efficiency for Zero Carbon Homes*. Tech. rep. Milton Keynes, UK: Zero Carbon Hub.

ZCH (2013). *Closing the gap between design & as-built performance - Interim Progress Report*. Tech. rep. London, UK: Zero Carbon Hub.

ZCH (2014a). *Closing the gap between design & as-built performance - End of Term Report*. Tech. rep. London, UK: Zero Carbon Hub.

ZCH (2014b). *Closing the gap between design & as-built performance - Evidence Review Report*. Tech. rep. London, UK: Zero Carbon Hub.

Zonen, Kipp & (2013). *Instruction Manual - CMP Series Pyranometer*. Tech. rep. Kipp & Zonen, Delft, The Netherlands.

Appendix A

Supporting Figures & Explanations

This section of the appendix provides additional examples, figures and explanations to the main text. These are contained in sections under the same titles as the chapters of the thesis.

A.1 Defining the *HLC*, *R*, *S* and uncertainty - supporting material

A.1.0.1 Orientation and incident solar radiation

In this section, the solar radiation incident upon a dwelling is considered in more detail. Diurnally, direct solar radiation will initially strike the east facade, followed by the south and then west. In the winter, as the sun is above the horizon for a shorter period in the middle of the day, the majority of solar radiation is incident upon the south facade. As daylight hours increase, more direct solar radiation will be incident on east and west facing facades, increasing their relative importance. This is demonstrated across a week in January and April in figure A.1.

In the winter, the sun's low position in the sky means that there is a low angle of incidence on south facing vertical surfaces. In the summer, with the sun's higher position in the sky, this angle increases. This means that whilst S_{GHR} increases significantly into the summer, S_{GVS} and S_{GVM} do not increase to the same extent (figure A.2).

Although this is all somewhat trivial, it is important to carefully consider when discussing the suitability of both the measurement of *S*, and the definition of *R*, as these values are considered in the context of co-heating tests.

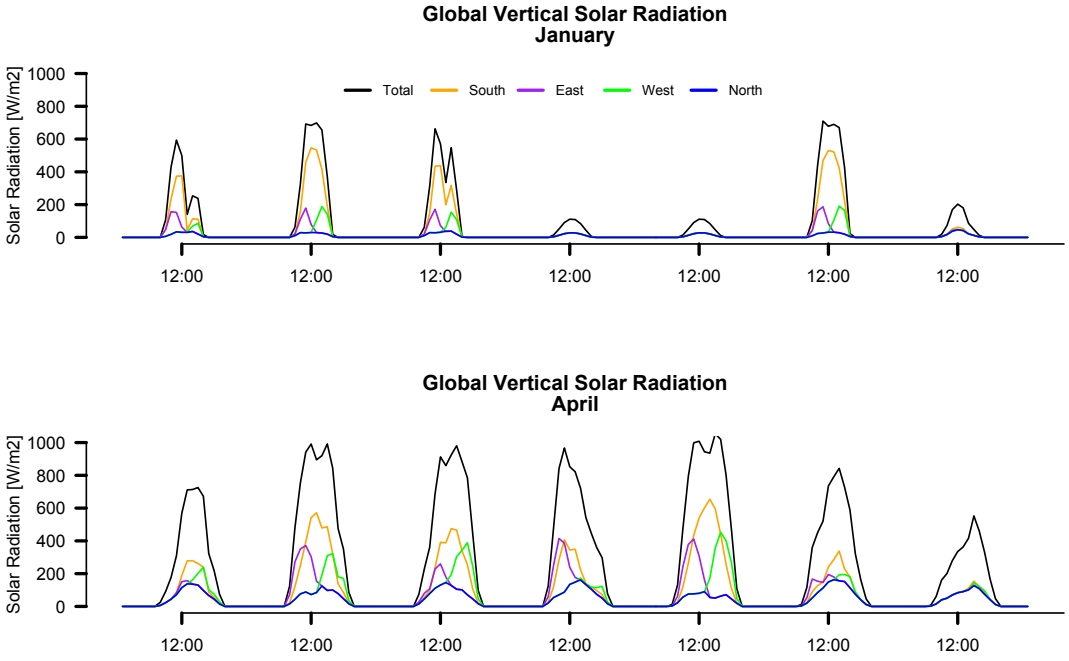

Figure A.1: *Incident Solar Radiation on each facade of a test building in January and April.*

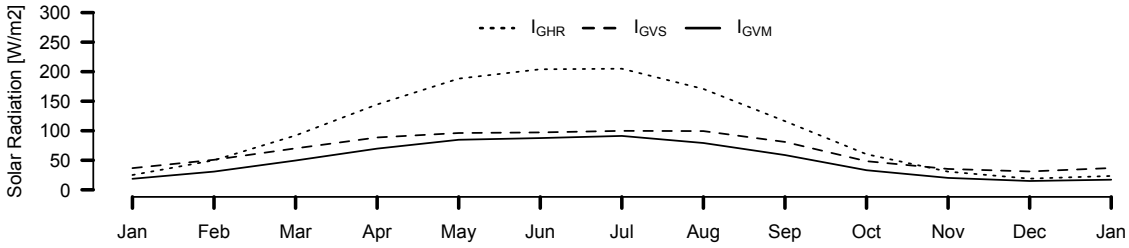

Figure A.2: S_{GHR}, S_{GVS} *and* S_{GVM} *across the year*

A.2 Solar driven sources of uncertainty - supporting material

A.2.1 Multiple solar regression terms

The use of multiple solar terms (i.e. both S_{GVE} & S_{GVW}) in MLR is shown in figure A.3 for an east-west orientated dwelling. This can be seen to be less accurate than the use of a single vertical measurement, or a single mean value.

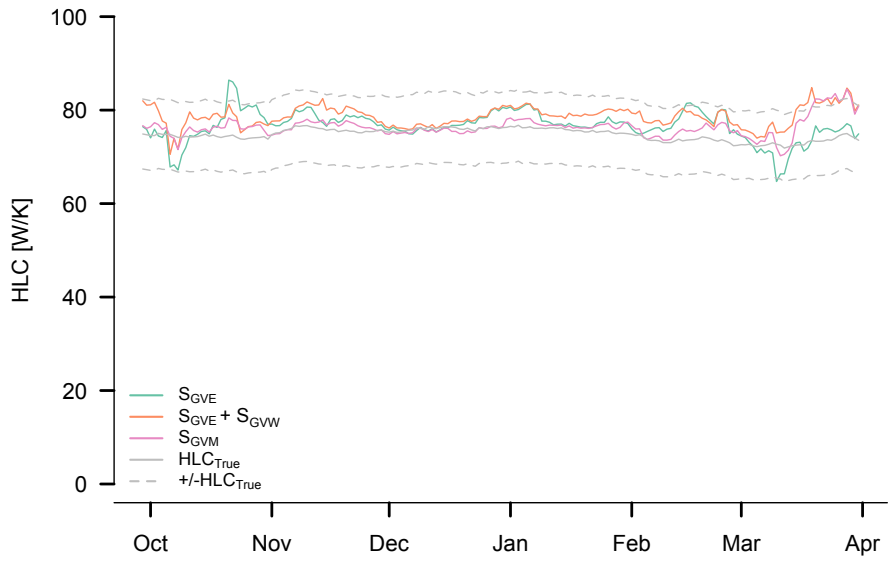

Figure A.3: *S_{GHR}, S_{GVM} and a regression using both S_{GVW} and S_{GVE} across the year.* (Simulation: BRE-NOT-SLW-FINN-EW-MLR-2w-24h-6agg)

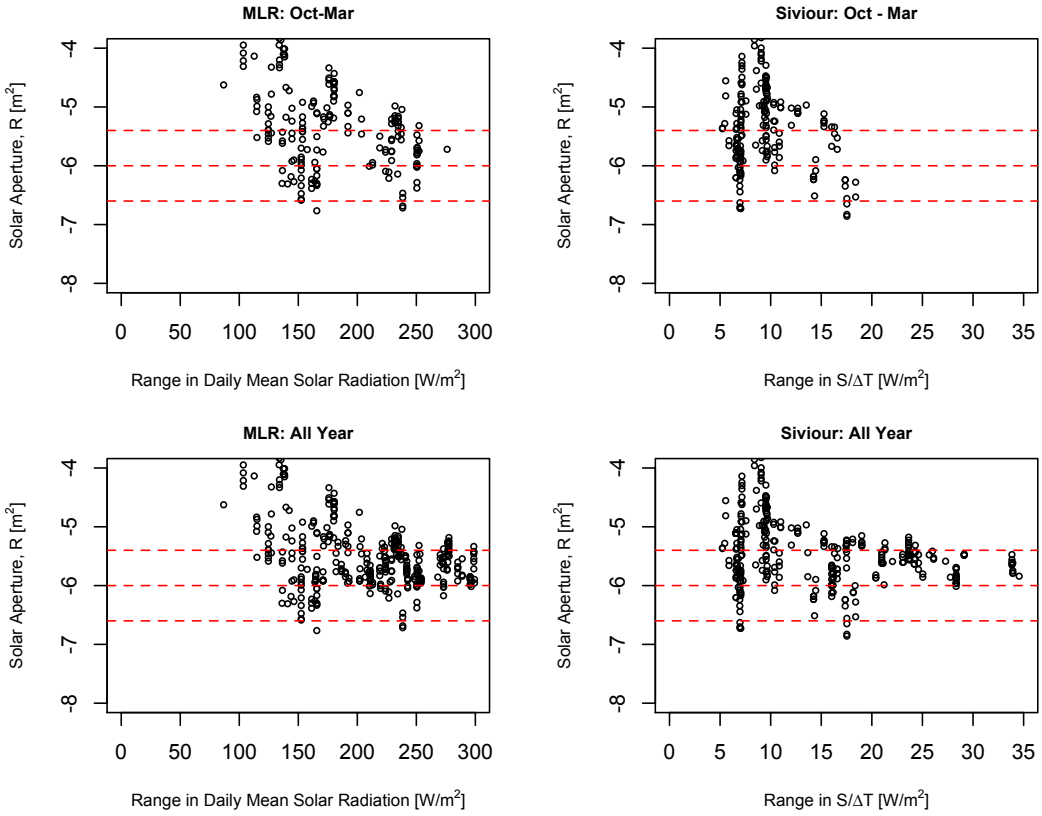

Figure A.4: *Estimated value of R plotted against range in ΔT or ($S/\Delta T$). Red lines indicate the value of R inputted into the model (6 m^2) and $\pm$ 10% bands about this. Random error applied to both Q and S.* (Modelled: FINN-2w-24h-6agg-S_{GVS})

A.2.2 Statistically determining *R* - attenuation bias

Figure A.4 shows a simple model (*HLC* = 80 W/K, *R* = 6 m^2) used to determine the accuracy of *R*, as seen in figure 5.10 of the main thesis. This time a 10% uncertainty is added to *S* (an independent regression variable[1]) not just to Q_{elec}. The attenuation bias (discussed in section 8.2) is clear, with *R* tending towards underestimation in both MLR and Siviour regression.

A.2.3 Statistically Determining *R* - Simulations using S_{GHR} and S_{GVM}

Figures A.5, A.6, A.7 and A.8 show the estimated value of *R* and the subsequently estimated solar gains, Q_{sol} when using S_{GHR} and S_{GVM} respectively. The overestimate of *R* and Q_{sol} when using S_{GHR} is apparent, resulting in the overestimated *HLC* in figures 5.3 and 5.5 of the main thesis. A smaller overestimate is seen when using S_{GVM}.

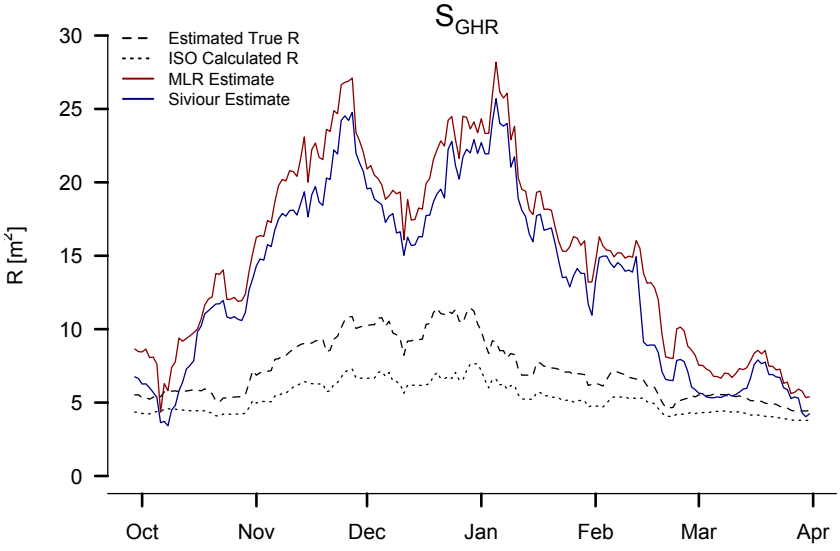

Figure A.5: *Estimated Solar Aperture from MLR and Siviour analysis, using* S_{GHR}.

[1] Standard deviation = 10% of *S*.

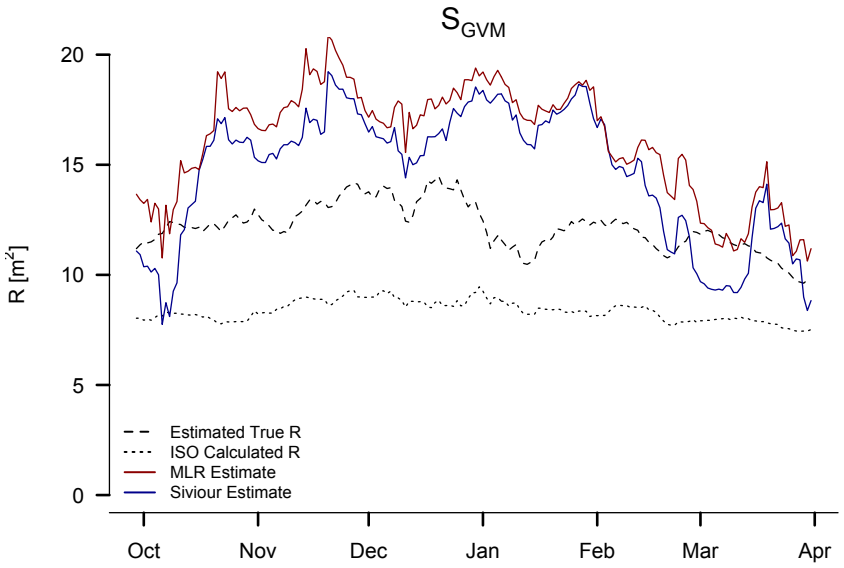

Figure A.6: *Estimated Solar Aperture from MLR and Siviour analysis, using* S_{GVM}.

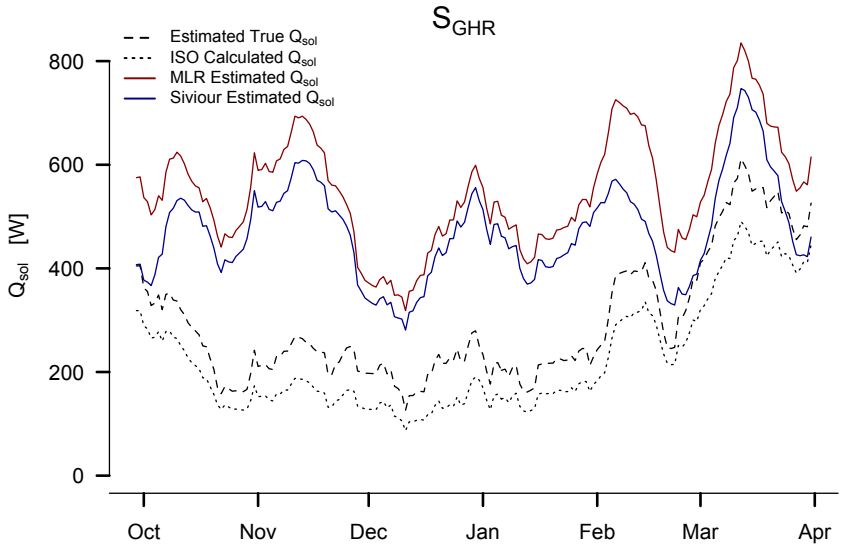

Figure A.7: *Estimated Solar Gains from MLR and Siviour analysis, using* S_{GHR}.

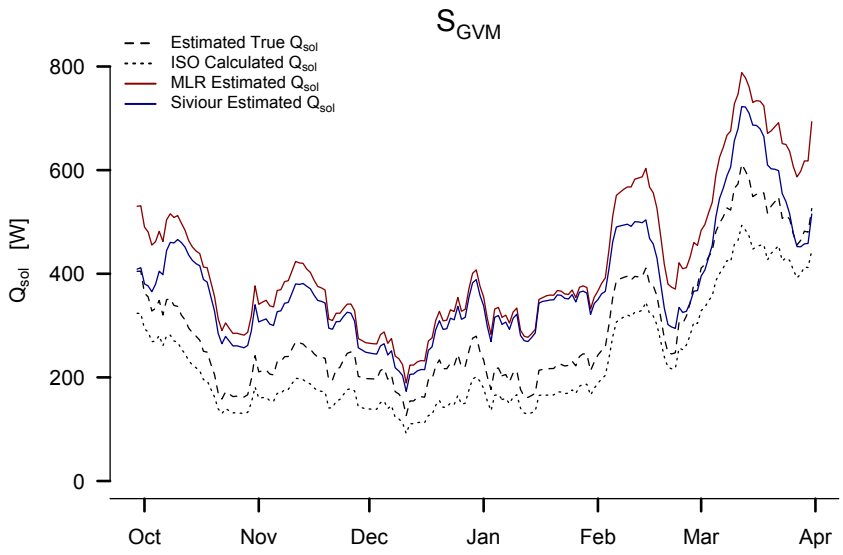

Figure A.8: *Estimated Solar Gains from MLR and Siviour analysis, using* S_{GVM}.

A.2.4 Solar driven overheating - Re-analysis of NHBC field trial shading data

After the NHBC round robin test, BRE conducted a series of tests using different shading devices. Whilst one test house featured no additional shading, remaining as a control, the other house was used to test shading on each glazed surface, including: external aluminium foil (25/06/2014-06/08/2014), external shading (06/08/2014-28/08/2014) and internally placed aluminium foil (28/08/2014-17/09/2014), figures A.10 - A.11.

As external conditions varied across this period, the experimental design does not allow testing of each device under the same conditions; this would require an additional identical dwelling for each shading strategy tested. Additionally, there were differences between the experimental conditions of each test house during this period. Specifically, the internal experimental set point temperature was raised from $\sim$25 °C proceeding the shading tests, to $\sim$ 30 °C during the testing of the solar shading tests. This will alter the SOLR, reduce any overheating but also increase the predicted HLC_{True}, for example, by increasing stack losses. Similarly, across the period there was a difference between the internal temperatures seen in either test house, with the control approximately 1.5 °C cooler than the shaded dwelling. It is therefore not entirely clear how much of the short-term overheating seen in the control dwelling is negated by the shading and how much by the increased $T_{setpoint}$. The increased temperatures for both dwellings are shown in figure A.9, where it can be seen that the higher internal temperature of the shaded dwelling (B04) may have reduced any periods of solar overheating across this period.

The data from these periods was provided to the researcher as part of the NHBC project and are briefly re-analysed here. Table A.1 shows the results from MLR examining all daily data points from each period. This also includes the mean for all valid 2 week tests that could be analysed within each period, accounting for the different lengths of each interval. The results can be seen in table A.1, with further details of the conditions during testing seen in table A.2.

Table A.1: Estimated *HLC* from periods testing various shading devices. (Field Test: BRE-NOT-FINN-MLR-2w-24h-6agg-S_{GHR})

Dwelling	Test Period	Days	All Data		Mean of 2 Week Tests		All Data		Mean of 2 Week Tests	
			HLC [W/K]	*95% c.i.* [W/K]	*HLC* [W/K]	*95% c.i.* [W/K]	*SA* [m²]	*95% c.i.* [m²]	*SA* [m²]	*95% c.i.* [m²]
B04	*Increased Internal Temp*	9	62	16	-	-	-0.8	0.9	-1.0	0.2
	External Foil	41	59	4	57	4	-0.3	0.3	-0.1	0.5
	External Shading	21	55	7	54	3	-0.5	0.5	-0.4	0.2
	Internal Foil	19	60	6	60	3	-1.2	0.6	-1.2	0.2
B03 - Reference	*Increased Internal Temp*	9	59	5	-	-	-0.2	0.7	-0.4	0.3
	External Foil	41	54	6	51	5	-0.8	0.4	-0.6	0.3
	External Shading	21	43	11	39	7	-0.5	0.7	-0.2	0.3
	Internal Foil	19	58	11	59	3	-1.5	1.0	-1.6	0.5

Table A.2: Corresponding experimental and environmental conditions. (Field Test: BRE-NOT-FINN-MLR-2w-24h-6agg-S_{GHR})

Dwelling	Test Period	Statistics Over Period					
		Mean T_i [°C]	*Mean* T_e [°C]	*Mean Solar* [W/m²]	*Mean Windspeed* [m/s]	*Mean ΔT* [K]	*Mean S/ΔT* [W/m²K]
B04	*Increased Internal Temp*	30.9	13.3	158.8	3.6	17.7	9.0
	External Foil	31.2	16.5	184.2	2.9	14.7	12.5
	External Shading	31.3	18.3	167.4	2.3	13.0	12.9
	Internal Foil	30.4	15.2	155.5	2.7	15.2	10.3
B03 - Reference	*Increased Internal Temp*	29.7	13.3	158.8	3.6	16.4	9.7
	External Foil	30.1	16.5	184.2	2.9	13.6	13.6
	External Shading	30.3	18.3	167.4	2.3	12.0	13.9
	Internal Foil	30.1	15.2	155.5	2.7	14.9	10.4

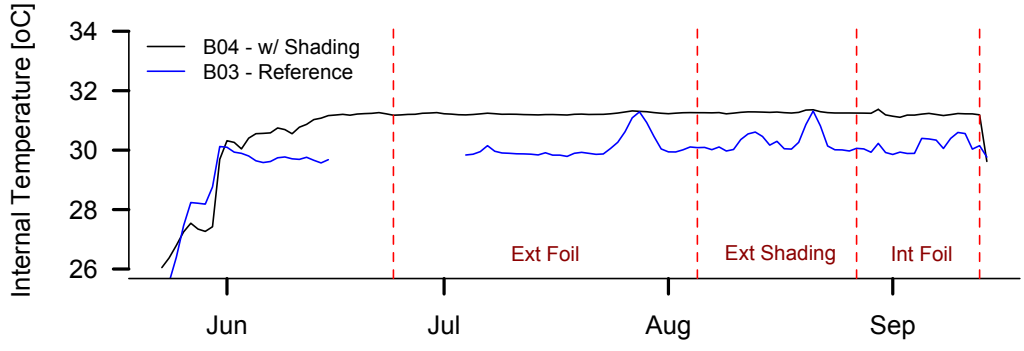

Figure A.9: *Mean internal temperatures during testing of various shading strategies.* (Field Test-BRE)

The measured *HLC* is consistently higher in the shaded dwelling, with the difference between estimates ranging from 2-12 W/K. The lower *HLC* estimates could be associated with the periods of short term overheating and stored solar contributions but may also result from the higher HLC_{True} of the test dwelling, either from its construction or differing internal conditions. The biggest difference seen is between the two dwellings when external cotton shading is used, despite the fact that this is not the sunniest period, although the horizontally measured solar radiation is not an ideal indicator of this.

It is therefore hard to draw conclusive results from this work. Generally, we can conclude that reducing overheating provides better results, but that results during high periods of high solar radiation still are likely to underestimate the *HLC* for further reasons. This work perhaps demonstrates that if sources of uncertainty and variations in protocol are to be investigated experimentally then a full understanding of sources of uncertainty and bias need to be considered and that experimental control needs to be precise. It is hoped that this thesis will help future researchers to design experiments that can provide more conclusive results.

Figure A.10: *Internal foil shading. Courtesy of BRE.*

Figure A.11: *External cotton shading. Courtesy of BRE.*

A.3 Further weather driven sources of uncertainty - Supporting figures & further details

A.3.1 Dynamic T_e

Below is a figure showing the estimated *HLC* resulting from a weather file in which only T_e varies. Both a simple linear regression (SLR) is performed (as there is no solar radiation to use in MLR) and a simple averaging (SA) method are used.

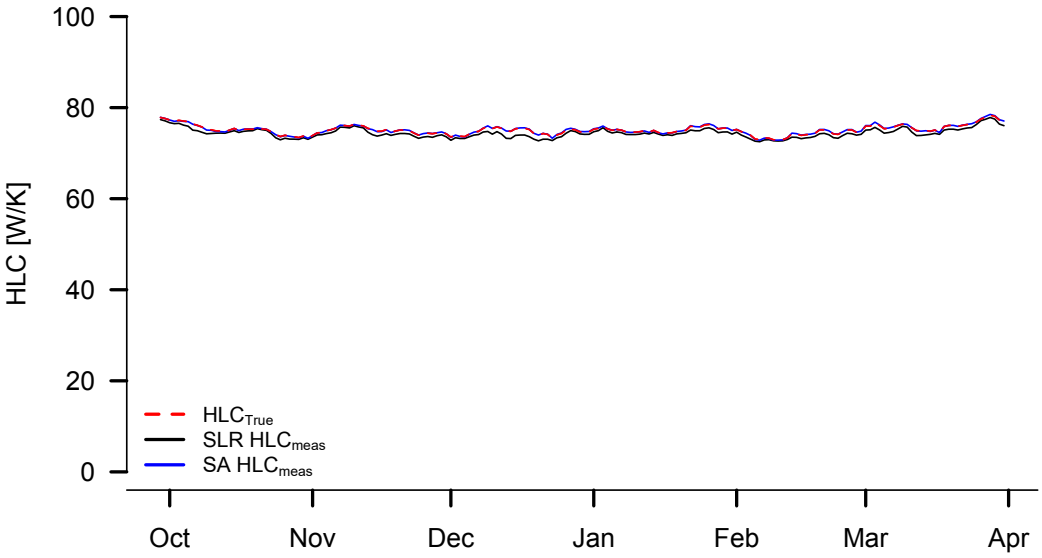

Figure A.12: *Estimated HLC due to dynamic T_e alone. HLC_{meas} for both SLR and SA accurately reflect HLC_{True} across this period with 2 week monitoring durations. It should however be remembered that the dynamic heat flows created by T_e are incorporated into the estimation of HLC_{True}. Nevertheless, little variation due to a dynamic T_e is seen (1 W/K or 1%).* (Simulation: BRE-NOT-MW-FINN.T_e-SN-2w-24h-6agg)

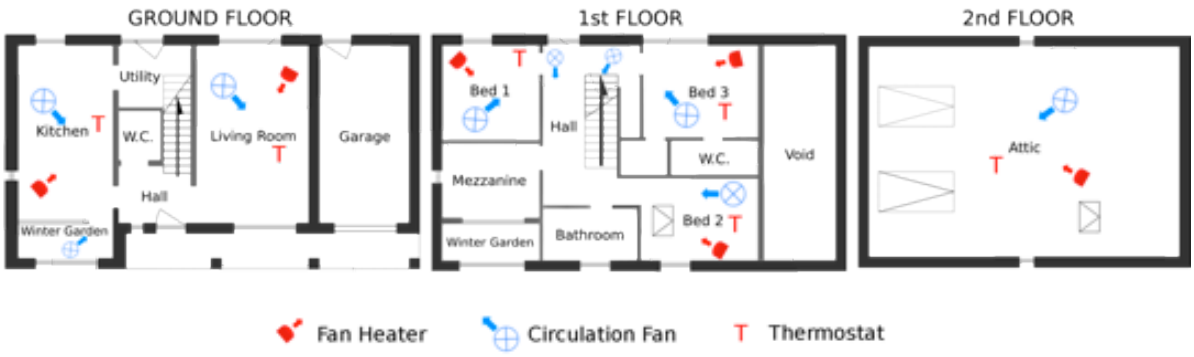

Figure A.13: *Floor plans for CASE-B relating to figure 7.9*

A.4 Experimental sources of uncertainty - Supporting figures

A.4.1 Floor plans for referenced internal temperature distributions in field tests

On the previous page (figure A.13), the floor plans and equipment locations for the internal test profiles in figure 7.9 of the main text are shown.

A.4.2 Equipment measurement errors

This additional plot relates to the modelled sensor error for solar radiation measurements. If the measuring device (pyranometer) features an absolute offset, e.g. +10 W/m^2, then the *HLC* (intercept) is overestimated whilst *R* remains the same as the ideal or zero error case. If the measurement uncertainty is proportional, e.g. 6% across all measurements, then the value of the *HLC* remains the same whilst the value of *R* is biased, see (A.14).

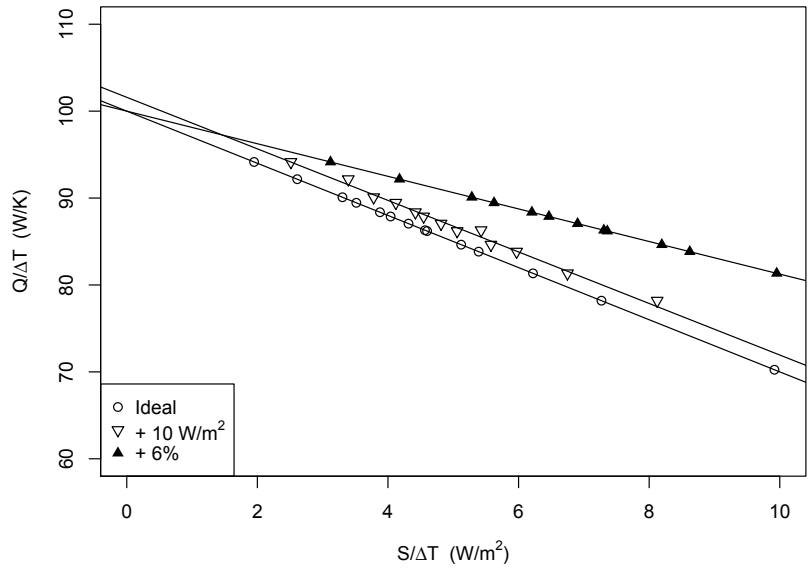

Figure A.14: *Offset and relative errors applied to measured solar radiation. An constant offset alters the HLC but not R, whilst a percentage error alters R but not the HLC.*

A.4.3 Moisture & latent loads: Monitoring RH

The monitored RH for all field tests is shown in figures A.15 and A.16.

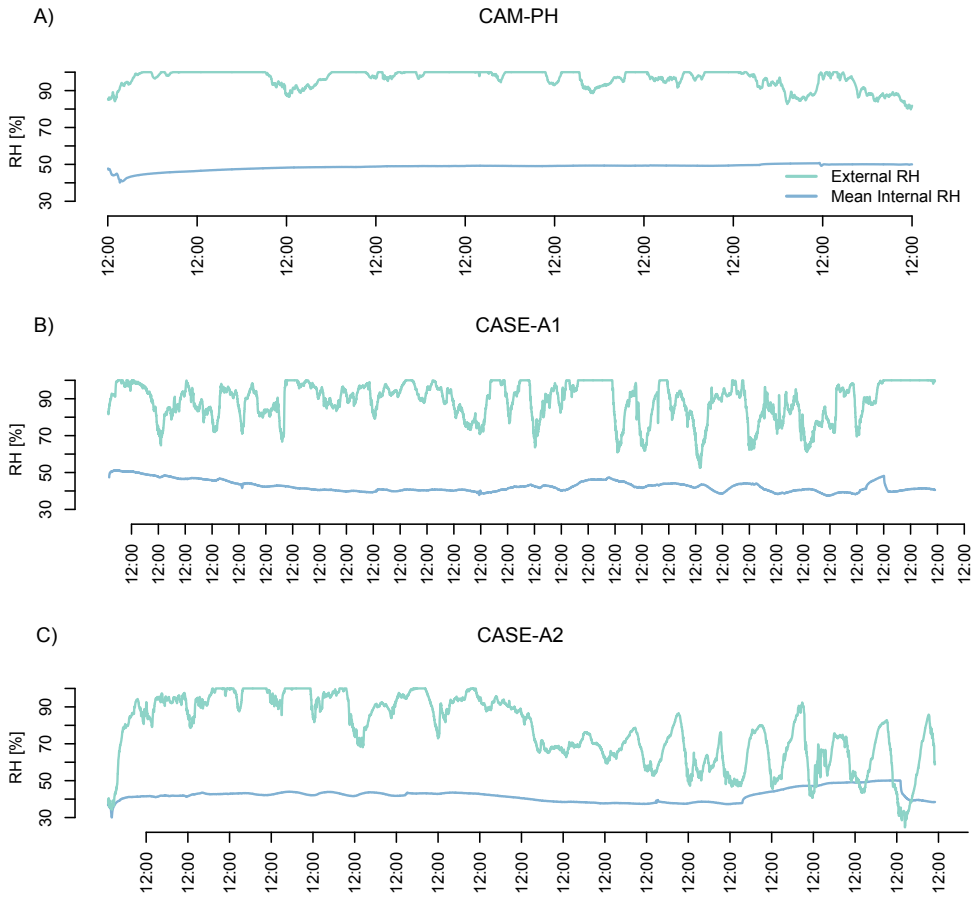

Figure A.15: *Mean internal and external RH for further field test dwellings.*

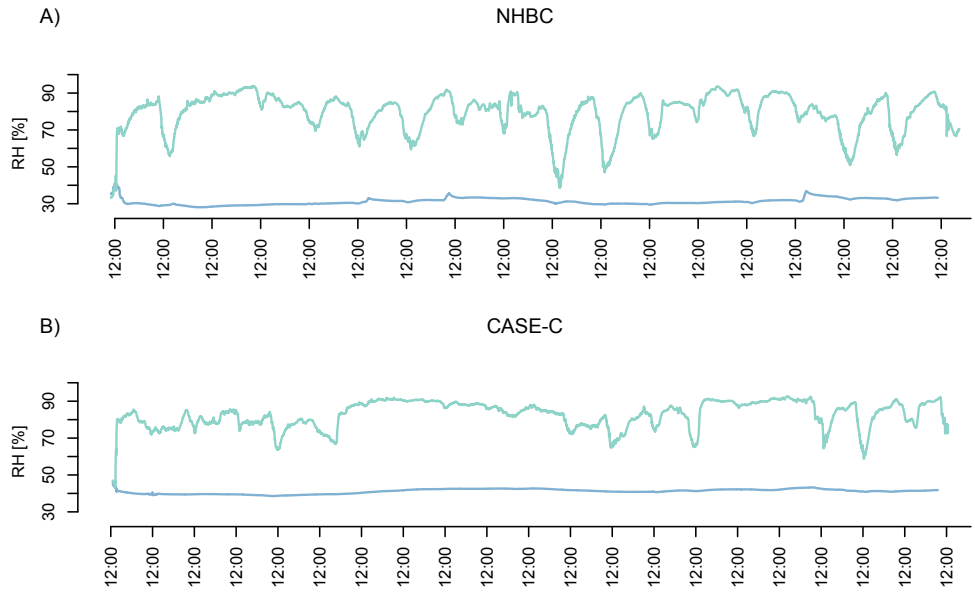

Figure A.16: *Mean internal and external RH for further field test dwellings - part 2.*

A.4.4 Operational Uncertainties

Tables showing the make up of the walls modelled in section 7.7.1 to examine the impact of increased internal temperatures upon the thermal conductivity of a dwelling.

Table A.3: Make up of uninsulated wall used in section 7.7.1.

BRICK - BRICK CAVITY WALL

	Layer	d	k	R	U	%	Cp	Density	Ref
1	Rse	-	-	0.040	25.000	5.7%	-	-	
2	Brick (Exposed)	0.105	0.770	0.136	7.333	19.6%	1000	1750	
3	Airspace	-	-	0.180	5.556	25.8%	800	1700	
4	Brick	0.105	0.560	0.188	5.333	26.9%	-	-	
5	Dense Plaster	0.013	0.570	0.023	43.846	3.3%	1000	1300	
6	-	-	-	-	-	-	-	-	
7	Rsi	-	-	0.130	7.692	18.7%	-	-	
Element		0.223	-	0.527	1.899				
Total				0.697	**1.435**				CIBSE GUIDE A

Table A.4: Make up of insulated wall used in section 7.7.1.

BRICK - BRICK CAVITY WALL - (INSULATED)

	Layer	d	k	R	U	%	Cp	Density	Ref
1	Rse	-	-	0.040	25.000	1.2%	-	-	
2	Brick (Exposed)	0.105	0.770	0.136	7.333	4.1%	1000	1750	
3	UF Foam	0.113	0.040	2.813	0.356	84.5%	1400	10	
4	Brick	0.105	0.560	0.188	5.333	5.6%	1000	1750	
5	Dense Plaster	0.013	0.570	0.023	43.846	0.7%	1000	1300	
6	-	-	-	-	-	-	-	-	
7	Rsi	4.000		0.130	7.692	3.9%	-	-	
Element		0.336	-	3.159	0.317				
Total				3.329	**0.300**				CIBSE GUIDE A

A.5 The Application of Co-heating - Supporting Figures & Further Details

A.5.1 Simulated BRE Test House

Details of the simulated BRE Swedish test house used in figure 9.5 are shown in the tables below. The weather file, is not included for copy write but was purchased from weatheranalytics.com, covering the year of the field test across the BRE Garston site.

A.5.2 Estimating uncertainty in NHBC field test

Tables A.10 and A.11 detail the calculation of the uncertainty in *R* for the NHBC field test, as in section 9.4.7 of the main thesis.

Table A.5: Combined uncertainty in NHBC field test *R* estimates. Sensitivity coefficients calculated in table A.11

Building Data	
Number of zones:	3
Heated/cooled floor area (m^2)	84.7
Volume (m^3)	209.7
External area (m^2)	172.4
Area-weighted average U-value (W/m^2K)	0.38
External surface area/Volume (m^{-1})	0.82

Table A.6: Combined uncertainty in NHBC field test *R* estimates. Sensitivity coefficients calculated in table A.11

	Area (m^2)	**U+Value (W/m^2K)**	**UA (W/K)**
Walls	115.6	0.21	24.3
Floor	42.4	0.19	8.1
Windows	13.0	1.85	24.1
Door	1.4	1.00	1.4
Roof	42.4	0.16	6.8
Ceiling	42.4	0.17	7.4
Walls	14.0	0.21	2.9
Pitched Roof	56.2	0.21	11.9
TOTAL FABRIC			**64.7**
Infiltration		0.57 $m^3/(hm^2)$	2
TOTAL			**66.7**

Table A.7: Ground floor make up.

Element	Adjacent condition	Area-Nett (m2)	Flow path	U-Value (W/K-m2)	U-Value*Area (W/K)	Air temperature (C)	Km (KJ/m2-K	Km*Area (KJ	SROut (m2-K	Orientation (	Slope (deg)	Heavyweight?
Infiltration	Outside	N/A	N/A	N/A	7.175	25	N/A	N/A	N/A	N/A	N/A	FALSE
Ground floor	Ground	42.368	ST - BRE INinsulated Suspended Timber Floor - UV - 0.21 - R	0.191	8.8859	25	0	0	0.01	0	180	TRUE
Ceiling	Block 2 - Zone 1	42.368	SS - Internal Floor Timber_Reversed	1.278	54.1504	25	0	0	0.17	0	0	TRUE
Wall	Outside	14.036	SS - Wall BRE Swedish - As designed UV = 0.21	0.21	2.9472	25	50.752	712.3454	0.04	270	90	TRUE
Wall	Outside	15.656	SS - Wall BRE Swedish - As designed UV = 0.21	0.21	3.2874	25	50.752	794.5643	0.04	180	90	TRUE
Wall	Outside	14.036	SS - Wall BRE Swedish - As designed UV = 0.21	0.21	2.9472	25	50.752	712.3454	0.04	90	90	TRUE
Wall	Outside	13.35	SS - Wall BRE Swedish - As designed UV = 0.21	0.21	2.8032	25	50.752	677.5394	0.04	0	90	TRUE
Door	Outside	1.443	SS - Door - UV=1	1.001	1.4448	25	9.612	13.8723	0.13	0	90	TRUE
Partition	Block 1 - Zone 1	39.011	Partition	3.017	117.7044	25	88.2	3440.7352	0.13	0	0	TRUE
Glazing	Outside	2.835	BRE - Swedish	1.85	5.2448	25	0	0	0.061	180	90	FALSE
Glazing	Outside	3.698	BRE - Swedish	1.85	6.8404	25	0	0	0.061	0	90	FALSE

Table A.8: 2nd floor make up.

Element	Adjacent condition	Area-Nett (m2)	Flow path	U-Value (W/K-m2)	U-Value*Area (W/K)	Air temperature (C)	Km (KJ/m2-K	Km*Area (KJ	SROut (m2-K	Orientation (	Slope (deg)	Heavyweight?
Infiltration	Outside	N/A	N/A	N/A	7.175	25	N/A	N/A	N/A	N/A	N/A	FALSE
Floor	Block 1 - Zone 1	42.368	SS - Internal Floor Timber	1.278	54.1504	25	18	762.624	0.1	0	0	TRUE
Ceiling	Block 4 - Zone 1	42.368	SS - BRE Swedish Flat Roof - As Designed - UV=0.174 - 0.16	0.17	7.2143	25	7.1	300.8128	0.17	0	0	TRUE
Wall	Outside	14.036	SS - Wall BRE Swedish - As designed UV = 0.21	0.21	2.9472	25	50.752	712.3454	0.04	270	90	TRUE
Wall	Outside	15.656	SS - Wall BRE Swedish - As designed UV = 0.21	0.21	3.2874	25	50.752	794.5643	0.04	180	90	TRUE
Wall	Outside	14.036	SS - Wall BRE Swedish - As designed UV = 0.21	0.21	2.9472	25	50.752	712.3454	0.04	90	90	TRUE
Wall	Outside	14.816	SS - Wall BRE Swedish - As designed UV = 0.21	0.21	3.111	25	50.752	751.9322	0.04	0	90	TRUE
Partition	Block 2 - Zone 1	85.496	Partition	3.017	257.9633	25	88.2	7540.7828	0.13	0	0	TRUE
Glazing	Outside	2.835	BRE - Swedish	1.85	5.2448	25	0	0	0.061	180	90	FALSE
Glazing	Outside	3.675	BRE - Swedish	1.85	6.7987	25	0	0	0.061	0	90	FALSE

Table A.9: Unheated attic make up.

Element	Adjacent condition	Area-Nett (m2)	Flow path	U-Value (W/K-m2)	U-Value*Area (W/K)	Air temperature (C)	Km (KJ/m2-K	Km*Area (KJ	SROut (m2-K	Orientation (	Slope (deg)	Heavyweight?
Infiltration	Outside	N/A	N/A	N/A	7.751	1.1035	N/A	N/A	N/A	N/A	N/A	FALSE
Floor	Block 2 - Zone 1	42.368	SS - BRE Swedish Flat Roof - As Designed - UV=0.174 - 0.16	0.17	7.2143	1.1035	17.877	757.4128	0.1	0	0	TRUE
Wall	Outside	7.018	SS - Wall BRE Swedish - As designed UV = 0.21	0.21	1.4736	1.1035	50.752	356.1752	0.04	90	90	TRUE
Roof	Outside	28.119	Pitched roof - Energy code standard - Medium weight (data	0.211	5.9337	1.1035	6.412	180.2865	0.04	0	41.12	TRUE
Wall	Outside	7.018	SS - Wall BRE Swedish - As designed UV = 0.21	0.21	1.4736	1.1035	50.752	356.1752	0.04	270	90	TRUE
Roof	Outside	28.119	Pitched roof - Energy code standard - Medium weight (data	0.211	5.9337	1.1035	6.412	180.2865	0.04	180	41.12	TRUE

Table A.10: Combined uncertainty in NHBC field test *R* estimates. Sensitivity coefficients calculated in table A.11

Input Quantity / Parameter of Uncertainty	Nominal Value	Expanded Uncertainty or limit relative	Expanded Uncertainty or limit absolute	Probability Distribution	Divisor	Standard Uncertainty	Sensitivity Coefficient	Contribution to Uncertainty	Correlated group contribution	Contribution Squared	Rank
	x_j	$U^*(x_j)$	$U(x_j)$		k	$u(x_j)$	$c(x_j)$	$u(x_j).c(x_j)$	$u(x_1).c(x_1)+u(x2).c(x2)...$	$(u(x_j).c(xj))^2$	
Ti	25.20	1.4%	0.36	Normal	2.00	0.18	0.1555	0.03		0.0008	*4*
Te	4.77	19.2%	0.92	Normal	2.00	0.46	-0.1193	-0.05		0.0030	*2*
Q	1236.56	2.5%	30.91	Normal	2.00	15.46	-0.0020	-0.03		0.0009	*3*
S	75.62	6.0%	4.54	Normal	2.00	4.54	0.0356	0.16		0.0260	*1*
		$U^*(y_j)$	$U(y_j)$			u(y)				$\sum(u(x_j).c(xj))^2$	
R	**2.64**	**14.5%**	**0.38**		**2**	**0.18**				**0.0308**	

Table A.11: NHBC *R* Sensitivity coefficients

Input Quantity	Nominal Value	Expanded Uncertainty or limit relative	Expanded Uncertainty or limit absolute	x+Δx	x-Δx	Ynominal	Y +: (x + Δx)	Y -: (x - Δx)	c	c*
	xj		*Δx*			*R*			*(y1+-y1-)/2Δx1*	*c1x1/ynorm*
Ti	25.20	1.4%	0.18	25.38	25.02	-2.64	-2.62	-2.67	0.1555	-5.89%
Te	4.77	19.2%	0.46	5.23	4.31	-2.64	-2.70	-2.59	-0.1193	4.52%
Q	1236.56	2.5%	15.46	1252.02	1221.10	-2.64	-2.67	-2.61	-0.0020	0.07%
S	75.622	6.0%	4.54	80.16	71.08	-2.64	-2.49	-2.81	0.0356	-1.35%

A.5.3 Estimating Uncertainty in CASE-A1 Field Test

Following are tables detailing the calculation of the uncertainty in R for the CASE-A1 field test, featuring party wall heat transfer, as in section 9.4.7.2 of the main thesis. Uncertainty estimates for each parameter can be found in tables A.12 to A.17 with the uncertainty in *HLC* calculated in table A.18 and R in table A.19. Sensitivity coefficients for *HLC* and R can be found in tables A.20 and A.21 respectively.

Table A.12: CASE-A1 Estimated uncertainty in T_i

Input Quantity / Parameter of Uncertainty	Nominal Value	Expanded Uncertainty or limit relative	Expanded Uncertainty or limit absolute	Probability Distribution	Divisor	Standard Uncertainty	Sensitivity Coefficient	Contribution to Uncertainty	Correlated group contribution	Contribution Squared	Rank
	x_j	$U^*(x_j)$	$U(x_j)$		k	$u(x_j)$	$c(x_j)$	$u(x_j).c(x_j)$	$u(x_1).c(x_1)+u(x2).c(x2)...$	$(u(x_j).c(xj))^2$	
T_i Spatial	23.93	-	-	Normal	2	0.946	1	0.9460	-	0.8949	*1*
T_i Calibration	23.93	-	-	Normal	2	0.085	1	0.0800	-	0.0064	*2*
T_i Sampling	23.93	-	-	Normal	2	0.012	1	0.0123	-	0.0002	*3*
T_i Resolution	23.93	-	-	Rectangular	1.732	0.000	1	0.0002	-	0.0000	*4*
		$U^*(y_j)$	$U(y_j)$			u(y)				$\sum(u(x_j).c(xj))^2$	
T_i	**23.93**	**7.9%**	**1.899**	**Normal**	**2**	**0.949**				**0.9014**	

Table A.13: CASE-A1 Estimated uncertainty in T_e

Input Quantity / Parameter of Uncertainty	Nominal Value	Expanded Uncertainty or limit relative	Expanded Uncertainty or limit absolute	Probability Distribution	Divisor	Standard Uncertainty	Sensitivity Coefficient	Contribution to Uncertainty	Correlated group contribution	Contribution Squared	Rank
	x_j	$U^*(x_j)$	$U(x_j)$		k	$u(x_j)$	$c(x_j)$	$u(x_j).c(x_j)$	$u(x_1).c(x_1)+u(x2).c(x2)...$	$(u(x_j).c(xj))^2$	
T_e Spatial	3.76	-	-	**Normal**	2	0.346	1	0.3462	-	0.1198	2
T_e Calibration	3.76	-	-	Normal	2	0.424	1	0.4243	-	0.1800	*1*
T_e Sampling	3.76	-	-	Normal	2	0.058	1	0.0577	-	0.0033	*3*
T_e Resolution	3.76	-	-	Rectangular	1.732	0.000	1	0.0002	-	0.0000	*4*
		$U^*(y_j)$	$U(y_j)$			u(y)				$\sum(u(x_j).c(xj))^2$	
Te	**3.76**	**29.3%**	**1.101**	**Normal**	**2**	**0.551**				**0.3032**	

Table A.14: CASE-A1 Estimated uncertainty in ΔT

Input Quantity / Parameter of Uncertainty	Nominal Value	Expanded Uncertainty or limit relative	Expanded Uncertainty or limit absolute	Probability Distribution	Divisor	Standard Uncertainty	Sensitivity Coefficient	Contribution to Uncertainty	Correlated group contribution	Contribution Squared	Rank
	x_j	$U^*(x_j)$	$U(x_j)$		k	$u(x_j)$	$c(x_j)$	$u(x_j).c(x_j)$	$u(x_1).c(x_1)+u(x2).c(x2)...$	$(u(x_j).c(xj))^2$	
Ti	23.93	7.9%	1.899	Normal	2	0.949	1	0.949	-	0.901	*2*
Te	3.76	29.3%	1.101	Normal	2	0.551	1	0.551	-	0.303	*1*
		$U^*(y_j)$	$U(y_j)$			u(y)				$\sum(u(x_j).c(xj))^2$	
ΔT	**20.17**	**10.9%**	**2.195**		**2**	**1.098**				**1.205**	

Table A.15: CASE-A1 Estimated uncertainty in Q_{adj}

Input Quantity / Parameter of Uncertainty	Nominal Value	Expanded Uncertainty or limit relative	Expanded Uncertainty or limit absolute	Probability Distribution	Divisor	Standard Uncertainty	Sensitivity Coefficient	Contribution to Uncertainty	Correlated group contribution	Contribution Squared	Rank
	x_j	$U^*(x_j)$	$U(x_j)$		k	$u(x_j)$	$c(x_j)$	$u(x_j).c(x_j)$	$u(x_1).c(x_1)+u(x2).c(x2)...$	$(u(x_j).c(xj))^2$	
q_{adj} Sensors	3.23	14.00%	0.45	Normal	1	0.45	-	-	-	-	
q_{adj} Variation	3.23	41.20%	1.33	Normal	2	0.67	-	-	-	-	
q_{adj} Total	3.23	49.83%	1.61	Normal	2	0.80	66.4	53.44	-	2855.34	*1*
Party Wall Area	66.40	10.00%	6.64	Normal	2	3.32	3.23	10.72	-	115.00	*2*
		$U^*(y_j)$	$U(y_j)$			u(y)				$\sum(u(x_j).c(xj))^2$	
Q_{adj}	**214.71**	**50.8%**	**109.00**	**Normal**	**2**	**54.50**				**2970.34**	

Table A.16: CASE-A1 Estimated uncertainty in Q_{elec}

Input Quantity / Parameter of Uncertainty	Nominal Value	Expanded Uncertainty or limit relative	Expanded Uncertainty or limit absolute	Probability Distribution	Divisor	Standard Uncertainty	Sensitivity Coefficient	Contribution to Uncertainty	Correlated group contribution	Contribution Squared	Rank
	x_j	$U^*(x_j)$	$U(x_j)$		k	$u(x_j)$	$c(x_j)$	$u(x_j).c(x_j)$	$u(x_1).c(x_1)+u(x2).c(x2)...$	$(u(x_j).c(xj))^2$	
Q_Calibration	4912.08	-	-	Normal	2	50.19	1	50.19	-	2518.90	*1*
Q_Resolution	4912.08	-	-	Rectangular	1.732	6.93	1	6.93	-	48.00	*2*
		$U^*(y_j)$	$U(y_j)$			u(y)				$\sum(u(x_j).c(xj))^2$	
Q	**4912.08**	**2.1%**	**101.33**	**Normal**	**2**	**50.66**				**2566.90**	

Table A.17: CASE-A1 Estimated uncertainty in S

Input Quantity / Parameter of Uncertainty	Nominal Value	Expanded Uncertainty or limit relative	Expanded Uncertainty or limit absolute	Probability Distribution	Divisor	Standard Uncertainty	Sensitivity Coefficient	Contribution to Uncertainty	Correlated group contribution	Contribution Squared	Rank
	x_j	$U^*(x_j)$	$U(x_j)$		k	$u(x_j)$	$c(x_j)$	$u(x_j).c(x_j)$	$u(x_1).c(x_1)+u(x2).c(x2)...$	$(u(x_j).c(xj))^2$	
S_Calibration	37.28	6.00%	2.24	Normal	1	2.24	1	2.24	-	5.00	*1*
S_Resolution	37.28	-	-	Rectangular	1	0.00	1	0.00	-	0.0000082944	*2*
		$U^*(y_j)$	$U(y_j)$			u(y)				$\sum(u(x_j).c(xj))^2$	
S	**37.28**	**12.0%**	**4.47**	**Normal**	**2**	**2.24**				**5.00**	

Table A.18: CASE-A1 *HLC* uncertainty estimate

Input Quantity / Parameter of	Nominal Value	Expanded Relative Uncertainty	Expanded Absolute Uncertainty	Probability Distribution	Divisor	Standard Uncertainty	Sensitivity Coefficient	Contribution to Uncertainty	Correlated group contribution	Contribution Squared	Rank
	x_j	$U^*(x_j)$	$U(x_j)$		k	$u(x_j)$	$c(x_j)$	$u(x_j).c(x_j)$	$u(x_1).c(x_1)+u(x2).c(x2)...$	$(u(x_j).c(xj))^2$	
T_i	23.93	7.9%	1.90	Normal	2	0.949	-3.979	-3.778	-	14.271773	*2*
T_e	3.76	29.3%	1.10	Normal	2	0.551	9.703	5.342	-	28.541	*1*
Q	4912.08	2.5%	122.80	Normal	2	50.665	0.050	2.541	-	6.455	*3*
Qadj	214.71	50.8%	109.00	Normal	2	54.501	-0.026	-1.440	-	2.074	*4*
S	37.28	6.0%	2.24	Normal	2	2.237	0.000	0.000	-	0.000	5
		$U^*(y_j)$	$U(y_j)$			$u(y)$				$\sum(u(x_j).c(xj))^2$	
HLC	**242.00**	**5.9%**	**14.33**		**2**	**7.165**				**51.342**	

Table A.19: CASE-A1 *R* uncertainty estimate

Input Quantity / Parameter of Uncertainty	Nominal Value	Expanded Uncertainty or limit relative	Expanded Uncertainty or limit absolute	Probability Distribution	Divisor	Standard Uncertainty	Sensitivity Coefficient	Contribution to Uncertainty	Correlated group contribution	Contribution Squared	Rank
	x_j	$U^*(x_j)$	$U(x_j)$		k	$u(x_j)$	$c(x_j)$	$u(x_j).c(x_j)$	$u(x_1).c(x_1)+u(x2).c(x2)...$	$(u(x_j).c(xj))^2$	
Ti	23.93	7.9%	1.90	Normal	2.00	0.95	0.964791	0.92		0.83906	*2*
Te	3.76	29.3%	1.10	Normal	2.00	0.55	-3.857496	-2.12		4.51099	*1*
Q	4912.08	2.5%	122.80	Normal	2.00	50.66	-0.000582	-0.03		0.00087	*5*
Qadj	214.71	50.8%	109.00	Normal	2.00	54.50	-0.008755	-0.48		0.22767	*3*
S	37.28	6.0%	2.24	Normal	2.00	2.24	0.150214	0.34		0.11290	*4*
		$U^*(y_j)$	$U(y_j)$			$u(y)$				$\sum(u(x_j).c(xj))^2$	
R	**-5.58**	**-85.5%**	**4.77**		**2**	**2.39**				**5.69149**	

Table A.20: CASE-A1 *HLC* Sensitivity Coefficients

Input Quantity	Nominal Value	Expanded Uncertainty or limit relative	Expanded Uncertainty or limit absolute	x+Δx	x-Δx	Ynominal	Y +: (x + Δx)	Y -: (x - Δx)	c	c*
	xj		*Δx*			*HLC*			*(y1+-y1-)/2Δx1*	*c1x1/ynorm*
Ti	23.93	7.9%	0.95	24.88	22.98	242.00	238.21	245.77	-3.9790	-1.64%
Te	3.76	29.3%	0.55	4.31	3.21	242.00	247.45	236.76	9.7030	4.01%
Q	4912.08	2.5%	50.66	4962.74	4861.42	242.00	244.54	239.46	0.0501	0.02%
Qadj	214.71	50.8%	54.50	269.21	160.21	242.00	240.56	243.44	-0.0264	-0.01%
S	37.28	6.0%	2.24	39.52	35.04	242.00	242.00	242.00	0.0000	0.00%

Table A.21: CASE-A1 *R* Sensitivity Coefficients

Input Quantity	Nominal Value	Expanded Uncertainty or limit relative	Expanded Uncertainty or limit absolute	x+Δx	x-Δx	Ynominal	Y +: (x + Δx)	Y -: (x - Δx)	c	c*
	xj		*Δx*			*R*			*(y1+-y1-)/2Δx1*	*c1x1/ynorm*
Ti	23.93	7.9%	0.95	24.88	22.98	-5.58	-4.64	-6.47	0.9648	-17.29%
Te	3.76	29.3%	0.55	4.31	3.21	-5.58	-7.64	-3.40	-3.8575	69.13%
Q	4912.08	2.5%	50.66	4962.74	4861.42	-5.58	-5.61	-5.55	-0.0006	0.01%
Qadj	214.71	50.8%	54.50	269.21	160.21	-5.58	-6.06	-5.10	-0.0088	0.16%
S	37.28	6.0%	2.24	39.52	35.04	-5.58	-5.26	-5.94	0.1502	-2.69%

A.5.4 Estimating uncertainty in HLC_{pred}

Following are tables detailing the calculation of the uncertainty in HLC_{pred}, section 9.5.1.1, according the the GUM procedure, using some nominal uncertainties.

Table A.22: Uncertainty in Thermal Resistance of Components.

Input Quantity	Nominal Value	Expanded Uncertainty or limit relative	Expanded Uncertainty or limit absolute	Probability Distribution	Divisor	Standard Uncertainty	Sensitivity Coefficient	Contribution to Uncertainty	Correlated group contribution	Contribution Squared	Rank
	xj				k	uxj or U*xj	cxj or c*xj	uxi . Cxi		(uxj . Cxj) 2	
External Brick, R	**0.157**	**5.4%**	**0.00846**	**Normal**	**2**	**0.00423**	**1.00000**			**0.00002**	
Thermal Conductivity, k	0.670	5.0%	0.03350	Normal	2	0.01675	-0.23449	-0.00393		0.00002	1
Thickness, d	0.105	2.0%	0.00210	Normal	2	0.00105	1.49254	0.00157		0.00000	2
Blown Mineral Wool Fibre, R	**2.500**	**10.3%**	**0.25743**	**Normal**	**2**	**0.12871**	**1.00000**			**0.01657**	
Thermal Conductivity, k	0.040	10.0%	0.00400	Normal	2	0.00200	-63.13131	-0.12626		0.01594	1
Thickness, d	0.100	2.0%	0.00200	Normal	2	0.00100	25.00000	0.02500		0.00063	2
Lighweight Aggregate Block, R	**0.525**	**5.4%**	**0.02833**	**Normal**	**2**	**0.01417**	**1.00000**			**0.00020**	
Thermal Conductivity, k	0.200	5.0%	0.01000	Normal	2	0.00500	-2.63158	-0.01316		0.00017	1
Thickness, d	0.105	2.0%	0.00210	Normal	2	0.00105	5.00000	0.00525		0.00003	2
Plaster, R	**0.062**	**11.2%**	**0.00692**	**Normal**	**2**	**0.00346**	**1.00000**			**0.00001**	
Thermal Conductivity, k	0.210	5.0%	0.01050	Normal	2	0.00525	-0.29552	-0.00155		0.00000	2
Thickness, d	0.013	10.0%	0.00130	Normal	2	0.00065	4.76190	0.00310		0.00001	1

Table A.23: Uncertainty in Wall U-value.

Input Quantity	Nominal Value	Expanded Uncertainty or limit relative	Expanded Uncertainty or limit absolute	Probability Distribution	Divisor	Standard Uncertainty	Sensitivity Coefficient	Contribution to Uncertainty	Correlated group contribution	Contribution Squared	Rank
	xj				k	uxj or U*xj	cxj or c*xj	uxi . Cxi		(uxj . Cxj) 2	
External Brick, R	0.157	5.4%	0.008	Normal	2	0.004	1.000	0.004		0.000018	4
Blown Mineral Wool Fibre, R	2.500	10.3%	0.257	Normal	2	0.129	1.000	0.129		0.016567	1
Lighweight Aggregate Block, R	0.525	5.4%	0.028	Normal	2	0.014	1.000	0.014		0.000201	2
Plaster, R	0.062	11.2%	0.007	Normal	2	0.003	1.000	0.003		0.000012	5
Internal Surface Resistance	0.130	10.0%	0.013	Normal	2	0.007	1.000	0.007		0.000042	3
External Surface Resistance	0.040	10.0%	0.004	Normal	2	0.002	1.000	0.002		0.000004	6
Wall R-Value	**3.414**	**6.5%**	**0.221**	**Normal**	**2**	**0.130**				**0.0168**	
Wall U-Value	**0.293**	**6.5%**	**0.019**	**Normal**	**2**						

Table A.24: Uncertainty in building elements.

Input Quantity	Nominal Value	Expanded Uncertainty or limit relative	Expanded Uncertainty or limit absolute	Probability Distribution	Divisor	Standard Uncertainty	Sensitivity Coefficient	Contribution to Uncertainty	Correlated group contribution	Contribution Squared	Rank
	xj				k	uxj or U*xj	cxj or c*xj	uxi . Cxi		(uxj . Cxj) 2	
Wall UA	**24.41**	**6.6%**	**1.61**	**Normal**	**2**	**0.80**				**0.64**	**1**
Wall U	0.21	6.5%	0.01	Normal	2	0.01	116.24	0.79		0.63	(1)
Wall A	116.24	1.0%	1.16	Normal	2	0.58	0.21	0.12		0.01	(2)
Roof UA	**6.71**	**5.1%**	**0.34**	**Normal**	**2**	**0.17**				**0.03**	**4**
Roof U	0.16	5.0%	0.01	Normal	2	0.00	41.96	0.17		0.03	(1)
Roof A	41.96	1.0%	0.42	Normal	2	0.21	0.16	0.03		0.00	(2)
Window UA	**24.27**	**5.1%**	**1.24**	**Normal**	**2**	**0.62**				**0.38**	**2**
Window U	1.85	5.0%	0.09	Normal	2	0.05	13.12	0.61		0.37	(1)
Window A	13.12	1.0%	0.13	Normal	2	0.07	1.85	0.12		0.01	(2)
Floor UA	**8.81**	**5.1%**	**0.45**	**Normal**	**2**	**0.22**				**0.05**	**3**
Floor U	0.21	5.0%	0.01	Normal	2	0.01	41.96	0.22		0.05	(1)
Floor A	41.96	1.0%	0.42	Normal	2	0.21	0.21	0.04		0.00	(2)
Door UA	**1.44**	**5.1%**	**0.07**	**Normal**	**2**	**0.04**				**0.00**	**5**
Door U	1.00	5.0%	0.05	Normal	2	0.03	1.44	0.04		0.00	(1)
Door A	1.44	1.0%	0.01	Normal	2	0.01	1.00	0.01		0.00	(2)
TOTAL HLC_{UA}	**65.65**										
		*U*c(y)*	*Expanded Uncertainty Uc(y)*			*Uncertainty uc(y)*				*sum (uxj.cxj)^2*	
TOTAL HLC_{UA}	**65.65**	**3.2%**	**2.11**	**Normal**	**2**	**1.05**				**1.11**	

Table A.25: Uncertainty in HLC_{UA}

Input Quantity	Nominal Value	Expanded Uncertainty or limit relative	Expanded Uncertainty or limit absolute	Probability Distribution	Divisor	Standard Uncertainty	Sensitivity Coefficient	Contribution to Uncertainty	Correlated group contribution	Contribution Squared	Rank
	xj				k	uxj or U*xj	cxj or c*xj	uxi . Cxi		(uxj . Cxj) 2	
Wall UA	24.41	6.58%	1.61	Normal	2	0.80	1	0.80		0.644	1
Roof UA	6.7136	5.10%	0.34	Normal	2	0.17	1	0.17		0.029	4
Window UA	24.272	5.10%	1.24	Normal	2	0.62	1	0.62		0.383	2
Floor UA	8.8116	5.10%	0.45	Normal	2	0.22	1	0.22		0.050	3
Door UA	1.44	5.10%	0.07	Normal	2	0.04	1	0.04		0.001	5
		*U*c(y)*	*Expanded Uncertainty Uc(y)*			*Uncertainty uc(y)*				*sum (uxj.cxj)^2*	
TOTAL HLC_{Fabric}	**65.65**	**3.2%**	**2.11**	**Normal**	**2**	**1.05**				**1.108**	

Table A.26: Uncertainty in thermal bridging calculations.

Input Quantity	Nominal Value	Expanded Uncertainty or limit relative	Expanded Uncertainty or limit absolute	Probability Distribution	Divisor	Standard Uncertainty	Sensitivity Coefficient	Contribution to Uncertainty	Correlated group contribution	Contribution Squared	Rank
	xj				k	uxj or U*xj	cxj or c*xj	uxi . Cxi		(uxj . Cxj) 2	
Y	0.15	50.00%	0.075	Normal	2	0.038	301.560	11.309		127.882	1
Envelope Area	301.56	2.00%	6.031	Normal	2	3.016	0.150	0.452		0.205	2
Thermal Bridges W/K	45.23	50.04%	22.635	Normal	2	11.318				128.087	

Table A.27: Uncertainty in air change rate calculated from pressure test.

Input Quantity	Nominal Value	Expanded Uncertainty or limit relative	Expanded Uncertainty or limit absolute	Probability Distribution	Divisor	Standard Uncertainty	Sensitivity Coefficient	Contribution to Uncertainty	Correlated group contribution	Contribution Squared	Rank
	xj				k	uxj or U*xj	cxj or c*xj	uxi . Cxi		(uxj . Cxj) 2	
Air Permeability	5.10	10.0%	0.51	Normal	2	0.255	0.050	0.013		0.000	
Conversion Factor = 20	20.00	50.0%	10.00	Normal	2	5.000	-0.017	-0.085		0.007	
n/20	**0.26**	**67.4%**	**0.17**		**2**	**0.086**				**0.007**	

Table A.28: Uncertainty in HLC_{inf}.

Input Quantity	Nominal Value	Expanded Uncertainty or limit relative	Expanded Uncertainty or limit absolute	Probability Distribution	Divisor	Standard Uncertainty	Sensitivity Coefficient	Contribution to Uncertainty	Correlated group contribution	Contribution Squared	Rank
	xj				k	uxj or U*xj	cxj or c*xj	uxi . Cxi		(uxj . Cxj) 2	
C_p*ρ_{air}	0.34	2.6%	0.009	Normal	2	0.004	53.499	0.240		0.058	(3)
Volume	209.80	5.0%	10.490	Normal	2	5.245	0.087	0.458		0.210	(2)
n/20	0.26	67.4%	0.172	Normal	2	0.086	71.819	6.173		38.104	(1)
HLC_{inf} = Cp*ρair*n*V	**18.31**	**67.6%**	**12.389**	**Normal**	**2**	**6.194**	**0.925**			**38.372**	**2**
Shelter	0.93	10.0%	0.093	Normal	2	0.046	18.314	0.847		0.717	4
Wind Speed	4.00	20.0%	0.800	Normal	2	0.400	16.940	6.776		45.915	1
Wind Factor	1.00	20.0%	0.200	Normal	2	0.100	16.940	1.694		2.870	3
Adjusted HLC_{inf} (W/K)	**16.94**	**76.5%**	**12.955**	**Normal**	**2**	**6.478**				**41.959**	

Table A.29: Uncertainty in HLC_{pred}.

Input Quantity	Nominal Value	Expanded Uncertainty or limit relative	Expanded Uncertainty or limit absolute	Probability Distribution	Divisor	Standard Uncertainty	Sensitivity Coefficient	Contribution to Uncertainty	Correlated group contribution	Contribution Squared	Rank
	xj				k	uxj or U*xj	cxj or c*xj	uxi . Cxi		(uxj . Cxj) 2	
TOTAL HLC_{UA} (W/K)	65.65	3.21%	2.11	Normal	2	1.05	1	1.05		1.11	3
Thermal Bridges (W/K)	45.23	50.04%	22.64	Normal	2	11.32	1	11.32		128.09	1
Adjusted HLC_{Inf} (W/K)	16.94	76.48%	12.96	Normal	2	6.48	1	6.48		41.96	2
TOTAL	**127.82**	**20.47%**	**26.17**	Normal	2	13.08				171.15	

Appendix B

Heat Loss Theory & Modelling

Providing further depth to the definition of the heat loss coefficient, mechanisms of heat transfer and the EnergyPlus modelling of heat losses, the following are considered in this section of the appendix:

- B.1 Transmission heat transfer coefficient.
- B.2 Infiltration heat transfer.
- B.3 Long wave radiation & the effective sky temperature.
- B.4 Solar radiation.

B.1 The transmission heat transfer coefficient

B.1.1 ISO definition of the transmission heat transfer coefficient

The transmission heat loss coefficient, HLC_{trans}, can be defined, as within the main thesis (section 3.1) as:

$$HLC_{trans} + HLC_d + HLC_g + HLC_{unc} + HLC_{adj} \tag{B.1}$$

Further depth is added to each of these four components, based on the ISO 13790:2008 (ISO, 2008) descriptions in the following sections:

- Direct conductive losses, HLC_d. (Section B.1.1.1)
- Heat transfer through the ground, HLC_g. (Section B.1.1.2)
- Heat transfer through unconditioned spaces, HLC_{unc}. (Section B.1.1.4)
- Heat transfer through adjoining spaces, HLC_{adj}. (Section B.1.1.5)

B.1.1.1 Direct conductive losses, HLC_d

The direct heat transfer is then calculated from summing over the building U-values and thermal bridges.

$$HLC_d = \sum_i A_i \cdot U_i + \sum_k l_k \cdot \Psi_k + \sum_j \chi_j \tag{B.2}$$

Where:

A_i is the area of element *i*, in m^2.

U_i is the thermal transmittance, or U-value, of element i, in W/m^2.

l_k is the length of linear thermal bridge *k*, in m.

Ψ is the linear thermal transmittance of thermal bridge *k* in W/mK (ISO 14683:2007; ISO 10211:2007)

χ_j is the point thermal transmittance of point thermal bridge *j*, in W/K (ISO 10211:2007)

B.1.1.2 Heat transfer through the ground, HLC_g

The steady state ground heat transfer coefficient is described in ISO 13370 as:

$$HLC_g = A_g \cdot U_g + P \cdot \Psi_g \tag{B.3}$$

Where:

Ψ_g (W/mK) is the linear thermal transmittance associated with the wall and junction and

P (m) is the exposed perimeter of the floor.

To allow for the three-dimensional nature of heat flow to the ground, a characteristic dimension is incorporated into heat loss equations and terms are also introduced to consider the thermal resistance of the ground. To estimate the heat flow rate on a seasonal or monthly basis, additional periodic components are then required to account for the thermal inertia of the ground. The method adopted in this thesis uses known mean monthly internal and external temperatures to determine the monthly heat flow rate (ISO 13370:2007, A.4):

$$Q_g, m = HLC_g(\bar{T_i} - \bar{T_e}) - H_{pi}(\bar{T_i} - T_{i,m}) + H_{pe}(\bar{T_e} - T_{e,m}) \tag{B.4}$$

Where $\bar{T_e}$ and $\bar{T_i}$ are the annual average external and internal temperatures, $T_{e,m}$ and $T_{e,m}$ are the monthly mean external and internal temperatures for month m.

H_{pi} is the internal periodic heat transfer coefficient (W/K), defined by:

$$H_{pi} = A\frac{\lambda}{d_t}\sqrt{\frac{2}{(1+\frac{\delta}{d_t})^2+1}} \tag{B.5}$$

H_{pe} is the external periodic heat transfer coefficient (W/K).

$$H_{pe} = 0.37 \cdot P\lambda \ln\frac{\delta}{d_t} + 1 \tag{B.6}$$

Where λ is the thermal conductivity of the ground, d_t is the total equivalent thickness of the ground and δ is the periodic penetration depth of the slab.

B.1.1.3 EnergyPlus Treatment of Ground Losses

Ground losses in EnergyPlus were modelled simply by monthly ground temperatures, T_g, and the heat loss coefficient of the ground, determined by its U.A value. Therefore, monthly ground temperatures were determined such that the heat flow through the ground floor match that defined in equation B.4.

B.1.1.4 Heat transfer through unconditioned spaces, HLC_{unc}

Many building constructions will feature heat flow paths in which heat is not transferred directly from a conditioned, heated space to the external environment but via an unheated or unconditioned space. This can include both ventilation and transmission heat transfer. Examples include attic spaces, garages and basements and can be evaluated by:

$$HLC_{unc} = HLC_{Uib} \tag{B.7}$$

Where,

$$b = \frac{H_{Ue}}{H_{Ui} + H_{Ue}} \tag{B.8}$$

Where, HLC_{Ui} is the the direct heat transfer coefficient between the conditioned space and the unconditioned space (W/K), HLC_{Ue} is the heat transfer coefficient between the unconditioned space and external environment (W/K) and *b* is an adjustment factor which allows the unconditioned space to be at a different temperature to the external environment.

Alternatively, the U-values describing the heat transfer across an element to the external environment via an unconditioned space can be determined by:

$$U = \frac{1}{\frac{1}{U_0} + R_U} \tag{B.9}$$

Where U_0 is the U-value of the dividing element and R_U is an added thermal resistance for the unconditioned space. This can take the form of a notional value (e.g. 0.5 for pitched roof attics) or be determined by ISO 6946:2007 (ISO, 2007).

$$R_U = \frac{A_i}{\sum_k (A_{e,k} \cdot U_{e,k}) + 0.33 \cdot nV} \tag{B.10}$$

Where, A_i is the total area of elements between the internal and unheated space (m^2), $A_{e,k}$ is the area of element *k* between the internal and unheated space (m^2), $U_{e,k}$ is the thermal transmittance of element *k*, (W/m^2K), *n* is the ventilation rate of the unheated space (h^{-1}) and *V* is the volume of the unheated space (m^3).

B.1.1.5 Heat transfer through adjoining spaces, HLC_{adj}

Similarly, many buildings will contain heat flow paths in which heat is exchanged between one or more heated adjoining space. In this case, the adjoining space can be at a temperature higher or lower than the space under consideration, meaning heat transfer can also operate in either direction. Additionally, in many cases this will involve an occupied neighbouring property, in which the temperature may follow dynamic heating and occupancy patterns. Heat transfer to adjoining spaces can be described by:

$$HLC_{adj} = HLC_{Ai}b \tag{B.11}$$

Where,

$$b = \frac{T_i - T_{adj}}{T_i - T_e} \tag{B.12}$$

B.1.2 EnergyPlus treatment of transmission losses

The heat flux through a wall is described by the conduction transfer function module in EnergyPlus. This, in the most basic time series solution, relates the flux at one surface of an element to an infinite series of temperature histories at both sides. Details can be found in (p.36 LBNL, 2014).

B.1.2.1 EnergyPlus: External surface balance & convection to the outdoors

The outside surface energy balance in EnergyPlus is model by (see also figure B.1):

$$q_{sol} + q_{LWR} + q_{conv} - q_{cond} = 0 \tag{B.13}$$

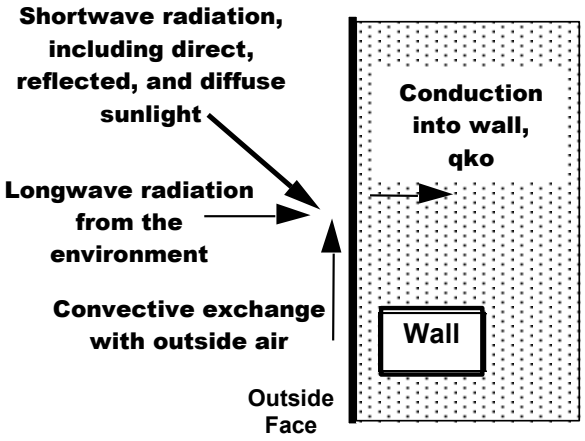

Figure B.1: *Energy Plus external surface energy balance (p.58 LBNL, 2014)*

The terms, q_{sol} and q_{LWR} are further defined in sections B.3 and B.4 respectively, with q_{cond} defined in the previous section. Here, the heat transfer due to surface convection at the external surface is further discussed.

Convection to the external environment

Heat transfer from surface convection is modelled using (LBNL, 2014, p.64):

$$Q_{conv} = A_s h_{c,e}(T_{se} - T_e) \tag{B.14}$$

Where $h_{c,e}$ is the exterior convection coefficient. Substantial research has gone into the formulation of models for estimating the exterior convection coefficient. Since the 1930s, there have been many different methods published for calculating this coefficient. EnergyPlus therefore offers a wide selection of different methods for determining values for $h_{c,ext}$. Options include:

- Simple Combined
- TARP
- MoWiTT
- DOE-2
- Adaptive Convection Algorithm

Within the simulations performed as part of this thesis the DOE-2 model for external convection was used.

B.1.2.2 EnergyPlus: Internal surface balance & convection to internal environment

The outside surface energy balance in Energy Plus is model as:

$$q_{LWX} + q_{SW} + q_{LWS} + q_{sol} + q_{conv} - q_{cond} = 0 \tag{B.15}$$

Where: q_{LWX} is the net longwave radiant exchange flux between zone surfaces.

q_{SW} is the net short wave radiation flux to the surface from lights, noting no lighting is present in the simulated co-heating tests.

q_{LWS} is the longwave radiation from equipment in the zone.

q_{sol} is the transmitted solar radition flux absorbed at the surface.

q_{conv} is the conduction through the wall.

q_{cond} is the convective heat flux to the zone.

And:

$$q_{conv} = h_c(T_{si} - T_i) \tag{B.16}$$

With h_c based upon correlations for either natural, mixed and forced convection. Again, a number of models can be deployed, with an adaptive convective algorithm used in the simulations in this thesis.

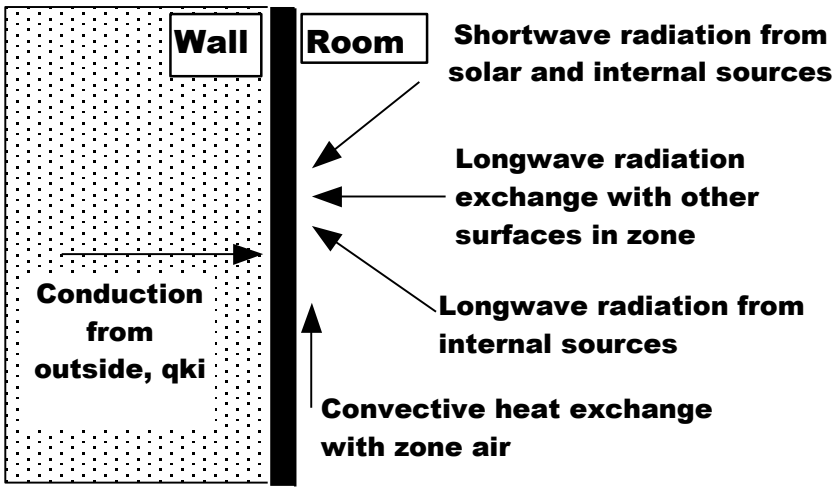

Figure B.2: *Energy Plus internal surface energy balance (LBNL, 2014, p.76)*

B.2 Infiltration Losses

The ventilation heat transfer coefficient can be calculated from:

$$HLC_{vent} = \rho_a c_p \dot{V} \tag{B.17}$$

Where:

$\dot{V}$ is the airflow rate through the heated or cooled space, typically in m^3/h.

$\rho_a c_p$ is the heat capacity of air per unit volume, equal to one-third if $\dot{V}$ is in units of m^3/h, from the density, ρ_a, and heat capacity of air, c_p.

Ventilation is usually used to refer to deliberate air exchange in order to provide a suitable internal environment. Infiltration then refers to unintentional air leakage. In the context of co-heating tests in unoccupied dwellings, the ventilation systems are normally switched off. Therefore, all air exchanged during co-heating tests can be considered as infiltration, and can therefore be denoted HLC_{inf}. Both wind pressures and buoyancy or stack effects within the dwelling will then drive the infiltration rate of a test dwelling.

B.2.1 Models of wind and stack driven losses

Wind and stack driven infiltration losses can be determined either through the 'basic' or 'enhanced' models (ASHRAE, 2013), although in reality wind driven infiltration losses can is one of the least understood and most difficult heat loss mechanisms to model (Deru and Burns, 2003).

The Basic Model (Sherman et al., 1980):

$$\dot{V} = \frac{A_L}{1000}\sqrt{C_s \Delta T + C_w U^2} \tag{B.18}$$

Where:

$\dot{V}$ is the airflow rate (m^3/s)

A_L is the effective leakage area at 4 Pa (cm^2)

C_s is the stack coefficient ($(L/s)^2/(cm^4\ K)$)

C_w is a wind coefficient ($(L/s)^2/(cm^4\ K)$)

U_w is the average wind speed (m/s)

The Enhanced Model (Walker and Wilson, 1997):

$$\dot{V} = \sqrt{\dot{V}_w^2 + \dot{V}_s^2} = \sqrt{(cC_w(sU)^{2n})^2 + (cC_s(\Delta T)^n)^2} \tag{B.19}$$

Here:

$\dot{V}_w$ is the wind airflow rate (m^3/s)

c is the flow coefficient ($m^3/(s/Pa^n)$)

C_w is the wind coefficient ($Pa.s^3/m^2)^n$

s is the stack coefficient $(Pa/K)^n$

n is a pressure exponent

$\dot{V}$ can be calculated via BSI 15242:2007.

B.2.1.1 Flow through openings

Alternatively, ventilation/infiltration rates are calculated via the pressure differences across cracks, from the Newtonian equations. The pressure on any point on the surface of a building facade can therefore be represented by (Lowe, 2000; CIBSE, 2007):

$$\Delta P_w = \frac{1}{2}\rho C_p U_z^2 \tag{B.20}$$

and

$$\Delta P_s = -\rho g(z - z_0)\frac{\Delta T}{T} \tag{B.21}$$

Where: U_z is the wind speed at height z, normally taken to be the undisturbed flow at the height of the building

C_p is a dimensionless pressure coefficient

z is the height of the point on the facade above some datum, typically the bottom of the building

z_0 is the mean height (m) of the neutral plane of the building

ρ is the density of air (kg m^3) at temperature equal to the mean of inside and outside

g is acceleration due to gravity (9.81 ms^{-2})

ΔT is the temperature difference across the thermal envelope (K)

T is the mean of the inside and outside temperatures ($\sim$ 300K)

The wind pressure coefficient, C_p, is a function of wind direction, position on the building surface and side exposure. Some typical approximate values for buildings subjected to varying

degrees of shelter and wind directions are given in the AIVC publication A guide to energy-efficient ventilation. This data is also quoted in the CIBSE A Guide (CIBSE, 2007).

The total pressure difference across an element of the thermal envelope is to a very good approximation equal to the sum of the stack and wind pressures (Lowe, 2000). The flow through a crack is then described by the power law (Etheridge, 1996):

$$q = C(\Delta P)^n \tag{B.22}$$

Where: q is the volumetric flow through the opening/crack.
ΔP is the pressure difference across the opening/crack.
$n$is the flow exponent varying between 0.5 for fully turbulent flow and 1 for fully laminar flow.
C represents a flow coefficient, related to the size of the opening/crack (m^3/s Pa^2n).

B.2.1.2 Modelling infiltration in EnergyPlus

Energy Plus contains four models for modelling infiltration (LBNL, 2014, p.363):

1. The *design flow rate* see (LBNL, 2014).
2. The *effective leakage area* model based upon Sherman et al. (1980), equation B.18.
3. *Flow coefficient* of Walker and Wilson (1997), equation B.19.
4. The *airflow network model*.

The AirflowNetwork or AIRNET model (LBNL, 2014, p.527) can also be used to model ventilation and infiltration, using equations B.20-B.21. This approach is used in the majority of full building simulations in this thesis. As the only airflows to be considered in the simulated co-heating tests are those between internal dwelling zones and infiltration to the external environment, these pressure differences are used to model the airflow through cracks and porous materials, i.e.:

- Airflow through the surface itself, which could be caused by cracks or by general fabric porosity.
- Cracks between windows, vents and doors and the main wall or roof surface.

The air leakage is therefore defined by the properties of the construction materials and crack sizes. Further assumptions and limitations of this infiltration model can then be considered.

Assumptions

- Any outdoor air that enters by way of infiltration is assumed to be immediately mixed with the zone air.
- In reality the porosity of walls is caused by a very large number of small cracks and holes. Porosity is modelled using a single equivalent crack whilst crack characteristics are normalised by surface area.
- Wind can be removed by setting a sheltering wing factor to zero.

Limitations The determination of the amount of infiltration air is quite complicated and subject to significant uncertainty (LBNL, 2014).

- The flow of infiltrating air through the building envelope also alters the thermal performance of the material in the building envelope (Powell et al., 1989). It also impacts the heat flow through insulating material in the building envelope and leads to an additional heat flow through the insulation (Claesson and Hellstrom, 1995).

B.3 Long wave sky radiation

Heat transferred through long wave radiation is not driven by the immediately surrounding external air temperature but by the temperature of surrounding surfaces that can be 'seen' by a given surface. Surrounding surfaces include the ground, neighbouring buildings and other terrestrial objects. Often the temperature difference between terrestrial objects is low, both being strongly coupled to the external air temperature. However, looking upwards to the sky, through long wave radiaiton a building surface will see a colder temperature at a much higher height.

Surfaces, which can see the sky, will see an apparent sky temperature that is lower than the surrounding ambient air temperature, typically 10 °C lower than the ambient air[1]. More significant long-wave radiative heat losses will then occur between the surface and this colder part of the sky seen by the surface. The greatest long wave losses occur from horizontal surfaces under cloudless conditions with a dry atmosphere, which can allow external surfaces to cool as much as 10 °C below the ambient air temperature.

Within this thesis, long-wave radiative sky losses are modelled from equation B.28 to examine the hypothetical effect of sky losses in isolation. Sky radiative losses are then modelled

[1] As calculated in the Finningley Weather file used predominantly in this thesis

in accordance with section B.3.1.2 within EnergyPlus.

B.3.1 Theoretical models of long wave radiative losses

Generally, the outgoing long-wave radiation flux emitted by any plane surface can be calculated from the Stefan-Boltzman law:

$$q_{sky} = \epsilon_s \sigma T_s^4 \tag{B.23}$$

Where q_{sky} is the flux emitted by a plane surface (W/m^2), $epsilon_s$ is the long-wave emissivity of the surface (0-1), σ is the Stefan-Boltzmann constant (5.6697 x 10^-8 W/m^{2}K$^-4$) and T_s is the absolute surface temperature (K).

The net heat transfer (Q_{sky}) is then dependent upon how much each surface can 'see' each other, introducing the concept of a view factor *F*, and upon the temperature different between the two surfaces. The net heat transfer rate between two surfaces, or a surface and the sky, is then given by:

$$Q_{sky} = \varepsilon_s \sigma A_{se} F_{sky} (T_{se}^4 - T_{sky}^4) \tag{B.24}$$

Where A_se is the area of a surface (m^2) and and F_{sky} is the view factor between surface 1 and 2 (0-1). Note temperatures here are in degrees Kelvin (K).

This is often linearised for convenience, introducing a radiative heat loss coefficient (h_r, W/(m^2/K)).

$$h_{r,sky} = \frac{\varepsilon_s \sigma F_{sky} \beta (T_{sky}^4 - T_{se}^4)}{T_{sky} - T_{se}} \tag{B.25}$$

Such that the heat flux, q_{sky} (W/m^2) can be defined as:

$$q_{sky} = h_{r,sky} (T_{sky} - T_{se}) \tag{B.26}$$

Or for the heat loss, Q_{sky} (W), as:

$$Q_{sky} = h_{r,sky} A_s (T_{sky} - T_{se}) \tag{B.27}$$

Long-wave radiative losses are therefore dependent upon the size and orientation of a surface, the surface temperature (a function of its U-value, the external air temperature and linked to the incident solar radiation) and the apparent sky temperature. To understand this heat flow path the apparent sky temperature therefore needs to be known and understood.

B.3.1.1 ISO 13790 calculation of thermal radiative losses to the sky

In ISO 13790:2008 thermal radiation to the sky is defined by the last component within equation B.28, determining solar gains (ISO, 2008, 11.3.2):

$$Q_{sol,k} = F_{sh,ob,k} \cdot A_{sol,k} \cdot I_{sol,k} - F_{r,k} \cdot \phi_{r,k} \tag{B.28}$$

Here:

$Q_{sol,k}$ is the total heat gains through building element *k* (W).

$F_{sh,ob,k}$ is a shading reduction factor for external obstacles for the solar effective collecting are of surface *k* (0-1).

$A_{sol,k}$ is the effective collecting area of surface *k*, with a given orientation and tilt angle, in the considered zone or space (for glazed or opaque) (m^2).

$I_{sol,k}$ is the solar irradiance, the mean energy of the solar irradiation over the time step of the calculation, per square meter of collecting area of surface *k*, with a given orientation and tilt angle (W/m^2).

$F_{r,k}$ is a form factor between the building element and the sky.

$\phi_{r,k}$ is the extra heat flow due to thermal radiation to the sky from building element *k* (W).

Here, thermal radiation to the sky is defined by a form factor, F_r, between the element and the sky and ϕ_r, a term describing the extra heat flow from thermal radiation, described by (ISO 13790:2008, 11.3.5):

$$Q_{sky} = F_{sky} R_{se} \cdot U_c \cdot A_c \cdot h_{r,sky} \cdot (T_{sky} - T_{se}) \tag{B.29}$$

The form factor, F_r, (equivalent to a view factor) then equals (ISO 13790:2008, 11.4.6):

- F_r = 1 for a horizontal unshaded roof and
- F_r = 0.5 for an unshaded vertical wall

Additionally, the radiative heat transfer coefficient, h_r, can be approximated by:

$$h_r = 4\epsilon\sigma(T_{ss} + 273)^3 \tag{B.30}$$

Where T_{ss} is the arithmetic average of the surface temperature and the sky temperature ($^\circ$C).

To a first approximation, h_r can be taken to equal 5ϵ W/m^{2}K, which corresponds to an average temperature of 10 $^\circ$C.

B.3.1.2 Sky Radiation Modelling in EnergyPlus

The external long wave sky radiation is described in eq, figure B.31. The following assumptions are assumed:

- Each surface emits diffusely and is gray and opaque ($\alpha = \epsilon$,$\tau = 0$ and $\rho = 1 - \epsilon$).
- Each surface is at a uniform temperature.
- Energy flux leaving a surface is distributed evenly across the surface.
- The medium within the surface is non-participating.

$$q_{LWR} = \varepsilon\sigma F_g({T_g}^4 - {T_{se}}^4) + \varepsilon\sigma F_{sky}({T_{sky}}^4 - {T_{se}}^4) + \epsilon\sigma F_{air}(T_{air}^4 - {T_{se}}^4) \tag{B.31}$$

$$F_{sky} = 0.5(1 + cos\phi) \tag{B.32}$$

$$F_g = 0.5(1 - cos\phi) \tag{B.33}$$

View factor, β to the sky is further split between sky and air radiation by:

$$\beta = \sqrt{0.5(1 = cos\phi)} \tag{B.34}$$

B.3.1.3 The apparent sky temperature

The sky is not a surface as such, but contains water vapour, which is a strong absorber and emitter of infrared radiation. A surface on the ground will see the temperature at a certain distance in the atmosphere above, hence a lower temperature than the ambient air. The height of the temperature seen depends upon the density of the water vapour within this line of sight. This means, in a clear sky, the temperature seen directly above will be colder than that at an angle, as the water vapour will be at a higher concentration along this line of sight. The apparent sky temperature is therefore a function of the humidity of the air in the atmosphere but it is also dependent upon cloud cover. A cloud will act to absorb and emit long-wave radiation in the same way, but as the clouds are lower in the sky their presence will dictate a lower apparent sky temperature in comparison to a clear sky.

If local long wave downward radiation (q_{LWR}, W/m^2), is measured then the apparent sky temperature (T_{sky}, $^\circ$C), can be calculated from equation B.35 (LBNL, 2014).

$$T_{sky} = (\frac{q_{down}}{\sigma})^{0.25} - T_{Kelvin} \tag{B.35}$$

Where q_{LWR} is the horizontal infrared radiation intensity (Wh/m^2) and T_{Kelvin} is a conversion term from Kelvin to ($^\circ$C), i.e. 273.15.

When the local long wave radiation is not measured, the apparent sky temperature can be evaluated via a number of models. One such approach is used within the EnergyPlus engine. This determines a sky emissivity from the local dew point temperature and cloud cover.

$$Sky_{emissivity} = (0.787 + 0.764 \cdot \ln \frac{T_{dew}}{273} \cdot (1 + 0.224 \cdot N - 0.0035 \cdot N^2 + 0.00028 \cdot N^3) \quad \text{(B.36)}$$

Where N = Opaque sky cover (10th?s where N=0 is clear sky) and T_{dew} is the dew point temperature, which itself can be calculated from the external air temperature and RH.

The Horizontal Infrared Radiation Intensity in Wh/m^2, can then be calculated from:

$$q_{down} = Sky_{emissivity} \cdot \sigma \cdot T^4_{drybulb} \quad \text{(B.37)}$$

Humidity and cloud cover will vary on an hourly basis, between days and also across wet and dry seasons.

B.4 Solar radiation and gains

B.4.1 Solar radiation theory

General theory on solar radiation and its measurement can be found in the main thesis, section 3.4.

B.4.2 EnergyPlus modelling of solar radiation

The total solar gain on any exterior surface is a combination of the absorption of direct and diffuse solar radiation given by (LBNL, 2014, p.161)

$$Q_{sol} = \alpha(S_{Dir} \cdot cos(\theta) \cdot \frac{A_s}{A} + S_{Diff} \cdot F_{ss} + S_{Ref} \cdot F_{sg} \quad \text{(B.38)}$$

Where, α is the solar absorptance of the surface (0-1), A_s is the sunlit area and *A* is the area of the surface, F_{ss} and F_{sg} are the surface view factors to the sky and ground respectively and are defined by:

$$F_{ss} = \frac{(1 + cos(\Sigma)}{2} \quad \text{(B.39)}$$

$$F_{sg} = \frac{(1 - cos(\Sigma)}{2} \quad \text{(B.40)}$$

Where Σ is the angle of the surface from the horizontal ground. Further details of sky radiation modelling can be found in LBNL (2014, p.161).

As LBNL (2014) states, EnergyPlus calculates the distribution of short-wave radiation in the interior of each thermal zone. This radiation consists of beam solar radiation, diffuse solar radiation, and short-wave radiation from electric lights. The program determines the amount of this radiation that is (1) absorbed on the inside face of opaque surfaces, (2) absorbed in the glass and shading device layers of the zone's exterior and interior windows, (3) transmitted through the zone's interior windows to adjacent zones, and (4) transmitted back out of the exterior windows. The effects of movable shading devices on the exterior windows are taken into account but not relevant to this thesis.

Furthermore, diffuse solar transmitted through exterior windows is first distributed to the interior heat transfer surfaces in the zone containing the external windows. This initial distribution apportions the transmitted diffuse solar to interior surfaces using the approximate view factors described by long wave radiation exchange within an internal space. The amount of this initially distributed diffuse solar that is reflected is accumulated for each zone and redistributed uniformly to the other surfaces. The amount of this initially distributed diffuse solar that is transmitted by interior windows to adjacent zones is initially distributed to the interior heat transfer surfaces in the adjacent zone in the same manner as just described.

Shadowing can be modelled via a number of model options. The simulations in this thesis used a 'Full interior and exterior with reflections' model, although it should be noted that their were no other shading objects, other buildings or terrestrial objects, in any of the simulations performed.

Appendix C

CAM-PH Report

Executive Summary

Camden Passivhaus is part of the Technology Strategy Board's Building Performance and Evaluation programme. Part of this programme includes a series of post-construction tests to evaluate the 'as-built' thermal performance of the dwelling. These tests are designed to evaluate any variation between design intent and as-built performance and to identify the causes of any such discrepancies. This report focuses on the results of two co-heating tests at Camden passivhaus. Co-heating tests experimentally determine the heat loss coefficient, a measure of the total heat loss across the entire building envelope. This quantitative measurement across the entire fabric separates it from other post-construction tools such as in situ u-values, which measure heat loss only at discrete points, and thermal imagery, which only provides a visual indication of heat loss. The measured heat loss coefficient from co-heating can carefully be compared to design predictions. When the measured and design heat loss coefficient show significant disagreement this can be an indication of issues with buildabilty/workmanship, design assumptions or real world material performance. When this is the case a variety of forensic tools can be used to attempt to determine the causes of such a disagreement.

To this purpose, at the end of March 2011 an initial co-heating test was undertaken at the Camden Passivhaus. There are two important points to note about this test. Firstly, the Camden Passivhaus has a low overall designed heat loss and a high glazing fraction, making it far more sensitive to uncertainties from the external environment than many other buildings. Secondly, the co-heating test, performed at the end of March, experianced high amounts of solar radiation. These two issues combined to cause difficulties in preserving the co-heating method and energy balance upon which the energy balance is based. Specifically due to large amounts of solar gains the house overheated beyond the co-heating set point of 25^{o}C. This caused a large amount of uncertainty in the co-heating result.

It was therefore determined that, if possible, a second co-heating test under more favourable conditions should be pursued. As the dwelling was fully occupied arranging this second co-heating period was difficult and depended on the cooperation and holiday arrangements of the occupants. As only a short amount of time was likely to be available it was important to avoid any of the problems of the first test. An evaluation of when the second test should be performed was carried out using simulated co-heating tests and is included in this report. The results of this showed that the test was more likely to be successful in December or January but this still depended on having dull weather conditions.

The second co-heating test at the Camden Passivhaus was therefore performed between the 21st and 30th December 2012. This test period coincided with a dull

spell of weather, reducing any risks of overheating. The second result could then be stated with far less uncertainty than the first.

Co-heating Result from first (2011) test:
Heat loss coefficient (HLC) = 35 ± 15[1] W/K

Co-heating Result from second (2012) test:
Heat loss coefficient (HLC) = 56 ± 5 W/K

The two results are significantly different. It is therefore important to understand the uncertainties in each measurement such that we can understand the true building performance. As fully discussed later in this report the first co-heating result is severely influenced by solar generated overheating in the test house. This overheating, which pushed internal temperatures above the co-heating set-point meant that the steady-state assumptions of the co-heating method were affected by dynamic thermal mass effects. In comparison the second co-heating test was performed under almost ideal test conditions for the Camden Passivhaus, being largely dull and overcast. This means the second test was far more successful and its result far more reliable.

The indication is that with a measured value of 56 W/K the Camden Pasivhaus is performing within its PHPP design heat loss value of 66 W/K. Previous air tightness, in situ u-value and thermography results support this conclusion. The indication is that the Camden Passivhaus is one of only a few co-heating tested dwellings that meets its design intent. This is a positive reflection on the design and build quality of the house and is especially encouraging considering the low heat loss that was targeted here.

[1] The error here is the standard deviation of the HLC calculated across each day in the test.

Table of Contents

1. Introduction

This report will document the second co-heating test in detail (section 2) and also briefly summarise the original test in order to draw comparisons between the two (section 3). This section will describe Camden Passivhaus and the process used in which to schedule the second co-heating test.

1.1 The Test House

The Camden passivhaus is regarded as the first house in London to be accredited to Passivhaus standards. Situated on a residential street in north London, the two-story house has an entirely open plan 1st floor with bedrooms and bathrooms located on the ground floor. Both floors have large amounts of glazing (37.8m^2 in total), almost exclusively on the south façade.

Figure 1: Ranulf Road Passivhaus, south elevation

The building fabric can be divided up into several different elements. The timber frame walls are highly insulated and feature exterior cladding. The ground floor walls have an additional concrete retaining element as the ground floor is partially excavated. There is also an insulated concrete floor slab and a green roof with both a flat and a sloping element to the rear.

Full details of the construction can be found elsewhere but there are several features of note in regards to the success of the co-heating method.

- **A large south-facing glazing area:** There are two implications here. The first is the high potential for overheating above the co-heating 25^{o}C setpoint. Secondly, potentially a large proportion of the heating input will come from solar gains, such that accurately determining the gains becomes increasingly important.
- **Low heat loss:** Designed to passivhaus standards Camden passivhaus is well insulated and has a low overall design heat loss coefficient. This low value means the measurement is more sensitive to some of the uncertainties in co-heating and the building is more susceptible to overheating.
- **Open Plan:** The 1st floor is an open plan living space. This facilitates good mixing under the co-heating method. The ground floor is more partitioned, particularly with a number of small WC's and cupboards.
- **Partially excavated:** Camden passivhaus is on a partially excavated site and therefore has a large proportion of its envelope in contact with the ground, rather than the air. The ground floor slab accounts for 15% of the total envelope and when incorporating the excavated external wall this increases to 35%.

1.2 Scheduling co-heating test

Work of the author involves investigating the uncertainty in co-heating through simulated tests. This allowed an Energy Plus model of Camden Passivhaus to be created and then a vast number of simulated co-heating tests to be performed. In particular these were used to determine the likelihood of achieving an accurate result and determining what weather conditions would achieve this. Continuous co-heating tests were simulated across a typical year, figure 2.

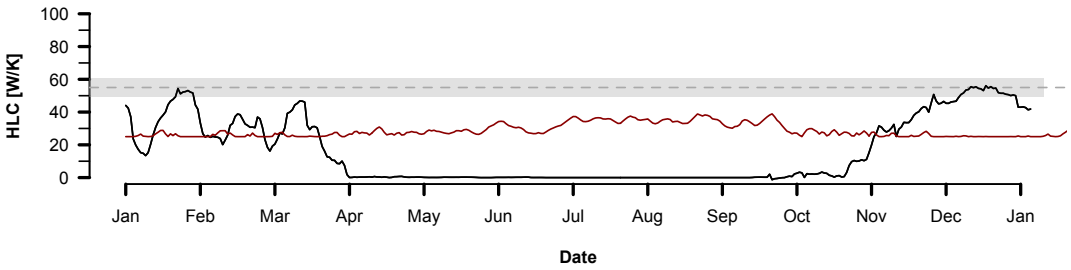

Figure 2: Results of simulated co-heating tests on Camden Passivhaus. The derived heat loss coefficient (black line) is shown throughout atypical year. The grey band represents a region ± 10% around the true HLC. The internal temperature (red) is also shown to identify overheating.

What is seen in figure 2 is that any significant overheating results in the co-heating method failing to achieve a result. Outside the typical co-heating test season of October-March there is no chance of achieving a result. In fact, there are only brief periods throughout the whole year when results were achieved to within 10% of the expected heat loss coefficient. These occur in December and January and represent periods with little solar radiation and no overheating. Furthermore, it is desirable that as high a proportion of heating input comes from electrical power, rather than solar gains. These two signals across the same simulated year are shown in figure 3. It is clear then that dull conditions are required and should be sought for the second co-heating test. Testing of the Camden Passivhaus is however very sensitive to the external weather conditions so any test carries with it an element of risk. Figure 2 really shows that performing a co-heating measurement in a house such as the Camden Passivhaus is extremely challenging and even at the best times of year there is a great risk the measurement will incorporate a large amount of uncertainty. This is in short the story that is told by the two co-heating tests documented here. Performing initial investigations such as this therefore seem increasingly prudent in sensitive test houses, where a little more foresight could avoid wasted tests.

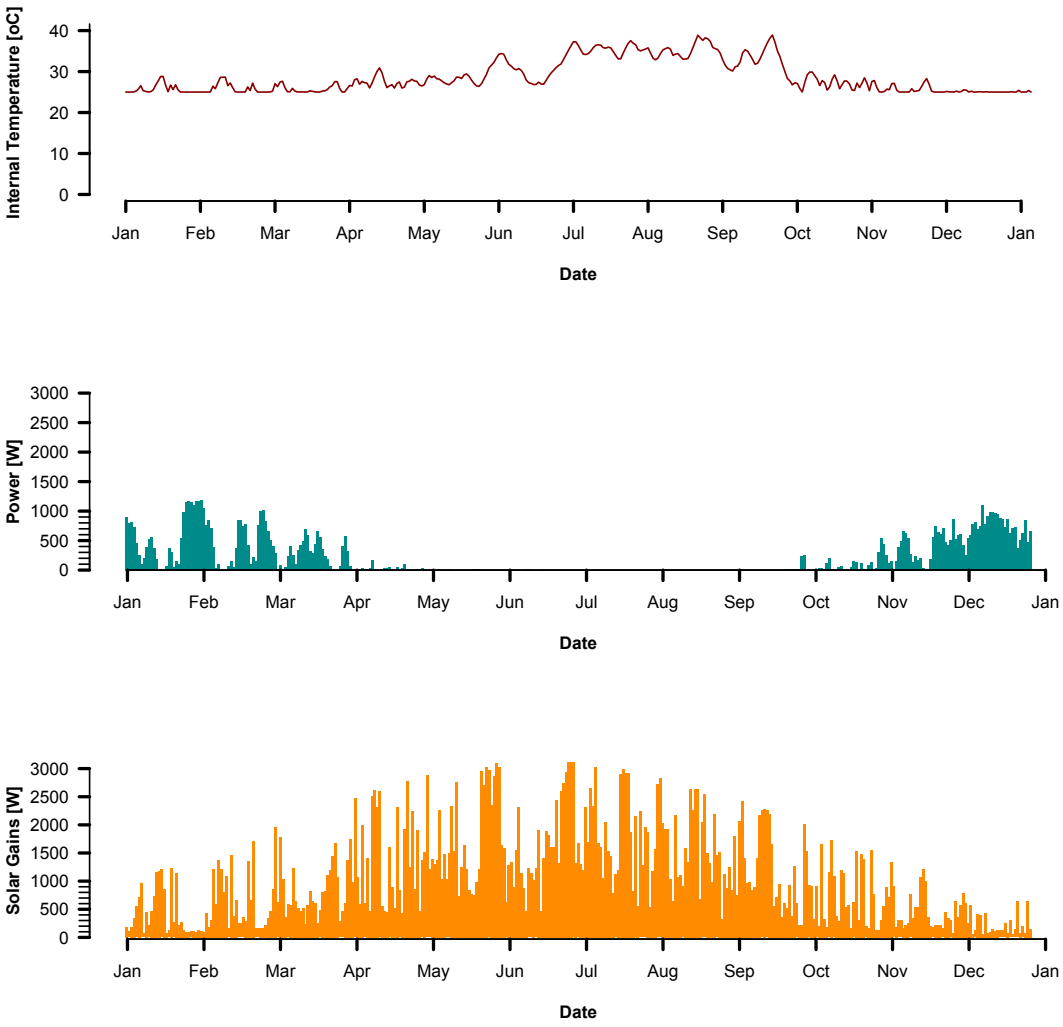

Figure 3: Simulated internal temperature, electrical heating power and solar gains across typical year.

2. 2012 Co-heating of Camden Passivhaus

2.1 Co-heating Principal

The co-heating method dates back to work in the US in the 1980's on the PStar and STEM methods (Subbarao et al., 1988) and to the work by Siviour & Everett in the UK (Everett, 1988; Siviour, 1981). This was then developed into the current set of experimental guidelines (Wingfield et al., 2010). The two co-heating tests described in this report are based on these guidelines.

The co-heating method is based on an energy balance at an approximated steady state. The test building is held at a constant internal temperature, typically 25°C, through the use of electric fan heaters and mixing fans, figure 6. This constant internal temperature minimises dynamic behaviour in the dwelling and means that, under co-heating approximations, the heat input equals the heat loss of the building across daily averaged measurements.

Heat input, Q [W], to all electrical equipment is recorded through the use of kilowatt-hour meters and pulse counters. There is additional heat input, from solar gains, that also need to be accounted for. Solar radiation, S [W/m^2], is measured externally by a pyranometer. This is then converted into the effective heating contribution [W] from solar gains by a solar aperture, R [m^2]. The solar aperture can itself be derived experimentally from the co-heating test or alternatively from the glazing characteristics of the dwelling.

Figure 4: Co-heating principal and analysis method. The energy balance the co-heating method uses is shown along side an example of data used in linear regression. Typically an additional independent variable and axis for solar radiation is included as part of a multiple linear regression.

$$Q + R.S = (\Sigma U.A + \tfrac{1}{3}nV)\Delta T \quad \text{(Equation 1.)}$$

Here, Q is the heat input from electric heaters or other heating device [W]
$R.S$ is the Solar Gains [W], where S is the solar radiation [W/m^2] and R is the solar aperture [m^{-2}]
ΔT is the temperature difference [K] between the internal and external conditions
$\Sigma A.U$ [W/K] is the sum of the U-values [W/m^2] and respective areas of the thermal envelope [m^2]
$\frac{1}{3}nV$ is the infiltration heat loss [W/K] comprising of n the air change rate [h^{-1}] and the volume, V.

By taking long enough averaging periods, 24 hours, the dynamic effects inside the test dwelling are assumed to be averaged out such that the energy balance equation 1 is satisfied. This allows the daily heat input (from electrical heating and solar gains) to be plotted against the daily averaged internal-external

temperature difference, ΔT, (figure 4). The slope of the line of best fit, which goes through these points, gives the buildings measured heat loss coefficient, [W/K]. This regression of power against ΔT can be performed as a simple linear regression with solar corrections as explained here or through a 'Siviour' or multiple linear regression, both of which separate out the electrical power and solar radiation. All three are demonstrated in section 2.3.

2.2 Camden Passivhaus Set Up

In total four sets of kW-hour meter, fan, heater and thermostat combinations were positioned in the house, figures 5 & 6. This is to provide sufficient heating power and control to maintain an internal temperature of 25°C. Additional temperature and relative humidity sensors were placed in all zones in the house to establish a representative internal temperature for use in analysis and to ensure a uniform temperature was achieved throughout the dwelling. Additionally, heat flux sensors were placed in pairs on sections of the lower and upper external wall as well as on the ground floor. As the house is occupied and it was not possible to affix the heat flux sensors with thermal paste these were not used to measure in situ u-values but more to understand heat flows throughout the co-heating test.

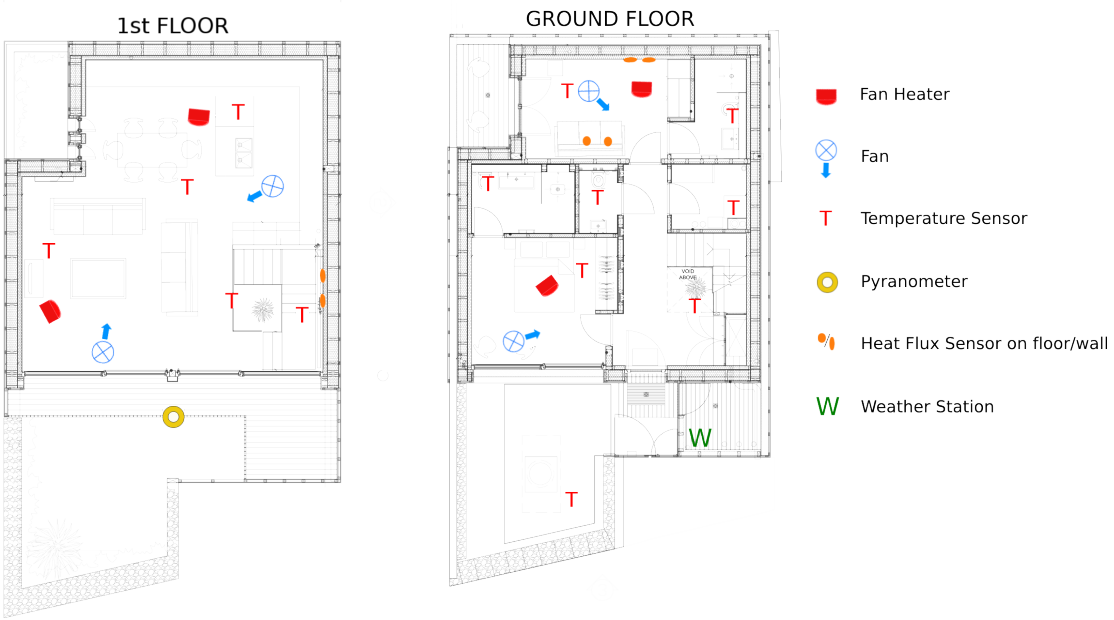

Figure 5: Equipment Layout for second (2012) co-heating test.

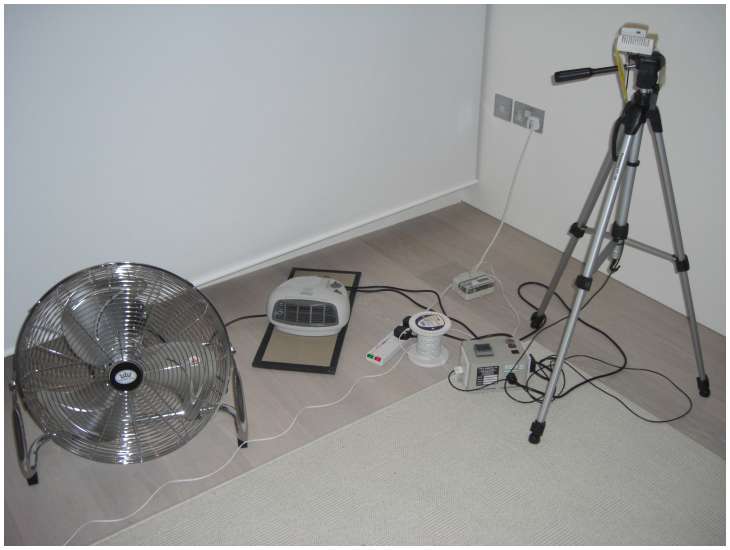

Figure 6: Co-heating zone equipment

The external environment needs to be monitored throughout the co-heating test, not only to record the external temperature required to establish a ΔT, but also to record other external variables which can be sources of uncertainty in the co-heating method. These external environment sensors included:

- An **external**, shielded, **temperature sensor:** located on a tripod stand in the front garden. (Note: this represents one of the few significant changes in equipment between the two tests. The original test did not include such a sophisticated external temperature sensor, this is discussed in the comparison section)
- **Local Weather Station**: Located on the 1st floor balcony. This included external temperature, relative humidity, wind speed & direction. Data from a second weather station, installed as part of the long term TSB monitoring programme located on the green roof was also available.
- **Pyranometer:** Vertical and in the plane of the south facing building façade. Measures solar radiation [W/m^2]

Figure 7:

Equipment used to monitor external environment. Clockwise from top left: Stevenson screen external temperature sensor, vertical facing pyranometer on balustrade, weather station, south façade showing weather station and pyranometer on balcony level.

2.3 Result of 2012 Co-heating Test

Camden passivhaus was unoccupied for a total of 10 days, of which 6 days are used in the full co-heating analysis. Including a day each end of the test for setting up and taking down equipment this left 8 days at test conditions. A further day at the beginning of testing was removed from analysis as the building's mass was still being heating to the set point temperature and was therefore a source of bias. Finally, a day was used to perform a cool down – warm up cycle, following that of the PStar method. This will be used later to evaluate the thermal mass of the dwelling but is not used in the co-heating data or included in this report.

The six days of co-heating data are analysed in four different ways:

1) Global Average

A simple average of total power input and average temperature difference across the test period can be calculated. This is often useful as a check on the regression process itself, particularly when there is not a wide spread in data points.

Global Average HLC = 56 ± 5[2] W/K

2) Simple Linear Regression

More traditionally co-heating data is analysed through regression. The simple linear regression model plots the heating power against ΔT. This is shown in a raw and solar corrected form in figure 8.

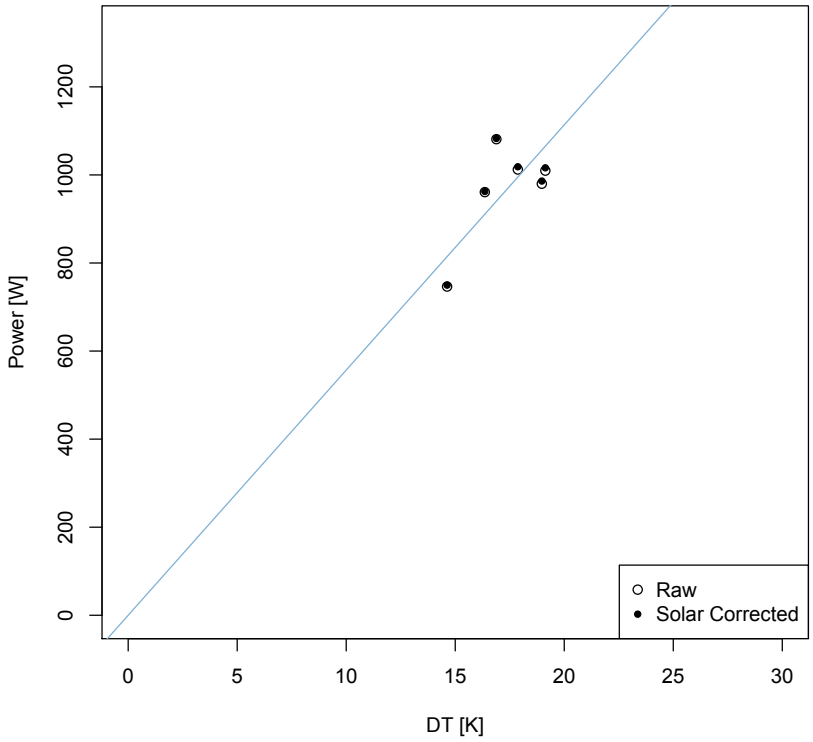

Figure 8: Simple Linear Regression co-heating analysis

[2] The error here is the standard deviation from each days data.

The results from the simple linear regression show:

Simple Linear Regression HLC = 56 ± 5 W/K

The solar correction seen in figure 8 is very small. This is a result of such a low level of solar radiation being experienced across the test period. In fact only about 1% of the total heating power is calculated to come from solar gains, the rest from electrical heating. This is in stark contrast to the first test, discussed in section 3.

3) 'Siviour Analysis'

Another form of regression analysis often used is 'Siviour' analysis. This rearranges the energy balance equation into the form seen in equation 2. Here the heat loss coefficient is the y-intercept of figure 9. An advantage of this method is that the solar aperture can also be derived from regression, forming the slope of the line of best fit in this case.

$$\frac{\boldsymbol{Q}}{\boldsymbol{\Delta T}} = -\boldsymbol{R}.\frac{\boldsymbol{S}}{\boldsymbol{\Delta T}} + \left((\boldsymbol{\Sigma A}.\boldsymbol{U}) + \frac{\mathbf{1}}{\mathbf{3}}\boldsymbol{nV}\right) \qquad \text{(Equation 2)}$$

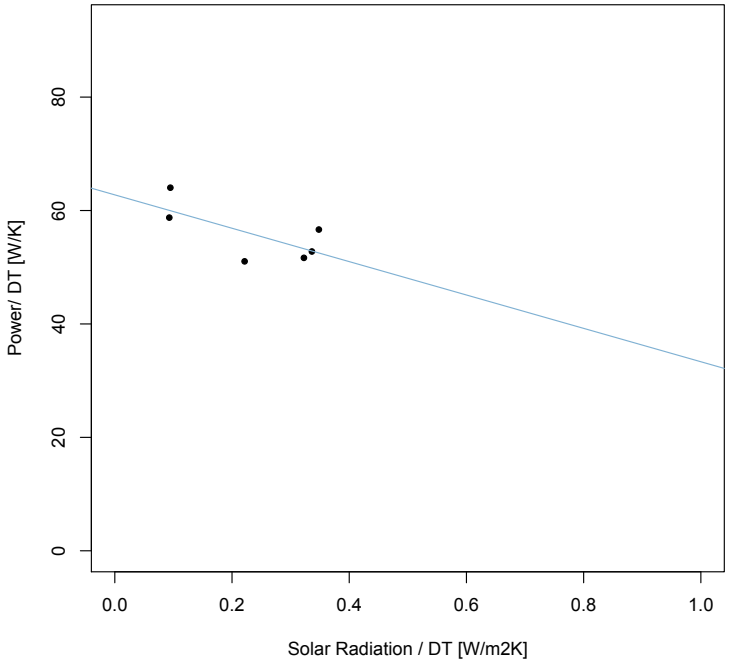

Figure 9: Siviour Co-heating Analysis

HLC = 63 ± 10 W/K
Solar Aperture = -29 ± 15 m^{-2}

It is important to note here that the derived solar aperture has a significant amount of error associated with it. This is in part because all days data featured very low levels of solar radiation. A small range in data such as this results in a higher degree of uncertainty. The solar aperture can also be derived from the

glazing properties, equation 3 (SAP 2009, pg 21).

$$G_{solar} = 0.9 \times A \times S \times g \times FF \times z \qquad \text{(Equation 3)}$$

Where:

0.9 is a factor representing the average transmittance to that at normal incidence
A is the glazed area [m^2]
S is the solar flux [W/m^2]
g total solar energy transmittance factor at normal incidence
FF is the frame factor, the fraction of the opening that is glazed
z is a solar access factor or shading factor

The solar apertures derived from regression in both the Siviour analysis and multiple linear regression differ from the calculated value here of 6.2 m^{-2}. This is not particularly significant in performing solar corrections in this second test as the amount of solar radiation was so small. It is however far more significant under high levels of solar radiation, as in the first co-heating test where is creates a significant uncertainty.

4) Multiple Linear Regression

Finally, and perhaps more commonly, multiple linear regression can be carried out between Power, ΔT and solar radiation. Again this extracts the heat loss coefficient and solar aperture through regression. The results are as follows:

HLC = 63 ± 10
Solar Aperture = -30 ± 14 m^{-2}

2.4 Discussion of results

The four methods of analysing the result here show a small variation between each other ranging from 55 – 63 W. Generally multiple linear regression can offer the more reliable results but can be biased by poor data in the regression variables. The poor range, and subsequent large error in solar radiation means its use as a regression variable is less reliable. As there was such a little amount of solar radiation and therefore the scale of any correction is very small the simple linear regression result offers a more reasonable result. Therefore the quoted value from this second co-heating test is to be taken as:

Simple Linear Regession HLC = 56 ± 5 W/K

2.5 External Conditions

The external environment is a key driver for sources of uncertainty in the co-heating result. High variation external temperature, solar radiation or wind speed can cause errors in the co-heating results. However, in this second test there was relatively little variation in wind speed and external temperature. There was also a very small amount of solar radiation across the test period.

Another point to note is that a large part of the building envelope is in contact with the ground, rather than the ambient air assumed in co-heating. This de-coupling of the two temperatures can cause an offset in the co-heating result and could be significant in the case of the Camden passivhaus. However, the ground temperature, measured at site, remains fairly steady across the test period. It also has an average value of 8°C which is close to the average air temperature of 7.6°C. It is therefore assumed no significant offset exists.

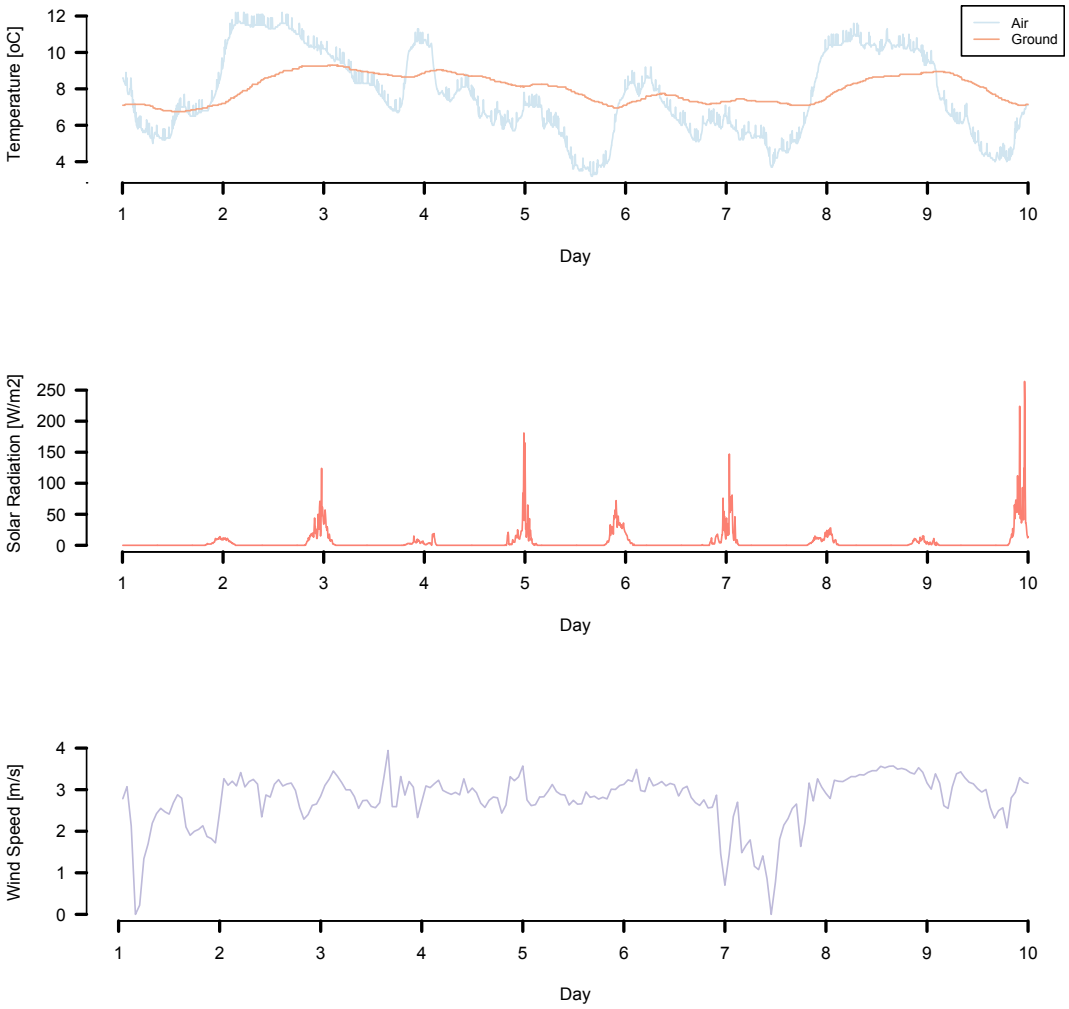

Figure 10: External Environment throughout the test period

2.6 Internal Conditions

The co-heating analysis is based on the assumption of a constant and uniform internal temperature. When the condition of constant temperature is broken thermal mass effects come into play, which can create lags and distort the energy balance. The initial Camden Passivhaus test is a prime example of this.

The second condition, of a uniform temperature can also create bias. If a particular area of the house experiences higher or lower temperatures than the average internal temperature then the heat loss through the associated building elements will equally be higher or lower respectively. If such an area has a substantially different heat loss this can significantly bias the results.

It is obviously impossible for a perfectly uniform and isotropic internal temperature to be maintained throughout testing. It is therefore important to assess the limitations to this assumption by viewing the internal temperatures throughout the test period.

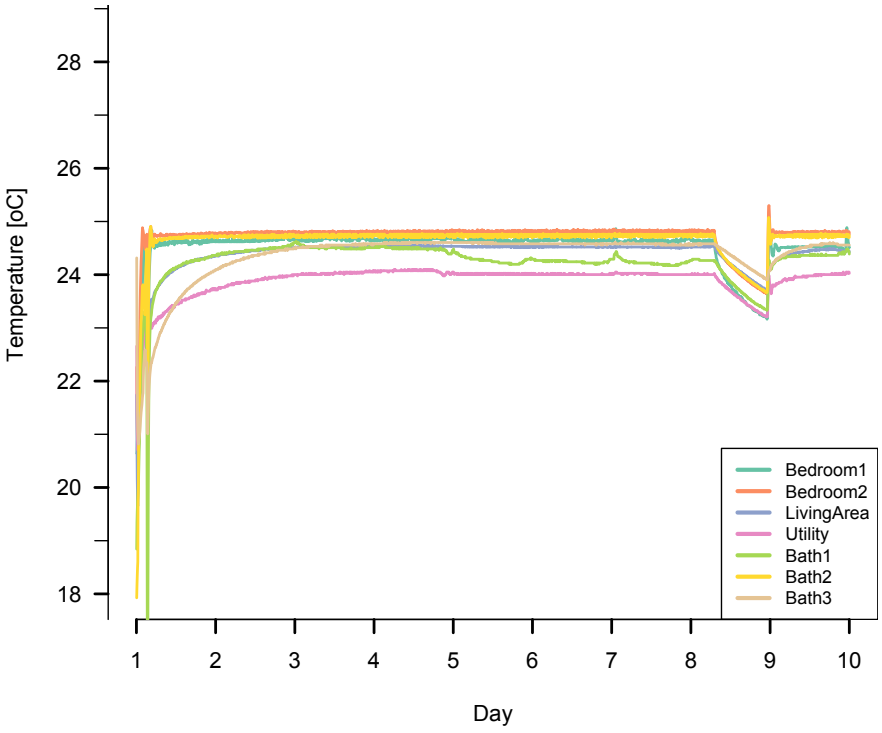

Figure 11: Internal temperature profiles throughout second co-heating test

Figure 11 shows most temperatures were maintained within a tight range, under half a degree. Some zones did take a longer period to heat up to the 25°C set point, either because they were not themselves directly heated (Bath1, Utility) or they incorporated a large volume in which to fully heat (Living Area).

The utility room, not being directly heated and being an enclosed space, did not reach a temperature as high as the internal mean. This, as mentioned, can cause a bias. A way of examining this problem and potentially correcting it is to take either volume weighted or heat loss weighted average internal temperatures – as opposed to a simple arithmetic mean. These were both examined but as the utility is only a degree different in temperature and represents a small proportion of the internal volume and external envelope this does not significantly alter the representative internal temperature.

Figure 11 shows a good degree of control in the internal temperature. This can often be upset by highs in midday solar radiation causing brief periods of overheating. If this persists at high levels then long term overheating can be seen, see section 3.3. This breaks down the assumption of a steady state thermal mass and can cause large amounts of error in the co-heating result, a steady state model that cannot handle this dynamic behaviour. The absence of any overheating in the second co-heating test affords us confidence that this assumption does still hold.

3. 2010 Co-heating of Camden Passivhaus

3.1 Introduction

The original co-heating test is documented in a previous report but some elements are again reported here to allow a comparison with the second test.

In general and as previously mentioned the timing of this second was far from ideal and featured high amounts of solar gains. This in turn led to overheating and undermined the accuracy of the derived heat loss coefficient. The stated result of 35 ± 15 W/K seemed to indicate the Camden Passivhaus was performing well but there was a large amount of uncertainty in this result. Further details can be found in the original report but relevant details are discussed in this section to provide a comparison to the second test.

3.2 Test Method

The same basic test method was followed for the first test as in the second. Again the house was occupied so scheduling a test was difficult. To allow for more co-heating data a pre-heating phase was used. This included heating the building to the 25°C set point temperature whilst still occupied. This was to reduce any loss of data to the building and its mass warming up. In total the pre-heating period lasted five days with a further 12 days of data used in the co-heating analysis.

Equipment used in both tests was largely the same although there were a couple of differences. The first test did not feature such a sophisticated external temperature sensor. This had meant external temperature measurements were more susceptible to the influence of solar radiation. To limit any inaccuracies these were also compared to an external local weather stations data. A dedicated on-site weather station was also not used in the first test. However, this is not too significant as there is little variation in heat loss with wind speed seen in the second test or similarly in the simulated co-heating tests.

The equipment layout can be seen in figure 12.

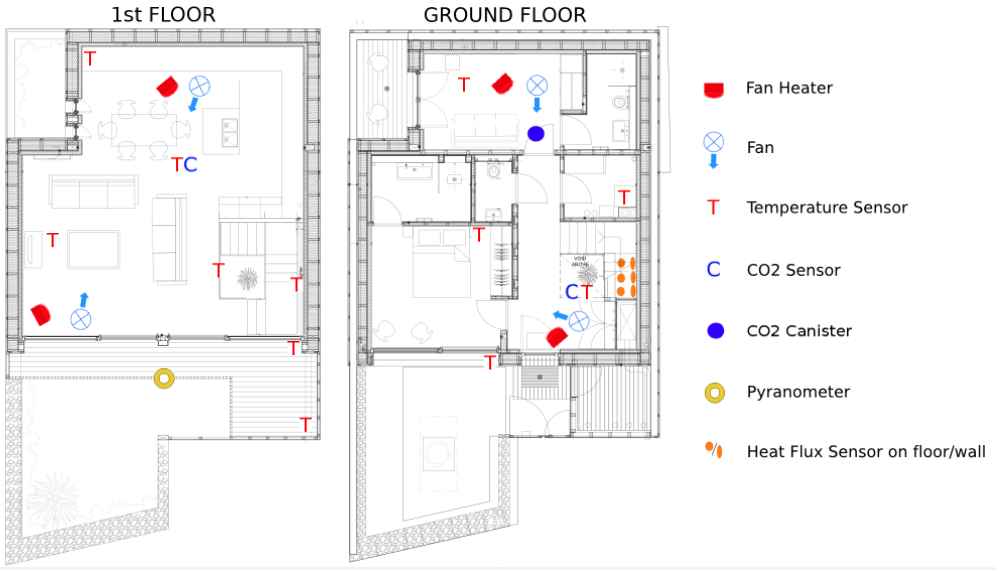

Figure 12: First Floor & Ground floor plans, with location of sensors and equipment for the first co-heating test.

3.3 Internal Conditions

The internal conditions and overheating in the first co-heating test of the Camden passivhaus need to be understood to put the result in context. The internal and external temperatures are shown in figure 13.

Significantly, after the overheating was observed the internal and external blinds were lowered. This was to see if further over heating could be avoided. Unfortunately, due to the low heat loss and thermal mass of the building it took a significant amount of time to cool down to 25°C again. This meant for an extended period the energy balance and steady-state co-heating assumptions broke down.

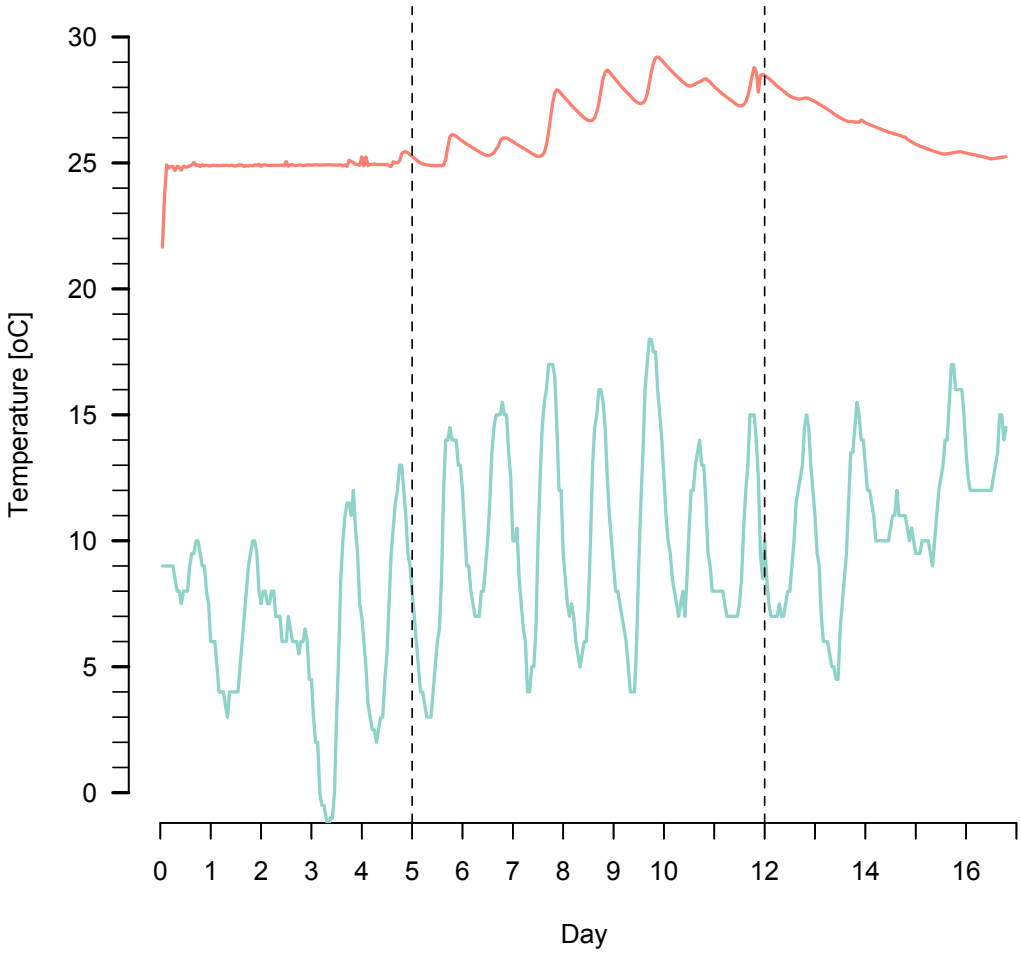

Figure 13: Internal Temperature profile from test 1. The first dashed line represents the end of the pre-heating phase and the second indicates when the blinds were shut.

As figure 13 shows the overheating started shortly after the beginning of the co-heating test proper on day 5. The overheating quickly meant that the internal temperature was rising and rising until day 12 when the blinds were shut. For the subsequent five days the building was still cooling down to the set point temperature. This all means that the steady state assumptions the co-heating test are based upon were not met and this significantly impacted the result.

3.4 Main Co-heating Result

The co-heating results from solar corrected linear regression, as originally reported, are shown in the two figures below. The data from days with the blinds shut is initially removed as during these days the highest heat input was not electrical power or even solar gains but in fact the thermal mass of the building itself. In the second plot a rudimentary correction to these days has been applied.

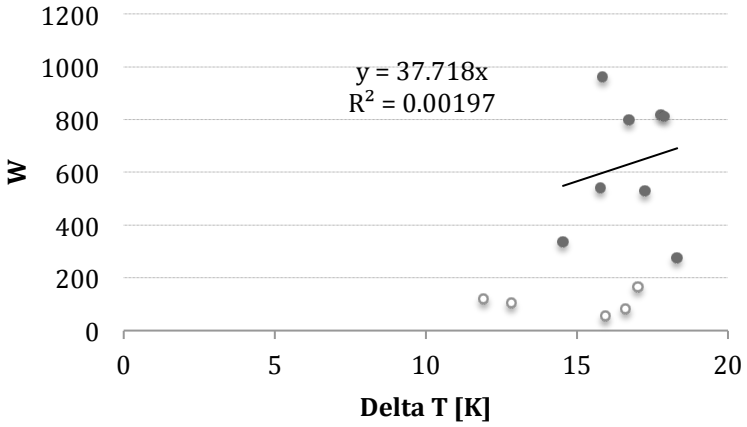

Figure 14: Plot to determine thermal heat loss coefficient. Solid data points represent the days 5-13 and the hollow points show the discarded points in the days 14-18 in which the blinds were shut.

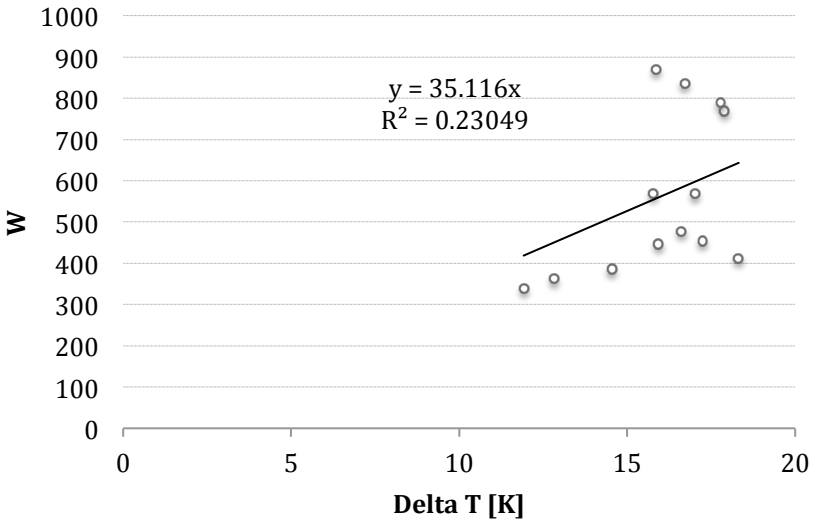

- **Figure 15: Result with corrections for thermal mass contributions**

This rudimentary correction involved the use of heat flux data. The change in heat flux seen during the cooling down of the building was associated with the thermal mass contribution to internal heating. This was then extrapolated and used to correct those five data points. This does rely on some heavy assumptions and carries with it a large amount of uncertainty. The result from this first test was therefore stated to be:

$$35 \pm 15 \text{ W/K}$$

Another large source of uncertainty is the extent of the solar corrections derived from the solar aperture. As previously mentioned the solar aperture can be experimentally calculated or calculated from the glazing characteristics of the dwelling. The data in both co-heating tests did not allow for this to be done experimentally so it has been calculated from glazing characteristics in the PHPP file. As with the heat loss coefficient there is likely to be a difference between the design and as-built solar aperture value. In this first test as such a high proportion of the heating came from solar gains any inaccuracy in the solar aperture can have a significant influence of the stated heat loss coefficient. This makes any test that features high proportions of solar gains inherently less accurate than a dull one, in which the solar aperture has far less influence. This is one of the main reasons the second co-heating result can be stated with far more confidence than the first.

3.5 External Conditions

To compare with the external conditions of the second test in figure 10 the external conditions of the first test are shown below. It is important to note the lower ΔT, related to higher external temperatures, and a larger variation in external temperature, which will lead to more thermal mass effects. Most significantly solar radiation regularly reaches values four times higher than the maximum seen in the second test.

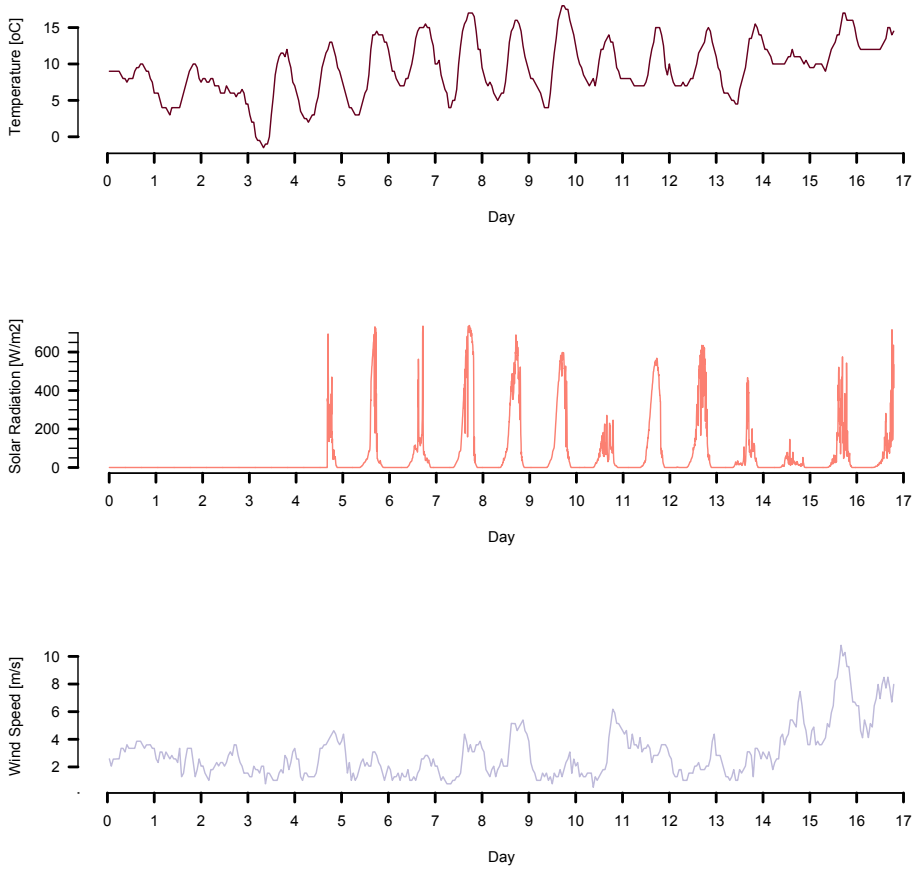

Figure 16: External weather conditions of the first co-heating test

4. Conclusions & Recommendations

Two co-heating tests were performed on Camden passivhaus, the first in March 2010 and the second December 2012. The result of the first test was 35 ± 15 W/K, indicating the building performed well in comparison to its design intent. However, this first test had a large amount of uncertainty due to high solar gains and overheating.

Therefore a second test was performed in December 2012. Simulated co-heating tests had show this was the most likely time to achieve an accurate result, although this depended on having dull conditions. Fortunately this second period was extremely dull and allowed a second result of 56 ± 5 W/K to be recorded with far less uncertainty.

This indicates that the Camden passivhaus is performing well in comparison to its PHPP design intent of 66 W/K. This is a good reflection on the design and build quality of Camden passivhaus and lessons from this process could be taken forward to ensure more buildings had as-built performances closer to design.

Co-heating is one of few post construction tools we have that are capable of evaluating actual performance in situ. The test method is fairly demanding in terms of test duration and requirements over the incumbent weather. The demands on modern energy efficient houses, particularly in passivhaus style designs, are even greater and the sensitivity to uncertainty higher. From simulation work in section 2 as well as both the co-heating tests it is clear that overheating above the co-heating set point temperature has massive implications on the co-heating result. The steady state co-heating model cannot handle the dynamic thermal mass effects induced when this overheating occurs. The solution, if the co-heating method is going to be used in dwellings similar to Camden passivhaus is that overheating needs to be avoided. This may mean lowering blinds throughout testing and accepting the limitations this causes. Or it may require a higher internal set point temperature and the repercussions to the building fabric cracking and drying out accepted. Performing simulated co-heating tests as in section 1.2 can allow the researchers greater understanding of both the uncertainty in the co-heating measurement and the likelihood of achieving an accurate result.

Even after avoiding overheating there still remain large amounts of uncertainty in the co-heating result from accurately determining solar gains and the solar aperture. The solar aperture itself may have more uses beyond the co-heating method, such as assessing the probability of summer time overheating. Therefore more research is needed into this type of building parameter measurement.

Appendix D

NHBC Co-heating Field Trial Report

NHBC Co-heating Project

UCL Co-heating Test February 2012

by

Samuel Stamp

samuel.stamp.10@ucl.ac.uk

3rd May 2012

Energy Institute
University College London

Table of Contents

1. Introduction

NHBC Foundation Co-heating Project

The co-heating test document in this reports falls under the context of the NHBC Foundation Co-heating Project, which aims to 'investigate sensitivity of variations in test methodology'.

A series of co-heating tests, by 6 different organizations, were run on the same test dwelling between January and April 2012. The quality of workmanship and materials used for the test dwelling's construction are well documented. Additionally a 'control' test was run for the same period by BRE in an identical and neighbouring house. It is hoped the findings of this series of tests and their subsequent reports will help to develop guidance on an 'optimal test method suitable for use in a range of buildings.'

UCL Test

The UCL Co-heating test of was carried out from the 10th to the 24th of February 2012. The previous test had finished a couple of days previously such that the building required a brief period to heat up and reach a steady internal temperature. Allowing for this warm up and dismantling the equipment the test data includes 13 days at steady state for analysis.

In addition to the co-heating several additional methods were undertaken. These included (1) in-situ U-value measurements of a selection of building elements, (2) background air infiltration measurements through CO2 tracer gas decay methods and (3) an infrared thermography survey.

BRE Test House B.04

The test house, B.04, was built as part of a pair of identical houses at the BRE Garston site, Watford, in 1995 and has been used for a series of tests ever since. The design and construction were set to meet the Swedish standard of performance at the time. The building sits on two floors with an empty attic space where insulation is provided at the ceiling layer.

Figure 1: Test house south façade (right) with its identical dwelling (left).

The construction is a brick clad timber frame structure with suspended timber floors. In total there is 13.12m^2 of glazing, split between the north and south facades. Cross-sectional details of the building elements are shown in figure 2 and their design u-values and respective heat loss are shown in table 1.

Table 1: Building design heat and u-value loss by element

	Envelop Area [m2]	*Design U-value [W/m2K]*	*Design HLC [W/K]*
Walls	116.88	0.210	24.54
Windows	13.12	1.850	24.27
Floor	42.37	0.210	8.90
Roof	42.37	0.160	6.78
Door	1.44	1.000	1.44
TOTAL	216.18		65.93

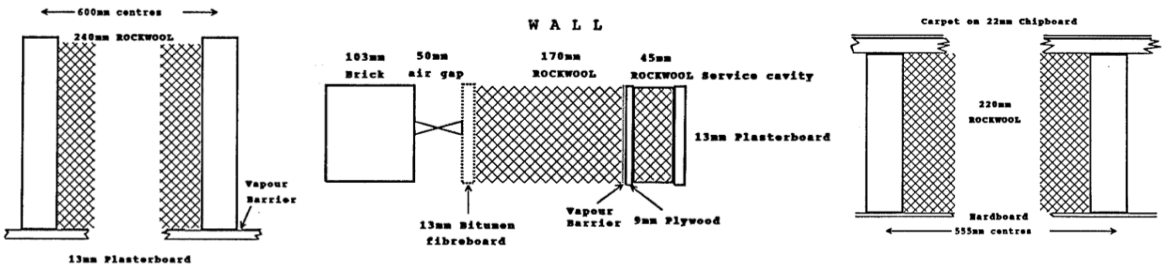

Figure 2: Cross sectional constructions of (left to right) ceiling, external wall and floor.

The following section documents the methods used in both the co-heating and additional tests used to investigate the thermal performance of the building. Section 3 will contain the analysis, first looking at temperature and environmental conditions during testing. The analysis of the co-heating result to extract the heat loss coefficient and solar aperture are then shown. Results from in situ u-values, infiltration and infrared thermography are presented in turn. Finally a conclusion will compare the different types of measurements made.

2. Test Method

2.1 Co-heating

Guidelines for the co-heating test protocol are laid out in the Leeds Metropolitan Protocol (2009) and form the basis of the method employed here. A significant departure from this was the absence of any pressurization tests, as it was deemed the CO_2 tracer gas decay measurements would be sufficient for determining air infiltration. The building was heated to a constant 25°C through electric heaters controlled by individual thermostats. Mixing was then encouraged by the placement of circulation fans throughout the dwelling. All electricity consumed by heaters and subsidiary equipment was recorded by kW-hour meters with pulse outputs.

In total 5 sets of kW-hour meter, fan, heater and thermostat combinations were positioned in the house. Their locations are described in figure 3. Additional temperature and relative humidity sensors were placed in all zones in the house. A full list of equipment used is available in the appendix.

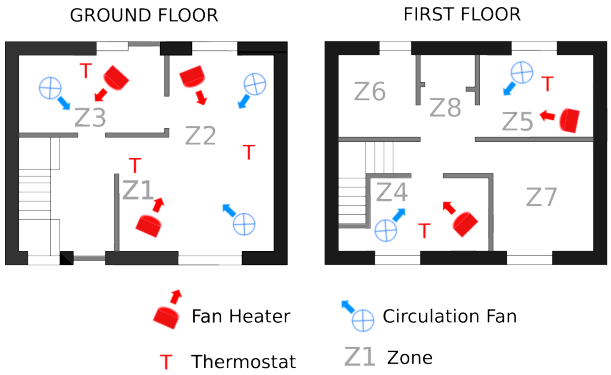

Figure 3: Floor plans and co-heating equipment positioning

The external environment was monitored through the use of a dedicated weather station placed centrally in front of the south façade. This included a vertically orientated pyranometer on a tripod-mounted pole. The weather station included the facilities to measure wind speed, direction, rainfall and external temperature and relative humidity. Two additional temperature sensors were housed in a Stevenson screen at the same location. A permanent weather station and additional horizontal pyranometer were also already in place at the site allowing for a consistent form of measurement throughout the series of tests and allowing a comparison with the local station data.

2.2 In-situ U-value

Heat flux plates were placed in a variety of locations throughout the house to measure in situ u-value and heat flows. As it takes a period of approximately a week under co-heating conditions to determine the U-values the sensors were moved at the midway point.

Six Hukseflux HF01 heat flux sensors were used and positioned on the walls, floor and ceiling via a non-silicon heat compound and tape. Images of a selection of sensors in position are shown below. Sensors were placed in pairs on each measured element and air temperature local to each pair was recorded. Additionally, areas tested were observed through an infrared camera such that any defects at the point of the sensor were noticed. Often sensors were placed to avoid any defects but some were deliberately placed to pick up the difference in heat flux at these defects or edge effects.

Figure 4: Heat flux sensors on external wall

2.3 CO2 Tracer Gas Decay

Carbon dioxide was used as a tracer gas in a decay method outlined by Roulet and Foradini (2006). This involves a release of CO_2 for a short period of time, followed by recording the exponential decay back to background levels. Three CO2 sensors were placed throughout the dwelling to record internal levels.

CO2 was released from cylinders in two locations in the dwelling (see figure 5) by a solenoid valve attached to the regulator on each cylinder. The solenoid would switched on and allow the release of CO2 for 15mins every 24 hours via an electronic timer. Due to a fault with the solenoids this was not performed daily and some releases were made manually whilst the tester was in the dwelling.

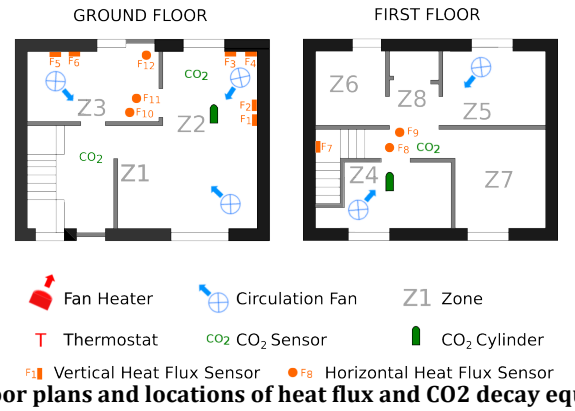

Figure 5: Floor plans and locations of heat flux and CO2 decay equipment

3. Analysis

3.1 Temperatures during testing

The dwelling was heated to 25°C within the first day of testing, having initially been 8°C internal air temperature. Internal temperature was than held at 25°C for the test period. The attic temperature (SE1) follows the profile of the external temperature, with a lag of around 2 hours and an average temperature difference of +8.5°C from the external air.

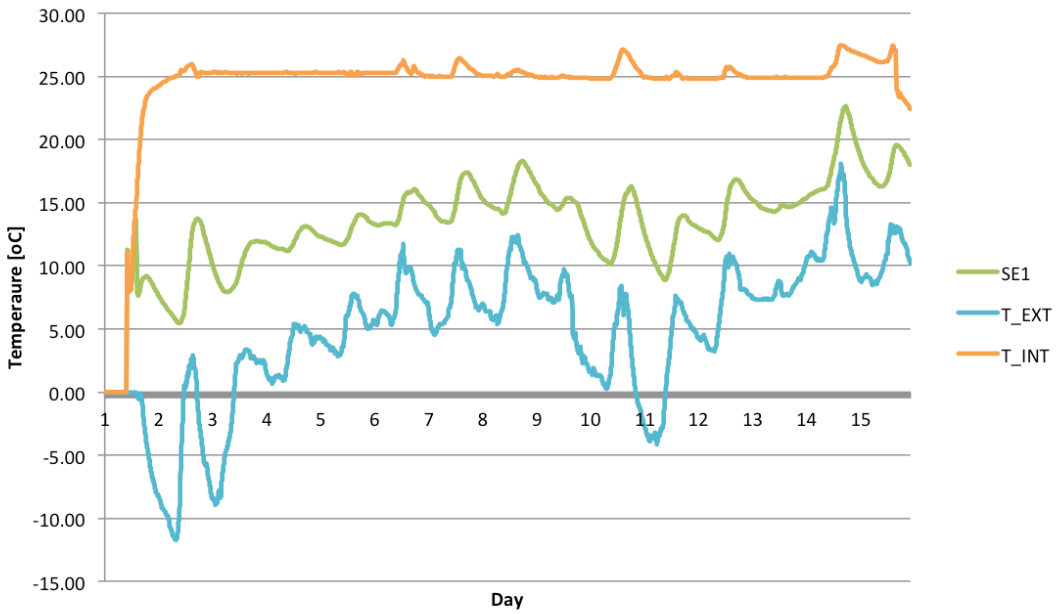

Figure 6: Temperature profiles throughout test period. Internal (T_INT), external (T_EXT) and the attic (SE1) temperatures are shown.

Several days show evidence of the midday peak in solar gains, forcing the internal air above the set temperature. This effect is most significant in day 14 where the temperature does not return to 25°C before the end of the day. This means energy has gone into heating the mass of the building, but as the building has not fully cooled the contribution to the mass has not been returned. We would therefore expect day 14 to have a higher power input than normal, which can be seen in figure 11.

3.2 Mixing & Temperature Stratification

Uneven temperature and stratification wants to be avoided as far as possible through the use of the mixing fans and employing a sufficient number of sets of heaters and thermostats. As a separate thermostatic controller controls each heater they need to be calibrated to each other once in position.

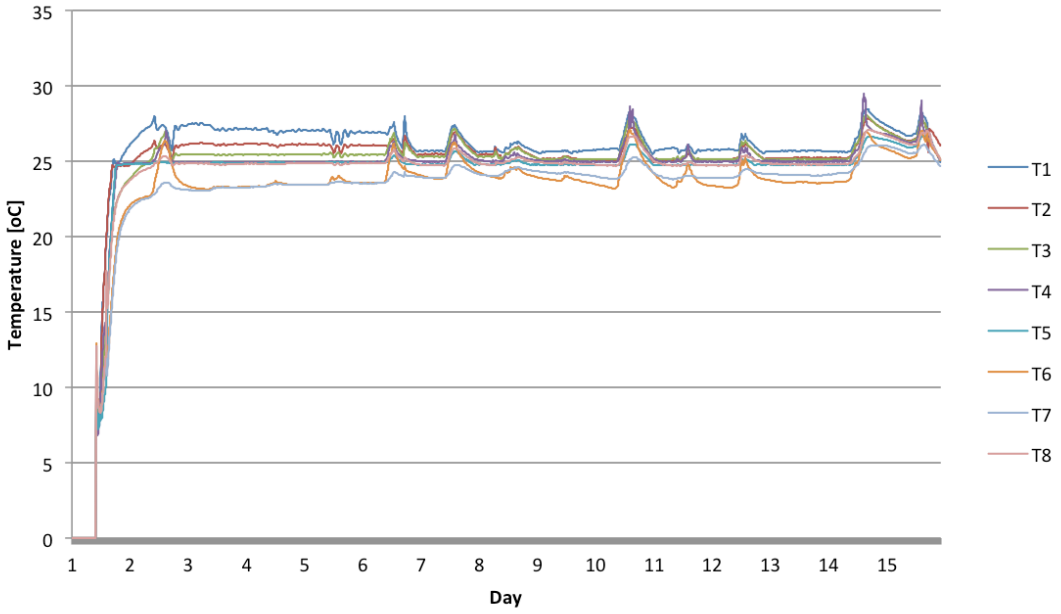

Figure 7: Zonal internal temperatures. Temperatures are labeled with numbers equivalent to their zones shown in figure 3.

Figure 7 shows range in temperatures in each zone defined in figure 3. Temperatures in zones throughout the house were not as close as desired, emanating from two factors. Firstly, the first six days show evidence of zones 1 & 2 overheating due to a thermostat that needed to be recalibrated once in position in the house. Secondly, the upper bedroom and bathroom, without their own designated heater remained cooler than the other rooms in the building. With a narrow floor layout it is advisable to incorporate more heaters and mixing fans to reduce this temperature difference, although due to equipment availability this was not possible on this occasion.

A heat loss weighted average internal temperature was used in the analysis, although this varied little from either a volume weighted or simple average value.

3.3 Relative Humidity

Internal relative humidity was also monitored, as it can be useful to determine if heating energy is used in the evaporation of moisture rather than directly heating the space. This can be particularly important on recently completed buildings when the drying out process is not yet complete.

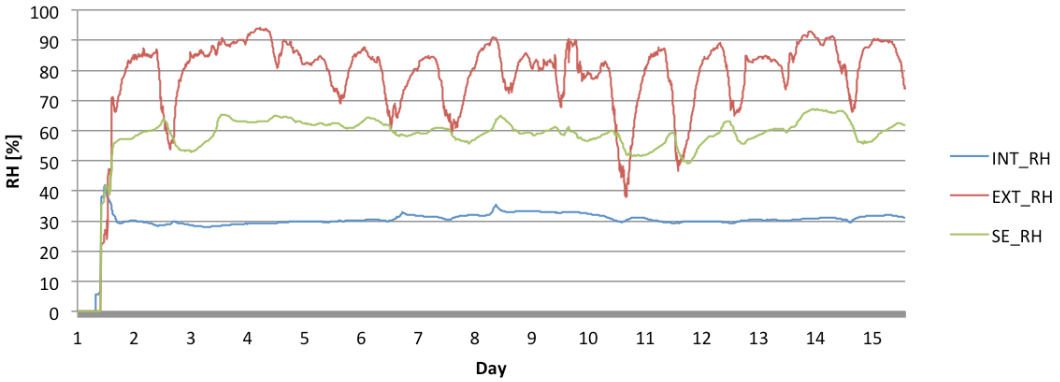

Figure 8: Relative Humidity throughout test period. Internal (INT_RH), external (EXT_RH) and attic (SE_RH) relative humidity are shown.

In this case there was a small quantity of water in both the sink and bath in the bathroom at the start of the test. As a result there is an initial peak in RH before it returns to a level around 30% for the duration of the test. This can be linked to the evaporation of this sitting water, as the peak is strongest in the sensor assigned to the bathroom. As this evaporation happen during the first day, forming the warm up phase and therefore excluded from analysis, this can be ignored.

3.4 Heat Loss Coefficient

The co-heating test operates on the principle of setting up a constant internal temperature and therefore energy balance, meaning the energy supplied towards heating is equal to the energy being lost from the building.

$$\textit{Space Heating + Solar Gains = Fabric Heat Loss + Infiltration Losses}$$

$$\boldsymbol{Q + R.S = (\Sigma A.U)\Delta T + \frac{1}{3}nV\Delta T}$$

Here: Q is the power [W], heat input from electric heaters or other heating device,
R is the solar aperture [m^2],
S is the vertical solar radiation [W/m^2],
ΔT is the temperature difference, delta T [K], between the internal and external conditions,
$\Sigma A.U$ is the sum of the U-values [W/m^2] and respective areas of the thermal envelope [m^2],
n is the air change rate (associated with the background infiltration rate) [h^{-1}],
V is the internal volume [m^3]

The heat loss coefficient can be found through regression of the power, solar radiation and temperature difference, delta T. To smooth out dynamic effects daily averaged values are used. A 6am-6am, rather than 12am-12am, averaging period is used as it provides a more balanced, natural time period with the daily weather cycle. In its simplest form this analysis involves the plotting of daily averaged electrical heating power against delta T, the internal – external temperature difference. This raw data plot is shown below, figure 9.

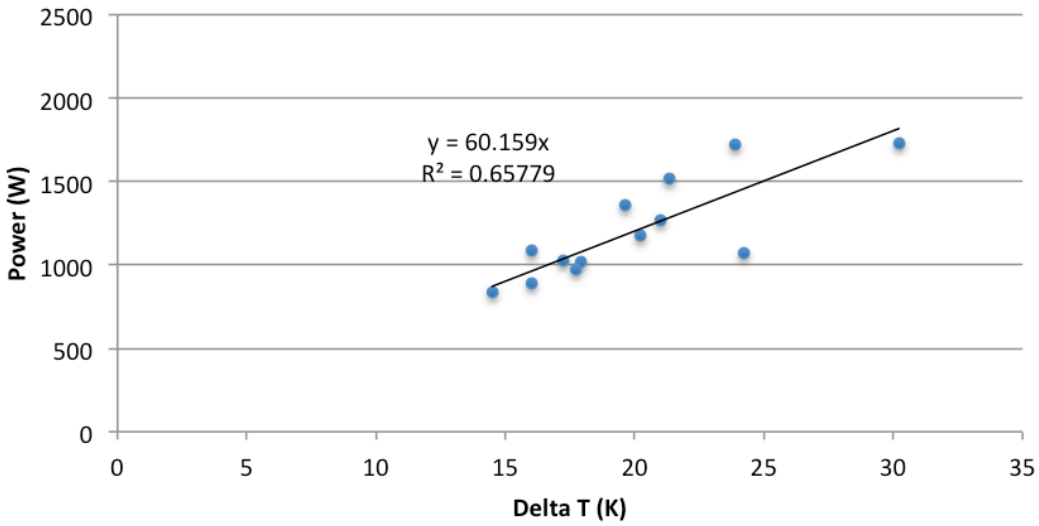

Figure 9: Analysis of raw co-heating data.

The slope of the regression line, which is suppressed through the origin, gives the calculated heat loss coefficient; in W/K. Simply from the raw data this gives a heat loss coefficient of 60.2 W/K. The strong range in delta T's due to varying weather is clear here and aids in the certainty we have in drawing the regression line.

However, this does not incorporate all the additional heating supplied by solar gains. To begin to look at incorporating this it is useful to look at a alternative analysis method, that first introduced by Siviour (Everett, 1985).

In figure 10, the heat balance equation is rearranged and power over delta T is plotted against solar radiation divided by delta T. Two key variables can be extracted from this figure. Firstly a heat loss coefficient of 69.9 W/K can be calculated from the y-intercept. Then the gradient of the slope, 2.376, gives the solar aperture. This identifies the amount of solar gain, i.e. Watts, delivered to the building for a given solar radiation. Effectively this analysis is a 2D projection along the 3D plane of delta T.

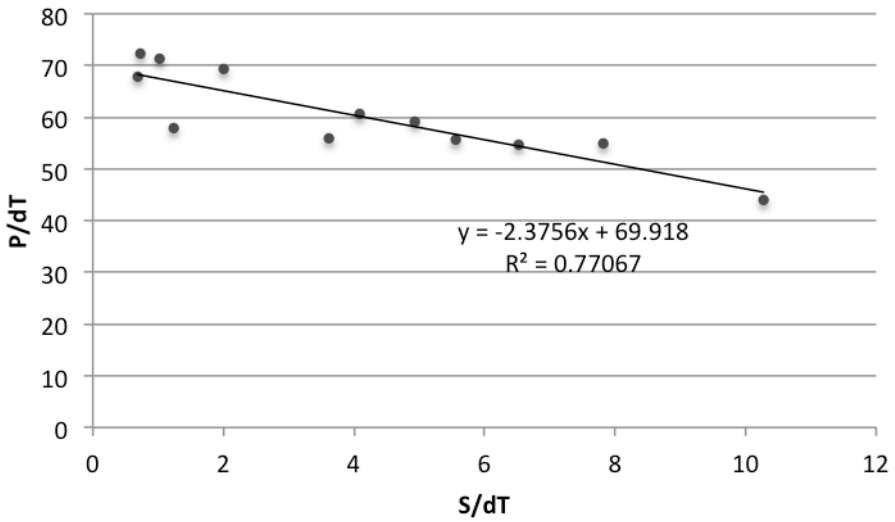

Figure 10: Siviour analysis of co-heating data

This solar aperture can be used to correct daily measurements in power for the solar gains calculated for the given solar radiation. This has been performed in figure 11. The heat loss coefficient in this instance is again determined by the gradient of the regression line and is given as 70 W/K, very close to the value given in the Siviour analysis.

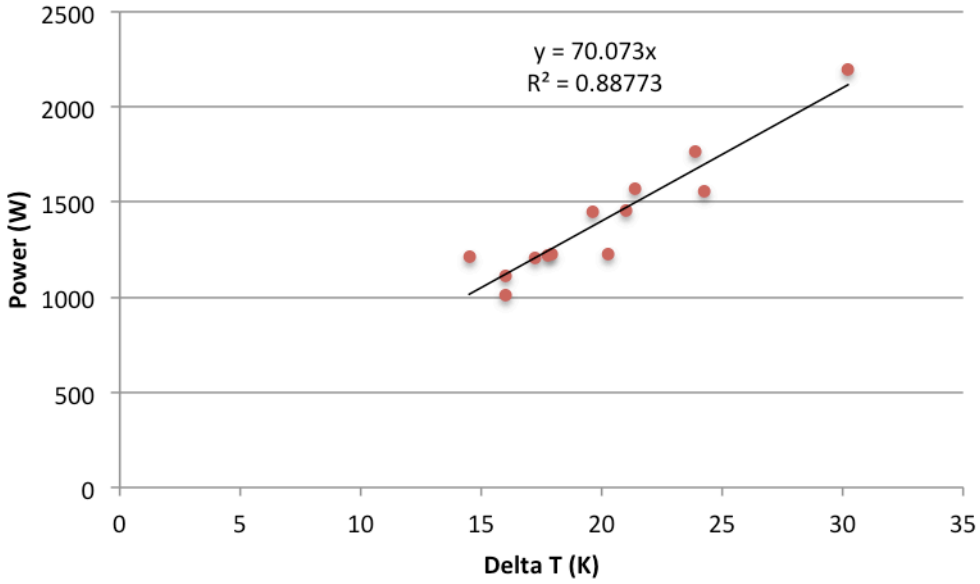

Figure 11: Solar corrected analysis of co-heating data

The overheating seen earlier in day 14 (figure 6), in which we expected additional power per K to be used, is evident in figure 11. Day 14 represents the furthest left point, and has a higher power than predicted by the regression line, as expected. It is also worth pointing out that when the regression line is not suppressed the gradient is given as 70.3 W/K and the intercept occurs at -5.1W.

Effectively this is a multiple regression of power, solar radiation and delta T. This can be analysed directly as a multiple regression and the results are shown in the table below.

Table 2: HLC & Solar Aperture through multiple regression

	Coefficient	*Standard Error*
Heat Loss Coefficient / Delta T Coefficient	69.3	2.6
Solar Aperture / Solar Radiation Coefficient	-2.2	0.5

Typically wind measurements, often including data with insolation, can be used to further correct the data. However, in this case the wind measurements from both the local and BRE station showed weak correlation with heat loss so no such correction was made.

The heat loss coefficient derived from the co-heating test is then taken to be:

$$\mathbf{69.3 \pm 2.6\ W/K}$$

And the solar aperture:

$$\mathbf{2.2 \pm 0.5\ m^2}$$

3.5 In situ U-value

In situ U-values were calculated for each element by averaging the heat flux over the temperature difference for the test period, see equation below (Baker, 2011). Cumulative averaged U-values are shown in figure 12.

$$U = \frac{\sum Q}{\sum T_i - \sum T_e}\ \mathrm{W/m^2K}$$

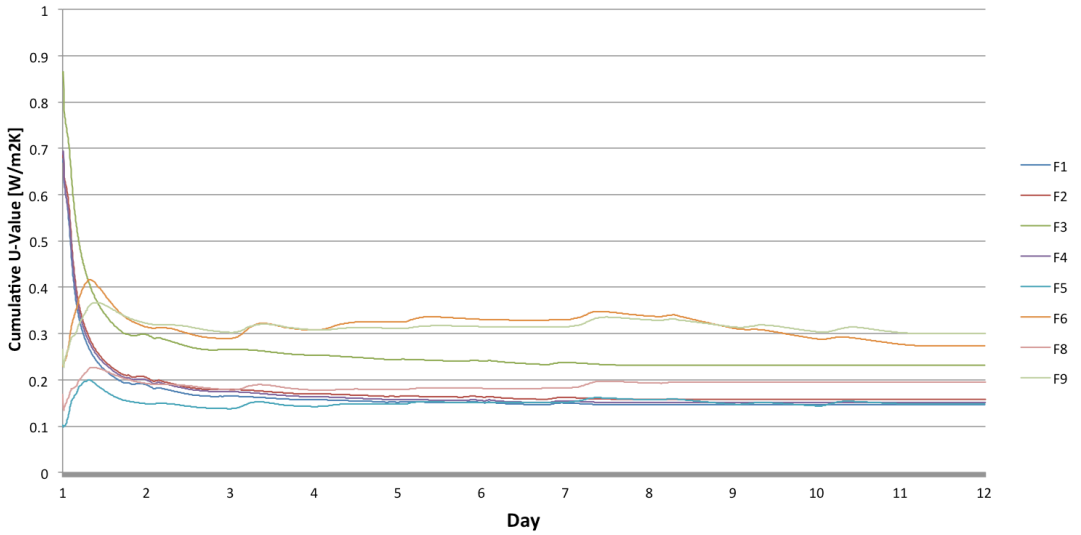

Figure 12: Cumulative u-value measurements

U-value measurements taken at central points in the wall, away from thermal bridges and defects, (F1, F2, F4, F5) show very consistent U-value measurements, showing an average value of 0.155 W/m²K (table 3).

Table 3: Design and measured external wall u-values

Sensor	*Position*	*Design U-Value [W/m2K]*	*Measured U-Value [W/m2K]*
F1	East Wall High	0.21	0.15
F2	East Wall Low	0.21	0.16
F3	North Wall Corner	0.21	0.23
F4	North Wall Window	0.21	0.15
F5	North Wall Kitchen	0.21	0.16
F6	North Wall Defect	0.21	0.35

Two sensors show considerably higher U-values for the external wall. F3 is positioned close to the junction of the east and north wall. Hence it measures a U-value 52% higher than the other wall sensors. Sensor F6 was placed deliberately over a defect detected through thermal imagery. This is believed to be a joint in the fabric or service cavity in the wall, meaning a reduction in thermal resistance. The U-value measured here was 133% higher than the other wall measurements.

This indicates that whilst the main body of the external wall is performing better than design, areas of the wall are performing significantly worse.

Table 4: Design and measured ceiling u-values

Sensor	*Position*	*Design U-Value [W/m2K]*	*Measured U-Value [W/m2K]*
F8	Ceiling 1	0.16	0.16
F9	Ceiling 2	0.16	0.35

Two sensors determined the u-value for the ceiling, this time utilising the attic temperature as the 'external' temperature. One measurement matches the design u-value whilst the other is significantly higher (table 4). It is likely this emanates from being placed on a roof joist or lower insulation, although thermal images did not confirm this.

Finally, floor heat flux was monitored. Whilst it was not possible to take a temperature measurement beneath the floor and hence determine U-value, the heat flux was observed. Flux measured at the edge was 60% higher than measured in the centre of the floor.

3.6 Recalculation of Performance Based on U-value

The heat loss coefficient as a sum of element u-values and envelop areas can be re-calculated based on in situ u-value measurements. Whilst not all elements were measured the design and re-calculated building heat loss can be compared. Due to the lower than design u-value of the walls, the largest envelope area, the total heat loss coefficient is marginally lower than design (table 5).

Table 5: Design and re-calculated building heat loss

	Envelop Area [m2]	*Design U-value [W/m2K]*	*Measured U-Value[W/m2K]*	*Design HLC [W/K]*	*Measured HLC [W/K]*
Walls	116.88	0.210	0.155	24.54	18.12
Windows	13.12	1.850	-	24.27	24.27
Floor	42.37	0.210	-	8.90	8.90
Roof	42.37	0.160	0.250	6.78	10.59
Door	1.44	1.000	-	1.44	1.44
TOTAL	216.18			65.93	63.32

(Note: Average wall u-value taken from sensors F1, F2, F4, F5, excluding the measurements of defects)

3.7 Infiltration

Suitable periods of decay in CO_2 concentration are selected and put into a normalized form, C_n, for each time step $C(t)$, using the initial concentration C_i and the outdoor base level C_o. The natural log of C_n is then plotted against time, in units of hours, as shown in figure 13. The gradient of the slope represents the measured air change rate.

$$C_n = \frac{(C(t) - C_o)}{(C_i - C_o)}$$

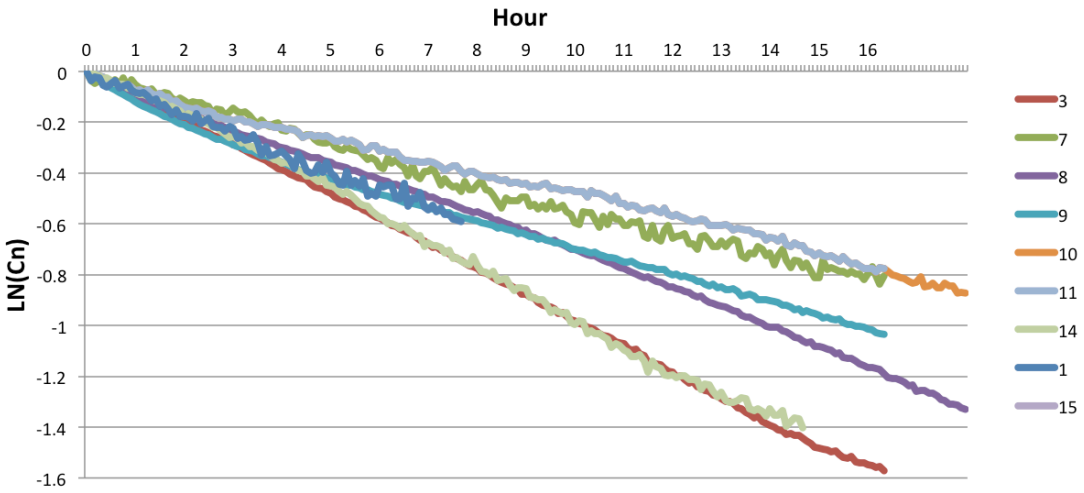

Figure 13: Logarithmic normalised CO2 decays labeled for different days

Table 6: Infiltration measurements throughout test period

Day	*Specific Air Flow Rate [h-1]*	*Outdoor Air Flow Rate [m3/h]*	*Specific Leakage Rate [m3/(hm2)]*	*Heat Loss (W/K)*
1	0.1022	21.6562	0.1246	7.15
2	-	-	-	-
3	0.0479	10.1500	0.0584	3.35
4	-	-	-	-
5	-	-	-	-
6	-	-	-	-
7	0.0747	15.8289	0.0910	5.22
8	0.0648	13.7311	0.0790	4.53
9	0.0498	10.5526	0.0607	3.48
10	0.0634	13.4345	0.0773	4.43
11	0.0576	12.2054	0.0702	4.03
12	-	-	-	-
13	-	-	-	-
14	0.0943	19.9822	0.1149	6.59
15	0.0853	18.0751	0.1040	5.96
Average	**0.0711**	**15.0684**	**0.0867**	**4.9726**
Stdev	0.0193	4.0988	0.0236	1.3526

The air change rate is given as 0.7 ACH_{50}. A rule of thumb attributed to Kronvall and Persily by Sherman (1987) generally relates blower door data to seasonal air change data in normal conditions:

$$ACH = \frac{ACH_{50}}{20}$$

This allows the design and measured infiltration rates to be compared (table 7), although it should be remembered the 'divide by 20' factor is a rule of thumb and this can vary due to sheltering effects.

Table 7: Design and measured infiltration heat loss

	Design Air Changes [h-1]	*Measured Air Changes [h-1]*	*Design HLC [W/K]*	*Measured HLC [W/K]*
Background Infiltration Rate	0.035	0.071	2.47	5.01
FABRIC + INFILTRATION HEAT LOSS			68.41	68.33

3.8 Infrared Thermography

Images were taken between 6 and 8am on the 17/02/2012 both externally and internally. During this period the average external wind speed was 0.7 m/s and the average internal – external temperature difference was 19.5°C. A selection of images are shown and annotated below. In general no major anomalies were found, perhaps a tribute to the higher attention paid to the build. The elevated and more stable internal temperatures provided by co-heating form an ideal platform in which to perform a infrared thermography survey and a great deal on information can often be found. There were periodic linear defects in the walls, slight issues with door and window fittings and losses around the boiler flue and its pipe work.

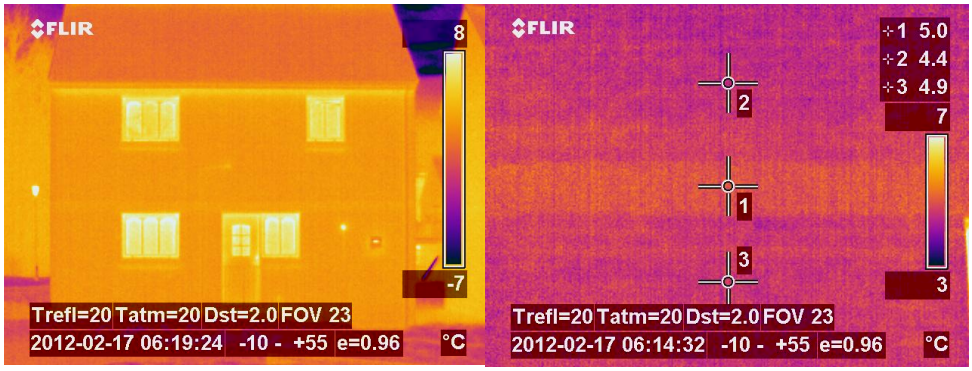

Figure 14: Left) External image of house (north facade), Right) Difference between types of bricks on external facade

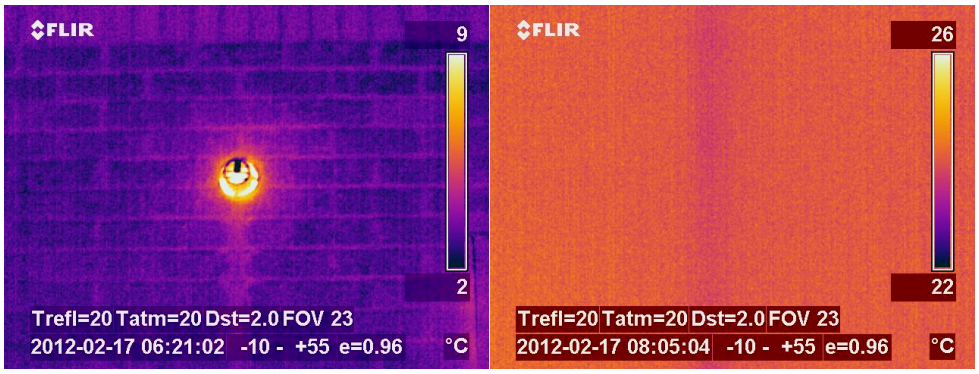

Figure 15: Left) Heat loss around, and below, boiler flue, Right) Defect shown from interior view of wall

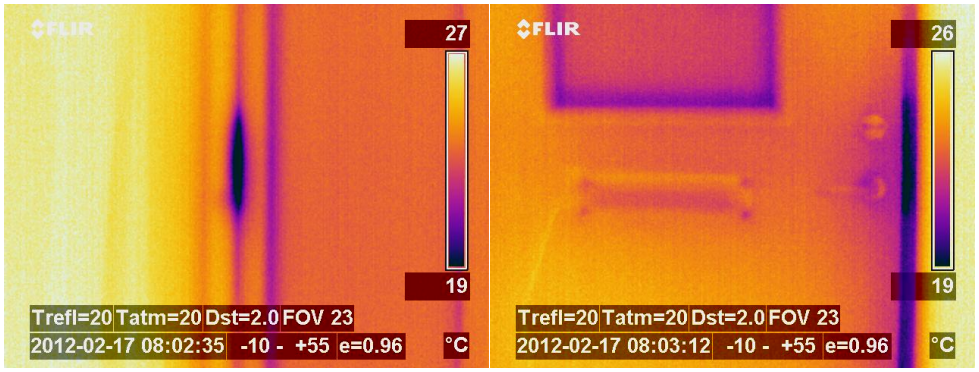

Figure 16: Left) Heat loss due to poor fitting in window frame joint, Right) Leakage around door handle fitting

4. Conclusion

The comparison can now be extended to include all the measured data. The heat loss coefficient in table 8 is calculated in three ways; from design, based on summing in situ u-value and measured infiltration or by using the co-heating total heat loss, from which infiltration based on CO_2 decays can be subtracted.

Table 8: Comparison of heat loss coefficients

		Heat Loss Coefficient HLC [W/K]
Design	*Fabric*	65.9
	Infiltration	2.5
	Total	68.4
U-Value & CO2	*Fabric*	63.3
	Infiltration	5.0
	Total	68.3
Co-heating & CO2	*Fabric*	65.1
	Infiltration	5.0
	Total	70.1

The results show similar measurements. In part, as a test house the design and construction process were more closely controlled. It would be expected that the as-built structure is almost identical to design. Often in practice changes are made during construction, or from original design calculations such that the two can significantly vary. Additionally, in its role as a test house it would be expected far more care was taken over construction details.

The co-heating test itself provided a total heat loss coefficient of 69.3 ± 2.6 W/K, with a solar aperture of 2.2 ± 0.5 m^2. The mix in external temperature and solar radiation experienced during the test period provided strong correlation and the ability to derive the solar aperture accurately, which was further improved by the solar correction applied.

Further investigations are likely to occur subsequent to this report, based on the assessment of other participating organisations findings and additional analysis performed from data collected in this test.

References

Baker, P., 2011. Technical Paper 10 U - values and traditional buildings, *Historic Scotland*

Everett, B., 1985. Rapid Thermal Calibration of Houses, *Science and Engineering Research Council*

Leeds Metropolitan University, 2009. Detailed Description of Coheating Test Procedure, *Good Homes Alliance*

Roulet, C. & Foradini, F., 2006, Simple and Cheap Air Change Rate Measurement Using CO 2 Concentration Decays. *International Journal Of Ventilation*, 1(1), pp.39-44.

Sherman M.H., 1987, Estimation of Infiltration from Leakage and Climate Indicators, *Energy and Buildings*.

Appendix

EQUIPMENT LIST
LOGGERS
Campbell Scientific CR10X Data logger
Campbell Scientific CR23X Data logger
Eltek RX250AL receiver logger with RX250AL receiver logger modem
SENSORS
Hobo U12-012
Eltek GD47 CO2, RH and Temp Transmitter
Hukseflux HFP01 Heat Flux Sensor
WEATHER STATION
6250UK Vantage Vue Weather Station
CMP3 Pyranometer
CO2 DECAY
Wave 2kg Cylinder / Disposable Cylinder
Wave Solenoid Regulator / D-D System
CO-HEATING EQUIPMENT
Elster A100C Electricity Generation Meter (1W/Pulse Output)
Delonghi 2kW Electric Heater
Air Circulator
Tripod
TMS Europe Temperature Control Box